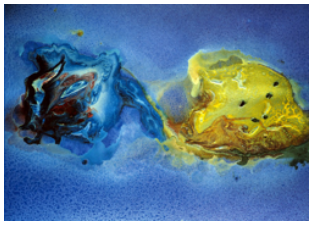

TECHNISCHE UNIVERSITÄT MÜNCHEN
PHYSIK-DEPARTMENT
INSTITUT FÜR THEORETISCHE PHYSIK T30F

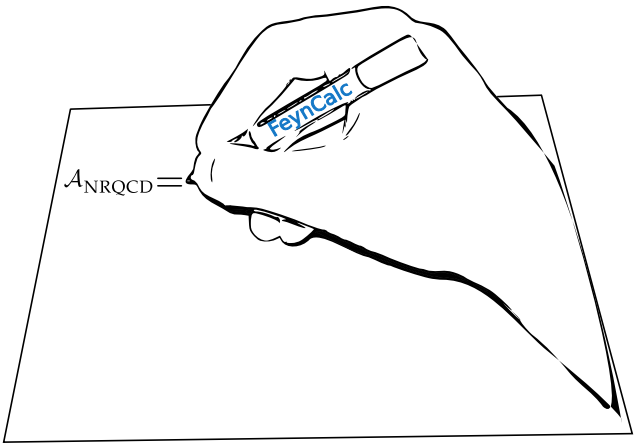

Nonrelativistic Effective Field Theories of QED and QCD: Applications and Automatic Calculations

DISSERTATION
BY
VLADYSLAV SHTABOVENKO

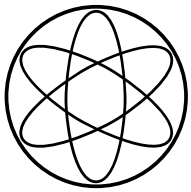

TECHNISCHE UNIVERSITÄT MÜNCHEN
PHYSIK-DEPARTMENT
INSTITUT FÜR THEORETISCHE PHYSIK T30F

Nonrelativistic Effective Field Theories of QED and QCD: Applications and Automatic Calculations

VLADYSLAV SHTABOVENKO

Vollständiger Abdruck der von der Fakultät für Physik der Technischen Universität München zur Erlangung des akademischen Grades eines

Doktors der Naturwissenschaften (Dr. rer. nat.)

genehmigten Dissertation.

Vorsitzender:		Prof. Dr. Lothar Oberauer
Prüfer der Dissertation:	1.	Prof. Dr. Nora Brambilla
	2.	Hon.–Prof. Dr. Wolfgang F. L. Hollik

Die Dissertation wurde am 10.05.2017 bei der Technischen Universität München eingereicht und durch die Fakultät für Physik am 22.05.2017 angenommen.

Publications related to this thesis

Refereed publications

- V. Shtabovenko, R. Mertig and F. Orellana, *New Developments in FeynCalc 9.0*, Comput. Phys. Commun. 207, 432-444 (2016), arXiv:1601.01167 [hep-ph].
- V. Shtabovenko, *FeynHelpers: Connecting FeynCalc to FIRE and Package-X*, arXiv:1611.06793 [physics.comp-ph], accepted for publication in Computer Physics Communications.
- N. Brambilla, V. Shtabovenko, J. Tarrús Castellà and A. Vairo, *Effective field theories for van der Waals interactions*, arXiv:1704.03476 [hep-ph], in publication on Physical Review D.

Preprints

- N. Brambilla, W. Chen, Y. Jia, V. Shtabovenko and A. Vairo, *Relativistic corrections to exclusive $\chi_{cJ} + \gamma$ production from e^+e^- annihilation*, in preparation for submission to Physical Review D.

Conference proceedings

- V. Shtabovenko, *Relativistic corrections to electromagnetic heavy quarkonium production*, Proceedings of Confinement XII in Thessaloniki, EPJ Web Conf. 137, 06023 (2017).
- V. Shtabovenko, *Van der Waals forces in pNRQED*, Proceedings of Confinement XI in St. Petersburg, AIP Conf. Proc. 1701, 080012 (2016).
- V. Shtabovenko, *FeynCalc 9*, Proceedings of ACAT 2016 in Valparaiso, J. Phys. Conf. Ser. 762 no.1, 012064 (2016), arXiv:1604.06709 [hep-ph].

Zusammenfassung

Diese Doktorarbeit beschäftigt sich mit der Anwendung von nichtrelativistischen Effektiven Feldtheorien auf die Physik der elektromagnetischen und der starken Wechselwirkung. Die Hauptergebnisse dieser Arbeit sind in drei Teile unterteilt.

Im ersten Teil benutzen wir Potenzial-Nichtrelativistische Quantenelektrodynamik (pNRQED), eine EFT der QED bei Energien viel kleiner als $m_e\alpha$ (wobei m_e für die Elektronenmasse steht und α die Feinstrukturkonstante bezeichnet), um eine konsistente Beschreibung der elektromagnetischen Van-der-Waals-Kräfte zwischen zwei Wasserstoffatomen zu entwickeln, deren Abstand R viel größer als der Bohrsche Radius ist. Dabei betrachten wir die Wechselwirkungen bei kurzen ($R \ll 1/m_e\alpha^2$), langen ($R \gg 1/m_e\alpha^2$) und mittleren Abständen ($R \sim 1/m_e\alpha^2$) und bestimmen die relevanten dynamischen Skalen, die für jedes von diesen drei Regimes charakteristisch sind. Für jedes Regime konstruieren wir eine passende Van-der-Waals-EFT, welche die einfachste Beschreibung der Niederenergiedynamik ermöglicht. Bei dieser Beschreibung kommen die Van-der-Waals-Potenziale auf natürliche Art und Weise als Matching-Koeffizienten der entsprechenden EFTs zum Vorschein. Sie lassen sich systematisch berechnen, Ordnung für Ordnung in den relevanten Entwicklungsparametern, so wie es in der vorliegenden Arbeit gemacht wurde. Des weiteren enthalten diese Potenziale Beiträge von Stahlungskorrekturen und müssen dementsprechend renormiert werden. Die Entwicklung eines konsistenten EFT-Rahmenwerks zur Beschreibung von Van-der-Waals-Kräften zwischen zwei Wasserstoffatomen und die Renormierung der Van-der-Waals-Potenziale stellen neue Ergebnisse dieser Studie dar.

Im zweiten Teil untersuchen wir relativistische $\mathcal{O}(\alpha_s^0 v^2)$ (wobei α_s für die starke Kopplungskonstante steht) Korrekturen zu der exklusiven elektromagnetischen Erzeugung von einem schweren Quarkonium χ_{cJ} und einem harten Photon im Rahmen der Nichtrelativistischen Quantenchromodynamik (NRQCD), einer EFT der QCD, welche die nichtrelativistische Natur der Charmonia und Bottomonia sowie die großen Unterschiede zwischen deren relevanten dynamischen Skalen vollständig ausnutzt. Diese Skalen sind $m_Q \gg m_Q v \gg m_Q v^2$, wobei m_Q die Masse eines schweren Quarks kennzeichnet, während v für die relative Geschwindigkeit der schweren Quarks im Quarkonium steht. Das Neue an dieser Untersuchung ist die Einbeziehung der Effekte von höheren Fockzuständen $|Q\bar{Q}g\rangle$, die in den vorherigen Studien der $\mathcal{O}(\alpha_s^0 v^2)$ relativistischen Korrekturen zu $e^+e^- \to \chi_{cJ}\,\gamma$ fälschlich nicht berücksichtigt wurden. Physikalisch entsprechen diese Effekte der Situation, bei der ein Paar von schweren Quarks und ein weiches Gluon sich gemeinsam nichtperturbativ zu einem schweren Quarkonium χ_{cJ} entwickeln. In dieser Arbeit wurden die Matching-Koeffizienten explizit berechnet, welche, mit den entsprechenden langreichweitigen Matrixelementen (LDME) multipliziert, in die NRQCD-faktorisierten Wirkungsquerschnitte eingehen. Die phänomenologische Bedeutung dieser Beiträge bleibt vorerst unklar, da noch keine experimentellen Messungen vorliegen und die Abschätzung der Größe von nichtperturbativen LDMEs mit großen Unsicherheiten verbunden ist. Das Belle II-Experiment in Japan sollte jedoch prinzipiell in der Lage sein, die elektromagnetische Produktion von χ_{cJ} zu vermessen.

Der letzte Teil dieser Doktorarbeit widmet sich der Entwicklung von Software-Werkzeugen, welche die Automatisierung von Rechnungen in relativistischen und nichtrelativistischen EFTs ermöglichen. Zunächst berichten wir von den Fortschritten im FeynCalc-Projekt. FeynCalc ist ein Mathematica-Paket für halbautomatische symbolische QFT-Rechnungen, das ursprünglich von Rolf Mertig im Jahr 1991 entwickelt wurde. Seit 2001 wurde die Software jedoch fast nicht mehr aktiv weiterentwickelt, obwohl sie unter Theoretikern und Phänomenologen noch große Beliebtheit genießt. Im Jahr 2014

übernahm der Autor dieser Dissertation die Entwicklung des Pakets. Abgesehen von der Ausbesserung zahlreicher Bugs, verbesserte er die Geschwindigkeit der Programms und implementierte viele neue Funktionen, die für Ein- und Vielschleifen-Rechnungen relevant sind. Als nächster Schritt wurde ein Interface namens FEYNHELPERS geschrieben. FEYNHELPERS verbindet FEYNCALC mit PACKAGE-X und FIRE. Ersteres bietet eine Datenbank von analytischen Ergebnissen für skalare Einschleifen-Integrale mit bis zu 4 Beinen, während Letzteres ein Universalwerkzeug für die Reduktion von skalaren Vielschleifen-Integralen mittels partieller Integration (IBP) darstellt. Die Kombination aus FEYNCALC und FEYNHELPERS führt zu einer signifikanten Vereinfachung von Matching-Rechnungen in relativistischen EFTs, bei denen es wichtig ist, vollständig analytische Ergebnisse für die Matching-Koeffizienten zu erhalten. Schließlich wurde FEYNCALC so erweitert, dass sich nun auch Rechnungen in solchen Theorien automatisieren lassen, die nicht manifest lorentzkovariant sind. Das ist z. B. bei den nichtrelativistischen EFTs der Fall, bei denen man explizit die räumlichen und zeitlichen Komponenten von Lorentztensoren betrachten muss. Funktionen, welche spezielle für die Matching-Rechnungen zwischen QCD und NRQCD gedacht sind, wurden dabei in eine separate Erweiterung namens FEYNONIUM ausgelagert. Anschließend ist zu bemerken, dass FEYNCALC, FEYNHELPERS und FEYNONIUM freie und quelloffene Software sind. Die Quellcodes sind unter `https://github.com/FeynCalc` öffentlich zugänglich.

Abstract

This thesis deals with the applications of nonrelativistic Effective Field Theories to electromagnetic and strong interactions. The main results of this work are divided into three parts.

In the first part, we use potential Nonrelativistic Quantum Electrodynamics (pNRQED), an EFT of QED at energies much below $m_e\alpha$ (with m_e being the electron mass and α the fine-structure constant), to develop a consistent description of electromagnetic van der Waals forces between two hydrogen atoms at a separation R much larger than the Bohr radius. We consider the interactions at short ($R \ll 1/m_e\alpha^2$), long ($R \gg 1/m_e\alpha^2$) and intermediate ($R \sim 1/m_e\alpha^2$) distances and identify the relevant dynamical scales that characterize each of the three regimes. For each regime we construct a suitable van der Waals EFT, that provides the simplest description of the low-energy dynamics. In this framework, van der Waals potentials naturally arise from the matching coefficients of the corresponding EFTs. They can be computed in a systematic way, order by order in the relevant expansion parameters, as is done in this work. Furthermore, the potentials receive contributions from radiative corrections and have to be renormalized. The development of a consistent EFT framework to treat electromagnetic van der Waals interactions between hydrogen atoms and the renormalization of the corresponding van der Waals potentials are the novel features of this study.

In the second part, we study relativistic $\mathcal{O}(\alpha_s^0 v^2)$ (with α_s being the strong coupling constant) corrections to the exclusive electromagnetic production of the heavy quarkonium χ_{cJ} and a hard photon in the framework of nonrelativistic Quantum Chromodynamics (NRQCD), an EFT of QCD that takes full advantage of the nonrelativistic nature of charmonia and bottomonia and exploits wide separation of the relevant dynamical scales. These scales are $m_Q \gg m_Q v \gg m_Q v^2$, where m_Q is the heavy quark mass and v is the relative velocity of the heavy quarks in the quarkonium. The novelty of this study is the inclusion of the effects from higher order Fock states $|Q\bar{Q}g\rangle$, that were incorrectly ignored in the previous investigations of the $\mathcal{O}(\alpha_s^0 v^2)$ relativistic corrections for $e^+e^- \to \chi_{cJ}\,\gamma$. Physically, these effects describe the situation, when a heavy quark pair and a soft gluon together undergo a nonperturbative evolution into the heavy quarkonium χ_{cJ}. In this work we explicitly compute the matching coefficients multiplying the corresponding long distance matrix elements (LDMEs) in the NRQCD-factorized production cross sections. The phenomenological importance of these contribution remains unclear, due to the lack of experimental data and large uncertainties in the estimates of the nonperturbative LDMEs. Good perspectives for the measurement of the electromagnetic χ_{cJ} production will exist at Belle II in Japan.

The last part of this thesis is dedicated to the development of software tools for automatic calculations in relativistic and nonrelativistic EFTs. First of all, we describe the recent progress in the FEYNCALC project. FEYNCALC is a MATHEMATICA package for semi-automatic symbolic QFT calculations that was originally developed by Rolf Mertig in 1991. Since 2001 the active development of the package almost halted, despite its large popularity among theorists and phenomenologists. In 2014 the author of this thesis became lead developer of the package. Apart from fixing numerous bugs, he has also improved the overall performance of FEYNCALC and added many new functions relevant for 1-loop and multi-loop calculations. In the next step, an interface called FEYNHELPERS was developed. FEYNHELPERS connects FEYNCALC to PACKAGE-X and FIRE. The former provides a library of analytic results for scalar 1-loop integrals with up to 4 legs, while the latter is a general-purpose tool for reduction of multi-loop scalar integrals using Integration-by-Parts (IBP) identities. The combination of FEYNCALC and

FEYNHELPERS greatly facilitates matching calculations in relativistic EFTs, where it is important to obtain fully analytic results for the matching coefficients. Finally, FEYNCALC was extended to automatize calculations in theories that lack manifest Lorentz covariance. This is the case for nonrelativistic EFTs, where one has to deal with explicit spatial and temporal components of Lorentz tensors. Functions, that are specific for matching calculations between QCD and NRQCD, were collected in a separate FEYNCALC add-on called FEYNONIUM. It is worth noting that FEYNCALC, FEYNHELPERS and FEYNONIUM are free and open source software. The source codes are publicly available at `https://github.com/FeynCalc`.

Contents

Part I

Introduction

Introduction

Two important ingredients of progress in theoretical physics are new methods and their applications to physical problems: It is necessary not only to develop new theoretical tools, but also to use them to explain experimental observations and make new predictions. One of the most modern and powerful tools that can be applied across many branches of physics is known under the name of the Effective Field Theory (EFT) [1, 2] approach. EFTs allow us to describe physics below the given energy scale Λ in a rigorous and systematic way, regardless of whether we know the correct theory at energies $E \gtrsim \Lambda$ or not. The separation of scales, that naturally arises in the EFT framework, makes calculations conceptually simpler, while the obtained results are fully equivalent to what one would have gotten from the more complicated high energy theory. Nevertheless, EFT calculations beyond leading order in the relevant expansion parameters often require a lot of effort. We face technical bottlenecks, such as large number of Feynman diagrams, complicated loop integrals or intricacies of different renormalization schemes, that limit our ability to apply EFTs to interesting phenomena and obtain new results in a reasonable amount of time. The only realistic way to overcome these and similar obstacles is to develop suitable software for automatic EFT calculations.

In this thesis we focus on nonrelativistic EFTs (NREFTs) [3, 4], that were developed to take the full advantage of the hierarchy of scales typically found in nonrelativistic systems, such as nonrelativistic bound states.

One of such systems is the hydrogen atom, that is characterized by the widely separated scales $m_e \gg m_e\alpha \gg m_e\alpha^2$, with m_e being the electron mass and $\alpha = e^2/4\pi$ the fine-structure constant, while e stands for the electric charge. Integrating out the hard scale m_e, we obtain Nonrelativistic QED (NRQED) [5], which is equivalent to full QED at energies $E \ll m_e$, with the advantage, that calculations of low-energy observables become much simpler. Still, NRQED is not the most useful theory if we are interested in physics at energies $E \ll m_e\alpha$. Integrating out the soft scale $m_e\alpha$ from NRQED, we obtain potential Nonrelativistic QED (pNRQED) [6], which will be our main tool for studying electromagnetic van der Waals forces between two hydrogen atoms.

Bound states of a heavy quark and a heavy antiquark of the same flavor are sometimes regarded as the "hydrogen atoms" of QCD. The hierarchy of scales that is believed to be realized in a heavy quarkonium is $m_Q \gg m_Qv \gg m_Qv^2$, where m_Q is the heavy quark mass and $v \ll 1$ is the relative velocity of the heavy quark and the heavy antiquark. Production and decays of heavy quarkonia can be described in an EFT known as nonrelativistic QCD (NRQCD) [7], which is obtained from full QCD by integrating out the hard scale m_Q. We will use NRQCD to study relativistic corrections to the production of heavy quarkonia in e^+e^- annihilation. Let us also remark that by integrating out the soft scale m_Qv from NRQCD, we obtain potential Nonrelativistic QCD (pNRQCD) [8, 9], which, among other achievements, has accomplished the long-term goal of quarkonium physics to systematically derive heavy quarkonium potentials from full QCD.

The wish to find a correct theoretical description of the hydrogen atom, that could reproduce the existing experimental results, was one of the main motivations for the development of the quantum theory [10] in the beginning of the last century. One of the early applications of the newly established quantum mechanics was the study of electromagnetic forces between two neutral systems without permanent electric dipole moments (e. g. two hydrogen atoms) at distances much larger than the size of each system [11]. The corresponding London potential, that behaves as $1/R^6$, was obtained under the assumption that the separation R between the systems is much smaller than their intrinsic time scale t. The opposite case, where R is much larger than t, so that

retardation effects become important, was considered in [12]. The obtained result is known as the Casimir–Polder potential, which, however, scales as $1/R^7$.

The London and the Casimir-Polder force belong to the category of van der Waals forces (sometimes also referred to as dispersive forces), which describe long-range electromagnetic interactions of neutral systems that are not subjected to external electric or magnetic fields. Despite the relative weakness of the van der Waals forces in comparison to other electromagnetic interactions, their long-range behavior makes them an important ingredient in the description of various phenomena in physics, chemistry, biology and other sciences [13]. Van der Waals forces are also studied in the context of QCD, where, e. g. heavy quarkonia and nucleons might interact with each other via the exchange of multiple gluons [14, 15]

The goal of this work is a systematic investigation of electromagnetic van der Waals forces between two hydrogen atoms in pNRQED. We will not only reproduce the existing results for $R \gg t$ and $R \ll t$, but also compute the subleading contributions to the corresponding potentials and, for the first time, explore the intermediate range regime, where $R \sim t$. Furthermore, we will discuss the issue of the renormalization of the van der Waals potentials, which, to our knowledge, has not been addressed in the existing studies of the van der Waals interactions.

As we will see, the presented framework can be regarded as a template to treat van der Waals interactions between different systems using NREFTs of QED and QCD. It has the potential to inspire new exciting research in this direction, especially in the realm of QCD. In particular, the insights gained in this work have already been employed in a study of gluonic van der Waals forces between two heavy quarkonia using pNRQCD [15].

The importance of heavy quarkonia [16] in the establishment of QCD as the correct theory of strong interactions is comparable to the role of the hydrogen atom in the establishment of quantum mechanics. The experimental discovery of the J/ψ meson in 1974 [17, 18] was soon followed by the first attempts to describe the production process $e^+e^- \to J/\psi$ in QCD [19]. Yet, it took almost two decades to develop methods, that would allow us to study heavy quarkonia using EFTs [3], such as NRQCD and pNRQCD. Comparing the theoretical tools, that we now have in our disposal, to what was available in the seventies and eighties, it is not an exaggeration to say that we are living in the golden age of heavy quarkonium. Nevertheless, calculations of quarkonium observables in NRQCD, especially NRQCD-factorized production cross sections, are technically very challenging and are mostly done using appropriate software tools, such as FeynCalc [20, 21] FeynCalcFormLink [22], FIRE [23, 24] or FDC [25] as well as unpublished private codes. Much theoretical effort is also dedicated to the goal of proving NRQCD factorization in quarkonium production (the proof for decays exists since many years [7]) to all orders in α_s, which has not yet been achieved: This is why for production we still speak of the NRQCD factorization conjecture, instead of the NRQCD factorization theorem. Measurements of heavy quarkonia also have a prominent position in the physics programs of current and future particle experiments [16], such as LHC at CERN in Geneve, SuperKEKB at KEK in Tsukuba, BESIII at IHEP in Beijing and VEPP4-M in Novosibirsk. The heavy quarkonium community is a successful collaboration of theorists and experimentalists from many institutions all over the world.

An important insight from NRQCD, is that the heavy quarkonium Fock state $|H\rangle$ should not be understood just as the dominant state $|Q\bar{Q}\rangle$ with the same quantum numbers as the physical quarkonium. Instead, $|H\rangle$ also contains subleading contributions with gluons, such that we should think of it as

$$|H\rangle \sim a_0 \, |Q\bar{Q}\rangle + a_1 \, |Q\bar{Q}g\rangle + a_2 \, |Q\bar{Q}gg\rangle + \dots . \tag{0.1}$$

In case of the P-wave heavy quarkonia produced or annihilated in exclusive electromagnetic processes, the subleading Fock state $|Q\bar{Q}g\rangle$ contributes through the 4-fermion operators with one chromoelectric or chromomagnetic field already at next-to-leading order in the relativistic expansion of the NRQCD-factorized cross sections and decay rates.

The matching coefficients of such "color octet" operators for the decay $\chi_{cJ} \to \gamma\gamma$ are known since long time [26, 27]. Surprisingly, all the existing studies [28–30] of the $\mathcal{O}(v^2)$ corrections to the corresponding production process $e^+e^- \to \gamma^* \to \chi_{cJ}\,\gamma$, where χ_{cJ} is produced together with a hard photon, completely ignored the contribution of $|Q\bar{Q}g\rangle$, taking into account only the dominant Fock state $|Q\bar{Q}\rangle$. Therefore, the aim of this work is to thoroughly analyze the exclusive production of χ_{cJ} in e^+e^- annihilation at $\mathcal{O}(\alpha_s^0 v^2)$ and to compute the previously unknown matching coefficients of operators that contribute through the subleading Fock state $|Q\bar{Q}g\rangle$.

To our knowledge, this is the first NRQCD calculation of this kind for a production process. We would also like to stress the main difference between this calculation and the existing calculations of color octet contributions in inclusive hadronic production and decays of heavy quarkonia. When people speak of color octet contributions in hadronic processes, what they mean is the creation of a $Q\bar{Q}$ pair in the color octet configuration. What we consider here is the creation of a $Q\bar{Q}g$ system, where the gluon is treated in NRQCD (i. e. it is not integrated out) as a part of the heavy quarkonium. This makes the calculation much more involved, since we need to expand the QCD amplitudes not only in the momenta of the heavy quarks but also in that of the gluon. Nevertheless, in this work we will not only determine the required matching coefficients, but also present two different ways to carry out the matching using the threshold expansion technique of Braaten and Chen [31].

While experimental measurements of the process $e^+e^- \to \gamma^* \to \chi_{cJ}\,\gamma$ are not yet available, such measurements should be possible with the Belle II detector at KEK. Therefore, we hope that our study will motivate our experimental colleagues to measure the exclusive electromagnetic production of χ_{cJ}. Furthermore, the presented methods to extract contributions from the subleading Fock state $|Q\bar{Q}g\rangle$ can be, of course, also applied to other production processes, such as e. g. heavy quarkonium production in Higgs decays [32, 33].

The complications that we may face when applying EFTs to physical phenomena are often of a rather technical nature. When dealing with many Feynman diagrams, especially at 1-loop and beyond, and possibly expanding them in some small parameters to a high order, it is very easy to make stupid mistakes (such as sign errors) that will jeopardize the final result. Apart from that, many calculations turn out to be too involved to be done entirely by pen and paper in a reasonable amount of time. Unless one is ready to spend weeks or even months doing dull algebraic manipulations, there are no alternatives to using software for automatic calculations. One of such software packages is FeynCalc [20, 21], that is widely used for symbolic evaluation of Feynman diagrams in relativistic QFTs.

In this thesis we will review the evolution of FeynCalc in the last three years and introduce two extensions, FeynHelpers and FeynOnium that were developed for the purpose of making the package more useful for automatic calculations in relativistic and nonrelativistic EFTs, especially in NRQCD. An important difference between this work and the existing *private* codes developed for similar purposes (c. f. e. g. [25]), is that all our software tools are open source and publicly available. This is why it is guaranteed, that they will be beneficial to the whole (NR)EFT community and not only to the collaborators of the author of this thesis.

This work is organized as follows. In Part II we review the main concepts of QCD, explain the conceptual and technical aspects of the EFT approach and introduce the relevant NREFTs of QED and QCD, which are NRQED, pNRQED, NRQCD and pNRQCD. Part III briefly reviews the main ideas behind automatic software for QFT calculations and discusses existing challenges in automatizing NREFTs, especially NRQCD. Part IV is devoted to the derivation of dispersive van der Waals forces between two hydrogen atoms in pNRQED. The study of $\mathcal{O}(\alpha_s^0 v^2)$ corrections to $e^+e^- \to \gamma^* \to \chi_{cJ}\,\gamma$ in NRQCD is presented in Part V. Part VI introduces software tools developed for automatic EFT calculations, including usage information and detailed examples. Finally, in Part VII we summarize the main results of this thesis and provide an outlook. Some technical details of the presented calculations can be found in the appendices.

Part II

Theoretical tools

1 Quantum Chromodynamics

1.1 Fundamentals of QCD

According to our present knowledge, the correct theory of strong interactions is called Quantum Chromodynamics (QCD) [34–36]. It is a nonabelian SU(3) gauge theory that describes interactions of massless vector bosons (gluons) and massive fermions (quarks). The Lagrangian of QCD can be written as

$$\mathcal{L}_{\mathrm{QCD}} = -\tfrac{1}{4} G^{a\mu\nu} G^a_{\mu\nu} + \sum_{f=1}^{N_f} \bar{\psi}_f (i \not{D} - m_f) \psi_f, \tag{1.1}$$

where ψ_f is a quark field of flavor f ($f = u, d, c, s, t, b$),N_f is the number of quark flavors and $\not{D} = \gamma^\mu D_\mu$. The covariant derivative is defined as $D^\mu = \partial^\mu - igA^\mu$ with A^μ being the gluon field. The field-strength tensor is given by $G^a_{\mu\nu} = \partial_\mu A^a_\nu - \partial_\nu A^a_\mu + g f^{abc} A^b_\mu A^c_\nu$, where a is the adjoint color index, f^{abc} denotes the SU(3) structure constant and g is the strong coupling constant. Furthermore, $A_\mu \equiv A^a_\mu T^a$ with T^a being a generator of SU(3) in the fundamental representation (usually denoted as *color matrix*).

To study the dynamics of gluon fields, it is often useful to consider QCD without matter fields, i. e.

$$\mathcal{L}_{\mathrm{YM}} = -\tfrac{1}{4} G^{a\mu\nu} G^a_{\mu\nu}, \tag{1.2}$$

which is known as SU(3) Yang-Mills theory [37]. In particle physics the theory described by Eq. (1.2) is usually called *pure QCD* in contrast to the *full QCD* from Eq. (1.1). Let us remark that pure QCD is not a trivial theory of noninteracting vector bosons, as it is the case for QED without matter fields. The reason for this is that the structure of $G^a_{\mu\nu}$ allows gluons to interact with each other via 3- and 4-gluon vertices.

QCD exhibits several remarkable properties that are not obvious from Eq. (1.1). One of them is the *asymptotic freedom* [38, 39], which characterizes the behavior of the QCD coupling constant $\alpha_s(E^2) \equiv g^2(E^2)/4\pi$ at different energies E. The formula for the energy dependence of α_s obtained from perturbative QCD with N_f quark flavors at 1-loop reads

$$\alpha_s(\mu_2^2) = \left(\frac{1}{\alpha_s(\mu_1^2)} + \beta_0 \log \frac{\mu_2^2}{\mu_1^2} \right)^{-1}, \tag{1.3}$$

with

$$\beta_0 = \frac{33 - 2N_f}{12\pi}. \tag{1.4}$$

Introducing

$$\Lambda_{\mathrm{QCD}} = \mu e^{-\frac{1}{2\alpha_s(\mu^2)\beta_0}}, \tag{1.5}$$

we can rewrite Eq. (1.3) as

$$\alpha_s(\mu^2) = 12\pi \left((33 - 2N_f) \log \frac{\mu^2}{\Lambda_{\mathrm{QCD}}} \right)^{-1} \tag{1.6}$$

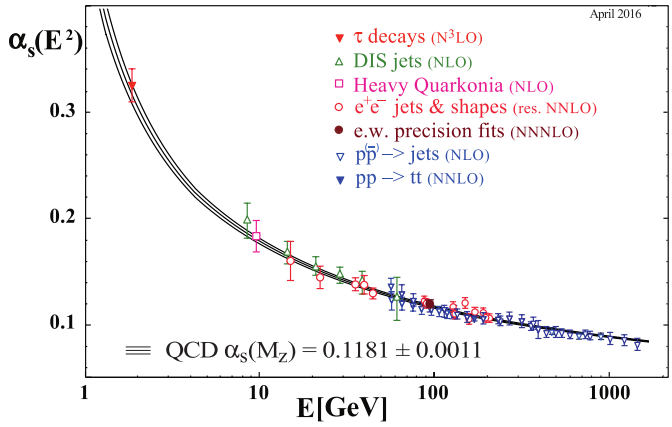

Figure 1.1: Behavior of $\alpha_s(E^2)$ at different energy scales E. The plot was taken from [40] and slightly edited. The values of α_s are obtained by comparing experimental measurements of indicated processes to the corresponding theoretical predictions obtained from QCD. The order in perturbation theory is given in the brackets.

Eq. (1.6) is remarkable for two reasons. First of all, we see that quantum effects link α_s, a dimensionless quantity, to a dimensionful parameter Λ_{QCD}. The value of α_s at the scale of the Z boson mass m_Z determined from experiment by comparing to theoretical predictions calculated in the $\overline{\text{MS}}$ renormalization scheme can be used to obtain [40]

$$\Lambda^{(5)}_{\text{QCD}} = (210 \pm 14)\,\text{MeV} \quad \text{for} \quad N_f = 5. \tag{1.7}$$

Second, Eq. (1.6) implies that for $N_f \leq 16$, $\alpha_s(E^2)$ goes to zero in the limit $E \to \infty$, so that in this regime quarks behave almost as if they were free particles. On the other hand, α_s increases for $E \to 0$ making QCD strongly coupled at energies around 1 GeV. Experimental measurements (c. f. Fig. 1.1) confirm this behavior of the theory at the energies that are currently accessible in particle accelerators. Lattice QCD [2] simulations combined with perturbative calculations can also be employed to determine the value of α_s at different energies [41, 42].

On the one hand, the smallness of α_s at high energies allows us to use it as an expansion parameter in perturbative QCD. On the other hand, at low energies perturbation theory in α_s breaks down and we need something else to understand the relevant physics. Depending on what observables we are interested in, we can use nonperturbative techniques (e. g. lattice simulations [2] or Dyson-Schwinger equations [43–45]) or try to separate perturbative and nonperturbative contributions from each other (factorization [46]). Both approaches can be also combined with the Effective Field Theory (EFT) [1, 2] methods, when we identify other small quantities than α_s and use them as expansion parameters in a suitable low-energy EFT. This way it is possible to use perturbation theory, to make predictions that depend on the values of some nonperturbative parameters.

Another interesting property of QCD is known as *color confinement*, which forbids hadronic states with nonzero color charge. This implies that unlike electrons and photons in QED, quarks and gluons can never be observed as free particles. Let us consider the gluonic interaction of a quark and an antiquark of the same flavor in the color singlet configuration. For simplicity, we can assume that the quarks are so heavy, that their relative velocity is very small compared to the speed of light. In this case we

are dealing with a nonrelativistic system, where the interaction of the heavy quarks proceeds through a static potential $V_S(r)$. The static potential is related to the static energy between a static quark and a static antiquark at distance r, which is an important quantity for the understanding of the QCD dynamics, especially in the context of EFTs for heavy quark bound states [16, 47].

The color singlet $V_{S,s}(r)$ static potential can be understood as a quantity that consists of a short-distance (Coulombic) and a long-distance (confining) part

$$V_s(r) = -\frac{C_F}{r}\kappa + \sigma r. \tag{1.8}$$

The value of the slope σ can be obtained from lattice simulations, e. g. $\sigma = 0.21\,\text{GeV}^2$ [4], while the value of κ can be computed in perturbation theory (c. f. [4, 47] for an overview of existing results).

To gain some feeling for the determination of κ, let us sketch this calculation at lowest order in perturbation theory. In this case, the perturbative (Coulombic) part of the static potential in the momentum space can be extracted from the nonrelativistic expansion of one tree-level $Q\bar{Q} \to Q\bar{Q}$ Feynman diagram shown in Fig. 1.2. Expanding the amplitude

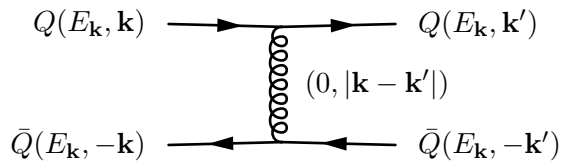

Figure 1.2: Leading order contribution to the interaction of two heavy quarks via 1-gluon exchange. The initial state quark and antiquark can be in the color singlet (both particles have the same color) or in the color octet (the particles have different colors) configurations. In the rest frame of the system we have $E_\mathbf{k} = \sqrt{m_Q + \mathbf{k}^2}$ and $|\mathbf{k}| = |\mathbf{k}'|$.

to leading order in the relative momenta $|\mathbf{k}|$ and $|\mathbf{k}'|$, we obtain

$$i\mathcal{M}_S = i\frac{4\pi\alpha_s}{|\mathbf{k}-\mathbf{k}'|^2} T^a_{c_1'\,c_1} T^a_{c_2\,c_2'} \equiv i\frac{4\pi}{\tilde{\mathbf{k}}^2}\frac{1}{2}\left(\delta_{c_1\,c_2}\delta_{c_1'\,c_2'} - \frac{1}{N_c}\delta_{c_1\,c_1'}\delta_{c_2\,c_2'}\right), \tag{1.9}$$

where $c_{1/2}$ and $c'_{1/2}$ denote the colors of the initial and final state quarks respectively and we have used the Fierz identity

$$T^a_{i_1\,i_2} T^a_{i_3\,i_4} = \frac{1}{2}\left(\delta_{i_1\,i_4}\delta_{i_2\,i_3} - \frac{1}{N_c}\delta_{i_1\,i_2}\delta_{i_3\,i_4}\right) \tag{1.10}$$

Fourier-transforming $\mathcal{M}_S$ into position space yields

$$V_S(r) = -\int \frac{d^3\tilde{k}}{(2\pi)^3} e^{i\tilde{\mathbf{k}}\cdot\mathbf{r}} \mathcal{M}_S = -\frac{1}{2}\left(\delta_{c_1\,c_2}\delta_{c_1'\,c_2'} - \frac{1}{N_c}\delta_{c_1\,c_1'}\delta_{c_2\,c_2'}\right)\frac{\alpha_s}{r}, \tag{1.11}$$

with $r \equiv |\mathbf{r}|$. If the initial state quarks are in the color singlet configuration, we set $c_1 = c_2$ and sum over c_1' and c_2', such that

$$V_{S,s}(r) = -\frac{C_F\alpha_s}{r}, \tag{1.12}$$

where $C_F = \frac{N_c^2-1}{2N_c}$ with N_c being the number of colors (in QCD $C_F = 4/3$). The color octet configuration of the heavy quarks means that $c_1 = c_1'$ and $c_2 = c_2'$ and hence

$$V_{S,o}(r) = \frac{1}{2N_c}\frac{\alpha_s}{r} = \frac{1}{2C_A}\frac{\alpha_s}{r}, \tag{1.13}$$

where $C_A = N_c$

Coming back to the singlet static potential in Eq. (1.8), we see that its linear part corresponds to a constant force that does not decrease with the distance between the quark and the antiquark. Any attempt to pull them apart would increase the energy density of the system, up to a point when a new $Q\bar{Q}$ pair can be created out of the vacuum. In this picture we can never liberate a quark out of a hadron and observe it as a free particle.

Nowadays, experimental observations but also the success of lattice simulations make it clear that color confinement is a fundamental property of QCD. Unfortunately, a rigorous mathematical proof of this property from the first principles of the theory is still lacking.

From the phenomenological point of view, QCD does a very good job in explaining the observed hadronic states by classifying them as bound states of quarks and gluons. Almost all hadrons found in experiment can be identified as bound states of two (mesons) or three (baryons) quarks. However, a priori there is no reason why the QCD spectrum should contain only di- and triquarks. One can also consider more exotic hadrons, such as tetraquarks, pentaquarks, hybrids ($q\bar{q}g$) or glueballs (gg). An observation of two pentaquark candidates $P_c(4380)^+$ and $P_c(4450)^+$ has been recently reported by the LHCb collaboration [48]. Some of the exotic X, Y and Z quarkonium-like states [47] can be considered as candidates for tetraquarks (e. g. $Z_c(3900)$ [49]), mesonic molecules (e. g. $X(3872)$) [50] or hybrids (e. g. $Y(4220)$ [51]). This shows that QCD still offers a lot of room for exciting theoretical and experimental work. The physics of strong interactions is likely to remain a challenging but gratifying field of research for many years, even if the discovery of the much anticipated new physics beyond the Standard Model will not happen soon.

1.2 Symmetries

Many aspects of strong interactions can be understood by looking at the symmetries of QCD. On the one hand, there are exact symmetries that correspond to transformations that leave the full QCD Lagrangian invariant. On the other hand, we can also gain new insights from approximate symmetries that hold only in some limit (e. g. for $m_q \to 0$ or $m_Q \to \infty$, with m_q and m_Q being the light and heavy quark masses respectively) and are therefore valid only up to corrections in the parameter that we are expanding in (e. g. $\mathcal{O}(m_q)$ or $\mathcal{O}\left(1/m_Q\right)$).

As every Lorentz invariant relativistic QFT, QCD respects charge conjugation (C), parity transformation (P) and time reversal (T), so that

$$(\mathrm{CPT})\, \mathcal{L}_{\mathrm{QCD}}(x)\, (\mathrm{CPT})^{-1} = \mathcal{L}_{\mathrm{QCD}}(-x), \tag{1.14}$$

which ensures that the action $\int d^4x \mathcal{L}_{\mathrm{QCD}}(x)$ is invariant under CPT. Moreover, C, P and T are also conserved separately, which is equally the case in QED but not in the electroweak theory where C and P are strongly violated and even CP is not conserved. In principle, CP violation might also be present in QCD. It is possible to augment the QCD Lagrangian with an additional operator

$$\mathcal{L}_\theta = \frac{\theta g^2}{32\pi^2} G^a_{\alpha\beta} \tilde{G}^{\alpha\beta}_A, , \tag{1.15}$$

with $\tilde{G}^{\alpha\beta}_a = \epsilon^{\alpha\beta\mu\nu} \tilde{G}_{a\mu\nu}$, where $\epsilon^{\alpha\beta\mu\nu}$ is the Levi-Civita symbol, which violates the CP invariance of the theory but does not spoil the renormalizability of QCD. Although this

term can be rewritten as a total derivative, the nontrivial topology of the nonperturbative QCD vacuum does not guarantee that such a surface term vanishes identically. However, it appears that the size of θ is so small ($|\theta| \leq 10^{-10}$ [40]), that experimentally we do not observe any CP violations in strong interactions. Such a violation would manifest itself e. g. in the nonzero value for the electric dipole moment of the neutron d_n. Yet the current experimental limit on this quantity is given by $d_n < -0.21 \pm 1.82 \times 10^{-26} e\,\text{cm}$ [52]. There seems to be no intrinsic reason why θ is not $\mathcal{O}(1)$. This puzzle is known as the strong CP problem. One possible explanation is to postulate an additional symmetry that makes θ very small [53, 54]. This introduces a new light particle, the axion, which however, has not been experimentally observed yet.

Another very important symmetry that is crucial for the nature of the theory is gauge invariance. The QCD Lagrangian is invariant under local SU(3) gauge transformations

$$q_{f,i}(x) \to \Lambda_{ij}(x) q_{f,j}(x), \tag{1.16}$$

$$A^c_\mu T^c_{ij} \to \frac{i}{g} \Lambda_{ia}(x) \left(\partial_\mu \delta_{ab} - i g A^c_\mu T^c_{ab}\right) \Lambda^\dagger_{bj}(x), \tag{1.17}$$

with

$$\Lambda_{ij}(x) = \left(e^{i\theta^c(x) T^c}\right)_{ij}, \tag{1.18}$$

where f is a quark flavor index, i and j are fundamental color indices and c is the adjoint color index, while $\theta^c(x)$ is a set of 8 functions that depend on the spacetime coordinates.

A mass term for the gluons would violate gauge invariance, so that these fields are massless in QCD. On the other hand, quark masses do not cause any problems, as $m_f \bar{\psi}\psi$ is clearly gauge invariant. This changes once we want to embed QCD into the Standard Model. In this case quark fields can interact with $W^\pm$ and Z bosons and must transform under the $\text{SU}_L(2)$ symmetry that governs electroweak interactions. Since the invariance under $\text{SU}_L(2)$ forbids mass terms for quark and leptons, Higgs mechanism [55–58] is required to explain how fermion fields acquire their masses via spontaneous symmetry breaking.

If we rotate all the quark fields by the same constant phase α

$$q_f \to e^{i\alpha} q_f, \tag{1.19}$$

we see that the QCD Lagrangian is also invariant under a global $\text{U}(1)_V$ transformation, that corresponds to the baryon number conservation. This conservation law has an important phenomenological consequence. Since proton is the lightest baryon, it cannot decay without violating the baryon number conservation. Experimental searches [59] indicate that the proton lifetime must be larger than 5.9×10^{33} years and no proton decays have been observed so far. Notice that there is no similar conservation law for mesons: the lightest meson π^0 predominantly decays into two photons and also heavier mesons (e. g. heavy quarkonia) can decay into final states that do not contain any other mesons.

Let us now turn our attention to the approximate symmetries of QCD. At energies much below the typical hadronic scale of $\mathcal{O}(1\,\text{GeV})$ (which corresponds to the mass of the proton) we may neglect the existence of the heavy quarks. For simplicity, let us also ignore the strange quark and look at the QCD Lagrangian that contains only u and d quarks,

$$\mathcal{L}_{\text{QCD}} = \sum_{f=u,d} \bar{q}_f (i \not{D} - m_f) q_f. \tag{1.20}$$

The masses of the light quarks are very small as compared to the typical hadronic scale, with $m_u \approx 2.2 \pm 0.7\,\text{MeV}$ and $m_d \approx 4.7 \pm 0.6\,\text{MeV}$ [40] for quark masses extracted from experimental data when comparing to theoretical predictions calculated in the $\overline{\text{MS}}$ renormalization scheme. Since $m_u - m_d \ll 1\,\text{GeV}$, we might approximate the mass matrix as

$$\begin{pmatrix} m_u & 0 \\ 0 & m_d \end{pmatrix} \approx m \begin{pmatrix} 1 & 0 \\ 0 & 1 \end{pmatrix} \tag{1.21}$$

with $m \approx m_u \approx m_d$. In this case Eq. (1.20) becomes

$$\mathcal{L}_{\text{QCD}} = \bar{q}(i\not{D} - m)q, \tag{1.22}$$

with $q = (u, d)^T$. Now we can transform the vector q as

$$q \to e^{i\alpha^j \frac{\boldsymbol{\sigma}^j}{2}} q, \quad \alpha^j = \text{const.}\,, \tag{1.23}$$

where $\boldsymbol{\sigma}^i$ denotes a Pauli matrix, without changing Eq. (1.22), which is corresponds to the $\text{SU}(2)_V$ isospin symmetry.

If the light quark masses are completely neglected, we obtain

$$\mathcal{L}_{\text{QCD}} = \bar{q} i\not{D} q = \bar{q}_L i\not{D} q_L + \bar{q}_R i\not{D} q_R, \tag{1.24}$$

with $q_L = \frac{1}{2}(1 - \gamma_5)q$ and $q_R = \frac{1}{2}(1 + \gamma_5)q$. Therefore, we can apply different $\text{SU}(2)$ transformations to the left- and right-handed fields, which is known as the chiral $\text{SU}_L(2) \otimes \text{SU}_R(2)$ symmetry. The same goes also for $\text{U}(1)$ transformations so that in the limit of vanishing quark masses we would expect QCD to be invariant under

$$\text{U}(1)_L \otimes \text{U}(1)_R \otimes \text{SU}(2)_L \otimes \text{SU}(2)_R = \text{U}(1)_V \otimes \text{U}(1)_A \otimes \text{SU}(2)_V \otimes \text{SU}(2)_A. \tag{1.25}$$

However, on the quantum level only the invariance under $\text{U}(1)_V \otimes \text{SU}(2)_V$ is preserved.

The chiral $\text{SU}_L(2) \otimes \text{SU}_R(2)$ symmetry is spontaneously broken by the nonvanishing vacuum expectation value of

$$\langle \bar{q}q \rangle = \langle \bar{u}u + \bar{d}d \rangle = \langle (\bar{u}_L + \bar{u}_R)(u_L + u_R) + (\bar{d}_L + \bar{d}_R)(d_L + d_R) \rangle\,, \tag{1.26}$$

which is known as the quark condensate. A recent average value of lattice simulations for 2+1 flavor QCD [60] reads

$$|\,\langle \bar{u}u \rangle\,|_{m_u, m_d \to 0} = 271(15)\,\text{MeV}. \tag{1.27}$$

Eq. (1.26) introduces mixing of left- and right-handed quark fields, so that the invariance under $\text{SU}_L(2) \otimes \text{SU}_R(2)$ reduces to the invariance under $\text{SU}(2)_V$.

In nature the approximate $\text{SU}(2)_V$ isospin symmetry manifests itself in the very small difference between the masses of the proton ($m_p = 938.3\,\text{MeV}$ [40]) and the neutron ($m_n = 939.6\,\text{MeV}$ [40]). Both particles have isospin $I = 1/2$ and would have the same masses if $\text{SU}(2)_V$ were an exact symmetry and if the electromagnetic interactions could be neglected. An approximate $\text{SU}(2)_A$ would induce the same effect for states with opposite parity. The opposite parity partner of the proton would be the $N(1520)$ baryon, that is, however, almost 40% heavier.

If the up and down quarks were massless in nature, this spontaneous symmetry breaking would produce three massless Goldstone bosons. Due to the finite masses of the light quarks we would expect the corresponding particles (pseudo-Goldstone bosons) to be massive but still very light as compared to the typical hadronic scale. These

pseudo-Goldstone bosons can be identified as pions ($\pi^{\pm}$ and π^0), which are indeed the lightest hadrons in the QCD spectrum.

The axial $\mathrm{U}(1)_A$ symmetry is broken due to the quantum effects, that lead to the nonconservation of the axial current. This is known as the axial anomaly. An explicit way to see this is to compute a 1-loop triangle diagram, where the axial current is coupled to two gluons via a quark loop. The divergence of the current does not vanish, which is usually referred to as the Adler-Bell-Jackiw anomaly [61, 62].

The $\mathrm{SU}(2)_V$ isospin symmetry can be used to classify mesons and baryons made of up and down quarks, and was discovered by Heisenberg [63] long before the establishment of QCD. In the context of QCD it can be understood as a flavor symmetry of the massless up and down quarks. In principle, one could enlarge the $\mathrm{SU}(2)_V$ flavor symmetry by considering heavier quarks and neglecting their masses. If we include the s quark, our symmetry group becomes $\mathrm{SU}(3)_V$ and the number of pseudo-Goldstone bosons increases to $3^2 - 1 = 8$. Although the strange quark is roughly 50 times heavier than the up and down quarks, $\mathrm{SU}(3)$ still can be useful for phenomenological applications, since m_s is smaller than the typical hadronic scale.

However, it does not make much sense to include even heavier quarks. For the charm quark we already have $m_c > 1\,\mathrm{GeV}$ so that it cannot be treated as a small perturbation. This is even more true for bottom and top quarks.

It is interesting to observe that massless QCD (c. f. Eq. (1.24) seems to be a scale invariant theory, as no explicit dimensionful scale is present in the Lagrangian. However, as we have already seen in Sec. 1.1, this property does not survive in the quantum theory, where a dimensionful parameter Λ_{QCD} is generated by the loop corrections.

Last but not least, there are also approximate QCD symmetries that are related to the heavy quarks. The two relevant symmetries are the $\mathrm{SU}(2N_h)$ heavy quark flavor symmetry and the $\mathrm{SU}(2N_h)$ heavy quark spin symmetry, where N_h denotes the number of heavy quark flavors. However, these symmetries are not manifest in the standard QCD Lagrangian. One can make them explicit in the context of Effective Field Theories that describe interactions of heavy quarks with gluons, light quarks or with each other inside hadrons. For this reason we would like to postpone the detailed discussion of these symmetries until we introduce the Heavy Quark Effective Theory (HQET) (c. f. Sec. 2.3).

1.3 Quantization

The usual strategy in quantizing a field theory is to start with the classical Lagrangian (e. g. Eq. (1.1) for QCD) that describes interactions of classical fields.

If the quantization is carried out in the operator formalism [64, 65], we interpret our fields $\phi_i(x)$ as noncommuting operators. Then we impose commutation (for bosons) and anticommutation (for fermions) relations that the fields should obey. The equations of motion for noninteracting (free) fields allow us to deduce their Fourier decompositions in terms of creation and annihilation operators. We can introduce n-point correlation functions (usually denoted as *Green's functions*)

$$G_{\phi_{i_1}\ldots\phi_{i_n}}(x_1,\ldots,x_n) \equiv \langle\Omega|\mathcal{T}\left\{\phi_{i_1}(x_1)\ldots\phi_{i_n}(x_n)\right\}|\Omega\rangle\,, \tag{1.28}$$

where $|\Omega\rangle$ is the vacuum of the interacting theory and $\mathcal{T}$ is the time-ordering operator that rearranges field operators to have decreasing time arguments from left to right, e. g.

$$\mathcal{T}\left\{\phi_i(x)\phi_j(y)\right\} = \theta(x^0-y^0)\phi_i(x)\phi_j(y) \pm \theta(y^0-x^0)\phi_j(y)\phi_i(x), \tag{1.29}$$

with $+$ for bosons and $-$ for fermions. The fields appearing in Eq. (1.28) are time dependent operators i. e. Heisenberg fields. This is because the Heisenberg picture of quantum interactions is defined in such a way, that there all operators depend on time, while states are time-independent.

Green's functions are most conveniently evaluated in the interaction picture, where we can write

$$\phi_i(t,\mathbf{x}) = \mathcal{T}\left\{e^{i\int_{t_0}^{t} dt' H_{\text{int}}(t')}\right\}\phi_{I,i}(t,\mathbf{x})\mathcal{T}\left\{e^{-i\int_{t}^{t_0} dt' H_{\text{int}}(t')}\right\}, \tag{1.30}$$

with $\phi_i(t,\mathbf{x})$ being the original Heisenberg field and $\phi_{I,i}(t,\mathbf{x})$ the field in the interaction picture. Here H_{int} denotes the interacting part of the Hamiltonian H of the theory

$$H = H_0 + H_{\text{int}}, \tag{1.31}$$

while H_0 describes noninteracting fields. The obvious advantage of using interaction picture is that the time evolution of $\phi_{I,i}$ is governed by the free Hamiltonian H_0

$$\frac{d}{dt}\phi_{I,i} = \frac{i}{\hbar}\left[H_0, \phi_{I,i}\right], \tag{1.32}$$

so that they can be represented as Fourier decompositions of free fields that we found earlier. Using Gell-Mann and Low theorem [66] one can relate $|\Omega\rangle$ to the vacuum of the free theory $|0\rangle$, so that Eq. (1.28) can be rewritten as [67]

$$G_{\phi_{i_1}\ldots\phi_{i_n}}(x_1,\ldots,x_n) = \lim_{T\to\infty(1-i\varepsilon)} \frac{\langle 0|\mathcal{T}\left\{\phi_{I,i_1}(x_1)\ldots\phi_{I,i_n}(x_n)e^{i\int_{-T}^{T} dt H_{\text{int}}(t)}\right\}|0\rangle}{\langle 0|\mathcal{T}\left\{e^{i\int_{-T}^{T} dt H_{\text{int}}(t)}\right\}0\rangle}, \tag{1.33}$$

where the limit $T\to\infty(1-i\varepsilon)$ signifies that we are considering asymptotic initial and final states. In the asymptotic past before the interaction, the separation between the ingoing fields is so large, that they can be regarded as free fields. The same holds also for the outgoing fields in the asymptotic future after the interaction. The denominator on the right-hand side of Eq. (1.33) ensures that all vacuum bubbles (i. e. diagrams without external legs) from the numerator cancel.

Perturbation theory arises from the expansion of $e^{i\int_{-T}^{T} dt H_{\text{int}}(t)}$ in $H_{\text{int}}(t)$

$$\begin{aligned}\mathcal{T}\left\{\ldots e^{i\int_{-T}^{T} dt H_{\text{int}}(t)}\right\} = \mathcal{T}\left\{\ldots\right\} + i\mathcal{T}\left\{\ldots\int_{-T}^{T} dt\, H_{\text{int}}(t)\right\} \\ + \frac{(-i)^2}{2!}\mathcal{T}\left\{\ldots\int_{-T}^{T} dt\int_{-T}^{t} dt'\, H_{\text{int}}(t)\, H_{\text{int}}(t')\right\},\end{aligned} \tag{1.34}$$

which is justified if H_{int} is a small perturbation, i. e. if it consists of interaction terms that are proportional to small coupling constants. Eq. (1.34) is known as the Dyson series [68].

Finally, we need to use Wick's theorem [69] to convert time-ordered products of fields into normal-ordered products. The normal-ordering operator $\mathcal{N}$ reorders products of operators in such a way, that all creation operators appear on the left and annihilation operators on the right, e. g.

$$\mathcal{N}\left\{aa^\dagger\right\} = \pm a^\dagger a, \tag{1.35}$$

with $+$ for commuting (bosonic) and $-$ for anticommuting (fermionic) operators.

When we apply perturbation theory to calculate the given Green's function using Eq. (1.33) and Wick's theorem, each term of the expansion can be assigned a pictorial representation, known as *Feynman diagram*. The idea of Feynman was that instead of calculating $G_{\phi_{i_1}\ldots\phi_{i_n}}(x_1,\ldots,x_n)$ from Eq. (1.33), it is simpler to draw all corresponding Feynman diagrams and then use a set of previously derived rules (*Feynman rules*) to recover terms of the perturbative series from the diagrams. This approach turned out to be extremely successful in organizing perturbative calculations in QFTs.

LSZ reduction formula [70] relates Green's functions to the S-matrix elements

$$S_{fi} = \langle f|i\rangle\,, \tag{1.36}$$

which are transition amplitudes for the initial state $|i\rangle$ to evolve into the final state $|f\rangle$. We can write

$$S_{fi} = \delta_{fi} + (2\pi)^4\delta^{(4)}\left(\sum_i p_i - \sum_i p_i'\right) i\mathcal{M}_{fi} \equiv \delta_{fi} + iT_{fi}, \tag{1.37}$$

where p_i (p_i') are the 4-momenta of the ingoing (outgoing) particles, while δ_{fi} accounts for the possibility that no interaction between initial state particles occurs. Therefore, the nontrivial interaction of particles is described by the T-matrix elements T_{fi}, while the amplitude $\mathcal{M}_{fi}$ is the quantity that one actually obtains when evaluating Feynman diagrams. Physical observables such as cross sections or decay rates are then obtained from squaring $\mathcal{M}_{fi}$, possibly averaging over initial state and summing over final state polarizations and finally integrating over the Lorentz invariant phase space of the process.

We may also choose to work in the path integral formalism [71], where our fundamental quantity is the generating functional

$$Z[J] = \int \mathcal{D}\phi_1\ldots\phi_n e^{i\int d^4x\left(\mathcal{L}+\sum_{i=1}^n J_i(x)\phi_i(x)\right)}, \tag{1.38}$$

where $J_i(x)$ are external sources. In this case boson fields are represented by ordinary c-numbers (i. e. real or complex numbers), while for fermion fields one has to introduce anticommuting Grassmann numbers.

Notice that the exact form of $J_i(x)$ also depends on the type of the corresponding field. For example, for a complex scalar field φ we would introduce two sources

$$J^*(x)\varphi(x) + J(x)\varphi^*(x). \tag{1.39}$$

Two sources are also needed for fermions, so that we would write

$$\bar\psi\eta + \bar\eta\psi, \tag{1.40}$$

while for a vector field there is only source, but is must carry a Lorentz index (and also a color index if we are considering gluons) $J_\mu(x)A^\mu(x)$.

Performing functional differentiation with respect to the external sources and setting them to zero afterwards, we can define Green's functions as

$$\begin{aligned} G_{\phi_{i_1}\ldots\phi_{i_n}}(x_1,\ldots,x_n) &= \frac{1}{Z_0}\frac{1}{i^n}\frac{\delta^n}{\delta J_{i_n}(x_1)\ldots\delta J_{i_n}(x_n)} Z[J]\Big|_{J=0} \\ &= \frac{1}{Z_0}\int \mathcal{D}\phi_1\ldots\phi_n\, e^{i\int d^4x\mathcal{L}}\phi_{i_1}\ldots\phi_{i_n}, \end{aligned} \tag{1.41}$$

with $Z_0 \equiv Z[0]$. In order to compute the second line of Eq. (1.41) explicitly, it is useful to rewrite the $Z[J]$ as

$$Z[J] = N_0 e^{\int dw \sum_i \left(\prod_j g_{i_j}\right)\left(\prod_j \frac{\delta}{i\delta J_{i_j}(w)}\right)} e^{-\int d^4x d^4y \sum_i c_i \tilde{J}_i(x)\Delta_{F,i}(x-y)J_i(y)}, , \tag{1.42}$$

where g_{i_j} are the couplings of the interaction terms and $\Delta_{F,i}(x-y)$ are the Feynman propagators of the fields in the position space. The numerical constants c_i depend on the field ϕ_i (i. e. $c_i = 1/2$ for vector fields). Also the form of $\tilde{J}_i(x)$ (where we have suppressed possible extra indices) depends on the fields we are considering: we would write $J^*(x)$ for bosonic but $\bar{J}(x)$ for fermionic fields. Furthermore, if an interaction terms contains derivatives with respect to the fields, they also must be included in the first exponential of Eq. (1.42).

The idea behind this procedure is to pull out all the interaction terms from $e^{i\int d^4x \mathcal{L}}$ so that the remaining expression contains only free fields and source terms. This leaves us with a Gaussian path integral that can be easily computed by completing the square. Remember that for the 1-dimensional Gaussian integral over the real variable x we have

$$\int_{-\infty}^{\infty} dx e^{-ax^2+bx+c} = e^{\frac{b^2}{4a}+c} \int_{-\infty}^{\infty} dy\, e^{-ay^2} \quad \text{for} \quad a > 0, \tag{1.43}$$

Here the $e^{\frac{b^2}{4a}+c}$ piece corresponds to the second exponential of Eq. (1.42), while the remaining integral with the exponent quadratic in the integration variable is factored out into N_0.

Now one can plug Eq. (1.42) into Eq. (1.41) and expand in the small coupling constants, so that

$$e^{\int dw \sum_i \left(\prod_j g_{i_j}\right)\left(\prod_{i_j} \frac{\delta}{i\delta J_{i_j}(w)}\right)} = 1 + \int dw \sum_i \left(\prod_j g_{i_j}\right)\left(\prod_j \frac{\delta}{i\delta J_{i_j}(w)}\right) + \dots \tag{1.44}$$

This way we obtain the same perturbation theory as in the operator approach. Again, we can avoid the tedious task of expanding exponentials and differentiating with respect to the sources by first deriving Feynman rules of the theory and then computing Feynman diagrams to obtain the amplitude $\mathcal{M}_{fi}$.

Gauge theories like QED or QCD are usually more difficult to quantize than theories that do not have the property of the gauge invariance. In the following we restrict ourselves to the situation in the continuum, since quantization of gauge theories on the lattice (e. g. Lattice QCD [2]) is outside of the scope of this work.

First of all, we cannot quantize QCD without first choosing a gauge condition, a procedure known as gauge fixing. Instead of choosing a particular gauge immediately, we can implement a large class of covariant gauges by augmenting the QCD Lagrangian with a gauge fixing term

$$L_{\text{GF}} = -\frac{1}{2\xi}(A^\mu A_\mu)^2, \tag{1.45}$$

where ξ is an arbitrary constant that enters the gluon propagator

$$\langle A^a_\mu(x) A^b_\nu(y)\rangle = \Delta^{ab}_{F\,\mu\nu}(x-y) = \delta^{ab} \int \frac{d^4k}{(2\pi)^4} i \frac{-g^{\mu\nu} + (1-\xi)\frac{k^\mu k^\nu}{k^2}}{k^2 + i\eta} e^{-ik\cdot(x-y)}, \tag{1.46}$$

where the choice $\xi = 1$ yields the familiar Feynman gauge propagator.

In QED one can show that the extra term in Eq. (1.45) is sufficient to ensure that the unphysical degrees of freedom (photons with longitudinal or temporal polarizations) do not contribute to physical observables. This procedure is known as the Gupta-Bleuler formalism [72, 73].

In QCD the situation is more complicated due to the nonabelian nature of the theory. It turns out that if we just introduce the gauge-fixing term and nothing else, then the unphysical gluonic degrees of freedom do not automatically cancel, which signals a serious problem in the consistency of the so quantized theory.

The proper way to quantize nonabelian gauge theories in the path integral formalism was worked out by Fadeev and Popov [74], while the quantization in the operator formalism can be achieved using Becchi–Rouet–Stora–Tyutin construction [75–77, 77]. The important point is that gauge fixing in general[1] leads to the appearance of new fields in the QCD Lagrangian, known as Fadeev–Popov ghosts. The full QCD Lagrangian including the ghost fields reads

$$\begin{aligned}\mathcal{L}_{\text{QCD}} = &-\tfrac{1}{4}G^{a\mu\nu}G^a_{\mu\nu} + \sum_{f=1}^{N_f}\bar{\psi}_f(i\not{D} - m_f)\psi_f - \frac{1}{2\xi}(\partial^\mu A_\mu)^2 \\ &+ \bar{c}^a(-\partial^2\delta^{ac} - g f^{abc}\partial^\mu A^b_\mu)c^c. \end{aligned} \tag{1.47}$$

The ghost fields c^a are scalars that transform under the adjoint representation of SU(3), but at the same time they are described by anticommuting fields, which is characteristic for fermions. Hence, they violate the spin-statistics theorem and cannot correspond to physical states. Nevertheless, in Feynman diagrams they appear as virtual particles (e. g. inside loops), where they cancel the contributions of unphysical polarizations of the gluons.

Since ghosts are not physical, it does not seem to make much sense to consider diagrams with external ghosts. However, in some cases the inclusion of such diagrams can be used as a convenient trick to make the calculation of the matrix element squared $|\mathcal{M}_{fi}|^2$ much simpler.

The reason is the following. It is well known, that a massless vector boson can have only two degrees of freedom, which are its transverse polarizations. Let us denote the corresponding polarization vectors with $\varepsilon^\mu(k,1)$ and $\varepsilon^\mu(k,2)$, where k is the four momentum of the boson with $k^2 = 0$. If we have a diagram with one massless vector boson in the initial or finite state and want to sum or average over its polarizations, we need to find an explicit expression for the polarization sum

$$\sum_{\lambda=1}^{2}\varepsilon_\mu(k,\lambda)\varepsilon^*_\nu(k,\lambda). \tag{1.48}$$

The issue with Eq. (1.48) is that to write it as a Lorentz covariant expression we need four linearly independent Lorentz vectors. Unfortunately, we have only three such vectors (k^μ, $\varepsilon^\mu(k,1)$ and $\varepsilon^\mu(k,2)$) to our disposal, which is not sufficient to completely span a 4-dimensional vector space. To solve this issue we can introduce an auxiliary vector n^μ that must not be a linear combination of k^μ, $\varepsilon^\mu(k,1)$ and $\varepsilon^\mu(k,2)$. This yields

$$\sum_{\lambda=1}^{2}\varepsilon_\mu(k,\lambda)\varepsilon^*_\nu(k,\lambda) = -g_{\mu\nu} + \frac{(k_\mu n_\nu + k_\nu n_\mu)}{(k\cdot n)} - \frac{n^2 k_\mu k_\nu}{(k\cdot n)^2}, \tag{1.49}$$

[1] QCD in the temporal or axial gauge is free of ghosts in the sense, that the ghost fields decouple. However, if we want to use Feynman, Landau or Coulomb gauge, ghosts must be taken into account.

where $k \cdot n \neq 0$ and n^2 depends on the choice of n^μ. For simplicity, one can always choose n^μ such that $n^2 = 0$, which removes the last term of Eq. (1.49). Still, in practical calculations the usage of Eq. (1.49) leads to a significant increase of intermediate terms. Consider for example an unpolarized process with four massless bosons in the final state. In this case we need to calculate

$$\sum_{\lambda_1=1}^{2} \varepsilon_\mu(k_1,\lambda_1)\varepsilon^*_\alpha(k_1,\lambda_1) \sum_{\lambda_2=1}^{2} \varepsilon_\nu(k_2,\lambda_2)\varepsilon^*_\beta(k_2,\lambda_2)$$
$$\times \sum_{\lambda_3=1}^{2} \varepsilon_\rho(k_3,\lambda_3)\varepsilon^*_\gamma(k_3,\lambda_3) \sum_{\lambda_4=1}^{2} \varepsilon_\sigma(k_4,\lambda_4)\varepsilon^*_\delta(k_4,\lambda_4)\mathcal{M}^{\mu\nu\rho\sigma}\mathcal{M}^{*\alpha\beta\gamma\delta} \tag{1.50}$$

which is a huge sum of sixteen matrix elements squared.

In QED processes one can safely do the replacement

$$\sum_{\lambda=1}^{2} \varepsilon_\mu(k,\lambda)\varepsilon^*_\nu(k,\lambda) \to \sum_{\lambda=0}^{3} \varepsilon_\mu(k,\lambda)\varepsilon^*_\nu(k,\lambda) = -g_{\mu\nu}, \tag{1.51}$$

i. e. sum not only over the physical but also over the unphysical polarizations. The reason for this is that in QED unphysical degrees of freedom always cancel, as was demonstrated by Gupta and Bleuler. However, as we have explained above, in QCD there is no such automatic cancellation of unphysical degrees of freedom in the final states, so that we really need to use Eq. (1.49) to sum over physical polarizations of the gluons. However, if we also include diagrams with gluons replaced by ghosts, then Eq. (1.51) becomes valid also in QCD, as the unphysical contributions from final state ghosts precisely cancel the contributions from unphysical final state gluons. Moreover, since there is no interference between gluon and ghost diagrams, Eq. (1.50) simplifies to

$$(-g_{\mu\alpha})(-g_{\nu\beta})(-g_{\rho\gamma})(-g_{\sigma\delta})\mathcal{M}^{\mu\nu\rho\sigma}\mathcal{M}^{*\alpha\beta\gamma\delta} - |\mathcal{M}_{\text{ghosts}}|^2, \tag{1.52}$$

which is obviously much easier to evaluate. This simple example shows that textbook formulas are often not the most effective way to tackle large computations, even if one can benefit from automatic programs.

Let us also give another example when formulas most suited for automatic calculations are not the most obvious ones. On the one hand, many theorists consider the path integral formalism to be the most elegant way to derive Feynman rules from the given Lagrangian.

On the other hand, Feynman rules can be, of course, also conveniently derived in the operator formalism. In order to do so, we need to know not only the interaction term, but also the free Fourier decompositions of the involved fields. With these ingredients the determination is straight-forward. In tree-level calculations relevant for the determination of the vertices (with all momenta incoming) we can use the following shortcut formula [67]

$$\langle 0|iT_{0i}|i\rangle \sim \lim_{T\to\infty(1-i\varepsilon)} \langle 0|\mathcal{T}\left\{i\int_{-T}^{T} dt \int d^3x \mathcal{L}_{\text{int}}(x,t)\right\}|i_0\rangle\,, \tag{1.53}$$

with the restriction that each field in the interaction term $\mathcal{L}_{\text{int}}$ also appears in the initial state $|i_0\rangle$. This state arises from the action of the corresponding creation operators on the vacuum state of the free theory $|0\rangle$. Moreover, when we apply Wick's theorem to replace time ordering by the normal ordering, all we need to do is to move all the

creation (annihilation) operators to the left (right) using the known commutation and anticommutation relations obeyed by the fields and operators. Then we multiply the remaining terms by i, drop the spinors and polarization vectors from external states and remove the momentum conserving delta function. What remains is the Feynman rule for the given interaction term $\mathcal{L}_{\text{int}}$.

This algorithm is implemented in FEYNRULES [78], which is currently the most popular software package for automatic derivation of Feynman rules from almost arbitrary relativistic Lagrangians. It goes without saying that the algorithm is equally applicable also to nonrelativistic theories and moreover it is very easy to implement[2] in any symbolic manipulation system such as MATHEMATICA or FORM.

For definiteness, let us do one simple nonrelativistic calculation using Eq. (1.53) for a theory called Nonrelativistic QCD (NRQCD) [7]. Although NRQCD will be introduced only in Sec. 3, to put Eq. (1.53) to work we do not really need to know much about it, except for the Fourier decompositions of the NRQCD fields. Let us determine the Feynman rule for

$$\chi^\dagger g\boldsymbol{\sigma}\cdot\mathbf{B}\psi, \tag{1.54}$$

where ψ (χ) denotes a Pauli field that annihilates (creates) a heavy quark (antiquark), $\boldsymbol{\sigma}^i$ is a vector of Pauli matrices and $\mathbf{B}^i = (\boldsymbol{\nabla}\times\mathbf{A})^i$ is the chromoelectric field. Furthermore, i and j are Cartesian indices.

The Fourier decompositions of the free fields ψ, χ and A read

$$\psi_i^\alpha(x) = \int\frac{d^3p}{(2\pi)^3}\frac{1}{\sqrt{2E_{\mathbf{p}}}}\sum_{s=1}^{2}\sum_{c=1}^{3} b(\mathbf{p},s,c)\,\xi_i(s)v^\alpha(c)\,e^{-ip\cdot x}, \tag{1.55a}$$

$$\chi_i^\alpha(x) = \int\frac{d^3p}{(2\pi)^3}\frac{1}{\sqrt{2E_{\mathbf{p}}}}\sum_{s=1}^{2} c^\dagger(\mathbf{p},s,c)\,\eta_i(s)v^\alpha(c)\,e^{ip\cdot x}, \tag{1.55b}$$

$$\begin{aligned}A^{k\mu}(x) = \int\frac{d^3p}{(2\pi)^3}\frac{1}{\sqrt{2E_{\mathbf{p}}}}\sum_{\lambda=0}^{3}\sum_{a=1}^{8}\Big(&d(\mathbf{p},\lambda,a)\varepsilon^\mu(p,\lambda)\tilde{v}^k(a)e^{-ip\cdot x}\\ &+d^\dagger(\mathbf{p},\lambda,a)\varepsilon^{*\mu}(p,\lambda)\tilde{v}^k(a)e^{ip\cdot x}\Big).\end{aligned} \tag{1.55c}$$

Here s and c denote spin and color quantum numbers of the heavy quark fields, while α and i stand for color and Pauli indices. The Pauli spinors are defined as

$$\xi(1) = \eta(1) = (1,0)^T \tag{1.56}$$

$$\xi(2) = \eta(2) = (0,1)^T, \tag{1.57}$$

while the unit color vectors can be written as

$$v(1)\equiv v(r) = (1,0,0)^T, \tag{1.58}$$

$$v(2)\equiv v(g) = (0,1,0)^T, \tag{1.59}$$

$$v(3)\equiv v(b) = (0,0,1)^T. \tag{1.60}$$

and

$$\tilde{v}(1) = (1,0,0,0,0,0,0,0)^T, \tag{1.61}$$

[2]Of course, one can also automatize the derivation of Feynman rules using functional differentiation in the path integral approach. In our view, it is ultimately a matter of taste and personal preference whether one prefers to derive Feynman rules using operator or path integral formalism.

$$\tilde{v}(2) = (0,1,0,0,0,0,0,0)^T, \tag{1.62}$$
$$\dots \tag{1.63}$$

The creation and annihilation operators that appear in Eqs. (1.55) obey the usual anti-commutation (for heavy quarks) and commutation (for gluons) relations

$$\{b(\mathbf{p},s,c), b^\dagger(\mathbf{p}',s',c')\} = \{c(\mathbf{p},s,c), c^\dagger(\mathbf{p},s',c')\} = (2\pi)^3\delta^{(3)}(\mathbf{p}-\mathbf{p}')\delta_{ss'}\delta_{cc'}, \tag{1.64}$$
$$[d(\mathbf{p},\lambda,a), d^\dagger(\mathbf{p}',\lambda',a')] = -(2\pi)^3\delta^{(3)}(\mathbf{p}-\mathbf{p}')g_{\lambda\lambda'}\delta_{aa'}. \tag{1.65}$$

From here we can easily follow that

$$[\mathbf{A}^{k\cdot i}(x), d^\dagger(\mathbf{p},\lambda,a)] = \frac{1}{\sqrt{2E_\mathbf{p}}}\boldsymbol{\varepsilon}^i(p,\lambda)\tilde{v}^k(a)e^{-ip\cdot x}, \tag{1.66}$$
$$\{\psi_i^\alpha(x), b^\dagger(\mathbf{p},s,c)\} = \frac{1}{\sqrt{2E_\mathbf{p}}}\xi_i(s)v^\alpha(c)e^{-ip\cdot x}, \tag{1.67}$$
$$\{\chi_i^{\dagger\alpha}(x), c^\dagger(\mathbf{p},s,c)\} = \frac{1}{\sqrt{2E_\mathbf{p}}}\eta_i(s)v^\alpha(c)e^{-ip\cdot x}. \tag{1.68}$$

Finally, the perturbative Fock states containing a quark, an antiquark or a gluon are defined as

$$|Q(\mathbf{p},s,c)\rangle = \sqrt{2E_\mathbf{p}}b^\dagger(\mathbf{p},s,c)\,|0\rangle\,, \tag{1.69}$$
$$|\bar{Q}(\mathbf{p},s,c)\rangle = \sqrt{2E_\mathbf{p}}c^\dagger(\mathbf{p},s,c)\,|0\rangle\,, \tag{1.70}$$
$$|g(\mathbf{p},\lambda,a)\rangle = \sqrt{2E_\mathbf{p}}d^\dagger(\mathbf{p},\lambda,a)\,|0\rangle\,. \tag{1.71}$$

This way we obtain

$$\begin{aligned}
&\langle 0|\chi^\dagger g\boldsymbol{\sigma}^i\mathbf{B}^j\psi|Q(\mathbf{p}_1,s_1,c_1)\bar{Q}(\mathbf{p}_2,s_2,c_2)g(\mathbf{p}_g,\lambda,a)\rangle \\
&= g\sqrt{8E_{\mathbf{p}_1}E_{\mathbf{p}_2}E_{\mathbf{p}_g}}\boldsymbol{\sigma}^i_{pq}\,\langle 0|\chi_p^{\dagger\alpha}\epsilon^{ijk}\partial_j\mathbf{A}^{k\,l}T^{l\alpha\beta}\psi_q^\beta b^\dagger(\mathbf{p}_1,s_1,c_1)c^\dagger(\mathbf{p}_2,s_2,c_2)d^\dagger(\mathbf{p}_g,\lambda,a)|0\rangle \\
&= g\sqrt{8E_{\mathbf{p}_1}E_{\mathbf{p}_2}E_{\mathbf{p}_g}}\boldsymbol{\sigma}^i_{pq}T^{l\alpha\beta}\epsilon^{ijk}\{\chi_p^{\dagger\alpha}, c^\dagger(\mathbf{p}_2,s_2,c_2)\} \\
&\times\boldsymbol{\partial}_j\left([\mathbf{A}^{k\,l}, d^\dagger(\mathbf{p}_g,\lambda,a)]\right)\{\psi_q^\beta, b^\dagger(\mathbf{p}_1,s_1,c_1)\} \\
&= ig\eta_p(s_2)\boldsymbol{\sigma}^i_{pq}\xi_q(s_1)\,\epsilon^{ijk}\mathbf{p}_g^j\varepsilon^k(p,\lambda)\,v^\alpha(c_2)T^l_{\alpha\beta}v^\beta(c_1)\tilde{v}^l(a)e^{-i(p_1+p_2+p_g)\cdot x}.
\end{aligned} \tag{1.72}$$

and the corresponding Feynman rule is given by

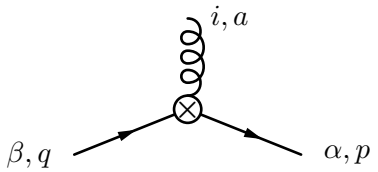

$$= -g\epsilon^{ijk}\boldsymbol{\sigma}^j_{pq}\mathbf{p}_g^k T^a_{\alpha\beta} \tag{1.73}$$

where p and q are the spin indices of the quark fields and i is the Cartesian index of the gluon field. The quark colors are denoted by α and β, while a specifies the color of the gluon.

While it is certainly tedious to keep track of all the indices by hand, the whole procedure can be easily automatized to avoid involuntary sign errors. For NRQCD this especially pays off when one needs to work out more involved interaction terms such as $\psi^\dagger(\boldsymbol{\nabla}-ig\mathbf{A})^4\psi$ or $\psi^\dagger\{\mathbf{D}^2, \boldsymbol{\sigma}\cdot g\mathbf{B}\}\psi$.

1.4 Regularization and Renormalization

In the calculation of QCD Feynman diagrams beyond tree level we encounter loop integrals that are divergent for large and small values of the loop momenta. These two kinds of divergences are usually referenced to as ultraviolet (UV) and infrared (IR). In the following we will primarily consider the former.

A divergent integral is not a mathematically well-defined object, so that manipulations of such quantities lead to meaningless results. We can, nevertheless, assign a divergent integral some finite value by introducing a regulator that renders it finite. The final result will of course depend on the regulator, so that different regularization prescriptions lead to different values of loop integrals. The physical predictions should be, of course, independent on the choice of the regulator (which is an unphysical parameter).

The most common regularization procedure in the context of gauge theories and hence also QCD is known as the dimensional regularization (DR) [79]. The main idea behind DR is to observe that UV divergent loop integrals in 4 space-time dimensions are convergent in lower dimensions, e. g. in $D = 4 - 2\epsilon$, where ϵ can be chosen to be a small positive number. This means that we can conveniently regularize divergent loop integrals by working with D-dimensional amplitudes and expanding them around $D = 4$, so that the UV divergences manifest themselves as $1/\epsilon$ poles.

The master formula for computing 1-loop integrals in D-dimensions reads

$$\int \frac{d^D l}{(2\pi)^D} \frac{1}{(l^2 + 2l \cdot q + m^2 \pm i\eta)^n} = (-1)^n \frac{i}{(4\pi)^{\frac{D}{2}}} \frac{\Gamma(n - \frac{D}{2})}{\Gamma(n)} (q^2 - m^2 \mp i\eta)^{\frac{D}{2} - n}, \quad (1.74)$$

while D-dimensional Dirac matrices satisfy

$$\{\gamma^\mu, \gamma^\nu\} = 2g^{\mu\nu} \quad (1.75)$$

$$\gamma^\mu \gamma_\mu = D \quad (1.76)$$

$$\gamma^\mu \gamma^\nu \gamma_\mu = -(D-2)\gamma^\nu = -2\gamma^\nu - (D-4)\gamma^\nu \quad (1.77)$$

$$\gamma^\mu \gamma^\nu \gamma^\rho \gamma_\mu = 4g^{\nu\rho} - (4-D)\gamma^\nu \gamma^\rho \quad (1.78)$$

$$\gamma^\mu \gamma^\nu \gamma^\rho \gamma^\sigma \gamma_\mu = -2\gamma^\sigma \gamma^\rho \gamma^\nu + (4-D)\gamma^\nu \gamma^\rho \gamma^\sigma \quad (1.79)$$

Special care is required when working with objects that cannot be naively generalized to D dimensions, such as γ_5 and $\varepsilon^{\mu\nu\rho\sigma}$. In this case one should use special regularization prescriptions e. g. [80].

The removal of divergences is achieved by a procedure called renormalization. The justification for renormalization is the observation that fields, masses and coupling constants appearing in the Lagrangian are *bare* i. e. not physical quantities. The latter are obtained by multiplying bare quantities with renormalization constants Z_i, which cancel the UV divergences from loop diagrams. An explicit example for renormalization of QED using software tools developed during this work will be presented in Part VI.

2 Effective Field Theories

2.1 Philosophy Behind the Effective Field Theory Approach

Most of the physical systems have a set of several characteristic scales that are relevant for their description. For example, in a hydrogen atom such scales [3, 5, 81] are the electron mass m_e, the typical size of the 3-momentum of the electron $m_e\alpha$ and the typical size of the binding energy $m_e\alpha^2$, where $\alpha \equiv e^2/4\pi$ is the fine structure constant and e is the electric charge. Let us neglect the motion of the proton[1] and describe the dynamics of the electron through its interaction with a potential. In this case the quantum mechanical Hamiltonian for the hydrogen atom reads

$$H = \frac{\mathbf{p}^2}{2m_e} + V(\mathbf{r}). \tag{2.1}$$

The leading contribution to $V(\mathbf{r})$ is of course the Coulomb potential

$$V_C(\mathbf{r}) = -\frac{e^2}{r} \tag{2.2}$$

with $r \equiv |\mathbf{r}|$. It is well known, that Eq. (2.2) provides only a very crude description of the hydrogen spectrum. Quantum mechanics textbooks (e. g. [82]) usually discuss additional corrections to the potential, that describe interaction of the electron spin with the magnetic field in the atom (spin-orbit coupling), relativistic corrections to the kinetic energy of the electron (due to $E_{\text{kin}} = \sqrt{m_e^2 + \mathbf{p}^2} - m_e \neq \mathbf{p}^2/2m_e$) and the smearing of the potential due to the quantum mechanical uncertainty in the position of the electron (Darwin term). However, the derivation of these corrections in quantum mechanics is nowhere systematic and involves hand-waving arguments. To define a bound state potential from the first principles, we clearly need to describe our nonrelativistic system in QFT. This is all the more important in view of the fact, that nonrelativistic quantum mechanics has difficulties to account for QFT effects, such as Lamb shift (loop corrections to the self-energy of the atom) and anomalous magnetic dipole moment (loop corrections to the electron-electron-photon vertex).

However, a high energy theory such as QED, is usually not the most appropriate tool to describe phenomena that occur at low energies. The issue is that the hierarchy of scales

$$m_e \gg m_e\alpha \gg m_e\alpha^2 \tag{2.3}$$

of the system is not manifest in the QED Lagrangian. This is why it is difficult to use this theory for the description of the low-energy dynamics of the hydrogen atom, e. g. interactions of electrons and photons with energies and momenta much below m_e.

In general, this raises the question of finding a rigorous and systematic quantum field theoretical description of phenomena that occur at energies much below some scale Λ (e. g. $\Lambda = m_e$ for the hydrogen atom). The natural answer to this question is provided by the Effective Field Theory (EFT) approach [1, 2].

An EFT is a low-energy QFT that approximates the given high energy theory at energies $E \ll \Lambda$, using the most appropriate degrees of freedom and thus providing the

[1] Owing to the large difference between the masses of the proton and the electron $m_p/m_e \sim 1836$ [40], one usually argues that the change in the momentum of the proton due to the interactions with the electron is negligible. If needed, one can also explicitly include the effects of the proton recoil (c. f. for example [5])

simplest description of the relevant physics. What is more, to construct an EFT we do not necessarily need to know the exact form of the relevant high energy theory. It is sufficient to correctly identify the relevant scales, symmetries and degrees of freedom and then consider all the interactions allowed by the symmetries. This procedure guarantees, that the so-obtained EFT will precisely reproduce the behavior of the high energy theory in the given low energy region. The power-counting rules of an EFT tell us how different operators scale with respect to the relevant expansion parameters. This allows for a systematic improvement of the EFT predictions, which is usually not feasible for a phenomenological model. A more technical description of the EFT framework will be given in Sec. 2.2.

The EFT philosophy provides a deeper and refreshing view on many QFT concepts that were developed long before the advent of EFTs.

One of them concerns the renormalizability of the given theory. In the traditional sense only theories with dimensionless couplings and operators of mass dimension less or equal to four are regarded as renormalizable. This means that all UV divergences of the theory can be absorbed into a finite number of renormalized parameters. For example, in QED these parameters are wave-function renormalization Z_ψ, photon-field renormalization Z_A, charge renormalization Z_e and mass renormalization Z_m. When we go beyond 1-loop renormalization of QED, no additional renormalization constants are required: at each higher loop order Z_i (organized as a series in the coupling constant) are adjusted in such a way, that they can absorb all the UV divergences that appear at the given order in the coupling constant.

In a theory that contains operators with mass dimension larger than four (which is usually the case for EFTs), the number of renormalization parameters increases with the inclusion of new operators. The problem is, hence, not the removal of UV divergences, but rather the necessity to carry out an infinite number of measurement that determine the values of the renormalized quantities at some scale. This is why it is traditionally argued that a nonrenormalizable theory is meaningless, as it lacks any predictive power.

Although EFTs are usually not renormalizable in this traditional sense, it is not true that they cannot be used to derive new predictions. In an EFT we always work at a given order in E/Λ, such that the number of renormalization parameters remains finite. Depending on the EFT, their values can be extracted from matching calculations, experimental measurements or lattice simulations and then used to predict the values of the physical observables. Certainly, the number of counterterms increases with each loop order, so that at some point we might end up with a very big number of unknown constants, whose values need to be fixed. However, this is rather a practical, than a fundamental complication and should not obscure the statement that nonrenormalizable theories are not irrelevant for the phenomenology.

In fact, in the EFT philosophy there is no fundamental difference between renormalizable and nonrenormalizable theories. We can regard every renormalizable QFT as an EFT, for which we know only the leading order part of the Lagrangian, up to the operators suppressed by powers of E/Λ. If the scale Λ is sufficiently large, as compared to the energies that we are interested in, the effects of higher order operators may be neglected and we end up with a theory that has no operators with mass dimension larger than four. For example, we know that QED, a renormalizable theory, ceases being accurate at energies around $100\,\text{GeV} \sim m_Z$, where the contributions of Z bosons to "pure" QED processes become significant, e. g. in $e^+e^- \to Z/\gamma^* \to e^+e^-$. This is not a practical issue, as we know that at these energies QED is superseded by the Electroweak theory.

Now imagine a world where physicists know only QED but not the Electroweak

theory and the experimentally available energies are still well below the m_Z threshold. At the same time their detector technology is so well developed, that the QED alone is not sufficient to describe highly precise experimental data. In this case, using EFT techniques, theorists could explain experimental measurements by improving the QED Lagrangian with higher dimensional operators, suppressed by powers of $1/m_Z$ [83]. Of course, at energies $E \sim m_Z$ their expansion in E/m_Z would break down and they would need to construct a new EFT that works at higher energies.

In this sense our whole physical understanding of the world can be represented by an infinite chain of EFTs. What we call Standard Model is just the leading part of some EFT Lagrangian. The theory appears renormalizable because the unknown scale Λ is sufficiently large so that the contributions of higher dimensional operators to the processes that we can measure are very small. Depending on the size of Λ, these effects may or may not be observable at the Large Hadron Collider at CERN. If every QFT is an EFT, the notion of full or high energy theory should be always understood in relation to some low-energy theory.

In principle, there exists a possibility that the chain of EFTs terminates when we discover the so-called Theory of Everything (TOE), an ultimate theory of nature that describes all physical phenomena up to infinitely high energies. Even if such a theory can be found and verified experimentally, it is highly unlikely that it would be simple to apply the TOE to low-energy phenomena, such as electromagnetic or hadronic bound states. We would still require all the previously developed EFTs to describe physics at lower energies in a simple but systematic way.

2.2 Construction of Effective Field Theories and Matching

EFTs is a very active field of research [83, 84]: In the last decades the EFT approach has been applied to electromagnetic (c. f. Sec. 4.1), weak [85], strong (c. f. Sec. 2.3) and gravitational [86, 87] interactions. In general, the construction of every EFT proceeds through several steps, that are worth being explained in some details. This knowledge greatly facilitates the development and the application of EFTs.

We can apply EFT methods to a system that contains several well separated dynamical scales

$$\Lambda \gg \Lambda_1 \gg \Lambda_2 \gg \dots , \tag{2.4}$$

where Λ is the largest scale. The first step is always to identify these scales and estimate the size of the dimensionless ratios

$$\frac{\Lambda_1}{\Lambda_2}, \quad \frac{\Lambda_1}{\Lambda}, \quad \dots . \tag{2.5}$$

For $\Lambda_i/\Lambda \ll 1$ the EFT expansion will obviously converge sufficiently fast. Otherwise, higher order corrections in the Λ_i/Λ expansion are important and should be included to obtain reliable predictions.

The second step is to enumerate the relevant symmetries. In case of strong and electromagnetic interactions it is natural to impose the separate conservation of C, P and T as well as that of the gauge symmetry. The given system might also obey additional exact or appropriate symmetries, such as the isospin symmetry in the interactions of up and down quarks or the heavy quark symmetries in the processes that involve charm or bottom quarks.

The third step is to identify the correct degrees of freedom in the relevant energy region. This is necessary to define the field content of the theory, i. e. the states that our

EFT will describe. These can be fields that equally appear at high energies, but also new fields that manifest themselves only in low energetic interactions. For example, QCD is formulated as a theory of quarks and gluons. In high energy collisions quarks and gluons are indeed the correct degrees of freedom to understand what happens in the interaction point. However, at energies below Λ_{QCD} and below, quarks and gluons are confined inside hadrons. In this case light hadrons such as pions and kaons are the appropriate degrees of freedom for the suitable EFT.

Once the proper scales, symmetries and degrees of freedom are known, we can begin with the step four, which involves the explicit construction of the EFT Lagrangian. In principle, the Lagrangian of an EFT is an infinite series in Λ_i/Λ, where each term contains an operator $\mathcal{O}_i$ multiplied by the matching coefficient c_i. The reason for this is that in the limit $\Lambda \to \infty$ the EFT should coincide with the full theory, so that every operator compatible with the underlying symmetries must be included. Schematically, we can write

$$\mathcal{L}_{\text{EFT}} = \sum_i \frac{c_i}{\Lambda^{d_i-4}} \mathcal{O}_i, \tag{2.6}$$

where d_i denotes the mass dimension of the operator $\mathcal{O}_i$.

The operators appearing in the EFT Lagrangian can be classified according to their mass dimensions into relevant ($d_i < 4$), marginal ($d_i = 4$) and irrelevant ($d_i > 4$). This naming scheme reflects the fact that at low energies irrelevant operators appear suppressed by inverse powers of the heavy scale Λ and hence they are less important than relevant and marginal operators. Although the effects of irrelevant operators are small at energies $E \ll \Lambda_{\text{QCD}}$, their presence is crucial for the systematics of the theory: In many cases interesting physical processes are described by irrelevant operators, so that they must be taken into account.

The presence of irrelevant operators in the Lagrangian is also the reason why EFTs are not renormalizable in the traditional sense. As was already explained in Sec. 2.1, this does not prevent us from using EFTs for precise and unambiguous phenomenological predictions.

The matching coefficients c_i are usually left unspecified. If the full theory is known and perturbative matching is possible, then the c_i can be computed explicitly to any desired accuracy. Unfortunately, these two conditions are not always satisfied. Think of Chiral Petrubation Theory (ChPT, c. f. Sec. 2.3) that describes interactions of hadrons at $E \ll \Lambda_{\text{QCD}}$. Here we know the full theory but cannot calculate the matching coefficients, because QCD is not perturbative in the relevant energy region. A different issue arises in the construction of EFTs for physics beyond the Standard Model: since we do not know the full theory, we obviously cannot calculate the matching coefficients in the usual way.

Sometimes values of some matching coefficients can be determined or at least constrained from symmetry considerations, as it is the case in the EFTs for heavy quarks, where the relevant symmetry is the Poincare invariance of the full theory (QCD) and its realization in form of the reparametrization invariance in the EFT [88].

It is important to note that usually not all the operators $\mathcal{O}_i$ that are compatible with the symmetries are linearly independent. Relations between different operators can be obtained from field redefinitions and equations of motions. Such relations can be sometimes used to completely eliminate a particular operator by expressing it as a linear combination of other operators that are already present in the basis. This automatically implies a redefinition of the corresponding matching coefficients. Consider, for example, a combination of

$$c_1\mathcal{O}_1 + c_2\mathcal{O}_2 + c_3\mathcal{O}_3, \tag{2.7}$$

where $\mathcal{O}_3$ can be eliminated via

$$\mathcal{O}_3 = a\mathcal{O}_1 + b\mathcal{O}_2. \tag{2.8}$$

Plugging Eq. (2.8) into Eq. (2.7) we obtain

$$c_1'\mathcal{O}_1 + c_2'\mathcal{O}_2 \tag{2.9}$$

with

$$c_1' = c_1 + a, \quad c_2' = c_2 + b \tag{2.10}$$

This means that someone doing calculations in the basis of Eq. (2.7) will find different matching coefficients than a person who works with the basis of Eq. (2.9). Since their matching coefficients are related to each other via Eq. (2.10), they can always cross-check each others results.

Although the Lagrangian presented in Eq. (2.6) contains an infinite number of terms, only a finite number of operators contributes at the given order in $\mathcal{O}\left(\left(\frac{\Lambda_1}{\Lambda}\right)^{n_1}\left(\frac{\Lambda_1}{\Lambda_2}\right)^{n_2}\dots\right)$. To determine these operators we need to introduce some power-counting rules, which is the fifth step in our process of constructing an EFT. These rules tell us how each operator scales in Λ_i/Λ, so that we can select all the operators that contribute to the process at the accuracy we are aiming at. Power counting is usually simple for theories that contain a single scale. In a theory with several scales, e. g. $\Lambda \gg \Lambda_1, \Lambda_2, \dots$, things tend to become more complicated. In this case loop momenta of order $\Lambda_1, \Lambda_2, \dots$ can equally appear in the loop integrals, so that by just looking at a loop diagram we cannot immediately tell how it will contribute to the given observable. Instead, we must carefully analyze the typical size of the momenta flowing through the internal propagators and their contributions to the value of the integral.

For definiteness, let us consider an EFT with a scalar particle ϕ of mass m. The theory is defined to work at energies below some large scale Λ_0 and we are interested in the contributions from the integral

$$\int \frac{d^D l}{(2\pi)^D} \frac{1}{\left(l^2 - m^2 + i\eta\right)^2 \left((l-p)^2 - m^2 + i\eta\right)}. \tag{2.11}$$

Let us first suppose that the hierarchy of scales in our EFT is given by

$$\Lambda_0 \gg \Lambda', \tag{2.12}$$

with $m \sim \Lambda'$. This means that apart from Λ' there are no further dynamical scales in the theory. In this case the typical energy and momentum of ϕ are of order Λ' and the size of the contribution from Eq. (2.11) can be easily estimated to be $(\Lambda')^{-2}$, where we count each propagator as $(\Lambda')^{-2}$ and the integral measure as $(\Lambda')^4$. Since we have only one dynamical scale Λ' , the counting is very simple or, in the EFT language, homogeneous.

Now we want to assume that our EFT contains two dynamical scales Λ_1 and Λ_2 with

$$\Lambda_0 \gg \Lambda_1 \gg \Lambda_2. \tag{2.13}$$

The integral from Eq. (2.11) can also appear in this other theory and it is interesting to see how we can determine its contributions. Suppose that we have

$$p^0 \sim \mathbf{p} \sim \Lambda_1, \tag{2.14}$$

$$m \sim \Lambda_2. \tag{2.15}$$

While we can specify the typical size of p^0 and $\mathbf{p}$ (since p is an external momentum), the temporal and spatial components of the loop momentum q can be in principle of order Λ_1 or Λ_2 or both.

To identify the dominant contributions[2] to the integral in Eq. (2.11) we can use the method of regions [89]. In the context of matching calculations, this technique allows us to split the full loop integral into regions determined by the typical size of the loop momentum. These regions can be identified by looking at the poles of the energy component of the loop momentum in the complex plain. Then, in each region we can expand in the masses and momenta that are smaller than the loop momentum. The resulting loop integrals are usually much simpler than the original one. Naively, one would expect that these integrals should be computed such, that the domain of the integration is adjusted to the size of each region. However, it turns out that in dimensional regularization this is not necessary: we can integrate over the entire integration domain and still obtain correct results for each expanded integral. This is a very nontrivial aspect of the method of regions, but it can be proven in a rigorous way [90]. It is also worth noting that in the context of NRQCD, the prescription to identify the correct region when doing matching between QCD and NRQCD was worked out [91] in the time, when the method of regions was not yet available.

The poles of l^0 from Eq. (2.11) are shown in Fig. 2.1. We choose to close the contour

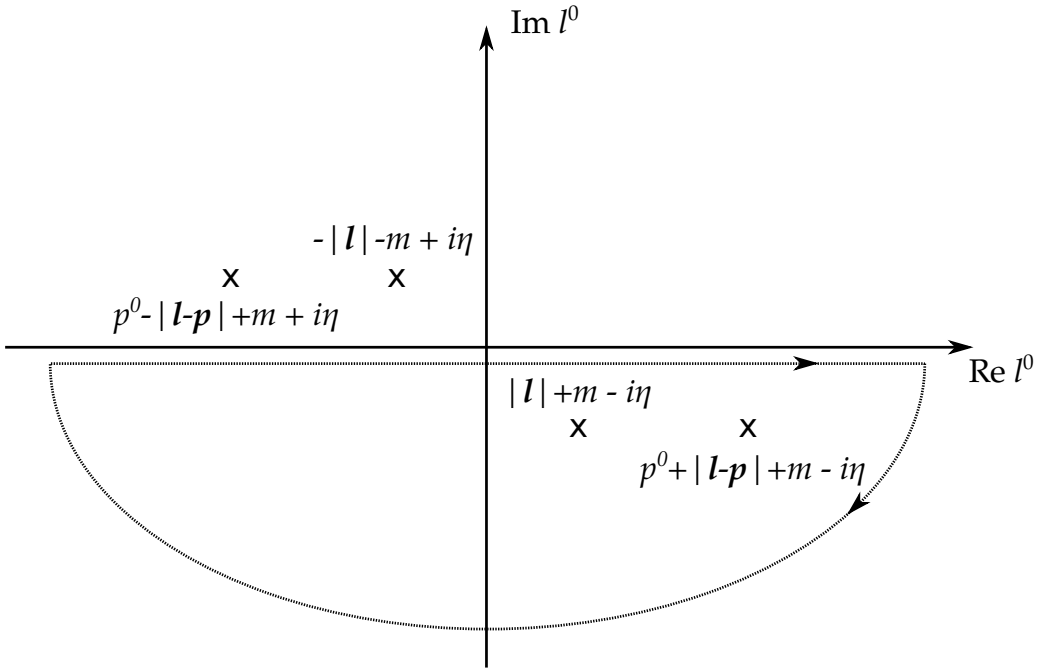

Figure 2.1: Poles of l^0 from Eq. (2.16) in the complex plane. The dotted line shows our choice of the integration contour.

from below such, that we pick up the residues from

$$l^0 = p^0 + |\mathbf{l} - \mathbf{p}| + m - i\eta \tag{2.16}$$

[2]Of course, for this simple example we could also directly expand the integral in the appropriate small quantities. However, since the method of regions is a quite useful technique in dealing with loop integrals, we would still like to introduce it here.

and

$$l^0 = |\mathbf{l}| + m - i\eta. \tag{2.17}$$

Eq. (2.17) tells us that we can have $l^0 \sim \mathbf{l}$, where l^0 and $\mathbf{l}$ are both of order Λ_1 or Λ_2. From Eq. (2.16) we see that $l^0 \sim \Lambda_1, \mathbf{l} \sim \Lambda_2$ is also possible. On the other hand, we apparently cannot have a contribution from $l^0 \sim \Lambda_2$, $\mathbf{l} \sim \Lambda_1$, since this would contradict the scaling of Eqs. (2.16) and (2.17). Therefore, the dominant contributions to the loop integral arise from three different regions, which are

$$l^0 \sim \mathbf{l} \sim \Lambda_1, \tag{2.18}$$

$$l^0 \sim \Lambda_1, \quad \mathbf{l} \sim \Lambda_2, \tag{2.19}$$

$$l^0 \sim \mathbf{l} \sim \Lambda_2. \tag{2.20}$$

In case of $l^0 \sim \mathbf{l} \sim \Lambda_1$, we may neglect m which is only of order Λ_2,

$$\int \frac{d^D l}{(2\pi)^D} \frac{1}{(l^2-m^2)^2((l-p)^2-m^2)} \approx \int \frac{d^D l}{(2\pi)^D} \frac{1}{l^4(l-p)^2} \sim \Lambda_1^{-2}\Lambda_2^0 \tag{2.21}$$

For $l^0 \sim \Lambda_1, \mathbf{l} \sim \Lambda_2$ the integral becomes scaleless with respect to the spatial integration in $D-1$ dimensions and hence vanishes.

$$\int \frac{d^D l}{(2\pi)^D} \frac{1}{(l^2-m^2)^2((l-p)^2-m^2)} \approx \int \frac{dl^0}{(2\pi)} \frac{d^{D-1}\mathbf{l}}{(2\pi)^{D-1}} \frac{1}{((l^0)^4)((l^0-p^0)^2-\mathbf{p}^2)} = 0. \tag{2.22}$$

Finally, for $l^0 \sim \mathbf{l} \sim \Lambda_2$ we end up with

$$\int \frac{d^D l}{(2\pi)^D} \frac{1}{(l^2-m^2)^2((l-p)^2-m^2)} \approx \int \frac{dl^0}{(2\pi)} \frac{d^{D-1}\mathbf{l}}{(2\pi)^{D-1}} \frac{1}{(l^2-m^2)^2 p^2} \sim \Lambda_1^0 \Lambda_2^{-2}. \tag{2.23}$$

We see that the scaling of the integral from Eq. (2.11) changes dramatically, depending on the region we are looking at. It is, therefore, very important to properly disentangle the contributions of different regions from each other. Needless to say, that the situation becomes even more complicated when we have more scales, more loops or more external momenta. In the EFT language this is known as inhomogeneous power-counting, which is a distinct feature of EFTs with several dynamical scales. In contrast, the power-counting of EFTs with a single dynamical scale is homogeneous, so that such complications do not occur.

Let us also remark that if we are predominantly interested in physics at the scale Λ_2, we could construct a new EFT that works at energies $\Lambda_1 \ll \Lambda_2$. In this case we are integrating out the scale Λ_1 out of our first EFT and obtain a second EFT that contains only one dynamical scale Λ_2 and hence has homogeneous power-counting.

Let us finally discuss the matching, which is usually the final step in the construction of an EFT. For simplicity[3], let us assume that we know the full theory and this theory is perturbative at $E \sim \Lambda$. The main purpose of the matching is to determine the coefficients c_i in Eq. (2.6) by comparing suitable quantities computed in the EFT and in the full theory. At energies $E \ll \Lambda$ the predictions of both theories should be identical by construction. However, only the full theory can also describe physics at $E \geq \Lambda$. As already explained in Sec. 2.1, if we want to describe low-energy phenomena at arbitrary precision, we must

[3] It is clear, that we cannot calculate matching coefficients if we do not know that full theory or if this theory is nonperturbative in the relevant energy region.

include contributions from the high energy region in a systematic way. Matching is what allows us to encode these contributions in the matching coefficients of the EFT. This is important, because a low energy EFT by definition does not know anything about physics at $E \geq \Lambda$. Through the matching coefficients it nevertheless can correctly take the high energy effects into account when doing predictions for low-energy observables.

The prescription that tells us what quantities in the full theory and in the EFT should be computed and compared to each other is called matching condition. In practice one encounters matching conditions formulated in terms of on-shell or off-shell amplitudes (Green's functions), total cross sections, decay rates or other suitable quantities.

To give an explicit nontrivial example, let us consider matching for the Euler-Heisenberg effective Lagrangian [92] at leading order in the $1/m_e$ expansion. The Lagrangian of this EFT reads

$$\mathcal{L}_{\text{EH}} = -\frac{1}{4}F^{\mu\nu}F_{\mu\nu} + \frac{a}{m_e^4}\left(F^{\mu\nu}F_{\mu\nu}\right)^2 + \frac{b}{m_e^4}F^{\mu\nu}F_{\nu\sigma}F^{\sigma\rho}F_{\rho\mu}. \tag{2.24}$$

In the modern understanding $\mathcal{L}_{\text{EH}}$ describes a low energy EFT of QED, which contains photons but no leptons. The energies and momenta of the photons are so small ($p^0, \mathbf{p} \ll m_e$), that pair creation or annihilation are impossible. These photons can interact with each other via light-by-light scattering, which is described by the two dimension eight operators in Eq. (2.24).

To determine the matching coefficients a and b we need to calculate the $\gamma\gamma \to \gamma\gamma$ scattering process (c. f. Fig. 2.2) in QED and Euler-Heisenberg EFT (EHEFT). The external

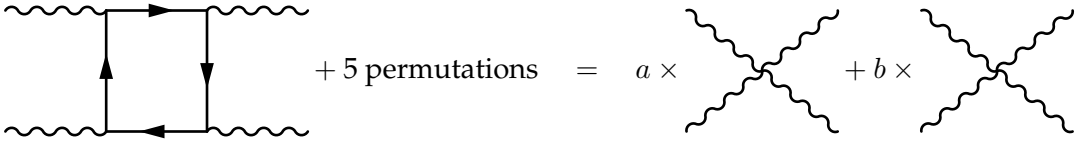

(2.25)

Figure 2.2: Matching between QED and EHEFT. The hard region ($l^0 \sim \mathbf{l} \sim m_e$) of six light-by-light scattering diagrams in QED determines the matching coefficients a and b of EHEFT.

photons can be put on-shell. A convenient shortcut [93] is to consider the forward scattering $\gamma(p_1)\gamma(p_2) \to \gamma(p_1)\gamma(p_2)$ and to amputate the external states (i. e. polarization vectors of the photons). In this case our matching condition reads

$$\mathcal{M}^{\mu\nu\alpha\beta}_{\text{QED}} = a\mathcal{M}^{\mu\nu\alpha\beta}_{1,\text{EHEFT}} + b\mathcal{M}^{\mu\nu\alpha\beta}_{2,\text{EHEFT}} \tag{2.26}$$

Contracting Eq. (2.26) with $g_{\mu\nu}g_{\alpha\beta}$ and $g_{\mu\alpha}g_{\nu\beta}$ we obtain a linear system with (after appropriate simplifications using FeynCalc (c. f. Sec. 22) and FeynHelpers (c. f. Sec. 22))

$$\begin{aligned}
\mathcal{M}^{\mu\nu\alpha\beta}_{\text{QED}} g_{\mu\nu}g_{\alpha\beta} = \frac{8i\pi^2 e^4}{(2\pi)^D}\frac{1}{(p_1\cdot p_2)}\Big(& \\
& \times \left((D^2-4D+2)(p_1\cdot p_2) - 4(D-3)m_e^2\right)B_0(2(p_1\cdot p_2), m_e^2, m_e^2) \\
& - \left((2D^2-11D+16)(p_1\cdot p_2) - 4(D-3)m_e^2\right)B_0(-2(p_1\cdot p_2), m_e^2, m_e^2) \\
& + \left((D^2-4D+8)(p_1\cdot p_2) + 4(p_1\cdot p_2)m_e^2 - 8m_e^4\right) \\
& \times C_0(0, 0, -2(p_1\cdot p_2), m_e^2, m_e^2, m_e^2)
\end{aligned}$$

$$
\begin{aligned}
&+ ((D^2-6D+4)(p_1\cdot p_2) + 4(p_1\cdot p_2)m_e^2 + 8m_e^4) \\
&\times C_0(0,0,2(p_1\cdot p_2), m_e^2, m_e^2, m_e^2) \\
&- \frac{(3D^2-20D+28)(p_1\cdot p_2)}{2m_e^2} A_0(m^2)\Big), \qquad (2.27a)\\
\mathcal{M}^{\mu\nu\alpha\beta}_{\text{QED}} g_{\mu\alpha}g_{\nu\beta} &= \frac{-8i\pi^2 e^4}{(2\pi)^D}\frac{1}{(p_1\cdot p_2)}\Big(\\
&\times (4(D-3)m_e^2 + (D-2)(p_1\cdot p_2))B_0(2(p_1\cdot p_2), m_e^2, m_e^2) \\
&+ ((D-2)(p_1\cdot p_2) - 4(D-3)m_e^2)B_0(-2(p_1\cdot p_2), m_e^2, m_e^2) \\
&+ (4(D-2)(p_1\cdot p_2)m_e^2 + (D-2)^2(p_1\cdot p_2)^2 - 8m_e^4) \\
&\times C_0(0,0,2(p_1\cdot p_2), m_e^2, m_e^2, m_e^2) \\
&+ (4(D-2)(p_1\cdot p_2)m_e^2 - (D-2)^2(p_1\cdot p_2)^2 + 8m_e^4) \\
&\times C_0(0,0,-2(p_1\cdot p_2), m_e^2, m_e^2, m_e^2) \\
&- \frac{(D-2)^3(p_1\cdot p_2)}{2m_e^2} A_0(m^2)\Big), \qquad (2.27b)
\end{aligned}
$$

$$
\left(a\mathcal{M}^{\mu\nu\alpha\beta}_{1,\text{EHEFT}} + b\mathcal{M}^{\mu\nu\alpha\beta}_{2,\text{EHEFT}}\right) g_{\mu\nu}g_{\alpha\beta} = \frac{32i(p_1\cdot p_2)^2}{m_e^4}(13a+6b)\,, \qquad (2.28a)
$$

$$
\left(a\mathcal{M}^{\mu\nu\alpha\beta}_{1,\text{EHEFT}} + b\mathcal{M}^{\mu\nu\alpha\beta}_{2,\text{EHEFT}}\right) g_{\mu\alpha}g_{\nu\beta} = \frac{32i(p_1\cdot p_2)^2}{m_e^4}(4a+3b)\,, \qquad (2.28b)
$$

where we have introduced Passarino–Veltman scalar integrals in the convention of [94]

$$
A_0(m_0^2) = \int \frac{d^Dl}{i\pi^2}\frac{1}{(l^2-m_0^2)}, \qquad (2.29)
$$

$$
B_0(p_1^2, m_0^2, m_1^2) = \int \frac{d^Dl}{i\pi^2}\frac{1}{(l^2-m_0^2)((l-p_1)^2-m_1^2)}, \qquad (2.30)
$$

$$
C_0(p_1^2,(p_1-p_2)^2,p_2^2,m_0^2,m_1^2,m_2^2) = \int \frac{d^Dl}{i\pi^2}\frac{1}{(l^2-m_0^2)((l-p_1)^2-m_1^2)((l-p_2)^2-m_2^2)}. \qquad (2.31)
$$

The values of the matching coefficients a and b are determined by the hard region of the 1-loop diagrams on the QED side, where

$$
l^0 \sim \mathbf{l} \sim m_e. \qquad (2.32)
$$

Owing to $\mathbf{p}_1, \mathbf{p}_2 \ll m_e$ we can expand the 1-loop QED amplitude in

$$
p_1\cdot p_2 = |\mathbf{p}_1||\mathbf{p}_2|(1-\hat{\mathbf{p}}_1\cdot\hat{\mathbf{p}}_2) \qquad (2.33)
$$

up to second order and match the result to the EFT amplitude. Although it is well known that the A_0 and B_0 integrals are divergent, the final result (i. e. sum of contributions from all the integrals) is finite. The expansions of the loop integrals are given by

$$
A_0(m_e^2) = \frac{m_e^2}{16\pi^4}\left(\Delta + 1 + \log\left(\frac{\mu^2}{m_e^2}\right)\right), \qquad (2.34)
$$

$$
B_0(\pm 2(p_1\cdot p_2), m_e^2, m_e^2) = \frac{1}{16\pi^4}\left(\Delta + \log\left(\frac{\mu^2}{m_e^2}\right) \pm \frac{(p_1\cdot p_2)}{3m_e^2} + \frac{(p_1\cdot p_2)^2}{15m_e^4}\right.
$$

$$\pm \frac{2(p_1\cdot p_2)^3}{105m_e^6} + \mathcal{O}\left(\frac{(p_1\cdot p_2)^4}{m_e^8}\right)\Bigg), \tag{2.35}$$

$$C_0(0,0\pm 2(p_1\cdot p_2),m_e^2,m_e^2,m_e^2) = \frac{1}{32\pi^4 m_e^2}\Bigg(1\pm\frac{(p_1\cdot p_2)}{6m_e^2}+\frac{2(p_1\cdot p_2)^2}{45m_e^4}\pm\frac{(p_1\cdot p_2)^3}{70m_e^6} + \mathcal{O}\left(\frac{(p_1\cdot p_2)^4}{m_e^8}\right)\Bigg), \tag{2.36}$$

with $\Delta = \frac{1}{\varepsilon} - \gamma_E + \log(4\pi)$. This yields

$$\mathcal{M}^{\mu\nu\alpha\beta}_{\text{QED}}\, g_{\mu\nu}g_{\alpha\beta} = \frac{19ie^4(p_1\cdot p_2)^2}{90\pi^2 m_e^4} + \mathcal{O}\left(\frac{(p_1\cdot p_2)^3}{m_e^6}\right), \tag{2.37a}$$

$$\mathcal{M}^{\mu\nu\alpha\beta}_{\text{QED}}\, g_{\mu\alpha}g_{\nu\beta} = \frac{11ie^4(p_1\cdot p_2)^2}{45\pi^2 m_e^4} + \mathcal{O}\left(\frac{(p_1\cdot p_2)^3}{m_e^6}\right). \tag{2.37b}$$

Comparing Eqs. (2.37) to Eqs. (2.28) we readily reproduce the known results

$$a = -\frac{\alpha^2}{36}, \qquad b = \frac{7\alpha^2}{90}, \tag{2.38}$$

which concludes our brief introduction to the general concepts of EFTs.

2.3 Effective Field Theories for Strong Interactions

The physics of hadronic interactions [95] belongs to the most fascinating but also most challenging sectors of the Standard Model. We know that hadrons are made of quarks and gluons and that their behavior is governed by QCD. However, perturbative QCD is of very limited use if we want to understand strong interactions of hadronic systems, as well as their formation from and decay into partons.

The description of many hadronic systems is based on the usage of EFTs and factorization theorems. For definiteness, let us consider the example of quarkonium production in a collision of two particles (e. g. $e + e^-$ or $q\bar{q}$). A sketch of this process is shown in Fig. 2.3. On the one hand, the formation of a heavy quark pair in a collision process is a

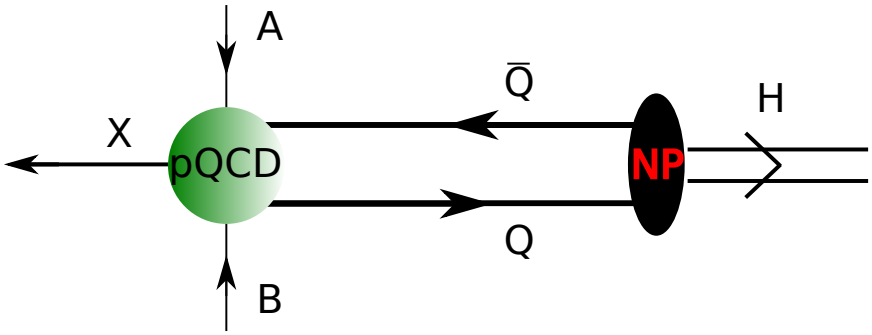

Figure 2.3: Schematic representation of quarkonium production. A $Q\bar{Q}$ pair plus anything else (X) are created in a perturbative short distance collision process. After that the pair can evolve into a heavy quarkonium. This evolution is a nonperturbative long distance effect that cannot be computed in perturbative QCD.

short distance effect that can be calculated in perturbative QCD on the level of partons,

as $A + B \to Q\bar{Q} + X$. On the other hand, the formation of a heavy quarkonium out of the $Q\bar{Q}$ pair is a long-distance process, which is beyond the scope of perturbative methods.

In Sec. 1.1 we have already briefly mentioned factorization theorems that are used to achieve a separation of short- and long-distance effects in hadronic reactions. If factorization is possible, the long distance part of the process can be expressed through nonperturbative parameters that enter the final result. However, factorization alone does not provide us with a precise field theoretical definition of the nonperturbative parameters, which is very important e. g. for their evaluation on the lattice. Such definition can, however, be given in the framework of a suitable EFT. This is why the combination of EFT methods and factorization techniques constitutes a powerful theoretical tool to approach relevant hadronic interactions e. g. production and decays of heavy quarkonia[4] or heavy-light mesons.

If we are interested in interactions of hadrons at very low energies ($E \ll \Lambda_{\rm QCD}$), there is no way we can apply perturbative QCD to any of such processes. Once QCD becomes strongly coupled, perturbative expansion in α_s obviously does not make any sense. Moreover, in this case quarks and gluons are not even appropriate degrees of freedom.

Here EFT techniques again come at rescue and allow us to study the low energy dynamics of hadrons in a meaningful and systematic way. As was already explained in Sec. 2.1, all we need to know to construct an EFT are the relevant scales, symmetries and correct degrees of freedom. If we choose to work with the approximate $\mathrm{SU}(2)_V$ symmetry of low-energy QCD (c. f. Sec. 1.2), then the relevant degrees of freedom are pions ($\pi^\pm$, π^0), the pseudo-Goldstone bosons of the spontaneous symmetry breaking. This EFT is known as Chiral Perturbation Theory (ChPT) [1, 96]. In ChPT perturbative calculations are organized as an expansion in E/Λ_χ, where $\Lambda_\chi \sim 1\,\mathrm{GeV}$ is the chiral symmetry breaking scale. This is why the theory is valid only at energies $E \ll \Lambda_{\rm QCD}$. The symmetry group can be also extended to include the strange quark [97], in which case $\mathrm{SU}_L(3) \otimes \mathrm{SU}_R(3)$ is broken to $\mathrm{SU}(3)_V$. This increases the number of pseudo-Goldstone bosons to eight($\pi^\pm$, π^0, η, $K^\pm$, K^0 and $\bar{K}^0$). The most general ChPT Lagrangian for interactions of pseudo-Goldstone bosons at $\mathcal{O}(p^2/\Lambda^2_{\rm QCD})$, where p is the typical size of the momentum of the particle, can be written as

$$\mathcal{L}_{\rm ChPT} = \frac{f_\pi^2}{4}\,\mathrm{Tr}\left(\partial_\mu U \partial^\mu U^\dagger\right), \tag{2.39}$$

with f_π being the pion decay constant and $U = e^{i\phi(x)/f_\pi}$, where

$$\phi(x) = \sqrt{2}\begin{pmatrix} \pi^0/\sqrt{2} & \pi^+ \\ \pi^- & \pi^0/\sqrt{2} \end{pmatrix} \quad \text{for} \quad \mathrm{SU}(2)\ \ \mathrm{ChPT}, \tag{2.40}$$

$$\phi(x) = \sqrt{2}\begin{pmatrix} \pi^0/\sqrt{2} + \eta/\sqrt{6} & \pi^+ & K^+ \\ \pi^- & -\pi^0/\sqrt{2} + \eta/\sqrt{6} & K^0 \\ K^- & \bar{K}^0 & -2\eta/\sqrt{6} \end{pmatrix} \quad \text{for} \quad \mathrm{SU}(3)\ \ \mathrm{ChPT}. \tag{2.41}$$

The kinetic and interaction terms follow from the expansion of the matrix exponentials U and $U^\dagger$.

Let us now turn our attention to the heavy quark sector. Interactions of heavy-light systems, i. e. mesons that consist of a heavy and a light quark, can be treated in the framework of the Heavy Quark Effective Theory (HQET) [98–102].

[4]The situation with heavy quarkonia is somewhat special. A generally accepted proof for the NRQCD factorization in production is still lacking[16], so it is more correct to speak of a factorization conjecture. NRQCD factorization in decays has been proven long time ago [7], c. f. also Sec. 3.

In this EFT the heavy quark masses are taken to be infinitely large, such that $m_Q \to \infty$. The reason for this is that in a heavy-light system the typical relative momentum between two quarks scales as Λ_{QCD}. Due to $\Lambda_{\text{QCD}} \ll m_Q$ the change of $\mathcal{O}(\Lambda_{\text{QCD}})$ is negligible for the momentum of the heavy quark.

From the point of view of the light quark, a heavy quark appears as a static source. Up to corrections of $\mathcal{O}(1/m_Q)$ the interaction between the two does not depend on the heavy quark mass, so that bottom and charm quarks behave exactly in the same way. This effect is known as the heavy quark flavor symmetry. The interactions of heavy quarks with gluons are not suppressed, so that a quark-quark-gluon vertex arises already at zeroth order in the $1/m_Q$ expansion. Nevertheless, up to corrections of $\mathcal{O}(1/m_Q)$ this interaction does not depend on the spin of the heavy quark, which is known as the heavy quark spin symmetry. The heavy quark part of the HQET Lagrangian at leading order in $1/m_Q$ is given by

$$\mathcal{L}_{\text{HQET}} = \sum_{i=1}^{N_h} \bar{Q}_v^{(i)} (iv \cdot D) Q_v^{(i)} \tag{2.42}$$

where $Q_v^{(i)}$ is the heavy quark spinor field, v^μ is the heavy quark 4-velocity and the summation goes over heavy quark flavors N_h. In $\mathcal{L}_{\text{HQET}}$ the heavy quark symmetries are manifest. Moreover, since the theory contains only one dynamical scale Λ_{QCD}, the power-counting is homogeneous.

In HQET the heavy quark is static in the $1/m_Q$ expansion, so that its kinetic energy is a small $\mathcal{O}(1/m_Q)$ correction. This picture does not hold anymore, when the heavy quark interacts with another heavy quark, as it is the case in heavy quarkonia. There the relative momentum between the heavy quarks can be of order Λ_{QCD} or larger, although it is still much smaller than m_Q, i. e. $\mathbf{q} \sim m_Q v \gtrsim \Lambda_{\text{QCD}}$ with $v \ll c$. Due to the smallness of v, a heavy quarkonium can be regarded as a nonrelativistic system. The appropriate EFT for this case is known as Nonrelativistic QCD (NRQCD) [5, 7] and will be discussed in the next chapter.

There of course exist many other EFTs of QCD, such as Soft-Collinear Effective Theory [103–108], potential NRQCD (pNRQCD) [8, 9], pNRQCD at finite temperature [109], Heavy Hadron ChPT [110–112] or XEFT [113] to name just a few of them. While QCD is believed to be the fundamental theory of strong forces, its strongly coupled nature at low energies does not allow us to understand the interactions of hadronic systems using only perturbative QCD. The EFT description not only gives us access to different aspects of hadronic interactions (including those, that are, in principle, not accessible with perturbative QCD) but also allows us to define important quantities (e. g. potentials) in a rigorous way. This is why the development of the EFT methods and their applications is of paramount importance for our understanding of strong interactions.

3 Non-Relativistic QCD and Potential Nonrelativistic QCD

3.1 Dynamical Scales and Degrees Of Freedom in Heavy Quarkonia

Heavy quarkonia are bound states of a heavy quark and a heavy antiquark [16, 47]. In this work we are primarily interested in the bound states of heavy quarks of the same flavor, so that when speaking of heavy quarkonia we will always have $Q\bar{Q}$ systems in mind. The only $Q\bar{Q}$ states so far observed in experiments are charmonia and bottomonia. The top quark also belongs to the category of heavy quarks, but its mass is too large to allow for QCD bound states[1].

A generic heavy quarkonium state can be labeled by its quantum numbers as [40]

$$N^{2S+1}L_J, \tag{3.1}$$

where S, L and J denote the spin, orbital angular momentum and total angular momentum quantum numbers respectively, while N is the principal quantum number defined as

$$N = n_r + 1, \tag{3.2}$$

with n_r being the number of nodes in the radial wave function. Notice that this convention is different [114] from the one used in the atomic physics (e. g. for labeling states of the positronium), where $N_{\text{atoms}} = n_r + L + 1$ applies. The quantum number N, S, L and J obey following relations

$$N = 1, 2, 3, \ldots, \tag{3.3}$$
$$L = 0, 1, 2, \cdots < N, \tag{3.4}$$
$$S = 0, 1, \tag{3.5}$$
$$|L - S| \leq J \leq L + S. \tag{3.6}$$

Different L-states can be conventionally labeled with capital letters (e. g. S for $L = 0$, P for $L = 1$, D for $L = 2$ etc.), which is the reason why corresponding heavy quarkonium states are often denoted as S-wave, P-wave, D-wave etc.

Another way to label heavy quarkonia is to observe that $Q\bar{Q}$ bound states are neutral mesons, hence they are eigenstates of the charge conjugation operator $\mathcal{C}$. The C-parity (eigenvalue of $\mathcal{C}$) of a bound state of two fermions is given by

$$C = (-1)^{L+S}. \tag{3.7}$$

Furthermore, the P-parity (eigenvalue of the parity operator $\mathcal{P}$) of a meson is

$$P = (-1)^{L+1}. \tag{3.8}$$

Together with J, the values of P and C can be used to uniquely label sets of $N^{2S+1}L_J$ states that differ only in N via

$$J^{PC} \tag{3.9}$$

L	S	J	P	C	J^{PC}	S^P	$N^{2S+1}L_J$	Examples
0	0	0	-1	$+1$	0^{-+}	0^- (pseudoscalar)	N^1S_0	η_c, η_b
0	1	1	-1	-1	1^{--}	1^- (vector)	N^3S_0	J/ψ, $\Upsilon(1S)$
1	0	1	$+1$	-1	1^{+-}	0^+ (scalar)	N^1P_1	h_c, h_b
1	1	0	$+1$	$+1$	0^{++}	1^+ (pseudovector)	N^2P_0	χ_{c0}, χ_{b0}
1	1	1	$+1$	$+1$	1^{++}	1^+ (pseudovector)	N^2P_1	χ_{c1}, χ_{b1}
1	1	2	$+1$	$+1$	2^{++}	1^+ (pseudovector)	N^2P_2	χ_{c2}, χ_{b2}

Table 3.1: Different ways to label of S- and P-wave quarkonia by their quantum numbers.

as is shown in Table 3.1 Notice that Eq. (3.7) and Eq. (3.8) constrain the allowed values of J^{PC}. Certain combinations such as 0^{--}, 0^{-+} or 1^{-+} apparently would not fit into this scheme. When particles that have such quantum numbers and behave like a heavy quarkonium are observed in experiments, they are often denoted as *exotic states*.

In the spectrum of charmonia and bottomonia we observe that most of the conventional S- and P-wave quarkonia have masses below that of $D\bar{D}$ (for charmonia) and $B\bar{B}$ (for bottomonia) mesons. The corresponding mass values are usually referred to as the open flavor threshold. Heavy quarkonia with masses below threshold can decay either through the annihilation of the $Q\bar{Q}$ pair or via radiative transitions to lighter $Q\bar{Q}$ bound states. A decay into a combination of $Q\bar{q}$ and $\bar{Q}q$ mesons is forbidden by the conservation of energy. The situation becomes much more complicated above the open flavor threshold, where heavy quarkonia can also decay into heavy-light mesons. In the last decade experiments have observed many exotic states [16, 47] with masses above the threshold. These states do not seem to fit into the traditional $Q\bar{Q}$ scheme (some of them are even charged), so that their true nature is still unclear. As was already mentioned in Sec. 1.1, they could be tetraquarks, hadronic molecules, hybrids or something else that we currently do not understand.

The large mass of the heavy quarks suggests, that heavy quarkonia can be treated as nonrelativistic systems, where the relative velocity between the quark and the antiquark v is small with $v_c^2 \sim 0.3$ in charmonia and $v_b^2 \sim 0.1$ in bottomonia[2]. One can identify the following three characteristic scales of the system: the heavy quark mass m_Q (hard scale), the relative momentum between the heavy quarks $|\mathbf{q}| \sim m_Q v$ (soft scale) and the binding energy of the bound state $E_B \sim m_Q v^2$ (ultrasoft scale). Since $v \ll 1$, these scales obey

$$m_Q \gg m_Q v \gg m_Q v^2. \tag{3.10}$$

Moreover, the large size of the heavy quark mass in comparison to the QCD scale

$$m_Q \gg \Lambda_{\text{QCD}} \tag{3.11}$$

ensures, that effects occuring at energies of order m_Q (e. g. annihilation of a $Q\bar{Q}$ pair) and above (e. g. creation of a $Q\bar{Q}$ pair in a particle collision) can be understood in perturbation theory. The relative size of Λ_{QCD} and $m_Q v$ depends on the heavy quarkonium state we are considering. The hierarchy $\Lambda_{\text{QCD}} \gg m_Q v$ is expected to hold for the lowest lying charmonium and bottomonium states, while $\Lambda_{\text{QCD}} \sim m_Q v$ appears to be realized for the excited states [3, 4, 47].

[1] t is the only quark that is so heavy, that it can decay into an on-shell W-boson and a b quark. Consequently, its lifetime is too short to hadronize and create a $t\bar{t}$ bound state.

[2] These estimates are also confirmed in lattice simulations [115].

QCD does not take the full advantage of the widely separated hierarchy of scales from Eq. (3.10), such that any amplitude relevant for the calculation of a heavy quarkonium observable will receive contributions from the hard, soft and ultrasoft scales. Disentangling these scales from each other in full QCD turned out to be very difficult[3] and some calculations (e. g. P-wave decays [116]) exhibited IR divergences that were poorly understood.

The key to a consistent, systematic and rigorous theoretical description of heavy quarkonia lies in the separation of scales: While the nonrelativistic dynamics of a heavy quarkonium is governed by modes with energies and momenta much smaller than m_Q, the relativistic process of creation or annihilation of $Q\bar{Q}$ pairs occurs at energies of order m_Q and larger.

The first step in this direction was the establishment of nonrelativistic QED (NRQED) [5], a nonrelativistic EFT that can be obtained from full QED by integrating out the hard scale m_e. The construction of suitable nonrelativistic EFTs for heavy quarkonium bound states soon followed. These theories are known as Nonrelativistic QCD (NRQCD) [7] (obtained by integrating out the scale m_Q) and potential Nonrelativistic QCD (pNRQCD) [8, 9] (obtained by integrating out the scales m_Q and $m_Q v$) and will be introduced in the next sections of this chapter.

3.2 Lagrangian of NRQCD

As was already mentioned in Sec 3.1, NRQCD is obtained from QCD by integrating out the hard scale m_Q, so that its Lagrangian is an expansion in $1/m_Q$. In the energy region $E \ll m_Q$ NRQCD is equivalent to QCD. The degrees of freedom of the theory are heavy quarks, gluons and light quarks with energies and momenta below m_Q.

The explicit construction of the NRQCD Lagrangian proceeds by considering all possible operators allowed by the symmetries. A systematic description of this procedure for the 2-fermion sector can be found in [117], while the 4-fermion sector is covered in [27, 118]. At $\mathcal{O}(1/m_Q^2)$ (including the kinetic terms $\mathbf{D}^4/(8m_Q^3)$) the Lagrangian of NRQCD (up to possible field redefinitions) reads [3–5, 7]

$$\mathcal{L}_{\text{NRQCD}} = \mathcal{L}_g + \mathcal{L}_{\text{l}} + \mathcal{L}_\psi + \mathcal{L}_\chi + \mathcal{L}_{\psi\chi}. \tag{3.12}$$

The pure gauge sector of the theory is described by $\mathcal{L}_g$

$$\mathcal{L}_g = -\frac{1}{4} G^a_{\mu\nu} G^{a\mu\nu} + c_1^g \frac{1}{4m_Q^2} g f^{abc} G^{a\mu\nu} G^{b\mu}{}_\alpha G^{c\nu\alpha}, \tag{3.13}$$

while $\mathcal{L}_{\text{l}}$ accounts for the light quarks q_i

$$\begin{aligned}
\mathcal{L}_l = & \sum_{i=1}^{n_f} \bar{q}_i i \not{D} q_i \\
& + c_1^{ll} \frac{g^2}{8m_Q^2} \sum_{i,j=1}^{n_f} \bar{q}_i T^a \gamma^\mu q_i \bar{q}_j T^a \gamma_\mu q_j + c_2^{ll} \frac{g^2}{8m_Q^2} \sum_{i,j=1}^{n_f} \bar{q}_i T^a \gamma^\mu \gamma_5 q_i \bar{q}_j T^a \gamma_\mu \gamma_5 q_j \\
& + c_3^{ll} \frac{g^2}{8m_Q^2} \sum_{i,j=1}^{n_f} \bar{q}_i \gamma^\mu q_i \bar{q}_j \gamma_\mu q_j + c_4^{ll} \frac{g^2}{8m_Q^2} \sum_{i,j=1}^{n_f} \bar{q}_i \gamma^\mu \gamma_5 q_i \bar{q}_j \gamma_\mu \gamma_5 q_j,
\end{aligned} \tag{3.14}$$

[3] c. f. introduction to [3] for a good overview of historical developments, especially regarding the attempts to define a heavy quarkonium potential from QCD.

with n_f bein the number of light quark flavors. The interactions of heavy quarks with gluons and light quarks are encoded in

$$\begin{aligned}\mathcal{L}_\psi = \psi^\dagger \left(iD_0 + c_2 \frac{\mathbf{D}^2}{2m_Q} + c_4 \frac{\mathbf{D}^4}{8m_Q^3} + c_F \frac{\boldsymbol{\sigma}\cdot g\mathbf{B}}{2m_Q} + c_D \frac{[\mathbf{D}\cdot, g\mathbf{E}]}{8m_Q^2} + c_S \frac{i\boldsymbol{\sigma}\cdot[\mathbf{D}\times, g\mathbf{E}]}{8m_Q^2} \right) \psi \\ + c_1^{hl} \frac{g^2}{8m_Q^2} \sum_{i=1}^{n_f} \psi^\dagger T^a \psi \bar{q}_i \gamma_0 T^a q_i + c_2^{hl} \frac{g^2}{8m_Q^2} \sum_{i=1}^{n_f} \psi^\dagger \gamma^\mu \gamma_5 T^a \psi \bar{q}_i \gamma_\mu \gamma_5 T^a q_i \\ + c_3^{hl} \frac{g^2}{8m_Q^2} \sum_{i=1}^{n_f} \psi^\dagger \psi \bar{q}_i \gamma_0 q_i + c_4^{hl} \frac{g^2}{8m_Q^2} \sum_{i=1}^{n_f} \psi \gamma^\mu \gamma_5 \psi \bar{q}_i \gamma_\mu \gamma_5 T^a q_i \end{aligned} \tag{3.15}$$

$$\mathcal{L}_\chi = \text{c.c.of } \mathcal{L}_\psi \tag{3.16}$$

Here ψ (χ) denotes a Pauli field that annihilates (creates) a heavy quark (antiquark). Furthermore, $\mathbf{B}^i \equiv \frac{1}{2}\varepsilon^{ijk}G^{kj}$, $\mathbf{E}^i \equiv G^{i0}$ and $\mathbf{D} = \boldsymbol{\nabla} - ig\mathbf{A}$, while c.c. stands for charge conjugate. Finally, the operators appearing in

$$\begin{aligned}\mathcal{L}_{\psi\chi} = \frac{f_1(^1S_0)}{m_Q^2} \psi^\dagger \chi \chi^\dagger \psi + \frac{f_1(^3S_1)}{m_Q^2} \psi^\dagger \boldsymbol{\sigma} \chi \chi^\dagger \boldsymbol{\sigma} \psi \\ + \frac{f_8(^1S_0)}{m_Q^2} \psi^\dagger T^a \chi \chi^\dagger T^a \psi + \frac{f_8(^3S_1)}{m_Q^2} \psi^\dagger \boldsymbol{\sigma} T^a \chi \chi^\dagger \boldsymbol{\sigma} T^a \psi, \end{aligned} \tag{3.17}$$

describe decays of heavy quarkonia into light hadrons. Electromagnetic decays can be described by inserting QCD vacuum between the heavy antiquark fields, i. e. via the replacement $\chi\chi^\dagger \to \chi^\dagger |0\rangle \langle 0| \chi$.

The matching coefficients c_i are determined my matching on-shell scattering amplitudes computed in perturbative QCD and perturbative NRQCD along the lines discussed in Sec. 2.2. The amplitudes are expanded in the external energies and momenta of the heavy quarks[4], so that by comparing the Pauli structures on both sides we can read off the values of c_i. The expansions can be carried out before or after doing the loop integration. An important subtlety is that in the matching the NRQCD propagator

$$\frac{i}{p^0 - \frac{\mathbf{p}^2}{2m_Q} + i\eta} \tag{3.18}$$

should be expanded in $1/m_Q$ [91]. Otherwise, one would obtain wrong results due to the contributions from regions where NRQCD is not valid. The values of the matching coefficients c_i for the pure gauge and heavy quark sectors can be found in [91, 119].

Since the matching coefficients are computed from perturbative processes, they should be understood as a series in α_s. At the same time NRQCD operators have a definite scaling in v (from $|\mathbf{q}|/m_Q \sim m_Q v/m_Q$), determined by the power-counting rules of the theory. This is why $\mathcal{L}_{\text{NRQCD}}$ is an expansion in two parameters: α_s and v.

The power-counting is, however, not unambiguous. NRQCD has two dynamical scales (soft and ultrasoft), which means that there are ambiguities in the way how we estimate the contributions of different operators to physical observables. The main difficulty comes from nonperturbative interactions between heavy quarks and soft or ultrasoft gluons. The issue is that NRQCD operators sandwiched between quarkonium or vacuum Fock states are nonperturbative quantities. Therefore, we cannot unambiguously deduce

[4] If the perturbative quarkonium is represented by $Q\bar{Q}$ and a gluon, then one should, of course, expand also in the energy and momentum of the gluon.

their scaling by just looking at the corresponding perturbative expressions e. g. by replacing heavy quarkonium Fock state by a pair of free heavy quarks fields.

The question, to which extent one can rely on perturbation theory, has lead to the existence of different sets of power-counting rules. The perturbative counting of [7] assumes that $\Lambda_{\rm QCD} \sim m_Q v^2$, while a more conservative prescription [27, 118] uses $\Lambda_{\rm QCD} \sim m_Q v$. The implications of different counting schemes have also been discussed in the literature [3, 120].

The choice of the correct counting is clearly not just an academic question. Different power-counting rules lead to a different number of operators that contribute at the given order in v. As was shown in [27, 118], the number of operators that contribute at the given order in v is much smaller in the perturbative counting as compared to the conservative one. In principle, one should be able to deduce the correct power-counting by comparing predictions from different countings to experimental measurements. In practice, the uncertainties in our knowledge of the nonperturbative parameters that enter NRQCD predictions for cross sections and decay rates, are still much larger than the uncertainties from different choices of the counting. Throughout this work we will use the perturbative counting of [7].

3.3 Application of NRQCD to Production and Decay of Heavy Quarkonia

NRQCD predictions for decays of heavy quarkonia can be expressed in form of NRQCD-factorized decay rate formulas

$$\Gamma = \sum_i \frac{2\,\mathrm{Im}\, c_i}{m_Q^{d_i-4}} \langle H|\mathcal{O}_n^{2S+1}L_J|H\rangle\,, \tag{3.19}$$

where is $\langle H|\mathcal{O}_n^{2S+1}L_J|H\rangle$ a nonperturbative long-distance matrix element (LDME). More explicitly, it is a 4-fermion operator from $\mathcal{L}_{\rm NRQCD}$ sandwiched between two heavy quarkonium Fock states. The general form of the LDME for hadronic[5] decays is given by

$$\langle H|\mathcal{O}_n^{2S+1}L_J)|H\rangle = \langle H|\psi^\dagger \mathcal{K}_n \chi\chi^\dagger \mathcal{K}_n'\psi|H\rangle\,, \tag{3.20}$$

where $\mathcal{K}_n^{(\prime)}$ are polynomials in $\mathbf{D}$, $\mathbf{E}$ and $\mathbf{B}$. Furthermore, in the spin and color space $\mathcal{K}_n^{(\prime)}$ are proportional to the unit matrices or to $\boldsymbol{\sigma}$ and T^a respectively. The Fock state $|H\rangle$ represents states with physical quarkonium H, while the spectroscopic notation ${}^{2S+1}L_J$ is used to specify that the operator $\mathcal{O}_n^{2S+1}L_J$ annihilates a heavy quarkonium with the same quantum numbers.

It is important to point out that $|H\rangle$ does not contain only a $Q\bar{Q}$ pair with the same quantum numbers as the physical quarkonium (as is assumed by the old Color Singlet Model (CSM) [121–123]). In NRQCD, the heavy quarkonium Fock state can schematically written as [124]

$$\begin{aligned}
|H({}^{2S+1}L_J)\rangle = {}& \mathcal{O}(v^0)\,|Q\bar{Q}({}^{2S+1}L_J)^{(1)}\rangle \\
&+ \mathcal{O}(v)\,|Q\bar{Q}({}^{2S+1}(L\pm1)'_J)^{(8)}g\rangle + \mathcal{O}(v^2)\,|Q\bar{Q}({}^{2(S\pm1)+1}L'_J)^{(8)}g\rangle \\
&+ \mathcal{O}(v^2)\,|Q\bar{Q}({}^{2S+1}L'_J)^{(1,8)}gg\rangle + \mathcal{O}(v^2)\,|Q\bar{Q}({}^{2S+1}(L\pm2)'_J)^{(1,8)}gg\rangle \\
&+ \mathcal{O}(v^2)\,|Q\bar{Q}\left({}^3(J-1)_J), ({}^3(J+1)_J)\right)^{(1)}\rangle + \ldots\,,
\end{aligned} \tag{3.21}$$

[5]The LDME for electromagnetic decays is obtained via the replacement $\chi\chi^\dagger \to \chi^\dagger\,|0\rangle\,\langle 0|\,\chi$

where $\mathcal{O}(v^n)$ denotes the relative suppression in v. The first term in Eq. (3.21) is the dominant Fock state that corresponds to the decay of a heavy quarkonium into two heavy quarks[6] in the color singlet configuration. A heavy quarkonium may also decay into two heavy quarks and gluons. The terms on the second line of Eq. (3.21) come into play when a heavy quarkonium emits a gluon through an electric (E1) or magnetic (M1) transition before decaying into a heavy quark pair. After the decay the heavy quark pair will appear in the color octet configuration. The last three terms in Eq. (3.21) describe double E1 or M1 transitions as well as mixing between quantum numbers with $L = J-1$ and $L = J+1$.

Eq. (3.21) is also the reason why an operator $\mathcal{O}_n^{2S+1}L_J$ may give a nonvanishing contribution to the total decay rate in Eq. (3.19), even though the quantum numbers of the decaying heavy quarkonium are different from ${}^{2S+1}L_J$.

Obviously, Eq. (3.19) implies that the short- and long-distance contributions to a quarkonium decay process can be factorized into the imaginary parts of the matching coefficients c_i and nonperturbative LDMEs $\langle H|\mathcal{O}_n^{2S+1}L_J|H\rangle$. This is a nontrivial statement, but it has been explicitly and rigorously proven in [7], so that NRQCD factorization is known to hold in quarkonium decays.

It is worth noting, that in NRQCD the LDMEs are assumed to be universal i. e. process-independent quantities, that depend only on the quantum numbers of the heavy quarkonium. For example, if we think of the decay of J/ψ into two leptons, the LDMEs extracted from the process $J/\psi \to e^+e^-$ could be used to make predictions for $J/\psi \to \mu^+\mu^-$ or vice versa. The matching coefficients are, on the contrary, process dependent quantities. The assumed universality of LDMEs is what gives NRQCD its predictive power.

Let us now turn our attention to the heavy quarkonium production. NRQCD suggests following factorization formula for production of heavy quarkonia

$$\sigma(H) = \sum_i \frac{C_i(\alpha_s(m_Q),\mu)}{m_Q^{d_i-4}} \langle 0|\mathcal{O}_n^H|0\rangle\,, \tag{3.22}$$

where a generic production LDME reads

$$\langle 0|\mathcal{O}_n^H|0\rangle = \langle 0|\,\chi^\dagger\mathcal{K}_n\psi\Big(\sum_X\sum_{m_J}|H+X\rangle\,\langle H+X|\Big)\psi^\dagger\mathcal{K}_n'\chi\,|0\rangle\,, \tag{3.23}$$

with $|H+X\rangle$ being a Fock state that contains a heavy quarkonium H and all other particles X that appear in the final state and have energy and momenta that are typically much smaller than the hard scale m_Q. The summations go over all allowed X states and $m_J = -J,\ldots,J$, where J denotes the total angular momentum quantum number of the quarkonium state.

The sum over X in Eq. (3.23) is the source of many complications related to our understanding of quarkonium production. In particular, it is difficult to find a rigorous field theoretical definition of production LDMEs, which would allow us to rewrite them in terms of a smaller number of nonperturbative quantities (as it has been done for decay LDMEs using pNRQCD, c. f. [125]) or reliably calculate them on the lattice [126]. One exception to this rule is the exclusive electromagnetic production, where the sum over X is not present. For a more detailed discussion of this class of production processes we refer to Part V of this work.

Although Eq. (3.22) has been applied in numerous studies of heavy quarkonia (c. f. [16] for a recent overview of the existing results), it is not a rigorous statement in the

[6] or formation of a heavy quarkonium out of two heavy quarks, if we think of production

framework of NRQCD. As of now, the factorization in heavy quarkonium production to all orders in α_s remains a conjecture, although much progress towards a solid proof has been made in the recent years [127–132]. In particular, factorization proofs exist for exclusive double quarkonium production in e^+e^- annihilation as well as exclusive quarkonium production from B-meson decays [133–135]. Factorization in inclusive hadronic production was explicitly shown to hold at 2-loop order [136, 137], albeit for the price of modifying NRQCD production LDMEs to include Wilson lines. The difficulties with factorization might be related to another issue in the context to heavy quarkonium production in NRQCD. That is, the tensions between values of production LDMEs extracted from different sets of experimental data [138], seem to challenge the assumed universality of these nonperturbative quantities. It remains to be seen, whether and how these difficulties can be resolved in future.

Leaving the issues related to the factorization aside, let us provide a basic explanation of how NRQCD describes production and decays of heavy quarkonia through its 4-fermion operators.

For definiteness, let us first consider the annihilation of a heavy quarkonium into two gluons. It is easy to see, that in a process like $Q\bar{Q} \to gg$, the momenta of the gluons must be of order m_Q, i. e. the gluons are hard. Yet in NRQCD all the hard modes have been already integrated out, which is why annihilation of heavy quarks cannot directly occur in the theory. The 4-fermion operators allow us to reproduce such effects from full QCD without introducing degrees of freedom that are not part of NRQCD: All the contributions from the hard modes are encoded int the matching coefficients multiplying the corresponding operators, as it is schematically shown in Fig. 3.1 Here we use the

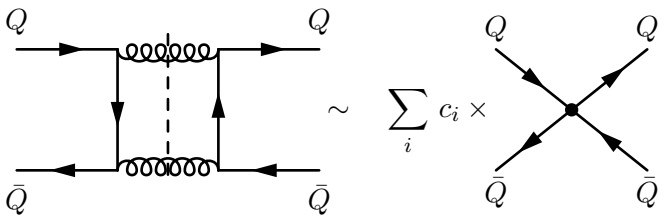

(3.24)

Figure 3.1: Schematic representation of matching between QCD and NRQCD for decay operators. Imaginary parts of the hard region of the $Q\bar{Q} \to Q\bar{Q}$ diagrams determine matching coefficients that enter NRQCD-factorized decay rates of heavy quarkonia

cut-diagram notation to represent the decay of a $Q\bar{Q} \to gg$ as an imaginary part of the $Q\bar{Q} \to Q\bar{Q}$ amplitude

$$\mathrm{Im}\mathcal{M}(Q\bar{Q} \to Q\bar{Q}) = m_{Q\bar{Q}} \sum_X \Gamma(Q\bar{Q} \to X), \tag{3.25}$$

From the point of view of NRQCD, the creation and annihilation of two hard gluons is a process that occurs at much shorter distances ($1/m_Q$ and smaller) than the typical scale of the theory which is $1/m_Q v$. Hence, it can be shrinked into a 4-fermion vertex, where all the effects of this process are encoded in the imaginary parts of the matching coefficients c_i.

The same argument is applicable also to the production of heavy quarkonia. The creation of a $Q\bar{Q}$ pair requires a short-distance process with the available center of mass energy s to be at least $s \geq 4m_Q^2$. We again can use the cut-diagram notation and the

optical theorem

$$\mathrm{Im}\,\mathcal{M}\,(p_A, p_B \to p_A, p_B) = 4\sqrt{s}|\mathbf{p}_{\mathrm{cm}}| \sum_X \sigma(p_A, p_B \to Q\bar{Q}), \tag{3.26}$$

where A and B are particles that collide to create a $Q\bar{Q}$ pair and $\mathbf{p}_{\mathrm{cm}}$ is the relative 3-momentum of A and B in the center-of-mass frame of the colliding particles. For definiteness, let us consider exclusive electromagnetic production of a heavy quarkonium in e^+e^- annihilation. A schematic representation of matching for this production process is shown in Fig. 3.2. Notice that the heavy quarkonium is "inside" the diagram, while the colliding leptons appear as initial and final states. In NRQCD the highly energetic short distance process $e^+e^- \to Q\bar{Q}$ can be shrinked to a point and factored into the matching coefficients C_i.

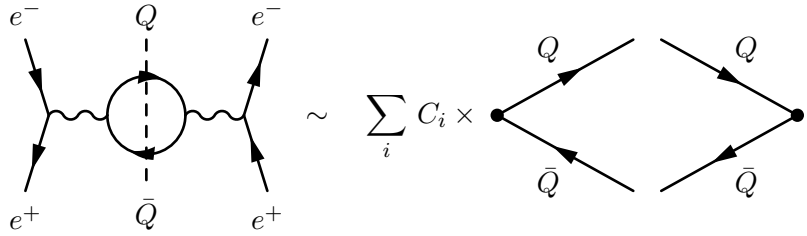

(3.27)

Figure 3.2: Schematic representation of the matching between QCD and NRQCD for production operators. The hard region of the total partonic cross section to produce a $Q\bar{Q}$ pair in a particle collision determines matching coefficients that enter NRQCD-factorized heavy quarkonium production cross sections.

3.4 Potential Nonrelativistic QCD

NRQCD is not the most useful theory if we are interested in studying phenomena that occur at energies much below the soft scale $m_Q v$: The soft and ultrasoft scales are entangled so that the power-counting is inhomogeneous. Integrating out the soft scale $m_Q v$ we obtain a new EFT, known as potential Nonrelativistic QCD (pNRQCD) [8, 9]. For simplicity, let us assume that $m_Q v \gg \Lambda_{\mathrm{QCD}}$, so that the soft scale can be integrated out in perturbation theory. In addition, we may also assume that $m_Q v^2 \geq \Lambda_{\mathrm{QCD}}$[7] which leads us to pNRQCD in the weak-coupling regime.

There are at least two possible ways to represent the Lagrangian of pNRQCD [3]:

1. Using the same degrees of freedom as in NRQCD, which are understood to be ultrasoft.

2. Using singlet and octet wave-function fields $S(t, \mathbf{r}, \mathbf{R})$ and $O(t, \mathbf{r}, \mathbf{R})$ that describe the $Q\bar{Q}$ system in the color singlet and color octet states respectively. The wave-function fields depend on the center-of-mass $\mathbf{R} = (\mathbf{x}_1 + \mathbf{x}_2)/2$ and the relative $\mathbf{r} = \mathbf{x}_1 - \mathbf{x}_2$ coordinates of the $Q\bar{Q}$ system.

For the purpose of matching NRQCD to pNRQCD, it is most convenient to use the first form, i. e. to write

$$L_{\mathrm{pNRQCD}} = L^{\mathrm{US}}_{\mathrm{NRQCD}} + L_{\mathrm{pot}}. \tag{3.28}$$

[7] The hierarchy $m_Q v \gg m_Q v^2 \geq \Lambda_{\mathrm{QCD}}$ is expected to be relevant for the lowest lying quarkonium states, especially for bottomonia.

Here $L^{\rm US}_{\rm NRQCD}$ is the familiar NRQCD Lagrangian, where all gluons are understood to be ultrasoft, while $L_{\rm pot}$ is the part that contains potential terms

$$L_{\rm pot} = -\int d^3\mathbf{x}_1 d^3\mathbf{x}_2 \psi^\dagger(t,\mathbf{x}_1)\chi(t,\mathbf{x}_2) V(\mathbf{r},\mathbf{p}_1,\mathbf{p}_2,\mathbf{S}_1,\mathbf{S}_2) \\ \times (\text{US gluon fiels})\chi^\dagger(t,\mathbf{x}_2)\psi(t,\mathbf{x}_1), \tag{3.29}$$

where $\mathbf{p}_i = -i\boldsymbol{\nabla}_i$ and $\mathbf{S}_i = \boldsymbol{\sigma}_i/2$ denote operators that act on fermion and antifermion fields. The appearance of potentials V[8], i. e. terms that are local in time but nonlocal in space, is a distinct feature of pNRQCD. This accomplishes the long term goal of deriving heavy quarkonium potentials from QCD and explains the limited success of potential models in reproducing spectra of heavy quarkonia. However, while those models had to use phenomenologically fine-tuned potentials without any solid theoretical justification, the potentials V are obtained from an EFT of QCD that is equivalent to the full theory in the relevant energy region.

Once the matching coefficients have been determined, we may want to switch to the second form of the pNRQCD Lagrangian, which is more suited for bound states calculations. To this end we can project the Hamiltonian of the theory on a subspace of the Fock space spanned by

$$\int d^3\mathbf{x}_1 d^3\mathbf{x}_2 \Psi(t,\mathbf{x}_1,\mathbf{x}_2)\psi^\dagger(t,\mathbf{x}_1)\chi(t,\mathbf{x}_2)\,|\text{US gluons}\rangle\,, \tag{3.30}$$

where $|\text{US gluons}\rangle$ is a state that contains an arbitrary number of ultrasoft gluons, but no quarks or antiquarks, while $\Psi(t,\mathbf{x}_1,\mathbf{x}_2)$ is a bilocal field that represents the $Q\bar{Q}$ system. This yields [3]

$$L_{\rm pNRQCD} = \int d^3\mathbf{x}_1 d^3\mathbf{x}_2\, \mathrm{Tr}\left(\Psi^\dagger(t,\mathbf{x}_1,\mathbf{x}_2)\left(iD_0 + \frac{\mathbf{D}_1^2}{2m_Q} + \frac{\mathbf{D}_2^2}{2m_Q} + \dots\right)\Psi(t,\mathbf{x}_1,\mathbf{x}_2)\right) \\ - \int d^3x \frac{1}{4} G^{a\mu\nu}G^a_{\mu\nu} + \int d^3x \sum_{i=1}^{n_f} \bar{q}_i(x) i\not{D} q_i(x) + \dots \\ + \int d^3\mathbf{x}_1 d^3\mathbf{x}_2\, \mathrm{Tr}\Big(\Psi^\dagger(t,\mathbf{x}_1,\mathbf{x}_2) V(\mathbf{r},\mathbf{p}_1,\mathbf{p}_2,\mathbf{S}_1,\mathbf{S}_2)(\text{US gluon fiels})\Psi(t,\mathbf{x}_1,\mathbf{x}_2)\Big), \tag{3.31}$$

with

$$iD_0\Psi(t,\mathbf{x}_1,\mathbf{x}_2) = i\partial_0\Psi(t,\mathbf{x}_1,\mathbf{x}_2) - gA_0(t,\mathbf{x}_1)\Psi(t,\mathbf{x}_1,\mathbf{x}_2) + \Psi(t,\mathbf{x}_1,\mathbf{x}_2)gA_0(t,\mathbf{x}_2). \tag{3.32}$$

Two more steps are needed to obtain the final form of the pNRQCD Lagrangian. First, we decompose the bilocal field $\Psi(t,\mathbf{x}_1,\mathbf{x}_2)$ into singlet and octet fields

$$\Psi(t,\mathbf{x}_1,\mathbf{x}_2) = P\big[e^{ig\int_{\mathbf{x}_2}^{\mathbf{x}_1}\mathbf{A}(t,\mathbf{x})\cdot d\mathbf{x}}\big] S(t,\mathbf{r},\mathbf{R}) \\ + P\big[e^{ig\int_{\mathbf{R}}^{\mathbf{x}_1}\mathbf{A}(t,\mathbf{x})\cdot d\mathbf{x}}\big] O(t,\mathbf{r},\mathbf{R}) P\big[e^{ig\int_{\mathbf{x}_2}^{\mathbf{R}}\mathbf{A}(t,\mathbf{x})\cdot d\mathbf{x}}\big], \tag{3.33}$$

where P stands for the path ordering and the Wilson lines $e^{ig\int \mathbf{A}\cdot d\mathbf{x}}$ are required to make the gauge invariance of the theory manifest. Second, to ensure that gluon fields are ultrasoft, we multipole expand them in $\mathbf{r}$

$$A^\mu(t,\mathbf{x}_{1/2}) = A^\mu(t,\mathbf{R}) \pm \frac{1}{2}\mathbf{r}^i(\boldsymbol{\nabla}^i_{\mathbf{R}} A^\mu(t,\mathbf{R})) + \mathcal{O}(\mathbf{r}^2), \tag{3.34}$$

[8] $V(\mathbf{r},\mathbf{p}_1,\mathbf{p}_2,\mathbf{S}_1,\mathbf{S}_2)$ are matching coefficients of the 4-fermion operators. The ultrasoft gluon fields become relevant only at higher orders.

$$i\mathbf{D}_{1/2} = \pm i\boldsymbol{\nabla}_{\mathbf{r}} + \frac{i}{2}\boldsymbol{\nabla}_{\mathbf{R}} + ig\mathbf{A}(t,\mathbf{R}) \pm \frac{1}{2}\mathbf{r}^i(\boldsymbol{\nabla}^i_{\mathbf{R}}\mathbf{A}(t,\mathbf{R})) + \mathcal{O}(\mathbf{r}^2). \tag{3.35}$$

One of the advantages of the multipole expansion, is that it makes the expansion of the pNRQCD Lagrangian in $1/m_Q$ and r (with $r = |\mathbf{r}|$) manifest. In the power-counting of the theory, $1/r$ and $\boldsymbol{\nabla}_{\mathbf{r}}$ scale as $m_Q v$, while the scaling of $\boldsymbol{\nabla}_{\mathbf{R}}$ and of the gluon fields is given by $m_Q v^2$. The size of α_s depends on the type of calculation in which it appears. In the matching between NRQCD and pNRQCD we have $\alpha_s(1/r)$, while in calculations with ultrasoft gluons the size of the strong coupling constant is $\alpha_s(m_Q v^2)$.

Finally, the most general pNRQCD Lagrangian at $\mathcal{O}(1/m_Q^2)$ and $\mathcal{O}(r)$ can be written as [3]

$$\begin{aligned}
\mathcal{L}_{\text{pNRQCD}} = \int d^3\mathbf{r}\,\mathrm{Tr}\Big(& S^\dagger(i\partial_0 - h_s(\mathbf{r},\mathbf{p},\mathbf{P}_{\mathbf{R}},\mathbf{S}_1,\mathbf{S}_2))S \\
& + O^\dagger(iD_0 - h_0(\mathbf{r},\mathbf{p},\mathbf{P}_{\mathbf{R}},\mathbf{S}_1,\mathbf{S}_2))O\Big) \\
& + V_A(r)\,\mathrm{Tr}\left(O^\dagger\,\mathbf{r}\cdot g\mathbf{E}\,S + S^\dagger\,\mathbf{r}\cdot g\mathbf{E}\,O\right) + \frac{V_B(r)}{2}\,\mathrm{Tr}\left(O^\dagger\mathbf{r}\cdot g\mathbf{E}\,O + O^\dagger O\,\mathbf{r}\cdot g\mathbf{E}\right) \\
& - \frac{1}{4}G^{a\mu\nu}G^a_{\mu\nu} + \sum_{i=1}^{n_f}\bar{q}_i(x)i\not{D}q_i(x) + \ldots
\end{aligned} \tag{3.36}$$

where for brevity we have suppressed the dependence of fields on t, $\mathbf{r}$ and $\mathbf{R}$. Furthermore, $\mathbf{P} = -i\mathbf{D}_{\mathbf{R}}$, $\mathbf{r} = -i\boldsymbol{\nabla}_{\mathbf{r}}$ and

$$h_{s/o}(\mathbf{r},\mathbf{p},\mathbf{P}_{\mathbf{R}},\mathbf{S}_1,\mathbf{S}_2)) = \frac{\mathbf{p}^2}{m_Q} + \frac{\mathbf{P}^2}{4m_Q} + V_{s/o}(\mathbf{r},\mathbf{p},\mathbf{P}_{\mathbf{R}},\mathbf{S}_1,\mathbf{S}_2), \tag{3.37}$$

with

$$V_{s/o} = V^{(0)}_{s/o} + \frac{V^{(1)}_{s/o}}{m_Q} + \frac{V^{(2)}_{s/o}}{m_Q^2} \tag{3.38}$$

The potentials $V_{s/o}$, V_A and V_B represent matching coefficients of pNRQCD. At leading order in α_s we have [9]

$$V_s^{(0)} = -C_F\frac{\alpha_s}{r}, \quad V_o^{(0)} = \frac{1}{2N_c}\frac{\alpha_s}{r}, \quad V_A = V_B = 1. \tag{3.39}$$

Notice that $V_s^{(0)}$ is the static potential, that has already been mentioned in Sec. 1.1.

Since the development of pNRQCD, this EFT has been successfully used to describe various aspects of the physics of heavy quarkonia both at zero and finite temperature. We refer to [3] and [47] for an overview of the existing results. In this work we will use potential Nonrelativistic QED (pNRQED) [8] the electromagnetic counterpart of pNRQCD to describe dispersive van der Waals forces between hydrogen atoms in Part IV.

4 Effective Field Theories for Electromagnetic Interactions

4.1 Nonrelativistic QED

So far we have been mainly concerned with EFTs of strong interactions. In particular, we introduced NRQCD and pNRQCD as useful tools to describe physics of $Q\bar{Q}$ bound states in a rigorous and systematic way.

Let us now depart from hadronic physics and consider electromagnetic interactions. In Sec. 2.1 we used the hydrogen atom as a motivation to introduce the concept of EFTs and to explain their usefulness for dealing with physics at low energies and especially with bound state calculations. Historically, the original approach to this problem was to treat the bound state completely in QED. The appropriate formalism was worked out by Bethe and Salpeter in the form of the Bethe-Salpeter equation [139]. Unfortunately, the application of this equation to nonrelativistic systems such as muonium ($e^-\mu^+$ bound state) or positronium (e^+e^- bound state) is not so simple, especially if one is interested in higher order corrections in α. The reasons for this have been already outlined in Sec. 2.1.

A useful alternative to the Bethe-Salpeter equation that does not suffer from these issues is nonrelativistic QED (NRQED) [5]. It is an EFT of electromagnetic interactions that was developed to work at energies relevant for nonrelativistic systems ($E \ll m_e$), while the effects of hard modes ($E \geq m_e$) are taken into account through the matching coefficients. The reason why we denote the electron mass m_e as our hard scale, is that in this work we are predominantly interested in the electromagnetic interactions of two hydrogen atoms.

The similarity of the notions NRQED and NRQCD is not accidental, since the formulation of NRQCD (which appeared some years after NRQED) was very much inspired by the work of Caswell and Lepage [5]. Apart from the apparent differences between electromagnetic and strong interactions, both theories are very similar in many ways. For example, the Lagrangian of NRQED readily follows from $\mathcal{L}_{\text{NRQCD}}$ once we replace gluons by photons and consequently omit all 4-fermion operators with color matrices. At $\mathcal{O}(1/m_e^2)$ this yields

$$\begin{aligned}
\mathcal{L}_{\text{NRQED}} = & -\frac{1}{4}F^{\mu\nu}F_{\mu\nu} \\
& + \psi^\dagger \left(i\mathbf{D}_0 + \frac{\mathbf{D}^2}{2m_e} + c_F \frac{\boldsymbol{\sigma}\cdot g\mathbf{B}}{2m_e} + c_D \frac{[\mathbf{D}\cdot, g\mathbf{E}]}{8m_e^2} + c_S \frac{i\boldsymbol{\sigma}\cdot[\mathbf{D}\times, g\mathbf{E}]}{8m_e^2} \right) \psi \\
& + \chi^\dagger \left(i\mathbf{D}_0 - \frac{\mathbf{D}^2}{2m_e} - c_F \frac{\boldsymbol{\sigma}\cdot g\mathbf{B}}{2m_e} + c_D \frac{[\mathbf{D}\cdot, g\mathbf{E}]}{8m_e^2} + c_S \frac{i\boldsymbol{\sigma}\cdot[\mathbf{D}\times, g\mathbf{E}]}{8m_e^2} \right) \chi \\
& + \frac{f_1(^1S_0)}{m_e^2}\psi^\dagger\chi\chi^\dagger\psi + \frac{f_1(^3S_1)}{m_e^2}\psi^\dagger\boldsymbol{\sigma}\chi\chi^\dagger\boldsymbol{\sigma}\psi,
\end{aligned} \tag{4.1}$$

where ψ (χ) denotes a Pauli field that annihilates (creates) a fermion (antifermion). Here $F^{\mu\nu} = \partial^\mu A^\nu - \partial^\nu A^\mu$ is the electromagnetic field-strength tensor and A^μ is the photon field.

NRQED greatly simplifies the systematic treatment of electromagnetic bound states, especially when compared to the methods based on the usage of the Bethe-Salpeter equation [3]. This has been used to obtain many new QED results, c. f. [140–145].

Nevertheless, NRQED is not the most useful theory if we want to study effects of typical energies and momenta much below $m\alpha$: The power-counting of the theory is

not homogeneous, since both scales $m\alpha$ and $m\alpha^2$ remain dynamical. As was already explained in Sec. 2.2, this issue can be resolved by integrating out the scale $m\alpha$, which leads to potential nonrelativistic QED (pNRQED) [8].

4.2 Potential Nonrelativistic QED

Potential nonrelativistic QED (pNRQED) [8] is a theory of ultrasoft $m_e\alpha^2$ degrees of freedom. The natural way to construct this EFT is to first obtain NRQED from QED by integrating out the hard scale m_e. After that we can integrate out the soft scale $m_e\alpha$ from NRQED to obtain pNRQED. The construction of pNRQED is very similar to that of pNRQCD, which has already been explained in Sec 3.4. Instead of discussing pNRQED for generic electromagnetic bound states, let us specialize to the hydrogen atom from the very beginning. The reason for doing so, is to introduce the formalism, that will be used for the calculation of dispersive van der Waals forces between two hydrogen atoms in Part IV.

Let us start with the NRQED Lagrangian that describes an electron ψ and a proton N at $\mathcal{O}(1/m_e)$

$$\mathcal{L}_{\text{NRQED}}^{\text{2-fermion}} = \psi^\dagger \left[iD^0 + \frac{\mathbf{D}^2}{2m} - c_F \frac{\boldsymbol{\sigma}\cdot e\mathbf{B}}{2m} \right] \psi + N^\dagger iD^0 N - \frac{1}{4} F^{\mu\nu}F_{\mu\nu}\,, \tag{4.2}$$

The covariant derivatives acting on the electron field are defined as $iD^0 = i\partial^0 + eA^0$, $i\boldsymbol{D} = i\boldsymbol{\nabla} - e\boldsymbol{A}$, and acting on the proton field as $iD^0 = i\partial^0 - eA^0$. The proton mass m_p is taken to be much larger than the electron mass, so that operators proportional to powers of $1/m_p$ are beyond the precision we are aiming at and will be neglected.

The matching coefficient c_F at $\mathcal{O}(\alpha)$ reads [91]

$$c_F = 1 + \frac{\alpha}{2\pi}\,. \tag{4.3}$$

Requiring that the electric charge in (4.2) is the one measured in low-energy experiments (e. g. Thomson scattering) guarantees that the matching coefficient of the operator $-F^{\mu\nu}F_{\mu\nu}/4$ remains one to all orders [8]. The matching coefficient of the kinetic energy operator is also constrained to be one to all orders by reparameterization/Poincaré invariance.

To have a proper renormalization of the van der Waals interactions, it is necessary to augment Eq. (4.2) with 4-electron operators. The corresponding operators of dimension six are

$$\mathcal{L}_{\text{NRQED}}^{\text{4-fermion}} = \frac{d_s}{m_e^2}\left(\psi^\dagger\psi\right)^2 + \frac{d_v}{m_e^2}\left(\psi^\dagger\boldsymbol{\sigma}\psi\right)^2. \tag{4.4}$$

The matching coefficients at one loop in the $\overline{\text{MS}}$ renormalization scheme read [3, 8]

$$d_s = \alpha^2\left[\log\left(\frac{m_e^2}{\nu^2}\right) - \frac{2}{3}\right], \qquad d_v = \alpha^2\,, \tag{4.5}$$

with ν being the renormalization scale. The divergence in d_s is an IR divergence and cancels in physical observables against UV divergences coming from low-energy modes.

pNRQED describing hydrogen atom is obtained by integrating out soft electrons and photons. Since the energies and momenta, that we are integrating out are of order $m\alpha$, the matching can be performed by using static propagators for the electron field. This allows us to match NRQED to pNRQED at any given order in $1/m_e$ and α.

It is convenient to introduce the center of mass coordinate $\mathbf{X} \approx \mathbf{x}_p(1 + \mathcal{O}(m_e/m_p))$ and the electron-proton distance $\mathbf{x} = \mathbf{x}_e - \mathbf{x}_p$, where $\mathbf{x}_e$ and $\mathbf{x}_p$ are the coordinates of the electron and the proton respectively. Variations in the center of mass coordinate due to recoiling of the atom against low-energy photons are of the order of the inverse of the ultrasoft scale, hence much smaller than the typical magnitude of $\mathbf{x}$, which is of the order of the inverse of the soft scale. The dynamical degrees of freedom of pNRQED are: the field $S(t, \mathbf{x}, \mathbf{X})$, which is invariant under $\mathrm{U}(1)$ gauge transformations, and encodes the proton and electron fields, and photons $A_\mu(t, \mathbf{X})$. The photon fields have been multipole expanded in $\mathbf{x}$ to guarantee that they are ultrasoft. The Lagrangian also contains potential terms, which naturally arise in the matching of NRQED to pNRQED.

Showing only operators that are relevant for our study, the pNRQED Lagrangian density at $\mathcal{O}(\mathbf{x}, 1/m_e)$ reads [6]

$$\mathcal{L}^{\text{1-atom}}_{\text{pNRQED}} = \int d^3\mathbf{x}\, S^\dagger(t, \mathbf{x}, \mathbf{X}) \left[i\partial_0 + \frac{\boldsymbol{\nabla}^{\mathbf{2}}_{\mathbf{x}}}{2m_e} + \frac{\alpha}{|\mathbf{x}|} - \mathbf{x} \cdot e\mathbf{E} - \frac{\boldsymbol{\mu} \cdot e\mathbf{B}}{2m_e} \right] S(t, \mathbf{x}, \mathbf{X}) - \frac{1}{4} F^{\mu\nu} F_{\mu\nu}\,, \tag{4.6}$$

where the total magnetic moment of the electron is defined as $\boldsymbol{\mu} = \boldsymbol{L} + 2c_F \boldsymbol{S}$, with $\boldsymbol{S} = \boldsymbol{\sigma}/2$ and $\boldsymbol{L} = -i(\mathbf{x} \times \boldsymbol{\nabla}_{\mathbf{x}})$ being the electron spin and orbital angular momentum operators. The operators $\mathbf{x} \cdot e\mathbf{E}$ and $\boldsymbol{\mu} \cdot e\mathbf{B}/(2m_e)$ are the electric and magnetic dipoles respectively. All electromagnetic fields in the Lagrangian density are located at $(t, \mathbf{X})$. The size of each term in Eq. (4.6) can be evaluated in the following way. Each relative momentum $-i\boldsymbol{\nabla}_{\mathbf{x}}$ and inverse relative coordinate $1/x$ have a size of $m_e\alpha$. Time derivatives acting on the atom field $S(t, \mathbf{x}, \mathbf{X})$ have a size of $m_e\alpha^2$. Each ultrasoft photon field and derivatives acting on it are of order $m_e\alpha^2$, which leads to $\mathbf{E} \sim \mathbf{B} \sim m_e^2\alpha^4$. In the two-atom sector the 4-electron operators of Eq. (4.4) induce at leading order in the multipole expansion a contact interaction between the S fields, given by

$$\mathcal{L}^{\text{2-atom}}_{\text{pNRQED}} = \int d^3\mathbf{x}_1 d^3\mathbf{x}_2 \left[\frac{d_s}{m_e^2} S^\dagger S(t, \mathbf{x}_1, \mathbf{X})\, S^\dagger S(t, \mathbf{x}_2, \mathbf{X}) + \frac{d_v}{m_e^2} S^\dagger \boldsymbol{\sigma} S(t, \mathbf{x}_1, \mathbf{X}) \cdot S^\dagger \boldsymbol{\sigma} S(t, \mathbf{x}_2, \mathbf{X}) \right]. \tag{4.7}$$

Part III

Computational tools

5 Computer-Assisted Analytic Calculations in Quantum Field Theory

5.1 The Main Idea of Symbolic Calculations

In the last decades the importance of computer tools for higher order perturbative calculations in quantum field theory (QFT) has increased tremendously. Indeed, many calculations at 1-loop and beyond would have been hardly possible to complete within a reasonable time frame, if such projects were to be carried out only by pen and paper. The question that most QFT practitioners pose themselves today is not whether to use software tools or not, but rather, which combination of tools will be the most efficient for the endeavored project. It is clear that, in principle, there can be no universal package to cover any demand of any particle theorist.

Many codes used for loop calculations are available only upon request or only for collaborators, e. g. `q2e/exp` [146, 147] or `FDC` [25]. On the one hand, this situation may seem to contradict the idea of sharing knowledge in science. On the other hand, one should keep in mind that loop calculations is a very competitive field. There are, however, also many publicly available tools, especially for 1-loop calculations.

Here one can distinguish between standalone tools and all-in-one packages. The former usually automatize only one particular step of QFT computations, e. g. generation of Feynman diagrams (FEYNARTS [148], QGRAF [149]), calculation of Dirac traces (TRACER [150]) or manipulation of color matrices (COLORMATH [151]). All-in-one packages try to handle most of these steps in one framework.

This category can be further subdivided into fully automatic and semi-automatic all-in-one packages. In the last decades, much effort was invested to develop packages (e. g. FORMCALC [152], GOSAM [153], GRACE [154]) that are able to perform all the steps needed to arrive to physical observables (e. g. decay rates or cross sections) in a highly automatized way. The level of the automation in such packages is so advanced, that in many cases the user just has to specify the incoming and outgoing particles, while the underlying code will take care of everything else and produce final results. Certainly, it is very gratifying to see how studies that would require weeks or even months decades ago, can be nowadays completed in a few minutes on a modern notebook. Unfortunately, this level of automation can be achieved only for certain types of calculations, for example 1-loop evaluations of cross sections or decay rates in the Standard Model and its extensions. If a particular calculation (e. g. matching in EFTs) does not fit into one of the predefined templates of a fully automatic package, there is usually no simple way to make it work. Of course, one may try to adjust the source code of the package accordingly or contact the developers and ask them to implement the desired functionality. The former requires good programming skills and very good familiarity with the internal structure of the package in question. The latter depends on the willingness of other people to work on something they might not be interested in.

Often, semi-automatic packages (FEYNCALC [20, 21], PACKAGE-X [155], HEPMATH [156]) might provide a good alternative to developing own code from scratch. While a fully automatic package can be imagined as a black box, a semi-automatic package should be understood as a toolbox. This makes semi-automatic packages very flexible so that they can be applied to very different types of calculations. The price to pay is that the user must have very good understanding of what he or she is doing and how the calculation should be carried out. In this sense, the usage of semi-automatic packages has many similarities with pen and paper computations.

Nevertheless, there are also situations when none of the available tools really suits one's needs. Computer algebra systems such as MATHEMATICA, MAPLE or REDUCE provide a convenient framework to implement new symbolic codes, but suffer performance problems when they need to deal with hundreds of thousands or even millions of terms. This is why most of the modern large scale perturbative calculations employ FORM [157]. FORM is a symbolic manipulation system that was developed with applications to high energy physics in mind. It was optimized to handle extremely large expressions in the fastest possible way and provides built-in support for many operations needed in perturbative calculations, such as index contractions and calculation of Dirac traces. Unfortunately, the range of features provided by FORM is not comparable with the capabilities of a regular computer algebra systems. Many basic operations, such as differentiation, integration, series expansion or solving of linear equations are not available in FORM out-of-the-box and have to be added via external libraries or implemented by the user.

Modern perturbative calculations often require a combination of many tools, where public and/or private packages are wired together with self-written codes implemented in FORM and a computer algebra system (e. g. MATHEMATICA).

5.2 Understanding Algorithms of Software for QFT Calculations

While everyone can be trained to use tools for perturbative calculations, it is also extremely important to develop some understanding of the underlying algorithms and their limitations. In the following we would like to briefly mention some important formulas that enter algorithms for the manipulation of Dirac and color matrices.

A chain of Dirac matrices can be simplified further, if it contains at least one pair of matrices contracted with each other

$$\gamma^{\mu_1} \dots \gamma^{\mu_l} \gamma^{\alpha} \gamma^{\nu_1} \dots \gamma^{\nu_n} \gamma_{\alpha} \gamma^{\rho_1} \dots \gamma^{\rho_m} \tag{5.1}$$

or with the same 4-vector

$$\gamma^{\mu_1} \dots \gamma^{\mu_l} \not{p} \gamma^{\nu_1} \dots \gamma^{\nu_n} \gamma_{\mu} \gamma^{\rho_1} \dots \gamma^{\rho_m} \not{p}. \tag{5.2}$$

The relevant formulas were worked out in [158–161] and summarized in [162]. Let us first discuss the purely 4-dimensional case. If the chain contains one or multiple occurrences of γ_5, it is convenient to move all of them to the very left or to the very right of the chain via

$$\{\gamma_5, \gamma^{\mu}\} = 0. \tag{5.3}$$

After that, the relevant part of the chain can be simplified to

$$\gamma^{\alpha} \gamma^{\nu_1} \dots \gamma^{\nu_n} \gamma_{\alpha} = -2\gamma^{\nu_n} \dots \gamma^{\nu_1} \text{ for } n \text{ odd}. \tag{5.4}$$

The formula for n even can be obtained directly from Eq. (5.4) and reads [20]

$$\gamma^{\alpha} \gamma^{\nu_1} \dots \gamma^{\nu_n} \gamma_{\alpha} = 2\gamma^{\nu_n} \gamma^{\nu_1} \dots \gamma^{\nu_{n-1}} + 2\gamma^{\nu_{n-1}} \dots \gamma^{\nu_1} \gamma^{\nu_n} \text{ for } n \text{ even}. \tag{5.5}$$

An alternative version is given by [162]

$$\gamma^{\nu_{n-1}} \dots \gamma^{\nu_1} \gamma^{\nu_n} = \mathrm{Tr}(\gamma^{\nu_1} \dots \gamma^{\nu_n}) - \mathrm{Tr}(\gamma^{\nu_1} \dots \gamma^{\nu_n} \gamma_5) \gamma_5 \text{ for } n \text{ even}. \tag{5.6}$$

The formulas given in Eq. (5.5) and Eq. (5.6) look very different and indeed if one applies them e. g. to

$$\gamma^\alpha\gamma^{\nu_1}\gamma^{\nu_2}\gamma^{\nu_3}\gamma^{\nu_4}\gamma^{\nu_5}\gamma^{\nu_6}\gamma_\alpha, \tag{5.7}$$

it is not so simple to show that the difference is zero, as it should be. The reason for this is the existence of the Schouten identity

$$\varepsilon^{\mu\nu\rho\sigma}q^\tau + \varepsilon^{\nu\rho\sigma\tau}q^\mu + \varepsilon^{\rho\sigma\tau\mu}q^\nu + \varepsilon^{\sigma\tau\mu\nu}q^\rho + \varepsilon^{\tau\mu\nu\rho}q^\sigma = 0, \tag{5.8}$$

where q is an arbitrary 4-vector. Together with

$$\gamma^\mu\gamma^\nu\gamma^\lambda = g^{\mu\nu}\gamma^\lambda + g^{\nu\lambda}\gamma^\mu - g^{\mu\lambda}\gamma^\nu + i\varepsilon^{\mu\nu\lambda\sigma}\gamma_\sigma\gamma_5 \tag{5.9}$$

Schouten identity can be used to show that the terms remaining in the difference between Eq. (5.5) and Eq. (5.6) add up to zero. Unfortunately, in large calculations this identity is very difficult to apply in a systematic way.

For Dirac matrices contracted with the same 4-vectors one can use [162]

$$\begin{aligned}&\not{p}\gamma^{\nu_1}\dots\gamma^{\nu_n}\not{p}\\ &= \begin{cases} -p^2\gamma^{\nu_n}\dots\gamma^{\nu_1} + \frac{1}{2}\not{p}\,\mathrm{Tr}(\not{p}\gamma^{\nu_n}\dots\gamma^{\nu_1}) + \frac{1}{2}\not{p}\gamma_5\,\mathrm{Tr}(\gamma_5\not{p}\gamma^{\nu_n}\dots\gamma^{\nu_1}) & \text{for } n \text{ odd} \\ -p^2\gamma^{\nu_n}\dots\gamma^{\nu_1} + \frac{1}{2}\gamma^\mu\not{p}\,\mathrm{Tr}(\not{p}\gamma_\mu\gamma^{\nu_n}\dots\gamma^{\nu_1}) & \text{for } n \text{ even} \end{cases}\end{aligned} \tag{5.10}$$

or [20]

$$\not{p}\gamma^{\nu_1}\dots\gamma^{\nu_n}\not{p} = (-1)^n p^2\gamma^{\nu_1}\dots\gamma^{\nu_n} + 2\sum_{i=1}^{n}(-1)^{i+1}\gamma^{\nu_1}\dots\gamma^{\nu_{i-1}}\gamma^{\nu_{i+1}}\dots\gamma^{\nu_n}\not{p}p^{\nu_i} \tag{5.11}$$

Notice that Eq. (5.11) also holds for D-dimensional matrices. The D-dimensional formulas for pairs of contracted Dirac matrices are given by [162]

$$\begin{aligned}\gamma^\mu\gamma^{\nu_1}\dots\gamma^{\nu_n}\gamma_\mu &= (D-4)(-1)^n\gamma^{\nu_1}\dots\gamma^{\nu_n} + 2(-1)^n\gamma^{\nu_3}\gamma^{\nu_2}\gamma^{\nu_1}\gamma^{\nu_4}\dots\gamma^{\nu_n}\\ &\quad + 2\sum_{j=4}^{n}(-1)^{n-j}\gamma^{\nu_j}\gamma^{\nu_1}\dots\gamma^{\nu_{j-1}}\gamma^{\nu_{j+1}}\dots\gamma^{\nu_n} \quad \text{for} \quad n \geq 3\end{aligned} \tag{5.12}$$

or alternatively [20]

$$\begin{aligned}\gamma^\alpha\gamma^{\nu_1}\dots\gamma^{\nu_n}\gamma_\alpha &= (-1)^n\Bigg((D-2n)\gamma^{\nu_1}\dots\gamma^{\nu_n}\\ &- 4\sum_{i=1}^{l-1}\sum_{j=i+1}^{l}(-1)^{j-i}\gamma^{\nu_1}\dots\gamma^{\nu_{i-1}}\gamma^{\nu_{i+1}}\dots\gamma^{\nu_{j-1}}\gamma^{\nu_{j+1}}\dots\gamma^{\nu_n}g^{\nu_i\nu_j}\Bigg) \quad \text{for} \quad n \geq 2.\end{aligned} \tag{5.13}$$

The situation becomes more involved once we have to deal with γ_5 in D dimensions. The issue is that one cannot consistently define a D-dimensional γ_5 that preserves the anicommutation relation in Eq. (5.3) and the cyclicity of the Dirac trace. It is easy to show [163, 164], that a D-dimensional γ_5 that anticommutes with all other Dirac matrices and does not violate the cyclicity of the trace automatically implies

$$(4-D)\,\mathrm{Tr}(\gamma_5\gamma^\mu\gamma^\nu\gamma^\rho\gamma^\sigma) = 0, \tag{5.14}$$

i. e. every trace that contains an odd number of γ_5 vanishes, unless $D = 4$. This definition is clearly very problematic, because it does not allow us to recover the 4-dimensional trace in the limit $D \to 4$.

An algebraically consistent way to treat γ_5 in dimensional regularization was worked out in [79, 80]. This can be achieved by decomposing D-dimensional Dirac matrices, metric tensors and 4-vectors into 4 and $D-4$ dimensional parts, such that

$$\begin{aligned} &\dim(\gamma^\mu) = D, && \gamma^\mu = \bar{\gamma}^\mu + \hat{\gamma}^\mu, \\ &\dim(\bar{\gamma}^\mu) = 4, && g^{\mu\nu} = \bar{g}^{\mu\nu} + \hat{g}^{\mu\nu}, \\ &\dim(\hat{\gamma}^\mu) = D-4, && p^\mu = \bar{p}^\mu + \hat{p}^\mu. \end{aligned} \tag{5.15}$$

Every contraction of a D-dimensional tensor with a 4- or $D-4$-dimensional object yields a 4- or $D-4$-dimensional tensor respectively. Contracting a 4-dimensional tensor with a $D-4$ dimensional tensor yields zero. The anticommutators between Dirac matrices in different dimensions are given by

$$\{\gamma^\mu, \gamma^\nu\} = 2g^{\mu\nu}, \tag{5.16}$$
$$\{\bar{\gamma}^\mu, \bar{\gamma}^\nu\} = \{\gamma^\mu, \bar{\gamma}^\nu\} = 2\bar{g}^{\mu\nu}, \tag{5.17}$$
$$\{\hat{\gamma}^\mu, \hat{\gamma}^\nu\} = \{\gamma^\mu, \hat{\gamma}^\nu\} = 2\hat{g}^{\mu\nu}, \tag{5.18}$$
$$\{\bar{\gamma}^\mu, \hat{\gamma}^\nu\} = 0. \tag{5.19}$$

Furthermore, γ_5 is defined as a purely 4-dimensional object that anticommutes with all other Dirac matrices in 4 dimensions, but commutes with Dirac matrices in $D-4$ dimensions. This is why the anticommutator of γ_5 and a D-dimensional Dirac matrix is not zero

$$\{\bar{\gamma}^\mu, \gamma_5\} = [\hat{\gamma}^\mu, \gamma_5] = 0 \tag{5.20}$$
$$\{\gamma^\mu, \gamma_5\} = \{\hat{\gamma}^\mu, \gamma_5\} = 2\hat{\gamma}^\mu\gamma_5 = 2\gamma_5\hat{\gamma}^\mu. \tag{5.21}$$

However, in perturbative calculations this scheme violates axial Ward identity. Additional counterterms are required to restore the conservation of the axial vector current. All these undesirable properties of γ_5 have led to a large number of prescriptions [164–168] for handling this object in D-dimensional calculations .

A trace of an odd number of Dirac matrices without γ_5 is zero in any number of dimensions. For an even number of matrices we have

$$\mathrm{Tr}(\gamma^{\nu_1} \dots \gamma^{\nu_n}) = \sum_{j=2}^{n} (-1)^j g^{\nu_1\nu_j} \,\mathrm{Tr}(\gamma^{\nu_2} \dots \gamma^{\nu_{j-1}} \gamma^{\nu_{j+1}} \dots \gamma^{\nu_n}), \tag{5.22}$$

which is again true both for D- and 4-dimensional Dirac matrices. Traces that involve γ_5 are somewhat more complicated. In 4 dimensions it is convenient to apply Eq. (5.9) repeatedly, until we have chains with less than five Dirac matrices and one γ_5. Once this is the case, we may use that

$$\mathrm{Tr}(\gamma^\mu\gamma_5) = \mathrm{Tr}(\gamma^\mu\gamma^\nu\gamma_5) = \mathrm{Tr}(\gamma^\mu\gamma^\nu\gamma^\rho\gamma_5) = 0, \tag{5.23}$$
$$\mathrm{Tr}(\gamma^\mu\gamma^\nu\gamma^\rho\gamma^\sigma\gamma_5) = -4i\varepsilon^{\mu\nu\rho\sigma}. \tag{5.24}$$

In D-dimensions the evaluation of the trace very much depends on the employed prescription for γ_5. For the scheme of [79, 80], the most efficient trace formula appears to be [169]

$$\mathrm{Tr}(\gamma^{\nu_1} \dots \gamma^{\nu_n}\gamma_5) = \frac{2}{D-4} \sum_{i=2}^{n} \sum_{j=1}^{i-1} (-1)^{i+j+1} g^{\nu_i\nu_j} \,\mathrm{Tr}\left(\prod_{k=1, k\neq i,j}^{n} \gamma^{n_k}\gamma_5 \right) \quad \text{for} \quad n \geq 6 \tag{5.25}$$

As far as color matrices are concerned, their contractions and traces can be effectively handled by the Cvitanovic algorithm [170]. The main idea behind this approach is to simplify traces and chains of SU(N) matrices in the fundamental representation by using corresponding Fierz identities

$$\delta_{ij}\delta_{kl} = 2T^a_{il}T^a_{kj} + \frac{1}{N}\delta_{il}\delta_{kj}, \tag{5.26}$$

$$T^a_{ij}T^a_{kl} = \frac{C_F}{N}\delta_{il}\delta_{kj} - \frac{1}{N}T^a_{il}T^a_{kj}. \tag{5.27}$$

For A, B, C and D being chains of color matrices, this yields following simple rules

$$AT^aBT^aC = \frac{1}{2}(AC)\,\mathrm{Tr}(B) - \frac{1}{2N}ABC, \tag{5.28}$$

$$(AT^aB)\,\mathrm{Tr}(CT^aD) = \frac{1}{2}(ADCB) - \frac{1}{2N}(AB)\,\mathrm{Tr}(CD), \tag{5.29}$$

$$\mathrm{Tr}(AT^aB)\,\mathrm{Tr}(CT^aD) = \frac{1}{2}\,\mathrm{Tr}(ADCB) - \frac{1}{2N}\,\mathrm{Tr}(AB)\,\mathrm{Tr}(CD). \tag{5.30}$$

that allow us to simplify color algebra in a systematic way.

The relations presented in this section can be implemented in a software package for the algebraic simplification of expressions containing Dirac and SU(N) matrices. In general, the correct formulas alone are not sufficient to design a useful software for automatic calculations. Testing and profiling are essential to ensure that the tool returns correct results and works sufficiently fast with all kinds of input expressions. Moreover, the syntax should be designed in such a way, that it can be easily extended when the software becomes more universal. Despite all these challenges, the development of tools for automation of QFT is a very rewarding activity that opens new opportunities for interesting calculations (c. f. Part VI) and provides many benefits to the particle physics community.

6 Automation of Calculations in Nonrelativistic EFTs

6.1 Nature of the Problem

EFTs simplify treatment of physical phenomena at low energies such that the effects of high energy modes are encoded in the matching coefficients. The determination of these matching coefficients often requires considerable effort, especially when loop contributions (that can be computed in different schemes) should be taken into account. This is why automation of matching calculations is not a luxury, but a necessity.

Unfortunately, there are no fully automatic packages to perform matching for almost arbitrary EFTs. This should not be surprising, since full automation always implies that all technical challenges of the theory have been correctly identified, understood and resolved. The plethora of existing EFTs with their different energy regions, degrees of freedom and matching prescriptions simply do not fit into several templates that one can implement in a reasonable amount of time. Even if we limit ourselves to strong interactions, it is clear that a package for fully automatic calculations in SCET or HQET will not work with ChPT or pNRQCD without significant modifications.

Each EFT should be approached in a particular way, but most of the required functionality (Lorentz, Dirac and SU(N) algebra, tensor reduction of loop integrals etc.) is often already present in semi-automatic packages for QFT calculations. The missing bits and pieces can be supplemented with standalone tools (e. g. reduction of scalar loop integrals using Integration-By-Parts identities [171]) and private codes written in FORM or MATHEMATICA.

This strategy works well for relativistic EFTs, i. e. QFTs that are formulated in a manifestly Lorentz covariant way. However, we know that many physical systems of interest (e. g. hydrogen atom or heavy quarkonia) are nonrelativistic. Consequently, they are most conveniently described in terms of nonrelativistic EFTs (NREFTs) such as NRQCD or pNRQED. From the technical point of view, automation of nonrelativistic QFTs is challenging, due to the variety of structures that can appear in the calculation. Additional complications arise when we need to work with tensors that can carry both Lorentz and Cartesian indices. This problem usually arises in the matching between a relativistic and a nonrelativistic theory, e. g. QCD and NRQCD. For definiteness, think of the metric tensor g. In a manifestly Lorentz covariant calculation, this object with both indices upstairs may appear only as

$$g^{\mu\nu}. \tag{6.1}$$

In a calculation that lacks manifest Lorentz covariance, we need to account for

$$g^{\mu\nu}, \quad g^{\mu 0}, \quad g^{\mu i}, \quad g^{00}, \quad g^{ij}, \tag{6.2}$$

where i and j represent Cartesian indices. Furthermore, one should distinguish between g^{ij} and the Kronecker delta δ^{ij},

$$g^{ij} = s\delta^{ij}, \tag{6.3}$$

and keep in mind that

$$g^{00} = t, \tag{6.4}$$

where the values of s and t (± 1) depend on the signature of the metric tensor (t, s, s, s). Things become even more involved once Dirac matrices and Levi-Civita tensors come into play, so that the program needs to know how to handle objects like

$$\epsilon^{0\mu\nu\rho}, \quad \epsilon^{\mu\nu i}, \quad \epsilon^{\mu i j}, \quad \gamma^0, \quad \gamma^i, \quad \not{p}. \tag{6.5}$$

Of course, all the related complications can be resolved in a meaningful way. In principle, there are no fundamental difficulties that prevent us from having automatic codes for nonrelativistic EFTs. On the other hand, we are not aware of any publicly available packages that offer support for this kind of calculations out-of-the-box.

There are several reasons for that. First of all, large-scale calculations in nonrelativistic EFTs are clearly not as mainstream as in relativistic EFTs. The latter can benefit from all the machinery that was developed to automatize Standard Model calculations, while the former do not have this advantage. NREFTs is a comparably small niche, so that the overlap between people working in the field and people interested in developing new packages for automatic calculations is quite small. Second, many practitioners are very much in favor of pen and paper calculation and/or have a collection of private codes that are employed for more elaborate cases.

One might argue, that the lack of general purpose public codes for nonrelativistic calculations is not really an issue. After all, everyone with sufficient experience in symbolic programming should be capable to write a FORM or MATHEMATICA code that automatizes a specific NREFT calculation in a sufficiently short amount of time. However, if this way of thinking would be prevalent in the particle physics community, there probably would be no publicly available packages for any kind of QFT calculations and every group would be forced to use in-house codes only.

It is important to realize, that this "nonpropagation of knowledge" not only makes it difficult to develop efficient algorithms for nonrelativistic calculations, but also to reproduce and check existing results. The only realistic way to improve the situation, is to set a good example for other to follow, i. e. develop suitable software tools and make them publicly available. As the lead developer of the well-known MATHEMATICA package FEYNCALC and a theorist doing calculations in NREFTs, the author of this work considers himself to be in a good position for doing so. The present status of this endeavor for NRQCD will be presented in Part VI.

6.2 Existing Approaches to Matching Calculations in NRQCD

Existing recipes to automatize matching between QCD and NRQCD mostly try to preserve the Lorentz covariance of the QCD amplitude until the very end of the calculation. A crucial ingredient of this approach is the usage of spin projectors [172–174]. The purpose of projectors is to extract contributions proportional to spin singlet or spin triplet parts of the QCD amplitude without going through the explicit rewriting of Dirac matrices in terms of Pauli matrices.

As an example, let us consider the decay of a heavy quarkonium. The QCD amplitude for this process will contain a Dirac structure

$$\bar{v}(p_2) O u(p_1), \tag{6.6}$$

where u and $\bar{v}$ and are Dirac spinors that describe the heavy quark with momentum p_1 and the heavy antiquark with momentum p_2, while O is a string of Dirac matrices. Here it is convenient to work in the rest frame of the heavy quarkonium, where

$$\mathbf{p}_1 = -\mathbf{p}_2 \equiv \mathbf{q}, \tag{6.7}$$

$$p_1^0 = p_2^0 = \sqrt{m_Q^2 + \mathbf{q}^2} \equiv E_{\mathbf{q}}. \tag{6.8}$$

For simplicity, let us assume that $O = \gamma^\mu$. Using explicit representation of Dirac spinors with nonrelativistic normalization

$$u(p,s) = \sqrt{\frac{E_{\mathbf{p}} + m_Q}{2E_{\mathbf{p}}}} \begin{pmatrix} \xi(s) \\ \frac{\mathbf{p}\cdot\boldsymbol{\sigma}}{E_{\mathbf{p}}+m_Q}\xi(s) \end{pmatrix}, \qquad v(p,s) = \sqrt{\frac{E_{\mathbf{p}} + m_Q}{2E_{\mathbf{p}}}} \begin{pmatrix} \frac{\mathbf{p}\cdot\boldsymbol{\sigma}}{E_{\mathbf{p}}+m_Q}\eta(s) \\ \eta(s) \end{pmatrix}, \tag{6.9}$$

where η and ξ are Pauli spinors, we obtain

$$\bar{v}(p_1)\gamma^0 u(p_2) = 0, \tag{6.10a}$$

$$\begin{aligned} \bar{v}(p_1)\gamma^i u(p_2) &= \frac{E_{\mathbf{q}} + m_Q}{2E_{\mathbf{q}}} \left(\eta^\dagger \boldsymbol{\sigma}^i \xi + \eta^\dagger \frac{-\mathbf{q}^i(\boldsymbol{\sigma}\cdot\mathbf{q}) + \mathbf{q}^2\boldsymbol{\sigma}^i}{(E_{\mathbf{q}} + m_Q)^2}\xi \right) \\ &= \eta^\dagger \boldsymbol{\sigma}^i \xi - \frac{\mathbf{q}^i \eta^\dagger(\boldsymbol{\sigma}\cdot\mathbf{q})\xi}{2m_Q^2} + \mathcal{O}(\mathbf{q}^3), \end{aligned} \tag{6.10b}$$

where we have expanded up to second order in $\mathbf{q}/m_Q$.

The same exercise can be repeated using projectors from [174]

$$\begin{aligned} \Pi_0(P,q) &= -\sum_{\lambda_1,\lambda_2} u(p_1,\lambda_1)\bar{v}(p_2,\lambda_2) \left\langle \tfrac{1}{2}\lambda_1, \tfrac{1}{2}, \lambda_2 | 0, 0 \right\rangle \\ &= \frac{1}{2\sqrt{2}E_{\mathbf{q}}(E_{\mathbf{q}} + m_Q)} (\tfrac{1}{2}\not{P} + \not{q} + m) \frac{\not{P} + 2E_{\mathbf{q}}}{4E_{\mathbf{q}}} \gamma_5 (\tfrac{1}{2}\not{P} - \not{q} - m), \end{aligned} \tag{6.11a}$$

$$\begin{aligned} \Pi_1(P,q,\epsilon) &= \sum_{\lambda_1,\lambda_2} u(p_1,\lambda_1)\bar{v}(p_2,\lambda_2) \left\langle \tfrac{1}{2}, \lambda_1, \tfrac{1}{2}, \lambda_2 | 1, \epsilon \right\rangle \\ &= \frac{-1}{2\sqrt{2}E_{\mathbf{q}}(E_{\mathbf{q}} + m)} (\tfrac{1}{2}\not{P} + \not{q} + m) \frac{\not{P} + 2E_{\mathbf{q}}}{4E_{\mathbf{q}}} \not{\epsilon} (\tfrac{1}{2}\not{P} - \not{q} - m), \end{aligned} \tag{6.11b}$$

where

$$p_1 = \frac{1}{2}P + q, \quad p_2 = \frac{1}{2}P - q, \quad P = (2E_{\mathbf{q}}, 0), \quad q = (0, \mathbf{q})^T \tag{6.12}$$

and $\epsilon = (0, \boldsymbol{\epsilon})^T$ is the polarization vector of the heavy quarkonium. Furthermore, we have

$$|\tfrac{1}{2}, -\tfrac{1}{2}, \tfrac{1}{2}, -\tfrac{1}{2}\rangle = |1, -1\rangle \tag{6.13}$$

$$|\tfrac{1}{2}, -\tfrac{1}{2}, \tfrac{1}{2}, \tfrac{1}{2}\rangle = \tfrac{1}{\sqrt{2}} |1, 0\rangle - \tfrac{1}{\sqrt{2}} |0, 0\rangle \tag{6.14}$$

$$|\tfrac{1}{2}, \tfrac{1}{2}, \tfrac{1}{2}, -\tfrac{1}{2}\rangle = \tfrac{1}{\sqrt{2}} |1, 0\rangle + \tfrac{1}{\sqrt{2}} |0, 0\rangle \tag{6.15}$$

$$|\tfrac{1}{2}, \tfrac{1}{2}, \tfrac{1}{2}, \tfrac{1}{2}\rangle = |1, 1\rangle \tag{6.16}$$

$$|1, \epsilon\rangle = \epsilon^- |1, 1\rangle - \epsilon^+ |1, -1\rangle - \epsilon^3 |1, 0\rangle, \tag{6.17}$$

with $\epsilon^\pm = \frac{1}{\sqrt{2}}(\epsilon^1 \pm i\epsilon^2)$. Notice that since

$$E_{\mathbf{q}} = \frac{1}{2}\sqrt{P^2} = \sqrt{m_Q^2 - q^2}, \tag{6.18}$$

Eqs. (6.11) can be written in a manifestly Lorentz covariant fashion. Applying projectors to

$$\bar{v}(p_2) O u(p_1) = \mathrm{Tr}\left(u(p_1)\bar{v}(p_2)O\right) \tag{6.19}$$

with $O = \gamma^\mu$ yields

$$\mathrm{Tr}\left(\Pi_0(P,q)\gamma^\mu\right) = 0, \tag{6.20a}$$

$$\mathrm{Tr}\left(\Pi_1(P,q,\epsilon)\gamma^\mu\right) = \sqrt{2}\left(\epsilon^\mu + \frac{q^\mu(q\cdot\epsilon)}{2m^2} + \mathcal{O}(q^3)\right). \tag{6.20b}$$

Comparing Eqs. (6.20) to Eqs. (6.10) we see that $\boldsymbol{\epsilon}$ corresponds[1] to

$$\frac{\eta^\dagger \boldsymbol{\sigma}^i \xi}{\sqrt{2}} \tag{6.21}$$

so that we can easily extract prefactors of different Pauli structures without breaking manifest Lorentz covariance.

With projectors the whole QCD calculation can be carried out pretty much in the usual covariant way. There is, however, one complication that arises in the treatment of loop integrals. As was already observed in [175], expansion of loop integrals in q generates integrals with linearly dependent propagators raised to integer powers e. g.

$$\begin{aligned}
&\int \frac{d^Dl}{(2\pi)^D} \frac{l^{\mu_1}\dots l^{\mu_n}}{l^2\left((l+p_1)^2-m_Q^2\right)\left((l-p_2)^2-m_Q^2\right)^2} \\
&= \int \frac{d^Dl}{(2\pi)^D} \frac{l^{\mu_1}\dots l^{\mu_n}}{l^2\left((l+\frac{P}{2})^2-m_Q^2\right)\left((l-\frac{P}{2})^2-m_Q^2\right)^2} + \mathcal{O}(q)
\end{aligned} \tag{6.22}$$

The author of [175] argued that direct Passarino–Veltman reduction of such integrals is not possible due to zero Gram determinants, which made it necessary to develop a more generalized reduction technique. However, this issue can be eliminated if one observes [176] that a loop integral with linearly dependent propagators can always be decomposed into a sum of loop integrals with linearly independent propagators. Using the algorithm presented in [176] it is very easy to show that

$$\begin{aligned}
&\int \frac{d^Dl}{(2\pi)^D} \frac{l^{\mu_1}\dots l^{\mu_n}}{l^2\left((l+\frac{P}{2})^2-m_Q^2\right)\left((l-\frac{P}{2})^2-m_Q^2\right)^2} \\
&= \frac{1}{2}\int \frac{d^Dl}{(2\pi)^D} \frac{l^{\mu_1}\dots l^{\mu_n}}{(l^2)^3\left((l-\frac{P}{2})^2-m_Q^2\right)} + \frac{1}{2}\int \frac{d^Dl}{(2\pi)^D} \frac{l^{\mu_1}\dots l^{\mu_n}}{(l^2)^2\left((l-\frac{P}{2})^2-m_Q^2\right)^2}.
\end{aligned} \tag{6.23}$$

This way conventional Pasarino-Veltman technique is fully sufficient to decompose such integrals into scalars and subsequently reduce them to the basic scalar integrals using Integration-By-Parts [177] identities. For example,

$$\begin{aligned}
&\int \frac{d^Dl}{(2\pi)^D} \frac{l^\mu l^\nu}{l^2\left((l+\frac{P}{2})^2-m_Q^2\right)\left((l-\frac{P}{2})^2-m_Q^2\right)^2} \\
&= \frac{(D-4)(D-2)}{64(D-5)(D-3)m_Q^6}\left((D-6)P^\mu P^\nu + 4m_Q^2 g^{\mu\nu}\right)\int \frac{d^Dl}{(2\pi)^D}\frac{1}{l^2-m_Q^2}.
\end{aligned} \tag{6.24}$$

While covariant projector technique certainly has many advantages, it is definitely not the only way to handle QCD amplitudes in matching calculations. First of all, since

[1] the extra $1/\sqrt{2}$ appears due to the normalization of the projectors chosen in [174].

the extraction of spin singlet and spin triplet contributions requires different projectors, two separate calculations are required to extract these parts of the QCD amplitude in the matching. Moreover, when projectors are applied at 1-loop and beyond, in the spin singlet case we are forced to deal with the problem of γ_5 in dimensional regularization, even though γ_5 does not actually appear in the full QCD amplitude.

An alternative technique to do matching on the QCD side in the noncovariant fashion as in Eqs. (6.10) is known under the name of *threshold expansion method* [31, 178] (c. f. Part V for practical applications). However, among practitioners this technique does not enjoy as much popularity as covariant projectors. This is unfortunate, since both approaches can be used as an important cross-check of the obtained results. On the other hand, it is also clear that calculations using projectors can be immediately automatized using existing tools, while no public packages provide automation of nonrelativistic calculations required for the threshold expansion method.

In this sense, software tools developed in the course of this work (c. f. Part VI) are meant to fill this gap and make it possible to automatize matching calculations that use the threshold expansion method. However, these tools are also very useful for calculations with projectors, so that both approaches are covered.

Let us also remark, that even though the QCD side of the matching can be done in a covariant fashion, this does not apply to the NRQCD side. Once we need to do calculations in this theory, or even match it to a lower energy EFT (e. g. pNRQCD), there is no way to avoid nonrelativistic calculations. It goes without saying that the opportunity to do such calculations with a well-tested software package can greatly simplify one's life.

Part IV

Effective Field Theory Approach to Electromagnetic Van der Waals forces

7 Motivation

Long-range electromagnetic forces between neutral particles in the absence of external electromagnetic fields have been studied since a long time, and are called *van der Waals interactions*. In this context, forces are of long range if they act at distances R between the neutral particles much larger than the typical size of the particles. In the case of atoms, van der Waals forces act at distances $R \gg a_0$, where a_0 is the Bohr radius.

Van der Waals interactions can be of different nature depending on whether they are generated by permanent dipoles (or higher multipole moments) or by instantaneously induced dipoles (or higher multipoles). In the latter case, the first studies were done by London in 1930 [11] and included only the electrostatic Coulomb interaction, i. e. in a field theory language, only potential or Coulombic photons. London realized that systems without permanent dipole moments can still interact electromagnetically at second order in quantum mechanical perturbation theory due to the mutually induced electric dipole moments. More precisely, they give rise to an attractive interaction that depends on the distance of the neutral particles as $1/R^6$:

$$W_{\text{Lon}} = -\frac{C_6}{R^6}, \tag{7.1}$$

which is known as the *London potential*. The positive coefficient C_6 is a function of the instantaneous dipole moments of the interacting systems computed for all intermediate states and their energies. The computation of C_6 may be quite challenging for complex atomic and molecular systems. Furthermore, London related the strength of this interaction to the oscillator strengths of the system. Since the oscillator strengths are also related to the dispersion of light by the system, this type of van der Waals interactions are sometimes referred to as *dispersion forces*. Dispersion forces in this framework are therefore electromagnetic forces acting between well-separated neutral, unpolarized and unmagnetized atoms or bodies in the absence of any applied electromagnetic field.

To consider only potential photons is a good approximation as long as the interactions occur over sufficiently distances, so that the photon travel time is negligible. Casimir and Polder (CP) showed that retardation effects are important for the long-range regime, i. e. when R is much larger than the typical time scale of the interacting particles [12]. They calculated a general form of the interaction from quantum mechanics using two-photons exchanges. Their result reproduces the London form at short distances, but at large distances, where retardation effects are important, the van der Waals potential shows a different R dependence:

$$W_{\text{CP}} = -\frac{C_7}{R^7}\,, \tag{7.2}$$

where C_7 is a positive coefficient. The potential (7.2) is also known as *Casimir–Polder potential*. The results for the shorter distance regime, Eq. (7.1), and for the longer distance regime, Eq. (7.2), have been later reproduced using dispersive methods by Feinberg and Sucher [179, 180].

Dispersive forces are the weakest and at the same time the most persistent of all electromagnetic interactions. For this reason they play an important role across molecular physics, surface physics, colloid science, biology and even astrophysics. For the strong interactions, van der Waals potentials play a similar prominent dynamical role in systems made of at least two heavy quarks as they do in quantum electrodynamics (QED). The long-range interaction of small color dipoles (well realized in nature by heavy quarkonium states like the J/ψ or $\Upsilon(1S)$) has been the object of studies since

the first years of quantum chromodynamics (QCD) [181]. The interest in these systems is motivated by computing nuclear cross sections for quarkonium propagating in nuclear matter (relevant, e. g. for experiments at FAIR) or disentangling cold matter from deconfinement effects in heavy-ion collisions (relevant, e. g. for experiments at RHIC and LHC). The heavy quarkonium-nucleon scattering appears to be dominated by gluonic van der Waals interactions [182–185]. The quarkonium-quarkonium van der Waals interactions contain nontrivial information about low energy QCD [14, 15] and about quarkonium (chromo)polarizabilities [186]. As in QED, the QCD van der Waals potential is attractive and, in principle, could lead to molecular-like bound states of heavy quarkonia with nuclei. This could explain [15, 187], for instance, the structure of the charmonium pentaquark observed at the LHCb experiment at CERN [48]. Van der Waals interactions are also prominent in studies of Feshbach resonances [188] and in the computation of quantum corrections to the gravitational potential between a pair of polarizable objects [189].

The broad interest for van der Waals interactions calls for a flexible, rigorous and systematic computational method that allows us to properly define and efficiently compute van der Waals interactions in quantum field theory at any precision. Nonrelativistic effective field theories (EFTs) [3] provide such a method. Recently there have been some studies of the electromagnetic van der Waals interactions in the framework of EFTs by Holstein [190]. In this work, we will construct a complete set of effective field theories suited to compute the van der Waals interactions between two hydrogen atoms in different regimes. As we will see, our approach gives a clear definition and a computational framework for the potentials, without additional requirements [191]. The EFT approach developed here for the simpler case of QED will possibly provide a useful guideline for more complicate cases, like the study of van der Waals interactions in QCD that may require dealing also with nonperturbative effects.

The most simple polarizable neutral system is the hydrogen atom. The hydrogen atom is a nonrelativistic bound state characterized by three well separated energy scales, which are the mass of the electron, m_e, the typical relative momentum, given by the inverse Bohr radius $1/a_0 \sim m_e\alpha$, and the typical binding energy, which is of order $m_e\alpha^2$, where $\alpha = e^2/(4\pi) \approx 1/137 \ll 1$ is the fine structure constant. These are usually referred to as *hard*, *soft* and *ultrasoft scales* respectively. The presence of a set of well separated energy scales makes the hydrogen atom a perfect system to apply nonrelativistic EFT techniques. Owing to their power counting, EFTs simplify significantly bound state calculations. Moreover, they are renormalizable (finite) order by order in the expansion parameters, which are α and ratios among the energy scales of the system.

When considering the van der Waals interactions between two hydrogen atoms, the distance R between them provides a new scale. As mentioned at the beginning, these interactions are well defined at a distance large enough that the internal structure of the atoms cannot be resolved, i. e. when R is much larger than the Bohr radius: $R \gg a_0$.

The interplay between the scale R and the typical time scale of the hydrogen atom, which is of order $1/(m_e\alpha^2)$, leads to different forms of the van der Waals interactions. There are three possible regimes:

1. the short distance regime when $R \ll 1/m_e\alpha^2$,
2. the long distance regime when $R \gg 1/m_e\alpha^2$ [192],
3. the intermediate distance regime when $R \sim 1/m_e\alpha^2$.

The aim of this study is to work out an appropriate EFT and to compute the van der Waals potential between two hydrogen atoms for each of these physical situations.

Results will be given in d space-time dimensions and renormalized. The proper renormalization of the van der Waals interactions is one of the original contributions of the present work. Here we will focus on atoms in S-wave states. More general results can be found in the appendices.

8 Effective Field Theory of Van der Waals Forces

The energy scale, Q, which is relevant for the dynamics of the two hydrogen atoms is of order $\boldsymbol{k}^2/m_p$, where $\boldsymbol{k}$ is the typical momentum transfer between the atoms and m_p is the proton mass, here a good approximation of the total mass of the electron-nucleus system. If we restrict ourselves to interactions over distances larger than the Bohr radius of the atoms, $R \gg a_0$, then the typical momentum $\boldsymbol{k}$ is much smaller than $m_e\alpha$ and the energy scale of the two-atom dynamics is much smaller than the ultrasoft scale. At an energy scale Q photons of higher energy are not resolved and their effect is taken into account by potential terms. We are going to refer to these latter terms as *van der Waals potentials* and to the EFT that lives at the scale Q and describes the dynamics of hydrogen atoms interacting through them as *van der Waals EFT* (WEFT). For the QCD equivalent of this EFT see [15].

The degrees of freedom of WEFT are U(1) singlet fields, S_n, describing atoms with quantum numbers n, and low-energy photons carrying momentum and energy of order Q. At energies much below the typical binding energy $E_n \sim m_e\alpha^2$, the different atomic states are frozen, since photons are not energetic enough to excite them, and have to be considered as independent fields. Hence, in the absence of external interactions, the fields S_n are plane waves of energy E_n, where E_n is the binding energy of the state $|n\rangle$ solution of the Schrödinger equation for the hydrogen atom, at leading order $E_n = -m_e\alpha^2/(2n^2)$. The Lagrangian is built by coupling these states to electromagnetic fields and to each other. Since S_n are nonrelativistic fields, the couplings to the electromagnetic fields are better expressed in terms of the electric field, $\boldsymbol{E}$, and magnetic field, $\boldsymbol{B}$. The couplings between S_n are expressed in the Lagrangian by potentials.

In the one-atom sector, proceeding from QED to WEFT we integrate out the scales m_e, $m_e\alpha$ and $m_e\alpha^2$, so that one should be able to organize the WEFT Lagrangian as a series in the ratios

$$\frac{m_e\alpha}{m_e},\ \frac{m_e\alpha^2}{m_e\alpha},\ \frac{Q}{m_e\alpha^2}\,. \tag{8.1}$$

The scaling of the singlet field is $S_n \sim Q^{3/2}$. Space and time derivatives acting on the electromagnetic field $\boldsymbol{A}$ and the field itself are of order Q. Temporal derivatives acting on the singlet field scale like Q but space derivatives scale like $\sqrt{m_pQ}$.

The Lagrangian of WEFT in the one-atom sector reads

$$\begin{aligned} L^{\text{1-atom}}_{\text{WEFT}} = \int d^3\boldsymbol{X} \sum_n S_n^\dagger(t,\,\boldsymbol{X}) \Bigg[& i\partial_0 - E_n + \frac{\boldsymbol{\nabla}^{\boldsymbol{2}}_{\boldsymbol{X}}}{2m_p} + 2\pi\alpha_n^{ij}\boldsymbol{E}^i\boldsymbol{E}^j \\ & + 2\pi\beta_n^{ij}\boldsymbol{B}^i\boldsymbol{B}^j - \frac{\langle n|\boldsymbol{\mu}|n\rangle\cdot e\boldsymbol{B}}{2m_e} + \dots \Bigg] S_n(t,\,\boldsymbol{X}), \end{aligned} \tag{8.2}$$

where the dots stand for multipolar couplings and higher-order terms. Notice that, in general, E_n is a matrix with an imaginary part accounting for transitions between energy levels. Because the mixing of states is irrelevant for this work, we have neglected it in (8.2).

In the one-atom sector the matching is performed by equating Green's functions calculated in WEFT to the ones calculated in pNRQED in the limit of the external energies being much smaller than the bound state energies. The matchings of the kinetic operator and of the coupling to the magnetic field are trivial. The two electromagnetic

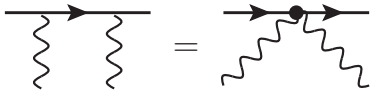

Figure 8.1: Tree-level matching of the couplings of the hydrogen atom with external radiation fields. On the left-hand side we have the pNRQED diagram (photons couple to atoms either via electric or magnetic dipoles, see Eq. (4.6)) and on the right-hand side the WEFT one.

field operators are obtained by matching the right-hand side of Fig. 8.1 with the left-hand side:

$$\alpha_n^{ij} = \frac{1}{2\pi} {\sum_m}' \frac{p_E(n,m)^{ij}}{\Delta E_{nm}}\,, \qquad \beta_n^{ij} = \frac{1}{2\pi} {\sum_m}' \frac{p_B(n,m)^{ij}}{\Delta E_{nm}}\,. \tag{8.3}$$

A prime in the sum sign, here and in the following, signifies that it runs over all values of the index/indices except the one/ones labeling the incoming energy (in Eq. (8.3) this is n). The sum is a short-hand notation that encompasses also the integral over the continuum states. Moreover, we have used the following notations: $\Delta E_{nm} = E_n - E_m$, and

$$p_E(n,m)^{ij} = e^2 \langle n|\boldsymbol{x}^i|m\rangle\langle m|\boldsymbol{x}^j|n\rangle\,, \tag{8.4}$$

$$p_B(n,m)^{ij} = \frac{e^2}{4m_e^2} \langle n|\boldsymbol{\mu}^i|m\rangle\langle m|\boldsymbol{\mu}^j|n\rangle\,. \tag{8.5}$$

The couplings α_n^{ij} and β_n^{ij} are called the *static electric and magnetic polarizability* tensors [193].

For the hydrogen atom the dipole moment $\langle n|\boldsymbol{x}|n\rangle$ vanishes due to parity, however, higher multipole moments are allowed. For instance, for states with $L \geq 2$ the quadrupole moment does not vanish. In the present work, we will mostly focus on the study of the dispersive van der Waals interactions between S-wave states in which all multipole moments vanish. In this case the electric polarizability takes a scalar form $\alpha_n^{ij} = \alpha_n \delta^{ij}$ and the magnetic dipole is given by the spin only: $\langle n|\boldsymbol{\mu}|n\rangle = 2c_F\langle n|\boldsymbol{S}|n\rangle$.

If both electric and magnetic polarizabilities take a scalar form, then the corresponding part of the Lagrangian simplifies to $2\pi\alpha_n \boldsymbol{E}^2 + 2\pi\beta_n \boldsymbol{B}^2$, which can be found in studies of neutral particles interacting with electromagnetic fields (see, e. g. [194–196]). However, for the hydrogen atom the magnetic polarizability never takes the scalar form since the hydrogen atom has a permanent magnetic dipole due to the spin of the electron.

In the two-atom sector the WEFT Lagrangian contains potential interactions between atoms:

$$\begin{aligned} L_{\text{WEFT}}^{\text{2-atom}} = -\int d^3\boldsymbol{X}_1\, d^3\boldsymbol{X}_2 \sum_{n_i,n_j} & S_{n_i}^\dagger(t,\boldsymbol{X}_1) S_{n_i}(t,\boldsymbol{X}_1) \\ & \times W_{n_i,n_j}(\boldsymbol{X}_1 - \boldsymbol{X}_2)\, S_{n_j}^\dagger(t,\boldsymbol{X}_2) S_{n_j}(t,\boldsymbol{X}_2)\,. \end{aligned} \tag{8.6}$$

The potential W_{n_i,n_j} corresponds to the van der Waals potential between two atoms in a $|n_i\rangle$ and $|n_j\rangle$ state respectively. Notice that, in general, the theory will also contain potential interactions that change the state of the hydrogen atoms involved, and couplings of the two atoms with photons of energy Q. However, neither of them is going to contribute to the atom-atom interaction at the accuracy of this work. In the following, we will often omit the indication of the states and denote the van der Waals potential simply by W and its Fourier transform in momentum space by $\widetilde{W}$.

A new physical scale appears in the van der Waals potentials of Eq. (8.6): the distance $\mathbf{R} = \boldsymbol{X_1} - \boldsymbol{X_2}$ between the two interacting atoms, whose conjugate variable is the momentum transfer between the atoms, which we denote by $\boldsymbol{k}$. The potential in the two-atom sector can be expressed as an expansion in the ratios of scales of Eq. (8.1) as well as an expansion in $(m_e\alpha^2\, R)$ for the short-distance regime ($R \ll 1/(m_e\alpha^2)$) and in $1/(m_e\alpha^2\, R)$ for the long-distance regime ($R \gg 1/(m_e\alpha^2)$). In the intermediate-distance regime, where $1/R \sim m_e\alpha^2$, we cannot expand R with respect to $1/(m_e\alpha^2)$. In the following sections, we will to obtain W for these different regimes.

9 Van der Waals Interactions at Short Distances

In this section, we study the van der Waals interactions in the short-distance regime. The physical situation is sketched in the left-hand panel of Fig. 9.1. The characteristic of this regime is that the distance between the atoms is much smaller than the time scale between the emission of the two photons, which is of the order of the inverse of the ultrasoft scale: $R \ll 1/(m_e\alpha^2)$. On the other hand, the distance between the atoms is much larger than the Bohr radius, namely the typical size of a hydrogen atom: $R \gg a_0$. Photons exchanged between the atoms carry a typical momentum, $\boldsymbol{k}$, that is of the order of the inverse of the distance between the atoms or $m_e\alpha^2$ or smaller. Finally, the energy scale of the atoms is set by the kinetic energy $Q \sim \boldsymbol{k}^2/m_p$. Since m_p provides a very strong suppression, the dynamics of the atoms occurs at a scale much smaller than any of the previous ones. In practice, for the purpose of computing the van der Waals potential we may consider the atoms as static. In the right-hand panel of Fig. 9.1 we have plotted the hierarchy of scales involved together with the corresponding EFTs.

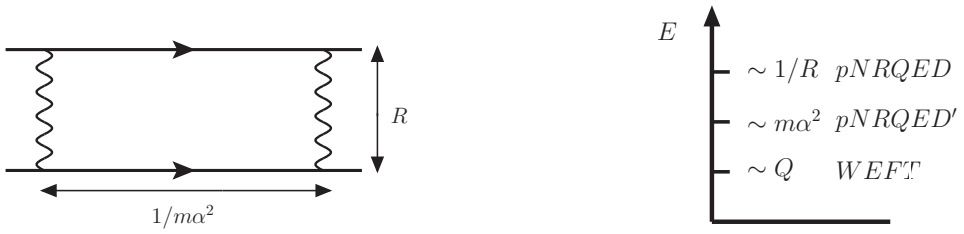

Figure 9.1: Left panel: Sketch of the physical picture of the van der Waals interactions in the short-range regime. The distance between the atoms is much smaller than the typical time scale of the hydrogen atom but much larger than the Bohr radius. Right panel: Hierarchy of scales and the corresponding EFTs in the short-distance regime.

In the following sections we will provide the details of the matching between the hierarchy of EFTs in the right-hand panel of Fig. 9.1. In Sec. 9.1 we integrate out photons carrying momentum of order $1/R$ and obtain pNRQED′. In the one-atom sector, pNRQED′ is similar to the theory described in Sec. 4.2, but in the two-atom sector new potentials appear. The van der Waals interactions are obtained in Sec. 9.2 by integrating out photons with energy and momentum of order $m_e\alpha^2$ and virtual atomic states, whose energy is also of order $m_e\alpha^2$, and matching pNRQED′ to WEFT.

In order to make the counting homogeneous, it is convenient to assign a specific size to $1/R$ in terms of m_e and α. A natural choice, given the scale hierarchy in the short-distance regime, is to take $1/R \sim m_e\alpha\sqrt{\alpha}$. From this assignment it follows that $(m_e\alpha^2\, R) \sim \sqrt{\alpha}$. In the short-distance regime, we aim at computing the van der Waals interactions, W (in coordinate space), up to order $m_e\alpha^6\sqrt{\alpha}$.

9.1 Matching pNRQED′

To obtain pNRQED′ we have to integrate out photons whose momentum and energy scale like $1/R$. The one-atom sector does not change in matching pNRQED to pNRQED′ and is given by Eq. (4.6). Whereas new potential interactions, V, arise in the two-atom

sector:

$$L^{\text{2-atom}}_{\text{pNRQED}'} = -\int d^3\boldsymbol{X}_1 d^3\boldsymbol{X}_2\, d^3\boldsymbol{x}_1 d^3\boldsymbol{x}_2\, S^\dagger S(t,\boldsymbol{x}_1,\boldsymbol{X}_1)\, V(\boldsymbol{X}_1-\boldsymbol{X}_2)\, S^\dagger S(t,\boldsymbol{x}_2,\boldsymbol{X}_2)\,. \tag{9.1}$$

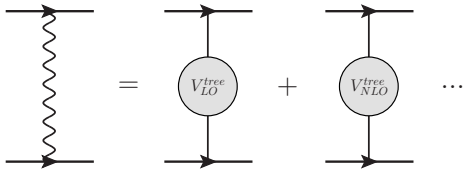

Figure 9.2: Tree-level matching of the two hydrogen atom potentials of pNRQED′. In the left-hand side the pNRQED diagram (the photon couples to electric or magnetic dipoles) and in the right-hand side the pNRQED′ ones.

The matching of pNRQED to pNRQED′ in the two-atom sector is given at tree-level by the exchange of one photon (Fig. 9.2) and (at the order we are interested in) the contact interaction of Eq. (4.7). First, we consider the one-photon exchange diagram. Since the energy of the atoms is the smallest scale in the problem, the photon propagator can be expanded in it. Hence, the momentum of the photon scales with the only scale in the diagram, which is $1/R \sim m_e\alpha\sqrt{\alpha}$.

The leading order (LO) contribution to Eq. (9.1) is an electric dipole exchange. This is of $\mathcal{O}\left(1/(m_e^2\alpha)\right)$ in momentum space and reads

$$\widetilde{V}^{\text{tree}}_{LO,\,E} = -e^2\frac{(\boldsymbol{x}_1\cdot\boldsymbol{k})(\boldsymbol{x}_2\cdot\boldsymbol{k})}{\boldsymbol{k}^2}\,, \tag{9.2}$$

where $\boldsymbol{x}_1$ and $\boldsymbol{x}_2$ are the electron-proton distances in the two atoms. Using the Fourier transforms of Appendix E.4 we can obtain the dipole potential in position space with its characteristic R^{-3} dependence. In coordinate space the potential is of order $m_e\alpha^3\sqrt{\alpha}$.

At next-to-leading order (NLO), $\mathcal{O}\left(1/m_e^2\right)$ in momentum space, we obtain

$$\widetilde{V}^{\text{tree}}_{NLO,\,E} = e^2\frac{(\boldsymbol{v}_1\cdot\boldsymbol{k})(\boldsymbol{v}_2\cdot\boldsymbol{k}) - (\boldsymbol{v}_1\cdot\boldsymbol{v}_2)\boldsymbol{k}^2}{\boldsymbol{k}^4}\,. \tag{9.3}$$

The NLO term is proportional to $\boldsymbol{v} = -i[\boldsymbol{x},\hat{h}_0]$, where $\hat{h}_0 = -\boldsymbol{\nabla}^2_{\boldsymbol{x}}/(2m_e) - \alpha/|\boldsymbol{x}|$. This dependence arises from the fact that the NLO contribution is proportional to the square of the energy carried by the photon. Using the equations of motion for the S field it can be shown that[1]

$$k_0 S^\dagger\boldsymbol{x}S = i\left(\partial_0 S^\dagger\boldsymbol{x}S + S^\dagger\boldsymbol{x}\partial_0 S\right) = -\left(S^\dagger\hat{h}_0\boldsymbol{x}S - S^\dagger\boldsymbol{x}\hat{h}_0 S\right) = S^\dagger[\boldsymbol{x},\hat{h}_0]S = iS^\dagger\boldsymbol{v}S\,. \tag{9.4}$$

In coordinate space the NLO potential is of order $m_e\alpha^4\sqrt{\alpha}$.

The tree-level diagram in the left-hand side of Fig. 9.2 may be also understood as an exchange between two magnetic dipoles or an electric dipole and a magnetic dipole. For the case of two magnetic dipoles we have

$$\widetilde{V}^{\text{tree}}_{LO,\,B} \;=\; \frac{e^2}{4m_e^2}\frac{1}{\boldsymbol{k}^2}\left(\boldsymbol{k}^2(\boldsymbol{\mu}_1\cdot\boldsymbol{\mu}_2) - (\boldsymbol{\mu}_1\cdot\boldsymbol{k})(\boldsymbol{\mu}_2\cdot\boldsymbol{k})\right), \tag{9.5}$$

[1] By means of Eq. (9.4) the subleading term in the expansion of the one-photon exchange can be identified with a pNRQED potential. In principle, one could absorb both energy factors in either singlet pair or one factor per singlet pair. These choices are related by partial integration and correspond to different operator basis. In (9.3) we have chosen to absorb one energy factor for each singlet pair as it leads to a simpler one-loop matching calculation.

where the subindices on $\boldsymbol{\mu}$ and $\boldsymbol{S}$ identify the atom. This is a contribution of order α/m_e^2 in momentum space (of order $m_e\alpha^5\sqrt{\alpha}$ in coordinate space).

Unlike the two former cases, the electric-magnetic dipole interaction is proportional to k^0 at leading order. We use Eq. (9.4) to convert the k^0 factor into a time derivative of S and write

$$\widetilde{V}^{\text{tree}}_{LO,\,M} \;=\; i\frac{e^2}{2m_e}\frac{\boldsymbol{k}}{\boldsymbol{k}^2}\cdot(\boldsymbol{v}_1\times\boldsymbol{\mu}_2-\boldsymbol{\mu}_1\times\boldsymbol{v}_2)\,. \tag{9.6}$$

This contribution is of order $\sqrt{\alpha}/m_e^2$ in momentum space (of order $m_e\alpha^5$ in coordinate space).

The matching of the contact interaction of Eq. (4.7) is trivial since it is independent of the momentum:

$$\widetilde{V}^{\text{cont.}} = -\frac{d_s}{m_e^2}-\frac{4d_v}{m_e^2}\boldsymbol{S}_1\cdot\boldsymbol{S}_2\,. \tag{9.7}$$

This contribution is of $\mathcal{O}\left(\alpha^2/m_e^2\right)$ in momentum space ($\mathcal{O}\left(m_e\alpha^6\sqrt{\alpha}\right)$ in coordinate space).

Notice that, by considering the power-counting only, further subleading contributions from electric dipole, magnetic dipole and electric-magnetic dipole tree-level exchanges could, in principle, be of order α^2/m_e^2 or larger in momentum space. Nevertheless, these terms do not eventually contribute to the van der Waals interactions. In fact, the characteristic feature of dispersive van der Waals interactions is that they appear at the one-loop level. The reason is that the expectation value of the electric dipole for eigenstates of the hydrogen atom vanishes due to parity, as well as higher multipole moments for S-wave states. Moreover, all contributions proportional to the energy transfer, like higher-order electric and magnetic dipole potentials, and electric-magnetic dipole potentials vanish once evaluated on static initial and final state atoms with the same quantum numbers. In the case of hydrogen atoms, the only tree-level exchange that contributes to the atom-atom interaction is the exchange of two magnetic dipoles: it does not depend on the energy transfer and the hydrogen atom has a permanent magnetic dipole generated by the spin of the electron. In addition, for nonzero orbital angular momentum, there is also an orbital contribution to the magnetic dipole. As a result, out of all potentials generated by a tree-level photon exchange, only $\widetilde{V}^{\text{tree}}_{LO,\,B}$ gives a nonvanishing contribution to the hydrogen-hydrogen interaction.

The situation changes at the loop level due to virtual intermediate states. Loops involving electric dipoles do not necessarily vanish because they are proportional to $\langle n|\boldsymbol{x}|m\rangle$ with $|m\rangle$ being an intermediate state different from $|n\rangle$. The intermediate states are the solutions of the Schrödinger equation with Hamiltonian $\hat{h}_0$ for the hydrogen atom; n collects all discrete and continuum quantum numbers necessary to label the spectrum of $\hat{h}_0$. To perform the one-loop matching is, therefore, of paramount importance to compute the van der Waals interactions.

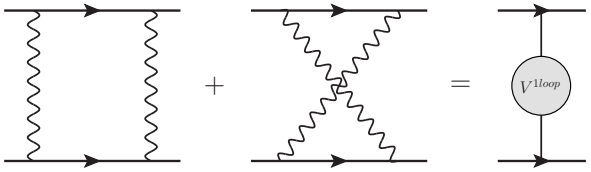

Figure 9.3: One-loop matching of the two-atom potential of pNRQED'. In the left-hand side we have the pNRQED diagrams and in the right-hand side the pNRQED' one.

We proceed to analyze the one-loop contributions to the two-atom potential of Eq. (9.1) up to $\mathcal{O}\left(\alpha^2/m_e^2\right)$ in momentum space. The scheme of the one-loop matching can be found in Fig. 9.3, with pNRQED diagrams in the left-hand side matching the pNRQED' diagram in the right-hand side. In the loop, we integrate over a photon momentum q^μ such that $q^0 \sim |\boldsymbol{q}| \sim 1/R$. The one-loop diagrams give rise to new terms for the potential of Eq. (9.1) starting at $\mathcal{O}(\alpha/m_e^2)$ in momentum space. Subleading contributions are suppressed by powers of $\sqrt{\alpha}$, thus the first three terms are needed to reach an accuracy of $\mathcal{O}(\alpha^2/m_e^2)$. Pinch singularities cancel against the two dipole potential exchanges in pNRQED' [3].

In these new potential terms powers of the energy gap factors ΔE_{nm} appear in the numerator, however the matching coefficients of pNRQED' cannot depend on a specific state. This dependence on ΔE_{nm} is fictitious and can be eliminated by using the results of Appendix E.3 to perform the sums over the intermediate states. In the case that all the vertices are electric dipole couplings, it turns out that after summing over the intermediate states the LO and NLO contributions vanish. Only the next-to-next-to-leading order (N^{2}LO) term survives:

$$\widetilde{V}^{\text{1loop}}_{N^2LO,\,E} = -\frac{2\pi^2\alpha^2}{3m_e^2}(d-2)(4d-9)A_{3/2}(\boldsymbol{k}^2)\,, \tag{9.8}$$

with $A_{3/2}$ a loop integral defined in Appendix E.1 and d the space-time dimension. The expression in (9.8) is, indeed, independent of the initial and final states considered. The potential $\widetilde{V}^{\text{1loop}}_{N^2LO,\,E}$ is of order α^2/m_e^2, whereas the corresponding expression in coordinate space, $V^{\text{1loop}}_{N^2LO,\,E}$, is of order $m_e\alpha^6\sqrt{\alpha}$. Analogous matching contributions can be obtained by replacing two or four of the electric dipole couplings by magnetic dipole ones. These are suppressed by α and α^3 respectively with respect to the four electric dipole interaction computed in (9.8), and are, therefore, beyond the precision we are aiming at. Nevertheless, the corresponding expressions are given in Appendix E.2.

9.2 Matching WEFT

The last remaining step to obtain the van der Waals potential in the short-distance regime consists in integrating out ultrasoft photons with energy and momentum of order $m_e\alpha^2$ and virtual atomic states, whose energy is also of order $m_e\alpha^2$. This is done by matching the two-atom sector of pNRQED' from the previous section to WEFT. The relevant contributions to the van der Waals potential defined in Eq. (8.6) can be found in the left-hand side of Fig. 9.4. The tree level contribution is the magnetic dipole potential of Eq. (9.5). There are four one-loop diagrams to be considered: diagram *(a)* with two LO electric dipole potential exchanges, which is of $\mathcal{O}(\sqrt{\alpha}/m_e^2)$ ($m_e\alpha^5$ in coordinate space), diagram *(b)* with one LO and one NLO electric dipole potential, which is of $\mathcal{O}(\alpha\sqrt{\alpha}/m_e^2)$ ($m_e\alpha^6$ in coordinate space), diagrams *(d)* and *(e)* with one LO electric dipole potential and one ultrasoft photon, which are of $\mathcal{O}(\alpha^2/m_e^2)$ ($m_e\alpha^6\sqrt{\alpha}$ in coordinate space). Of the same order as the latter are also diagram *(c)*, which is the potential of Eq. (9.8), and the last diagram, which is the contact term of Eq. (9.7). Diagrams involving more than two potential exchanges, either vanish because of parity or give contributions beyond our accuracy. Diagrams consisting of the exchange of two ultrasoft photons contribute at order α^2/m_e^2 in momentum space but only at order $m_e\alpha^8$ in coordinate space and are therefore also beyond our accuracy for the computation of W.

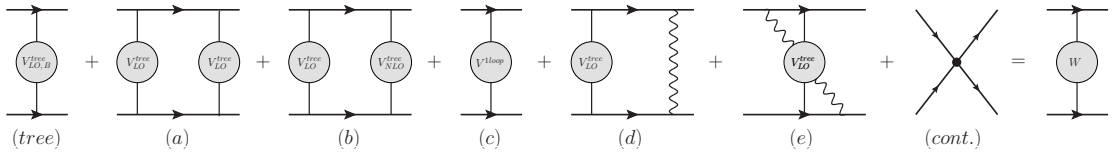

Figure 9.4: Matching of the van der Waals potential between two hydrogen atoms. In left-hand side are the pNRQED' diagrams and in the right-hand side the WEFT one. The symmetric diagrams of *(b)*, *(d)* and *(e)* have not been displayed, but are understood.

The contribution from diagram *(a)* reads

$$\widetilde{W}_E^{(a)} = \frac{\boldsymbol{k}^4 A_2(\boldsymbol{k}^2)}{4} \sum_{m_1,m_2}{}' \frac{p_E(n_1,m_1) p_E(n_2,m_2)}{\Delta E_{n_1 m_1} + \Delta E_{n_2 m_2}}\,, \tag{9.9}$$

where n_1 and n_2 label the hydrogen atom states and A_2 is a loop integral defined in Appendix E.1. We have used that for S-wave states, due to rotational symmetry, $p_E(n,m)^{ij} = p_E(n,m)\delta^{ij}$ (where a sum over all degenerate intermediate Coulomb states is understood).

The contribution from diagram *(b)* reads

$$\widetilde{W}_E^{(b)} = \boldsymbol{k}^2 A_2(\boldsymbol{k}^2) \sum_{m_1,m_2}{}' p_E(n_1,m_1) p_E(n_2,m_2) \frac{\Delta E_{n_1 m_1} \Delta E_{n_2 m_2}}{\Delta E_{n_1 m_1} + \Delta E_{n_2 m_2}}\,, \tag{9.10}$$

where we have used $\langle n|\boldsymbol{v}|m\rangle = i\Delta E_{nm}\langle n|\boldsymbol{x}|m\rangle$.

Diagrams *(d)* and *(e)* involve one ultrasoft photon. Their contribution reads

$$\begin{aligned}\widetilde{W}_E^{(d+e)} = \frac{4(d-2)}{d-1} \sum_{m_1,m_2}{}' & p_E(n_1,m_1) p_E(n_2,m_2) \frac{\Delta E_{n_1 m_1} \Delta E_{n_2 m_2}}{\Delta E_{n_1 m_1}^2 - \Delta E_{n_2 m_2}^2} \\ & \times \left[\Delta E_{n_1 m_1} J(\Delta E_{n_1 m_1}) - \Delta E_{n_2 m_2} J(\Delta E_{n_2 m_2})\right], \end{aligned} \tag{9.11}$$

where $J(\Delta E_{nm})$ is a loop integral that can be found in Appendix E.1 and d is the space-time dimension.

Finally, adding the contributions from the left-hand side of Fig. 9.4, we obtain all terms relevant to compute the van der Waals potential, W, up to order $m_e\alpha^6\sqrt{\alpha}$. In the momentum space they read

$$\widetilde{W}^{(0)} = \widetilde{W}_E^{(a)}\,, \tag{9.12}$$

$$\widetilde{W}^{(1/2)} = \langle n_1, n_2|\widetilde{V}^{\text{tree}}_{LO,\,B}|n_1,n_2\rangle\,, \tag{9.13}$$

$$\widetilde{W}^{(1)} = \widetilde{W}_E^{(b)}\,, \tag{9.14}$$

$$\widetilde{W}^{(3/2)} = \widetilde{W}_E^{(d+e)} + \langle n_1,n_2|\left(\widetilde{V}^{\text{1loop}}_{N^2LO,\,E} + \widetilde{V}^{\text{cont.}}\right)|n_1,n_2\rangle\,, \tag{9.15}$$

where $|n_1\rangle$ and $|n_2\rangle$ are the hydrogen atom states. The LO term is $\widetilde{W}^{(0)}$. The suppressions of Eqs. (9.13), (9.14) and (9.15) relative to Eq. (9.12) are $\sqrt{\alpha}$, α and $\alpha\sqrt{\alpha}$ respectively, as indicated by the superindeces.

The first two terms of Eq. (9.15) carry divergent pieces. These can be recast into local terms by using the results of Appendix E.3 and after $\overline{\text{MS}}$ subtraction the residual scale dependence cancels against the one of d_s in $\widetilde{V}^{\text{cont.}}$ (see Eq. (4.5)):

$$\widetilde{W}_E^{(d+e)} + \langle n_1,n_2|\widetilde{V}^{\text{1loop}}_{N^2LO,\,E}|n_1,n_2\rangle + \langle n_1,n_2|\widetilde{V}^{\text{cont.}}|n_1,n_2\rangle\Big|_{\log\nu}$$

$$= \frac{8\alpha^2}{3m_e^2}\log\nu - \frac{14\alpha^2}{3m_e^2}\log\nu + \frac{2\alpha^2}{m_e^2}\log\nu = 0\,. \tag{9.16}$$

The one-loop contributions including magnetic dipole vertices are strongly suppressed. The first one, involving two electric-magnetic dipole potentials, is α^3 suppressed with respect to the LO term $W^{(0)}$. The expressions for the analogous diagrams of Fig. 9.4 with magnetic dipole interactions are given in Appendix E.2.

Using the Fourier transforms of Appendix E.4, the van der Waals potential can be written in position space. The LO van der Waals potential, given in Eq. (9.12), corresponds to the exchange of two electric dipole potentials and has an R^{-6} dependence in position space

$$W^{(0)} = \frac{3}{8\pi^2 R^6}\sum_{m_1,\,m_2}{}' \frac{p_E(n_1,m_1)p_E(n_2,m_2)}{\Delta E_{n_1m_1}+\Delta E_{n_2m_2}}\,. \tag{9.17}$$

Comparing with the London potential (7.1) we obtain

$$C_6 = -\frac{3}{8\pi^2}\sum_{m_1,\,m_2}{}' \frac{p_E(n_1,m_1)p_E(n_2,m_2)}{\Delta E_{n_1m_1}+\Delta E_{n_2m_2}}\,. \tag{9.18}$$

If the hydrogen atoms are in the ground state the London potential (9.17) is attractive, and a numerical evaluation that includes discrete and continuum intermediate states gives $C_6 = 1.73123\ldots\ 10^{-3}$ keV^{-5} [197]. Moreover, an approximation that holds for the ground state $n_1 = n_2 = 1$,

$$\frac{3}{8}E_1 \geq \frac{\Delta E_{1m_1}\Delta E_{1m_2}}{\Delta E_{1m_1}+\Delta E_{1m_2}} \geq \frac{1}{2}E_1\,, \tag{9.19}$$

with E_1 the ground state energy, allows us to write Eq. (9.17) in the traditional form obtained by London [11] using second-order time-independent perturbation theory:

$$W^{(0)} \approx -\frac{3}{2}\frac{w_0\,\alpha_1^2}{R^6}\,, \tag{9.20}$$

where $w_0 \approx -E_1/2$ and α_1 is the polarizability of the ground state hydrogen atom.

Following the counting, after the LO London potential the most important interaction is given by the magnetic dipole potential $W^{(1/2)}$:

$$W^{(1/2)} = \frac{\alpha}{m_e^2}\left[\frac{2\pi}{3}\delta^{(3)}(\boldsymbol{R})\,\langle n_1|\boldsymbol{\mu}|n_1\rangle\cdot\langle n_2|\boldsymbol{\mu}|n_2\rangle + \frac{3}{4R^3}\hat{\boldsymbol{R}}\cdot\langle n_1|\boldsymbol{\mu}|n_1\rangle\,\hat{\boldsymbol{R}}\cdot\langle n_2|\boldsymbol{\mu}|n_2\rangle\right]. \tag{9.21}$$

This term does not appear in Ref. [180], since only spinless particles were considered there. The magnetic dipole potential can be attractive or repulsive depending on the orientation of the angular momenta of the atoms.

The first correction to the London potential that does not depend on the intrinsic magnetic dipole moments of the atoms is given by $W^{(1)}$, which reads

$$W^{(1)} = -\frac{1}{8\pi^2 R^4}\sum_{m_1,m_2}{}' p_E(n_1,m_1)p_E(n_2,m_2)\frac{\Delta E_{n_1m_1}\Delta E_{n_2m_2}}{\Delta E_{n_1m_1}+\Delta E_{n_2m_2}}\,. \tag{9.22}$$

$W^{(1)}$ is also attractive for atoms in the ground state. This subleading term for S-wave states was derived by Hirschfelder and Meath [198] and also by Feinberg, Sucher and Au [199] using dispersion theory. However, in those previous works the potentials were presented depending on integrals over the Compton scattering form factors of a neutral

spinless particle. These form factors can be obtained for S-wave hydrogen atoms by adding to the diagram in the left-hand side of Fig. 8.1 (with incoming energy $E_n + \omega$) the equivalent one with the photon lines crossed:

$$F_E(\omega) = \sum_m{}' \, p_E(n,m) \frac{2\Delta E_{nm}}{\Delta E_{nm}^2 - \omega^2} \,, \qquad F_M(\omega) = \sum_m{}' \, p_B(n,m) \frac{2\Delta E_{nm}}{\Delta E_{nm}^2 - \omega^2} \,. \quad (9.23)$$

Using the form factors of Eq. (9.23) in the formulas of Ref. [199] for the short-distance potentials we obtain the leading and subleading terms of the London potential of Eqs. (9.12) and (9.14) (c. f. Appendix E.2 for the formulas with magnetic dipoles). The form factors of Eq. (9.23) can be interpreted as a frequency dependent version of the polarizabilities of Eq. (8.3).

The remaining contribution from $W^{(3/2)}$ contains both a R^{-3} part and a Dirac-delta potential:

$$W^{(3/2)} = -\frac{7\alpha^2}{6\pi m_e^2 R^3} + \dots \,, \quad (9.24)$$

where the dots denote the Dirac-delta piece.

10 Van der Waals Interactions at Long Distances

In this section, a different physical setting is explored. We consider the case of the long-distance van der Waals interactions. We have sketched the physical picture in the left-hand panel of Fig. 10.1. In this regime the distance between the atoms is much larger than the time scale between the emission of the two photons, which is of the order of the inverse of the ultrasoft scale: $R \gg 1/(m_e\alpha^2)$. Photons exchanged between the atoms carry a typical momentum, $\boldsymbol{k}$, that is of the order of $m_e\alpha^2$ or the inverse of the distance between the atoms or smaller. Again, the energy scale of the atoms, $Q \sim \boldsymbol{k}^2/m_p$, is much smaller than any other scale due to the strong suppression in m_p. In the right-hand panel of Fig. 10.1 we show the hierarchy of scales in the long-distance regime together with the suitable EFT at each scale. The results in this section are valid for arbitrarily long distances, since the hierarchy between the scales in the right-hand panel of Fig. 10.1 does not change as the distance R increases.

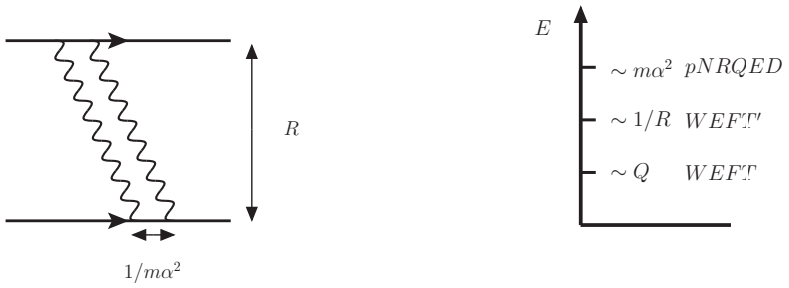

Figure 10.1: Left panel: Sketch of the physical picture of the van der Waals interactions in the long-range regime. The distance between the two atoms is much larger than the typical time interval in which the photons are exchanged. Right panel: Hierarchy of scales and the corresponding EFTs in the long-range regime.

In the following sections, we will provide the details of the matching between the hierarchy of EFTs in the right-hand panel of Fig. 10.1. In Sec. 10.1 we integrate out ultrasoft photons carrying energy and momentum of order $m_e\alpha^2$ and virtual atomic states, whose energy is also of order $m_e\alpha^2$, and obtain WEFT'. In the one-atom sector WEFT' is equivalent to WEFT (see Sec. 8). In the two-atom sector WEFT' differs from WEFT in that photons with momenta of order $1/R$ are still dynamical. The van der Waals potential between hydrogen atoms in S-wave states is obtained in Sec. 10.2 by integrating out photons with momenta of order $1/R$ and matching WEFT' to WEFT.

In order to make the counting homogeneous, it is convenient to assign a specific size to $1/R$ in terms of m_e and α. A natural choice, given the scale hierarchy in the long-distance regime, is to take $1/R \sim m_e\alpha^2\sqrt{\alpha}$. From this assignment it follows that $(m_e\alpha^2\, R) \sim 1/\sqrt{\alpha}$. In the long-distance regime, we aim at computing the nonlocal van der Waals interactions up to order $m_e\alpha^{11}\sqrt{\alpha}$ in coordinate space.

10.1 Matching WEFT′

To aid in the computation of the van der Waals potential we introduce WEFT', an EFT for momenta much smaller than the typical binding energies, but of the same order

as the inverse distance between hydrogen atoms. WEFT′ follows from pNRQED by integrating out ultrasoft photons carrying energy and momentum of order $m_e\alpha^2$ and virtual atomic states, whose energy is also of order $m_e\alpha^2$. The Lagrangian for WEFT′ in the one-atom sector is the same as for WEFT, and is given in Eq. (8.2). We will compute now the two-atom sector of WEFT′.

Since we are integrating out photons and virtual atomic states carrying an energy of order $m_e\alpha^2$, and since the energy scale $m_e\alpha^2$ is generated only in loops if the initial and final state atoms have the same quantum numbers, the only tree-level contributions to consider are potentials taken over from pNRQED to WEFT′. The leading potential from pNRQED is the contact interaction of Eq. (4.7), which gives

$$(\widetilde{W}')^{\text{cont.}} = -\frac{d_s}{m_e^2} - \frac{4d_v}{m_e^2}\langle n_1|\boldsymbol{S}|n_1\rangle\cdot\langle n_2|\boldsymbol{S}|n_2\rangle\,. \tag{10.1}$$

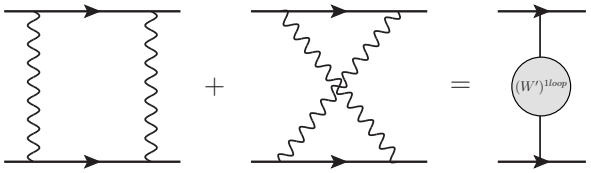

Figure 10.2: One-loop matching of the two hydrogen atom potentials of WEFT′. In the left-hand side we have the pNRQED diagrams and in the right-hand side the WEFT′ one.

The dominant one-loop contributions to the two-atom potential of WEFT′ are given by the two-photon exchange diagrams in the left-hand side of Fig. 10.2. The two photons are ultrasoft, which means that they carry a momentum q^μ that scales like $q^0 \sim |\boldsymbol{q}| \sim m_e\alpha^2$. The LO contribution, involving four electric-dipole vertices is of order α^2/m_e^2 in momentum space ($m_e\alpha^9\sqrt{\alpha}$ in coordinate space according to the counting $1/R \sim m_e\alpha^2\sqrt{\alpha}$). Subsequent contributions are suppressed by powers of $1/(m_e\alpha^2\,R)^2 \sim \alpha$. Furthermore, replacing an electric dipole coupling by a magnetic one adds at least an extra α suppression.

As we will see in the next section, the Casimir–Polder potential is generated by the one-loop diagram with two-photon exchange through the electric-polarizability seagull vertices of WEFT′ (fourth diagram in Fig. 10.3), and it is α^2 suppressed with respect to the LO contribution. To match that precision we have to compute the one-loop diagrams of Fig. 10.2 up to N^{2}LO. The different contributions to the WEFT′ potential for S-wave states read in momentum space

$$\begin{aligned}
(\widetilde{W}')^{\text{1loop}}_{LO,\,E} &= -(d^2-5d+6)\sum_{m_1,m_2}{}' \frac{p_E(n_1,m_1)p_E(n_2,m_2)}{\Delta E_{n_1m_1}^2-\Delta E_{n_2m_2}^2} \\
&\quad\times \Delta E_{n_1m_1}\Delta E_{n_2m_2}\left[\Delta E_{n_1m_1}J(\Delta E_{n_1m_1})-\Delta E_{n_2m_2}J(\Delta E_{n_2m_2})\right], \qquad (10.2)\\
(\widetilde{W}')^{\text{1loop}}_{NLO,\,E} &= -(d-2)(d^2-8d+27)\frac{\boldsymbol{k}^2}{12}\sum_{m_1,m_2}{}' \frac{p_E(n_1,m_1)p_E(n_2,m_2)}{\Delta E_{n_1m_1}^2-\Delta E_{n_2m_2}^2} \\
&\quad\times \left[\Delta E_{n_1m_1}J(\Delta E_{n_2m_2})-\Delta E_{n_2m_2}J(\Delta E_{n_1m_1})\right], \qquad (10.3)\\
(\widetilde{W}')^{\text{1loop}}_{N^2LO,\,E} &= (d-3)(d-2)(d^2-12d+55) \\
&\quad\times \frac{\boldsymbol{k}^4}{240}\sum_{m_1,m_2}{}' \frac{p_E(n_1,m_1)p_E(n_2,m_2)}{\Delta E_{n_1m_1}^2\Delta E_{n_2m_2}^2\left[\Delta E_{n_1m_1}^2-\Delta E_{n_2m_2}^2\right]}
\end{aligned}$$

$$\times \left[\Delta E_{n_1 m_1}^3 J(\Delta E_{n_2 m_2}) - \Delta E_{n_2 m_2}^3 J(\Delta E_{n_1 m_1})\right], \tag{10.4}$$

$$(\widetilde{W}')_{LO,\,M}^{\text{1loop}} = -(d-2) \sum_{m_1,m_2}{}' \frac{p_E(n_1,m_1)p_B(n_2,m_2)_{ii} + p_B(n_1,m_1)_{ii}p_E(n_2,m_2)}{\Delta E_{n_1 m_1}^2 - \Delta E_{n_2 m_2}^2}$$
$$\times \Delta E_{n_1 m_1} \Delta E_{n_2 m_2} \left[\Delta E_{n_1 m_1} J(\Delta E_{n_1 m_1}) - \Delta E_{n_2 m_2} J(\Delta E_{n_2 m_2})\right], \tag{10.5}$$

where J is a loop integral whose explicit expression can be found in Appendix E.1, d is the space-time dimension and summation over the index i is understood. We have used the subscript E to indicate that the contribution is generated in pNRQED by four electric dipole couplings and M by two electric and two magnetic dipoles.

10.2 Matching WEFT

The matching of WEFT′ to WEFT consists in integrating out photons with momenta scaling like $1/R$. This is shown diagrammatically in Fig. 10.3.

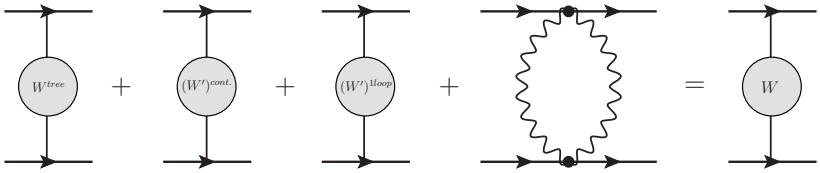

Figure 10.3: Matching of the van der Waals potential between two hydrogen atoms in the long-range regime. In the left-hand side we have the WEFT′ diagrams and in the right-hand side the WEFT one.

The first contribution to the two-atom potential of WEFT is given by the one-photon exchange diagram when the momentum transfer is of order $1/R$. Since we are interested in the case when initial and final state atoms have the same quantum numbers, the energy transfered by the photon in the tree-level diagram is zero. Furthermore, the electric dipole vertex vanishes when evaluated between initial and final states that are equal. Hence, the only contribution comes from the two magnetic dipole potential:

$$\widetilde{W}^{\text{tree}} = \frac{e^2}{4m_e^2}\left(\langle n_1|\boldsymbol{\mu}|n_1\rangle \cdot \langle n_2|\boldsymbol{\mu}|n_2\rangle - \frac{\langle n_1|\boldsymbol{\mu}|n_1\rangle \cdot \boldsymbol{k}\, \langle n_2|\boldsymbol{\mu}|n_2\rangle \cdot \boldsymbol{k}}{\boldsymbol{k}^2}\right). \tag{10.6}$$

The second and third contribution take over the potentials in Eqs. (10.1)-(10.5) of WEFT′. The fourth contribution is a one-loop diagram in WEFT′ made of the seagull vertices defined in the right-hand side of Fig. 8.1. Further higher-order contact terms like radiative corrections to the matching coefficients d_s and d_v, higher-order terms in the multipole expansion of the four-electron operators of NRQED or four-electron operators of dimension eight have not been displayed.

The different contributions to the WEFT potential for S-wave states read in momentum space

$$\widetilde{W}^{(-1)} = \widetilde{W}^{\text{tree}}, \tag{10.7}$$

$$\widetilde{W}^{(0)} = (\widetilde{W}')_{LO,\,E}^{\text{1loop}} + (\widetilde{W}')^{\text{cont.}}, \tag{10.8}$$

$$\widetilde{W}^{(1)} = (\widetilde{W}')_{NLO,\,E}^{\text{1loop}} + \dots, \tag{10.9}$$

$$\widetilde{W}^{(2)} = (\widetilde{W}')_{N^2LO,\,E}^{\text{1loop}} + \widetilde{W}_E^{\text{seg}} + (\widetilde{W}')_{LO,\,M}^{\text{1loop}} + \dots, \tag{10.10}$$

where the dots stand for the higher-order contact interactions that have not been computed here. The superindex in brackets indicates the suppression in powers of α with respect to Eq. (10.8), which is of order α^2/m_e^2 in momentum space and of order $m_e\alpha^9\sqrt{\alpha}$ in coordinate space.

The term $\widetilde{W}_E^{\rm seg}$ is the contribution from the fourth diagram of Fig. 10.3. The photon momenta and energies scale like $1/R$. In dimensional regularization $\widetilde{W}_E^{\rm seg}$ reads in momentum space

$$\widetilde{W}_E^{\rm seg} = -\frac{(d-2)(4d+7)\pi^2}{8(d-1)(d+1)}\alpha_{n_1}\alpha_{n_2}\boldsymbol{k}^4 A_{3/2}(\boldsymbol{k}^2), \tag{10.11}$$

where α_n is the electric polarizability of the hydrogen atom as defined in Sec. 8, $A_{3/2}$ can be found in Appendix E.1 and d is the space-time dimension.

Ultraviolet divergences are present in Eqs. (10.8)-(10.10). In the case of the seagull diagram, the divergence and scale dependence in $\widetilde{W}_E^{\rm seg}$ cancels with the corresponding ones in $(\widetilde{W}')^{\rm 1loop}_{N^2LO,\,E}$:

$$\begin{aligned}\widetilde{W}_E^{\rm seg} + (\widetilde{W}')^{\rm 1loop}_{N^2LO,\,E}\bigg|_{1/(4-d),\,\log\nu} &= -\frac{46}{240}\boldsymbol{k}^4\alpha_{n_1}\alpha_{n_2}\left(\frac{1}{4-d}+\log\nu\right)\\ &+\frac{46}{240}\boldsymbol{k}^4\frac{1}{4\pi^2}{\sum_{m_1,m_2}}'\frac{p_E(n_1,m_1)}{\Delta E_{n_1m_1}}\frac{p_E(n_2,m_2)}{\Delta E_{n_2m_2}}\left(\frac{1}{4-d}+\log\nu\right)=0\,.\end{aligned} \tag{10.12}$$

The divergence in $(\widetilde{W}')^{\rm 1loop}_{LO,\,E}$ can be recast as a local term when summing over the intermediate states (see Appendix E.3) and, once $\overline{\rm MS}$ renormalized, its scale dependence cancels against that one of $(\widetilde{W}')^{\rm cont.}$:

$$(\widetilde{W}')^{\rm 1loop}_{LO,\,E} + (\widetilde{W}')^{\rm cont.}\Big|_{\log\nu} = -\frac{2\alpha^2}{m_e^2}\log\nu + \frac{2\alpha^2}{m_e^2}\log\nu = 0\,. \tag{10.13}$$

The divergences in $(\widetilde{W}')^{\rm 1loop}_{NLO,\,E}$ carried by the J loop integrals cancel each other making $(\widetilde{W}')^{\rm 1loop}_{NLO,\,E}$ finite. Finally, divergences in $(\widetilde{W}')^{\rm 1loop}_{LO,\,M'}$ are at least of order α^6/m_e^2 and hence beyond our accuracy.

The position space representation of the potentials can be obtained using the results of Appendix E.4. All contributions proportional to positive even powers of the transfer momentum are proportional to Dirac-delta potentials except for the ones that contain a $\log\boldsymbol{k}^2$. Therefore, for long-distance van der Waals interactions the only nonlocal term is $W_E^{\rm seg}$ and the magnetic dipole potential, $W^{(-1)}$, given in coordinate space in Eq. (9.21).

The part of $W_E^{\rm seg}$ containing $\log\boldsymbol{k}^2$ is proportional to R^{-7}, whereas the part containing the finite pieces of the loop integral is proportional to a Dirac-delta in position space. The former corresponds to the van der Waals potential derived by Casimir and Polder by using two-photon exchange and fourth-order noncovariant perturbation theory [12]:

$$W_E^{\rm seg} = -\frac{23}{4\pi R^7}\alpha_{n_1}\alpha_{n_2} + \dots\,. \tag{10.14}$$

Comparing with the Casimir–Polder potential (7.2) we obtain

$$C_7 = \frac{23}{4\pi}\alpha_{n_1}\alpha_{n_2}\,. \tag{10.15}$$

A derivation of the Casimir–Polder potential in Eq. (10.14) using dispersive methods was given by Feinberg and Sucher in Refs. [179, 199]. Feinberg and Sucher also

provided the long-range potentials due to magnetic polarizabilities and mixed interactions between electric and magnetic polarizabilities. These can be recovered respectively from our results for $W_B^{\rm seg}$ and $W_M^{\rm seg}$ in Appendix E.2. Assuming scalar magnetic polarizabilities, $\beta_n^{ij} = \beta_n \delta^{ij}$, we can write $W_B^{\rm seg} = -\dfrac{23}{4\pi R^7}\beta_{n_1}\beta_{n_2} + \dots$ and $W_M^{\rm seg} = \dfrac{7}{4\pi R^7}\left(\alpha_{n_1}\beta_{n_2} + \beta_{n_1}\alpha_{n_2}\right) + \dots$. According to our counting, these two cases are suppressed by a factor α^4 and α^2 respectively compared to $W_E^{\rm seg}$. We note, however, that the magnetic polarizability of a hydrogen atom cannot be a scalar since hydrogen possesses a permanent magnetic dipole. The above results for $W_E^{\rm seg}$, $W_B^{\rm seg}$ and $W_M^{\rm seg}$ were also obtained by Holstein [190] using a phenomenological Hamiltonian for the Compton scattering of neutral scalar particles constrained by gauge symmetry, invariance under parity and time reversal.

11 Van der Waals Interactions at Intermediate Distances

The last possible physical situation to consider is when the range of the van der Waals interactions, R, is of the same order as the intrinsic time scale of the hydrogen atom, $1/(m_e\alpha^2)$. A visual representation of this case is sketched in the left panel of Fig. 11.1. In this regime the distance between the atoms is of the same order as the time scale between the emission of the two photons, which is of the order of the inverse of the ultrasoft scale: $R \sim 1/(m_e\alpha^2)$. The hierarchy of the two energy scales in the intermediate-distance regime is plotted in the right-hand panel of Fig. 11.1. In this section we obtain the van der Waals potential by integrating out at the same time photons and virtual atomic states with momenta and energies of order $1/R$ and $m_e\alpha^2$, and matching pNRQED directly to WEFT.

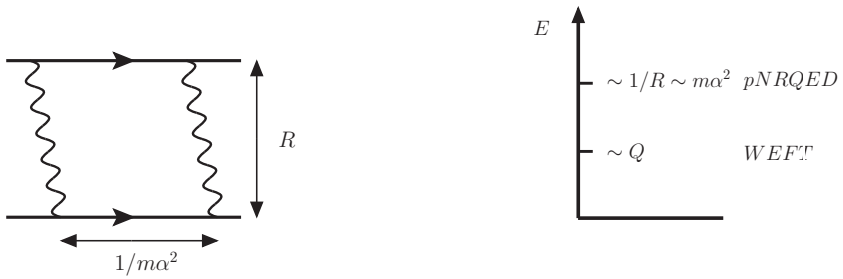

Figure 11.1: Left panel: Sketch of the physical picture of the van der Waals interactions in the intermediate-range regime. The distance between the two atoms is of the same size as the intrinsic time scale of the hydrogen atom. Right panel: Hierarchy of scales and the corresponding EFTs in the intermediate-distance regime.

The diagrams involved in the matching are shown in Fig. 11.2. The dominant contribution for interactions between atoms in S-wave states is given by a photon exchange between the permanent magnetic dipoles. The expression is in Eq. (10.6). It is of $\mathcal{O}(\alpha/m_e^2)$ in momentum space and of $\mathcal{O}(m_e\alpha^7)$ in coordinate space.

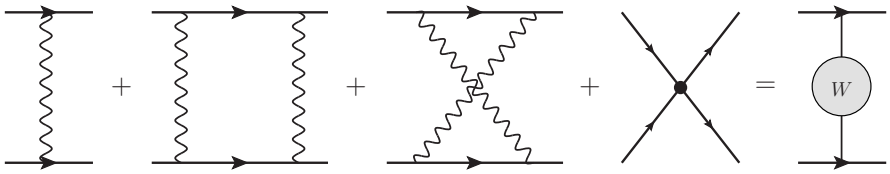

Figure 11.2: Matching of the van der Waals potential between two hydrogen atoms in the intermediate-range regime. In the left-hand side we draw the pNRQED diagrams and in the right-hand side the WEFT one.

The contribution of the 1-loop pNRQED diagrams is

$$\widetilde{W}_E^{\rm 1loop} = \sum_{m_1,m_2}{}' \, p_E(n_1,m_1) p_E(n_2,m_2) \times \left\{ \frac{1}{2\left(\Delta E_{n_1m_1}^2 - \Delta E_{n_2m_2}^2\right)} \left[\boldsymbol{k}^2 \left(\Delta E_{n_2m_2} J(\Delta E_{n_1m_1}) - \Delta E_{n_1m_1} J(\Delta E_{n_2m_2}) \right) \right. \right.$$

$$
\begin{aligned}
&- \left(\boldsymbol{k}^4 - 4\boldsymbol{k}^2\Delta E_{n_1m_1}^2 + 4(d-2)\Delta E_{n_1m_1}^4\right)\Delta E_{n_2m_2} K(\boldsymbol{k}^2, \Delta E_{n_1m_1}) \\
&+ \left(\boldsymbol{k}^4 - 4\boldsymbol{k}^2\Delta E_{n_2m_2}^2 + 4(d-2)\Delta E_{n_2m_2}^4\right)\Delta E_{n_1m_1} K(\boldsymbol{k}^2, \Delta E_{n_2m_2})\big] \\
&- \frac{d-2}{2}\Delta E_{n_1m_1}\Delta E_{n_2m_2} A_{3/2}(\boldsymbol{k}^2)\Big\}. \qquad (11.1)
\end{aligned}
$$

The explicit definitions of the loop integrals J, K and $A_{3/2}$ can be found in Appendix E.1.

The remaining contribution is the contact term

$$
\widetilde{W}^{\text{cont.}} = -\frac{d_s}{m_e^2} - \frac{4d_v}{m_e^2}\langle n_1|\boldsymbol{S}|n_1\rangle\cdot\langle n_2|\boldsymbol{S}|n_2\rangle\,. \qquad (11.2)
$$

The 1-loop electric dipole diagrams and the contact term are of $\mathcal{O}(\alpha^2/m_e^2)$ in momentum space and of $\mathcal{O}(m_e\alpha^8)$ in coordinate space. The rest of the terms are suppressed by one power of α for each magnetic dipole replacing an electric dipole.

In summary, we have that

$$
\begin{aligned}
\widetilde{W}^{(-1)} &= \widetilde{W}^{\text{tree}}\,, \qquad (11.3)\\
\widetilde{W}^{(0)} &= \widetilde{W}_E^{\text{1loop}} + \widetilde{W}^{\text{cont.}}\,, \qquad (11.4)
\end{aligned}
$$

where the superindex indicates that $\widetilde{W}^{(0)}$ is suppressed by one power of α compared to $\widetilde{W}^{(-1)}$. The ultraviolet divergence in $\widetilde{W}^{\text{1loop}}$ can be recast as a local term when summing over the intermediate states (see Appendix E.3) and, once $\overline{\text{MS}}$ renormalized, its scale dependence cancels against that one of $\widetilde{W}^{\text{cont.}}$

$$
\widetilde{W}_E^{\text{1loop}} + \widetilde{W}^{\text{cont.}}\Big|_{\log\nu} = -\frac{2\alpha^2}{m_e^2}\log\nu + \frac{2\alpha^2}{m_e^2}\log\nu = 0\,. \qquad (11.5)
$$

As a cross-check, the expression in Eq. (11.1) can be expanded in powers of $\Delta E_{nm}/|\boldsymbol{k}|$, yielding the short-distance van der Waals interactions of Eqs. (9.8)-(9.11) from Sec. 9. Analogously, expanding in powers of $|\boldsymbol{k}|/\Delta E_{nm}$ results in the long-distance van der Waals expressions of Eqs. (10.2)-(10.4) and Eq. (10.11) from Sec. 10.

The potential in coordinate space is obtained by Fourier transforming Eq. (11.4). However, in the 1-loop term $\widetilde{W}_E^{\text{1loop}}$ there are nonanalytic pieces that cannot be transformed using the results of Appendix E.4. The coordinate space potential associated to these pieces can be obtained by using a dispersive representation of the momentum space potential (see, e. g. [15, 199]).

The coordinate space potential is given by

$$
W(R) = \int \frac{d^3k}{(2\pi)^3}\, e^{i\boldsymbol{k}\cdot\boldsymbol{R}}\,\widetilde{W}(k)\,. \qquad (11.6)
$$

Since for $\boldsymbol{k}^2 \to \infty$ the momentum space potential $\widetilde{W}_E^{\text{1loop}}$ diverges as $\boldsymbol{k}^4$, its corresponding dispersion relation should be twice subtracted. The subtraction constants are independent of the momentum and as such correspond to Dirac-delta potentials. The nonlocal part of potential is given by the following dispersive representation corresponding to the two-photon cut

$$
\widetilde{W}(k) = \frac{2}{\pi}\int_0^\infty d\mu\,\frac{\mu\,\text{Im}\left[\widetilde{W}(\eta - i\mu)\right]}{\mu^2 + k^2}\,, \qquad (11.7)
$$

where the limit $\eta \to 0$ is understood. Plugging (11.7) into (11.6) and changing the order of the dispersive and Fourier integrals we arrive at

$$W(R) = \frac{1}{2\pi^2 R} \int_0^\infty d\mu \, e^{-\mu R} \mu \, \mathrm{Im} \left[\widetilde{W}(\eta - i\mu) \right]. \tag{11.8}$$

The imaginary part of $\widetilde{W}_E^{\mathrm{1loop}}$ can be easily obtained after inserting the explicit values of the loop integrals J, K and $A_{3/2}$ from Appendix E.1 into Eq. (11.1). This yields

$$\begin{aligned} \mathrm{Im} \left[\widetilde{W}_E^{\mathrm{1loop}}(\eta - i\mu) \right] = -{\sum_{m_1,m_2}}' \frac{p_E(n_1,m_1) p_E(n_2,m_2)}{16\pi} \Bigg\{ & 4\Delta E_{n_1 m 1} \Delta E_{n_2 m_2} \\ & + \frac{1}{\mu \left(\Delta E_{n_1 m_1}^2 - \Delta E_{n_2 m_2}^2 \right)} \\ & \times \Bigg[\left(\mu^4 + 4\mu^2 \Delta E_{n_1 m_1}^2 + 8 \Delta E_{n_1 m_1}^4 \right) \Delta E_{n_2 m_2} \, \mathrm{arccot} \left(\frac{2|\Delta E_{n_1 m_1}|}{\mu} \right) \\ & - \left(\mu^4 + 4\mu^2 \Delta E_{n_2 m_2}^2 + 8 \Delta E_{n_2 m_2}^4 \right) \Delta E_{n_1 m_1} \, \mathrm{arccot} \left(\frac{2|\Delta E_{n_2 m_2}|}{\mu} \right) \Bigg] \Bigg\}. \end{aligned} \tag{11.9}$$

In Fig. 11.3 we plot the relative difference between the intermediate-range van der Waals potential given in Eqs. (11.8) and (11.9) with the London potential from Eq. (9.17) and the Casimir–Polder potential from Eq. (10.14) for both atoms in the ground state. As expected, the London potential and the Casimir–Polder potential are a good approximation in the short and long distances respectively. Due to a conspiracy of numerical factors and cancellations, the convergence towards the London potential is, however, somewhat faster than the one towards the Casimir–Polder potential.

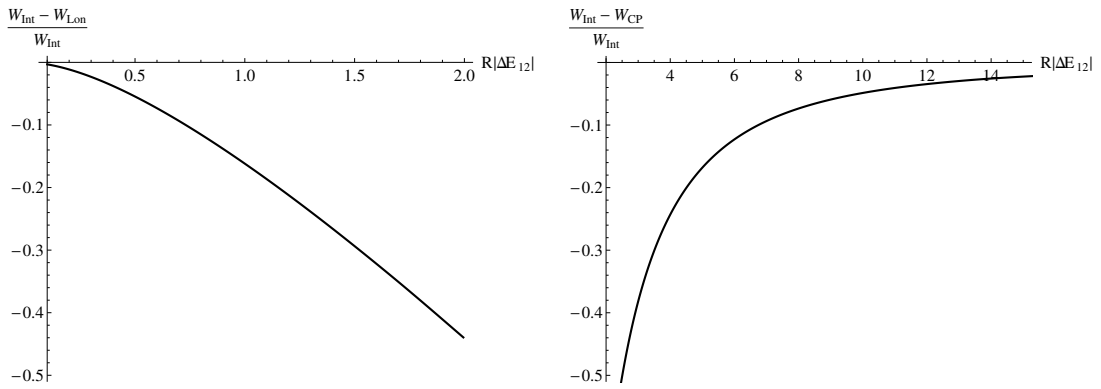

(a) *(b)*

Figure 11.3: Plots of the relative difference between the intermediate van der Waals potential and the London *(a)* and Casimir–Polder *(b)* potentials for both atoms in the ground state as a function of the distance R in units of $1/|\Delta E_{12}|$. W_{Int} is the intermediate-range potential in Eq. (11.8), W_{Lon} is the London potential in Eq. (9.17) and W_{CP} is the Casimir–Polder potential in Eq. (10.14).

12 Summary

A hydrogen atom is a nonrelativistic bound state characterized by a hierarchy of well separated scales. These are the mass of the particle that forms the bound state (hard), the inverse of the Bohr radius, namely the relative momentum (soft), and the typical bound state energy (ultrasoft). Integrating out the hard scale produces NRQED, and integrating out the soft scale leads to pNRQED, which is the theory best suited to study the bound state.

In systems with two hydrogen atoms two distinct physical regimes exist depending on the distance between the nuclei. If the distance between the nuclei is of the order of the Bohr radius, the system is configured as a diatomic molecule. On the other hand, if this distance is larger than the Bohr radius, the system consists of two atoms interacting through van der Waals interactions. In both cases a new energy scale, different from the intrinsic ones characterizing a single atom, appears. In diatomic molecules, the two nuclei dynamics takes place at a lower energy scale than the ultrasoft scale in which the electrons bind to the nuclei. This is nothing else that restating the usual assumption that the electron and nuclei dynamics occur at very different time scales, which is at the basis of the Born–Oppenheimer approximation [200]. In the van der Waals case, the new scale is the distance between the atoms, which can be larger or smaller than the ultrasoft scale.

In this work, we have presented a study of the dispersive van der Waals interactions between two hydrogen atoms in the framework of nonrelativistic EFTs of QED. We have focused on S-wave states, since these do not have permanent electric multipole moments and their interaction proceeds through dispersive van der Waals forces in addition to the magnetic-dipole coupling. We have introduced a new EFT, WEFT, to describe the dynamics of the degrees of freedom that live at the low energy scale where a van der Waals potential is naturally defined. Then the van der Waals potential has been obtained by sequentially integrating out the physical scales of the two hydrogen atoms. The EFT setting allows to compute all local terms needed to renormalize the van der Waals interactions, which is the most original result of the present work.

Different hierarchies of scales correspond to different physical scenarios and lead to different results for the dispersive van der Waals potential. We have explored three possible scenarios: short-, long- and intermediate-distances between the atoms.

In the short distance regime, $1/R \gg m_e\alpha^2$, integrating out modes scaling like $1/R$ leads to the well-known electric and magnetic dipole potentials as well as to subleading velocity dependent potentials. Integrating out the ultrasoft scale leads to the van der Waals potential. The leading contribution of Eq. (9.17) stems from the exchange of two electric-dipole potentials and corresponds to the London potential [11]. The NLO term, Eq. (9.22), is obtained by replacing one of the leading dipole potentials by a subleading one. This term is equivalent to the one obtained by Hirschfelder and Meath [198, 199]. In addition, we have investigated the NNLO van der Waals potential, previously unknown, which turns out to contain a R^{-3} term, shown in Eq. (9.24), and a local term.

The long-distance regime corresponds to $1/R \ll m_e\alpha^2$. Integrating out the ultrasoft scale defines in the one-atom sector the polarizability operators, while in the two-atom sector several local terms are generated. Integrating out the $1/R$ scale, the two-photon exchange induced by the polarizability operators generates the Casimir–Polder potential [12, 179, 190] of Eq. (10.14). The newly computed local terms turn out to be crucial to cancel all ultraviolet divergences in the Casimir–Polder diagram, which, to our knowledge, has been renormalized in this context here for the first time.

In the last part of this work, we have explored for the first time the intermediate-distance regime $1/R \sim m_e\alpha^2$. In this regime the van der Waals potential is obtained

by integrating out the ultrasoft and $1/R$ scales simultaneously. We have obtained a coordinate space representation for the nonlocal part of the van der Waals potential by using a dispersive representation of the momentum space potential. Figure 11.3 summarizes our findings. It shows the relative difference between the intermediate-range van der Waals potential and the London and the Casimir–Polder potentials for both atoms in the ground state as a function of R. The plot shows that the intermediate-range potential is needed to accurately describe (with an accuracy better than about 15%) the van der Waals interaction in the distance range between 400 to 2000 times the Bohr radius. Results for the dispersive van der Waals potentials in the three different regimes have been generalized to states with any angular momentum in Appendix E.2.

We conclude with a possible outlook. The EFT description of the van der Waals interactions between two hydrogen atoms obtained here offers a framework to appropriately define and systematically calculate also van der Waals interactions for other physical systems starting from the underlying quantum field theory. A prominent case is that of the hadronic van der Waals interactions, whose underlying field theory is QCD. The multigluon interaction is a QCD analogue of the van der Waals force of atomic physics. A color van der Waals force arises in hadron-hadron interactions due to the chromopolarizability of the color-neutral hadrons, similar to the electric polarizability in the case of the hydrogen atom. Contrary to the situation in QED, not much is presently known about color van der Waals forces: one reason is that they are a long-wavelength feature of QCD and therefore of nonperturbative nature, which makes it difficult to assess them from first principles. The potential relevance of color van der Waals forces for the study of the new hadrons, which may arise as a result of such interaction, demands a better understanding of their properties within QCD.

Quarkonia are hadrons made of a heavy quark and a heavy antiquark. The relative quark-antiquark velocity v may be identified with the strong coupling constant, α_s, only if the quarkonium is a Coulombic bound state, which holds for the lowest quarkonium states. Moreover, color provides a richer set of degrees of freedom with respect to QED. In particular, static quark-antiquark pairs may exist at small distances in two possible color configurations. Nevertheless, the hierarchy of EFTs relevant for describing quarkonium-quarkonium interactions is similar to the one discussed in this work for QED, starting from potential nonrelativistic QCD (pNRQCD) [8, 9] to the ultimate van der Waals EFT [15]. We have investigated van der Waals interactions for Coulombic quarkonia in [15], whereas van der Waals interactions for nonperturbatively bound quarkonia have been addressed with numerical methods [201] and lattice QCD [202]. Effective field theories may provide further insights into these systems and link the findings with other processes and systems like quarkonium hadronic transitions, quarkonium-nuclei interactions and exotic multiquark systems.

Part V

Relativistic corrections to exclusive $\chi_{cJ} + \gamma$ production from e^+e^- annihilation in NRQCD

13 Motivation

More than four decades have passed since experimental groups of Samuel Ting and Burton Richter [17, 18] discovered the J/ψ, the first observed bound state formed by a heavy (charm) quark and a heavy antiquark. This event was of crucial importance for the establishment of Quantum Chromodynamics (QCD) as the correct theory of strong interactions. Even though heavy quarkonia are sometimes regarded as the "hydrogen atoms" of QCD, our present understanding of these hadronic systems is by far not as good as our insight about bound states of electrons and protons in Quantum Electrodynamics (QED). The nonperturbative nature of QCD at low energy makes the theoretical description of heavy quarkonium on the one hand more challenging on the other hand also more interesting. Heavy quarkonia are indeed special probes of strong interactions and the recent progress in nonrelativistic Effective Field Theories (EFTs) and lattice calculations make this statement even more significant [3, 16, 47].

In particular, the theoretical description of the production mechanism for charmonia and bottomonia is challenging. While the creation of a heavy quark pair in a high energy collision can be very well described in perturbative QCD, this is not the case for the evolution of this pair into a heavy quarkonium, which is governed by nonperturbative long-distance effects.

EFT framework provides an elegant way to treat this problem by exploiting the nonrelativistic nature of the system and the large separation of the relevant scales. The resulting EFT, known as Nonrelativistic QCD (NRQCD) [7] conjectures a factorization theorem that allows us to write down the quarkonium production cross section as a series in α_s and the relative heavy quark velocity v, where each term is a product of a short-distance coefficient and a long-distance matrix element (LDME). The former are computed from matching to perturbative QCD and incorporate effects of the hard scale m (heavy quark mass) and above. The latter are of nonperturbative nature but can be obtained from fits to the experimental data. The LDMEs are assumed to be universal and to obey velocity power-counting rules, so that one always can estimate the relative importance of a particular matrix element at the given order in α_s and v. This gives NRQCD its predictive power and allows for a systematic inclusion of relativistic and loop effects.

NRQCD also predicts that quarkonium formation is not limited to heavy quark pairs in the color singlet configuration, as is assumed by the old color singlet model [121–123]. Instead, the Fock state of a heavy quarkonium can be schematically understood as a sum over several contributions

$$|H\rangle \sim a_0\,|Q\bar{Q}\rangle + a_1\,|Q\bar{Q}g\rangle + a_2\,|Q\bar{Q}gg\rangle + \dots. \tag{13.1}$$

where higher Fock states that involve gluons are suppressed by powers of v. Nevertheless, in higher order calculations such contributions become relevant and must be included to obtain a consistent result.

Electromagnetic quarkonium production can be regarded as a comparably simple and clean process, which makes it a perfect test ground for verifying predictions made by NRQCD. Electromagnetic quarkonium production is an important subject of study at BESIII at the tau-charm factory at IHEP in China and at Belle II at the beauty factory at KEK in Japan. One of such processes is the exclusive production of a heavy quarkonium and a hard ($|\mathbf{k}| \sim m_Q$) photon in the electron-positron annihilation.

Let us briefly review the existing NRQCD predictions for $e^+e^- \to \gamma^* \to \chi_{cJ}\,\gamma$. The leading order $\mathcal{O}(\alpha_s^0 v^0)$ cross section was obtained in [203]. Subsequently, corrections

of order $\mathcal{O}(\alpha_s v^0)$ [204, 205], $\mathcal{O}(\alpha_s^0 v^2)$ [28, 29] and finally $\mathcal{O}(\alpha_s v^2)$ [30] were computed as well. One of the reasons why this process has attracted so much interest from the theory side in the last years, is the anticipated connection between C-even quarkonia and some exotic XYZ particles [3, 206–208], although such identifications are still controversial [209, 210]. In any case, there is a clear experimental evidence [211] that the C-even state $X(3872)$ can be measured in the same channel ($e^+e^- \to X(3872)\,\gamma$) as our process of interest. Therefore, irrespective of the true nature of $X(3872)$, to study this state in more details it is very useful to have precise and unambiguous predictions for $e^+e^- \to \gamma^* \to \chi_{cJ}\,\gamma$. This is all the more important in view of the fact that no experimental measurements for the electromagnetic production of χ_{cJ} are yet available, while good perspectives for this measurement will exist at Belle II.

It is worth noting that all the above-mentioned NRQCD studies considered only operators that contribute through the dominant Fock state $|Q\bar{Q}\rangle$. However, for consistency reasons already at $\mathcal{O}(\alpha_s^0 v^2)$ operators that are related to the sub-leading Fock state $|Q\bar{Q}g\rangle$ should be taken into account. The importance of such effects is well known. In particular, they were explicitly considered in the studies of the decay $\chi_{cJ} \to \gamma\gamma$ [26, 27], which is very similar to $\gamma^* \to \chi_{cJ}\,\gamma$.

In the present work we will investigate these missing contributions to the production cross section by determining the matching coefficients of the corresponding operators at $\mathcal{O}(\alpha_s^0 v^2)$ in NRQCD. This chapter is organized in the following way. In Sec. 14 we discuss the relevant operators and LDMEs and introduce the NRQCD-factorized cross sections for this process at the precision in the α_s and v expansion we are aiming at. Different strategies for the determination of the NRQCD matching coefficients are discussed in Sec. 15. In Sec. 16 we explain the calculation of the NRQCD amplitudes, while Sec. 17 describes the QCD side of the matching and presets short-distance coefficients obtained with two independent methods. A long-standing discrepancy between the results of [26] and [27] regarding some matching coefficients that enter NRQCD-factorized decay rates for $\chi_{cJ} \to \gamma\gamma$ at $\mathcal{O}(\alpha_s^0 v^2)$ is resolved in Sec. 18. Sec. 19 and Sec. 20 contain the final cross sections and numerical predictions. Finally, a summary of the obtained results and their impact is presented in Sec. 21.

In Appendix G we present additional short-distance coefficients that arise from the matching. They are not functional to our calculation but they are new and appear at $\mathcal{O}(\alpha_s^0 v^4)$ contributing to the dominant Fock state. Appendix F contains the details of the calculation made with the threshold expansion method of Braaten and Chen.

14 NRQCD Cross Section

14.1 Properties of NRQCD Operators for Exclusive Electromagnetic Production

A generic NRQCD operator of mass dimension d_n that describes heavy quarkonium production can be conventionally denoted as [7]

$$\tilde{O}_n = \chi^\dagger \mathcal{K}_n \psi \left(\sum_X \sum_{m_J} |H + X\rangle \langle H + X| \right) \psi^\dagger \mathcal{K}'_n \chi, \tag{14.1}$$

where $\mathcal{K}_n^{(\prime)}$ consists of a spin matrix (1 or $\boldsymbol{\sigma}$), a color matrix (1 or T^a) and a polynomial in $\mathbf{B}^i \equiv \frac{1}{2}\varepsilon^{ijk} G^{kj}$, $\mathbf{E}^i \equiv G^{i0}$ and $\mathbf{D} = \boldsymbol{\nabla} - ig\mathbf{A}$ with $\mathbf{A}$ being the gluon field and g the gauge coupling constant [1]. Here ψ (χ) denotes a Pauli field that annihilates (creates) a heavy quark (antiquark), while $|H + X\rangle$ is a Fock state that contains a quarkonium H and all other particles X that appear in the final state and have energy and momenta that are typically much smaller than the hard scale m_Q. The summations run over all allowed X states and $m_J = -J, \ldots, J$, where J denotes the total angular momentum quantum number of the quarkonium state. The operators $\tilde{O}_n$ enter NRQCD production cross section as vacuum expectation values

$$\langle 0|\tilde{O}_n|0\rangle_{\text{BBL}} = \langle 0| \chi^\dagger \mathcal{K}_n \psi \left(\sum_X \sum_{m_J} |H + X\rangle \langle H + X| \right) \psi^\dagger \mathcal{K}'_n \chi |0\rangle_{\text{BBL}}\,, \tag{14.2}$$

where $|0\rangle$ denotes the QCD vacuum and the subscript BBL is used to specify that these matrix elements have nonrelativistic normalization, i. e.

$$\langle H(\mathbf{P})|H(\mathbf{P}')\rangle_{\text{BBL}} = (2\pi)^3 \delta^3(\mathbf{P} - \mathbf{P}'), \tag{14.3}$$

with $\mathbf{P}^{(\prime)}$ being the total 3-momentum of the heavy quarkonium.

The sum over X in Eq. (14.2) is one of the reasons why production matrix elements $\langle 0|\tilde{O}_n|0\rangle_{\text{BBL}}$ cannot be easily calculated in lattice simulations [126]. However, in exclusive electromagnetic production this sum is not present, such that a corresponding LDME reads

$$\langle 0|O_n|0\rangle_{\text{BBL}} = \langle 0| \chi^\dagger \mathcal{K}_n \psi \left(\sum_{m_J} |H\rangle \langle H| \right) \psi^\dagger \mathcal{K}'_n \chi |0\rangle_{\text{BBL}}\,. \tag{14.4}$$

Eq. (14.4) can be further simplified using rotational invariance of matrix elements [7, 31]. Since all matrix elements that differ only in the quantum number m_J are identical, the sum over m_J trivially reduces to $(2J + 1)$ and the LDME factorizes into a product of two quarkonium-to-vacuum matrix elements

$$\langle 0|O_n|0\rangle_{\text{BBL}} = (2J + 1) \langle 0| \chi^\dagger \mathcal{K}_n \psi |H\rangle_{\text{BBL}} \langle H| \psi^\dagger \mathcal{K}'_n \chi |0\rangle_{\text{BBL}}\,. \tag{14.5}$$

The matrix elements $\langle 0| \chi^\dagger \mathcal{K}_n \psi |H\rangle_{\text{BBL}}$ and $\langle H| \psi^\dagger \mathcal{K}'_n \chi |0\rangle_{\text{BBL}}$ are exactly the same that enter NRQCD formulas for exclusive electromagnetic decays [212]. Hence, up to the

[1] In case of polarized production $\mathcal{K}_n^{(\prime)}$ may also depend on corresponding polarization vectors [7]. Explicit NRQCD calculations of such processes can be found e. g. in [31]. In this work we are, however, interested only in unpolarized production.

prefactor $(2J+1)$ a LDME for exclusive electromagnetic production $\langle 0|O_n|0\rangle_{\text{BBL}}$ is identical to the corresponding LDME for exclusive electromagnetic decay $\langle H|O_n|H\rangle_{\text{BBL}}$

$$\langle 0|O_n|0\rangle_{\text{BBL}} = (2J+1)\,\langle H|\,\psi^\dagger \mathcal{K}'_n \chi\,|0\rangle_{\text{BBL}}\,\langle 0|\,\chi^\dagger \mathcal{K}_n \psi\,|H\rangle_{\text{BBL}} = (2J+1)\,\langle H|O_n|H\rangle_{\text{BBL}}\,. \tag{14.6}$$

This is why in the NRQCD-factorized cross section for exclusive electromagnetic production it is convenient to rewrite $\langle 0|O_n|0\rangle_{\text{BBL}}$ in terms of $\langle 0|\,\chi^\dagger \mathcal{K}_n \psi\,|H\rangle_{\text{BBL}}\,\langle H|\,\psi^\dagger \mathcal{K}'_n \chi\,|0\rangle_{\text{BBL}}$ and absorb $(2J+1)$ into the matching coefficients F_n

$$\frac{F_n}{m_Q^{d_n-4}}\,\langle 0|O_n|0\rangle_{\text{BBL}} = \frac{F'_n}{m_Q^{d_n-4}}\,\langle 0|\,\chi^\dagger \mathcal{K}_n \psi\,|H\rangle_{\text{BBL}}\,\langle H|\,\psi^\dagger \mathcal{K}'_n \chi\,|0\rangle_{\text{BBL}}\,, \tag{14.7}$$

with $F'_n \equiv (2J+1)F_n$.

14.2 Definition of Color Singlet and Color Octet Production Operators

In NRQCD it is customary to classify production operators according to the color configuration of the $Q\bar{Q}$ pair in the leading Fock state through which these operators contribute to the process. In the dominant Fock state $|Q\bar{Q}\rangle$ the heavy quark pair is always a color singlet, hence operators that contribute through this state are denoted as singlet operators. An octet operator is therefore an operator that gives a nonvanishing contribution only when the $Q\bar{Q}$ pair is a color octet. This is the case for the subleading Fock state $|Q\bar{Q}g\rangle$ but also for higher Fock states. A simple example for a color octet operator is

$$\chi^\dagger \boldsymbol{\sigma} T^a \psi \left(\sum_X \sum_{m_J} |H+X\rangle\,\langle H+X| \right) \psi^\dagger \boldsymbol{\sigma} T^a \chi, \tag{14.8}$$

which contributes to the inclusive production of spin-triplet P-wave quarkonium at leading order in v. In exclusive electromagnetic production there are no color octet operators similar to Eq. (14.8). This is because a matrix element like $\langle 0|\,\chi^\dagger \boldsymbol{\sigma} T^a \psi\,|H\rangle_{\text{BBL}}$ vanishes, which can be seen explicitly by replacing $|H\rangle_{\text{BBL}}$ with $|Q\bar{Q}g\rangle$. However, if we replace T^a with the chromoelectric field multiplied by the gauge coupling constant, we obtain

$$\langle 0|\,\chi^\dagger \boldsymbol{\sigma} \cdot g\mathbf{E} \psi\,|H\rangle_{\text{BBL}}\,, \tag{14.9}$$

which gives a nonvanishing contribution to the exclusive electromagnetic production of P-wave quarkonium at subleading order in v. The corresponding operator reads

$$\frac{1}{3}\left(\chi^\dagger (-\frac{i}{2} \overleftrightarrow{\mathbf{D}} \cdot \boldsymbol{\sigma}) \psi\,|H\rangle\,\langle H|\,\psi^\dagger (g\mathbf{E} \cdot \boldsymbol{\sigma}) \chi + \text{h.c.} \right) \tag{14.10}$$

with $\psi^\dagger \overleftrightarrow{\mathbf{D}} \chi \equiv \psi^\dagger (\mathbf{D}\chi) - (\mathbf{D}\psi)^\dagger \chi$, where h.c. stands for hermitian conjugate. According to the usual NRQCD classification, the operator in Eq. (14.10) is a color octet operator, because it contributes only through the subleading Fock state $|Q\bar{Q}g\rangle$. Of course, we are also aware of the fact that many NRQCD practitioners prefer to use the word color octet to denote operators similar to the one in Eq. (14.8), which are irrelevant for exclusive electromagnetic production. To avoid possible confusion, we therefore will not use the notion of color singlet and color octet operators in this work. Instead, we will speak of operators that contribute through the leading or subleading quarkonium Fock state $|Q\bar{Q}\rangle$ or $|Q\bar{Q}g\rangle$ respectively.

Let us also stress that operators with chromoelectric or chromomagnetic fields are not a specific feature of exclusive electromagnetic production. Such operators contribute also to hadronic processes, but their contributions are suppressed by powers of v. For inclusive decays, their matching coefficients were determined in [118]. However, we are not aware of any similar results for production. In this sense, to our knowledge, this is the very first study that computes matching coefficients of production operators with chromoelectric fields in exclusive electromagnetic production.

14.3 Production Cross Section and Power-Counting Rules

After having clarified the terminology and explained the relevance of this work, let us proceed with applying NRQCD factorization to the exclusive process $e^+e^- \to \gamma^* \to \chi_{cJ}\,\gamma$. To asses the relative importance of the NRQCD matrix elements we adopt power counting rules from [7]. Each of our formulas depends on three LDMEs, where two of them are v^2 suppressed as compared to the third one. When we refer to $\mathcal{O}(v^2)$ corrections, we always do so with respect to the absolute size of the leading order matrix element. Hence, at $\mathcal{O}(v^2)$ the NRQCD-factorized cross sections for $e^+e^- \to \gamma^* \to \chi_{cJ}\,\gamma$ can be written as

$$\begin{aligned}
\sigma(e^+e^- \to \chi_{c0}\gamma) &= \frac{F_1(^3P_0)}{3m_Q^2}\,\langle 0|\chi^\dagger(-\frac{i}{2}\overleftrightarrow{\mathbf{D}}\cdot\boldsymbol{\sigma})\psi|\chi_{c0}\rangle\,\langle\chi_{c0}|\psi^\dagger(-\frac{i}{2}\overleftrightarrow{\mathbf{D}}\cdot\boldsymbol{\sigma})\chi|0\rangle \\
&+ \frac{G_1(^3P_0)}{6m_Q^4}\left(\langle 0|\chi^\dagger(-\frac{i}{2}\overleftrightarrow{\mathbf{D}}\cdot\boldsymbol{\sigma})\psi|\chi_{c0}\rangle\,\langle\chi_{c0}|\psi^\dagger(-\frac{i}{2}\overleftrightarrow{\mathbf{D}}\cdot\boldsymbol{\sigma})(-\frac{i}{2}\overleftrightarrow{\mathbf{D}})^2\chi|0\rangle + \text{h.c.}\right) \\
&+ \frac{iT_8(^3P_0)}{3m_Q^3}\left(\langle 0|\chi^\dagger(-\frac{i}{2}\overleftrightarrow{\mathbf{D}}\cdot\boldsymbol{\sigma})\psi|\chi_{c0}\rangle\,\langle\chi_{c0}|\psi^\dagger(g\mathbf{E}\cdot\boldsymbol{\sigma})\chi|0\rangle + \text{h.c.}\right) \\
&\equiv \frac{F_1(^3P_0)}{m_Q^2}\,\langle 0|\mathcal{O}_1(^3P_0)|0\rangle + \frac{G_1(^3P_0)}{m_Q^4}\,\langle 0|\mathcal{P}_1(^3P_0)|0\rangle + \frac{T_8(^3P_0)}{m_Q^3}\,\langle 0|\mathcal{T}_8(^3P_0)|0\rangle\,, \quad (14.11a)
\end{aligned}$$

$$\begin{aligned}
\sigma(e^+e^- \to \chi_{c1}\gamma) &= \frac{F_1(^3P_1)}{2m_Q^2}\,\langle 0|\chi^\dagger(-\frac{i}{2}\overleftrightarrow{\mathbf{D}}\times\boldsymbol{\sigma})\psi|\chi_{c1}\rangle\,\langle\chi_{c1}|\psi^\dagger(-\frac{i}{2}\overleftrightarrow{\mathbf{D}}\times\boldsymbol{\sigma})\chi|0\rangle \\
&+ \frac{G_1(^3P_1)}{4m_Q^4}\left(\langle 0|\chi^\dagger(-\frac{i}{2}\overleftrightarrow{\mathbf{D}}\times\boldsymbol{\sigma})\psi|\chi_{c1}\rangle\,\langle\chi_{c1}|\psi^\dagger(-\frac{i}{2}\overleftrightarrow{\mathbf{D}}\times\boldsymbol{\sigma})(-\frac{i}{2}\overleftrightarrow{\mathbf{D}})^2\chi|0\rangle + \text{h.c.}\right) \\
&+ \frac{iT_8(^3P_1)}{2m_Q^3}\left(\langle 0|\chi^\dagger(-\frac{i}{2}\overleftrightarrow{\mathbf{D}}\times\boldsymbol{\sigma})\psi|\chi_{c1}\rangle\,\langle\chi_{c1}|\psi^\dagger(g\mathbf{E}\times\boldsymbol{\sigma})\chi|0\rangle + \text{h.c.}\right) \\
&\equiv \frac{F_1(^3P_1)}{m_Q^2}\,\langle 0|\mathcal{O}_1(^3P_1)|0\rangle + \frac{G_1(^3P_1)}{m_Q^4}\,\langle 0|\mathcal{P}_1(^3P_1)|0\rangle + \frac{T_8(^3P_1)}{m_Q^3}\,\langle 0|\mathcal{T}_8(^3P_1)|0\rangle\,, \quad (14.11b)
\end{aligned}$$

$$\begin{aligned}
\sigma(e^+e^- \to \chi_{c2}\gamma) &= \frac{F_1(^3P_2)}{m_Q^2}\,\langle 0|\chi^\dagger(-\frac{i}{2}\overleftrightarrow{\mathbf{D}}^{(i}\boldsymbol{\sigma}^{j)})\psi|\chi_{c2}\rangle\,\langle\chi_{c2}|\psi^\dagger(-\frac{i}{2}\overleftrightarrow{\mathbf{D}}^{(i}\boldsymbol{\sigma}^{j)})\chi|0\rangle \\
&+ \frac{G_1(^3P_2)}{2m_Q^4}\left(\langle 0|\chi^\dagger(-\frac{i}{2}\overleftrightarrow{\mathbf{D}}^{(i}\boldsymbol{\sigma}^{j)})\psi|\chi_{c2}\rangle\,\langle\chi_{c2}|\psi^\dagger(-\frac{i}{2}\overleftrightarrow{\mathbf{D}}^{(i}\boldsymbol{\sigma}^{j)})(-\frac{i}{2}\overleftrightarrow{\mathbf{D}})^2\chi|0\rangle + \text{h.c.}\right) \\
&+ \frac{iT_8(^3P_2)}{m_Q^3}\left(\langle 0|\chi^\dagger(-\frac{i}{2}\overleftrightarrow{\mathbf{D}}^{(i}\boldsymbol{\sigma}^{j)})\psi|\chi_{c2}\rangle\,\langle\chi_{c2}|\psi^\dagger(g\mathbf{E}^{(i}\boldsymbol{\sigma}^{j)})\chi|0\rangle + \text{h.c.}\right) \\
&\equiv \frac{F_1(^3P_2)}{m_Q^2}\,\langle 0|\mathcal{O}_1(^3P_2)|0\rangle + \frac{G_1(^3P_2)}{m_Q^4}\,\langle 0|\mathcal{P}_1(^3P_2)|0\rangle + \frac{T_8(^3P_2)}{m_Q^3}\,\langle 0|\mathcal{T}_8(^3P_2)|0\rangle\,, \quad (14.11c)
\end{aligned}$$

with $\mathbf{a}^{(i}\mathbf{b}^{j)} \equiv \frac{\mathbf{a}^i\mathbf{b}^j+\mathbf{a}^j\mathbf{b}^i}{2} - \frac{1}{3}\delta^{ij}(\mathbf{a}\cdot\mathbf{b})$. The subscript 1 in the names of operators is used to indicate that the operator contributes through the dominant Fock $|Q\bar{Q}\rangle$, while an operator with the subscript 8 is nonvanishing only for the subleading Fock state $|Q\bar{Q}g\rangle$. The absence of the BBL subscript means that we use matrix elements normalized relativistically, i. e.

$$\langle H(\mathbf{P})|H(\mathbf{P}')\rangle = 2E_{\mathbf{P}}(2\pi)^3\delta^3(\mathbf{P}-\mathbf{P}'). \tag{14.12}$$

The exact nonperturbative relation between quarkonium-to-vacuum matrix elements with relativistic and nonrelativistic normalizations is given by [213]

$$\langle H|\psi^\dagger\mathcal{K}\chi|0\rangle = \sqrt{2M_H}\,\langle H|\psi^\dagger\mathcal{K}\chi|0\rangle_{\text{BBL}}\,, \tag{14.13}$$

where $M_{\chi_{cJ}}$ denotes the physical quarkonium mass. Relativistic normalization of matrix elements is very convenient in perturbative matching calculations, while final results are usually given in terms of LDMEs with nonrelativistic normalization. In this work we will also follow this strategy.

According to the power counting rules, the scaling of $\langle 0|\mathcal{O}_1(^3P_J)|0\rangle$ is v^5, while $\langle 0|\mathcal{P}_1(^3P_J)|0\rangle$ scales as v^7 due to the presence of two additional covariant derivatives. In comparison to $\langle 0|\mathcal{O}_1(^3P_J)|0\rangle$ the matrix element $\langle 0|\mathcal{T}_8(^3P_J)|0\rangle$ contains one covariant derivative less, but depends on the chromoelectric field, which scales as v^3 so that the absolute size of this LDME is also v^7.

It is worth noting that vacuum expectation values of operators like Eq. (14.8) that contribute through the subleading Fock state $|Q\bar{Q}g\rangle$ contain additional suppression of $\mathcal{O}(v)$, if the $Q\bar{Q}$ pair in the color octet configuration is produced with a different angular momentum than the $Q\bar{Q}$ pair in the dominant Fock state. The reason for this is that in the corresponding short-distance process we create a color octet $Q\bar{Q}$ pair that emits a soft gluon during its nonperturbative evolution into a heavy quarkonium. The emission of the gluon that changes the orbital angular momentum of the pair by one unit and converts it into a color singlet, corresponds to an E1 transition, which leads to the extra suppression.

However, according to the power counting rules from [7], for LDMEs that contain chromoelectric fields, the additional $\mathcal{O}(v)$ suppression is already accounted for in the power counting rule for $\mathbf{E}^2$. This is why $\langle 0|\mathcal{T}_8(^3P_J)|0\rangle$ is only $\mathcal{O}(v^2)$ suppressed as compared to $\langle 0|\mathcal{O}_1(^3P_J)|0\rangle$ and hence as important as $\langle 0|\mathcal{P}_1(^3P_J)|0\rangle$.

Eqs. (14.11) depend on 9 matching coefficients. The matching coefficients $F_1(^3P_J)$ and $G_1(^3P_J)$ at $\mathcal{O}(\alpha_s^0)$ were reported in [203] and [28, 29] respectively. The authors of [28, 29] worked at $\mathcal{O}(v^2)$ and therefore should have included the operators $\langle 0|\mathcal{T}_8(^3P_J)|0\rangle$ in their cross section formulas. Since this was not done, the corresponding matching coefficients $T_8(^3P_J)$ remain unknown, which means that the $\mathcal{O}(\alpha_s^0 v^2)$ and $\mathcal{O}(\alpha_s v^2)$ corrections to $e^+e^- \to \gamma^* \to \chi_{cJ}\,\gamma$ reported in [28–30] are incomplete.

In this work we for the first time compute the values of $T_8(^3P_J)$ at $\mathcal{O}(\alpha_s^0)$. This is the last missing piece to have the complete $\mathcal{O}(v^2)$ corrections for exclusive electromagnetic production of χ_{cJ} and a hard photon. The calculation is essentially tree-level, but nontrivial, as we need to work with a quarkonium composed of two heavy quarks and a gluon. The strategies to determine $T_8(^3P_J)$ from matching between QCD and NRQCD will be discussed in the next section.

[2] We thanks G. Bodwin for communications on this point, c. f. also [174]

15 Strategies to Determine NRQCD Matching Coefficients

15.1 Possible Matching Conditions

There exist different approaches to calculate the NRQCD matching coefficients in a quarkonium production process. In all of them matching is done between perturbative QCD and perturbative NRQCD, relying on the same behavior of both theories at low energies. The NRQCD matrix elements are evaluated in such a way, that the quarkonium Fock states are replaced by the perturbative Fock states that contain on-shell quarkonium constituents, e. g.

$$\langle 0|\chi^\dagger \mathcal{K}_n \psi|H\rangle \langle H|\psi^\dagger \mathcal{K}'_n \chi|0\rangle \to \langle 0|\chi^\dagger \mathcal{K}_n \psi|Q\bar{Q}\rangle \langle Q\bar{Q}|\psi^\dagger \mathcal{K}'_n \chi|0\rangle \,. \tag{15.1}$$

The explicit calculation of matrix elements on the right-hand side of Eq. (15.1) in perturbative NRQCD will be explained in Sec. 16. To deduce the values of the coefficients multiplying such matrix elements, we need to impose a relation between suitable quantities (e. g. Green's functions, cross sections, on-shell amplitudes etc.) in QCD and NRQCD. In EFTs such relations are called matching conditions.

In [7] the matching condition for quarkonium production was given as

$$\sigma(Q\bar{Q})|_{\text{pert. QCD}} = \sum_n \frac{F_n}{m_Q^{d_n-4}} \langle 0|\mathcal{O}_n^{Q\bar{Q}}|0\rangle \,|_{\text{pert. NRQCD}}, \tag{15.2}$$

which imposes an equality between the partonic cross section to produce an on-shell heavy quark pair in perturbative QCD and the sum of suitable LDMEs multiplied by matching coefficients F_n and inverse powers of the heavy quark mass in perturbative NRQCD. Assuming that the relative momentum of the heavy quarks in the rest frame $\mathbf{q}$ is small, one can expand both sides of Eq. (15.2) in $|\mathbf{q}|/m_Q$. With this nonrelativistic expansion one can read-off the values of the matching coefficients F_n and then substitute them into the NRQCD-factorized production cross section. A more technical explanation of this approach can be found in [214].

One of the difficulties related to practical applications of Eq. (15.2) is the necessity to perform nonrelativistic expansion of the phase-space measure on the QCD side of the matching. In processes, where the heavy quarkonium is produced together with other particles, such expansions tend to become complicated and require great care.

In case of exclusive reactions (such as our process of interest) it is also possible to employ NRQCD factorization at the amplitude level [213, 215],

$$\mathcal{A}_{\text{pert. QCD}} = \sum_n c_n^{i_1\ldots i_k} \langle Q\bar{Q}|\, \psi^\dagger \mathcal{K}_n^{i_1\ldots i_k} \chi\, |0\rangle \equiv \mathcal{A}_{\text{pert. NRQCD}}, \tag{15.3}$$

where $c_n^{i_1\ldots i_k}$ is a short-distance coefficient, which, depending on the form of $\mathcal{K}_n^{i_1\ldots i_k}$ can be a scalar or a tensor. Eq. (15.3) is an equality between the on-shell amplitude to produce a heavy quark pair in perturbative QCD and a sum of quarkonium-to-vacuum matrix elements multiplied or contracted with short-distance coefficients in perturbative NRQCD. Once the short-distance coefficients c_n are known, they can be substituted into the NRQCD-factorized production amplitude

$$\mathcal{A}_{\text{NRQCD}} = \sum_n c_n^{i_1\ldots i_k} \langle H|\, \psi^\dagger \mathcal{K}_n^{i_1\ldots i_k} \chi\, |0\rangle \,. \tag{15.4}$$

Squaring Eq. (15.4) and integrating over the phase space of the physical quarkonium we obtain NRQCD production cross sections as in Eqs. (14.11). Notice that, in general, not all matrix elements present in $\mathcal{A}_{\text{pert. NRQCD}}$ will also appear in $\mathcal{A}_{\text{NRQCD}}$. Since QCD amplitudes do not have definite angular momentum, in the matching we will determine more short-distance coefficients than required in Eqs. (14.11).

The great advantage of this method is that the matching can be done in a much simpler way, since it does not require us to compute the QCD matrix element squared and expand the phase space measure in $|\mathbf{q}|/m_Q$. Unfortunately, amplitude level matching is not applicable to inclusive processes. Since we are not affected by this limitation, in this work we calculate our matching coefficients by employing NRQCD factorization at the amplitude level.

15.2 Kinematics

Let us now explain the kinematics that will be used throughout this work. We need to distinguish between two frames of reference. The laboratory frame is the center of mass (CM) frame of the colliding leptons, where the heavy quarkonium and the photon fly away from the interaction point in opposite directions. The rest frame is the frame in which the heavy quarkonium is at rest.

Let us denote the 4-momenta of the heavy quarks and the gluon in the laboratory frame as p_1, p_2 and p_g respectively. Then k stands for the 4-momentum of the photon, while the momenta of the colliding leptons are given by l_1 and l_2. We will also make use of the polarization vectors for the photon ε, the gluon ε_g and the dilepton system $\ell^\mu \equiv e\bar{v}(l_2)\gamma^\mu u(l_1)$. The direction of photon 3-momentum is referred to as $\hat{\mathbf{k}} \equiv \mathbf{k}/|\mathbf{k}|$. In the matching all the external momenta are put on-shell and the masses of the leptons are neglected as compared to the CM energy s. Hence,

$$p_1^2 = p_2^2 = m_Q^2, \tag{15.5}$$

$$l_1^2 = l_2^2 = k^2 = p_g^2 = 0, \tag{15.6}$$

$$\varepsilon_p \cdot k = \varepsilon_g \cdot p_g = (l_1 + l_2) \cdot \ell = 0. \tag{15.7}$$

Finally, the 4-momentum of the heavy quarkonium is denoted by P. In the perturbative matching P is usually expressed in terms of the momenta of the quarkonium constituents, i. e. $P = p_1 + p_2$ for a $Q\bar{Q}$ system and $P = p_1 + p_2 + p_g$ for a $Q\bar{Q}g$ system. The same holds also for the value of P^2. In the nonperturbative context, however, P is regarded as the 4-momentum of the *physical* quarkonium, such that $P^2 = M_{\chi_{cJ}}^2$, where $M_{\chi_{cJ}}$ denotes the mass of χ_{cJ} measured in experiments. We will explicitly state, which meaning we assign to P at different stages of this work.

To distinguish the laboratory frame momenta from the rest frame momenta, the latter carry an additional subscript R. For example, when considering the $Q\bar{Q}$ system, it is convenient to introduce the relative momentum of the heavy quarks in the rest frame, defined as $\mathbf{q} \equiv \frac{1}{2}(\mathbf{p}_{1,R} - \mathbf{p}_{2,R})$. In case of the $Q\bar{Q}g$ system, two relative momenta are needed, given by

$$\mathbf{q}_1 = \frac{1}{2}\left(\mathbf{p}_{1,R} - \mathbf{p}_{2,R}\right), \qquad \mathbf{q}_2 = \frac{1}{6}\left(2\mathbf{p}_{g,R} - \mathbf{p}_{1,R} - \mathbf{p}_{2,R}\right). \tag{15.8}$$

More details regarding the kinematics of the $Q\bar{Q}$ and $Q\bar{Q}g$ systems can be found in the Appendix F.

15.3 Treatment of the QCD amplitudes

As all matching prescriptions involve nonrelativistic expansion of the perturbative QCD amplitudes, let us also briefly discuss different strategies to approach this task.

In [7] matching calculations for decays were done in such a way, that the expanded QCD amplitudes were explicitly rewritten in terms of energies, Cartesian 3-vectors, Pauli matrices and Pauli spinors. Since such objects naturally arise on the NRQCD side of the matching, having both sides of the matching equation expressed as products of 3-vectors and Pauli structures facilitates the extraction of the matching coefficients. This approach to NRQCD matching calculations was developed further and generalized to be applicable both to production and decays in [216] and [178]. In accordance with [178] we will denote it as threshold expansion method. Applying the technique developed by Braaten and Chen is conceptually simple, yet the calculations tend to become rather cumbersome when one goes beyond tree-level or leading order in v. In particular, the necessity to work with noncovariant objects on the QCD side of the matching makes such calculations quite tedious not only when done by hand but also when automatized with FORM [157] or similar symbolic manipulation systems.

The manifest Lorentz covariance of the QCD amplitudes can be preserved if one uses covariant projector technique [174]. This property is especially useful when the evaluation should be automatized using existing software for symbolic calculations in relativistic QFTs (e. g. FEYNCALC [20, 21], REDBERRY [217] or FDC [25] to name those that are often use in NRQCD calculations). This is one of the main reasons why almost all modern NRQCD matching calculations are done using projectors.

For the present calculation we, however, decided not to use this approach. The reason for this, is that it is not so clear how to use projector technique to extract matching coefficient multiplying matrix elements such as $\langle 0|\mathcal{T}_8(^3P_J)|0\rangle$. On the other hand, the calculation of matching coefficients $T_8(^3P_J)$ using the threshold expansion method and matching at the amplitude level is straightforward, albeit tedious. Similar calculations have already been done in the investigation of the electromagnetic decay $\chi_{cJ} \to \gamma\gamma$ [26, 27], such that one can benefit from the existing knowledge on this subject.

To automatize our matching calculations we use FEYNARTS [148], FEYNCALC, FORM and FEYNCALCFORMLINK [22] as well as self-written MATHEMATICA codes.

16 Calculation of the NRQCD Amplitudes

16.1 NRQCD-factorized Production Amplitudes and Cross Sections

In order to apply the threshold expansion method at the amplitude level, we introduce NRQCD production amplitudes at $\mathcal{O}(v^2)$ relative to the scaling of the leading order quarkonium-to-vacuum matrix element

$$\mathcal{A}^{J=0}_{\rm NRQCD} = \frac{c_1^{J=0}}{m_Q^2}\,\langle\chi_{c0}|\psi^\dagger\left(-\frac{i}{2}\overleftrightarrow{\mathbf{D}}\cdot\boldsymbol{\sigma}\right)\chi|0\rangle + \frac{c_3^{J=0}}{m_Q^4}\,\langle\chi_{c0}|\psi^\dagger\left(-\frac{i}{2}\overleftrightarrow{\mathbf{D}}\cdot\boldsymbol{\sigma}\right)\left(-\frac{i}{2}\overleftrightarrow{\mathbf{D}}\right)^2\chi|0\rangle$$
$$+\frac{d_1^{J=0}}{m_Q^3}\,\langle\chi_{c0}|\psi^\dagger g\mathbf{E}\cdot\boldsymbol{\sigma}\chi|0\rangle\,, \tag{16.1a}$$

$$\mathcal{A}^{J=1}_{\rm NRQCD} = \frac{(c_1^{J=1})^i}{m_Q^2}\,\langle\chi_{c1}|\psi^\dagger\left(-\frac{i}{2}\overleftrightarrow{\mathbf{D}}\times\boldsymbol{\sigma}\right)^i\chi|0\rangle$$
$$+\frac{(c_3^{J=1})^i}{m_Q^4}\,\langle\chi_{c1}|\psi^\dagger\left(-\frac{i}{2}\overleftrightarrow{\mathbf{D}}\times\boldsymbol{\sigma}\right)^i\left(-\frac{i}{2}\overleftrightarrow{\mathbf{D}}\right)^2\chi|0\rangle + \frac{(d_1^{J=1})^i}{m_Q^3}\,\langle\chi_{c1}|\psi^\dagger(g\mathbf{E}\times\boldsymbol{\sigma})^i\chi|0\rangle\,, \tag{16.1b}$$

$$\mathcal{A}^{J=2}_{\rm NRQCD} = \frac{(c_1^{J=2})^{ij}}{m_Q^2}\,\langle\chi_{c2}|\psi^\dagger\left(-\frac{i}{2}\overleftrightarrow{\mathbf{D}}^{(i}\boldsymbol{\sigma}^{j)}\right)\chi|0\rangle$$
$$+\frac{(c_3^{J=2})^{ij}}{m_Q^4}\,\langle\chi_{c2}|\psi^\dagger\left(-\frac{i}{2}\overleftrightarrow{\mathbf{D}}^{(i}\boldsymbol{\sigma}^{j)}\right)\left(-\frac{i}{2}\overleftrightarrow{\mathbf{D}}\right)^2\chi|0\rangle + \frac{(d_1^{J=})^{ij}}{m_Q^3}\,\langle\chi_{c2}|\psi^\dagger g\mathbf{E}^{(i}\boldsymbol{\sigma}^{j)}\chi|0\rangle\,. \tag{16.1c}$$

The scaling of these matrix elements in v is estimated according to the same power-counting rules as used in the discussion of Eqs. (14.11). For example, the matrix element $\langle\chi_{c0}|\psi^\dagger\left(-\frac{i}{2}\overleftrightarrow{\mathbf{D}}\cdot\boldsymbol{\sigma}\right)\chi|0\rangle$ scales as $v^{5/2}$, while the scaling of $\langle\chi_{c0}|\psi^\dagger g\mathbf{E}\cdot\boldsymbol{\sigma}\chi|0\rangle$ is $v^{9/2}$. As explained in Sec. 15, to arrive to production cross sections, we need to square the amplitudes in Eq. (16.1), average over the polarizations of the leptons, sum over the polarizations of the photon and integrate over the phase space for producing a heavy quarkonium and a photon

$$\sigma(e^+e^-\to\chi_{cJ}\gamma) = (2J+1)\int d\Phi_J\frac{1}{4}\sum_{\rm pols}|\mathcal{A}^J_{\rm NRQCD}|^2, \tag{16.2}$$

where pols refers to the photon polarizations. The prefactor $(2J+1)$ appears because of our redefinition of the matching coefficients in Eq. (14.7) and the phase space measure is given by

$$d\Phi_J = \frac{s-M_{\chi_{cJ}}^2}{64\pi^2 s^2}d\Omega_k \tag{16.3}$$

with the integration done over the solid angle of the photon 3-momentum $\mathbf{k}$. This yields

$$\sigma(e^+e^-\to\chi_{c0}\gamma) = \int d\Phi_0\frac{1}{4}\sum_{\rm pols}\left(3\frac{|c_1^{J=0}|^2}{m_Q^4}\,\langle 0|\mathcal{O}_1(^3P_0)|0\rangle\right.$$

$$+ 6\frac{c_1^{J=0}(c_3^{*J=0})}{m_Q^6}\langle 0|\mathcal{P}_1(^3P_0)|0\rangle - 3i\frac{c_1^{J=0}(d_1^{*J=0})}{m_Q^5}\langle 0|\mathcal{T}_8(^3P_0)|0\rangle\Big), \tag{16.4a}$$

$$\sigma(e^+e^-\to\chi_{c1}\gamma) = \int d\Phi_1\frac{1}{4}\sum_{\text{pols}}\Big(2\frac{(c_1^{J=1})^i(c_1^{*J=1})^i}{m_Q^4}\langle 0|\mathcal{O}_1(^3P_1)|0\rangle$$
$$+ 4\frac{(c_1^{J=1})^i(c_3^{*J=1})^i}{m_Q^6}\langle 0|\mathcal{P}_1(^3P_1)|0\rangle - 2i\frac{(c_1^{J=1})^i(d_1^{*J=1})^i}{m_Q^5}\langle 0|\mathcal{T}_8(^3P_1)|0\rangle\Big), \tag{16.4b}$$

$$\sigma(e^+e^-\to\chi_{c2}\gamma) = \int d\Phi_2\frac{1}{4}\sum_{\text{pols}}\Big(\frac{1}{m_Q^4}\left[(c_1^{J=2})^{ij}(c_1^{*J=2})^{ij} - \frac{1}{3}(c_1^{J=2})^{ii}(c_1^{*J=2})^{jj}\right]$$
$$\times\langle 0|\mathcal{O}_1(^3P_2)|0\rangle + \frac{2}{m_Q^6}\left[(c_1^{J=2})^{ij}(c_3^{*J=2})^{ij} - \frac{1}{3}(c_1^{J=2})^{ii}(c_3^{*J=2})^{jj}\right]\langle 0|\mathcal{P}_1(^3P_2)|0\rangle$$
$$- \frac{i}{m_Q^5}\left[(c_1^{J=2})^{ij}(d_1^{*J=2})^{ij} - \frac{1}{3}(c_1^{J=2})^{ii}(d_1^{*J=2})^{jj}\right]\langle 0|\mathcal{T}_8(^3P_2)|0\rangle\Big), \tag{16.4c}$$

where we used that $c_1c_3^* = c_3c_1^*$ and $c_1^*d_1 = -c_1d_1^*$.

Comparing Eq. (16.4) with Eq. (14.11) we can express the matching coefficients $F_1(^3P_J)$, $G_1(^3P_J)$ and $T_8(^3P_J)$ through the short-distance coefficients c_1, c_3 and d_1

$$F_1(^3P_0) = \int d\Phi_0\frac{1}{4}\sum_{\text{pols}}3\frac{|c_1^{J=0}|^2}{m_Q^2}, \tag{16.5a}$$

$$G_1(^3P_0) = \int d\Phi_0\frac{1}{4}\sum_{\text{pols}}6\frac{c_1^{J=0}(c_3^{*J=0})}{m_Q^2}, \tag{16.5b}$$

$$T_8(^3P_0) = -i\int d\Phi_0\frac{1}{4}\sum_{\text{pols}}3\frac{c_1^{J=0}(d_1^{*J=0})}{m_Q^2}, \tag{16.5c}$$

$$F_1(^3P_1) = \int d\Phi_1\frac{1}{4}\sum_{\text{pols}}2\frac{(c_1^{J=1})^i(c_1^{*J=1})^i}{m_Q^2}, \tag{16.5d}$$

$$G_1(^3P_1) = \int d\Phi_1\frac{1}{4}\sum_{\text{pols}}4\frac{(c_1^{J=1})^i(c_3^{*J=1})^i}{m_Q^2}, \tag{16.5e}$$

$$T_8(^3P_1) = -i\int d\Phi_1\frac{1}{4}\sum_{\text{pols}}2\frac{(c_1^{J=1})^i(d_1^{*J=1})^i}{m_Q^2}, \tag{16.5f}$$

$$F_1(^3P_2) = \int d\Phi_2\frac{1}{4}\sum_{\text{pols}}\frac{(c_1^{J=2})^{ij}(c_1^{*J=2})^{ij} - \frac{1}{3}(c_1^{J=2})^{ii}(c_1^{*J=2})^{jj}}{m_Q^2}, \tag{16.5g}$$

$$G_1(^3P_2) = \int d\Phi_2\frac{1}{4}\sum_{\text{pols}}\frac{(c_1^{J=2})^{ij}(c_3^{*J=2})^{ij} - \frac{1}{3}(c_1^{J=2})^{ii}(c_3^{*J=2})^{jj}}{m_Q^2}, \tag{16.5h}$$

$$T_8(^3P_2) = -i\int d\Phi_2\frac{1}{4}\sum_{\text{pols}}\frac{(c_1^{J=2})^{ij}(d_1^{*J=2})^{ij} - \frac{1}{3}(c_1^{J=2})^{ii}(d_1^{*J=2})^{jj}}{m_Q^2}. \tag{16.5i}$$

Our task is to calculate $T_8(^3P_J)$ at $\mathcal{O}(\alpha_s^0)$, which can be inferred from the knowledge

of c_1 and d_1. To determine these short-distance coefficients we need to carry out the matching between perturbative QCD and perturbative NRQCD at the amplitude level.

16.2 Computation of the NRQCD Amplitudes

The perturbative NRQCD matrix elements are most conveniently evaluated in the operator formalism by rewriting heavy quark fields in terms of Pauli spinors and single fermion creation and annihilation operators, as explained in [124]. In variance with [124], in the matching we use relativistic normalization of the Fock states. The evaluation of matrix elements that enter perturbative NRQCD amplitudes is straightforward. For example, replacing $|H\rangle$ with $|Q(\mathbf{p}_{1,R})\bar{Q}(\mathbf{p}_{2,R})\rangle$ and $|Q(\mathbf{p}_{1,R})\bar{Q}(\mathbf{p}_{2,R})g(\mathbf{p}_{g,R})\rangle$ in $\mathcal{A}^{J=0}_{\text{NRQCD}}$ from Eq. (16.1a) we find

$$\langle Q(\mathbf{p}_{1,R})\bar{Q}(\mathbf{p}_{2,R})|\psi^\dagger\left(-\frac{i}{2}\overleftrightarrow{\mathbf{D}}\cdot\boldsymbol{\sigma}\right)\chi|0\rangle = \xi^\dagger(\boldsymbol{\sigma}\cdot\mathbf{q})\eta, \tag{16.6}$$

$$\langle Q(\mathbf{p}_{1,R})\bar{Q}(\mathbf{p}_{2,R})|\psi^\dagger\left(-\frac{i}{2}\overleftrightarrow{\mathbf{D}}\cdot\boldsymbol{\sigma}\right)\left(-\frac{i}{2}\overleftrightarrow{\mathbf{D}}\right)^2\chi|0\rangle = \mathbf{q}^2\xi^\dagger(\boldsymbol{\sigma}\cdot\mathbf{q})\eta, \tag{16.7}$$

$$\langle Q(\mathbf{p}_{1,R})\bar{Q}(\mathbf{p}_{2,R})|\psi^\dagger g\mathbf{E}\cdot\boldsymbol{\sigma}\chi|0\rangle = 0, \tag{16.8}$$

$$\langle Q(\mathbf{p}_{1,R})\bar{Q}(\mathbf{p}_{2,R})g(\mathbf{p}_{g,R})|\psi^\dagger\left(-\frac{i}{2}\overleftrightarrow{\mathbf{D}}\cdot\boldsymbol{\sigma}\right)\chi|0\rangle = -g\xi^\dagger(\boldsymbol{\sigma}\cdot\boldsymbol{\varepsilon}^*_{g,R})\eta, \tag{16.9}$$

$$\begin{aligned}\langle Q(\mathbf{p}_{1,R})\bar{Q}(\mathbf{p}_{2,R})g(\mathbf{p}_{g,R})|\psi^\dagger\left(-\frac{i}{2}\overleftrightarrow{\mathbf{D}}\cdot\boldsymbol{\sigma}\right)\left(-\frac{i}{2}\overleftrightarrow{\mathbf{D}}\right)^2\chi|0\rangle &= -g\xi^\dagger\boldsymbol{\sigma}^i\eta \\ &\quad\times(2\mathbf{q}^i(\mathbf{q}\cdot\boldsymbol{\varepsilon}^{*i}_{g,R}) + \boldsymbol{\varepsilon}^{*i}_{g,R}\mathbf{q}^2),\end{aligned} \tag{16.10}$$

$$\langle Q(\mathbf{p}_{1,R})\bar{Q}(\mathbf{p}_{2,R})g(\mathbf{p}_{g,R})|\psi^\dagger g\mathbf{E}\cdot\boldsymbol{\sigma}\chi|0\rangle = -ig|\mathbf{k}_g|\xi^\dagger(\boldsymbol{\sigma}\cdot\boldsymbol{\varepsilon}^*_{g,R})\eta. \tag{16.11}$$

Notice that although matrix elements that are free of $\mathbf{E}$ contribute through the leading Fock state $|Q\bar{Q}\rangle$, because of the covariant derivative that contains the gluon field they also give a nonvanishing contribution to the subleading Fock state $|Q\bar{Q}g\rangle$.

The full calculation on the NRQCD side of the matching is, however, slightly more involved. As explained in Sec. 15, in the matching we usually determine more matching coefficients than needed to compute production cross sections. Therefore, it is not surprising that our perturbative NRQCD amplitudes contain more quarkonium-to-vacuum matrix elements than the amplitudes in Eqs. (16.5). For example, apart from the P-wave spin triplet quarkonium (χ_{cJ}) we may also produce the S-wave spin singlet quarkonium (η_c). Even though we are actually not interested in the latter, we still have to determine short-distance coefficients of the corresponding operators. In fact, this property of the threshold expansion method provides an important consistency check of the whole matching calculation: if the short-distance coefficients were determined correctly, the difference

$$\mathcal{A}_{\text{pert. QCD}} - \mathcal{A}_{\text{pert. NRQCD}} \tag{16.12}$$

is exactly zero order by order in v. The NRQCD amplitudes relevant for the perturbative matching read

$$\mathcal{A}^{J=0}_{\text{pert. NRQCD}} = \frac{c_0^{J=0}}{m_Q}\langle H|\psi^\dagger\chi|0\rangle + \frac{c_1^{J=0}}{m_Q^2}\langle H|\psi^\dagger\left(-\frac{i}{2}\overleftrightarrow{\mathbf{D}}\cdot\boldsymbol{\sigma}\right)\chi|0\rangle$$

$$
\begin{aligned}
&+\frac{c_2^{J=0}}{m_Q^3}\,\langle H|\psi^\dagger\left(-\frac{i}{2}\overleftrightarrow{\mathbf{D}}\right)^2\chi|0\rangle+\frac{c_3^{J=0}}{m_Q^4}\,\langle H|\psi^\dagger\left(-\frac{i}{2}\overleftrightarrow{\mathbf{D}}\cdot\boldsymbol{\sigma}\right)\left(-\frac{i}{2}\overleftrightarrow{\mathbf{D}}\right)^2\chi|0\rangle\\
&+\frac{d_0^{J=0}}{m_Q^3}\,\langle H|\psi^\dagger g\mathbf{B}\cdot\boldsymbol{\sigma}\chi|0\rangle+\frac{d_1^{J=0}}{m_Q^3}\,\langle H|\psi^\dagger g\mathbf{E}\cdot\boldsymbol{\sigma}\chi|0\rangle\\
&+\frac{c_0^{J=0}}{m_Q}\,\langle H|\psi^\dagger\chi|0\rangle_{\mathcal{L}_{2-f}}+\frac{c_1^{J=0}}{m_Q^2}\,\langle H|\psi^\dagger\left(-\frac{i}{2}\overleftrightarrow{\mathbf{D}}\cdot\boldsymbol{\sigma}\right)\chi|0\rangle_{\mathcal{L}_{2-f}}\\
&+\frac{c_2^{J=0}}{m_Q^3}\,\langle H|\psi^\dagger\left(-\frac{i}{2}\overleftrightarrow{\mathbf{D}}\right)^2\chi|0\rangle_{\mathcal{L}_{2-f}}
\end{aligned}
\tag{16.13a}
$$

$$
\begin{aligned}
\mathcal{A}^{J=1}_{\text{pert. NRQCD}}&=\frac{(c_1^{J=1})^i}{m_Q^2}\,\langle H|\psi^\dagger\left(-\frac{i}{2}\overleftrightarrow{\mathbf{D}}\times\boldsymbol{\sigma}\right)^i\chi|0\rangle\\
&+\frac{(c_3^{J=0})^i}{m_Q^4}\,\langle H|\psi^\dagger\left(-\frac{i}{2}\overleftrightarrow{\mathbf{D}}\times\boldsymbol{\sigma}\right)^i\left(-\frac{i}{2}\overleftrightarrow{\mathbf{D}}\right)^2\chi|0\rangle+\frac{(d_0^{J=0})^i}{m_Q^3}\,\langle H|\psi^\dagger(g\mathbf{B}\times\boldsymbol{\sigma})^i\chi|0\rangle\\
&+\frac{(d_1^{J=0})^i}{m_Q^3}\,\langle H|\psi^\dagger(g\mathbf{E}\times\boldsymbol{\sigma})^i\chi|0\rangle+\frac{(c_1^{J=1})^i}{m_Q^2}\,\langle H|\psi^\dagger\left(-\frac{i}{2}\overleftrightarrow{\mathbf{D}}\times\boldsymbol{\sigma}\right)^i\chi|0\rangle_{\mathcal{L}_{2-f}},
\end{aligned}
\tag{16.13b}
$$

$$
\begin{aligned}
\mathcal{A}^{J=2}_{\text{pert. NRQCD}}&=\frac{(c_1^{J=0})^{ij}}{m_Q^2}\,\langle H|\psi^\dagger\left(-\frac{i}{2}\overleftrightarrow{\mathbf{D}}^{(i}\boldsymbol{\sigma}^{j)}\right)\chi|0\rangle+\frac{(c_2^{J=0})^{ij}}{m_Q^3}\,\langle H|\psi^\dagger\left(-\frac{i}{2}\right)^2\overleftrightarrow{\mathbf{D}}^{(i}\overleftrightarrow{\mathbf{D}}^{j)}\chi|0\rangle\\
&+\frac{(c_3^{J=0})^{ij}}{m_Q^4}\,\langle H|\psi^\dagger\left(-\frac{i}{2}\overleftrightarrow{\mathbf{D}}^{(i}\boldsymbol{\sigma}^{j)}\right)\left(-\frac{i}{2}\overleftrightarrow{\mathbf{D}}\right)^2\chi|0\rangle\\
&+\frac{(d_0^{J=0})^{ij}}{m_Q^3}\,\langle H|\psi^\dagger g\mathbf{B}^{(i}\boldsymbol{\sigma}^{j)}\chi|0\rangle+\frac{(d_1^{J=0})^{ij}}{m_Q^3}\,\langle H|\psi^\dagger g\mathbf{E}^{(i}\boldsymbol{\sigma}^{j)}\chi|0\rangle\\
&+\frac{(c_1^{J=0})^{ij}}{m_Q^2}\,\langle H|\psi^\dagger\left(-\frac{i}{2}\overleftrightarrow{\mathbf{D}}^{(i}\boldsymbol{\sigma}^{j)}\right)\chi|0\rangle_{\mathcal{L}_{2-f}}+\frac{(c_2^{J=0})^{ij}}{m_Q^3}\,\langle H|\psi^\dagger\left(-\frac{i}{2}\right)^2\overleftrightarrow{\mathbf{D}}^{(i}\overleftrightarrow{\mathbf{D}}^{j)}\chi|0\rangle_{\mathcal{L}_{2-f}}.
\end{aligned}
\tag{16.13c}
$$

Some explanations are in order. The matrix elements with the subscript $\mathcal{L}_{2-f}$ contain Lagrangian insertions, where the relevant part of the NRQCD Lagrangian (2-fermion sector only) is

$$
\begin{aligned}
\mathcal{L}_{2-f}=\psi^\dagger&\left(\frac{\mathbf{D}^2}{2m}+\frac{\boldsymbol{\sigma}\cdot g\mathbf{B}}{2m_Q}+\frac{[\mathbf{D}\cdot,g\mathbf{E}]}{8m_Q^2}+\frac{i\boldsymbol{\sigma}\cdot[\mathbf{D}\times,g\mathbf{E}]}{8m_Q^2}+\frac{\mathbf{D}^4}{8m_Q^3}+\frac{\{\mathbf{D}^2,\boldsymbol{\sigma}\cdot g\mathbf{B}\}}{8m_Q^3}\right)\psi\\
+\chi^\dagger&\left(-\frac{\mathbf{D}^2}{2m}-\frac{\boldsymbol{\sigma}\cdot g\mathbf{B}}{2m_Q}+\frac{[\mathbf{D}\cdot,g\mathbf{E}]}{8m_Q^2}+\frac{i\boldsymbol{\sigma}\cdot[\mathbf{D}\times,g\mathbf{E}]}{8m_Q^2}-\frac{\mathbf{D}^4}{8m_Q^3}+\frac{\{\mathbf{D}^2,\boldsymbol{\sigma}\cdot g\mathbf{B}\}}{8m_Q^3}\right)\chi.
\end{aligned}
\tag{16.14}
$$

In the diagrammatic representation of the NRQCD vacuum-to-matrix elements, Lagrangian insertions correspond to the emission of a gluon from one of the external heavy quark lines. For example, for $\langle H|\psi^\dagger\chi|0\rangle$ and $\langle H|\psi^\dagger\chi|0\rangle_{\mathcal{L}_{2-f}}$ we have

$$
=i\,\langle Q(\mathbf{p}_{1,R})\bar{Q}(\mathbf{p}_{2,R})|\psi^\dagger\chi|0\rangle
\tag{16.15a}
$$

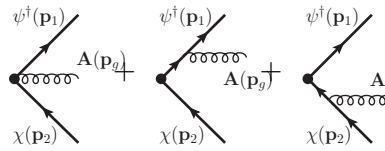

$$= i \langle Q(\mathbf{p}_{1,R}) \bar{Q}(\mathbf{p}_{2,R}) g(\mathbf{p}_{g,R}) | \psi^\dagger \chi | 0 \rangle_{\mathcal{L}_{2-f}} , \qquad (16.15b)$$

where the quark-quark-gluon vertex on the heavy quark (antiquark) line is understood as a sum of all the 6 vertices from quark-quark-gluon (antiquark-antiquark-gluon) interaction terms in Eq. (16.14). Hence, to calculate diagrams on the left hand side of Eq. (16.15b) we need to apply Feynman rules for the $\psi^\dagger \chi$ operator and for the interaction terms in Eq. (16.14).

The derivation of such Feynman rules in the operator approach is a simple QFT exercise: we sandwich the operator between vacuum and a Fock state that contains our fields (so that all momenta are ingoing), calculate the matrix element, amputate external states (Pauli spinors and polarization vectors) and multiply the result by i. For example, for the operator $\psi^\dagger \frac{\{\mathbf{D}^2, \boldsymbol{\sigma}\cdot g\mathbf{B}\}}{8m_Q^3}\psi$ we obtain

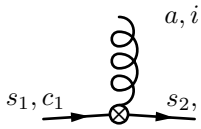

$$= \frac{1}{8m_Q^3}(2(\mathbf{p}_{g,R}\cdot\mathbf{p}_{1,R}) + 2\mathbf{p}_{1,R}^2 + \mathbf{p}_{g,R}^2)\varepsilon^{ijk}\boldsymbol{\sigma}^j_{s_1 s_2}\mathbf{p}^k_{g,R}T^a_{c_1 c_2}. \qquad (16.16)$$

Once we have the full expressions for the amplitudes in Eq. (16.13) with $|H\rangle$ replaced by perturbative $|Q\bar{Q}\rangle$ and $|Q\bar{Q}g\rangle$ Fock states, we can expand them in the relative momenta of quarkonium constituents. For the $Q\bar{Q}$ system we expand up to the third order in $|\mathbf{q}|/m_Q$, which permits us to determine the values of c_0, c_1, c_2 and c_3. In case of the $Q\bar{Q}g$ system it is sufficient to expand the amplitude up to the first order in $|\mathbf{q}_1|/m_Q$ and $|\mathbf{q}_2|/m_Q$, so that we can extract d_0 and d_1.

17 Calculation of the QCD Amplitudes

In this section we explain the nonrelativistic expansions of the relevant QCD amplitudes (c. f. Fig. 17.1) that describe exclusive electromagnetic production of $Q\bar{Q}$

$$e^-(l_1)\,e^+(l_2) \to Q(p_1)\,\bar{Q}(p_2)\,\gamma(k) \tag{17.1}$$

and $Q\bar{Q}g$

$$e^-(l_1)e^+(l_2) \to Q(p_1)\,\bar{Q}(p_2)\,g(p_g)\,\gamma(k). \tag{17.2}$$

The process in Eq. (17.1) is described by two QCD Feynman diagrams so that

$$\begin{aligned}\mathcal{A}^{Q\bar{Q}}_{\text{pert. QCD}} = &-\frac{ie^3Q^2g}{s}\bar{v}(l_2)\gamma_\mu\bar{u}(l_1)\\ &\times\left(\frac{\bar{u}(p_1,m_Q)\not{\epsilon}^*(\not{p}_1+\not{k}+m_Q)\gamma^\mu v(p_2,m_Q)}{((p_1+k)^2-m_Q^2)}\right.\\ &\left.+\frac{\bar{u}(p_1,m_Q)\gamma^\mu(-\not{p}_2-\not{k}+m_Q)\not{\epsilon}^* v(p_2,m_Q)}{((p_2+k)^2-m_Q^2)}\right),\end{aligned} \tag{17.3}$$

while the reaction in Eq. (17.2) requires six diagrams

$$\begin{aligned}\mathcal{A}^{Q\bar{Q}g}_{\text{pert. QCD}} = &-\frac{ie^3Q^2g}{s}\bar{v}(l_2)\gamma_\mu\bar{u}(l_1)T^a\Bigg(\\ &\times\frac{\bar{u}(p_1,m_Q)\not{\epsilon}_g^*(\not{p}_g+\not{p}_1+m_Q)\not{\epsilon}^*(\not{p}_1+\not{p}_g+\not{k}+m_Q)\gamma^\mu v(p_2,m_Q)}{((p_1+p_g)^2-m_Q^2)((p_1+p_g+k)^2-m_Q^2)}\\ &+\frac{\bar{u}(p_1,m_Q)\not{\epsilon}^*(\not{k}+\not{p}_1+m_Q)\not{\epsilon}^*(k_g)(\not{p}_1+\not{p}_g+\not{k}+m_Q)\gamma^\mu v(p_2,m_Q)}{((p_1+p_g)^2-m_Q^2)((p_1+p_g+k)^2-m_Q^2)}\\ &+\frac{\bar{u}(p_1,m_Q)\not{\epsilon}_g^*(\not{p}_1+\not{p}_g+m_Q)\gamma^\mu(-\not{p}_2-\not{k}+m_Q)\not{\epsilon}^* v(p_2,m_Q)}{((p_1+p_g)^2-m_Q^2)((p_2+k)^2-m_Q^2)}\\ &+\frac{\bar{u}(p_1,m_Q)\not{\epsilon}^*(\not{p}_1+\not{k}+m_Q)\gamma^\mu(-\not{p}_2-\not{p}_g+m_Q)\not{\epsilon}_g^* v(p_2,m_Q)}{((p_2+p_g)^2-m_Q^2)((p_1+k)^2-m_Q^2)}\\ &+\frac{\bar{u}(p_1,m_Q)\gamma^\mu(-\not{p}_2-\not{k}-\not{p}_g+m_Q)\not{\epsilon}^*(-\not{p}_2-\not{p}_g+m_Q)\not{\epsilon}_g^* v(p_2,m_Q)}{((p_2+p_g)^2-m_Q^2)((p_2+p_g+k)^2-m_Q^2)}\end{aligned} \tag{17.4}$$

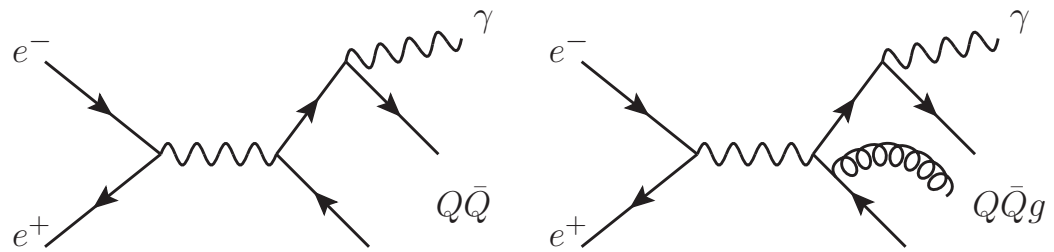

Figure 17.1: Representative QCD diagrams for the processes $e^+e^- \to Q\bar{Q}\gamma$ and $e^+e^- \to Q\bar{Q}g\gamma$ that are relevant for the matching to NRQCD. For the production of $Q\bar{Q}$ there are only two diagrams in total: the one displayed here and a second one where the photon is emitted from the heavy antiquark line. The production of $Q\bar{Q}g$ is described by six diagrams, where the gluon can be emitted before the photon or from a different heavy fermion line.

$$+\frac{\bar{u}(p_1,m_Q)\gamma^\mu(-\not{p}_2-\not{k}-\not{p}_g+m_Q)\not{\epsilon}_g^*(-\not{k}-\not{p}_2+m_Q)\not{\epsilon}^* v(p_2,m_Q)}{((p_2+k)^2-m_Q^2)((p_2+p_g+k)^2-m_Q^2)}\Bigg), \quad (17.5)$$

where Q denotes the heavy quark charge. The amplitudes $\mathcal{A}^{Q\bar{Q}}_{\text{pert. QCD}}$ and $\mathcal{A}^{Q\bar{Q}g}_{\text{pert. QCD}}$ can be evaluated in the laboratory frame or in the rest frame, although both approaches have their advantages and disadvantages. In the course of this study we carried out our calculations in both frames and arrived to the same results for the final matching coefficients.

In this calculation it is convenient to decompose all Dirac structures involving heavy quarks into scalar, pseudoscalar, vector, axial-vector and tensor components. Since this is a tree-level calculation in 4 dimensions, such decomposition is always possible. Then the amplitudes can be rewritten as

$$\mathcal{A}^{Q\bar{Q}}_{\text{pert. QCD}} = -\frac{ie^3Q^2g}{s}\left(j_1^\mu \bar{u}(p_1,m_Q)\gamma_\mu v(p_2,m_Q) + j_2^\mu \bar{u}(p_1,m_Q)\gamma_\mu\gamma_5 v(p_2,m_Q)\right), \quad (17.6)$$

$$\mathcal{A}^{Q\bar{Q}g}_{\text{pert. QCD}} = -\frac{ie^3Q^2g}{s}T^a\left(j_3^\mu \bar{u}(p_1,m_Q)\gamma_\mu v(p_2,m_Q) + j_4^\mu \bar{u}(p_1,m_Q)\gamma_\mu\gamma_5 v(p_2,m_Q)\right), \quad (17.7)$$

where the coefficients j_i^μ are free of heavy quark spinors. The vector and axial-vector structures $\bar{u}(p_1,m_Q)\gamma_\mu v(p_2,m_Q)$ and $\bar{u}(p_1,m_Q)\gamma_\mu\gamma_5 v(p_2,m_Q)$ can be rewritten in terms of Pauli matrices and spinors using formulas given in Appendix F. Furthermore, all the propagators and scalar products in j_i^μ have to be expressed in terms $\mathbf{q}$ (for $Q\bar{Q}$) or $\mathbf{q}_1$ and $\mathbf{q}_2$ (for $Q\bar{Q}g$). As in Sec. 16 we expand up to the third order in $|\mathbf{q}|/m_Q$ and up to the first order in $|\mathbf{q}_1|/m_Q$ and $|\mathbf{q}_2|/m_Q$.

The NRQCD amplitudes in Eq. 16.13 are given for different values of the total angular momentum J, but $\mathcal{A}^{Q\bar{Q}}_{\text{pert. QCD}}$ and $\mathcal{A}^{Q\bar{Q}g}_{\text{pert. QCD}}$ do not have definite angular momentum. However, on the QCD side we can identify Cartesian tensors that correspond to the matrix elements on the NRQCD side and decompose them into irreducible spherical tensors. For example, a term that contains the rank 2 tensor $\boldsymbol{\sigma}^i\mathbf{q}^j$ contracted with $\mathbf{a}^i\mathbf{b}^j$ and no further occurrences of $\mathbf{q}$ contributes to

$$\frac{c_1^{J=0}}{m_Q^2}\langle Q\bar{Q}|\psi^\dagger\left(-\frac{i}{2}\overleftrightarrow{\mathbf{D}}\cdot\boldsymbol{\sigma}\right)\chi|0\rangle \quad (17.8)$$

from $\mathcal{A}^{J=0}_{\text{pert. NRQCD}}$ but also to

$$\frac{(c_1^{J=1})^i}{m_Q^2}\langle Q\bar{Q}|\psi^\dagger\left(-\frac{i}{2}\overleftrightarrow{\mathbf{D}}\times\boldsymbol{\sigma}\right)^i\chi|0\rangle \quad (17.9)$$

from $\mathcal{A}^{J=1}_{\text{pert. NRQCD}}$ and

$$\frac{(c_1^{J=0})^{ij}}{m_Q^2}\langle Q\bar{Q}|\psi^\dagger\left(-\frac{i}{2}\overleftrightarrow{\mathbf{D}}^{(i}\boldsymbol{\sigma}^{j)}\right)\chi|0\rangle \quad (17.10)$$

from $\mathcal{A}^{J=2}_{\text{pert. NRQCD}}$. We can disentangle these contributions by explicitly projecting out the $J=0,1,2$ components of the tensor, i. e.

$$\mathbf{a}^i\mathbf{b}^j\boldsymbol{\sigma}^i\mathbf{q}^j \to \begin{cases} \frac{1}{3}\delta^{ij}a^ib^j(\boldsymbol{\sigma}\cdot\mathbf{q}) & \text{for } J=0 \\ \mathbf{a}^i\mathbf{b}^j\frac{\boldsymbol{\sigma}^i\mathbf{q}^j-\boldsymbol{\sigma}^j\mathbf{q}^i}{2} & \text{for } J=1 \\ \mathbf{a}^i\mathbf{b}^j\left(\frac{\boldsymbol{\sigma}^i\mathbf{q}^j+\boldsymbol{\sigma}^j\mathbf{q}^i}{2}-\frac{1}{3}\delta^{ij}(\boldsymbol{\sigma}\cdot\mathbf{q})\right) & \text{for } J=2 \end{cases} \quad (17.11)$$

Applying such projections to the whole QCD amplitudes allows us to do the matching between QCD and NRQCD for each J-value separately and successfully extract the short-distance coefficients order by order in the relative momenta.

Before presenting our results for the short-distance coefficients, we would like to mention that on the QCD side of the matching we encounter terms that are singular in the limit $|\mathbf{p}_g| \to 0$, i. e. proportional to $1/|\mathbf{p}_g|$. Such singularities arise when the gluon is emitted from one of the external heavy quark lines and should cancel in the matching. Indeed, matrix elements with Lagrangian insertions given in Eqs. (16.13) on the NRQCD side of the matching generate terms that precisely reproduce the singularities of the QCD amplitude. The cancellation of the $1/|\mathbf{p}_g|$ singularities on both sides of the matching was explicitly checked in the laboratory frame and in the rest frame. A more detailed discussion on this subject can be found in [27] and [118].

17.1 Matching in the Laboratory Frame

In the laboratory frame it is straightforward to carry out the phase space integration over products of the so determined short-distance coefficients in Eq. (16.5) and thus arrive to the final matching coefficients. The more complicated part of the calculation is the manipulation of the QCD amplitudes. Obviously, potentially large laboratory frame momenta of the heavy quarks and the gluon are not suitable parameters for doing nonrelativistic expansions. The correct expansion can be done only after these momenta are rewritten in terms of the small rest frame momenta, which greatly increases the number of intermediate terms.

Lorentz boost transformations that relate potentially large laboratory frame momenta of a $Q\bar{Q}$ system to the small rest frame momenta in a way, that is useful for NRQCD matching calculations, were introduced in [31]. In this work we generalize the formulas for a $Q\bar{Q}g$ system and summarize them in the Appendix F.

The matching procedure yields following values for the short-distance coefficients

$$c_0^{J=0} = -\bar{Q}(\boldsymbol{\ell} \cdot (\hat{\mathbf{k}} \times \boldsymbol{\varepsilon}^*)), \tag{17.12a}$$

$$c_1^{J=0} = \frac{i}{3}(1-3r)\bar{r}\bar{Q}(\boldsymbol{\ell} \cdot \boldsymbol{\varepsilon}^*), \tag{17.12b}$$

$$c_2^{J=0} = \frac{2}{3}\bar{Q}(\boldsymbol{\ell} \cdot (\hat{\mathbf{k}} \times \boldsymbol{\varepsilon}^*)), \tag{17.12c}$$

$$c_3^{J=0} = -\frac{i}{30}(9-24r+35r^2)\bar{r}^2\bar{Q}(\boldsymbol{\ell} \cdot \boldsymbol{\varepsilon}^*), \tag{17.12d}$$

$$d_0^{J=0} = -\bar{r}\bar{Q}(\boldsymbol{\ell} \cdot (\hat{\mathbf{k}} \times \boldsymbol{\varepsilon}^*)), \tag{17.12e}$$

$$d_1^{J=0} = \frac{1}{6}(1+3r)\bar{r}\bar{Q}(\boldsymbol{\ell} \cdot \boldsymbol{\varepsilon}^*), \tag{17.12f}$$

$$(c_1^{J=1})^i = -i\bar{Q}\bar{r}\left((1-\sqrt{r})(\boldsymbol{\ell} \cdot \hat{\mathbf{k}})(\hat{\mathbf{k}} \times \boldsymbol{\varepsilon}^*)^i - (\boldsymbol{\ell} \times \boldsymbol{\varepsilon}^*)^i\right), \tag{17.12g}$$

$$(c_3^{J=1})^i = \frac{i}{10}\bar{Q}\bar{r}^2\left((1-\sqrt{r})^2(8+13\sqrt{r})(\boldsymbol{\ell} \cdot \hat{\mathbf{k}})(\hat{\mathbf{k}} \times \boldsymbol{\varepsilon}^*)^i - 2(4-9r)(\boldsymbol{\ell} \times \boldsymbol{\varepsilon}^*)^i\right), \tag{17.12h}$$

$$(d_0^{J=1})^i = -\bar{Q}\bar{r}\left(\sqrt{r}\,\boldsymbol{\varepsilon}^{*i}(\boldsymbol{\ell} \cdot \hat{\mathbf{k}}) - \hat{\mathbf{k}}^i(\boldsymbol{\ell} \cdot \boldsymbol{\varepsilon}^*)\right), \tag{17.12i}$$

$$(d_1^{J=1})^i = \frac{1}{2}\bar{Q}\bar{r}\left((2-\sqrt{r})(\boldsymbol{\ell} \cdot \hat{\mathbf{k}})(\hat{\mathbf{k}} \times \boldsymbol{\varepsilon}^*)^i - 2(\boldsymbol{\ell} \times \boldsymbol{\varepsilon}^*)^i\right), \tag{17.12j}$$

$$(c_1^{J=2})^{ij} = -i\bar{Q}\bar{r}\left((1-\sqrt{r})\sqrt{r}(\boldsymbol{\ell}\cdot\hat{\mathbf{k}})(\hat{\mathbf{k}}^i\boldsymbol{\varepsilon}^{*j}+i\leftrightarrow j)+r(\boldsymbol{\ell}^i\boldsymbol{\varepsilon}^{*j}+i\leftrightarrow j)\right.$$
$$\left.-(1-r)(\boldsymbol{\ell}\cdot\boldsymbol{\varepsilon}^*)\hat{\mathbf{k}}^i\hat{\mathbf{k}}^j\right), \tag{17.12k}$$
$$(c_2^{J=2})^{ij} = -\bar{Q}(\boldsymbol{\ell}\cdot(\hat{\mathbf{k}}\times\boldsymbol{\varepsilon}^*)\,\hat{\mathbf{k}}^i\hat{\mathbf{k}}^j), \tag{17.12l}$$
$$(c_3^{J=2})^{ij} = \frac{i}{10}\bar{Q}\bar{r}^2\left(5\sqrt{r}(1+2\sqrt{r})(1-\sqrt{r})^2(\boldsymbol{\ell}\cdot\hat{\mathbf{k}})(\hat{\mathbf{k}}^i\boldsymbol{\varepsilon}^{*j}+i\leftrightarrow j)\right.$$
$$\left.-10r^2(\boldsymbol{\ell}^i\boldsymbol{\varepsilon}^{*j}+i\leftrightarrow j)-6(1-r)^2(\boldsymbol{\ell}\cdot\boldsymbol{\varepsilon}^*)\hat{\mathbf{k}}^i\hat{\mathbf{k}}^j\right), \tag{17.12m}$$
$$(d_0^{J=2})^{ij} = 0, \tag{17.12n}$$
$$(d_1^{J=2})^{ij} = \frac{1}{2}\bar{Q}\bar{r}\left(\sqrt{r}(\boldsymbol{\ell}\cdot\hat{\mathbf{k}})(\hat{\mathbf{k}}^i\boldsymbol{\varepsilon}^{*j}+i\leftrightarrow j)-2\hat{\mathbf{k}}^i\hat{\mathbf{k}}^j(\boldsymbol{\ell}\cdot\boldsymbol{\varepsilon}^*)\right), \tag{17.12o}$$

with $\bar{Q}\equiv\frac{e^2Q^2}{s}$ and $\bar{r}\equiv\frac{1}{1-r}$, where $r\equiv\frac{4m_Q^2}{s}$ is the kinematic suppression factor.

17.2 Matching in the Heavy Quarkonium Rest Frame

Matching in the rest frame of the heavy quarkonium is very similar to the calculation of the $\mathcal{O}(\alpha_s^0v^2)$ corrections to the decay process $\chi_{cJ}\to\gamma\gamma$. The production of χ_{cJ} at rest can be regarded as the decay of a heavy vector boson γ^* into a photon and a quarkonium, so that in the limit were γ^* becomes massless ($s\to 0$), one expects to find the same short-distance coefficients as in the decay of χ_{cJ} into two photons. In our calculation this is indeed the case. Here the rest frame short-distance coefficients carry an additional subscript R to distinguish them from those obtained in the laboratory frame

$$c_{0,R}^{J=0} = -\bar{Q}(\mathbf{V}\cdot(\hat{\mathbf{k}}_R\times\boldsymbol{\varepsilon}_R^*)), \tag{17.13a}$$
$$c_{1,R}^{J=0} = \frac{i}{3}(1-2a)\bar{Q}(\mathbf{V}\cdot\boldsymbol{\varepsilon}_R^*), \tag{17.13b}$$
$$c_{2,R}^{J=0} = \frac{2}{3}\bar{Q}(\mathbf{V}\cdot(\hat{\mathbf{k}}_R\times\boldsymbol{\varepsilon}_R^*)), \tag{17.13c}$$
$$c_{3,R}^{J=0} = -\frac{i}{30}(9-16a)\,\bar{Q}(\mathbf{V}\cdot\boldsymbol{\varepsilon}_R^*), \tag{17.13d}$$
$$d_{0,R}^{J=0} = -(1+a)\bar{Q}(\mathbf{V}\cdot(\hat{\mathbf{k}}_R\times\boldsymbol{\varepsilon}_R^*)), \tag{17.13e}$$
$$d_{1,R}^{J=0} = \frac{1}{6}(1+6a+4a^2)\bar{Q}(\mathbf{V}\cdot\boldsymbol{\varepsilon}_R^*), \tag{17.13f}$$

$$(c_{1,R}^{J=1})^i = \frac{i}{2}\bar{Q}\left(2(1+a)(\mathbf{V}\times\boldsymbol{\varepsilon}_R^*)^i-(\mathbf{V}\cdot\hat{\mathbf{k}}_R)(\hat{\mathbf{k}}_R\times\boldsymbol{\varepsilon}_R^*)^i\right), \tag{17.13g}$$
$$(c_{3,R}^{J=1})^i = -\frac{i}{10}\bar{Q}\left((8+3a)(\mathbf{V}\times\boldsymbol{\varepsilon}_R^*)^i-4(\mathbf{V}\cdot\hat{\mathbf{k}}_R)(\hat{\mathbf{k}}_R\times\boldsymbol{\varepsilon}_R^*)^i\right), \tag{17.13h}$$
$$(d_{0,R}^{J=1})^i = \frac{1}{2}\bar{Q}\left(2(1+a)(\mathbf{V}\cdot\boldsymbol{\varepsilon}_R^*)\hat{\mathbf{k}}_R^i-(1+2a)(\mathbf{V}\cdot\hat{\mathbf{k}}_R)\boldsymbol{\varepsilon}_R^{*i}\right), \tag{17.13i}$$
$$(d_{1,R}^{J=1})^i = -\frac{1}{2}\bar{Q}\left((2+3a+2a^2)(\mathbf{V}\times\boldsymbol{\varepsilon}_R^*)^i-(1+a)(\mathbf{V}\cdot\hat{\mathbf{k}}_R)(\hat{\mathbf{k}}_R\times\boldsymbol{\varepsilon}_R^*)^i\right), \tag{17.13j}$$

$$(c_{1,R}^{J=2})^{ij} = -\frac{i}{2}\bar{Q}\left(2a(\mathbf{V}^i\boldsymbol{\varepsilon}_R^{*j}+i\leftrightarrow j)+(\mathbf{V}\cdot\hat{\mathbf{k}}_R)(\hat{\mathbf{k}}_R^i\boldsymbol{\varepsilon}_R^{*j}+i\leftrightarrow j)\right.$$
$$\left.-2(\mathbf{V}\cdot\boldsymbol{\varepsilon}_R^*)\hat{\mathbf{k}}_R^i\hat{\mathbf{k}}_R^j\right), \tag{17.13k}$$
$$(c_{2,R}^{J=2})^{ij} = -\bar{Q}(\mathbf{V}\cdot(\hat{\mathbf{k}}_R\times\boldsymbol{\varepsilon}_R^*))\,\hat{\mathbf{k}}_R^i\hat{\mathbf{k}}_R^j, \tag{17.13l}$$

$$(c_{3,R}^{J=2})^{ij} = \frac{i}{10}\bar{Q}\Big(5a(\mathbf{V}^i\boldsymbol{\varepsilon}_R^{*j} + i \leftrightarrow j) + 5(\mathbf{V}\cdot\hat{\mathbf{k}}_R)(\hat{\mathbf{k}}_R^i\boldsymbol{\varepsilon}_R^{*j} + i \leftrightarrow j)$$
$$-6(\mathbf{V}\cdot\boldsymbol{\varepsilon}_R^*)\hat{\mathbf{k}}_R^i\hat{\mathbf{k}}_R^j\Big), \tag{17.13m}$$
$$(d_{0,R}^{J=2})^{ij} = 0, \tag{17.13n}$$
$$(d_{1,R}^{J=2})^{ij} = \frac{1}{2}\bar{Q}\Big((1+a)(\mathbf{V}\cdot\hat{\mathbf{k}}_R)(\hat{\mathbf{k}}_R^i\boldsymbol{\varepsilon}_R^{*j} + i \leftrightarrow j) + a(1+2a)(\mathbf{V}^i\boldsymbol{\varepsilon}_R^{*j} + i \leftrightarrow j)$$
$$-2(1+a)(\mathbf{V}\cdot\hat{\mathbf{k}}_R)\hat{\mathbf{k}}_R^i\hat{\mathbf{k}}_R^j\Big), \tag{17.13o}$$

with $a \equiv \frac{m_Q}{|\mathbf{k}_R|}$ and $V^i \equiv \big(\delta^{ij} - \frac{\mathbf{k}_R^i\mathbf{k}_R^j}{\sqrt{s+\mathbf{k}_R^2}}\big)\boldsymbol{\ell}_R^j$. The connection to the laboratory frame can be established by means of the following Lorentz boost transformations

$$\mathbf{k}_R^i = \frac{\sqrt{s}}{M_{\chi_{cJ}}}\mathbf{k}^i, \quad \boldsymbol{\varepsilon}_R^{*i} = \boldsymbol{\varepsilon}^{*i}, \quad \boldsymbol{\ell}_R^i = \boldsymbol{\ell}^i + \frac{(M_{\chi_{cJ}} - \sqrt{s})^2}{2M_{\chi_{cJ}}\sqrt{s}}(\boldsymbol{\ell}\cdot\hat{\mathbf{k}})\hat{\mathbf{k}}^i, \tag{17.14}$$

where the appearance of the physical quarkonium mass stems from the fact that we employed kinematics of the physical quarkonium, i. e. used $P^2 = M_{\chi_{cJ}}^2$. In Sec. 17.3 we will explain how the dependence on $M_{\chi_{cJ}}$ can be eliminated up to the desired order in v.

17.3 Relations between Long Distance Matrix Elements and Heavy Quarkonium Masses

From the NRQCD point of view, LDMEs should be regarded as independent nonperturbative parameters. Nevertheless, symmetries and approximations can be used to establish relations between different LDMEs that are valid up to a certain order in v.

A particularly useful set of approximations can be derived from the equations of motion of NRQCD and is known as Gremm-Kapustin relations [218]. Since our LDMEs are identical to those that appear in the electromagnetic decay $\chi_{cJ} \to \gamma\gamma$, we can use Gremm-Kapustin relations that were first obtained in [26] and can be written as

$$\langle 0|\mathcal{P}_1(^3P_J)|0\rangle = m_Q E_{\chi_{cJ}} \langle 0|\mathcal{O}_1(^3P_J)|0\rangle + m_Q \langle 0|\mathcal{T}_8(^3P_J)|0\rangle, \tag{17.15}$$

where $E_{\chi_{cJ}} = M_{\chi_{cJ}} - 2m_Q$ is the binding energy of χ_{cJ}. Eq. (17.15) is valid up to $\mathcal{O}(v^4)$ and is useful for two reasons. First of all, we can solve for $M_{\chi_{cJ}}$

$$M_{\chi_{cJ}} = 2m_Q + \frac{1}{m_Q}\frac{\langle 0|\mathcal{P}_1(^3P_J)|0\rangle}{\langle 0|\mathcal{O}_1(^3P_J)|0\rangle} - \frac{\langle 0|\mathcal{T}_8(^3P_J)|0\rangle}{\langle 0|\mathcal{O}_1(^3P_J)|0\rangle} \tag{17.16}$$

and utilize the obtained relation to completely eliminate the dependence of matching coefficients in Eq. (16.5) on the heavy quarkonium mass. We use this to check that the matching coefficients obtained from the expansion of QCD amplitudes in the laboratory frame and in the rest frame are identical. Second, Eq. (17.15) allows us to reduce the number of unknown matrix elements in the final NRQCD-factorized production cross sections at the cost of making our numerical predictions depend on the heavy quarkonium binding energy.

18 Electromagnetic Decay of $\chi_{cJ} + \gamma$ into Photons

We report that our matching calculations in the rest frame also contribute to the resolution of the known discrepancy between the results of [26] and [27], which do not agree on the values of some matching coefficients that enter NRQCD-factorized decay rates for $\chi_{cJ} \to \gamma\gamma$ at $\mathcal{O}(\alpha_s^0 v^2)$

$$\begin{aligned}
\Gamma(\chi_{c0} \to \gamma\gamma) &= \frac{2\,\mathrm{Im}\, f_1(^3P_0)}{3m_Q^4} \langle \chi_{c0}|\psi^\dagger(-\frac{i}{2}\overleftrightarrow{\mathbf{D}}\cdot\boldsymbol{\sigma})\chi|0\rangle \langle 0|\chi^\dagger(-\frac{i}{2}\overleftrightarrow{\mathbf{D}}\cdot\boldsymbol{\sigma})\psi|\chi_{c0}\rangle \\
&+ \frac{2\,\mathrm{Im}\, g_1(^3P_0)}{6m_Q^6}\left(\langle \chi_{c0}|\psi^\dagger(-\frac{i}{2}\overleftrightarrow{\mathbf{D}}\cdot\boldsymbol{\sigma})(-\frac{i}{2}\overleftrightarrow{\mathbf{D}})^2\chi|0\rangle \langle 0|\chi^\dagger(-\frac{i}{2}\overleftrightarrow{\mathbf{D}}\cdot\boldsymbol{\sigma})\psi|\chi_{c0}\rangle + \text{h.c.}\right) \\
&+ i\frac{2\,\mathrm{Im}\, t_{8\,\mathrm{em}}(^3P_0)}{3m_Q^5}\left(\langle \chi_{c0}|\psi^\dagger(g\mathbf{E}\cdot\boldsymbol{\sigma})\chi|0\rangle \langle 0|\chi^\dagger(-\frac{i}{2}\overleftrightarrow{\mathbf{D}}\cdot\boldsymbol{\sigma})\psi|\chi_{c0}\rangle + \text{h.c.}\right) \\
&\equiv \frac{2\,\mathrm{Im}\, f_1(^3P_0)}{m_Q^4}\langle \chi_{c0}|\mathcal{O}_1(^3P_0)|\chi_{c0}\rangle + \frac{2\,\mathrm{Im}\, g_1(^3P_0)}{m_Q^6}\langle \chi_{c0}|\mathcal{P}_1(^3P_0)|\chi_{c0}\rangle \\
&+ \frac{2\,\mathrm{Im}\, t_{8\,\mathrm{em}}(^3P_0)}{m_Q^5}\langle \chi_{c0}|\mathcal{T}_{8\,\mathrm{em}}(^3P_0)|\chi_{c0}\rangle\,, \qquad (18.1a)
\end{aligned}$$

$$\begin{aligned}
\Gamma(\chi_{c2} \to \gamma\gamma) &= \frac{2\,\mathrm{Im}\, f_1(^3P_2)}{m_Q^4} \langle \chi_{c2}|\psi^\dagger(-\frac{i}{2}\overleftrightarrow{\mathbf{D}}^{(i}\boldsymbol{\sigma}^{j)})\chi|0\rangle \langle 0|\chi^\dagger(-\frac{i}{2}\overleftrightarrow{\mathbf{D}}^{(i}\boldsymbol{\sigma}^{j)})\psi|\chi_{c2}\rangle \\
&+ \frac{2\,\mathrm{Im}\, g_1(^3P_2)}{2m_Q^6}\left(\langle \chi_{c2}|\psi^\dagger(-\frac{i}{2}\overleftrightarrow{\mathbf{D}}^{(i}\boldsymbol{\sigma}^{j)})(-\frac{i}{2}\overleftrightarrow{\mathbf{D}})^2\chi|0\rangle \langle 0|\chi^\dagger(-\frac{i}{2}\overleftrightarrow{\mathbf{D}}^{(i}\boldsymbol{\sigma}^{j)})\psi|\chi_{c2}\rangle + \text{h.c.}\right) \\
&+ \frac{2\,\mathrm{Im}\, t_{8\,\mathrm{em}}(^3P_2)}{m_Q^3}\left(\langle \chi_{c2}|\psi^\dagger(g\mathbf{E}^{(i}\boldsymbol{\sigma}^{j)})\chi|0\rangle \langle 0|\chi^\dagger(-\frac{i}{2}\overleftrightarrow{\mathbf{D}}^{(i}\boldsymbol{\sigma}^{j)})\psi|\chi_{c2}\rangle + \text{h.c.}\right) \\
&\equiv \frac{2\,\mathrm{Im}\, f_1(^3P_2)}{m_Q^4}\langle \chi_{c2}|\mathcal{O}_1(^3P_2)|\chi_{c2}\rangle + \frac{2\,\mathrm{Im}\, g_1(^3P_2)}{m_Q^6}\langle \chi_{c2}|\mathcal{P}_1(^3P_2)|\chi_{c2}\rangle \\
&+ \frac{2\,\mathrm{Im}\, t_{8\,\mathrm{em}}(^3P_2)}{m_Q^5}\langle \chi_{c2}|\mathcal{T}_{8\,\mathrm{em}}(^3P_2)|\chi_{c2}\rangle\,, \qquad (18.1b)
\end{aligned}$$

While both collaborations obtained the same expressions for

$$\mathrm{Im}\, f_1(^3P_0) = 3\alpha^2 Q^4 \pi, \qquad (18.2a)$$

$$\mathrm{Im}\, f_1(^3P_2) = \frac{4}{5}\alpha^2 Q^4 \pi, \qquad (18.2b)$$

$$\mathrm{Im}\, g_1(^3P_0) = -7\alpha^2 Q^4 \pi, \qquad (18.2c)$$

they disagree on the values of other coefficients, c. f. Table 18.1. In 2013, it was reported [219] that an independent investigation of the $\chi_{cJ} \to \gamma\gamma$ decay confirmed the results of [27]. In the course of this study we have also repeated the calculation of the $\mathcal{O}(\alpha_s^0 v^2)$ corrections to this decay process. Using matching at the amplitude level and matching at the level of total decay rates we equally agree with the values of matching coefficients obtained in [27]. Notice that in [26] the decay rate of χ_{c2} contained an additional matrix element

$$\langle \chi_{c2}|\psi^\dagger\left(\left(-\frac{i}{2}\right)^2 \overleftrightarrow{\mathbf{D}}^{(i}\overleftrightarrow{\mathbf{D}}^{j)}\right)(-\frac{i}{2}\overleftrightarrow{\mathbf{D}}\cdot\boldsymbol{\sigma})\chi|0\rangle \langle 0|\chi^\dagger(-\frac{i}{2}\overleftrightarrow{\mathbf{D}}^{(i}\boldsymbol{\sigma}^{j)})\psi|\chi_{c2}\rangle + \text{h.c.}\,. \qquad (18.3)$$

Matching coefficient	Value from [26]	Value from [27]
$\mathrm{Im}\, g_1(^3P_2)$	$-\frac{86}{105}\alpha^2 Q^4\pi$	$-\frac{8}{5}\alpha^2 Q^4\pi$
$\mathrm{Im}\, t_8(^3P_0)$	$-2\alpha^2 Q^4\pi$	$-\frac{3}{2}\alpha^2 Q^4\pi$
$\mathrm{Im}\, t_8(^3P_2)$	$-\alpha^2 Q^4\pi$	0

Table 18.1: Discrepancy in the results of [26] and [27].

However, in [27] it was shown that the contribution of this operator to the total decay rate is already accounted for by the inclusion of $\langle\chi_{c2}|\mathcal{P}_1(^3P_2)|\chi_{c2}\rangle$. Following this argument we also do not include the operator from Eq. 18.3.

19 NRQCD Production Cross Section for $\chi_{cJ} + \gamma$ at $\mathcal{O}(v^2)$

Plugging our laboratory frame short-distance coefficients from Eqs. (17.12) into Eqs. (16.5) we readily obtain the values of matching coefficients that enter the factorized cross sections given in Eqs. (14.11)

$$F_1(^3P_0) = \frac{8\pi^2\alpha^3Q^4(1-3r)^2(s-M_{\chi_{c0}}^2)}{9m_Q^2s^3(1-r)^2}, \tag{19.1a}$$

$$G_1(^3P_0) = -\frac{8\pi^2\alpha^3Q^4(1-3r)(9-24r+35r^2)(s-M_{\chi_{c0}}^2)}{45m_Q^2s^3(1-r)^3}, \tag{19.1b}$$

$$T_8(^3P_0) = \frac{4\pi^2\alpha^3Q^4(1-9r^2)(s-M_{\chi_{c0}}^2)}{9m_Q^2s^3(1-r)^2}, \tag{19.1c}$$

$$F_1(^3P_1) = \frac{16\pi^2\alpha^3Q^4(1+r)(s-M_{\chi_{c1}}^2)}{3m_Q^2s^3(1-r)^2}, \tag{19.1d}$$

$$G_1(^3P_1) = -\frac{16\pi^2\alpha^3Q^4(8-15r-13r^2)(s-M_{\chi_{c1}}^2)}{15m_Q^2s^3(1-r)^3}, \tag{19.1e}$$

$$T_8(^3P_1) = -\frac{8\pi^2\alpha^3Q^4(2+r)(s-M_{\chi_{c1}}^2)}{3m_Q^2s^3(1-r)^2}, \tag{19.1f}$$

$$F_1(^3P_2) = \frac{16\pi^2\alpha^3Q^4(1+3r+6r^2)(s-M_{\chi_{c2}}^2)}{9m_Q^2s^3(1-r)^2}, \tag{19.1g}$$

$$G_1(^3P_2) = -\frac{8\pi^2\alpha^3Q^4(2+3r)(3-3r-20r^2)(s-M_{\chi_{c2}}^2)}{45m_Q^2s^3(1-r)^3}, \tag{19.1h}$$

$$T_8(^3P_2) = -\frac{8\pi^2\alpha^3Q^4(2+3r)(s-M_{\chi_{c2}}^2)}{9m_Q^2s^3(1-r)^2}, \tag{19.1i}$$

where the dependence on $M_{\chi_{cJ}}$ arises from the phase space integration (c. f. Eq. (16.3)). Furthermore, as was already mentioned in Sec. (14), our matrix elements are normalized relativistically, so that to compare to the literature we must first convert them to the nonrelativistic normalization of [7]. Using Eq. (14.13) and Eq. (17.15) we arrive to the cross sections that do not explicitly depend on the mass of χ_{cJ}

$$\sigma(e^+e^- \to \chi_{c0} + \gamma) = \frac{(4\pi\alpha)^3Q^4(1-3r)^2}{18\pi m_Q^3s^2(1-r)}\left(\left(1+C_0^0(r)\frac{\alpha_s}{\pi}\right)\langle 0|\mathcal{O}_1(^3P_0)|0\rangle_{\text{BBL}}\right.$$
$$\left. - \frac{(13-18r+25r^2)}{10m_Q^2(1-4r+3r^2)}\langle 0|\mathcal{P}_1(^3P_0)|0\rangle_{\text{BBL}} + \frac{2r(2-3r)}{m_Q(1-4r+3r^2)}\langle 0|\mathcal{T}_8(^3P_0)|0\rangle_{\text{BBL}}\right) \tag{19.2a}$$

$$\sigma(e^+e^- \to \chi_{c1} + \gamma) = \frac{(4\pi\alpha)^3Q^4(1+r)}{3\pi m_Q^3s^2(1-r)}\left(\left(1+\frac{C_1^0(r)+rC_1^1(r)}{1+r}\frac{\alpha_s}{\pi}\right)\langle 0|\mathcal{O}_1(^3P_1)|0\rangle_{\text{BBL}}\right.$$
$$\left. - \frac{(11-20r-11r^2)}{10m_Q^2(1-r^2)}\langle 0|\mathcal{P}_1(^3P_1)|0\rangle_{\text{BBL}} - \frac{(3-3r-4r^2)}{2m_Q(1-r^2)}\langle 0|\mathcal{T}_8(^3P_1)|0\rangle_{\text{BBL}}\right), \tag{19.2b}$$

$$\sigma(e^+e^-\to\chi_{c2}+\gamma)=\frac{(4\pi\alpha)^3Q^4(1+3r+6r^2)}{9\pi m_Q^3 s^2(1-r)}$$
$$\times\left(\left(1+\frac{C_2^0(r)+3rC_2^1(r)+6r^2C_2^2(r)}{1+3r+6r^2}\frac{\alpha_s}{\pi}\right)\langle 0|\mathcal{O}_1(^3P_2)|0\rangle_{\text{BBL}}\right.$$
$$\left.-\frac{(1+4r-30r^2)}{10m_Q^2(1+3r+6r^2)}\langle 0|\mathcal{P}_1(^3P_2)|0\rangle_{\text{BBL}}-\frac{(3+r-6r^2-18r^3)}{2m_Q(1-r)(1+3r+6r^2)}\langle 0|\mathcal{T}_8(^3P_2)|0\rangle_{\text{BBL}}\right), \tag{19.2c}$$

Here, the values of the matching coefficients multiplying $\langle 0|\mathcal{T}_8(^3P_J)|0\rangle_{\text{BBL}}$ constitute the main result of this work. Moreover, for consistency reasons we have included the known $\mathcal{O}(\alpha_s v^0)$ [204, 205] correction to $F_1(^3P_J)$, where explicit values of the coefficients $C_j^i(r)$ can be found the Appendix B of [204]. The corrections $\mathcal{O}(\alpha_s v^2)$ [30] are omitted. First of all, in our view the corrections reported in [30] are incomplete, as they do not include contributions from $\langle 0|\mathcal{T}_8(^3P_2)|0\rangle_{\text{BBL}}$. Second, to be consistent with the NRQCD power-counting rules at that order in α_s and v one would also require $\mathcal{O}(\alpha_s^0 v^4)$ and $\mathcal{O}(\alpha_s^2 v^0)$ corrections, that are not available yet.

Comparing our results to the literature, we see that our matching coefficients $F_1(^3P_J)$ agree with those reported in [203] and all subsequent studies. As far as the values of $G_1(^3P_J)$ are concerned, comparing to [220] and using their K-factor notation we agree on the values of $G_1(^3P_{0,1})$ but disagree on the value of $G_1(^3P_2)$. More specifically, we obtain

$$K_{v^2}[\chi_{c2}]=-\frac{(1+3r-34r^2+30r^3)v^2}{10(1-r)(1+3r+6r^2)} \tag{19.3}$$

as compared to

$$K_{v^2}[\chi_{c2}]=-\frac{(7+6r-83r^2-30r^3)v^2}{10(1-r)(1+3r+6r^2)} \tag{19.4}$$

reported in [220].

For comparisons to the experimental measurements we also present our differential cross sections in the laboratory frame, where θ denotes the angle between the beam line and the outgoing photon. Here, the $\mathcal{O}(\alpha_s v^0)$ corrections from [204] are included as well

$$\frac{d}{d\cos\theta}\sigma(e^+e^-\to\chi_{c0}+\gamma)=\frac{(4\pi\alpha)^3Q^4(1-3r)^2(1+\cos^2\theta)}{48\pi m_Q^3 s^2(1-r)}\Bigg($$
$$\left(1+C_0^0(r)\frac{\alpha_s}{\pi}\right)\langle 0|\mathcal{O}_1(^3P_0)|0\rangle_{\text{BBL}}-\frac{(13-18r+25r^2)}{10m_Q^2(1-4r+3r^2)}\langle 0|\mathcal{P}_1(^3P_0)|0\rangle_{\text{BBL}}$$
$$+\frac{2r(2-3r)}{m_Q(1-4r+3r^2)}\langle 0|\mathcal{T}_8(^3P_0)|0\rangle_{\text{BBL}}\Bigg), \tag{19.5a}$$

$$\frac{d}{d\cos\theta}\sigma(e^+e^-\to\chi_{c1}+\gamma)=\frac{(4\pi\alpha)^3Q^4}{8\pi m_Q^3 s^2(1-r)}\Bigg(\Bigg((1+\cos^2\theta)\left(1+\frac{\alpha_s}{\pi}C_1^0(r)\right)$$
$$+2r(1-\cos^2\theta)\left(1+\frac{\alpha_s}{\pi}C_1^{\pm1}(r)\right)\Bigg)\langle 0|\mathcal{O}_1(^3P_1)|0\rangle_{\text{BBL}}$$
$$-\frac{(11-19r-22r^2)+(11-23r+22r^2)\cos^2\theta}{10m_Q^2(1-r)}\langle 0|\mathcal{P}_1(^3P_1)|0\rangle_{\text{BBL}}$$
$$-\frac{(3-r-8r^2)+(3-9r-8r^2)\cos^2\theta}{2m_Q(1-r)}\langle 0|\mathcal{T}_8(^3P_1)|0\rangle_{\text{BBL}}\Bigg), \tag{19.5b}$$

$$\frac{d}{d\cos\theta}\sigma(e^+e^-\to\chi_{c2}+\gamma)=\frac{(4\pi\alpha)^3Q^4}{24\pi m_Q^3 s^2(1-r)}\Bigg(\Bigg((1+\cos^2\theta)\left(1+\frac{\alpha_s}{\pi}C_2^0(r)\right)$$
$$+6r(1-\cos^2\theta)\left(1+\frac{\alpha_s}{\pi}C_2^{\pm1}(r)\right)+6r^2(1+\cos^2\theta)\left(1+\frac{\alpha_s}{\pi}C_2^{\pm2}(r)\right)\Bigg)\langle 0|\mathcal{O}_1(^3P_2)|0\rangle_{\text{BBL}}$$
$$-\frac{(1+4r-30r^2)(1+\cos^2\theta)}{10m_Q^2}\langle 0|\mathcal{P}_1(^3P_2)|0\rangle_{\text{BBL}}$$
$$-\frac{(3+7r-18r^2-18r^3)+(1-3r)(3-8r+6r^2)\cos^2\theta}{2m_Q(1-r)}\langle 0|\mathcal{T}_8(^3P_2)|0\rangle_{\text{BBL}}\Bigg). \qquad (19.5c)$$

20 Numerical Estimates

In view of the fact, that no reliable determinations of the LDMEs $\langle 0|\mathcal{P}_1(^3P_J)|0\rangle_{\text{BBL}}$ and $\langle 0|\mathcal{T}_8(^3P_J)|0\rangle_{\text{BBL}}$ are available, we do not see ourselves in the position to provide reliable numerical predictions for the size of the $e^+e^- \to \gamma^* \to \chi_{cJ}\,\gamma$ production cross sections. On the other hand, we can apply some reasonable assumptions and approximations to estimate how large the contribution of $\langle 0|\mathcal{T}_8(^3P_J)|0\rangle_{\text{BBL}}$ to the total cross section at $\mathcal{O}(v^2)$ could be.

For $\langle 0|\mathcal{O}_1(^3P_J)|0\rangle_{\text{BBL}}$ we can use the values quoted in [215] which follow from Buchmüller-Tye (BT) potential model calculation [221].

$$\langle 0|\mathcal{O}_1(^3P_J)|0\rangle_{\text{BBL}} = 0.107\,\text{GeV}^5. \tag{20.1}$$

To some extent we can justify this choice by referring to the recent study [222] of $\mathcal{O}(\alpha_s^2 v^0)$ corrections to the decay $\chi_{cJ} \to 2\gamma$. The value of $\langle 0|\mathcal{O}_1(^3P_0)|0\rangle_{\text{BBL}}$ determined from fits to experimental data in [222] appears to be in a good agreement with the prediction from BT potential model, when the renormalization scale μ is chosen to be large enough ($\mu \geq 2m_Q$). For $\langle 0|\mathcal{O}_1(^3P_2)|0\rangle_{\text{BBL}}$ the agreement is much worse and the value of this LDME even becomes negative for small values of μ. Since it is not clear, how large $\langle 0|\mathcal{O}_1(^3P_1)|0\rangle_{\text{BBL}}$ and $\langle 0|\mathcal{O}_1(^3P_2)|0\rangle_{\text{BBL}}$ really are and no lattice determinations are available, the usage of values from Eq. (20.1) appears acceptable.

The number of the remaining independent LDMEs can be reduced by applying heavy-quark spin symmetry [7], which relates matrix elements with same orbital momenta but different spin values and is valid up to corrections of $\mathcal{O}(v^2)$. Since $\langle 0|\mathcal{P}_1(^3P_J)|0\rangle_{\text{BBL}}$ and $\langle 0|\mathcal{T}_8(^3P_J)|0\rangle_{\text{BBL}}$ are already v^2 suppressed as compared to $\langle 0|\mathcal{O}_1(^3P_J)|0\rangle_{\text{BBL}}$, the corrections from heavy-quark spin-symmetry to the total cross section are of $O(v^4)$ and hence irrelevant for the accuracy that we are aiming at

$$\langle 0|\mathcal{P}_1(^3P_J)|0\rangle_{\text{BBL}} = \langle 0|\mathcal{P}_1(^3P_0)|0\rangle_{\text{BBL}} \left(1 + \mathcal{O}(v^2)\right), \tag{20.2}$$

$$\langle 0|\mathcal{T}_8(^3P_J)|0\rangle_{\text{BBL}} = \langle 0|\mathcal{T}_8(^3P_0)|0\rangle_{\text{BBL}} \left(1 + \mathcal{O}(v^2)\right). \tag{20.3}$$

The values of $\langle 0|\mathcal{P}_1(^3P_0)|0\rangle_{\text{BBL}}$ and $\langle 0|\mathcal{T}_8(^3P_0)|0\rangle_{\text{BBL}}$ can be, in principle, determined from the electromagnetic decay $\chi_{c0} \to \gamma\gamma$ that has been recently measured by the BESIII [223] experiment with high precision

$$\Gamma(\chi_{c0} \to \gamma\gamma) = (2.33 \pm 0.20 \pm 0.22) \times 10^{-3}\,\text{MeV}. \tag{20.4}$$

Combining the NRQCD result for the total decay rate $\Gamma(\chi_{c0} \to \gamma\gamma)$ from Eq. (18.1) with the Gremm-Kapustin relation Eq. (17.15) we obtain

$$\begin{aligned}\Gamma(\chi_{c0} \to \gamma\gamma) = {} & \frac{6\alpha^2 Q^4 \pi}{m_Q^4}\left(1 + \frac{3\pi^2 - 28}{9}\frac{\alpha_s}{\pi}\right)\langle 0|\mathcal{O}_1(^3P_0)|0\rangle_{\text{BBL}} \\ & - \frac{14\alpha^2 Q^4 \pi}{m_Q^6}\langle 0|\mathcal{P}_1(^3P_0)|0\rangle_{\text{BBL}} - \frac{3\alpha^2 Q^4 \pi}{m_Q^5}\langle 0|\mathcal{T}_8(^3P_0)|0\rangle_{\text{BBL}}, \end{aligned} \tag{20.5a}$$

$$\langle 0|\mathcal{P}_1(^3P_0)|0\rangle_{\text{BBL}} = m_Q E_{\chi_{cJ}}\langle 0|\mathcal{O}_1(^3P_0)|0\rangle_{\text{BBL}} + m_Q\langle 0|\mathcal{T}_8(^3P_0)|0\rangle_{\text{BBL}}. \tag{20.5b}$$

Notice that the decay rate formula in Eq. (20.5a) contains not only corrections of $\mathcal{O}(\alpha_s^0 v^0)$ and $\mathcal{O}(\alpha_s^0 v^2)$ but also the $\mathcal{O}(\alpha_s v^0)$ correction [116, 224] to Im $f_1(^3P_0)$. This is required to be consistent with the NRQCD power-counting, where corrections of $\mathcal{O}(\alpha_s v^0)$ and $\mathcal{O}(\alpha_s^0 v^2)$ are assumed to be equally important.

x	$\langle 0\vert\mathcal{P}_1(^3P_0)\vert 0\rangle_{\text{BBL}}$	$\langle 0\vert\mathcal{T}_8(^3P_0)\vert 0\rangle_{\text{BBL}}$	$\frac{\langle 0\vert\mathcal{P}_1(^3P_0)\vert 0\rangle_{\text{BBL}}}{m_{Q,\text{OS}}\langle 0\vert\mathcal{T}_8(^3P_0)\vert 0\rangle_{\text{BBL}}}$
0	0.043 ± 0.005	0.03 ± 0.004	1.
0.1	0.044 ± 0.005	0.026 ± 0.004	1.2
0.3	0.046 ± 0.005	0.018 ± 0.004	1.8
0.5	0.049 ± 0.005	0.011 ± 0.004	3.2
0.7	0.051 ± 0.005	0.003 ± 0.004	12
1.0	0.054 ± 0.005	-0.008 ± 0.004	-4.5
1.3	0.058 ± 0.005	-0.020 ± 0.004	-2
1.5	0.060 ± 0.005	-0.027 ± 0.004	-1.5

Table 20.1: Dependence of $\langle 0\vert\mathcal{P}_1(^3P_0)\vert 0\rangle_{\text{BBL}}$ (in GeV^7) and $\langle 0\vert\mathcal{T}_8(^3P_0)\vert 0\rangle_{\text{BBL}}$ (in GeV^6) on the value of the binding energy.

Eqs. (20.5) describe a linear system of 2 equations with 3 unknowns: $\langle 0\vert\mathcal{P}_1(^3P_0)\vert 0\rangle_{\text{BBL}}$, $\langle 0\vert\mathcal{T}_8(^3P_0)\vert 0\rangle_{\text{BBL}}$ and $E_{\chi_{cJ}}$. Solving the system for the unknown LDMEs yields

$$\begin{aligned}\langle 0\vert\mathcal{P}_1(^3P_0)\vert 0\rangle_{\text{BBL}} &= \frac{m_Q}{51\pi}\langle 0\vert\mathcal{O}_1(^3P_0)\vert 0\rangle_{\text{BBL}}\left(9\pi(2m_Q+E_{\chi_{c0}})+2(3\pi^2-28)m_Q\alpha_s\right)\\ &\quad-\frac{m_Q^6}{17\pi\alpha^2Q^4}\Gamma(\chi_{c0}\to\gamma\gamma), \qquad (20.6a)\\ \langle 0\vert\mathcal{T}_8(^3P_0)\vert 0\rangle_{\text{BBL}} &= \frac{2m_Q}{51\pi}\langle 0\vert\mathcal{O}_1(^3P_0)\vert 0\rangle_{\text{BBL}}\left(3\pi(3m_Q-7E_{\chi_{c0}})+(3\pi^2-28)m_Q\alpha_s\right)\\ &\quad-\frac{m_Q^6}{17\pi\alpha^2Q^4}\Gamma(\chi_{c0}\to\gamma\gamma). \qquad (20.6b)\end{aligned}$$

To evaluate Eqs. (20.6) numerically, we use the most recent PDG [40] value for the charm mass $m_{Q,\overline{\text{MS}}} = 1.27 \pm 0.03$ and employ `RunDec` [225, 226] to convert it to the pole mass at 1-loop accuracy

$$m_{Q,\text{OS}} = 1.44 \pm 0.03 \text{ GeV}. \qquad (20.7)$$

Furthermore, we choose

$$\alpha = 1/137, \qquad (20.8a)$$
$$\alpha_s(m_{Q,\text{OS}}) = 0.31, \qquad (20.8b)$$

where the value of α_s was also obtained with `RunDec`. The main issue with this determination, is that $\langle 0\vert\mathcal{T}_8(^3P_0)\vert 0\rangle_{\text{BBL}}$ turns out to be very sensitive to the value of the binding energy $E_{\chi_{c0}}$. This dependence originates from the Gremm-Kapustin relation Eq. (17.15) and constitutes a large source of uncertainty. Before adopting a particular value for $E_{\chi_{c0}}$, we find it useful to explore the dependence of our LDMEs on this parameter. According to the hierarchy of scales in a heavy quarkonium, the binding energy should be of order $m_Q v^2$, where v^2 is usually assumed to be about 0.3 for charmonia [7]. Therefore, we can introduce a dimensionless parameter x of $\mathcal{O}(1)$ and rewrite the binding energy as

$$E_{\chi_{c0}} = 0.3\, x\, m_{Q,\text{OS}}. \qquad (20.9)$$

The values of $\langle 0\vert\mathcal{P}_1(^3P_0)\vert 0\rangle_{\text{BBL}}$ and $\langle 0\vert\mathcal{T}_8(^3P_0)\vert 0\rangle_{\text{BBL}}$ depending on the choice of x are given in Table 20.1. All the uncertainties in this section are estimated using Gaussian error propagation rule. We observe that $\langle 0\vert\mathcal{T}_8(^3P_0)\vert 0\rangle_{\text{BBL}}$ decreases for growing x, until it finally becomes unphysical around $x = 1.0$. Although we do not know the correct value of x, we choose $x = 0.3$ as a good compromise between zero binding energy

	$\mathcal{O}(\alpha_s^0 v^0)$ and $\mathcal{O}(\alpha_s v^0)$	$\mathcal{O}(\alpha_s^0 v^0)$, $\mathcal{O}(\alpha_s v^0)$ and $\mathcal{O}^*(\alpha_s^0 v^2)$	$\mathcal{O}(\alpha_s^0 v^0)$, $\mathcal{O}(\alpha_s v^0)$ and $\mathcal{O}(\alpha_s^0 v^2)$	$\frac{\sigma_8}{\sigma_1} - 1$
$\sigma(\chi_{c0})$	$(2.49 \pm 0.20 \pm 0.06)$	$(1.72 \pm 0.14 \pm 0.06)$	$(1.82 \pm 0.14 \pm 0.06)$	5.6%
$\sigma(\chi_{c1})$	$(18.8 \pm 1.15 \pm 1.22)$	$(14.1 \pm 0.82 \pm 1.22)$	$(10.2 \pm 1.20 \pm 1.22)$	-27.6%
$\sigma(\chi_{c2})$	$(3.71 \pm 0.19 \pm 1.38)$	$(3.54 \pm 0.17 \pm 1.38)$	$(2.11 \pm 0.39 \pm 1.38)$	-40.4%

Table 20.2: Estimates for $\sigma(e^+e^- \to \chi_{cJ}\gamma)$ (in fb) at $\sqrt{s} = 10.6\,\text{GeV}$ with $\mu = \sqrt{s}/2$. The second columns shows results, where both $\langle 0|\mathcal{P}_1(^3P_0)|0\rangle_{\text{BBL}}$ and $\langle 0|\mathcal{T}_8(^3P_0)|0\rangle_{\text{BBL}}$ are omitted. In the third column we include contributions from $\langle 0|\mathcal{P}_1(^3P_0)|0\rangle_{\text{BBL}}$ but not from $\langle 0|\mathcal{T}_8(^3P_0)|0\rangle_{\text{BBL}}$. In the fourth column all three LDMEs are included. The last column displays the change of the full cross section in percent, when $\langle 0|\mathcal{T}_8(^3P_0)|0\rangle_{\text{BBL}}$ is included (σ_8) or omitted (σ_1).

and vanishing value of $\langle 0|\mathcal{T}_8(^3P_0)|0\rangle_{\text{BBL}}$. This choice seems reasonable, as it satisfies the requirement, that the ratio of $\langle 0|\mathcal{P}_1(^3P_0)|0\rangle_{\text{BBL}}$ and $m_Q \langle 0|\mathcal{T}_8(^3P_0)|0\rangle_{\text{BBL}}$ should be of $\mathcal{O}(1)$ according to the conventional NRQCD power-counting rules [7]. With

$$\langle 0|\mathcal{P}_1(^3P_0)|0\rangle_{\text{BBL}} = 0.046 \pm 0.005\,\text{GeV}^7 \tag{20.10}$$

$$\langle 0|\mathcal{T}_8(^3P_0)|0\rangle_{\text{BBL}} = 0.018 \pm 0.004\,\text{GeV}^6 \tag{20.11}$$

we provide numerical estimates for $\sigma(e^+e^- \to \chi_{cJ}\gamma)$ that incorporate our new results but also the known $\mathcal{O}(\alpha_s v^0)$ [204, 205] corrections. The process can be measured at a B-factory with a sufficiently high CM energy to produce χ_{cJ} and a hard photon, e. g. at Belle II. Hence, we select our input parameters as

$$\sqrt{s} = 10.6\,\text{GeV}, \tag{20.12}$$

$$\alpha(10.6\,\text{GeV}) = 1/131. \tag{20.13}$$

To estimate the uncertainty in the choice of the renormalization scale μ that enters α_s, we use three possible values of μ

$$\alpha_s(\sqrt{s}) = 0.17, \tag{20.14}$$

$$\alpha_s(\sqrt{s}/2) = 0.20, \tag{20.15}$$

$$\alpha_s(2m_{Q,\text{OS}}) = 0.24. \tag{20.16}$$

Here $\alpha_s(\sqrt{s}/2)$ is taken as the central value, while $\alpha_s(\sqrt{s})$ and $\alpha_s(2m_{Q,\text{OS}})$ are used to obtain the errors.

Our results are summarized in Table 20.2. In order to emphasize the estimated size of the contribution from $\langle 0|\mathcal{T}_8(^3P_0)|0\rangle_{\text{BBL}}$, we use $\mathcal{O}^*(\alpha_s^0 v^2)$ to denote NLO relativistic corrections where $\langle 0|\mathcal{T}_8(^3P_0)|0\rangle_{\text{BBL}}$ is omitted. The first error originates from the uncertainties in $m_{Q,\text{OS}}$ and in the determination of $\langle 0|\mathcal{P}_1(^3P_0)|0\rangle_{\text{BBL}}$ and $\langle 0|\mathcal{T}_8(^3P_0)|0\rangle_{\text{BBL}}$ (assuming that the chosen values for $\langle 0|\mathcal{O}_1(^3P_J)|0\rangle_{\text{BBL}}$ and $E_{\chi_{c0}}$ are exact). The second error is due to the uncertainties in the choice of μ.

The contributions of different LDMEs to the total cross section in the energy region of Belle II are also shown in Fig. 20.1. The contribution of $\langle 0|\mathcal{T}_8(^3P_J)|0\rangle_{\text{BBL}}$ is positive for χ_{c0} and increases the size of the cross section at $\sqrt{s} = 10.6$ by 5.6%. The cross section for χ_{c1} decreases by roughly one third and that of χ_{c2} by 40%. However, our estimate for χ_{c2} is also the least reliable one, which is why one should better avoid any unjustified speculations. Once again, we would like to emphasize that we do

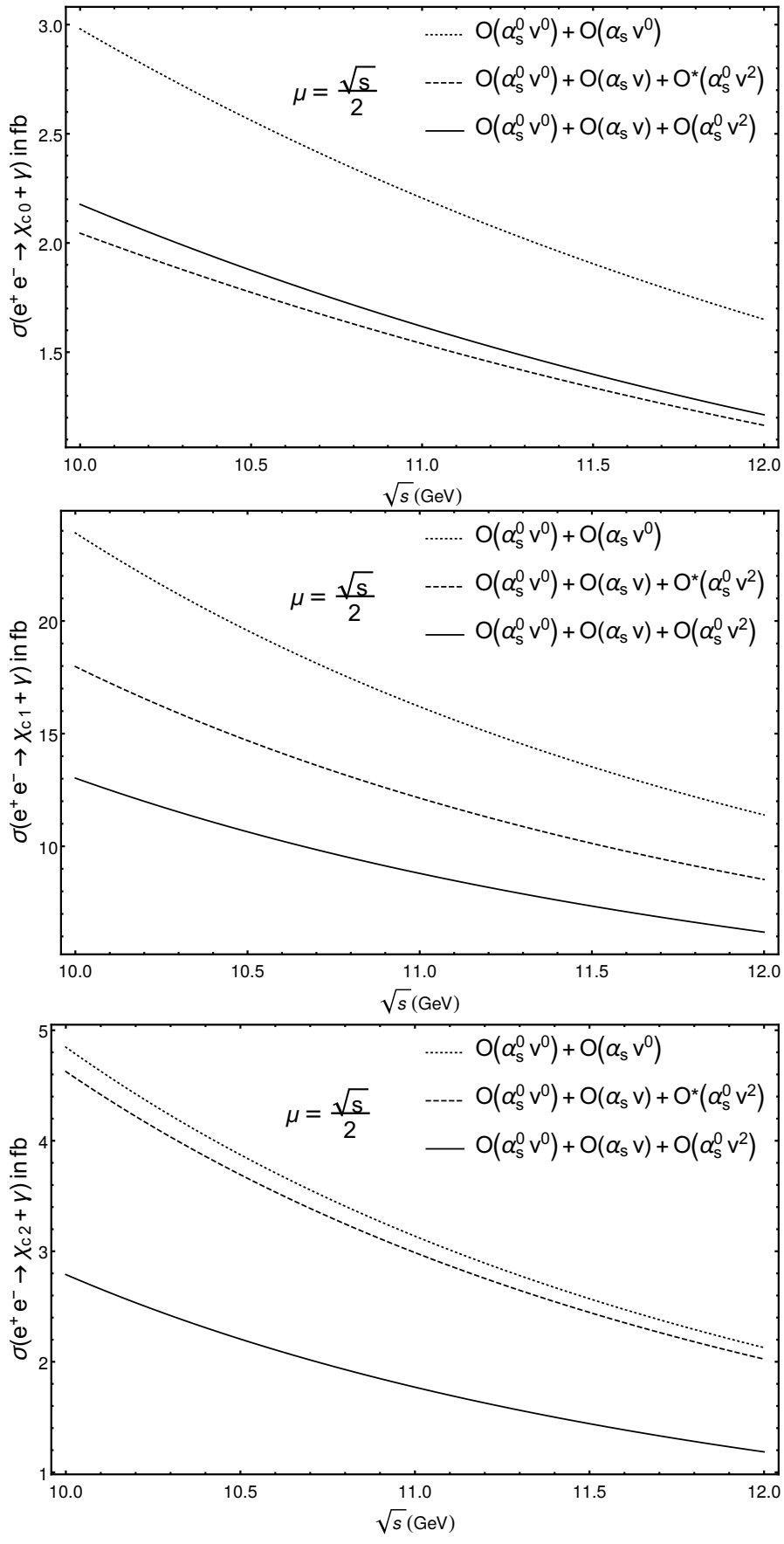

Figure 20.1: Cross sections for the production of χ_{cJ} in the energy region of Belle II. The dotted curve shows contributions only from the $\langle 0|\mathcal{O}_1(^3P_0)|0\rangle$ matrix element. The dashed curve includes also $\langle 0|\mathcal{P}_1(^3P_0)|0\rangle$, while the solid curve displays our final result with all the three contributions.

not consider our numerical estimates for the cross sections to be a reliable prediction for experimental searches. While our analytic results for the matching coefficients are unambiguous, the numerical results strongly depend on the estimated size of the quarkonium binding energy and the assumed value of $\langle 0|\mathcal{O}_1(^3P_J)|0\rangle_{\text{BBL}}$. A reliable determination of $\langle 0|\mathcal{P}_1(^3P_0)|0\rangle_{\text{BBL}}$ and $\langle 0|\mathcal{T}_8(^3P_0)|0\rangle_{\text{BBL}}$ from the experimental data or lattice simulations is therefore highly desirable.

21 Summary

NRQCD factorization provides a systematic prescription to compute production cross sections of heavy quarkonia order by order in α_s and v. Higher order corrections in α_s arise from loop effects, while higher order corrections in v are generated by the inclusion of higher-dimensional operators. Both quantities are not independent, such that a consistent computation of higher order corrections requires both loop corrections to matching coefficients of lower dimensional operators and relativistic corrections from higher dimensional operators.

In this work we determined the $\mathcal{O}(\alpha_s^0 v^2)$ contribution to the electromagnetic quarkonium production of χ_{cJ} induced by the higher Fock state $|Q\bar{Q}g\rangle$. For this we calculated the matching coefficients $T_8(^3P_J)$ that multiply LDMEs, which depend on the chromoelectric field. To this end we used perturbative matching between QCD and NRQCD at the amplitude level, where we treated the ultrasoft final state gluon as a part of the quarkonium system, together with the heavy quark pair. In the course of the calculation we encountered IR singularities induced by the emission of the ultrasoft gluon from a heavy quark line. We explicitly verified that such terms exactly cancel in the matching. As a further consistency check we performed the matching calculation in two different frames of reference: the CM frame of the colliding leptons and the rest frame of the heavy quarkonium. Although these two calculations are technically very different, they lead to the same matching coefficients.

The process $e^+e^- \to \gamma^* \to \chi_{cJ}\,\gamma$ should be observable at B-factories with sufficiently high CM-energy, e. g. Belle II. As no published experimental results are available so far, the phenomenological relevance of contributions from higher Fock states remains to be seen. A correction of $\mathcal{O}(v^2)$ should be sizable for charmonia, which is why expect it to be an important ingredient to the production cross section.

Part VI

Automatic Calculations with FeynCalc and FeynOnium

22 Mathematica Package FeynCalc

22.1 Overview of the Package

FeynCalc is a Mathematica package for algebraic calculations in QFT and semi-automatic evaluation of Feynman diagrams. The very first public version of FeynCalc, developed by Rolf Mertig with guidance from Ansgar Denner and Manfred Böhm, appeared in 1991. The main developments and improvements between 1991 and 1996 were triggered by the work of Mertig in electroweak theory [227–230] and perturbative QCD [231]. In 1998 Rolf Mertig and Rainer Scharf released TARCER [232], a Mathematica package that implements reduction of 2-loop propagator type integrals with arbitrary masses using O. V. Tarasov's recurrence algorithm [233, 234]. Since then TARCER is a part of FeynCalc, that can be loaded on-demand. Between 1997 and 2000, important contributions to the project came from Frederik Orellana, who, besides working on the general code, contributed the sub-package PHI for using FeynCalc in Chiral Perturbation Theory [235] and interfacing to FeynArts 3 [148]. From 2001 until 2014, the development of FeynCalc was mostly constrained to bug fixing and providing support through the mailing list [1], although some interesting projects with external collaborators still were conducted [22]. In 2014 the developer team was joined by the author of this thesis, who started to work on improving the existing code and implementing new features. In the same year the source code repository of FeynCalc was moved to GitHub [2], where the master branch of the repository represents the current development snapshot of the package. Not only the stable releases, but also the development version of FeynCalc can be anonymously downloaded by everyone at any time free of charge. The code is licensed under the General Public License (GPL) version 3. To minimize the number of new bugs and regressions, an extensive unit testing framework [3] with over 3000 tests was introduced.

In view of the existence of several well-known symbolic packages (FormCalc [152], GoSam [153], FDC [25], GRACE [154], Diana [236]) that offer almost fully automatic evaluation of Feynman diagrams at 1-loop from Lagrangian till the cross section, it appears necessary to explain how FeynCalc differs from such tools and why it is useful.

FeynCalc by itself does not provide a fully automatic way of computing cross sections or decay rates. Indeed, FeynCalc cannot generate Feynman diagrams and has no built-in capabilities for the numerical evaluation of master integrals and for the phase space integration. Therefore, these two important steps should be done using other tools.

Second, FeynCalc normally performs all the algebraic manipulations using Mathematica. This leads to a slower performance when compared to tools that rely e. g. on FORM [157] for most of the symbolic manipulations. Despite some possibilities [22] to link FeynCalc with FORM, one should keep in mind that FeynCalc is not very well suited for evaluating hundreds, thousands or even millions of Feynman diagrams.

Finally, FeynCalc does not impose any particular ordering in which different parts (Dirac matrices, SU(N) matrices, loop integrals etc.) of the amplitudes are supposed to be computed. It is always up to the user to decide what is the most useful way to carry out the calculation. This particular feature makes FeynCalc very different from tools

[1] http://www.feyncalc.org/forum
[2] https://github.com/FeynCalc
[3] https://github.com/FeynCalc/feyncalc/tree/master/Tests

that attempt to automatize all the steps of the evaluation process. Such tools usually stick to a particular workflow, which roughly consists of the following steps:

1. The user specifies the process that needs to be computed.
2. If the given process is available in the standard configuration, load the corresponding model (e. g. Standard model (SM)). Otherwise, the user must create a new model that contains this process.
3. Using the loaded model, generate relevant Feynman diagrams for the given process.
4. Evaluate the amplitudes by performing all the necessary algebraic simplifications.
5. Square the amplitude and sum/average over the spins of the involved particles.
6. Integrate over the phase space.

In this list, already the second step might turn out to be problematic. The list of built-in models usually includes SM and some popular (e. g. SUSY inspired) extensions, while more exotic theories require custom model files to be added by the user. If the Lagrangian of such a theory looks very different from $\mathcal{L}_{\text{SM}}$ (e. g. various EFTs of strong interactions), then its implementation becomes a formidable task. On the other hand, even if the model can be implemented with a limited amount of effort, is still might cost more time than just writing down the amplitudes by hand and then manually entering them into the program. Although it is possible to make fully automatic tools accept such amplitudes as input, this is usually much less straight-forward than the standard way of just specifying the process, launching the diagram generator and letting the automatics do the rest.

FEYNCALC avoids such difficulties by accepting any kind of input that consists of valid FEYNCALC objects. Hence, one can enter e. g. standalone Dirac traces, Lorentz vectors or loop integrals and then manipulate them with suitable FEYNCALC functions. In this sense FEYNCALC can be used much like a "calculator" for QFT expressions.

For manual input of Feynman diagrams FEYNCALC contains some functions (`FeynRule`, `FunctionalD`, `CovariantD`, `QuantumField` etc.) for deriving Feynman rules from Lagrangians that are manifestly Lorentz covariant. Furthermore, it is also possible to evaluate Feynman diagrams that were generated automatically (e. g. by FEYNARTS), so that the user always can choose the most efficient strategy to get the calculation done.

Steps 4 and 5 usually imply that the user is not supposed to interfere too much with the evaluation process. Instead, one should rely on the available options to influence the outcome of the calculation. For example, when an automatic tool handles the Dirac algebra, it would normally try to simplify everything it can. While in general, this approach is perfectly fine, sometimes one would like to simplify only some of the Dirac structures, leaving the others (e. g. all the traces involving an odd number of γ_5) untouched. In principle, provided that the particular tool is open source, one can always modify its code accordingly to obtain the desired output. Depending on the complexity of the code and the amount of documentation, this might, however, take some time and even introduce new bugs.

With FEYNCALC, the same result can be achieved in a more simple way, as one always has full access to all kind of intermediate expressions. For this purpose FEYNCALC also provides various helper functions (e. g. `Collect2`, `Expand2`, `Factor2`, `Isolate`, `ExpandScalarProduct`, `DiracGammaExpand`, `MomentumCombine`, `FCLoopSplit`,

`FCLoopIsolate`, `FCLoopExtract`) that can be used to expand, sort, abbreviate and collect the given expressions with respect to particular structures.

Thus, we see that FEYNCALC should not be regarded as a direct competitor to highly automatized packages like e. g. FORMCALC, because it neither provides routines for numerical evaluation nor offers a fully automatic workflow to evaluate a scattering process.

For studies that can be carried out using an automatic tool from the beginning to the end, it obviously would not be very efficient to stick to FEYNCALC. While one certainly can chain FEYNCALC with appropriate tools and libraries to obtain the same result, this would require more time and effort - which could be invested elsewhere.

There are indeed also other publicly available software packages (HEPMATH [156] and PACKAGE-X [155]) that follow the semi-automatic approach to QFT calculations and exhibit many similarities to FEYNCALC. Therefore, let us provide a short comparison between those two packages and FEYNCALC.

Just as FEYNCALC, HEPMATH is an open-source project licensed under GPL version 3. This way the users are able to study the source code and possibly modify HEPMATH to suit their specific needs. PACKAGE-X is on the contrary distributed as a closed source freeware. It can be downloaded directly from the project homepage, but the source code is encrypted, which prevents any possible modifications or extensions by the user. Like FEYNCALC both HEPMATH and PACKAGE-X can manipulate standalone expressions that do not need to represent a valid Feynman diagram. This is done by providing special functions for index contractions, treatment of Dirac algebra and manipulations of loop integrals. In D-dimensions all three packages can work with anticommuting γ_5, but only HEPMATH and FEYNCALC can also treat γ_5 using the Breitenlohner–Maison–t'Hooft-Veltman scheme [79, 80]. Tensor reduction of 1-loop integrals via Passarino–Veltman technique [237] and subsequent simplification of Passarino–Veltman coefficient functions are implemented in each package. FEYNCALC 9 and PACKAGE-X can work with arbitrarily high-rank tensor integrals, but HEPMATH is currently limited to rank 4. As far as the color algebra in concerned, while FEYNCALC can deal with general SU(N) generators, HEPMATH only supports SU(3) and PACKAGE-X does not offer any routines for working with color structures. Both FEYNCALC and HEPMATH provide an interface to FEYNARTS for generating Feynman diagrams. HEPMATH, however, also contains built-in interfaces to LOOPTOOLS [152] and LHAPDF [238] that are missing in the two other packages. On the other hand, PACKAGE-X comes with a library of explicit *analytic* results for 1-, 2-, 3- and 4-point Passarino–Veltman functions with almost arbitrary kinematics. This is a very useful feature that is, to our knowledge, not present in any other automatic or semi-automatic packages.

The above comparison shows that all three packages have somewhat different capabilities, but follow essentially the same philosophy to provide the user with convenient and flexible tools for doing calculations in QFT. Since HEPMATH and PACKAGE-X were released quite recently, they are still not so widely used in research as FEYNCALC. However, as future versions of these packages will likely introduce new useful features and improvements, they will also become more visible in the high energy physics community and thus further promote the idea of using semi-automatic tools in suitable computations.

The niche that FEYNCALC often fills are calculations that are too specific to be done in a fully automatic fashion but also too challenging to be done (only) by pen and paper, so that semi-automatic evaluation is very welcome.

One example for such problems is the determination of matching coefficients in EFTs. Such calculations are usually too special to be automatized in a full generality, but they

can benefit a lot from functions provided by FeynCalc. This is one of the reasons, why FeynCalc enjoys certain popularity in the heavy quarkonium physics community, where it is used to perform the matching between QCD and NRQCD for production [239–241] or decay [212, 242] of heavy quarkonia. Other studies where FeynCalc was used involve such fields as Higgs [243–245] and top quark physics [246], leptonic decays [247] phenomena in hadronic interactions [248, 249], dark matter [250, 251], neutrino physics [252–254] and gravity [255]. It is worth noticing that FeynCalc was also used at some stages of NNLO [256, 257] calculations. Indeed, FeynCalc can be well employed for small or medium size multi-loop processes if one connects it to suitable tools for IBP-reduction (e. g. FIRE [23]) and numeric evaluation of multi-loop integrals (e. g. FIESTA [258] or SecDec [259]).

Last but not least, FeynCalc can be also useful for educational purposes. The possibility of easily getting hands-on experience with computing Feynman diagrams and exploring the different steps involved can be very helpful and motivating for students of quantum field theory.

22.2 New Features in FeynCalc 9.0

In the following we would like to highlight some new features of FeynCalc that were introduced in version 9.0, the first version of the package that was mainly developed by the author of this thesis between 2014 and 2016.

22.2.1 Improved Tensor Decomposition

In the very early versions of FeynCalc, tensor decomposition of 1-loop integrals (via Passarino–Veltman technique [237]) could be done only using the function `OneLoop`, where the maximal rank of the integrals was limited to 4 and the output was always written in terms of Passarino–Veltman coefficient functions. Although one could reduce Passarino–Veltman coefficient functions with rank higher than 4 using `PaVeReduce`, the tensor basis for such higher rank integrals had to be constructed by hand.

While working on [231], Rolf Mertig added to FeynCalc 3.0 a tool (`Tdec`) for tensor decomposition of multi-loop integrals of arbitrary rank and multiplicity (for nonzero Gram determinants) and even included a database (`TIDL`) to load already computed decompositions, but only a very small amount of this functionality was turned into a user-friendly routine `TID` (1-loop only), while the rest remained to "lie idle" in the source code. `TID` was limited to 4-point functions of rank 4 and could not handle kinematic configurations with zero Gram determinants, so that for such cases one was forced to use `OneLoop`. However, in FeynCalc 4 the reduction of rank 4 tensor integrals via `OneLoop` was disabled due to its poor efficiency. As a consequence of all these developments the tensor reduction of 1-loop integrals (especially with rank higher than 3) in the recent FeynCalc versions often turned to be cumbersome and inconvenient.

In FeynCalc 9.0 `TID` was rewritten almost from scratch to allow for 1-loop tensor decompositions of any rank and multiplicity. At the beginning, the function computes Gram determinants for all the unique 1-loop integrals in the expression. If the determinant vanishes, the decomposition for that integral is done in terms of the Passarino–Veltman coefficient functions.

```
In[1]:= FCClearScalarProducts[];
        ScalarProduct[p1, p1] = 0;
        int = FCI[SPD[p2, q] FAD[{q, m0}, {q + p1, m1}]]
```

Out[1]:= $\frac{\text{p2}\cdot q}{\left(q^2-\text{m0}^2\right).\left((\text{p1}+q)^2-\text{m1}^2\right)}$

In[2]:= **TID**[int , q]

Out[2]:= $i\pi^2(\text{p1}\cdot\text{p2})\text{B}_1\left(0,\text{m0}^2,\text{m1}^2\right)$

Otherwise, `TID` will output the result in terms of scalar 1-loop integrals.

In[1]:= **FCClearScalarProducts**[];
int = **FCI**[**SPD**[p2, q] **FAD**[{q, m0}, {q + p1, m1}]]

Out[1]:= $-\frac{\left(\text{m0}^2-\text{m1}^2+\text{p1}^2\right)(\text{p1}\cdot\text{p2})}{2\text{p1}^2\left(q^2-\text{m0}^2\right).\left((q-\text{p1})^2-\text{m1}^2\right)}+\frac{\text{p1}\cdot\text{p2}}{2\text{p1}^2\left(q^2-\text{m0}^2\right)}-\frac{\text{p1}\cdot\text{p2}}{2\text{p1}^2\left(q^2-\text{m1}^2\right)}$

If needed, those scalar integrals can be converted to Passarino–Veltman scalar functions by using `ToPaVe`, which is also available since FEYNCALC 9.0.

In[2]:= **TID**[int , q] // **ToPaVe**[#, q] &

Out[2]:= $-\frac{i\pi^2\left(\text{m0}^2-\text{m1}^2+\text{p1}^2\right)(\text{p1}\cdot\text{p2})\text{B}_0\left(\text{p1}^2,\text{m0}^2,\text{m1}^2\right)}{2\text{p1}^2}+\frac{i\pi^2\text{A}_0\left(\text{m0}^2\right)(\text{p1}\cdot\text{p2})}{2\text{p1}^2}-\frac{i\pi^2\text{A}_0\left(\text{m1}^2\right)(\text{p1}\cdot\text{p2})}{2\text{p1}^2}$

The decompositions in terms of scalar integrals tend to become very large already for 3-point functions, so to obtain more compact expressions it might be desirable to use the basis of Passarino–Veltman coefficient functions, even if there are no zero Gram determinants. This can be easily achieved via the option `UsePaVeBasis`.

In[1]:= int = **FCI**[**FVD**[q, mu] **FVD**[q, nu] **FAD**[{q, m0}, {q + p1, m1}, {q + p2, m2}]]

Out[1]:= $\frac{q^{\text{mu}}q^{\text{nu}}}{\left(q^2-\text{m0}^2\right).\left((\text{p1}+q)^2-\text{m1}^2\right).\left((\text{p2}+q)^2-\text{m2}^2\right)}$

In[2]:= **TID**[int /(**I**∗**Pi**^2), q, **UsePaVeBasis** −> **True**]

Out[2]:= $g^{\text{munu}}\text{C}_{00}\left(\text{p1}^2,-2(\text{p1}\cdot\text{p2})+\text{p1}^2+\text{p2}^2,\text{p2}^2,\text{m0}^2,\text{m1}^2,\text{m2}^2\right)$
$+\text{p1}^{\text{mu}}\text{p1}^{\text{nu}}\text{C}_{11}\left(\text{p1}^2,-2(\text{p1}\cdot\text{p2})+\text{p1}^2+\text{p2}^2,\text{p2}^2,\text{m0}^2,\text{m1}^2,\text{m2}^2\right)$
$+\left(\text{p2}^{\text{mu}}\text{p1}^{\text{nu}}+\text{p1}^{\text{mu}}\text{p2}^{\text{nu}}\right)\text{C}_{12}\left(\text{p1}^2,-2(\text{p1}\cdot\text{p2})+\text{p1}^2+\text{p2}^2,\text{p2}^2,\text{m0}^2,\text{m1}^2,\text{m2}^2\right)$
$+\text{p2}^{\text{mu}}\text{p2}^{\text{nu}}\text{C}_{22}\left(\text{p1}^2,-2(\text{p1}\cdot\text{p2})+\text{p1}^2+\text{p2}^2,\text{p2}^2,\text{m0}^2,\text{m1}^2,\text{m2}^2\right)$

All the Passarino–Veltman functions are defined as in LOOPTOOLS [152] and explicit definitions are encoded for functions with up to 5 legs. For integrals with even higher multiplicities the coefficient functions (denoted as `GenPaVe`) simply include the dependence on the external momenta that can be used to convert them to the LOOPTOOLS or any other convention.

In[1]:= int = **FCI**[**FVD**[q, mu] **FVD**[q,nu] **FAD**[{q, m0}, {q, m1}, {q, m2}, {q, m3}, {q + p4, m4}, {q + p5, m5}, {q + p6, m6}]]

Out[1]:= $\left(q^{\text{mu}}q^{\text{nu}}\right)/\left(q^2-\text{m0}^2\right).\left(q^2-\text{m1}^2\right).\left((\text{p2}+q)^2-\text{m2}^2\right).\left((\text{p3}+q)^2-\text{m3}^2\right).$
$\left((\text{p4}+q)^2-\text{m4}^2\right).\left((\text{p5}+q)^2-\text{m5}^2\right).\left((\text{p6}+q)^2-\text{m6}^2\right)$

In[2]:= **TID**[int /(**I**∗**Pi**^2), q, **UsePaVeBasis** −> **True**]

Out[2]:=

$$g^{\text{munu}}\text{GenPaVe}\left[\{0,0\},\left\{\begin{array}{cc}0 & \text{m0}\\ \text{p1} & \text{m1}\\ \text{p2} & \text{m2}\\ \text{p3} & \text{m3}\\ \text{p4} & \text{m4}\\ \text{p5} & \text{m5}\\ \text{p6} & \text{m6}\end{array}\right\}\right] + \text{p1}^{\text{mu}}\text{p1}^{\text{nu}}\text{GenPaVe}\left[\{1,1\},\left\{\begin{array}{cc}0 & \text{m0}\\ \text{p1} & \text{m1}\\ \text{p2} & \text{m2}\\ \text{p3} & \text{m3}\\ \text{p4} & \text{m4}\\ \text{p5} & \text{m5}\\ \text{p6} & \text{m6}\end{array}\right\}\right] + \ldots$$

Here, `GenPaVe[{1,1},{{0,m0},{Momentum[p1],m1}, ...,{Momentum[p6],m6}}]` stands for the coefficient function of $p_1^\mu p_1^\nu$ in the tensor decomposition of

$$\int d^D q \, \frac{q^\mu q^\nu}{[q^2-m_0^2][(q-p_1)^2-m_1^2][(q-p_2)^2-m_2^2]\cdots[(q-p_6)^2-m_6^2]}. \tag{22.1}$$

Since this kind of output is useful if one explicitly wants to obtain coefficient functions defined in a different way than in LOOPTOOLS, it can be activated also for functions with lower multiplicities by setting the option `GenPaVe` of `TID` to `True`.

In[1]:= int = **FCI**[**FVD**[q, mu] **FVD**[q, nu] **FAD**[{q, m0}, {q + p1, m1}]]

Out[1]:= $\frac{q^{\text{mu}}\,q^{\text{nu}}}{\left(q^2-\text{m0}^2\right).\left((\text{p1}+q)^2-\text{m1}^2\right)}$

In[2]:= **TID**[int /(I∗**Pi**^2), q, **UsePaVeBasis** −> **True**, **GenPaVe** −> **True**]

Out[2]:=

$$g^{\text{munu}}\text{GenPaVe}\left(\{0,0\},\left\{\begin{array}{cc}0 & \text{m0}\\ \text{p1} & \text{m1}\end{array}\right\}\right) + \text{p1}^{\text{mu}}\text{p1}^{\text{nu}}\text{GenPaVe}\left(\{1,1\},\left\{\begin{array}{cc}0 & \text{m0}\\ \text{p1} & \text{m1}\end{array}\right\}\right)$$

One should also keep in mind that FEYNCALC cannot perform any further simplifications of `GenPaVe` functions, because internally they are not recognized as Passarino–Veltman integrals (`PaVe`).

It is well known, that for a general multi-loop multi-scale integral, tensor decomposition does not allow us to cancel all the scalar products containing loop momenta in the numerator, as it is the case at 1-loop. Nevertheless, this technique is widely used also in calculations beyond 1-loop, especially if one needs to deal with integrals that have loop momenta contracted to Dirac matrices or epsilon tensors or even loop momenta with free Lorentz indices. FEYNCALC uses a special reduction algorithm (implemented in `Tdec`) that consists of decomposing the integral into all tensor structures allowed by the symmetries and using a modified version of Gaussian elimination to obtain the coefficients of each tensor.

Since tensor decomposition of multi-loop integrals with FEYNCALC's function `Tdec` is not very straight-forward and usually requires some additional MATHEMATICA code, in FEYNCALC 9.0 a new function `FCMultiLoopTID` was added, that makes multi-loop tensor reduction work out of the box.

In[1]:= int = **FCI**[**FVD**[q1, mu] **FVD**[q2, nu] **FAD**[q1, q2, {q1 − p1}, {q2 − p1}, {q1 − q2}]]

Out[1]:= $\frac{\text{q1}^{\text{mu}}\text{q2}^{\text{nu}}}{\text{q1}^2.\text{q2}^2.(\text{q1}-\text{p1})^2.(\text{q2}-\text{p2})^2.(\text{q1}-\text{q2})^2}$

In[2]:= **FCMultiLoopTID**[int, {q1, q2}]

Out[2]:=

$$\frac{D\text{p1}^{\text{mu}}\text{p1}^{\text{nu}}-\text{p1}^2 g^{\text{munu}}}{4(D-1)\text{q2}^2.\text{q1}^2.(\text{q2}-\text{p1})^2.(\text{q1}-\text{q2})^2.(\text{q1}-\text{p1})^2} - \frac{D\text{p1}^{\text{mu}}\text{p1}^{\text{nu}}-\text{p1}^2 g^{\text{munu}}}{2(D-1)\text{p1}^4\text{q1}^2.(\text{q2}-\text{p1})^2.(\text{q1}-\text{q2})^2}$$

$$+\frac{\text{p1}^2 g^{\text{munu}}-\text{p1}^{\text{mu}}\text{p1}^{\text{nu}}}{(D-1)\text{p1}^2\text{q2}^2.\text{q1}^2.(\text{q1}-\text{q2})^2.(\text{q1}-\text{p1})^2} - \frac{\text{p1}^2 g^{\text{munu}}-\text{p1}^{\text{mu}}\text{p1}^{\text{nu}}}{2(D-1)\text{p1}^2\text{q2}^2.\text{q1}^2.(\text{q2}-\text{p1})^2.(\text{q1}-\text{p1})^2}$$

Unfortunately, the reduction breaks down when the corresponding Gram determinant vanishes. For such cases, in a future version it is planned to include a more useful algorithm.

22.2.2 New Partial Fractioning Algorithm

Since the version 3, FEYNCALC includes `ScalarProductCancel` and `Apart2` that can be used to rewrite loop integrals in a simpler form. `ScalarProductCancel` essentially applies the well-known identity [237]

$$q \cdot p = \frac{1}{2}[(q+p)^2 + m_2^2 - (q^2 + m_1^2) - p^2 - m_2^2 + m_1^2] \tag{22.2}$$

repeatedly, until all scalar products containing loop momenta that can be canceled in this way are eliminated. `Apart2` uses the trivial identity

$$\frac{1}{(q^2 - m_1^2)(q^2 - m_2^2)} = \frac{1}{m_1^2 - m_2^2}\left(\frac{1}{q^2 - m_1^2} - \frac{1}{q^2 - m_2^2}\right) \tag{22.3}$$

to simplify suitable denominators. In principle, these two functions implement some aspects of partial fractioning, i. e. the decomposition of a loop integral with linearly dependent propagators into a sum of integrals where each integral contains only linearly independent propagators. Notice that here we count scalar products that involve loop momenta as propagators with negative exponents. Unfortunately, there are plenty of examples where neither `ScalarProductCancel` nor `Apart2` can partial fraction an integral with linearly dependent propagators, e. g.

$$\int d^D q \, \frac{1}{q^2 (q-p)^2 (q+p)^2} = \frac{1}{p^2} \int d^D q \left(\frac{1}{q^2 (q-p)^2} - \frac{1}{(q-p)^2 (q+p)^2}\right) \tag{22.4}$$

A general partial fractioning algorithm that is suitable for multi-loop integrals including its MATHEMATICA implementation (APART[4]) was presented in [176]. The author has also shown how his code can be used together with FEYNCALC in order to decompose different loop integrals. For this the user is required to convert a loop integral in the FEYNCALC notation (with denominator encoded in `FeynAmpDenominator`) to a somewhat different form and to specify all the scalar products that contain loop momenta and appear in this loop integral. After the decomposition the resulting integrals need to be converted back into FEYNCALC notation.

In FEYNCALC 9.0 the algorithm from [176] was adopted and reimplemented to be the standard partial fractioning routine. As such, it is fully integrated with all other FEYNCALC functions and objects and does not require any explicit conversion of the input or output.

In[1]:= `int = FAD[{q}, {q - p}, {q + p}]`

Out[1]:= $\frac{1}{q^2.(q-p)^2.(p+q)^2}$

In[2]:= `ApartFF[int1, {q}]`

Out[2]:= $\frac{1}{p^2 q^2.(q-p)^2} - \frac{1}{p^2 q^2.(q-2p)^2}$

The name of the corresponding function is `ApartFF`, which stands for "Apart Feng Feng" and serves as an additional acknowledgment of the original author. One should

[4] `https://github.com/F-Feng/APart`

also notice that while the original APART can be used for partial fractioning of general multivariate polynomials, the FEYNCALC version is limited only to polynomials that appear in Feynman diagrams as propagators and scalar products. Thus, it is much less general than APART but is also more convenient when used with FEYNCALC.

22.2.3 Tools for Interfacing FEYNCALC with Packages for IBP-reduction

In modern multi-loop calculations, reduction of scalar loop integrals via integration-by-parts (IBP) identities [171] is a regular step needed to arrive to a smaller set of master integrals.

Although FEYNCALC does not include a general purpose tool for IBP reduction (the built-in TARCER [232] is suitable only for 2-loop self-energy type integrals), this omission can be compensated by using one of the publicly available IBP-packages (FIRE [23], LITERED [260], REDUZE [261], AIR [262]). However, one should keep in mind that such tools usually expect their input to contain only loop integrals with linearly independent propagators that form a basis. For example, the integral

$$\int d^D q_1\, d^D q_2\, d^D q_3\, \frac{1}{[q_1^2 - m^2]^2[(q_1+q_3)^2 - m^2](q_2 - q_3)^2 q_2^2} \tag{22.5}$$

cannot be processed by FIRE in this form because q_1^2, q_2^2, $(q_1+q_3)^2$ and $(q_2-q_3)^2$ alone do not form a basis.

```
In[1]:= << FIRE5`FIRE5`
        Internal = {q1, q2, q3};
        External = {};
        Propagators = {q1^2 - m^2, (q1 + q3)^2 - m^2, (q2 - q3)^2, q2^2};
        PrepareIBP[];

Out[1]:= FIRE, version 5.1
         DatabaseUsage: 0
         UsingFermat: False
         Not enough propagators. Add irreducible nominators
```

If one includes also q_3^2 and $q_1 \cdot q_2$ with zero exponentials, then we have a proper basis and the reduction works as it should. Also the integral

$$\int d^D q_1\, d^D q_2\, \frac{(p\cdot q_1)^2 (p\cdot q_2)^2}{[q_1^2 - m^2][q_2^2 - m^2](q_1 - p)^2 (q_2 - p)^2 (q_1 - q_2)^2} \tag{22.6}$$

cannot be reduced right away, this time because its propagators are linearly dependent.

```
In[1]:= << FIRE5`FIRE5`
        Internal = {q1, q2};
        External = {};
        Propagators = {q1^2 - m^2, q2^2 - m^2, (q1 - p)^2, (q2 - p)^2, (q1 - q2)^2, p q1, p q2};
        PrepareIBP[];

Out[1]:= FIRE, version 5.1
         DatabaseUsage: 0
         UsingFermat: False
         Linearly  dependant propagators. Perform reduction first
```

To detect such problems before the reduction actually fails, FEYNCALC 9.0 introduces two new special functions. When `FCLoopBasisIncompleteQ` is applied to a loop integral, it returns `True` if this integral does not contain enough irreducible propagators.

```
In[1]:= intP1 = FCI[FAD[{q1, m, 2}, {q1 + q3, m}, {q2 - q3}, q2]]
```

Out[1]:= $\frac{1}{(\text{q1}^2-m^2).(\text{q1}^2-m^2).((\text{q1}+\text{q3})^2-m^2).(\text{q2}-\text{q3})^2.\text{q2}^2}$

In[2]:= **FCLoopBasisIncompleteQ**[intP1, {q1, q2, q3}]
Out[2]:= **True**

In[3]:= **FCLoopBasisIncompleteQ**[**SPD**[q3, q3] **SPD**[q1, q2] intP1, {q1, q2, q3}]
Out[3]:= **False**

An integral with linearly dependent propagators will be detected by `FCLoopBasisOverdeterminedQ`,

In[1]:= intP2 = **FCI**[**SPD**[p, q1]^2 **SPD**[p, q2]^2 **FAD**[{q1, m}, {q2, m}, q1 − p, q2 − p, q1 − q2]]

Out[1]:= $\frac{(p\cdot\text{q1})^2(p\cdot\text{q2})^2}{(\text{q1}^2-m^2).(\text{q2}^2-m^2).(\text{q1}-p)^2.(\text{q2}-p)^2.(\text{q1}-\text{q2})^2}$

In[2]:= **FCLoopBasisOverdeterminedQ**[intP2, {q1, q2, q3}]
Out[2]:= **True**

so that only an integral for which both functions return `False` can be reduced in a straight-forward way.

In a practical calculation where one knows what integral topologies are involved, such issues can be easily resolved. In particular, a clever choice of additional propagators that are needed to have a basis, can greatly simplify the reduction. On the other hand, depending on the size of the problem and the number of topologies involved, a less clever but fully automatic solution may also be useful.

For an integral with linearly dependent propagators we can use `ApartFF`, that is guaranteed to decompose it into integrals where all propagators are linearly independent.

In[1]:= **ApartFF**[intP2, {q1, q2}]

Out[1]:= $\frac{\left(m^2+p^2\right)^4}{16\left(\text{q1}^2-m^2\right).\left(\text{q2}^2-m^2\right).(\text{q2}-p)^2.(\text{q1}-\text{q2})^2.(\text{q1}-p)^2}$
$-\frac{\left(m^2+p^2\right)^3}{8\left(\text{q1}^2-m^2\right).\left(\text{q2}^2-m^2\right).(\text{q1}-\text{q2})^2.(\text{q1}-p)^2}$
$-\frac{\left(m^2+p^2\right)(p\cdot\text{q1})}{8\left(\text{q2}^2-m^2\right).(\text{q1}-\text{q2})^2.(\text{q1}-p)^2}+\cdots$

For integrals with an incomplete basis of propagators one can use the new function `FCLoopBasisFindCompletion` that finds out which irreducible propagators (with zero exponents) are missing.

In[1]:= **FCLoopBasisFindCompletion**[intP1, {q1, q2, q3}]

Out[1]:= $\left\{\frac{1}{(\text{q1}^2-m^2).(\text{q1}^2-m^2).((\text{q1}+\text{q3})^2-m^2).(\text{q2}-\text{q3})^2.\text{q2}^2}, \{-(\text{q1}\cdot\text{q3})+\text{q2}\cdot\text{q3}+2\text{q3}^2, \text{q1}\cdot\text{q2}\}\right\}$

With the suggested propagators the integral is guaranteed to have a complete basis, but the choice of the propagators themselves is usually not very clever. This is because in general FeynCalc cannot guess the topology of the given integral without any additional input. It is planned to provide a possibility for specifying the topology, which would admittedly make `FCLoopBasisFindCompletion` much more useful than it is now.

Still, with `ApartFF` and `FCLoopBasisFindCompletion` it is now possible to automatically bring any scalar multi-loop integral in FeynCalc notation to a form that can be directly (modulo notation conversion) forwarded to an IBP tool.

22.2.4 Advanced Extraction of Loop Integrals

The idea to use FEYNCALC as a sort of switch board for different computational tools in a larger framework (c. f. e. g. [263]) is further developed in version 9.0 by the introduction of new functions that can extract different loop integrals from the given expression.

One of them, `FCLoopSplit`, breaks the given expression into four pieces, which are

1. Terms that contain no loop integrals.
2. Terms that only contain scalar loop integrals without any loop momenta in the denominators, e. g.
$$\int d^D q \, \frac{1}{q^2 - m^2}. \tag{22.7}$$
3. Terms that contain scalar loop integrals with loop momenta dependent scalar products in the denominators, e. g.
$$\int d^D q \, \frac{(q \cdot p)}{q^2 (q-p)^2}. \tag{22.8}$$
4. Terms that contain tensor loop integrals, e. g.
$$\int d^D q \, \frac{q^\mu q^\nu}{q^2 - m^2} \quad \text{or} \quad \int d^D q \, \frac{(\gamma \cdot q)}{q^2 (q-p)^2}. \tag{22.9}$$

In [1]:= int = **FCI**[(**GSD**[q − p] + m).**GSD**[x] **FAD**[q, {q − p, m}] + (m^2 + **SPD**[q, q]) **FAD**[{q, m,2}]];
Out[1]:= $\frac{(m+\gamma\cdot(q-p)).(\gamma\cdot x)}{q^2.\left((q-p)^2-m^2\right)} + \frac{m^2+q^2}{\left(q^2-m^2\right).\left(q^2-m^2\right)}$

In [2]:= **FCLoopSplit**[int, {q}]

Out[2]:= $\left\{0, \frac{m\gamma\cdot x-(\gamma\cdot p).(\gamma\cdot x)}{q^2.\left((q-p)^2-m^2\right)} + \frac{m^2}{\left(q^2-m^2\right).\left(q^2-m^2\right)}, \frac{q^2}{\left(q^2-m^2\right).\left(q^2-m^2\right)}, \frac{(\gamma\cdot q).(\gamma\cdot x)}{q^2.\left((q-p)^2-m^2\right)}\right\}$

This splitting makes it easier to handle different types of loop integrals and to simplify them with FEYNCALC or other tools. For example, if one wants to perform tensor reduction of multi-loop integrals with FARE [264] instead of `FCMultiLoopTID`, it can be done by applying `FCLoopSplit` to the given expression and working with the fourth element of the resulting list, while the other elements remain unchanged and can be later added to the final expression.

To handle a larger number of loop diagrams efficiently, `FCLoopSplit` alone is not sufficient. This is because same integrals may appear multiple times in different diagrams and ignoring this fact would make the evaluation more complex than it actually is. To avoid this kind of problems one should better first analyze the amplitude and extract all the unique integrals. Then each unique integral needs to be evaluated only once, no matter how often it appears in the full expression. In FEYNCALC 9.0 this can be conveniently done with `FCLoopIsolate`. The function wraps loop integers with the given head, such that the list of unique integrals can be quickly created with MATHEMATICA's `Cases` and `Union` or just FEYNCALC's `Cases2`

In [1]:= int = **FCI**[**GSD**[q − p1].(**GSD**[q − p2] + M).**GSD**[p3] **SPD**[q, p2] **FAD**[q, q − p1, {q − p2, m}]];

Out[1]:= $\frac{(\text{p2}\cdot q)(\gamma\cdot(q-\text{p1})).(M+\gamma\cdot(q-\text{p2})).(\gamma\cdot\text{p3})}{q^2.(q-\text{p1})^2.\left((q-\text{p2})^2-m^2\right)}$

In [2]:= res = **FCLoopIsolate**[int, {q}, **Head** −> loopInt]

Out[2]= loopInt $\left(\frac{\text{p2}\cdot q}{q^2.(q-\text{p1})^2.\left((q-\text{p2})^2-m^2\right)}\right)((\gamma\cdot\text{p1}).(\gamma\cdot\text{p2}).(\gamma\cdot\text{p3})-M(\gamma\cdot\text{p1}).(\gamma\cdot\text{p3}))+$

MloopInt $\left(\frac{(\text{p2}\cdot q)(\gamma\cdot q).(\gamma\cdot\text{p3})}{q^2.(q-\text{p1})^2.\left((q-\text{p2})^2-m^2\right)}\right)$ − loopInt $\left(\frac{(\text{p2}\cdot q)(\gamma\cdot\text{p1}).(\gamma\cdot q).(\gamma\cdot\text{p3})}{q^2.(q-\text{p1})^2.\left((q-\text{p2})^2-m^2\right)}\right)$

−loopInt $\left(\frac{(\text{p2}\cdot q)(\gamma\cdot q).(\gamma\cdot\text{p2}).(\gamma\cdot\text{p3})}{q^2.(q-\text{p1})^2.\left((q-\text{p2})^2-m^2\right)}\right)$ + loopInt $\left(\frac{(\text{p2}\cdot q)(\gamma\cdot q).(\gamma\cdot q).(\gamma\cdot\text{p3})}{q^2.(q-\text{p1})^2.\left((q-\text{p2})^2-m^2\right)}\right)$

In[3]:= Cases2[res, loopInt]

Out[3]= $\left\{\text{loopInt}\left(\frac{\text{p2}\cdot q}{q^2.(q-\text{p1})^2.\left((q-\text{p2})^2-m^2\right)}\right),\ \text{loopInt}\left(\frac{(\text{p2}\cdot q)(\gamma\cdot q).(\gamma\cdot\text{p3})}{q^2.(q-\text{p1})^2.\left((q-\text{p2})^2-m^2\right)}\right),\right.$

$\text{loopInt}\left(\frac{(\text{p2}\cdot q)(\gamma\cdot\text{p1}).(\gamma\cdot q).(\gamma\cdot\text{p3})}{q^2.(q-\text{p1})^2.\left((q-\text{p2})^2-m^2\right)}\right),\ \text{loopInt}\left(\frac{(\text{p2}\cdot q)(\gamma\cdot q).(\gamma\cdot\text{p2}).(\gamma\cdot\text{p3})}{q^2.(q-\text{p1})^2.\left((q-\text{p2})^2-m^2\right)}\right),$

$\left.\text{loopInt}\left(\frac{(\text{p2}\cdot q)(\gamma\cdot q).(\gamma\cdot q).(\gamma\cdot\text{p3})}{q^2.(q-\text{p1})^2.\left((q-\text{p2})^2-m^2\right)}\right)\right\}$

The combined application of `FCLoopIsolate` and `FCLoopSplit` is provided by `FCLoopExtract`. This function returns a list of three entries. The first one contains the part of the expression, which is free of loop integrals. The second entry consists of the remaining expression where every loop integral is wrapped with the given head. Finally, the last entry contains a list of all the unique loop integrals in the expression.

In[4]:= **FCLoopExtract**[int, {q}, loopInt][[1]]

Out[4]= 0

In[5]:= **FCLoopExtract**[int, {q}, loopInt][[2]] ===
FCLoopIsolate[int, {q}, **Head** −> loopInt]

Out[5]= **True**

In[6]:= **FCLoopExtract**[int, {q}, loopInt][[3]] ===
Cases2[res, loopInt]

Out[6]= **True**

Suppose that we want to evaluate these loop integrals using some custom function `loopEval` (in this example it is just a dummy function that computes the hash of each loop integral). All we need to do is to apply `FCLoopExtract` to the initial expression, map the list of the unique integrals to `loopEval`, create a substitution rule and apply this rule to our expression in order to get the final result.

In[7]:= {rest, loops, intsUnique} = **FCLoopExtract**[int, {q}, loopInt];

In[8]:= loopEval[x_] := **ToString**[**Hash**[x]];

In[9]:= solsList = loopEval /@ uniqueInts

Out[9]= {2069116068,115167616,776830638,1878762839,1337833147}

In[10]:= repRule = **MapThread**[**Rule**[#1, #2] &, {intsUnique, solsList}]

Out[10]= $\left\{\text{loopInt}\left(\frac{\text{p2}\cdot q}{q^2.(q-\text{p1})^2.\left((q-\text{p2})^2-m^2\right)}\right)\to 2069116068,\right.$

$\left.\text{loopInt}\left(\frac{(\text{p2}\cdot q)(\gamma\cdot q).(\gamma\cdot\text{p3})}{q^2.(q-\text{p1})^2.\left((q-\text{p2})^2-m^2\right)}\right)\to 115167616,\right.$

$$\text{loopInt}\left(\frac{(\text{p2}\cdot q)(\gamma\cdot\text{p1}).(\gamma\cdot q).(\gamma\cdot\text{p3})}{q^2.(q-\text{p1})^2.\left((q-\text{p2})^2-m^2\right)}\right) \to 776830638,$$
$$\text{loopInt}\left(\frac{(\text{p2}\cdot q)(\gamma\cdot q).(\gamma\cdot\text{p2}).(\gamma\cdot\text{p3})}{q^2.(q-\text{p1})^2.\left((q-\text{p2})^2-m^2\right)}\right) \to 1878762839,$$
$$\text{loopInt}\left(\frac{(\text{p2}\cdot q)(\gamma\cdot q).(\gamma\cdot q).(\gamma\cdot\text{p3})}{q^2.(q-\text{p1})^2.\left((q-\text{p2})^2-m^2\right)}\right) \to 1337833147\Bigg\}$$

```
In[11]:= res = rest + loops /. repRule
```

Out[11]:= $115167616M + 1337833147 - 1878762839 +$

$$2069116068((\gamma\cdot\text{p1}).(\gamma\cdot\text{p2}).(\gamma\cdot\text{p3}) - M(\gamma\cdot\text{p1}).(\gamma\cdot\text{p3})) - 776830638$$

With `FCLoopSplit`, `FCLoopIsolate` and `FCLoopExtract` it is now much easier not only to manipulate loop integrals, but also to check, which integrals actually appear in an expression. Unique loop integrals can be evaluated with tools outside of FEYNCALC and then substituted back by just a couple of lines of MATHEMATICA code.

22.2.5 Better Interface to FEYNARTS

If FEYNCALC needs to be used with a Feynman diagram generator, then FEYNARTS is usually the most convenient choice. Initially the syntax of both packages was adjusted to make them fully compatible with each other. In fact, for the very first version of FEYNARTS [265], FEYNCALC was referred to as the standard tool to evaluate the generated amplitudes. As FEYNARTS was developed further, the full compatibility was lost, but even now, the output of FEYNARTS can be converted into valid FEYNCALC input with only little effort. A more severe problem in using this setup arises when FEYNARTS and FEYNCALC are loaded in the same MATHEMATICA session. Unfortunately, both packages contain objects with same names but different contexts, definitions and properties (e. g. `FourVector`, `DiracMatrix` or `FeynAmpDenominator`) such that it is not possible to use them together without risking inconsistencies. To avoid these issues FEYNCALC is able to automatically patch the source code of FEYNARTS by renaming all the conflicting symbols, such that e. g. `FourVector` becomes `FAFourVector` and no variable shadowing can occur. This patching mechanism was greatly improved in FEYNCALC 9.0 both in terms of user-friendliness and compatibility to other MATHEMATICA packages. The patched copy of FEYNARTS now resides in the *FeynArts* directory inside the FEYNCALC installation. By default, this directory is empty. The user is expected to manually download the latest FEYNARTS tarball from the official website[5] and unpack its content to *FeynCalc/FeynArts*. When FEYNCALC is loaded via

```
$LoadFeynArts=True;
<<FeynCalc`
```

it will automatically detect FEYNARTS installation and offer the user to patch it. This procedure is required only once and after that one can use FEYNARTS and FEYNCALC together without any problems.

After all the required diagrams have been generated and turned into amplitudes with FEYNARTS ' function `CreateFeynAmp`, the output still needs to be converted into valid FEYNCALC input. In FEYNCALC 9.0 this is handled by the new function `FCFAConvert` that takes the output of `CreateFeynAmp` and generates proper FEYNCALC expressions based on the given options. With `IncomingMomenta`, `OutgoingMomenta` and

[5] http://www.feynarts.de

`LoopMomenta` the user can specify how the corresponding momenta should be named. Otherwise they will be denoted as `InMom1`, `InMom2`, ..., `OutMom1`, `OutMom2`, ...and `LoopMom1`, `LoopMom2`, ... Polarization vectors of external massless bosons are by default not transverse, but can be made so if the momenta of the bosons are listed in `TransversePolarizationVectors`. The splitting of fermion-fermion-boson couplings into left and right handed chirality projectors (default in FEYNARTS) can be undone with the option `UndoChiralSplittings`. For example, the amplitude for the tree level process $\gamma^* u \to u g$ is obtained via

```
In[1]:= $LoadFeynArts = True;
        $FeynCalcStartupMessages = False;
        << FeynCalc`;
        $FAVerbose = 0;

In[2]:= diags = InsertFields[ CreateTopologies[0, 2 -> 2], {F[3, {1}],
         V[1]} -> {V[5], F[3, {1}]}, InsertionLevel -> {Classes},
         Model -> "SMQCD"];

In[3]:= FCFAConvert[CreateFeynAmp[diags], IncomingMomenta -> {p1, kp},
        OutgoingMomenta -> {kg, p2}, UndoChiralSplittings -> True,
        TransversePolarizationVectors -> {kg}, DropSumOver -> True,
         List -> False] // Contract
```

$$\text{Out[3]:= } -\frac{2\text{EL}\,g_s\,T^{\text{Glu3}}_{\text{Col4Col1}}\left(\varphi(\overline{\text{p2}},\text{MU})\right).\left(\bar{\gamma}\cdot\bar{\varepsilon}^*(\text{kg})\right).\left(\bar{\gamma}\cdot\left(\overline{\text{kg}}+\overline{\text{p2}}\right)+\text{MU}\right).\left(\bar{\gamma}\cdot\bar{\varepsilon}(\text{kp})\right).\left(\varphi(\overline{\text{p1}},\text{MU})\right)}{3\left((-\text{kg}-\text{p2})^2-\text{MU}^2\right)}$$
$$-\frac{2\text{EL}\,g_s\,T^{\text{Glu3}}_{\text{Col4Col1}}\left(\varphi(\overline{\text{p2}},\text{MU})\right).\left(\bar{\gamma}\cdot\bar{\varepsilon}(\text{kp})\right).\left(\bar{\gamma}\cdot\left(\overline{\text{p2}}-\overline{\text{kp}}\right)+\text{MU}\right).\left(\bar{\gamma}\cdot\bar{\varepsilon}^*(\text{kg})\right).\left(\varphi(\overline{\text{p1}},\text{MU})\right)}{3\left((\text{kp}-\text{p2})^2-\text{MU}^2\right)}$$

22.2.6 Finer-grained Expansions

To expand scalar products of Lorentz vectors FEYNCALC provides the function `Expand-ScalarProduct`. The standard behavior of this command is to expand every scalar product in the expression.

```
In[1]:= exp = SPD[q1, p1 + p2] SPD[q2, p3 + p4] SPD[p5 + p6, p7 + p8]
```

$$\text{Out[1]:= } ((\text{p1}+\text{p2})\cdot\text{q1})((\text{p3}+\text{p4})\cdot\text{q2})((\text{p5}+\text{p6})\cdot(\text{p7}+\text{p8}))$$

```
In[2]:= ExpandScalarProduct[exp]
```

$$\text{Out[2]:= } (\text{p1}\cdot\text{q1}+\text{p2}\cdot\text{q1})(\text{p3}\cdot\text{q2}+\text{p4}\cdot\text{q2})(\text{p5}\cdot\text{p7}+\text{p5}\cdot\text{p8}+\text{p6}\cdot\text{p7}+\text{p6}\cdot\text{p8})$$

which might lead to an unnecessary increase of terms, if the user wants to expand only some particular scalar products. FEYNCALC 9.0 improves `ExpandScalarProduct` by introducing the option `Momentum` which allows to specify a list of momenta that need to be contained in a scalar product that will be expanded. All the other scalar products will remain untouched.

```
In[1]:= exp = SPD[q1, p1 + p2] SPD[q2, p3 + p4] SPD[p5 + p6, p7 + p8]
```

$$\text{Out[1]:= } ((\text{p1}+\text{p2})\cdot\text{q1})((\text{p3}+\text{p4})\cdot\text{q2})((\text{p5}+\text{p6})\cdot(\text{p7}+\text{p8}))$$

```
In[2]:= ExpandScalarProduct[exp, Momentum -> {q1}]
```

$$\text{Out[2]:= } (\text{p1}\cdot\text{q1}+\text{p2}\cdot\text{q1})((\text{p3}+\text{p4})\cdot\text{q2})((\text{p5}+\text{p6})\cdot(\text{p7}+\text{p8}))$$

```
In[3]:= ExpandScalarProduct[exp, Momentum -> {q2}]
```

$$\text{Out[2]:= } (\text{p3}\cdot\text{q2}+\text{p4}\cdot\text{q2})((\text{p1}+\text{p2})\cdot\text{q1})((\text{p5}+\text{p6})\cdot(\text{p7}+\text{p8}))$$

The same option is now present also in `DiracGammaExpand` that is used to expand Lorentz vectors contracted with Dirac matrices

In [1]:= exp = **GSD**[q1 + p1 + p2].**GSD**[q2 + p3 + p4].**GSD**[p5 + p6 + p7 + p8]

Out[1]:= $(\gamma \cdot (\text{p1} + \text{p2} + \text{q1})).(\gamma \cdot (\text{p3} + \text{p4} + \text{q2})).(\gamma \cdot (\text{p5} + \text{p6} + \text{p7} + \text{p8}))$

In [2]:= **DiracGammaExpand**[exp]

Out[2]:= $(\gamma \cdot \text{p1} + \gamma \cdot \text{p2} + \gamma \cdot \text{q1}).(\gamma \cdot \text{p3} + \gamma \cdot \text{p4} + \gamma \cdot \text{q2}).(\gamma \cdot \text{p5} + \gamma \cdot \text{p6} + \gamma \cdot \text{p7} + \gamma \cdot \text{p8})$

In [3]:= **DiracGammaExpand**[exp, **Momentum** −> {q1}]

Out[3]:= $(\gamma \cdot \text{p1} + \gamma \cdot \text{p2} + \gamma \cdot \text{q1}).(\gamma \cdot (\text{p3} + \text{p4} + \text{q2})).(\gamma \cdot (\text{p5} + \text{p6} + \text{p7} + \text{p8}))$

In [4]:= **DiracGammaExpand**[exp, **Momentum** −> {q2}]

Out[4]:= $(\gamma \cdot (\text{p1} + \text{p2} + \text{q1})).(\gamma \cdot \text{p3} + \gamma \cdot \text{p4} + \gamma \cdot \text{q2}).(\gamma \cdot (\text{p5} + \text{p6} + \text{p7} + \text{p8}))$

22.2.7 $SU(N)$ Generators with Explicit Fundamental Indices

FeynCalc denotes $SU(N)$ generators in the fundamental representation as `SUNT[a]` where `a` stands for the adjoint index. The fundamental indices are suppressed, so that a chain of `SUNT`-matrices is understood to have only two free fundamental indices, e. g. `SUNT[a,b,c]` stands for $T^a_{ij}T^b_{jk}T^c_{kl}$ and it is not possible to express, say $T^a_{ij}T^b_{kl}$ with `SUNT` objects only.

Due to this limitation, evaluation of Feynman amplitudes with more than two free fundamental color indices (e.g $q\bar{q} \to q\bar{q}$ scattering in QCD) was very inconvenient and usually required additional Mathematica code to obtain the correct result. For this reason FeynCalc 9.0 introduces a new object `SUNTF[{a},i,j]` that stands for T^a_{ij}, an $SU(N)$ generator in the fundamental representation with explicit fundamental indices `i` and `j` and the adjoint index `a`. Hence, expressions like $T^a_{ij}T^b_{kl}$ or $T^a_{ij}T^b_{jk}T^c_{lm}$ can be now conveniently expressed with `SUNTF[{a},i,j]*SUNTF[{b},k,l]` and `SUNTF[{a,b},i,k]*SUNTF[{c},l,m]` respectively. The new `SUNTF` objects are fully compatible with `SUNSimplify`, the standard routine for simplifying $SU(N)$ algebra.

In [1]:= exp1 = **SUNTF**[{a}, i, j] **SUNTF**[{b}, j, k] **SUNTF**[{c}, k, l]

Out[1]:= $T^a_{ij}T^b_{jk}T^c_{kl}$

In [2]:= **SUNSimplify**[exp1]

Out[2]:= $\left(T^a T^b T^c\right)_{il}$

In [3]:= exp2 = exp1 **SUNFDelta**[i, l]

Out[3]:= $\delta_{il}T^a_{ij}T^b_{jk}T^c_{kl}$

In [4]:= **SUNSimplify**[exp2]

Out[4]:= $\text{tr}(T^c.T^a.T^b)$

23 FeynHelpers

23.1 Motivation

Due to the fact that FeynCalc by itself is mostly limited to algebraic manipulations, it is often used together with other packages, e. g. FeynArts, LoopTools [152] or FeynRules [78]. While there is a built-in interface for converting amplitudes generated by FeynArts into valid FeynCalc input, for all the other tools one usually has to do such conversion by oneself.

As long as the other software is also written in Mathematica and the user has some programming experience with Wolfram language, it should be not too difficult to create a simple converter that does the job for the current project. However, there is a big difference between writing limited code for personal use, with all its potential limitations and pitfalls and creating a robust, tested and well-maintained interface that can be useful for the HEP community.

The long-term maintenance is always important because subsequent versions of a particular tool may introduce changes in syntax, changes in normalization, new features or simply workflow improvements that require appropriate adjustments in the interface code. Also, the interface itself might require updates to be compatible with the latest releases of Mathematica.

In the following we will present FeynHelpers, an interface that connects FeynCalc to the Mathematica packages Package-X [155] and FIRE [23]. The combination of FeynCalc and FeynHelpers allows one to obtain fully analytic results for most 1-loop amplitudes with up to 4 external legs and to rewrite many multi-loop amplitudes in terms of master loop integrals. Since the author of FeynHelpers is also the lead FeynCalc developer, we believe that this interface can provide a stable long-term solution for using FeynCalc, Package-X and FIRE in one framework, at least as long as the latter two packages are actively developed.

The main purpose for introducing FeynHelpers is not to compete with other established frameworks for loop calculations (e. g. FormCalc [152], GoSam [153], FDC [25], GRACE [154], Diana [236]) but rather to improve the usefulness of FeynCalc for specific calculations, which require semi-automatic approach and therefore cannot be easily done using fully automatic all-in-one tools.

23.2 Package-X and FIRE

23.2.1 Package-X

Even though the Passarino–Veltman technique [237] for evaluation of 1-loop tensor integrals was introduced almost four decades ago and alternative approaches are available (e. g. unitarity methods [266]), tensor decomposition is still widely used in many loop calculations. The key idea here is to convert all the occurring 1-loop tensor integrals into scalar ones, which are conventionally denoted as Passarino–Veltman coefficient functions. Thus, the calculation of an arbitrary 1-loop integral can be reduced to the evaluation of the resulting scalar functions. Often (e. g. in calculations of decay rates, cross sections or asymmetries) numerical evaluation of such functions is sufficient and many suitable tools for doing this are publicly available, e. g. FF [267], LoopTools [152], QCDLoop [268], OneLOop [269], Golem95C [270], PJFry [271] and Collier [272].

However, there are also cases (e. g. calculation of matching coefficients in effective field theories (EFTs), renormalization, etc.) where one would like to have fully analytic expressions for all the scalar functions that appear in the calculation. In general, it is desirable to have results for arbitrary kinematics, including zero Gram determinants but also for cases with vanishing and/or coinciding masses and scalar products of external momenta.

Although most of these results can be found in the literature (c. f. [273] and [274], as well as references in [155]), until recently there was no easy and convenient way to make use of them in automatic calculations. Public packages such as ANT [275] and LOOL [276] aimed to provide selected results for particular kinematical limits (e. g. vanishing external momenta or very large masses inside loops) are available since several years, but their applicability is limited to special cases.

This situation has changed with the release of PACKAGE-X [155], a MATHEMATICA package for semi-automatic 1-loop calculations. A unique feature of this package is the built-in library of analytic expressions for Passarino–Veltman functions with up to 4 legs and almost arbitrary kinematics. In a tedious work the author of PACKAGE-X has collected numerous analytic formulas from the literature and meticulously cross-checked everything by comparing with both analytic and numerical results. All this was then systematically implemented in an easy to use MATHEMATICA package. Although PACKAGE-X can do much more than just analytically evaluate coefficient functions, in this work we would like to concentrate only on this aspect of the package.

Let us provide several examples for the usefulness of the built-in 1-loop library. When computing the 1-loop gluon self-energy in QCD (in Feynman gauge), the result depends on 3 coefficient functions:

$$B_0(p^2, 0, 0), \quad B_0(p^2, m^2, m^2), \quad A_0(m^2), \tag{23.1}$$

where p is the external momentum and m is the mass of the quarks in the loops. Provided that PACKAGE-X has already been loaded via

```
In[1]:= <<X`

        Package−X v2.0.1, by Hiren H. Patel
        For more information, see the guide
```

it is very easy to obtain explicit results for these coefficient functions

```
In[2]:= li={PVB[0, 0, p.p, 0, 0], PVB[0, 0, p.p, m, m],
        PVA[0, m]}

Out[2]= {B0(p^2; 0, 0), B0(p^2; m, m), A0(m)}

In[3]:= res=(LoopRefine/@li);
        res//TableForm
```

Out[4]//TableForm=

$$\frac{1}{\tilde{\epsilon}}+\log\left(-\frac{\mu^2}{p^2}\right)+2$$

$$\frac{1}{\tilde{\epsilon}}+\Lambda(p^2;m,m)+\log\left(\frac{\mu^2}{m^2}\right)+2$$

$$m^2\left(\frac{1}{\tilde{\epsilon}}+\log\left(\frac{\mu^2}{m^2}\right)\right)+m^2$$

where `LoopRefine` is the function that replaces coefficient functions with analytic expressions. Notice that the results returned by PACKAGE-X are computed using $D = 4-2\epsilon$. Furthermore, for brevity the overall factor $i/16\pi^2$ is omitted and $1/\epsilon - \gamma_E + \log(4\pi)$ is abbreviated by $1/\tilde{\epsilon}$. For the same reason, the result for $B_0(p^2, m^2, m^2)$ is given as a function of Λ, which is defined as

$$\Lambda(p^2; m_0, m_1) = \frac{\sqrt{\lambda(p^2, m_0^2, m_1^2)}}{p^2} \ln\left(\frac{2m_0 m_1}{-p^2 + m_0^2 + m_1^2 - \sqrt{\lambda(p^2, m_0^2, m_1^2)}} + i\varepsilon\right), \quad (23.2)$$

with

$$\lambda(a, b, c) = a^2 + b^2 + c^2 - 2ab - 2ac - 2bc \quad (23.3)$$

being the Källén function. The explicit expressions can be obtained by applying `DiscExpand`

```
In[5]:= res[[2]]//DiscExpand

Out[5]= 1/ε̃ + (√(p²(p²−4m²)) log((√(p²(p²−4m²))+2 m²−p²)/(2 m²))) / p² + log(μ²/m²) + 2
```

More examples and explanations can be found in the official tutorial[1].

A FEYNCALC user who is not interested in switching to a different package may naturally wonder about different possibilities to continue doing calculations in FEYNCALC and use PACKAGE-X only to obtain analytic results for the coefficient functions. One would, of course, like to automatize the whole procedure in such a way, that an easy and direct evaluation of `PaVe` functions with PACKAGE-X can be achieved without interrupting the current FEYNCALC session. This wish was indeed one of the original motivations for the development of FEYNHELPERS.

23.2.2 FIRE

Let us now turn to another important task that arises in many loop calculations, especially when one goes beyond 1-loop. It is well known that loop integrals with propagators that are raised to integer powers usually can be reduced to simpler ones by using integration-by-parts identities (IBP) [171]. The underlying formula that generates IBP relations is just a consequence of the divergence theorem in D-dimensional spaces

$$\int \frac{d^D k_1}{(2\pi)^D} \cdots \int \frac{d^D k_n}{(2\pi)^D} \frac{\partial}{\partial k_j^\mu} \left(r^\mu \prod_i \frac{(p \cdot k)_i^{b_i}}{(q_i^2 + m_i^2)^{a_i}} \right) = 0, \qquad a_i, b_i \in \mathbb{Z}_0 \quad (23.4)$$

where q_i is a linear combination of loop and external momenta (with at least one loop momentum), $(p \cdot k)_i$ denote scalar products of a loop momentum with another loop or external momentum, r^μ can be a loop or an external momentum and j can take any values between 1 and n. Finding a useful way to combine numerous IBP relations generated by Eq. (23.4) such, that many complicated integrals can be reduced to a small set of master integrals, is a nontrivial task that requires special algorithms like Laporta algorithm [277], Baikov's method [278] or S-bases [279] to name just a few of them. Often a combination of several algorithms is used to obtain the most efficient reduction for different families of loop integrals.

[1] `http://packagex.hepforge.org/tutorial-2.0.0.pdf`

Several public packages (e. g. AIR [262], LITERED [260], FIRE [23], REDUZE [261]) for doing IBP-reduction are available, but in this work we would like to focus specifically on FIRE. It is a specialist package that was developed for doing IBP-reduction in a very general and efficient way. FIRE comes with various options for fine-tuning the reduction procedure and extra utilities for using `Fermat`[2] computer algebra system to speed up the calculations, and `KyotoCabinet`[3] to organize the integrals in a database. Furthermore, since version 5 of the package, one has a choice between doing reduction only by means of MATHEMATICA or via the (much faster) C++ back-end. In the following we would like to provide several simple examples for using FIRE 5.2 with 1- and 2-loop integrals (c. f. [24] for the official manual).

Let us begin with the almost trivial case of $\int \frac{d^D q}{(q^2-m^2)^\alpha}$. The computation proceeds in 2 steps, where we first need to prepare *start* files that encode the information about the given topology

```
In[1]:= <<FIRE5‘
        SetDirectory[NotebookDirectory[]];

        FIRE, version 5.2
        DatabaseUsage: 0
        UsingFermat: False

In[2]:= Internal= {q};
        External={};
        Propagators= {q^2−m^2};
        PrepareIBP[];
        Prepare[AutoDetectRestrictions→True];
        SaveStart["tadpole"];

        Prepared
        Dimension set to 1
        No symmetries
        Saving initial data

In[3]:= Quit[];
```

Notice that according to the official manual, after doing so we need to restart MATHEMATICA kernel, which is why the command `Quit[]` was added to the end of the code snippet. The information about the resulting integral family was saved to the file `tadpole.start`. In the next step we can perform the reduction by starting FIRE again, loading `tadpole.start` and supplying explicit integer numbers for α

```
In[2]:= LoadStart["tadpole", 1];
        Burn[]

        Initial data loaded

Out[2]= True

In[3]:= {F[1, {2}], F[1, {3}]}

        EVALUATING {1,{2}}
        Working in sector 1/1: {1,{1}}
        LAPORTA STARTED: 1 integrals for evaluation
        Maximal levels: (10)
```

[2] `http://www.bway.net/lewis`
[3] `http://fallabs.com/kyotocabinet`

```
{1,1}
Preparing points, symmetries and 2 IBP's: 0.005024‘4.152594624225113 seconds.
2 new relations produced: 0.004835‘4.135941471914991 seconds.
IRREDUCIBLE INTEGRAL: {1,{1}}
Sector complete
SORTING THE LIST OF 2 INTEGRALS: 0.000035‘1.9956130378462462 seconds.
Substituting 2 values: 0.000124‘2.544966678658208 seconds.
Total time: 0.022635‘4.806325492327244 seconds
Working in sector 1/1: {1,{1}}
Sector complete
SORTING THE LIST OF 2 INTEGRALS: 0.000038‘2.031328590112781 seconds.
Substituting 2 values: 0.000121‘2.534330363812423 seconds.
Total time: 0.002505‘3.850352723699239 seconds
```

Out[3]= $\{\frac{(d-2)G(1,\{1\})}{2m^2}, \frac{(d-4)(d-2)G(1,\{1\})}{8m^4}\}$

Here the first argument of G identifies the integral family (the same integer was also used as the second argument of `LoadStart`), while the numbers in the brackets denote inverse powers of the original propagators. Hence, $G(1,\{1\})$ stands for $\int \frac{d^Dq}{q^2-m^2}$.

Next, let us consider the integral $\int \frac{d^Dq_1 d^Dq_2\,(p\cdot q_2)^2}{q_1^2[q_2^2]^2[(q_1-p)^2]^3[(q_1-q_2-p)^2]^3}$ which appears e. g. in the computation of the ghost self-energy at 2-loops in pure QCD. With the appropriate input for `Internal`, `External` and `Propagators`

In[3]:=
```
Internal={q1, q2};
External={p};
Propagators={q1^2, (-p + q1)^2, (-p + q1 - q2)^2, q2^2, p q2};
PrepareIBP[];
Prepare[AutoDetectRestrictions→True];
SaveStart["se2loop"];

Prepared
Dimension set to 5
No symmetries
Saving initial data
```

the result of the reduction reads

Out[5]= $-\frac{(3d-10)(3d-8)(d^2-12d+38)G(1,\{1,0,1,1,0\})}{(d-10)(d-8)(d-6)p^4}$

In the above examples the reduction was carried out within MATHEMATICA in a reasonably small amount of time. For large calculations involving thousands or even millions of complicated multi-loop integrals, the performance of MATHEMATICA is usually not sufficient such that the use of the C++ engine becomes mandatory. However, in this work we do not want to go into details of using FIRE in large scale higher loop calculations. The reason for this is that people interested in such projects mostly use in-house FORM [157] codes and would hardly consider FEYNCALC to be appropriate for the task.

On the other hand, small and medium-sized loop calculations that are feasible with FEYNCALC often may involve integrals that can be further simplified by using IBP-relations. Since FEYNCALC can perform such reduction only for 2-loop propagator-type integrals (via the TARCER [232] sub-package), the idea to utilize FIRE as a general IBP-reduction back-end for FEYNCALC appears tempting.

23.3 Implementation and Usage

23.4 Implementation

Our goal is to be able to use PACKAGE-X and FIRE from an existing FEYNCALC session without worrying about different syntax, conventions, and normalizations. The interface should be seamless and easy to use, while still providing access to advanced configuration options. It is not intended to provide a pass-through for every possible function present in PACKAGE-X and FIRE, but rather to concentrate on those functions that appear to be most useful for FEYNCALC users. For example, in case of PACKAGE-X we completely ignore the Lorentz and Dirac algebra modules of the package, as similar functionality is already present in FEYNCALC.

First observation to make is that we cannot naively load PACKAGE-X, FIRE and FEYNCALC in the same MATHEMATICA kernel. As the symbols `DiracMatrix` and `Contract` are present both in FEYNCALC and PACKAGE-X, one quickly runs into shadowing issues. It is also not possible to patch PACKAGE-X and change the conflicting names (as done with FEYNARTS), because the package is closed-source. Fortunately, it is possible to load just the 1-loop library of PACKAGE-X which does not contain any conflicting symbol names and was tested to safely coexist with FEYNCALC on the same MATHEMATICA kernel[4]. On the other hand, the internal design of FIRE which puts many of the symbols introduced by the package into the `Global`` context of MATHEMATICA, makes it rather impractical to use it together with FEYNCALC within one kernel session. Even if that would be feasible, the necessity to quit the kernel before starting an IBP-reduction (c. f. Sec. 23.2.2) renders the whole idea of a seamless interface meaningless. Here one can take advantage of MATHEMATICA's parallel architecture that permits us to evaluate different parts of the calculation on separate kernels. This way it is possible to execute FIRE on a parallel kernel and safely communicate with it using the kernel that runs FEYNCALC and FEYNHELPERS. Before a parallel kernel is started, for each loop integral the interface creates three files: `FIREp1-intXXX.m`, `FIREp2-intXXX.m` and `FIRERepList-intXXX.m`, where `XXX` denotes an integer number assigned to that integral. The first two files are required to run FIRE according to the instructions given in Sec. 23.2.2. They can be also evaluated outside of FEYNHELPERS, i. e. directly with MATHEMATICA and FIRE. The third file contains replacement rules that are used to convert the result back into FEYNCALC notation. The files are located in `FeynCalc/Database` and can be examined for logging or debugging purposes. While this approach may appear too complicated and does induce time penalties for starting and stopping parallel kernels, it allows us to avoid unnecessary restarts of the main kernel, effectively prevents variable shadowing and does not require any modifications in the source code of FIRE.

Another subtlety to be taken into account when calling PACKAGE-X from FEYNCALC is the different normalization of 1-loop integrals. In Table 23.1, we summarize the existing ways to enter a 1-loop integral in FEYNCALC and PACKAGE-X.

Command in FEYNCALC	Meaning
`FAD[{q,m1},{q-p,m2}]`	$\int d^D q \, \frac{1}{[q^2-m1^2][(q-p)^2-m2^2]}$
`PaVe[0,{SPD[p,p]},{m1^2,m2^2}]`	$\int \frac{d^D q}{i\pi^2} \, \frac{1}{[q^2-m1^2][(q-p)^2-m2^2]}$

[4]The author is grateful to Hiren Patel, the developer of PACKAGE-X, for explaining how to load only the `OneLoop.m` part of the package and for accounting for the compatibility with FEYNHELPERS while developing PACKAGE-X 2.0.

B0[SPD[p,p],m1^2,m2^2] [5]	$\int \frac{d^Dq}{i\pi^2} \frac{1}{[q^2-m1^2][(q-p)^2-m2^2]}$
Command in PACKAGE-X	Meaning
LoopIntegrate[1,q,{q,m1},{q-p,m2}]	$\frac{(4\pi)^{D/2}}{ie^{-\gamma_E\epsilon}} \int \frac{d^Dq}{(2\pi)^D} \frac{1}{[q^2-m1^2][(q-p)^2-m2^2]}$
PVB[0, 0, p.p, m1, m2]	$\frac{(4\pi)^{D/2}}{ie^{-\gamma_E\epsilon}} \int \frac{d^Dq}{(2\pi)^D} \frac{1}{[q^2-m1^2][(q-p)^2-m2^2]}$

Table 23.1: Different ways of entering 1-loop integrals in FEYNCALC and PACKAGE-X.

PACKAGE-X multiplies all loop integrals by $\left(\frac{ie^{-\gamma_E\epsilon}}{(4\pi)^{D/2}}\right)^{-1}$ to conveniently remove the overall $i/(16\pi^2)$ prefactor as well as terms with γ_E and $\log(4\pi)$ that accompany poles in ϵ. To convert a coefficient function from FEYNCALC to PACKAGE-X and obtain the full result, we therefore need to multiply every `PaVe`-object by

$$\left(\frac{i}{16\pi^2}\right)^{-1} \frac{i\pi^2}{(2\pi)^D} \overset{D=4-2\epsilon}{=} (2\pi)^{-2\epsilon} \tag{23.5}$$

and perform the substitutions

$$\frac{1}{\epsilon} \to \frac{1}{\epsilon} - \gamma_E + \log(4\pi), \tag{23.6}$$

$$\frac{1}{\epsilon^2} \to \frac{1}{\epsilon^2} + \frac{1}{\epsilon}(-\gamma_E + \log(4\pi)) + \frac{\gamma_E^2}{2} - \gamma_E \log(4\pi) + \frac{1}{2}\log^2(4\pi). \tag{23.7}$$

When interfacing with FIRE we need to keep in mind that as of version 5.2, the package is not capable to perform reduction of integrals with linearly dependent propagators or propagators that do not form a basis. This should not be regarded as a flaw of FIRE, since both decomposition into integrals with linearly independent propagators and completion of the propagator basis are operations that can be done in many ways. The choice often depends on the details of the calculation and especially on the preferred basis of master integrals.

In Sec. 22.2.3 it was shown how one can handle these issues in FEYNCALC by using the functions `ApartFF`, `FCLoopBasisFindCompletion`, `FCLoopBasisIncompleteQ` and `FCLoopBasisOverdeterminedQ`. The interface takes advantage of this new functionality by always checking the completeness of the propagator basis before passing the integrals to FIRE. Automatic completion is performed when necessary, although it is also possible to supply a list of extra propagators by hand. For integrals with linearly dependent propagators the user receives a message to perform partial fractioning with `ApartFF` first.

Finally, let us briefly mention the existing alternatives to FEYNHELPERS. As far as PACKAGE-X is concerned, we are not aware of any other publicly available interface between this package and FEYNCALC. For FIRE several attempts to facilitate the transition from FEYNCALC exist. The APART[6] [176, 280] package can do both partial fractioning (`ApartAll`) and basis completion (`ApartComplete`). It is also possible to convert loop integrals from FEYNCALC into the FIRE notation via `FireArguments`. Another package, called FARE[7] [264], is intended for tensor reduction of loop integrals. The resulting scalar integrals can be converted to the FIRE notation via `FIREType`. It

[5] `PaVe` is the standard way to enter coefficient functions in FEYNCALC. For historical reasons it is also possible to enter several functions directly, namely via `A0`, `A00`, `B0`, `B1`, `B00`, `B11`, `C0` and `D0`.

[6] `https://github.com/F-Feng/APart`

[7] `https://sourceforge.net/projects/feyntoolfare`

is worth noting, however, that neither APART nor FARE currently make it possible to automatize the whole workflow, which includes not only converting the integrals but also preparing input files, running FIRE, fetching the results and sending them back to FEYNCALC, as it is done in FEYNHELPERS.

23.5 Installation and Usage

23.5.1 Installation

FEYNHELPERS is implemented as an add-on for FEYNCALC 9.2 and above and is licensed under the General Public License (GPL) version 3. We would like to stress that this license applies only to the interface itself, but not to PACKAGE-X and FIRE. Their licensing conditions are outlined on the corresponding websites[8]. Questions with regard to the usage of FEYNHELPERS can be posted to the FEYNCALC mailing list[9]. To install FEYNHELPERS using the online installer, it is sufficient to evaluate

```
In[1]:= Import["https://raw.githubusercontent.com/FeynCalc/feynhelpers/master/install.m"]
        InstallFeynHelpers[]
```

The installer automatically suggests downloading and installing PACKAGE-X and FIRE if the packages are not found. To use the add-on, one should specify that it should be loaded before starting FEYNCALC.

```
In[1]:= $LoadAddOns={"FeynHelpers"};
        << FeynCalc`
```

Essentially there are only two functions that handle all the communication between FEYNCALC and the two other packages: `PaXEvaluate` and `FIREBurn`.

23.5.2 `PaXEvaluate`

`PaXEvaluate` is the main function of the PACKAGE-X-interface. It works on scalar loop integrals without any loop-momentum dependent scalar products in the numerator and on Passarino–Veltman functions. If one wants to obtain only the UV- or the IR-divergent part of the result, one can use `PaXEvaluateUV` and `PaXEvaluateIR`. Finally, `PaXEvaluateUVIRSplit` returns the full result with an explicit distinction between ϵ_{UV} and ϵ_{IR}. All four functions share the same set of options.

`PaXEvaluate`[*expr*, *q*]	converts all the scalar 1 -loop integrals with loop momentum q in *expr* to Passarino–Veltman functions, which are then analytically evaluated using PACKAGE-X. Both UV- and IR-singularities are regulated with ϵ. If q is omitted, no conversion is done and only already present Passarino–Veltman functions are evaluated.

[8] `http://packagex.hepforge.org`
`http://science.sander.su/FIRE.htm`
[9] `https://feyncalc.github.io/forum`

PaXEvaluateUV[*expr*, *q*]	like PaXEvaluate, but only the $1/\epsilon_{\text{UV}}$-piece of the result is returned.
PaXEvaluateIR[*expr*, *q*]	like PaXEvaluate, but only the $1/\epsilon_{\text{IR}}$-piece of the result is returned.
PaXEvaluateUVIRSplit[*expr*, *q*]	like PaXEvaluate, but with the explicit distinction between $1/\epsilon_{\text{UV}}$ and $1/\epsilon_{\text{IR}}$ in the final result.

Option	Default value	Description
Collect	True	whether the result should be collected with respect to scalar products, metric tensors and the Levi-Civita tensors.
Dimension	D	the symbol that denotes D-dimensions in the loop integrals.
FCE	False	whether the result should be converted into FeynCalcExternal-notation.
FCVerbose	False	allows us to activate the debugging output.
FinalSubstitutions	{}	list of replacements to be applied to the final result.
PaVeAutoOrder	True	automatic ordering of arguments inside FeynCalc's PaVe functions.
PaVeAutoReduce	True	automatic reduction of certain PaVe functions into simpler ones.
PaXC0Expand	False	whether the full analytic result for the C_0 function should be inserted.

PaXD0Expand	False	whether the full analytic result for the D_0 function should be inserted.
PaXDiscExpand	True	whether the DiscB function of PACKAGE-X should be replaced with its explicit expression.
PaXExpandInEpsilon	True	whether the final results multiplied by PaXImplicitPrefactor should be expanded around $4 - 2\epsilon$.
PaXImplicitPrefactor	1	a D-dependent prefactor that multiplies the final result.
PaXKallenExpand	True	whether the Kallenλ function of PACKAGE-X should be replaced with its explicit expression.
PaXLoopRefineOptions	{}	allows us to directly specify options for LoopRefine of PACKAGE-X.
PaXPath	FileNameJoin[{ $UserBase- Directory,"App lications","X"}]	path to PACKAGE-X.
PaXSimplifyEpsilon	True	whether the finite and the divergent parts of the result should be simplified via Simplify.
PaXSubstituteEpsilon	True	whether the result should be given with standard normalization, i. e. without the prefactor $\left(\frac{ie^{-\gamma_E\varepsilon}}{(4\pi)^{D/2}}\right)^{-1}$ introduced by PACKAGE-X.
PaXSeries	False	offers the possibility to expand a Passarino–Veltman function around given parameters via LoopRefineSeries of PACKAGE-X.

PaXAnalytic	True	allows LoopRefineSeries to construct series expansions near Landau singularities by means of analytic continuation.

PaXEvaluate is designed in such a way that the function requires only a minimal amount of user input. For example, to compute the integral $\int \frac{d^D q}{(2\pi)^D} \frac{1}{q^2-m^2}$ it is sufficient to write

```
In[2]:= int=PaXEvaluate[FAD[{q,m}],q,PaXImplicitPrefactor→1/(2Pi)^D]
```

$$\text{Out[2]=} \quad \frac{\text{im}^2}{16\pi^2\varepsilon} - \frac{\text{im}^2\left(-\log\left(\frac{\mu^2}{\text{m}^2}\right)+\gamma-1-\log(4\pi)\right)}{16\,\pi^2}$$

where the first argument is our integral, the second is the loop momentum and the third is the option to specify the normalization. To make the result look more compact, we can introduce the abbreviation $\Delta \equiv 1/\epsilon - \gamma_E + \log(4\pi)$. This can be done with the FeynCalc function FCHideEpsilon

```
In[3]:= int//FCHideEpsilon
```

$$\text{Out[3]=} \quad \frac{\text{i}\Delta\text{m}^2}{16\pi^2} + \frac{\text{im}^2\left(\log\left(\frac{\mu^2}{\text{m}^2}\right)+1\right)}{16\pi^2}$$

In practical calculations one is usually interested in the evaluation of different Passarino–Veltman functions. In this case it is not needed to specify the loop momentum, such that to compute e. g. $B_0(p^2, 0, m^2)$ we use

```
In[4]:= PaXEvaluate[B0[SPD[p,p],0,m^2]]
```

$$\text{Out[4]=} \quad \frac{1}{\varepsilon}+\log\left(\frac{\mu^2}{\pi\text{m}^2}\right)-\frac{\text{m}^2\log\left(\frac{\text{m}^2}{\text{m}^2-\text{p}^2}\right)}{\text{p}^2}+\log\left(\frac{\text{m}^2}{\text{m}^2-\text{p}^2}\right)-\gamma+2$$

PaCkage-X can also expand coefficient functions in their parameters (masses or external momenta). To expand $B_0(p^2, 0, m^2)$ around $p^2 = m^2$ up to first order with PaXEvaluate we first need to assign an arbitrary symbolic value to the scalar product p^2, e. g. pp

```
In[5]:= SPD[p,p]=pp;
```

Then we use the option PaXSeries to specify the expansion parameters and activate the option PaXAnalytic to ensure that the derivatives of loop integrals are taken appropriately

```
In[6]:= PaXEvaluate[B0[SPD[p,p],0,m^2],PaXSeries→{{pp,m^2,1}},PaXAnalytic→True]
```

$$\text{Out[6]=} \quad \frac{3\,\text{m}^2-\text{pp}}{2\varepsilon\text{m}^2} - \frac{(3\,\text{m}^2-\text{pp})\left(-\log\left(\frac{\mu^2}{\text{m}^2}\right)+\gamma-2+\log(\pi)\right)}{2\text{m}^2}$$

If we are interested only in the UV-part of this series, it is sufficient to replace PaXEvaluate with PaXEvaluateUV

```
In[7]:= PaXEvaluateUV[B0[SPD[p,p],0,m^2],PaXSeries→{{pp,m^2,1}},PaXAnalytic→True]
```

```
Out[7]= 1/εUV
```

Similarly, we can also obtain the IR-part of the series

```
In[8]:= PaXEvaluateIR[B0[SPD[p,p],0,m^2],PaXSeries→{{pp,m^2,1}},PaXAnalytic→True]

Out[8]= (m^2-pp)/(2m^2 εIR)
```

Finally, `PaXEvaluateUVIRSplit` returns the result with explicit distinction between UV and IR singularities

```
In[9]:= PaXEvaluateUVIRSplit[B0[SPD[p,p],0,m^2],PaXSeries→{{pp,m^2,1}},PaXAnalytic
        →True]

Out[9]= (m^2-pp)/(2m^2 εIR) - ((3 m^2-pp)(-log(μ^2/m^2)+γ-2+log(π)))/(2 m^2) + 1/εUV
```

A comment is in place here. It is well known that in dimensional regularization (DR) it is possible to regularize both ultraviolet (UV) and infrared (IR) divergences with the same regulator ϵ. To disentangle both types of divergences one can use different regulators, i. e. keep ϵ for the UV divergences and regulate the IR divergences with a fictitious mass. On the other hand, it is also possible to distinguish between UV and IR divergences in DR by using ϵ_{UV} and ϵ_{IR}, as is done e. g. in [91]. Such a distinction is often useful in matching calculations for EFTs, but also in renormalization calculations. With this prescription the rule that scaleless integrals vanish in DR does not hold anymore. For example, the logarithmically divergent scaleless 1-loop integral

$$\int \frac{d^D l}{(2\pi)^D} \frac{1}{l^4} = \int \frac{d^D l}{(2\pi)^D} \left(\frac{1}{l^2(l^2-m^2)} - \frac{m^2}{l^4(l^2-m^2)} \right) \tag{23.8}$$

cannot be set to zero, as it is proportional to $1/\epsilon_{\text{UV}} - 1/\epsilon_{\text{IR}}$. FeynCalc 9.2 features a new global option `$KeepLogDivergentScalelessIntegrals`, which prevents the internal functions from setting such scaleless 1-loop integrals to zero. Together with `PaXEvaluateUVIRSplit` this can be used to consistently distinguish between UV and IR singularities regulated dimensionally at 1-loop. For example, we can see that after setting

```
In[10]:= $KeepLogDivergentScalelessIntegrals=True;
```

the integral $\int \frac{d^D l}{(2\pi)^D} \frac{1}{l^4}$ does not vanish anymore but evaluates to

```
In[11]:= PaXEvaluateUVIRSplit[FAD[{l,0,2}],l, PaXImplicitPrefactor->1/(2Pi)^D]

Out[11]= i/(16π^2 εUV) - i/(16π^2 εIR)
```

Notice that this prescription is implemented in FeynCalc for 1-loop integrals only. Furthermore, to ensure that the results are consistent, one should not use `FIREBurn`, as by default FIRE always sets all the scaleless integrals to zero.

23.5.3 `FIREBurn`

`FIREBurn` is the main function of the FIRE-interface. It reduces scalar multi-loop integrals to simpler ones using IBP-techniques.

FIREBurn[*expr*, {q_1, q_2,...}, {p_1, p_2,...}]	reduces all loop integrals in *expr* that depend on the loop momenta q_1, q_2, ... and external momenta p_1, p_2,....

Option	Default value	Description
Collect	True	whether the result should be collected with respect to the loop integrals.
FCE	False	whether the result should be converted into FeynCalcExternal-notation.
FCLoopIBPReducableQ	False	whether FIRE should try to reduce every loop integral in the expression (default) or only those that contain propagators raised to integer powers.
FCVerbose	False	allows us to activate the debugging output.
FIREAddPropagators	Automatic	whether extra propagators with zero powers needed to complete the basis should be added automatically or by hand.
FIREConfigFiles	{ToFileName[$FeynCalc-Directory, "Database", "FIREp1.m"], ToFileName[$FeynCalc-Directory, "Database", "FIREp2.m"], ToFileName[$FeynCalc-Directory, "Database", "FIRERepList.m	where to save scripts for running FIRE.

FIREPath	FileNameJoin[$UserBase- Directory, "Applications" "FIRE5", "FIRE5.m"]	path to FIRE.
FIRERun	True	whether the reduction should be started after all the configuration files have been created (default). Otherwise, the interface would just create the files but not run FIRE afterwards.
FIRESilentMode	True	whether the (rather verbose) text output of FIRE should be suppressed.
FIREStartFile	ToFileName[$FeynCalc- Directory, "Database", "FIREStartFile	where to save start file for the FIRE engine.
Timing	True	informs the user about the progress of the IBP-reduction.

The function requires only three arguments, which are the input expression, the list of loop momenta and the list of external momenta. For example, to IBP-reduce the 1-loop integral $\int \frac{d^D l}{[l^2]^2[(l-p)^2-m^2]^2}$ we need to enter

```
In[12]:= FIREBurn[FAD[{l,0,2},{l-p,m,2}],{l},{p}]
```

$$\text{Out[12]}= \frac{(D-2)(2\,D\,m^2-9\,m^2-pp)}{2m^2(m^2-pp)^3((l-p)^2-m^2)}-\frac{(D-3)(D\,m^2+D\,pp-4m^2-6\,pp)}{(m^2-pp)^3 l^2.((l-p)^2-m^2)}$$

If the integral has no dependence on external momenta, as for example the 3-loop integral $\int \frac{d^D q_1 d^D q_2 d^D q_3}{[q1^2-m^2]^2[(q_1+q_3)^2-m^2][(q_2-q_3)^2][q_2^2]^2}$, then the list of external momenta should be left empty

```
In[13]:= FIREBurn[FAD[{q1,m,2},{q1+q3,m},{q2-q3},{q2,0,2}],{q1,q2,q3},{}]
```

$$\text{Out[13]}= -\frac{(D-3)(3\,D-10)(3\,D-8)}{16(2\,D-7)m^4(q1^2-m^2).q2^2.(q2-q3)^2.((q1+q3)^2-m^2)}$$

In the current implementation of the interface to FIRE, each loop integral is evaluated separately, which is of course rather inefficient. Unfortunately, FeynCalc is still not able to automatically recognize multi-loop integrals that belong to the same topology, which is undoubtedly a crucial requirement to make the program more useful in multi-loop calculations. Despite this limitation, we believe that FIREBurn can be well employed in smaller calculations with a low number of loops, where the IBP-reduction makes it possible to arrive to simpler results.

23.6 Examples

So far we explained how to use FEYNHELPERS to evaluate single loop integrals. To demonstrate the usefulness of the interface in more realistic scenarios, we will provide four examples that make extensive use of the new functions introduced with FEYNHELPERS. The complete working codes for these calculations can be found in Appendix I. These codes are shipped together with FEYNHELPERS[10] and can be also viewed online[11]. To avoid cluttering up this chapter we will not copy the full code here but rather merely explain the most important steps and present the final results.

23.6.1 Renormalization of QED at 1-loop

Our first example is the 1-loop renormalization of QED in three different schemes: minimal subtraction (MS), modified minimal subtraction ($\overline{\text{MS}}$) and on-shell (OS). This calculation should be familiar to every QFT practitioner and can be found in many books, e. g. [281] which we will follow here.

We start with

$$\mathcal{L}_{\text{QED}} = \mathcal{L}_{\text{R,QED}} + \mathcal{L}_{\text{CT}}, \tag{23.9}$$

$$\mathcal{L}_{\text{R,QED}} = -\frac{1}{4}F_{\mu\nu}F^{\mu\nu} - \frac{1}{2\xi}(\partial^\mu A_\mu)^2 + \bar{\psi}(i\partial\!\!\!/ - m)\psi + e\bar{\psi}A\!\!\!/\psi, \tag{23.10}$$

$$\begin{aligned}\mathcal{L}_{\text{CT}} = &-(Z_A - 1)\frac{1}{4}F_{\mu\nu}F^{\mu\nu} - \frac{1}{2\xi}(Z_A Z_\xi^{-1} - 1)(\partial^\mu A_\mu)^2 \\ &+ (Z_\psi - 1)\bar{\psi}i\partial\!\!\!/\psi - (Z_\psi Z_m - 1)m\bar{\psi}\psi + (Z_\psi Z_A^{1/2} Z_e - 1)e\bar{\psi}\gamma^\mu\psi A_\mu.\end{aligned} \tag{23.11}$$

where $\mathcal{L}_{\text{R,QED}}$ contains only renormalized quantities and $\mathcal{L}_{\text{CT}}$ provides the counter terms. The renormalization constants are defined as

$$e_0 = Z_e e, \quad m_0 = Z_m m, \quad \xi_0 = Z_\xi \xi, \quad \psi_0 = Z_\psi^{1/2}\psi, \quad A_{0,\mu} = Z_A^{1/2} A_\mu, \tag{23.12}$$

where the subscript 0 denotes bare quantities. From the Ward identities for the photon propagator and for the electron-photon vertex we obtain that

$$Z_\xi = Z_A, \quad Z_e = 1/\sqrt{Z_A}. \tag{23.13}$$

Our task is, therefore, to determine Z_A, Z_ψ and Z_m at 1-loop in three different schemes.

In the minimal subtraction schemes we demand that the two-point functions of the electron and the photon are finite at 1-loop, i. e.

$$i\Gamma_R^{\psi\bar{\psi}}(p,-p) = \quad + \quad + \quad + \mathcal{O}(\alpha^2) \stackrel{!}{=} \text{finite} \tag{23.14}$$

$$\begin{aligned}\leftrightarrow \Gamma_R^{\psi\bar{\psi}}(p,-p) &= (p\!\!\!/ - m) + \Sigma(p\!\!\!/) + (Z_\psi^{\text{MS}/\overline{\text{MS}}} - 1)p\!\!\!/ \\ &\quad - (Z_\psi^{\text{MS}/\overline{\text{MS}}} Z_m^{\text{MS}/\overline{\text{MS}}} - 1)m + \mathcal{O}(\alpha^2) \stackrel{!}{=} \text{finite}\end{aligned} \tag{23.15}$$

and

$$-i\left(\Gamma_R^{AA}\right)^{\mu\nu}(q,-q) = \quad + \quad + \quad + \mathcal{O}(\alpha^2) \stackrel{!}{=} \text{finite} \tag{23.16}$$

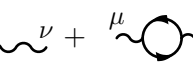

$$\leftrightarrow \left(\Gamma_R^{AA}\right)^{\mu\nu}(q,-q) = (q^2 g^{\mu\nu} - q^\mu q^\nu(1-\xi)) + \Pi^{\mu\nu}(q)$$

[10] When FEYNHELPERS is loaded, the greeting message contains the sentence "Have a look at the supplied examples". Clicking on the word "examples" opens the directory with sample calculations.

[11] https://github.com/FeynCalc/feynhelpers/tree/master/Examples

$$+ (q^2 g^{\mu\nu} - q^\mu q^\nu)(Z_A^{\text{MS}/\overline{\text{MS}}} - 1) + \mathcal{O}(\alpha^2) \stackrel{!}{=} \text{finite} \tag{23.17}$$

Using that

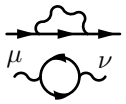

$$\equiv i\Sigma(\not{p}) = i(\not{p}\Sigma_V(p^2) + m\Sigma_S(p^2)), \tag{23.18}$$

$$\equiv -i\Pi^{\mu\nu}(q) = -i(q^2 g^{\mu\nu} - q^\mu q^\nu)\Pi(q^2) \tag{23.19}$$

and $Z_i = 1 + \delta_i + \mathcal{O}(\alpha^2)$ we can rewrite Eqs. (23.15) and (23.17) as

$$\not{p}(\delta_\psi^{\text{MS}/\overline{\text{MS}}} + \Sigma_V(p^2)) - m(\delta_\psi^{\text{MS}/\overline{\text{MS}}} + \delta_m^{\text{MS}/\overline{\text{MS}}} - \Sigma_S(p^2)) + \mathcal{O}(\alpha^2) \stackrel{!}{=} \text{finite}, \tag{23.20}$$

$$\Pi(q^2) + \delta_A^{\text{MS}/\overline{\text{MS}}} + \mathcal{O}(\alpha^2) \stackrel{!}{=} \text{finite}, \tag{23.21}$$

where we dropped the manifestly finite terms $(\not{p} - m)$ and $(q^2 g^{\mu\nu} - q^\mu q^\nu(1-\xi))$, since in minimal subtraction schemes we are interested only in subtracting the singularity $1/\epsilon$ (MS scheme) or $1/\epsilon - \gamma_E + \log(4\pi)$ ($\overline{\text{MS}}$ scheme).

The renormalization condition for the electron-photon vertex reads

$$ie\left(\Gamma_R^{A\psi\bar{\psi}}\right)^\mu(p_1, -p_2) =$$

$$+ \mathcal{O}(\alpha^2) \stackrel{!}{=} \text{finite} \tag{23.22}$$

$$\leftrightarrow \left(\Gamma_R^{A\psi\bar{\psi}}\right)^\mu(p_1, -p_2) = \gamma^\mu + \mathcal{V}^\mu(p_1, p_2) + \left(Z_\psi^{\text{MS}/\overline{\text{MS}}}\sqrt{Z_A^{\text{MS}/\overline{\text{MS}}}}Z_e^{\text{MS}/\overline{\text{MS}}} - 1\right)\gamma^\mu + \mathcal{O}(\alpha^2) \stackrel{!}{=} \text{finite}, \tag{23.23}$$

where

$$\equiv ie\mathcal{V}^\mu(p_1, p_2). \tag{23.24}$$

The condition given in Eq. (23.23) is equivalent to

$$\mathcal{V}^\mu(p_1, p_2) + \left(\frac{1}{2}\delta_A^{\text{MS}/\overline{\text{MS}}} + \delta_e^{\text{MS}/\overline{\text{MS}}} + \delta_\psi^{\text{MS}/\overline{\text{MS}}}\right)\gamma^\mu \stackrel{!}{=} \text{finite}. \tag{23.25}$$

Since Z_e has already been fixed by the Ward's identity, it is not necessary to explicitly evaluate the vertex function. On the other hand, nothing prevents us from doing so as a cross-check for the whole calculation.

In the on-shell scheme one demands that the renormalized self-energies satisfy

$$\lim_{p^2 \to m^2}\left(\frac{1}{\not{p} - m}\Gamma_R^{\psi\bar{\psi}}(p, -p)u(p) \stackrel{!}{=} u(p)\right), \tag{23.26}$$

$$\lim_{q^2 \to 0}\left(\frac{\left(\Gamma_R^{AA}\right)^{\mu\nu}(q, -q)}{q^2}\varepsilon_\nu(q) \stackrel{!}{=} -\varepsilon^\mu(q)\right). \tag{23.27}$$

It is easy to show that this corresponds to the following conditions

$$\delta_m^{\text{OS}} \stackrel{!}{=} \Sigma_S(m^2) + \Sigma_V(m^2), \tag{23.28}$$

$$\delta_\psi^{\text{OS}} \stackrel{!}{=} -\Sigma_V(m^2) + 2m^2(\Sigma_S'(m^2) + \Sigma_V'(m^2)), \tag{23.29}$$

$$\delta_A^{\text{OS}} \stackrel{!}{=} -\lim_{q^2\to 0} \frac{\partial}{\partial q^2}\left(q^2 \Pi(q^2)\right). \tag{23.30}$$

The on-shell condition for the vertex is given by

$$\bar{u}(p)\left(\Gamma_R^{A\psi\bar{\psi}}\right)^{\mu}(p,-p)u(p) = \bar{u}(p)\gamma^{\mu}u(p), \tag{23.31}$$

with $p^2 = m^2$. It should also be remarked that, apart from the renormalization, the evaluation of the on-shell vertex function allows us to extract some beautiful piece of physics. Owing to Lorentz invariance, the vertex function sandwiched between two spinors with $p_1 \neq p_2$ can be parametrized as

$$\bar{u}(p_2)\left(\Gamma_R^{A\psi\bar{\psi}}\right)^{\mu}(p_1,-p_2)u(p_1) \stackrel{!}{=} \bar{u}(p_2)\left(\gamma^{\mu}F_1(q^2) + \frac{i\sigma^{\mu\nu}q_{\nu}}{2m}F_2(q^2)\right)u(p_1), \tag{23.32}$$

with $q \equiv p_2 - p_1$ and $\sigma^{\mu\nu} = \frac{i}{2}[\gamma^{\mu},\gamma^{\nu}]$. Here, $F_2(0)$ is the 1-loop quantum correction to the anomalous magnetic moment of the electron in QED that was first obtained by Schwinger [282] in 1948

$$\frac{g-2}{2} = F_2(0) = \frac{\alpha}{2\pi} \tag{23.33}$$

and is often considered to be one of the greatest triumphs of QFT.

For $p_2 = p_1 \equiv p$ the term proportional to $F_2(0)$ vanishes and we are left with $F_1(0)$ only, i. e.

$$\begin{aligned}
&\bar{u}(p)\left(\Gamma_R^{A\psi\bar{\psi}}\right)^{\mu}(p,-p)u(p) = \\
&\bar{u}(p)\gamma^{\mu}u(p) + \bar{u}(p)\mathcal{V}^{\mu}u(p) + \left(\frac{1}{2}\delta_A^{\text{OS}} + \delta_e^{\text{OS}} + \delta_{\psi}^{\text{OS}}\right)\bar{u}(p)\gamma^{\mu}u(p) = \\
&= F_1(0)\bar{u}(p)\gamma^{\mu}u(p) \stackrel{!}{=} \bar{u}(p)\gamma^{\mu}u(p).
\end{aligned} \tag{23.34}$$

This leads to the renormalization condition

$$\bar{u}(p)\mathcal{V}^{\mu}(p,p)u(p) = -\left(\frac{1}{2}\delta_A^{\text{OS}} + \delta_e^{\text{OS}} + \delta_{\psi}^{\text{OS}}\right). \tag{23.35}$$

Now that we fully understand what we want to compute, it is time to carry out the calculation. When doing things by pen and paper, this is usually the most dull part, which however requires great care. With FEYNCALC and FEYNHELPERS one, of course, still has to pay attention to what one is doing, but the calculation itself can be done much faster.

Although FEYNARTS already contains the full Standard Model Lagrangian including the counter-terms, for this example we choose to create a model file that contains only QED. This can be conveniently done via FEYNRULES [78], a MATHEMATICA package that generates Feynman rules out of the given Lagrangian. The reason for doing so is to show how FEYNRULES can be chained with FEYNARTS, FEYNCALC and FEYNHELPERS to generate new models and study their phenomenology, including the determination of the renormalization coefficients in different schemes. The results can be also used as a cross-check for NLOCT [283], a FEYNRULES extension for fully automatic 1-loop renormalization of arbitrary models.

The FEYNRULES-model file `QED.fr` is already included in FEYNCALC 9.2 and can be found in `FeynCalc/Examples/FeynRules/QED`. Evaluating `GenerateModelQED.m` converts the input file `QED.fr` into a working FEYNARTS model and saves it to `FeynCalc/FeynArts/Models/QED`. Then we start a new MATHEMATICA kernel and load FEYNCALC, FEYNARTS and FEYNHELPERS in the usual way

```
In[14]:= $LoadAddOns={"FeynHelpers"};
         $LoadFeynArts= True;
         <<FeynCalc‘
         $FAVerbose = 0;
```

First of all we need to patch the new FEYNARTS QED model in order to make it compatible with FEYNCALC. Since in this calculation we will explicitly distinguish between UV and IR divergences regulated by ϵ_{UV} and ϵ_{IR}, we also need to activate the corresponding option

```
In[15]:= FAPatch[PatchModelsOnly->True];
         $KeepLogDivergentScalelessIntegrals=True;

         Patching FeynArts models... done!
```

From our QED model we can generate the required 1-loop diagrams and the corresponding counter-terms with FEYNARTS and then evaluate them with FEYNCALC and FEYNHELPERS. The conversion of a FEYNARTS amplitude into FEYNCALC notation can be conveniently done with `FCFAConvert`, where we explicitly keep the gauge parameter ξ. Our starting point is the electron self-energy $i\Sigma(\not{p})$. Tensor reduction with `TID` allows us to express this amplitude in terms of the Passarino–Veltman functions A_0, B_0 and C_0, while `PaXEvaluateUVIRSplit` provides the full analytic result for $i\Sigma(\not{p})$.

According to Eq. (23.20) we need to determine δ_ψ and δ_m in such a way, that the singularity is subtracted. This can be achieved by adding the amplitudes for the 1-loop self-energy and the counter-term and discarding all the finite terms, which gives

$$\text{Out[15]=}\quad -\text{i}\delta_\psi \text{m}_\text{e} - \text{im}_\text{e}\delta_\text{m} + \frac{\text{i}\alpha\Delta_{\text{UV}}\left(-\text{m}_\text{e}\xi_{\text{V(1)}} - 3\ \text{m}_\text{e} + \xi_{\text{V(1)}}\gamma\cdot\text{p}\right)}{4\pi} + \text{i}\delta_\psi \gamma\cdot\text{p}$$

Equating this to zero and solving for δ_ψ and δ_m we obtain

$$\text{Out[16]=}\quad \{\delta_\psi^{\text{MS}} \to -\frac{\alpha\xi_{\text{V(1)}}}{4\pi\varepsilon_{\text{UV}}},\ \delta_\text{m}^{\text{MS}} \to -\frac{3\alpha}{4\pi\varepsilon_{\text{UV}}}\}$$

$$\text{Out[17]=}\quad \{\delta_\psi^{\overline{\text{MS}}} \to -\frac{\alpha\Delta_{\text{UV}}\xi_{\text{V(1)}}}{4\pi},\ \delta_\text{m}^{\overline{\text{MS}}} \to -\frac{3\alpha\Delta_{\text{UV}}}{4\pi}\}$$

In order to compute these renormalization constants in the on-shell scheme we need to extract $\Sigma_S(p^2)$ and $\Sigma_V(p^2)$ first. Eq. 23.28 tells us that the mass renormalization constant follows from the sum of Σ_S and Σ_V evaluated at $p^2 = m^2$. To compute this integral we expand $\Sigma_S(p^2) + \Sigma_V(p^2)$ around $p^2 = m^2$ to zeroth order with `PaXSeries` and obtain

$$\text{Out[18]=}\quad \{\delta_\text{m}^{\text{OS}} \to -\frac{\alpha\left(3\log\left(\frac{\mu^2}{\text{m}_\text{e}^2}\right) + 3\Delta_{\text{UV}} + 4\right)}{4\pi}\}$$

In the same manner we can also compute the values of $\Sigma_S'(m^2) + \Sigma_V'(m^2)$ and $\Sigma_V(m^2)$. Plugging them into Eq. (23.29) yields

$$\text{Out[19]=}\quad \{\delta_\psi^{\text{OS}} \to -\frac{\alpha\left(3\log\left(\frac{\mu^2}{\text{m}_\text{e}^2}\right) - \Delta_{\text{IR}}(\xi_{\text{V(1)}} - 3) + \Delta_{\text{UV}}\xi_{\text{V(1)}} + 4\right)}{4\pi}\}$$

As is familiar from the literature [284], for $\Delta_{\text{UV}} = \Delta_{\text{IR}} = \Delta$ the parameter ξ drops out, leaving us with a gauge independent fermion wave-function renormalization constant $\delta_\psi^{\text{OS}} = \delta_m^{\text{OS}}$.

The evaluation of the photon self-energy proceeds similarly. From Eq. (23.21) we get the renormalization constant δ_A in the minimal subtraction schemes

Out[20]= $\{\delta_A^{MS} \to -\frac{\alpha}{3\pi\varepsilon_{UV}}\}$

Out[21]= $\{\delta_A^{\overline{MS}} \to -\frac{\alpha\Delta_{UV}}{3\pi}\}$

Then we again use `PaXSeries` to compute $\lim_{q^2\to 0}\frac{\partial}{\partial q^2}\left(q^2\Pi(q^2)\right)$ and thus determine δ_A in the on-shell scheme

Out[22]= $\{\delta_A^{OS} \to -\frac{\alpha\left(\log\left(\frac{\mu^2}{m_e^2}\right)+\Delta_{UV}\right)}{3\,\pi}\}$

Let us now also do some calculations with the vertex function. Although `TID` can of course reduce it into basic scalar integrals, the resulting expression will be huge, as we keep the kinematics completely general. We can, however, obtain a much more compact expression by sticking to coefficient functions, i. e. by activating the option `UsePaVeBasis`. Furthermore, as we are interested only in the UV-part of the whole expression, it is sufficient (and also much faster) to use `PaXEvaluateUV` instead of `PaXEvaluateUVIRSplit`. Then the UV-part of the vertex diagram reads

Out[23]= $\frac{i\alpha e\gamma^{Lor1}\xi_{V(1)}}{4\pi\varepsilon_{UV}}$

and with Eq. (23.23) we arrive to

Out[24]= $-\frac{2\pi\varepsilon_{UV}(\delta_A+2(\delta_\psi+\delta_e))+\alpha\xi_{V(1)}}{4\,\pi\,\varepsilon_{UV}} = 0$

Plugging our results for δ_ψ and δ_m into this relation yields

Out[25]= $\delta_A+2\delta_e = 0$

which explicitly confirms the relation $Z_e = 1/\sqrt{Z_A}$ in the minimal subtraction schemes.

To confirm this relation also in the on-shell scheme we need to look at the vertex function sandwiched between two spinors with their 4-momenta being put on-shell. At first, we choose the momenta to be p_1 and p_2 with $p_1 \neq p_2$. After having applied Gordon decomposition

$$\bar{u}(p_2)\gamma^\mu u(p_1) = \bar{u}(p_2)\left(\frac{(p_1+p_2)^\mu}{2m} + \frac{i\sigma^{\mu\nu}(p_2-p_1)_\nu}{2m}\right)u(p) \tag{23.36}$$

we can bring the amplitude to the form dictated by Eq. (23.32). As neither the counter-term nor the tree-level vertex contain a term proportional to $\sigma^{\mu\nu}$, the 1-loop vertex amplitude alone is sufficient to extract $F_2(q^2)$

Out[26]= $16\pi^3\alpha m_e^2(2C_1(m_e^2, 2m_e^2-2(p1\cdot p2), m_e^2, 0, m_e^2, m_e^2)+(D-2)(C_{11}(m_e^2, 2m_e^2-2(p1\cdot p2), m_e^2, 0, m_e^2, m_e^2)+C_{12}(m_e^2, 2m_e^2-2(p1\cdot p2), m_e^2, 0, m_e^2, m_e^2)))$

Evaluating it at $q^2 = 0$ we recover the famous result for $F_2(0) = \frac{g-2}{2}$

In[27]:=
```
PaXEvaluateUVIRSplit[tmp[15]/.{FCI[SPD[p1,p2]]→SMP["m_e"]^2},
  PaXImplicitPrefactor→1/(2Pi)^D]
```

Out[27]= $\frac{\alpha}{2\pi}$

When we set $p_1 = p_2 \equiv p$, the term proportional to $F_2(0)$ vanishes. Extracting $F_1(0)$ from $\bar{u}(p)\left(\Gamma_R^{A\psi\bar{\psi}}\right)^\mu(p,-p)u(p)$ according to Eq. (23.34) tells us that

Out[28]= $-\frac{2\pi\varepsilon_{UV}(\delta_A+2(\delta_\psi+\delta_e))+\alpha\xi_{V(1)}}{4\pi\varepsilon_{UV}} = 0$

and hence again

Out[29]= $\delta_A+2\delta_e = 0$

as it should.

This concludes the 1-loop renormalization of QED in 3 different schemes, carried out with FEYNCALC, FEYNHELPERS, FEYNARTS and FEYNRULES. Needless to say that similar calculations can also be done for more complicated theories (e. g. new models for physics beyond the Standard Model).

23.6.2 Quark-gluon vertex Expanded in the Relative Momentum Squared at 1-loop

The ability of FEYNHELPERS to distinguish between dimensionally regulated UV and IR divergences at 1-loop and to expand coefficient functions in their parameters can be also used to reproduce parts of the 1-loop matching between QCD and NRQCD. Here we concentrate on the 1-loop matching by following the famous work of Manohar [91], where on the QCD side of the matching the on-shell vertex function was evaluated using background field formalism [285, 286] and expanded up to the first order in the relative momentum squared.

As FEYNARTS does not contain a model for background-field QCD, we chose to implement it ourselves using FEYNRULES and to include the model file `QCDBGF.fr` to FEYNCALC 9.2[12]. A working FEYNARTS model can be generated via `GenerateModelQCDBGF.m`.

The abelian and nonabelian diagrams can be parametrized as

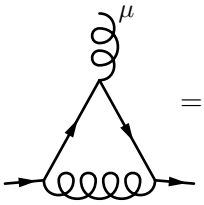

$$= -igT^a\bar{u}(p_2)\left(F_1^{(V)}(q^2)\gamma^\mu + iF_2^{(V)}(q^2)\frac{\sigma^{\mu\nu}q_\nu}{2m}\right)u(p_1), \tag{23.37}$$

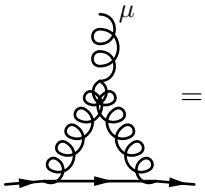

$$= -igT^a\bar{u}(p_2)\left(F_1^{(g)}(q^2)\gamma^\mu + iF_2^{(g)}(q^2)\frac{\sigma^{\mu\nu}q_\nu}{2m}\right)u(p_1), \tag{23.38}$$

where $q \equiv p_2 = p_1$. Our goal is to compute the form-factors $F_{1/2}^{(V)}(q^2)$ and $F_{1/2}^{(g)}(q^2)$ expanded up to $\mathcal{O}(q^2/m^2)$. In this case the whole calculation can be essentially split into 5 distinct steps

1. Generate the diagrams with FEYNARTS and prepare amplitudes for FEYNCALC.
2. Perform tensor decomposition of 1-loop integrals and simplify the Dirac algebra.
3. Apply Gordon decomposition.
4. Expand the amplitudes in q^2 with FEYNHELPERS.

[12]The model file is located in `FeynCalc/Examples/FeynRules/QCDBGF`.

5. Extract the form-factors.

Someone familiar with FEYNCALC can prepare the corresponding code with minimal effort. Applying it to each of the diagrams we find that $F_1^{(V)}(q^2)$ and $F_2^{(V)}(q^2)$ are given by

Out[30]= $$\frac{1}{\pi}\alpha_s\left(C_F-\frac{C_A}{2}\right)\left(\frac{\Delta_{IR}}{2}-\frac{q2\Delta_{IR}}{6m^2}+\frac{3}{4}\log\left(\frac{\mu^2}{m^2}\right)-\frac{q2(4\log(\frac{\mu^2}{m^2})+3)}{24m^2}+\frac{\Delta_{UV}}{4}+1\right)$$

and

Out[31]= $$\frac{\left(\frac{q2}{12m^2}+\frac{1}{2}\right)\alpha_s\left(C_F-\frac{C_A}{2}\right)}{\pi}$$

respectively, while the nonabelian form-factors $F_1^{(g)}(q^2)$ and $F_2^{(g)}(q^2)$ read

Out[32]= $$\frac{1}{8\,\pi}C_A\alpha_s\left(2\Delta_{IR}-\frac{3\,q2\Delta_{IR}}{2m^2}+3\log\left(\frac{\mu^2}{m^2}\right)-\frac{q2(3\log(\frac{\mu^2}{m^2})+2)}{2\,m^2}+\Delta_{UV}+4\right)$$

and

Out[33]= $$\frac{1}{8\,\pi}C_A\alpha_s\left(2\Delta_{IR}+\frac{2\,q2\Delta_{IR}}{m^2}+2\left(\log\left(\frac{\mu^2}{m^2}\right)+3\right)+\frac{q2(2\log(\frac{\mu^2}{m^2})+1)}{m^2}\right)$$

where $\mathrm{q2} \equiv q^2$. To compare this to the results presented in [91], we need to switch from $D = 4 - 2\epsilon$ to $D = 4 - \epsilon$ via $1/\epsilon \to 2/\epsilon$ and eliminate γ_E and $\log(4\pi)$ by substituting μ^2 with $\mu^2 \frac{e^{\gamma_E}}{4\pi}$. After doing so we precisely recover Eqs. (24)-(25) and Eqs. (29)-(30) from [91].

23.6.3 Higgs Decay to Two Gluons

Let us consider the partial decay width of the Higgs boson into two gluons via a top-quark loop[13]. With FEYNCALC, FEYNARTS and FEYNHELPERS the calculation is very similar to the two previous examples, the main difference being that for the generation of the diagrams we use `SM.mod`, the default Standard Model implementation shipped with FEYNARTS. As the amplitude for this process is finite, it is sufficient to use `PaXEvaluate` only. Squaring the amplitude, averaging over the polarizations of the on-shell gluons and multiplying by the phase space factor we arrive at the following expression for $\Gamma(H \to gg)$

Out[34]= $$\frac{G_F m_H^3 \alpha_s^2\left((\tau-1)\log^2\left(2\left(\sqrt{\frac{\tau-1}{\tau}}-1\right)\tau+1\right)-4\tau\right)^2}{256\sqrt{2}\pi^3\tau^4}$$

with $\tau = \frac{m_H^2}{4m_t^2}$, where m_H denotes the Higgs mass, m_t the mass of the top quark and G_F stands for the Fermi constant. According to the literature [287], $\Gamma(H \to gg)$ (taking into account all quark flavors) can be written as

$$\Gamma(H \to gg) = \frac{G_F \alpha_s^2}{36\sqrt{2}\pi^3} m_H^3 \left|\frac{3}{4}\sum_{\substack{Q=u,d,\\ c,s,t,b}} A_Q(\tau_Q)\right|^2, \tag{23.39}$$

[13] The calculation of this process with PACKAGE-X alone can be found in the official tutorial of the package, Sec 5.2.

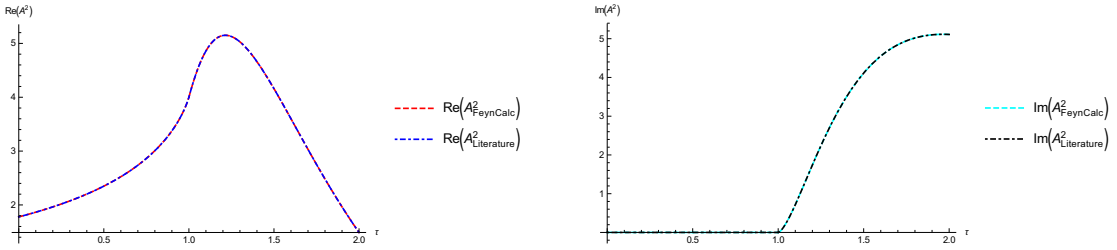

Figure 23.1: Real and imaginary parts of $A(\tau)$ from the literature and from the result obtained with FEYNHELPERS.

where $\tau_Q = \frac{m_H^2}{4m_Q^2}$ and A_Q is defined as

$$A_Q(\tau_Q) = \frac{2}{\tau_Q^2}\left[\tau_Q + (\tau_Q - 1) f(\tau_Q)\right] \tag{23.40}$$

with

$$f(\tau_Q) = \begin{cases} \arcsin^2(\sqrt{\tau_Q}) & \text{if } \tau_Q \leq 1 \\ -\frac{1}{4}\left[\log\left(\frac{1+\sqrt{1+\tau^{-1}}}{1-\sqrt{1-\tau^{-1}}}\right) - i\pi\right]^2 & \text{if } \tau_Q > 1 \end{cases} \tag{23.41}$$

Depending on the quark mass, one can have $\tau_Q \leq 1$ or $\tau_Q > 1$, while for the top quark and the known Higgs mass only the former case is relevant. Nevertheless, extracting $A_t^2(\tau_t) \equiv A^2(\tau)$ from our result and comparing it to Eq. (23.40) we can convince ourselves (c. f. Fig. 23.1) that the analytic expression returned by PACKAGE-X is indeed valid both for $\tau \leq 1$ and $\tau > 1$, such that our result is correct.

23.6.4 2-loop Self-energies in Massless QED

Our last example deals with the photon and electron self-energies (with full gauge dependence) in massless QED at 2-loops. This requires evaluation of six 2-loop diagrams

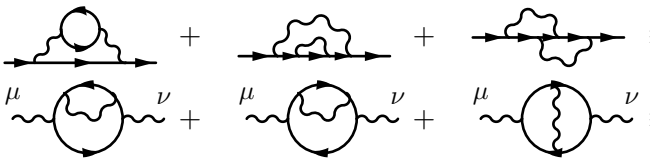

$$\equiv i\not{p}\Sigma_{2V}(p^2), \tag{23.42}$$

$$\equiv -i(p^2 g^{\mu\nu} - p^\mu p^\nu)\Pi_2(p^2), \tag{23.43}$$

that can be rewritten in terms of only two master integrals. Here we need to handle the amplitudes in a slightly different way, as compared to the previous examples. In particular, for the decomposition of 2-loop tensor integrals we use `FCMultiLoopTID` instead of `TID`, that works only at 1-loop. IBP-reduction with `FIREBurn` is then used to reduce all the resulting scalar integrals into two master integrals. These main steps can be summarized in only three lines of code for each class of diagrams. For definiteness, let us consider self-energy amplitudes from Eq. (23.42) and denote the expression obtained from FEYNARTS and processed with `FCFAConvert` with `ampsSE`. The sum of the amplitudes depends on the loop momenta l_1 and l_2 and the external momentum p. With

```
In[35]:= ampsSE1 = (ampsSE /. DiracTrace → Tr) // FCMultiLoopTID[#, {l1, l2}] & //
           DiracSimplify
```

we evaluate Dirac traces, carry out the tensor decomposition and simplify the resulting Dirac structures. Then, in

```
In[36]:= ampsSE2 = ampsSE1 // FDS[#, l1, l2] &
```

we use `FDS` to simplify loop integrals by shifting their loop momenta. The IBP-reduction is started by applying `FIREBurn` to the resulting expression

```
In[37]:= ampsSE3 = FIREBurn[ampsSE2, {l1, l2}, {p}] // FDS[#, l1, l2] &
```

Finally, after sorting terms using FeynCalc's `Collect2` (more advanced version of Mathematica's `Collect`)

```
In[38]:= ampsSE4=ampsSE3//Collect2[#,{FeynAmpDenominator},Factoring → FullSimplify]&
```

and factoring out $i\not{p}$

```
In[39]:= resSE=Cancel[ampsSE4/(-I FCI[(GSD[p])])]//FullSimplify
```

we find that the 2-loop contribution[14] to $\Sigma_{2V}(p^2)$ equals

$$\text{Out[39]=}\quad \frac{(D-2)e^4\left(\frac{2((D-6)(D-3)(3D-8)\xi_A^2-D((D-9)D+6)-40)}{l1^2.(l1-l2)^2.(l2-p)^2}-\frac{(D-6)(D-4)p^2((D-2)\xi_A^2+D-6)}{l1^2.l2^2.(l1-p)^2.(l2-p)^2}\right)}{4(D-6)(D-4)p^2}$$

The treatment of vacuum polarization diagrams proceeds in the same fashion and yields

$$\text{Out[40]=}\quad \frac{2(D-2)e^4\left(\frac{4(D-3)((D-4)D+8)}{l1^2.(l1-l2)^2.(l2-p)^2}-\frac{(D-4)((D-7)D+16)p^2}{l1^2.l2^2.(l1-p)^2.(l2-p)^2}\right)}{(D-4)^2(D-1)p^2}$$

for $\Pi_2(p^2)$.

As expected, the vacuum polarization amplitude is gauge invariant, while the electron self-energy depends on the gauge parameter ξ. These results precisely agree with the literature, e. g. Eq. 5.18 and Eq. 5.51 from [288].

[14] with $1/(2\pi)^{2D}$ omitted.

24 FeynOnium

24.1 Automatic Nonrelativsitc Calculations with FeynCalc and FeynOnium

In the previous sections we have explained how FEYNCALC can be used to automatize calculations in relativistic theories, including matching calculations in EFTs.

As long as we need to work only with manifestly Lorentz covariant expressions, there is, of course, no special reason to stick to FEYNCALC. Other semi-automatic packages such as HEPMATH or PACKAGE-X can be also well employed for this task, although they might lack the flexibility and features of FEYNCALC. In any case, there are alternatives to choose from.

As was already explained in Sec. (6.1), the real challenge begins when we need to automatize calculations in theories that lack manifest Lorentz covariance, such as nonrelativistic EFTs. It turns out, that the existing general purpose packages for semi-automatic and fully automatic calculations are not useful for this task: Those tools were simply not designed to handle expressions, where it is necessary to explicitly distinguish between temporal and spatial components of Lorentz tensors or to manipulate Pauli matrices contracted with Cartesian vectors, including those in $D-1$ dimensions. Hence, to perform such calculations in an automatic fashion, there are currently no alternatives to self-written codes.

On the one hand, the lack of publicly available automatic tools for nonrelativistic EFTs is an issue that needs to be addressed by the EFT community. On the other hand, one should understand, that it would require a lot of effort to develop such tools from scratch. A more pragmatic approach, is to extend one of the existing packages, so that it can be used also for nonrelativistic calculations. Ideally, this should be done by people familiar with the code and willing to provide long-term support, i. e. developers of the respective package. Unfortunately, most of the people behind well-established packages mentioned in Sec. 5.1 do not work in the field of nonrelativistic EFTs. Therefore, it is understandable that they have little interest to work on something that costs a lot time and effort and has no relevance for their daily research.

In this sense, the author of this thesis is in the fortunate position of using NREFTs in his research and being one of the developers of FEYNCALC. This is why automation of nonrelativistic calculations has become one of the directions in which FEYNCALC will evolve. Here one should keep in mind, that FEYNCALC provides over hundred functions to simplify and manipulate various types of expressions (vectors, scalar products, matrices, fields, loop integrals etc.) that appear in relativistic calculations. Therefore, it is not an easy task to extend the package in such a way, that all those functions can also work with noncovariant expressions out-of-the-box.

Instead, the extension is planned to be done in several steps, while the first step is presented in this work. At this stage we introduce support for basic noncovariant objects (Cartesian vectors and tensors, temporal and spatial components of Dirac and Pauli matrices) and their manipulations (contractions, expansions of scalar products, simplifications of matrix chains). Even though new objects can be also defined in D-dimensions, for now the simplification of nonrelativistic loop integrals is left aside. The reason for this is the necessity to account for all the various forms of propagators that appear in NREFTs, such as the heavy quark propagator in NRQCD

$$\frac{i}{p^0 - \frac{\mathbf{p}^2}{2m_Q} + i\eta}. \tag{24.1}$$

or the singlet propagator in pNRQCD

$$\frac{i}{p^0 - \widehat{h}_s + i\eta} = \sum_m \frac{i}{p^0 - E_m + i\eta} |m\rangle \langle m| , \tag{24.2}$$

with $E_m = \widehat{h}_s |m\rangle$, to name just a few of them. The ability to handle loop integrals with denominators as in Eq. (24.1) or Eq. (24.2) will be implemented in one of the future versions of FEYNCALC.

In Sec. 6.1 we have argued, that a realistic way to automatize EFT calculations, is to develop specific tools for specific EFTs, such that one can address the technical challenges of each theory in the best possible way. Following this line of argument, it was decided to separate new FEYNCALC functions for nonrelativistic calculations into two sets. Functions, that are sufficiently generic to be useful for any nonrelativistic QFT (e. g. contraction of Cartesian vectors or simplification of chains of Pauli matrices) were made part of the main package. Functions, that are specific to automatic calculations in NRQCD and pNRQCD, are collected in a separate FEYNCALC add-on called FEYNONIUM. In the next sections of this chapter we will provide an overview of new functions and give explicit examples of NRQCD calculations that can be now automatized with FEYNCALC and FEYNONIUM.

24.2 Overview of the New Developments

The internal implementation of the Lorentz and Dirac algebras in FEYNCALC has received only very little changes since the initial public release of the package in 1991 [20]. It proved itself as a flexible and convenient way to deal with symbolic Lorentz tensors and Dirac matrices in Wolfram language and is not likely to be altered in the future versions of FEYNCALC.

The most important Lorentz structures are represented by an object called `Pair` (c. f. Table 24.1). Depending on its two arguments, `Pair` may represent a metric tensor, a 4-vector or a scalar product of two 4-vectors. Allowed arguments are `LorentzIndex` and `Momentum`, which are used to denote Lorentz indices and four momenta respectively. These quantities can be defined in 4, D and $D-4$ dimensions. FEYNCALC uses the notation that was already introduced in Sec. 5.2 to distinguish between tensors that live in different dimensions, i. e.

$$\begin{aligned} &\dim(g^{\mu\nu}) = D, && \dim(p^\mu) = D, \\ &\dim(\bar{g}^{\mu\nu}) = 4, && \dim(\bar{p}^\mu) = 4, \\ &\dim(\hat{g}^{\mu\nu}) = D-4, && \dim(\hat{p}^\mu) = D-4. \end{aligned} \tag{24.3}$$

Contractions of tensors from different dimensions are resolved according to the rules from [80]. For example, FEYNCALC knows that

$$\bar{p} \cdot \hat{q} = 0 \tag{24.4}$$

for any 4-vectors p and q, or that

$$\bar{g}^{\mu\nu} p_\nu = \hat{p}^\mu. \tag{24.5}$$

Command in FEYNCALC	Meaning

`Pair[LorentzIndex[`μ`],LorentzIndex[`ν`]]`	$\bar{g}^{\mu\nu}$
`Pair[LorentzIndex[`μ, D`],LorentzIndex[`ν`],`D`]`	$g^{\mu\nu}$
`Pair[LorentzIndex[`$\mu, D-4$`],LorentzIndex[`ν`],`$D-4$`]`	$\hat{g}^{\mu\nu}$
`Pair[Momentum[`p`],LorentzIndex[`μ`]]`	$\bar{p}^{\mu}$
`Pair[Momentum[`p, D`],LorentzIndex[`μ, D`]]`	p^{μ}
`Pair[Momentum[`$p, D-4$`],LorentzIndex[`$\mu, D-4$`]]`	$\hat{p}^{\mu}$
`Pair[Momentum[`p`],Momentum[`q`]]`	$\bar{p}\cdot\bar{q}$
`Pair[Momentum[`p, D`],Momentum[`q, D`]]`	$p\cdot q$
`Pair[Momentum[`$p, D-4$`],Momentum[`$q, D-4$`]]`	$\hat{p}\cdot\hat{q}$

Table 24.1: Various Lorentz structures in 4, D and $D-4$ dimensions, that can be represented with `Pair`.

Let us also mention the Levi-Civita symbol, which is represented by `Eps` with four arguments. Those can be `LorentzIndex` or `Momentum`, c. f. Table 24.2.

Command in FeynCalc	Meaning
`Eps[LorentzIndex[`μ`],LorentzIndex[`ν`], LorentzIndex[`ρ`] LorentzIndex[`σ`]]`	$\bar{\epsilon}^{\mu\nu\rho\sigma}$
`Eps[LorentzIndex[`μ, D`],LorentzIndex[`ν, D`], LorentzIndex[`ρ, D`] LorentzIndex[`σ, D`]]`	$\epsilon^{\mu\nu\rho\sigma}$
`Eps[LorentzIndex[`μ`],LorentzIndex[`ν`], Momentum[`p`] Momentum[`q`]]`	$\bar{\epsilon}^{\mu\nu\rho\sigma}\bar{p}_\rho\bar{q}_\sigma$
`Eps[LorentzIndex[`μ, D`],LorentzIndex[`ν, D`], Momentum[`p, D`] Momentum[`q, D`]]`	$\epsilon^{\mu\nu\rho\sigma}p_\rho q_\sigma$

Table 24.2: 4- and D-dimensional Levi-Civita symbols in FeynCalc. For brevity, we do not list all possible combinations `LorentzIndex` and `Momentum` in the arguments of `Eps`.

As far as Dirac matrices are concerned, their internal representation is handled by `DiracGamma` (c. f. Table 24.3). The syntax is almost identical to the one used for `Pair`. Standalone Dirac matrices as well as contractions of a Dirac matrix and 4-vector can be defined in 4, D and $D-4$ dimensions.

Command in FeynCalc	Meaning
`DiracGamma[LorentzIndex[`μ`]]`	$\bar{\gamma}^{\mu}$
`DiracGamma[LorentzIndex[`μ, D`],`D`]`	γ^{μ}
`DiracGamma[LorentzIndex[`$\mu, D-4$`],`$D-4$`]`	$\hat{\gamma}^{\mu}$
`DiracGamma[Momentum[`p`]]`	$\bar{\gamma}\cdot\bar{p}$

`DiracGamma[Momentum[p, D], D]`	$\gamma \cdot p$
`DiracGamma[Momentum[μ, D − 4], D − 4]`	$\hat{\gamma} \cdot \hat{p}$

Table 24.3: Representation of Dirac matrices in 4-, D- and $D-4$ dimensions using `DiracGamma`.

Our goal is a consistent extension of this framework to include support for tensors and matrices with Cartesian indices. First of all, let us remark that internally FEYNCALC does not distinguish between upper and lower indices. This is not an issue for Lorentz tensors. As long as we work with manifestly Lorentz covariant expressions and respect Einstein summation convention, there are no inconsistencies regarding the position of a particular Lorentz index. For example, let us consider the trace of two Dirac matrices. In FEYNCALC the expression

```
Tr[DiracGamma[LorentzIndex[μ]],DiracGamma[LorentzIndex[ν]]]
```
(24.6)

evaluates to

```
4 Pair[LorentzIndex[μ]],LorentzIndex[ν]]
```
(24.7)

Although it is not specified, whether μ and ν are upper or lower indices, it is clear, that if a free Lorentz index appears upstairs or downstairs on the one side of an equality, it must appear in the same position on other side. Anything else would violate manifest Lorentz covariance. In this sense, Eq. (24.6) and Eq. (24.7) can be interpreted as

$$\mathrm{Tr}(\bar{\gamma}^{\mu}\bar{\gamma}^{\nu}) = 4\bar{g}^{\mu\nu} \text{ or } \mathrm{Tr}(\bar{\gamma}^{\mu}\bar{\gamma}_{\nu}) = 4\bar{g}^{\mu}{}_{\nu} \text{ or } \mathrm{Tr}(\bar{\gamma}_{\mu}\bar{\gamma}_{\nu}) = 4\bar{g}_{\mu\nu} \text{ or } \mathrm{Tr}(\bar{\gamma}_{\mu}\bar{\gamma}^{\nu}) = 4\bar{g}_{\mu}{}^{\nu} \tag{24.8}$$

without loss of generality. If a term contains two identical Lorentz indices, Einstein summation convention guarantees that one of them must be upstairs and the other downstairs. Again, in FEYNCALC we write

```
DiracGamma[LorentzIndex[μ]].DiracGamma[LorentzIndex[μ]]
```
(24.9)

which can be understood as

$$\bar{\gamma}^{\mu}\bar{\gamma}_{\mu} \text{ or } \bar{\gamma}_{\mu}\bar{\gamma}^{\mu} \tag{24.10}$$

without introducing any ambiguities.

Unfortunately, things become more complicated once we want to include Cartesian vectors. For example, if we use the metric signature $(1, -1, -1, -1)$, then

$$\mathbf{p}^{i} = -\mathbf{p}_{i} \tag{24.11}$$

and

$$\mathbf{p}^{i}\mathbf{q}^{i} = -\mathbf{p}^{i}\mathbf{q}_{i} \tag{24.12}$$

are perfectly valid expressions where the position of the Cartesian index i matters. Therefore, to avoid any possible inconsistencies, the new FEYNCALC adopts following convention regarding Lorentz and Cartesian indices

- Free Lorentz or Cartesian indices are always understood as upper indices.
- If a Lorentz index appears twice in a term (dummy Lorentz index), it is understood that one of the indices is upstairs and another downstairs.
- If a Cartesian index appears twice in a term (dummy Cartesian index), it is understood that both indices are upstairs.

With these rules all the input and output expressions are now unambiguous and we may go on and introduce new FEYNCALC objects for nonrelativistic calculations. The most important of them is `CartesianPair` that represents Kronecker deltas, Cartesian vectors and scalar products of Cartesian vectors. Just as the ordinary `Pair` it takes two arguments, which can be `CartesianIndex` or `CartesianMomentum`. In addition to that, we also have `TemporalPair` (with the arguments `TemporalIndex` and `TemporalMomentum`) that implements temporal components of 4-vectors.

Cartesian vectors and Kronecker deltas are 3-dimensional objects. However, for the purpose of the dimensional regularization we also need to define them in $D-1$ and $(D-1)-3 = D-4$ dimensions. The notation and contraction rules for such objects can be readily deduced from [80], such that

$$\delta^{ij} = \bar{\delta}^{ij} + \hat{\delta}^{ij}, \qquad \mathbf{p}^i = \bar{\mathbf{p}}^i + \hat{\mathbf{p}}^i, \tag{24.13}$$

with

$$\begin{aligned} &\dim(\delta^{ij}) = D-1, && \dim(\mathbf{p}^i) = D-1, \\ &\dim(\bar{\delta}^{ij}) = 3, && \dim(\bar{\mathbf{p}}^i) = 3, \\ &\dim(\hat{\delta}^{ij}) = D-4, && \dim(\hat{\mathbf{p}}^i) = D-4. \end{aligned} \tag{24.14}$$

It is interesting to see how Eq. (24.13) is related to the decomposition of a D-dimensional 4-vector into 4- and $D-4$-dimensional components. On the one hand, we have

$$p^\mu = \bar{p}^\mu + \hat{p}^\mu. \tag{24.15}$$

On the other hand, we may also write

$$p^\mu = g^{\mu 0} p^0 + g^{\mu i} \mathbf{p}^i = \bar{g}^{\mu 0} \bar{p}^0 + \bar{g}^{\mu i} \bar{\mathbf{p}}^i + \hat{g}^{\mu i} \hat{\mathbf{p}}^i, \tag{24.16}$$

where we used that tensors with temporal components do not have any $D-4$-dimensional parts, i. e.

$$\hat{g}^{\mu 0} = 0, \qquad \hat{p}^0 = 0. \tag{24.17}$$

Comparing Eq. (24.15) and Eq. (24.16) we see that

$$\bar{p}^\mu = \bar{g}^{\mu 0} \bar{p}^0 + \bar{g}^{\mu i} \bar{\mathbf{p}}^i, \tag{24.18}$$

$$\hat{p}^\mu = \hat{g}^{\mu i} \hat{\mathbf{p}}^i. \tag{24.19}$$

Even though the new FEYNCALC is currently not able to simplify nonrelativistic loop integrals, it is aware of Eq. (24.13) and similar relations, so that one can consistently work with spatial and temporal components of Lorentz tensors in dimensional regularization. The list of new objects that involve `Pair`, `CartesianPair` and `TemporalPair` is provided in Table 24.4.

Command in FEYNCALC	Meaning
`Pair[LorentzIndex[`μ`],TemporalIndex[]]`	$\bar{g}^{\mu 0}$
`Pair[LorentzIndex[`μ`],CartesianIndex[`i`]]`	$\bar{g}^{\mu i}$
`Pair[LorentzIndex[`μ`,D],CartesianIndex[`i`,D-1]]`	$g^{\mu i}$
`Pair[LorentzIndex[`μ`,D-4],CartesianIndex[`i`,D-4]]`	$\hat{g}^{\mu i}$
`Pair[TemporalIndex[],TemporalIndex[]]`	$\bar{g}^{00}$
`Pair[CartesianIndex[`i`],CartesianIndex[`j`]]`	$\bar{g}^{ij}$
`Pair[CartesianIndex[`i`,D-1],CartesianIndex[`j`,D-1]]`	g^{ij}
`Pair[CartesianIndex[`i`,D-4],CartesianIndex[`j`,D-4]]`	$\hat{g}^{ij}$
`CartesianPair[CartesianIndex[`i`],CartesianIndex[`j`]]`	$\bar{\delta}^{ij}$
`CartesianPair[CartesianIndex[`i`,D-1], CartesianIndex[`j`,D-1]]`	δ^{ij}
`CartesianPair[CartesianIndex[`i`,D-4], CartesianIndex[`j`,D-4]]`	$\hat{\delta}^{ij}$
`TemporalPair[TemporalMomentum[`p`],TemporalIndex[]]`	$\bar{p}^0$
`Pair[CartesianMomentum[`p`],LorentzIndex[`μ`]]`	$\bar{\mathbf{p}}^i \bar{g}^{i\mu}$
`Pair[CartesianMomentum[`p`,D-1],LorentzIndex[`μ`,D]]`	$\mathbf{p}^i g^{i\mu}$
`Pair[CartesianMomentum[`p`,D-4],LorentzIndex[`μ`,D-4]]`	$\hat{\mathbf{p}}^i \hat{g}^{i\mu}$
`CartesianPair[CartesianMomentum[`p`], CartesianIndex[`i`]]`	$\bar{\mathbf{p}}^i$
`CartesianPair[CartesianMomentum[`p`,D-1], CartesianIndex[`i`,D-1]]`	$\mathbf{p}^i$
`CartesianPair[CartesianMomentum[`p`,D-4], CartesianIndex[`i`,D-4]]`	$\hat{\mathbf{p}}^i$
`CartesianPair[CartesianMomentum[`p`], CartesianMomentum[`q`]]`	$\bar{\mathbf{p}} \cdot \bar{\mathbf{q}}$
`CartesianPair[CartesianMomentum[`p`,D-1], CartesianIndex[`i`,D-1]]`	$\mathbf{p} \cdot \mathbf{q}$
`CartesianPair[CartesianMomentum[`p`,D-4], CartesianIndex[`i`,D-4]]`	$\hat{\mathbf{p}} \cdot \hat{\mathbf{q}}$

Table 24.4: Representation of new tensors with Cartesian and mixed (Lorentz and Cartesian) indices using `Pair`, `CartesianPair` and `TemporalPair`.

Of course, Levi-Civita symbols and Dirac matrices may also carry a Cartesian index or appear contracted with a Cartesian vector. Allowed combinations of `Eps` or `DiracGamma` and `CartesianIndex`, `CartesianMomentum` or `TemporalIndex` are listed in Table 24.5 and Table 24.6 respectively.

Command in FeynCalc	Meaning
`Eps[TemporalIndex[],LorentzIndex[ν], LorentzIndex[ρ] LorentzIndex[σ]]`	$\bar{\epsilon}^{0\nu\rho\sigma}$
`Eps[TemporalIndex[],CartesianIndex[i], LorentzIndex[μ] LorentzIndex[ν]]`	$\bar{\epsilon}^{0i\mu\nu}$
`Eps[CartesianIndex[i],CartesianIndex[j], LorentzIndex[μ] LorentzIndex[ν]]`	$\bar{\epsilon}^{ij\mu\nu}$
`Eps[CartesianIndex[i,D-1], CartesianIndex[j,D-1], LorentzIndex[μ,D] LorentzIndex[ν,D]]`	$\epsilon^{ij\mu\nu}$
`Eps[ LorentzIndex[μ] LorentzIndex[ν], LorentzIndex[ρ]]`	$\bar{\epsilon}^{\mu\nu\rho}$
`Eps[ LorentzIndex[μ,D] LorentzIndex[ν,D], LorentzIndex[ρ,D]]`	$\epsilon^{\mu\nu\rho}$
`Eps[ CartesianIndex[i] LorentzIndex[μ], LorentzIndex[ν]]`	$\bar{\epsilon}^{i\mu\nu}$
`Eps[ CartesianIndex[i,D-1],LorentzIndex[μ,D], LorentzIndex[ν,D]]`	$\epsilon^{i\mu\nu}$
`Eps[ CartesianIndex[i],CartesianIndex[j], CartesianIndex[k]]`	$\bar{\epsilon}^{ijk}$
`Eps[ CartesianIndex[i,D-1],CartesianIndex[j,D-1], CartesianIndex[k,D-1]]`	ϵ^{ijk}
`Eps[ CartesianIndex[i],CartesianMomentum[p], CartesianMomentum[q]]`	$\bar{\epsilon}^{ijk}\bar{\mathbf{p}}^j\bar{\mathbf{q}}^k$
`Eps[ CartesianIndex[i,D-1],CartesianMomentum[p,D-1], CartesianMomentum[q,D-1]]`	$\epsilon^{ijk}\mathbf{p}^j\mathbf{q}^k$

Table 24.5: Representation of Levi-Civita symbols with spatial and temporal indices in FeynCalc. For brevity, we do not list all possible combinations of `LorentzIndex`, `Momentum`, `CartesianIndex`, `CartesianMomentum` and `TemporalIndex` in the arguments of `Eps`.

Command in FeynCalc	Meaning
`DiracGamma[TemporalIndex[]]`	$\bar{\gamma}^0$
`DiracGamma[CartesianIndex[i]]`	$\bar{\boldsymbol{\gamma}}^i$
`DiracGamma[CartesianIndex[i,D-1],D]`	$\boldsymbol{\gamma}^i$
`DiracGamma[CartesianIndex[i,D-4],D-4]`	$\hat{\boldsymbol{\gamma}}^i$
`DiracGamma[CartesianMomentum[p]]`	$\bar{\boldsymbol{\gamma}}\cdot\bar{\mathbf{p}}$
`DiracGamma[CartesianMomentum[p,D-1],D]`	$\boldsymbol{\gamma}\cdot\mathbf{p}$

DiracGamma[CartesianMomentum[p, $D-4$], $D-4$]	$\hat{\gamma}\cdot\hat{\mathbf{p}}$

Table 24.6: Representation of Dirac matrices with temporal or Cartesian indices in 4-, D- and $D-4$ dimensions using DiracGamma.

The new FEYNCALC also introduces Pauli matrices (represented with PauliSigma) with Lorentz or Cartesian indices, which were not available in the previous versions. The syntax of PauliSigma is very similar to that of DiracGamma and is summarized in Table 24.7.

Command in FEYNCALC	Meaning
PauliSigma[LorentzIndex[μ]]	$\bar{\sigma}^{\mu}$
PauliSigma[LorentzIndex[μ, D], $D-1$]	σ^{μ}
PauliSigma[LorentzIndex[μ, $D-4$], $D-4$]	$\hat{\sigma}^{\mu}$
PauliSigma[Momentum[p]]	$\bar{\sigma}\cdot\bar{p}$
PauliSigma[Momentum[p, D], D]	$\sigma\cdot p$
PauliSigma[Momentum[μ, $D-4$], $D-4$]	$\hat{\sigma}\cdot\hat{p}$
PauliSigma[CartesianIndex[i]]	$\bar{\boldsymbol{\sigma}}^{i}$
PauliSigma[CartesianIndex[i, $D-1$], $D-1$]	$\boldsymbol{\sigma}^{i}$
PauliSigma[CartesianIndex[i, $D-4$], $D-4$]	$\hat{\boldsymbol{\sigma}}^{i}$
PauliSigma[CartesianMomentum[p]]	$\bar{\boldsymbol{\sigma}}\cdot\bar{\mathbf{p}}$
PauliSigma[CartesianMomentum[p, D], D]	$\boldsymbol{\sigma}\cdot\mathbf{p}$
PauliSigma[CartesianMomentum[μ, $D-4$], $D-4$]	$\hat{\boldsymbol{\sigma}}\cdot\hat{\mathbf{p}}$

Table 24.7: Representation of Pauli matrices in 4-, D- and $D-4$ dimensions using PauliSigma.

Furthermore, we also have Pauli spinors (c. f. Table 24.8), so that one can conveniently represent Pauli structures that appear in nonrelativistic QFTs and especially in NRQCD.

Command in FEYNCALC	Meaning
PauliXi[I]	ξ
PauliXi[-I]	$\xi^{\dagger}$
PauliEta[I]	η
PauliEta[-I]	$\eta^{\dagger}$

Table 24.8: Pauli spinors in FEYNCALC.

The internal representation of FEYNCALC is obviously not the most convenient way to enter expressions. This is why the package also defines some convenient shortcuts that make user input fast and concise. In addition to the existing shortcuts (c. f. Table 24.9)

Shortcut in FeynCalc	Meaning
MT[μ,ν],MTD[μ,ν] MTE[μ,ν]	$\bar{g}^{\mu\nu}$, $g^{\mu\nu}$, $\hat{g}^{\mu\nu}$
FV[p,μ],FVD[p,μ],FVE[p,μ]	$\bar{p}^{\mu}$, p^{μ}, $\hat{p}^{\mu}$
SP[p,q],SPD[p,q],SPE[p,q]	$\bar{p}\cdot\bar{q}$, $p\cdot q$, $\hat{p}\cdot\hat{q}$
GA[μ],GAD[μ],GAE[μ]	$\bar{\gamma}^{\mu}$, γ^{μ}, $\hat{\gamma}^{\mu}$
GS[p],GSD[p],GSE[p]	$\bar{\gamma}\cdot\bar{p}$, $\gamma\cdot p$, $\hat{\gamma}\cdot\hat{p}$
LC[μ,ν,ρ,σ],LC[μ,ν][p,q]	$\bar{\epsilon}^{\mu\nu\rho\sigma}$, $\bar{\epsilon}^{\mu\nu\rho\sigma}p_{\rho}q_{\sigma}$
LCD[μ,ν,ρ,σ],LCD[μ,ν][p,q]	$\epsilon^{\mu\nu\rho\sigma}$, $\epsilon^{\mu\nu\rho\sigma}\hat{p}_{\rho}\hat{q}_{\sigma}$

Table 24.9: Some of the existing FeynCalc shortcuts.

the new FeynCalc also features additional shortcuts for the new objects. Those are listed in Table 24.10.

Shortcut in FeynCalc	Meaning
KD[i,j],KDD[i,j],KDE[i,j]	$\bar{\delta}^{ij}$, δ^{ij}, $\hat{\delta}^{ij}$
CV[p,i],CVD[p,i],CVE[p,i]	$\bar{\mathbf{p}}^{i}$, $\mathbf{p}^{i}$, $\hat{\mathbf{p}}^{i}$
CSP[p,q],CSPD[p,q],CSPE[p,q]	$\bar{\mathbf{p}}\cdot\bar{\mathbf{q}}$, $\mathbf{p}\cdot\mathbf{q}$, $\hat{\mathbf{p}}\cdot\hat{\mathbf{q}}$
TGA[]	$\bar{\gamma}^{0}$
CGA[i],CGAD[i],CGAE[i]	$\bar{\boldsymbol{\gamma}}^{i}$, $\boldsymbol{\gamma}^{i}$, $\hat{\boldsymbol{\gamma}}^{i}$
CGS[p],CGSD[p],CGSE[p]	$\bar{\boldsymbol{\gamma}}\cdot\bar{p}$, $\boldsymbol{\gamma}\cdot\mathbf{p}$, $\hat{\boldsymbol{\gamma}}\cdot\hat{\mathbf{p}}$
CLC[i,j,k],CLC[i,j][p]	$\bar{\epsilon}^{ijk}$, $\bar{\epsilon}^{ijk}\bar{\mathbf{p}}^{k}$
CLCD[i,j,k],CLCD[i,j][p]	ϵ^{ijk}, $\epsilon^{ijk}\mathbf{p}^{k}$
SI[μ],SID[μ],SIE[μ]	$\bar{\sigma}^{\mu}$, σ^{μ}, $\hat{\sigma}^{\mu}$
SIS[p],SISD[p],SISE[p]	$\bar{\sigma}\cdot\bar{p}$, $\sigma\cdot p$, $\hat{\sigma}\cdot\hat{p}$
CSI[i],CSID[i],CSIE[i]	$\bar{\sigma}^{i}$, σ^{i}, $\hat{\sigma}^{i}$
CSIS[p],CSISD[p],CSISE[p]	$\bar{\boldsymbol{\sigma}}\cdot\bar{\mathbf{p}}$, $\boldsymbol{\sigma}\cdot\mathbf{p}$, $\hat{\boldsymbol{\sigma}}\cdot\hat{\mathbf{p}}$

Table 24.10: New FeynCalc shortcuts for nonrelativistic calculations.

It is clear, that the most challenging part in making FeynCalc useful for nonrelativistic calculations is not the introduction of new objects, but the extension of the existing functions to manipulate those new objects in a proper way. Again, this is intended to be done in several steps. All functions, that are currently not ready to handle Cartesian tensors will identify those objects in the input and abort further evaluation. On the other hand, as we will see in the next sections, many existing functions are already capable of working with the new objects.

24.3 Manipulations of Nonrelativistic Expressions

In this section we will illustrate the usage of FEYNCALC and FEYNONIUM on standalone expressions. After having loaded the package

```
In[41]:= $LoadAddOns={"FeynOnium"};
         <<FeynCalc`
```

we can manipulate Cartesian vectors

```
In[42]:= CV[p,i]CV[q,j]KD[i,j]
         Contract[%]
```

Out[42]= $\bar{\mathbf{p}}^{i}\ \bar{\mathbf{q}}^{j}\ \bar{\delta}^{ij}$

Out[43]= $\bar{\mathbf{p}}\cdot\bar{\mathbf{q}}$

or Levi-Civita tensors

```
In[44]:= CLC[i,j,k]CLC[i,l,m]
         Contract[%]
```

Out[44]= $\bar{\epsilon}^{ijk}\ \bar{\epsilon}^{ilm}$

Out[45]= $\bar{\delta}^{jl}\ \bar{\delta}^{km} - \bar{\delta}^{jm}\ \bar{\delta}^{kl}$

in the same way as Lorentz objects. This includes undoing contractions of indices

```
In[46]:= CSP[p,q]
         Uncontract[%,q,CartesianPair→All]
```

Out[46]= $\bar{\mathbf{p}}\cdot\bar{\mathbf{q}}$

Out[47]= $\bar{\mathbf{p}}^{\$AL(\$24)}\ \bar{\mathbf{q}}^{\$AL(\$24)}$

and expanding Cartesian scalar products

```
In[48]:= CSP[p1+p2,q1+q2]
         ExpandScalarProduct[%]
```

Out[48]= $(\bar{\mathbf{p1}}+\bar{\mathbf{p2}})\cdot(\bar{\mathbf{q1}}+\bar{\mathbf{q2}})$

Out[49]= $\bar{\mathbf{p1}}\cdot\bar{\mathbf{q1}}+\bar{\mathbf{p1}}\cdot\bar{\mathbf{q2}}+\bar{\mathbf{p2}}\cdot\bar{\mathbf{q1}}+\bar{\mathbf{p2}}\cdot\bar{\mathbf{q2}}$

```
In[50]:= MomentumCombine[%]
```

Out[50]= $(\bar{\mathbf{p1}}+\bar{\mathbf{p2}})\cdot(\bar{\mathbf{q1}}+\bar{\mathbf{q2}})$

It is also possible to rewrite Lorentz objects in terms of Cartesian objects

```
In[51]:= FV[p,μ]
         LorentzToCartesian[%]
```

Out[51]= $\bar{\mathrm{p}}^{\mu}$

Out[52]= $\mathrm{p}^{0}\ \bar{\mathrm{g}}^{0\mu} - \bar{\mathbf{p}}^{\$}\ \bar{\mathrm{g}}^{\$\mu}$

```
In[53]:= SP[p,q]
         LorentzToCartesian[%]
```

Out[53]= $\bar{p}\cdot\bar{q}$

Out[54]= $p^0\, q^0 - \bar{\mathbf{p}}\cdot\bar{\mathbf{q}}$

In[55]:=
```
GS[p]
LorentzToCartesian[%]
```

Out[55]= $\bar{\gamma}\cdot\bar{p}$

Out[56]= $p^0\, \bar{\gamma}^0 - \bar{\boldsymbol{\gamma}}\cdot\bar{\mathbf{p}}$

or do the inverse

In[57]:=
```
CSP[p,q]
CartesianToLorentz[%]
```

Out[57]= $\bar{\mathbf{p}}\cdot\bar{\mathbf{q}}$

Out[58]= $p^0\, q^0 - \bar{\mathbf{p}}\cdot\bar{\mathbf{q}}$

In[59]:=
```
CGS[p]
CartesianToLorentz[%]
```

Out[59]= $\bar{\boldsymbol{\gamma}}\cdot\bar{\mathbf{p}}$

Out[60]= $p^0\, \bar{\gamma}^0 - \bar{\gamma}\cdot\bar{p}$

The dimensionality of Cartesian objects can be changed in the same way as for Lorentz objects

In[61]:=
```
CV[p,i]
ChangeDimension[%,D]
```

Out[61]= $\bar{\mathbf{p}}^{\mathbf{i}}$

Out[62]= $\mathbf{p}^{\mathbf{i}}$

Furthermore, the new FeynCalc can also perform summations over polarization vectors, that are contracted with Cartesian vectors

In[63]:=
```
SP[kp,kp]=0;
PolarizationSum[i,j,kp,n,Heads→{CartesianIndex,CartesianIndex}]
```

Out[63]= $\bar{\delta}^{\mathbf{ij}} - \frac{\bar{\mathbf{n}}^2\, \bar{\mathbf{kp}}^{\mathbf{i}}\, \bar{\mathbf{kp}}^{\mathbf{j}}}{(\bar{kp}\cdot\bar{n})^2} + \frac{\bar{\mathbf{n}}^{\mathbf{i}}\bar{\mathbf{kp}}^{\mathbf{j}} + \bar{\mathbf{kp}}^{\mathbf{i}}\, \bar{\mathbf{n}}^{\mathbf{j}}}{\bar{kp}\cdot\bar{n}}$

`DiracSimplify` is capable of simplifying chains of Dirac matrices with temporal or spatial components

In[64]:=
```
TGA[].TGA[]
DiracSimplify[%]
```

Out[64]= $\bar{\gamma}^0.\bar{\gamma}^0$

Out[65]= 1

In[66]:=
```
CGA[i].CGS[p].CGA[j].CGA[i]
DiracSimplify[%]
```

```
Out[66]= γ̄^i.(γ̄·p̄).γ̄^j.γ̄^i

Out[67]= (γ̄·p̄).γ̄^j+4 p̄^j
```

The same goes also for Dirac traces

```
In[68]:= CGA[i,j,k,l]
         DiracTrace[%,DiracTraceEvaluate→True]

Out[68]= γ̄^i.γ̄^j.γ̄^k.γ̄^l

Out[69]= 4 (δ̄^il δ̄^jk−δ̄^ik δ̄^jl+δ̄^ij δ̄^kl)
```

A new function that simplifies chains of Pauli matrices is called `PauliTrick`

```
In[70]:= CSI[i,i]
         PauliTrick[%]

Out[70]= σ̄^i.σ̄^i

Out[71]= 3

In[72]:= CSIS[p,p]
         PauliTrick[%]

Out[72]= (σ̄·p̄).(σ̄·p̄)

Out[73]= p̄^2

In[74]:= CSI[i,j,i]
         PauliTrick[%]
         Contract[%]

Out[74]= σ̄^i.σ̄^j.σ̄^i

Out[75]= σ̄^j+i ε̄^ij$MU($26) (δ̄^i$MU($26)+i σ̄^$MU($27) ε̄^$MU($26)i$MU($27))

Out[76]= −σ̄^j
```

Notice that with the option `PauliReduce` we can inhibit the usage of the well-known identity

$$\boldsymbol{\sigma}^i\boldsymbol{\sigma}^j = i\varepsilon^{ijk}\boldsymbol{\sigma}^k + \delta^{ij}, \tag{24.20}$$

such that

```
In[77]:= PauliTrick[CSI[i,j,i],PauliReduce→False]
         Contract[%]

Out[77]= 2 σ̄^i δ̄^ij−3 σ̄^j

Out[78]= −σ̄^j
```

Special care is required when handling Pauli matrices in $D-1$ dimensions. While the anticommutation relation

$$\{\boldsymbol{\sigma}^i, \boldsymbol{\sigma}^j\} = 2\delta^{ij} \tag{24.21}$$

can be directly generalized to $D-1$ dimensions with $(\delta^{ij})^2 = D-1$, the same is not true [178] for the commutation relation

$$[\boldsymbol{\sigma}^i, \boldsymbol{\sigma}^j] = i\epsilon^{ijk}\boldsymbol{\sigma}^k. \tag{24.22}$$

The issue is that ϵ^{ijk} is a purely 3 dimensional object that is not well-defined in $D-1$ dimensions. Nevertheless, the relation from Eq. (24.22) is sometimes also used in the literature [119], so that a tool as versatile as FEYNCALC should somehow account for that. The strategy implemented in FEYNCALC is to first simplify everything using Eq. (24.21), which is unambiguous

```
In[79]:= CSID[i,j,i]
         PauliTrick[%]

Out[79]= σ^i.σ^j.σ^i

Out[80]= 2 σ^i δ^ij-(D-1) σ^j
```

The anticommutation relation is not employed by default in $D-1$ dimensions

```
In[81]:= CSID[i,j]
         PauliTrick[%]

Out[81]= σ^i.σ^j

Out[82]= σ^i.σ^j
```

However, we can also tell FEYNCALC to naively apply Eq. (24.22), where the $D-1$ dimensional Levi-Civita tensor satisfies

$$(\epsilon^{ijk})^2 = (D-3)(D-2)(D-1), \tag{24.23}$$

such that

```
In[83]:= FCSetPauliSigmaScheme["Naive"];
         PauliTrick[CSID[i,j]]

Out[83]= δ^ij+i σ^$MU($28) ϵ^ij$MU($28)
```

In this sense, the user always can decide how such subtleties should be handled.

Let us also mention some functions provided by the FEYNONIUM extension. With `FMSpinorChainExplicit2` we can rewrite arbitrary Dirac spinor chains in terms of Pauli matrices and Pauli spinors, which is very useful for matching calculations between QCD and NRQCD. The general results turn out to be quite large, which is why we do not display them here

```
In[84]:= SpinorUBar[p1,m].GA[mu].SpinorV[p2,m]
         FMSpinorChainExplicit2[%,FMSpinorNormalization→"nonrelativistic"]

Out[84]= ū(p1,m).γ̄^mu.v(p2,m)
         ...
```

For practical purposes it is more useful to specify the kinematics explicitly, e. g. to consider

$$\bar{u}(p_1, m)\gamma^\mu v(p_2, m) \tag{24.24}$$

at 0th order in the relative momentum between p_1 and p_2, which returns a very short result

```
In[85]:= FCClearScalarProducts[]
         TC[p1]=m;
         TC[p2]=m;
         CartesianMomentum[p1|p2]=0;
         FMSpinorChainExplicit2[SpinorUBar[p1,m].GA[mu].SpinorV[p2,m],
             FMSpinorNormalization→"nonrelativistic"]
```

Out[85]= $\bar{g}^{\$MU(\$34)mu}\ \xi^\dagger.\bar{\sigma}^{\$MU(\$34)}.\eta$

Another important operation is the projection of different angular components from the given Cartesian tensor. This is again often needed in the matching, where we want to equate QCD and NRQCD amplitudes of the same total angular momentum J. The trivial example, is to consider the tensor

$$\mathbf{k}_1^i \mathbf{k}_2^j \tag{24.25}$$

and to extract its components that correspond to $J = 0$, $J = 1$ and $J = 2$ using `FMCartesianTensorDecomposition`

```
In[86]:= CV[k1,i]CV[k2,j]
         FMCartesianTensorDecomposition[%,{k1,k2},0]
         FMCartesianTensorDecomposition[%%,{k1,k2},1]
         FMCartesianTensorDecomposition[%%%,{k1,k2},2]
```

Out[86]= $\bar{\mathbf{k1}}^i\ \bar{\mathbf{k2}}^j$

Out[87]= $\frac{1}{3}\ \bar{\delta}^{ij}\ (\bar{\mathbf{k1}}\cdot\bar{\mathbf{k2}})$

Out[88]= $\frac{1}{2}\ \bar{\mathbf{k1}}^i\ \bar{\mathbf{k2}}^j - \frac{1}{2}\ \bar{\mathbf{k2}}^i\ \bar{\mathbf{k1}}^j$

Out[89]= $-\frac{1}{3}\ \bar{\delta}^{ij}\ (\bar{\mathbf{k1}}\cdot\bar{\mathbf{k2}}) + \frac{1}{2}\ \bar{\mathbf{k2}}^i\ \bar{\mathbf{k1}}^j + \frac{1}{2}\bar{\mathbf{k1}}^i\ \bar{\mathbf{k2}}^j$

Currently, FEYNONIUM can project out the $J = 0, 1, 2$ components of tensors up to rank 5. If needed, higher ranks or J-values can be easily added to the code.

Finally, in complex nonrelativistic calculations one often encounters spurious terms that vanish by the virtue of the 3-dimensional Schouten identity

$$\varepsilon^{ijk}\mathbf{p}^l - \varepsilon^{jkl}\mathbf{p}^i + \varepsilon^{kli}\mathbf{p}^j - \varepsilon^{lij}\mathbf{p}^k = 0, \tag{24.26}$$

where $\mathbf{p}$ is an arbitrary Cartesian vector. In general, it is very difficult to apply this identity in a systematic way, which is why FEYNONIUM features a tool that facilitates this task. `FMCartesianSchoutenBruteForce` tries out all possible combinations that can be formed out of the given list of Cartesian vectors and checks if this helps to reduce the number of terms in the expression. This is illustrated in the following simple example, where we have

$$(\hat{\mathbf{k}}\cdot\hat{\mathbf{q}})\left((\hat{\mathbf{k}}\cdot\hat{\mathbf{q}})(\hat{\mathbf{k}}\cdot(\varepsilon^*(k_1)\times\varepsilon^*(k_2))) - (\hat{\mathbf{q}}\cdot(\varepsilon^*(k_1)\times\varepsilon^*(k_2)))\right), \tag{24.27}$$

with

$$(\hat{\mathbf{k}} \cdot \hat{\mathbf{k}}) = (\hat{\mathbf{q}} \cdot \hat{\mathbf{q}}) = 1, \tag{24.28}$$

$$(\hat{\mathbf{k}} \cdot \boldsymbol{\varepsilon}^*(k_1)) = (\hat{\mathbf{k}} \cdot \boldsymbol{\varepsilon}^*(k_2)) = 0. \tag{24.29}$$

Here `FMCartesianSchoutenBruteForce` can readily find the correct version of Schouten identity that reduces the given expression to zero.

```
In[90]:= FCClearScalarProducts[];
         CSP[khat,Polarization[k1,-I,Transversality→True]]=0;
         CSP[khat,Polarization[k2,-I,Transversality→True]]=0;
         CSP[khat,khat]=1;
         CSP[qhat,qhat]=1;

         CSP[khat,qhat] (CSP[khat,qhat] CLC[][khat,Polarization[k1,-I,Transversality→True],
             Polarization[k2,-I,Transversality→True]]-
         CLC[][qhat,Polarization[k1,-I,Transversality→True],Polarization[k2,-I,Transversality
             →True]])

         FMCartesianSchoutenBruteForce[%,{khat,khat,qhat,Polarization[k1,-I,Transversality
             →True],Polarization[k2,-I,Transversality→True]}]

Out[90]= (khat·qhat) ((khat·qhat) ε̄^(khat ε*(k1) ε*(k2)) - ε̄^(qhat ε*(k1) ε*(k2)))

         FMCartesianSchoutenBruteForce: 2 terms were removed using {ε̄^(qhat ε*(k1) ε*(k2)) →
             (khat·qhat) ε̄^(khat ε*(k1) ε*(k2))}

         0
```

Of course, the function is also useful in more complicated cases.

24.4 Applications to NRQCD and pNRQCD

24.4.1 Exclusive Electromagnetic Decay $J/\psi \to 3\gamma$ at $\mathcal{O}(\alpha_s^0 v^0)$

Let us begin with the calculation of the exclusive electromagnetic decay $J/\psi \to 3\gamma$ at $\mathcal{O}(\alpha_s^0 v^0)$. The contribution that we are interested in, is known since almost 70 years [289], i. e. long before the establishment of NRQCD. The most recent study of this process in the framework of NRQCD at $\mathcal{O}(\alpha_s v^2)$ can be found in [290]. Using NRQCD factorization we can write the total decay rate at $\mathcal{O}(v^0)$ as

$$\Gamma(J/\psi \to 3\gamma) = \frac{2\,\mathrm{Im}\, f_1(^3S_1)}{m_Q^2} \langle J/\psi | \psi^\dagger \boldsymbol{\sigma} \chi | 0 \rangle \langle 0 | \chi^\dagger \boldsymbol{\sigma} \psi | J/\psi \rangle \tag{24.30}$$

In perturbative NRQCD (under the replacement $|J/\psi\rangle \to |Q\bar{Q}\rangle$) Eq. (24.30) trivially evaluates to

$$\Gamma_{\text{pert. NRQCD}}(Q\bar{Q} \to 3\gamma) = \frac{2\,\mathrm{Im}\, f_1(^3S_1)}{m_Q^2} \eta^\dagger \boldsymbol{\sigma} \xi\, \xi^\dagger \boldsymbol{\sigma} \eta. \tag{24.31}$$

The matching coefficient $\mathrm{Im}\, f_1(^3S_1)$ can be determined from the matching condition [7]

$$\mathrm{Im}\, \mathcal{A}_{\text{pert. QCD}}(Q\bar{Q} \to Q\bar{Q}) \stackrel{!}{=} \Gamma_{\text{pert. NRQCD}}(Q\bar{Q} \to 3\gamma), \tag{24.32}$$

or, alternatively

$$m_{Q\bar{Q}}\Gamma_{\text{pert. QCD}}(Q\bar{Q}\to 3\gamma)\stackrel{!}{=}\Gamma_{\text{pert. NRQCD}}(Q\bar{Q}\to 3\gamma), \tag{24.33}$$

where we have employed the optical theorem. In order to calculate $\Gamma_{\text{pert. QCD}}(Q\bar{Q}\to 3\gamma)$ in perturbative QCD at $\mathcal{O}(\alpha_s^0 v^0)$, we start with the amplitude

$$Q(p_1)\bar{Q}(p_2)\to\gamma(k_1)\gamma(k_2)\gamma(k_3), \tag{24.34}$$

which is represented by six Feynman diagrams (c. f. Fig. 24.1). We will work in the rest

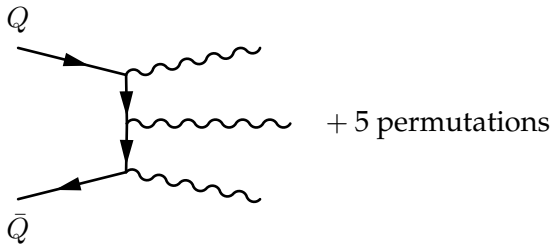

Figure 24.1: QCD diagrams that contribute to the decay $Q\bar{Q}\to 3\gamma$ at $\mathcal{O}(\alpha_s^0)$.

frame of the heavy quarkonium

$$\mathbf{p}_1+\mathbf{p}_2=\mathbf{k}_1+\mathbf{k}_2+\mathbf{k}_3=0, \tag{24.35}$$

with

$$\mathbf{p}_1=-\mathbf{p}_2\equiv\mathbf{q},\quad p_1^0=p_2^0=\sqrt{\mathbf{q}^2+m_Q^2}\equiv E_{\mathbf{q}} \tag{24.36}$$

Furthermore, it is useful to keep in mind that

$$|\mathbf{k}_3|=2E_{\mathbf{q}}-|\mathbf{k}_1|-|\mathbf{k}_2|, \tag{24.37}$$

$$\mathbf{k}_1\cdot\mathbf{k}_2=\frac{\mathbf{k}_3^2-\mathbf{k}_1^2-\mathbf{k}_2^2}{2}=2E_{\mathbf{q}}^2-2E_{\mathbf{q}}(|\mathbf{k}_1|+|\mathbf{k}_2|)+|\mathbf{k}_1||\mathbf{k}_2| \tag{24.38}$$

Let us also briefly discuss the parametrization of the phase space integral in

$$\Gamma_{\text{pert. QCD}}(Q\bar{Q}\to 3\gamma)=\frac{1}{3!}\frac{1}{2m_{Q\bar{Q}}}\int d\Phi\sum_{\text{pols}}|\mathcal{A}_{\text{pert. QCD}}(Q\bar{Q}\to 3\gamma)|^2 \tag{24.39}$$

Following [291] we can introduce the parametrization

$$x_i=\frac{|\mathbf{k}_i|}{E_{\mathbf{q}}}, \tag{24.40}$$

which yields

$$\begin{aligned}\int d\Phi\sum_{\text{pols}}|\mathcal{A}_{\text{pert. QCD}}(Q\bar{Q}\to 3\gamma)|^2&=\frac{d^3k_1}{(2\pi)^3 2|\mathbf{k}_1|}\frac{d^3k_2}{(2\pi)^3 2|\mathbf{k}_2|}\frac{d^3k_3}{(2\pi)^3 2|\mathbf{k}_3|}\\&\times(2\pi)^4\delta^{(4)}(p_1+p_2-k_1-k_2-k_3)\sum_{\text{pols}}|\mathcal{A}_{\text{pert. QCD}}(Q\bar{Q}\to 3\gamma)|^2\\&=\int_0^1 dx_1\int_1^{1-x_1}dx_2\,\frac{E_{\mathbf{q}}^2}{16\pi^3}\sum_{\text{pols}}|\mathcal{A}_{\text{pert. QCD}}(Q\bar{Q}\to 3\gamma)|^2,\end{aligned} \tag{24.41}$$

where we have implicitly performed the angular averaging in the directions of $\mathbf{k}_1$ and $\mathbf{k}_2$.

The calculation using FEYNCALC and FEYNONIUM (c. f. Appendix I for the complete source code) begins with the obligatory steps of generating the required QCD amplitudes with FEYNARTS and converting them to FEYNCALC. Then, using momentum conservation we can eliminate k_3 from the QCD amplitude

```
In[91]:= amps = MomentumExpand[MomentumExpand[ampsRaw] /. Momentum[k3] ->
            Momentum[p1 + p2 - k1 - k2]]
```

To make the calculation as efficient as possible, it is very important to implement all the kinematical conditions. In FEYNCALC it has always been possible to specify the values of the Lorentzian scalar products

```
In[92]:= FCClearScalarProducts[];
         SP[k1, k1] = 0;
         SP[k2, k2] = 0;
         SP[k3, k3] = 0;
         SP[p1, p1] = QMass^2;
         SP[p2, p2] = QMass^2;
```

but the new FEYNCALC allows us to be much more explicit: now we can also fix the values of the Cartesian scalar products (`CSP`) as well as spatial (`CartesianMomentum`) and temporal (`TC`, `TemporalMomentum`) components of various 4-vectors

```
In[13]:= TemporalMomentum[Polarization[k1 | k2 | k3, ___]] = 0;
         TC[q] = 0;
         TC[p1] = Eq;
         TC[p2] = Eq;
         TC[k1] = k1abs;
         TC[k2] = k2abs;
         TC[k3] = k3abs;
         TC[aux] = 1;
         CSP[k1hat, Polarization[k1, -I]] = 0;
         CSP[k2hat, Polarization[k2, -I]] = 0;
         CSP[k3hat, Polarization[k3, -I]] = 0;
         CSP[k1hat, k1hat] = 1;
         CSP[k2hat, k2hat] = 1;
         CSP[k3hat, k3hat] = 1;
         CSP[k1hat, k2hat] = (1/(k1abs*k2abs))*(2*Eq^2 - 2*Eq*(k1abs + k2abs) + k1abs*
             k2abs);
         CartesianMomentum[k1] := k1abs*CartesianMomentum[k1hat];
         CartesianMomentum[k2] := k2abs*CartesianMomentum[k2hat];
         CartesianMomentum[k3] := k3abs*CartesianMomentum[k3hat];
         CartesianMomentum[p1] := qabs*CartesianMomentum[qhat];
         CartesianMomentum[p2] := (-qabs)*CartesianMomentum[qhat];
         CartesianMomentum[q] := qabs*CartesianMomentum[qhat];
         CartesianMomentum[aux] = 0;
         Eq = PowerExpand[Normal[Series[Sqrt[qabs^2 + QMass^2], {qabs, 0, 0}]]];
         k1abs = Eq*x1;
         k2abs = Eq*x2;
```

After that we can simplify the Dirac algebra and rewrite all the occurring Dirac structures in terms of Pauli structures.

```
In[14]:= amps2=amps//DiracSimplify//FMSpinorChainExplicit2[#,
         FMSpinorNormalization->"nonrelativistic"]&//
         Contract//PropagatorDenominatorExplicit//LorentzToCartesian;
```

Then, we expand the resulting expression in $|\mathbf{q}|$ (`qabs`) to 0th order

```
In[44]:= amps3=amps2//EpsEvaluate//ExpandScalarProduct//DotSimplify//
         Series[#,{qabs,0,0}]&//Normal;
```

and isolate the spin triplet contribution (i. e. terms with one Pauli matrix), that corresponds to the decay of J/ψ

```
In[45]:= ampST=Collect2[SelectNotFree2[amps3,PauliSigma],PauliSigma,Polarization,
             FCFactorOut->QCharge^3]//
         ReplaceAll[#,{PauliEta[-I].PauliSigma[x_].PauliXi[I]:>
         CartesianPair[CartesianMomentum[ST],x],
         PauliXi[-I].PauliSigma[x_].PauliEta[I]:>
         CartesianPair[CartesianMomentum[STcc],x]}]&;
```

Finally, we square the amplitude

```
In[46]:= First[AbsoluteTiming[ampSTSquared1 = ComplexConjugate[ampST /. ST -> STcc]*
             ampST; ]]
```

and sum over the polarizations of the outgoing photons

```
In[47]:= ampSTSquared2=ampSTSquared1//DoPolarizationSums[#,k1,aux]&//
             DoPolarizationSums[#,k2,aux]&//
         DoPolarizationSums[#,k3,aux]&//LorentzToCartesian//Collect2[#,{ST,STcc}]&;
```

according to

$$\sum_{\lambda=1}^{2} \varepsilon^i(\mathbf{k},\lambda)\varepsilon^{*j}(\mathbf{k},\lambda) = \delta^{ij} + \frac{(\mathbf{k}^i\boldsymbol{\eta}^j + \mathbf{k}^j\boldsymbol{\eta}^i)}{(\mathbf{k}\cdot\eta)} - \frac{\eta^2\mathbf{k}^i\mathbf{k}^j}{(k\cdot\eta)^2}. \tag{24.42}$$

Obviously, in this case it is most convenient to choose the auxiliary vector η to be

$$\eta = (1,0,0,0)^T. \tag{24.43}$$

In the code η, it is denoted as `aux` and we have already defined its properties when setting up the kinematics. Summing over polarizations reintroduces $\mathbf{k}_3$ in our amplitude, so that we have to eliminate it once again

```
In[48]:= ampSTSquared3=ampSTSquared2//Uncontract[#,k3hat,CartesianPair->All]&//
         ReplaceRepeated[#,{CartesianMomentum[k3hat]:>-k1abs/k3abs
             CartesianMomentum[k1hat]-
         k2abs/k3abs CartesianMomentum[k2hat],k3abs->2Eq-k1abs-k2abs}]&//
             ExpandScalarProduct//Contract//
         Collect2[#,k1hat,k2hat]&;
```

Finally, performing angular averaging in the directions of $\mathbf{k}_1$ and $\mathbf{k}_2$

```
In[49]:= ampSTSquared4=FMCartesianTensorDecomposition[ampSTSquared3,
         {k1hat,k2hat},0]//Simplify;
```

and integrating over x_1 and x_2 we obtain

$$m_{Q\bar{Q}}\Gamma_{\text{pert. QCD}}(Q\bar{Q}\to 3\gamma) = \frac{8(\pi^2-9)\alpha^3 e_Q^6}{9m_Q^2}\eta^\dagger\boldsymbol{\sigma}\xi\,\xi^\dagger\boldsymbol{\sigma}\eta \tag{24.44}$$

Comparing Eq. (24.44) to Eq. (24.32) we immediately get

$$\text{Im}\, f_1(^3S_1) = \frac{4}{9}(\pi^2-9)\alpha^3 e_Q^6 \tag{24.45}$$

and hence

$$\Gamma(J/\psi\to 3\gamma) = \frac{8(\pi^2-9)\alpha^3 e_Q^6}{9m_Q^2}\,\langle J/\psi|\psi^\dagger\boldsymbol{\sigma}\chi|0\rangle\,\langle 0|\chi^\dagger\boldsymbol{\sigma}\psi|J/\psi\rangle \tag{24.46}$$

in full agreement with the literature [290].

24.4.2 Exclusive Electromagnetic Decays $\eta_c \to 2\gamma$ and $\chi_{cJ} \to 2\gamma$ at $\mathcal{O}(\alpha_s^0 v^4)$

Another interesting example is the electromagnetic decay of η_c or χ_{cJ} into two photons, that was already mentioned in Sec. 18. For simplicity, we will consider only contributions from the leading Fock state $|Q\bar{Q}\rangle$ and invoke NRQCD factorization at the amplitude level as in case of $e^+e^- \to \chi_{cJ}\,\gamma$ (c. f. Sec. 15). Ignoring operators that contribute only through the subleading Fock state $|Q\bar{Q}g\rangle$, the relevant NRQCD amplitudes at $\mathcal{O}(v^4)$ are given by

$$\begin{aligned}
\mathcal{A}^{J=0}_{\rm NRQCD} &= \frac{c_0^{J=0}}{m}\,\langle 0|\psi^\dagger\chi|H\rangle + \frac{c_1^{J=0}}{m^2}\,\langle 0|\psi^\dagger\left(-\frac{i}{2}\overleftrightarrow{\mathbf{D}}\cdot\boldsymbol{\sigma}\right)\chi|H\rangle \\
&+ \frac{c_2^{J=0}}{m^3}\,\langle 0|\psi^\dagger\left(-\frac{i}{2}\overleftrightarrow{\mathbf{D}}\right)^2\chi|H\rangle + \frac{c_3^{J=0}}{m^4}\,\langle 0|\psi^\dagger\left(-\frac{i}{2}\overleftrightarrow{\mathbf{D}}\right)^2\left(-\frac{i}{2}\overleftrightarrow{\mathbf{D}}\cdot\boldsymbol{\sigma}\right)\chi|H\rangle \\
&+ \frac{c_4^{J=0}}{m^5}\,\langle 0|\psi^\dagger\left(-\frac{i}{2}\overleftrightarrow{\mathbf{D}}\right)^4\chi|H\rangle\,,
\end{aligned} \tag{24.47a}$$

$$\begin{aligned}
\mathcal{A}^{J=2}_{\rm NRQCD} &= \frac{(c_1^{J=0})^{ij}}{m^2}\,\langle 0|\psi^\dagger\left(-\frac{i}{2}\overleftrightarrow{\mathbf{D}}^{(i}\boldsymbol{\sigma}^{j)}\right)\chi|H\rangle + \frac{(c_2^{J=0})^{ij}}{m^3}\,\langle 0|\psi^\dagger\left(-\frac{i}{2}\right)^2\overleftrightarrow{\mathbf{D}}^{(i}\overleftrightarrow{\mathbf{D}}^{j)}\chi|H\rangle \\
&+ \frac{(c_3^{J=0})^{ij}}{m^4}\,\langle 0|\left(-\frac{i}{2}\overleftrightarrow{\mathbf{D}}\right)^2\psi^\dagger\left(-\frac{i}{2}\overleftrightarrow{\mathbf{D}}^{(i}\boldsymbol{\sigma}^{j)}\right)\chi|H\rangle \\
&+ \frac{(c_4^{J=0})ij}{M^5}\,\langle 0|\psi^\dagger\left(-\frac{i}{2}\overleftrightarrow{\mathbf{D}}\right)^2\left(-\frac{i}{2}\right)^2\overleftrightarrow{\mathbf{D}}^{(i}\overleftrightarrow{\mathbf{D}}^{j)}\chi|H\rangle \\
&+ \frac{(c_5^{J=0})^{ij}}{M^4}\left(\langle 0|\psi^\dagger\left(-\frac{i}{2}\overleftrightarrow{\mathbf{D}}\cdot\boldsymbol{\sigma}\right)\left(-\frac{i}{2}\right)^2\overleftrightarrow{\mathbf{D}}^{(i}\overleftrightarrow{\mathbf{D}}^{j)}\chi|H\rangle\right. \\
&\left.-\frac{2}{5}\,\langle 0|\psi^\dagger\left(-\frac{i}{2}\overleftrightarrow{\mathbf{D}}\right)^2\left(-\frac{i}{2}\right)^2\overleftrightarrow{\mathbf{D}}^{(i}\overleftrightarrow{\mathbf{D}}^{j)}\chi|H\rangle\right).
\end{aligned} \tag{24.47b}$$

They need to be matched to the QCD amplitude for the process

$$Q(p_1)\bar{Q}(p_1) \to \gamma(k_1)\gamma(k_2) \tag{24.48}$$

shown in Fig. 24.2.

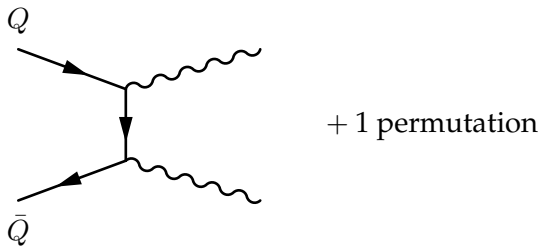

Figure 24.2: QCD diagrams that contribute to the decay $Q\bar{Q} \to 2\gamma$ at $\mathcal{O}(\alpha_s^0)$.

In the rest frame of the heavy quarkonium

$$\mathbf{p}_1 + \mathbf{p}_2 = \mathbf{k}_1 + \mathbf{k}_2 = 0, \tag{24.49}$$

we have

$$\mathbf{p}_1 = -\mathbf{p}_2 \equiv \mathbf{q}, \quad p_1^0 = p_2^0 = \sqrt{\mathbf{q}^2 + m_Q^2} \equiv E_{\mathbf{q}} \tag{24.50}$$

and

$$\mathbf{k}_1 = -\mathbf{k}_2 \equiv \mathbf{k} = E_{\mathbf{q}} \tag{24.51}$$

The determination of the short-distance coefficients c_i at the tree-level using FEYNCALC and FEYNONIUM (c. f. Appendix I for the complete source code) is very similar to the previous calculation: we specify the kinematical constraints

```
In[50]:= FCClearScalarProducts[];
         SP[k1, k1] = 0;
         SP[k2, k2] = 0;
         SP[p1, p1] = QMass^2;
         SP[p2, p2] = QMass^2;

In[51]:= TemporalMomentum[Polarization[k1 | k2, ___]] = 0;
         TC[q] = 0;
         TC[p1] = Eq;
         TC[p2] = Eq;
         TC[k1] = kabs;
         TC[k2] = kabs;
         CSP[khat, Polarization[k1, -I, Transversality -> True]] = 0;
         CSP[khat, Polarization[k2, -I, Transversality -> True]] = 0;
         CSP[khat, khat] = 1;
         CSP[qhat, qhat] = 1;
         CSP[qhatp, qhatp] = 1;
         CartesianMomentum[k1] := kabs*CartesianMomentum[khat];
         CartesianMomentum[k2] := (-kabs)*CartesianMomentum[khat];
         CartesianMomentum[p1] := qabs*CartesianMomentum[qhat];
         CartesianMomentum[p2] := (-qabs)*CartesianMomentum[qhat];
         CartesianMomentum[q] := qabs*CartesianMomentum[qhat];
         CartesianMomentum[qp] := qabs*CartesianMomentum[qhatp];
         CartesianMomentum[aux] = 0;
         Eq = PowerExpand[Normal[Series[Sqrt[qabs^2 + QMass^2], {qabs, 0, 4}]]];
         kabs = Eq;
```

switch to the nonrelativistic form of the amplitude

```
In[52]:= amps2=amps//DiracSimplify//
         FMSpinorChainExplicit2[#,FMSpinorNormalization->"nonrelativistic"]&//
         ntract//PropagatorDenominatorExplicit//LorentzToCartesian;
```

and expand it in $|\mathbf{q}|$ up to 4th order

```
In[53]:= amps3=amps2//EpsEvaluate//ExpandScalarProduct//DotSimplify//
         Series[#,{qabs,0,4}]&//Normal;
```

Then, as already explained in Sec. 17, we project out components of the QCD amplitude that correspond to $J = 0$ and $J = 2$

```
In[54]:= ampQCDJ0=FMCartesianTensorDecomposition[amps4,{qhat,ST},0]//
         Collect2[#,qhat,ST,qabs]&;
         ampQCDJ1=FMCartesianTensorDecomposition[amps4,{qhat,ST},1]//
         Collect2[#,qhat,ST,qabs]&;
         ampQCDJ2tmp=FMCartesianTensorDecomposition[amps4,{qhat,ST},2]//
         Collect2[#,qhat,ST,qabs]&;
```

Notice that the $J = 2$ piece can be simplified further using `FMCartesianSchouten-BruteForce` by the virtue of the 3-dimensional Schouten identity

```
In[55]:= ampQCDJ2=FixedPoint[FMCartesianSchoutenBruteForce[#,{khat,khat,qhat,qhat,
             Polarization[k1,-I,Transversality->True],
         larization[k2,-I,Transversality->True]},FCVerbose->-1]&,ampQCDJ2tmp];
```

This concludes that calculation on the QCD side of the matching. On the NRQCD side we essentially enter the perturbative amplitudes by hand, e. g. for $J = 0$

```
In[56]:= ampNRQCDJ0 = FCI[
         (c0J0/QMass)*PauliEta[-I] . PauliXi[I] +
         (c1J0/QMass^2)*CSP[q, ST] +
         (c2J0/QMass^3)*CSP[q, q]*PauliEta[-I] . PauliXi[I] +
         (c3J0/QMass^4)*CSP[q, ST]*CSP[q, q] +
         (c4J0/QMass^5)*CSP[q, q]^2*PauliEta[-I] . PauliXi[I]];
```

so that at the end we can deduce the short distance coefficients by comparing our QCD and NRQCD amplitudes for $J = 0$ and $J = 2$ order by order in $|\mathbf{q}|$. For the determination of the scalar short distance coefficients one can conveniently use MATHEMATICA's `Solve` function as in

```
In[57]:= tmp = Coefficient[ampQCDJ0, qabs, 3] == Coefficient[ampNRQCDJ0, qabs, 3]
         sdCoeff[c3J0] = Flatten[Solve[tmp, c3J0]]
```

In case of the tensor short distance coefficients, it is faster to "guess" the correct coefficient from looking at the difference of the QCD and NRQCD amplitudes. With the correct coefficients this difference is zero order by order in $|\mathbf{q}|$. Our final results for the short distance coefficients are given by

$$c_0^{J=0} = -e^2 e_Q^2 (\hat{\mathbf{k}} \cdot (\boldsymbol{\varepsilon}^*(k_1) \times \boldsymbol{\varepsilon}^*(k_2))), \tag{24.52a}$$

$$c_1^{J=0} = -ie^2 e_Q^2 (\boldsymbol{\varepsilon}^*(k_1) \cdot \boldsymbol{\varepsilon}^*(k_2)), \tag{24.52b}$$

$$c_2^{J=0} = \frac{2e^2 e_Q^2}{3} (\hat{\mathbf{k}} \cdot (\boldsymbol{\varepsilon}^*(k_1) \times \boldsymbol{\varepsilon}^*(k_2))), \tag{24.52c}$$

$$c_3^{J=0} = \frac{7ie^2 e_Q^2}{6} (\boldsymbol{\varepsilon}^*(k_1) \cdot \boldsymbol{\varepsilon}^*(k_2)), \tag{24.52d}$$

$$c_4^{J=0} = -\frac{8e^2 e_Q^2}{15} (\hat{\mathbf{k}} \cdot (\boldsymbol{\varepsilon}^*(k_1) \times \boldsymbol{\varepsilon}^*(k_2))), \tag{24.52e}$$

$$(c_1^{J=2})^{ij} = -ie^2 e_Q^2 \left((\varepsilon^{*i}(k_1)\varepsilon^{*j}(k_2) + i \leftrightarrow j) + \hat{\mathbf{k}}^i \hat{\mathbf{k}}^j (\boldsymbol{\varepsilon}^*(k_1) \cdot \boldsymbol{\varepsilon}^*(k_2)) \right), \tag{24.52f}$$

$$(c_2^{J=2})^{ij} = -e^2 e_Q^2 \hat{\mathbf{k}}^i \hat{\mathbf{k}}^j (\hat{\mathbf{k}} \cdot (\boldsymbol{\varepsilon}^*(k_1) \times \boldsymbol{\varepsilon}^*(k_2))), \tag{24.52g}$$

$$(c_3^{J=2})^{ij} = \frac{i}{5} e^2 e_Q^2 \left(5(\varepsilon^{*i}(k_1)\varepsilon^{*j}(k_2) + i \leftrightarrow j) + 3\hat{\mathbf{k}}^i \hat{\mathbf{k}}^j (\boldsymbol{\varepsilon}^*(k_1) \cdot \boldsymbol{\varepsilon}^*(k_2)) \right), \tag{24.52h}$$

$$(c_4^{J=2})^{ij} = \frac{8e^2 e_Q^2}{7} \hat{\mathbf{k}}^i \hat{\mathbf{k}}^j (\hat{\mathbf{k}} \cdot (\boldsymbol{\varepsilon}^*(k_1) \times \boldsymbol{\varepsilon}^*(k_2))), \tag{24.52i}$$

$$(c_5^{J=2})^{ij} = \frac{i}{42} e^2 e_Q^2 \left(25(\varepsilon^{*i}(k_1)\varepsilon^{*j}(k_2) + i \leftrightarrow j) - 17\hat{\mathbf{k}}^i \hat{\mathbf{k}}^j (\boldsymbol{\varepsilon}^*(k_1) \cdot \boldsymbol{\varepsilon}^*(k_2)) \right). \tag{24.52j}$$

Squaring the amplitudes in Eqs. (24.47) and comparing them to the NRQCD-factorized total decay rates (as is done in the code) we can precisely reproduce the corresponding matching coefficients from [27], which was already mentioned in Sec. 18.

24.4.3 Matching Coefficients of the Dimension six 4-fermion Operators in NRQCD (Unequal Mass Case)

Our last example is the determination of the matching coefficients that multiply NRQCD dimension six 4-fermion operators in the unequal mass case [119]. The corresponding operators are given by

$$\delta\mathcal{L}_{\text{NRQCD}} = \frac{d_{ss}}{m_1 m_2} \psi^\dagger \psi \chi^\dagger \chi + \frac{d_{sv}}{m_1 m_2} \psi^\dagger \boldsymbol{\sigma} \psi \chi^\dagger \boldsymbol{\sigma} \chi$$

$$+\frac{d_{vs}}{m_1 m_2}\psi^\dagger T^a \psi \chi^\dagger T^a \chi + \frac{d_{vv}}{m_1 m_2}\psi^\dagger \boldsymbol{\sigma} \psi \chi^\dagger \boldsymbol{\sigma} \chi, \tag{24.53}$$

where m_1 (m_2) denotes the mass of a heavy quark (antiquark). The matching coefficients are determined by the hard region of the corresponding QCD box diagrams for

$$Q(p_1)\bar{Q}'(p_2) \to Q(p_3)\bar{Q}'(p_4), \tag{24.54}$$

that are shown in Fig. 24.3. To extract the values of d_{ss}, d_{sv}, d_{vs} and d_{vv}, it is necessary to

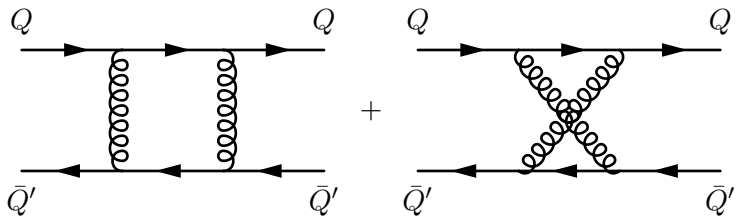

Figure 24.3: QCD diagrams representing $Q\bar{Q}' \to Q\bar{Q}'$, that are relevant for the matching coefficients of the dimension six 4-fermion operators in the unequal mass case.

expand the QCD amplitudes at 0th order in the relative momenta between p_1 and p_2 and between p_3 and p_4. Using FEYNCALC, FEYNHELPERS and FEYNONIUM this calculation can be done with minimal effort (c. f. Appendix I for the complete source code).

Again, we first setup the kinematics

```
In[58]:= FCClearScalarProducts[];
         SPD[p1, p1] = m1^2;
         SPD[p2, p2] = m2^2;
         SPD[p3, p3] = m1^2;
         SPD[p4, p4] = m2^2;
         SPD[p1, p2] = m1*m2;
         SPD[p3, p4] = m1*m2;
         SPD[p1, p3] = m1^2;
         SPD[p2, p4] = m2^2;
         SPD[p1, p4] = m1*m2;
         SPD[p2, p3] = m1*m2;

In[59]:= TC[p1] = m1;
         TC[p2] = m2;
         TC[p3] = m1;
         TC[p4] = m2;
         CartesianMomentum[p1, D - 1] = 0;
         CartesianMomentum[p2, D - 1] = 0;
         CartesianMomentum[p3, D - 1] = 0;
         CartesianMomentum[p4, D - 1] = 0;
         CartesianMomentum[p1] = 0;
         CartesianMomentum[p2] = 0;
         CartesianMomentum[p3] = 0;
         CartesianMomentum[p4] = 0;
```

The next step is to perform tensor decomposition of the loop integrals and to simplify the Dirac algebra

```
In[60]:= mp1=TID[amp,l,UsePaVeBasis->True,ToPaVe->True,Isolate->False]//DiracSimplify//
           DiracSimplify;
```

Following the original choice of the authors of [119], we will simplify the Pauli algebra using the commutation relation in $D-1$ dimensions from Eq. (24.22)

```
In[61]:= FCSetPauliSigmaScheme["Naive"];

In[62]:= amp2=amp1//Collect2[#,DiracSpinor]&//
         FMSpinorChainExplicit2[#,FMSpinorNormalization->"nonrelativistic"]&//
         ReplaceAll[#,{PauliEta[-I].PauliSigma[x_,D-1].PauliEta[I]:>
         CartesianPair[CartesianMomentum[ST1,D-1],x],
         PauliXi[-I].PauliSigma[x_,D-1].PauliXi[I]:>
         CartesianPair[CartesianMomentum[ST2,D-1],x]}]&//
         Contract//Collect2[#,{ST1,ST2}]&;
```

and then evaluate the Passarino–Veltman coefficient functions with the aid of FEYNHELPERS

```
In[63]:= amp3=amp2//Collect2[#,{PaVe,D0}]&//
         ReplaceAll[#,(x:_PaVe|_D0):>
         PaXEvaluateUVIRSplit[x,PaXAnalytic->True,
         PaXImplicitPrefactor->1/( 2Pi)^D]]&//FCHideEpsilon;
```

In [119], $D-1$-dimensional Levi-Civita tensors were defined such, that

$$\varepsilon^{ijk}\varepsilon^{ijk'} = (D-2)\delta^{kk'}, \tag{24.55}$$

which does not agree with the prescription used in FEYNCALC

$$\varepsilon^{ijk}\varepsilon^{ijk'} = (D-3)(D-2)\delta^{kk'}. \tag{24.56}$$

However, we can easily reproduce the effect of Eq. (24.55) on the final results via the replacement

$$\eta^\dagger \boldsymbol{\sigma}\eta\xi^\dagger\boldsymbol{\sigma}\xi \to \frac{1}{D-3}\eta^\dagger\boldsymbol{\sigma}\eta\xi^\dagger\boldsymbol{\sigma}\xi \tag{24.57}$$

```
In[64]:= amp4 = amp3 /. {FCI[CSPD[ST1, ST2]] -> FCI[CSPD[ST1, ST2]]/(D - 3)};
```

Finally, we expand $D = 4-2\epsilon$ around $\epsilon = 0$ and pick up the finite part. Here we also need to separate color singlet and color octet contributions from each other, according to [7]

$$T^aT^b \otimes T^bT^a = \frac{C_F}{2N_c}1\otimes 1 + \frac{N_c^2-2}{2N_c}T^a\otimes T^a, \tag{24.58}$$

$$T^aT^b \otimes T^aT^b = \frac{C_F}{2N_c}1\otimes 1 - \frac{1}{N_c}T^a\otimes T^a, \tag{24.59}$$

which is implemented in the replacement Rule `ruleColor`. Hence,

```
In[65]:= amp5=Series[amp4//FCReplaceD[#,D->4-2EpsilonIR]&//DotSimplify//
             FCShowEpsilon,{EpsilonIR,0,0}]//Normal//FCHideEpsilon;

In[66]:= {finitePart, divergentPart} = FCSplit[amp5, {SMP["Delta_IR"]}];

         finitePartEval=(finitePart/.D->4)//SUNSimplify//Expand2[#,SUNTF]&//
         ReplaceAll[#,ruleColor]&;
```

Finally, we split the result into spin singlet color singlet, spin singlet color octet, spin triplet color singlet and spin triplet color octet pieces

```
In[67]:= {spinSingletFin, spinTripletFin} = FCSplit[finitePartEval, {ST1, ST2}];
         {spinSingletColorSingletFin, spinSingletColorOctetFin} =
          FullSimplify /@ FCSplit[spinSingletFin, {SUNTF}];
         {spinTripletColorSingletFin, spinTripletColorOctetFin} =
          FullSimplify /@ FCSplit[spinTripletFin, {SUNTF}];
```

Comparing with the literature [119]

$$d_{ss} = -C_F\left(\frac{C_A}{2} - C_F\right)\frac{\alpha_s^2}{m_1^2 - m_2^2}\left(m_1^2\left(\log\frac{m_2^2}{\mu^2} + \frac{1}{3}\right) - m_2^2\left(\log\frac{m_1^2}{\mu^2} + \frac{1}{3}\right)\right), \tag{24.60}$$

$$d_{sv} = C_F\left(\frac{C_A}{2} - C_F\right)\frac{\alpha_s^2}{m_1^2 - m_2^2} m_1 m_2 \log\frac{m_1^2}{m_2^2}, \tag{24.61}$$

$$\begin{aligned} d_{vs} = &-\frac{2C_F\alpha_s^2}{m_1^2 - m_2^2}\left(m_1^2\left(\log\frac{m_2^2}{\mu^2} + \frac{1}{3}\right) - m_2^2\left(\log\frac{m_1^2}{\mu^2} + \frac{1}{3}\right)\right) \\ &+ \frac{C_A\alpha_s^2}{4(m_1^2 - m_2^2)}\left(3\left(m_1^2\left(\log\frac{m_2^2}{\mu^2} + \frac{1}{3}\right) - m_2^2\left(\log\frac{m_1^2}{\mu^2} + \frac{1}{3}\right)\right)\right. \\ &\left. + \frac{1}{m_1 m_2}\left(m_1^4\left(\log\frac{m_2^2}{\mu^2} + \frac{10}{3}\right) - m_2^4\left(\log\frac{m_1^2}{\mu^2} + \frac{10}{3}\right)\right)\right), \end{aligned} \tag{24.62}$$

$$\begin{aligned} d_{vv} = &\frac{2C_F\alpha_s^2}{m_1^2 - m_2^2} m_1^2 m_2^2 \log\frac{m_1^2}{m_2^2} \\ &+ \frac{C_A\alpha_s^2}{4(m_1^2 - m_2^2)}\left(\left(m_1^2\left(\log\frac{m_2^2}{\mu^2} + 3\right) - m_2^2\left(\log\frac{m_1^2}{\mu^2} + 3\right)\right) - 3m_1 m_2 \log\frac{m_1^2}{m_2^2}\right), \end{aligned} \tag{24.63}$$

we see that we precisely reproduce the known results.

Part VII

Conclusions

25 Summary

In the first part of this work we have investigated the dispersive van der Waals forces between two S-wave hydrogen atoms in the EFT framework. Our starting point was the description of hydrogen atoms in pNRQED, a low-energy EFT of QED that works at energies $E \ll m_e\alpha$. For a single hydrogen atom, the only relevant scale that remains dynamical in this energy region is $m_e\alpha^2$. However, once we allow two hydrogen atoms to interact with each other at distances R much larger than the Bohr radius (i. e. $R \gg r \sim 1/m_e\alpha$), another dynamical scale emerges. The inverse of R corresponds to the typical momentum transfer between the atoms $|\mathbf{k}| \sim 1/R$. The size of $|\mathbf{k}|$ in comparison to the intrinsic atomic scale $m_e\alpha^2$ determines the character of the van der Waals interaction. Each regime exhibits a different hierarchy of scales and can be described in a suitable EFT.

The EFT of the short-distance van der Waals forces is characterized by the hierarchy $1/R \gg m_e\alpha^2$. Integrating out the scale $1/R$ we obtained well-known electric and magnetic dipole potentials, as well as subleading velocity dependent potentials. To calculate the corresponding van der Waals potential we went one step further and integrated out the scale $m_e\alpha^2$ as well. Our LO result from Eq. (9.17) is the consequence of the exchange of two leading electric-dipole potentials and reproduces the well-known London potential [11]. The exchange of a leading and a subleading dipole potential generates an NLO contribution shown in Eq. (9.22). This contribution corresponds to the result previously obtained by Hirschfelder and Meath [198, 199]. Finally, we have also obtained an NNLO contribution, which, to our knowledge, has not been computed before. This contribution consists of a term that behaves as R^{-3} (c. f. Eq. (9.24)) and a local term (i. e. a term proportional to the Dirac-delta function).

For $1/R \ll m_e\alpha^2$ the relevant physics is described by an EFT of the long-distance van der Waals forces. Proceeding in the same manner as in the short-distance case, we first integrate out the largest scale $m_e\alpha^2$. In the one-atom sector this allows us to define polarizability operators, while in the two-atom sector we generate several local terms. Once we integrate out the scale $1/R$, we obtain a term that behaves as R^{-7}, which is nothing else than the Casimir–Polder potential [12, 179, 190]. The newly computed local terms are necessary to cancel the UV divergences of the diagram that generates the Casimir–Polder potential. This corresponds to the renormalization of the long distance van der Waals potential, which to our knowledge, has not been done before.

The most computationally challenging regime is the one with $1/R \sim m\alpha^2$, which has not been considered in the previous studies of van der Waals forces. The corresponding EFT of intermediate-distance van der Waals interactions contains two scales that are roughly of the same size and must be integrated out simultaneously. The resulting potential in the momentum space representation contains parts that are nonanalytic in $\mathbf{k}$. Using their dispersive representation we obtained the position space representation of the full potential and evaluated it numerically.

On the whole, we have a developed a consistent EFT formalism, in which dispersive van der Waals forces between two hydrogen atoms can be studied in a systematic way, order by order in α and $\mathbf{k}$. The NNLO contribution to the short range van der Waals potential, the renormalization of the long range potential and the computation of the intermediate range potential are the most interesting new results of this study. Finally, in Appendix E.2 we have generalized our results for the dispersive van der Waals potentials in the three different regimes to states with any angular momentum.

The second part of this thesis was devoted to the study of the relativistic $\mathcal{O}(\alpha_s^0 v^2)$ corrections to the exclusive electromagnetic production of the heavy quarkonium χ_{cJ}

and a hard photon in the framework of NRQCD. At the moment, there is no experimental data for this process, although the Belle II experiment in Japan should be able to measure it in the future. This is desirable, since precise and unambiguous predictions for the process $e^+e^- \to \chi_{cJ}\,\gamma$ are also very important for the study of the exotic $X(3872)$ state. The true nature of $X(3872)$ is still very much debated, but according to the experimental results of the BESIII Collaboration, it can be produced in the same channel as χ_{cJ}, namely $e^+e^- \to X(3872)\,\gamma$.

Unfortunately, the previous studies [28, 29, 204, 205] of $\mathcal{O}(v^2)$ relativistic corrections to $e^+e^- \to \chi_{cJ}\,\gamma$ in NRQCD did not take into account the effect of operators that contribute through the higher Fock state $|Q\bar{Q}g\rangle$. Yet the power-counting rules of NRQCD imply that at $\mathcal{O}(v^2)$ the corresponding operators are as important as operators that contribute through the leading Fock state $|Q\bar{Q}\rangle$.

This means that the $\mathcal{O}(v^2)$ NRQCD-factorized cross sections for the exclusive electromagnetic production of χ_{cJ} depend on three and not on two (as implicitly assumed in [28, 29, 204, 205]) nonperturbative long distance matrix elements (LDMEs). The determination of the matrix coefficients multiplying the third LDME for χ_{c0}, χ_{c1} and χ_{c2} even at tree-level is, however, nontrivial. The point is that to extract these matching coefficients from perturbative matching between QCD and NRQCD, we must consider the QCD process $e^+e^- \to Q\bar{Q}g\gamma$, where the gluon is ultrasoft and is regarded as a part of the quarkonium system. To our knowledge, the only similar calculation in the context of NRQCD was done for the exclusive electromagnetic decay $\chi_{cJ} \to 2\gamma$ [26, 27], but never before for a production process.

In this work we have not only determined the previously unknown matching coefficients $T_8(^3P_J)$ but also developed new strategies to approach such calculations in NRQCD. We showed, that using the threshold expansion method of Braaten and Chen [31], the matching can be performed in the rest or in the laboratory frame of the heavy quarkonium. In both cases, the final matching coefficient should agree with each other, which can be used as an important nontrivial cross-check of the final results. Combining our results with the already known $\mathcal{O}(\alpha_s v^0)$ [204, 205] corrections, we presented the complete $\mathcal{O}(v^2)$ total (c. f. Eq. (19.2)) and differential (c. f. Eq. (19.5)) NRQCD-factorized production cross sections for the exclusive electromagnetic production of χ_{cJ} and a hard photon. We believe that this can be very useful for comparisons to the future experimental measurements. Due to the very large uncertainties in the values of the LDMEs that enter production cross sections, we were not able to provide precise numerical predictions. Nevertheless, we made some reasonable numerical estimates, which imply that the new contributions computed in this work might have measurable effects on the final cross sections. In this sense, our results are of relevance both for the methodology and for the phenomenology of heavy quarkonia in the framework of NRQCD.

The last part of this thesis describes the development of computer codes for semi-automatic calculations in relativistic and nonrelativistic EFTs.

FEYNCALC, a well known MATHEMATICA package for symbolic QFT calculations and evaluation of Feynman diagrams, has received a large amount of improvements, many of which are related to the manipulation of 1-loop and multi-loop integrals. Much of the code was improved or rewritten from scratch, which resulted into better performance and stability. A lot of effort was invested into making the development of the package more transparent and robust. The development progress can be now followed through a public code repository. An extensive test suite and many real-life examples are used to minimize new bugs and prevent regressions. In 2016, FEYNCALC 9.0, the first stable release since version 8.2 (released 2012) was finally made public [21] and was met with a warm reception by the particle physics community.

At the same time, we have also recognized and addressed the existing limitations of FeynCalc in the context of EFT calculations. Being able to express a 1-loop amplitude in terms of Passarino–Veltman coefficient functions (as is done in FeynCalc) is certainly useful, if those functions are meant to be evaluated numerically. However, if we are doing an EFT matching calculation, we are clearly interested in the full analytic results, which FeynCalc cannot provide. The common workaround was to evaluate the coefficient functions by hand and then plug the results back into the FeynCalc calculation.

This unsatisfactory situation has lead to the development of the FeynHelpers interface. The main idea behind FeynHelpers it to chain FeynCalc with two other Mathematica packages, Package-X and FIRE. The unique feature of Package-X is the built-in library of analytic results for Passarino–Veltman coefficient functions with up to 4-legs. The package can not only handle singular kinematics but also expand in the arguments of the coefficient functions and separately extract their UV, IR and finite parts. As far as FIRE is concerned, it is a tool for automatic reduction of scalar multi-loop integrals using integration-by-parts (IBP) identities. FeynHelpers seamlessly integrates the most relevant features of these two packages into FeynCalc. Only one simple command is required to start the analytic evaluation of Passarino–Veltman functions (`PaXEvaluate`) or the IBP reduction of multi-loop integrals (`FIREBurn`), while the interface code takes care of all the required conversions and normalizations. With the aid of FeynCalc and FeynHelpers many types of matching calculations between relativistic EFTs can be done in a much simpler and convenient way, as compared to calculations by pen and paper, which are still popular among many EFT practitioners. What is more, since FeynHelpers is not only publicly available but also open source, it is guaranteed that the whole EFT community and not only the collaborators of the author can benefit from it.

Just as all the other publicly available packages for automatic calculations that we are aware of, FeynCalc was initially developed as a tool for relativistic QFTs. This implies that the expressions we are dealing with are manifestly Lorentz covariant, so that we do not need to single out temporal or spatial components of Lorentz tensors. We use Lorentz vectors to represent momenta of the particles, but we are not really interested in Cartesian vectors. Likewise, we may obtain 4-dimensional Levi-Civita tensors from traces of Dirac matrices, but it is not necessary to work with 3-dimensional ϵ^{ijk}. However, once we need to do calculations in nonrelativistic EFTs, we do need to manipulate all those Cartesian objects. Moreover, when doing nonrelativistic expansions of Lorentz covariant amplitudes, we will encounter tensors that carry both Lorentz and Cartesian indices, such as $g^{\mu i}$.

Up to now, such calculations were handled using private codes, since neither FeynCalc nor other public packages for automatic or semi-automatic calculations were suited for working with nonrelativistic QFTs. In order to ameliorate this situation, we have started the extension of FeynCalc to nonrelativistic calculations. The corresponding new features of the upcoming FeynCalc 9.3 include handling of Cartesian vectors, simplification of Pauli matrices and the ability to specify temporal and spatial components of Lorentz tensors. For the time being we omitted the simplification of nonrelativistic loop integrals, but all the new nonrelativistic objects can be defined in 3, $D-1$ or $D-4$ dimensions. The development version of FeynCalc 9.3 and a new extension for NRQCD calculations called FeynOnium are already available for testing in the main repository of the project. The examples included in this thesis demonstrate how the combination of FeynCalc 9.3 and FeynOnium can be used to reproduce existing tree-level NRQCD results with very small amount of effort.

The original motivation for most of these new developments was the desire to use

FeynCalc for the EFT studies conducted in the research group of the author of this thesis. This required a lot of time and effort but this effort was worthwhile. The work invested into the above-mentioned improvements and extensions of the FeynCalc package made this software tool more convenient and versatile than before, especially in the context of EFT calculations.

26 Outlook

We would like to conclude this thesis with a brief outlook.

The presented EFT description of the van der Waals interactions between two hydrogen atoms can be used a starting point to study van der Waals interactions of other physical systems in a rigorous and systematic way. In the context of strong interactions one may think of gluonic van der Waals forces between hadrons, e. g. a quarkonium and a nucleus or two heavy quarkonia, where the relevant EFT is pNRQCD. For example, the insight obtained in this work was used to investigate Van der Waals interactions for Coulombic quarkonia in [15], i. e. quarkonia where v can be identified with α_s, which holds for the lowest quarkonium states. The case of nonperturbatively bound quarkonia still remains to be studied in the EFT framework, whereas currently one has to resort to other methods [201, 202].

Our study of the $e^+e^- \to \chi_{cJ}\,\gamma$ production process motivates two further research directions. First of all, contributions from the subleading Fock state $|Q\bar{Q}g\rangle$ become relevant for numerous other heavy quarkonium production and decay processes, once we are interested in the higher order relativistic corrections to the corresponding observables. These corrections are especially important for charmonia, where $v^2 \sim 0.3$, such that even a v^4 correction to the cross section or a decay rate is not negligible. In fact, $\mathcal{O}(v^4)$ corrections are still missing for many relevant processes, such as e. g. quarkonium production in Higgs boson decay [32, 33]. A systematic investigation of these higher order corrections using the insight but also software tools developed during this work appears feasible and useful.

Last but least, the capabilities of FEYNCALC to interact with other useful packages for high energy physics calculations and to automatize nonrelativistic calculations (especially at 1-loop) will be definitely improved in the future versions of the program. The latter can be conveniently bench-tested by reproducing existing results of calculations in NRQCD, NRQED, pNRQCD, pNRQED but also other nonrelativistic QFTs. Clearly, once we are interested in large or very large calculations, the performance of MATHEMATICA alone tends to become insufficient. Therefore, for such cases it would be desirable to have a seamless interface to FORM, so that one can benefit from its performance while still using the user-friendly MATHEMATICA interface. Here FEYNCALCFORMLINK [22] or FORMTRACER [292] could provide a good starting point for future developments in this direction.

VIII Appendices

A Conventions

Unless otherwise specified, following conventions are used throughout this thesis

- $\hbar = c = 1$
- Signature of the metric tensor $g^{\mu\nu}$ in flat spacetime is $(+,-,-,-)$
- Sign choice for the Levi-Civita-tensor is $\varepsilon^{0123} = 1$, $\varepsilon_{0123} = -1$
- Bold font specifies Cartesian components of 4-vectors, e. g. $\mathbf{p}^i$ denotes spatial component of $p^\mu = (p^0, \mathbf{p})^T$
- Definition of the partial derivative

$$\partial_\mu = (\partial_0, \boldsymbol{\nabla})^T, \qquad \partial^\mu = \left(\partial^0, -\boldsymbol{\nabla}\right)^T, \qquad \boldsymbol{\nabla}^i = \boldsymbol{\partial}_i = -\boldsymbol{\partial}^i$$

- Definition of Pauli matrices

$$\boldsymbol{\sigma}^1 = \begin{pmatrix} 0 & 1 \\ 1 & 0 \end{pmatrix}, \qquad \boldsymbol{\sigma}^2 = \begin{pmatrix} 0 & -i \\ i & 0 \end{pmatrix}, \qquad \boldsymbol{\sigma}^3 = \begin{pmatrix} 1 & 0 \\ 0 & -1 \end{pmatrix},$$
$$\mathbf{p} \cdot \boldsymbol{\sigma} \equiv \begin{pmatrix} \mathbf{p}^3 & \mathbf{p}^1 - i\mathbf{p}^2 \\ \mathbf{p}^1 + i\mathbf{p}^2 & -\mathbf{p}^3 \end{pmatrix}$$

- Definition of Dirac matrices

$$\gamma^0 = \begin{pmatrix} \mathbb{1} & 0 \\ 0 & -\mathbb{1} \end{pmatrix}, \qquad \boldsymbol{\gamma}^i = \begin{pmatrix} 0 & \boldsymbol{\sigma}^i \\ -\boldsymbol{\sigma}^i & 0 \end{pmatrix},$$
$$\gamma_5 = \begin{pmatrix} 0 & \mathbb{1} \\ \mathbb{1} & 0 \end{pmatrix}, \qquad \gamma_5 = -\frac{i}{4!}\varepsilon_{\mu\nu\rho\sigma}\gamma^\mu\gamma^\nu\gamma^\rho\gamma^\sigma$$

- Definition of gauge covariant derivatives $D^\mu = (D^0, -\mathbf{D})^T$ in QED and QCD

$$D^\mu_{\text{QED}} = \partial^\mu + ieA^{A\mu}, \qquad D^\mu_{\text{QCD}} = \partial^\mu - igA^{a\mu}T^a$$

- Definition of field-strength tensors in QED and QCD

$$F_{\mu\nu} = \partial_\mu A_\nu - \partial_\nu A_\mu,$$
$$G^a_{\mu\nu} = \partial_\mu A^a_\nu - \partial_\nu A^a_\mu + gf^{abc}A^b_\mu A^c_\nu$$

- Definition of electric and magnetic fields

$$\mathbf{E}^i = F^{i0} = \boldsymbol{\partial}^i A^0 - \partial^0 \mathbf{A}^i = -\left(\boldsymbol{\nabla}A^0 + \partial_0 \mathbf{A}\right)^i,$$
$$\mathbf{B}^i = -\frac{1}{2}\varepsilon^{ijk}F^{jk} = \varepsilon^{ijk}\boldsymbol{\partial}_j \mathbf{A}^k = (\boldsymbol{\nabla} \times \mathbf{A})^i$$

- Definition of chromoelectric and -magnetic fields

$$E^{ai} = G^{ai0} = \boldsymbol{\partial}^i A^{a0} - \partial^0 \mathbf{A}^{ai} + gf^{abc}\mathbf{A}^{bi}A^{c0} = -\left(\boldsymbol{\nabla}A^{a0} + \partial_0 \mathbf{A} - g^{abc}\mathbf{A}^b A^{c0}\right)^i,$$
$$B^{ai} = \frac{1}{2}\varepsilon^{ijk}G^{akj} = \varepsilon^{ijk}\boldsymbol{\partial}_j \mathbf{A}^{ak} = (\boldsymbol{\nabla} \times \mathbf{A}^a)^i$$

- The branch cuts of the complex square root and the complex logarithm are defined along the negative real axis, such that for $r, \eta \in \mathbb{R}_+$ in the limit $\eta \to 0$ we have

$$\begin{aligned}\sqrt{r \pm i\eta} &= \sqrt{r},\\ \sqrt{-r \pm i\eta} &= \pm i\sqrt{r},\\ \log(r \pm i\eta) &= \log(r),\\ \log(-r \pm i\eta) &= \log(r) \pm i\pi\end{aligned}$$

B List of Acronyms

Below we list the acronyms used in this thesis

- **ChPT**: Chiral Perturbation Theory
- **DR**: Dimensional regularization
- **EFT**: Effective Field Theory
- **IBP**: Integration by parts
- **IR**: Infrared
- **HQET**: Heavy quark effective theory
- **LDME**: Long distance matrix element
- **LO**: Leading order
- **MS**: Minimal subtraction
- $\overline{\text{MS}}$: Modified minimal subtraction
- **NNLO**: Next-to-next-to-leading order
- **NLO**: Next-to-leading order
- **NRQCD**: Nonrelativistic QCD
- **NRQED**: Nonrelativistic QED
- **NREFT**: Nonrelativistic Effective Field Theory
- **NRQFT**: Nonrelativistic Quantum Field Theory
- **OS**: On-shell
- **pNRQED**: potential Nonrelativistic QED
- **pNRQCD**: potential Nonrelativistic QCD
- **QFT**: Quantum Field Theory
- **SCET**: Soft collinear effective theory
- **US**: Ultrasoft
- **UV**: Ultraviolet

C QCD Feynman Rules

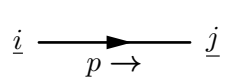

$$= \frac{i(\not{p} + m)}{p^2 - m^2 + i\eta}\delta_{\underline{ij}}$$

$$= \frac{i\delta^{ab}}{p^2 + i\eta}$$

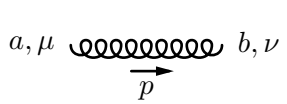

$$= \frac{-i}{p^2 + i\eta}\left(g^{\mu\nu} - (1-\xi)\frac{p^\mu p^\nu}{p^2}\right)\delta^{ab} \underset{\xi=1}{=} \frac{-ig^{\mu\nu}}{p^2 + i\eta}\delta^{ab}$$

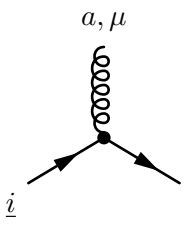

$$= ig\gamma^\mu t^a_{\underline{ij}}$$

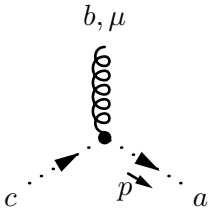

$$= -gf^{abc}p^\mu$$

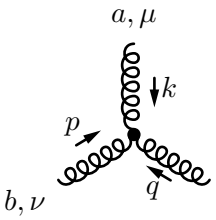

$$= gf^{abc}[g^{\mu\nu}(k-p)^\rho + g^{\nu\rho}(p-q)^\mu + g^{\rho\mu}(q-k)^\nu]$$

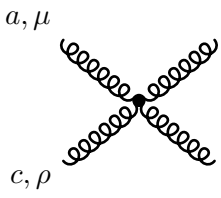

$$\begin{aligned} &-ig^2[f^{abe}f^{cde}(g^{\mu\rho}g^{\nu\sigma} - g^{\mu\sigma}g^{\nu\rho}) \\ = \quad &+ f^{ace}f^{bde}(g^{\mu\nu}g^{\rho\sigma} - g^{\mu\sigma}g^{\nu\rho}) \\ &+ f^{ade}f^{bce}(g^{\mu\nu}g^{\rho\sigma} - g^{\mu\rho}g^{\nu\sigma})] \end{aligned}$$

QCD Symmetry factors

$$S = \frac{1}{2}$$

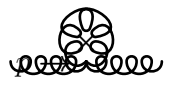

$$S = \frac{1}{2}$$

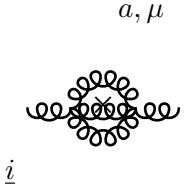

$$S = \frac{1}{3!}$$

D Foldy-Wouthuysen-Tani Transformations

Foldy-Wouthuysen-Tani (FWT) [293, 294] transformations are unitary time-dependent transformations that allow us to redefine Dirac fields in such a way, that the heavy particle and antiparticle components decouple from each other.

In a noninteracting theory this can be done to all orders in $1/m$ with a single unitary transformation. For definiteness, let us consider free Dirac fermions that obey the Dirac equation

$$(i\partial\!\!\!/ - m)\psi = 0 \tag{D.1}$$

with $\psi = (\varphi, \chi)^T$. It is useful to rewrite Eq. (D.1) in a Schrödinger-like form, so that

$$i\partial_t\psi = \gamma^0(\boldsymbol{\gamma}\cdot\mathbf{p} + m)\psi \equiv H\psi \Leftrightarrow i\begin{pmatrix}\partial_t\varphi\\ \partial_t\chi\end{pmatrix} = \begin{pmatrix} m & \boldsymbol{\sigma}\cdot\mathbf{p}\\ \boldsymbol{\sigma}\cdot\mathbf{p} & -m\end{pmatrix}\begin{pmatrix}\varphi\\ \chi\end{pmatrix}. \tag{D.2}$$

This gives us a system of two coupled equations

$$i\partial_t\varphi = m\varphi + (\boldsymbol{\sigma}\cdot\mathbf{p})\chi, \tag{D.3a}$$
$$i\partial_t\chi = -m\chi + (\boldsymbol{\sigma}\cdot\mathbf{p})\varphi. \tag{D.3b}$$

Applying a time-dependent unitary transformation

$$\psi \to \psi' = U(t)\psi \tag{D.4}$$

we can rewrite Eq. (D.2) as

$$i\partial_t\psi' = H'\psi', \tag{D.5}$$

with

$$H' = U(t)(H + i\partial_t)U^\dagger(t). \tag{D.6}$$

If we choose

$$U(t) = e^{\frac{\boldsymbol{\gamma}\cdot\mathbf{p}}{|\mathbf{p}|}\theta}\psi, \tag{D.7}$$

where

$$\sin\theta = \sqrt{\frac{E_\mathbf{p} - m}{2E_\mathbf{p}}}, \quad \cos\theta = \sqrt{\frac{E_\mathbf{p} + m}{2E_\mathbf{p}}}, \tag{D.8}$$

then the system in Eq. (D.3) decouples into

$$i\partial_t\varphi' = E\varphi', \tag{D.9}$$
$$i\partial_t\chi' = -E\chi', \tag{D.10}$$

with

$$\varphi' = \phi\cos\theta + (\boldsymbol{\sigma}\cdot\mathbf{p})\chi\sin\theta, \tag{D.11}$$
$$\chi' = \chi\cos\theta + (\boldsymbol{\sigma}\cdot\mathbf{p})\phi\sin\theta, \tag{D.12}$$
$$H' = \gamma^0 E. \tag{D.13}$$

This allows us to rewrite the Dirac Lagrangian in terms of φ' and χ' as

$$\begin{aligned}\mathcal{L}_{\text{Dirac}} &= \bar{\psi}(i\partial\!\!\!/ - m)\psi = \psi^\dagger(i\partial_0 - H)\psi \to \psi'^\dagger(i\partial_0 - H')\psi' \\ &= \varphi'^\dagger(i\partial_0 - E_{\mathbf{p}})\varphi' + \chi'^\dagger(i\partial_0 + E_{\mathbf{p}})\chi' \\ &= \varphi'^\dagger\left(i\partial_0 - m - \frac{\mathbf{p}^2}{2m} + \frac{\mathbf{p}^4}{8m^3}\right)\varphi' + \chi'^\dagger\left(i\partial_0 + m + \frac{\mathbf{p}^2}{2m} - \frac{\mathbf{p}^4}{8m^3}\right)\chi' + \mathcal{O}(\mathbf{p}^6),\end{aligned} \tag{D.14}$$

where the mass terms can be eliminated via additional unitary transformations

$$\varphi' \to e^{-imt}\varphi', \tag{D.15}$$

$$\chi' \to e^{imt}\chi', \tag{D.16}$$

which leave the remaining part of the Lagrangian unchanged. Things tend to become more complicated in an interacting theory, where many consequent unitary transformations are needed to decouple the upper and lower components of the Dirac spinor at each order in the $1/m_Q$ expansion.

E Additional Results for van der Waals EFT

E.1 Loop Integrals

Throughout our work we have used dimensional regularization. We define

$$\mathcal{K} = \boldsymbol{q}^2 + x(1-x)\boldsymbol{k}^2 \,. \tag{E.1}$$

The loop integrals that depend only on $\boldsymbol{k}^2$ are of the form

$$A_f(\boldsymbol{k}^2) = \nu^{4-d} \int_0^1 dx \int \frac{d^{(d-1)}q}{(2\pi)^{(d-1)}} \frac{1}{\mathcal{K}^f} \,, \tag{E.2}$$

with ν the renormalization scale. Only $A_{3/2}(\boldsymbol{k}^2)$ and $A_2(\boldsymbol{k}^2)$ appear in our results:

$$A_{3/2}(\boldsymbol{k}^2) = \frac{1}{4\pi^2}\left[\lambda + 2 - \log\left(\frac{\boldsymbol{k}^2}{\nu^2}\right)\right], \qquad \text{with} \quad \lambda = \frac{2}{4-d} - \gamma_E + \log 4\pi \,, \tag{E.3}$$

$$A_2(\boldsymbol{k}^2) = \frac{1}{8|\boldsymbol{k}|} \,, \tag{E.4}$$

where here and in the following one-loop results of this appendix (Eqs. (E.6), (E.10)-(E.14)) we have neglected terms of $\mathcal{O}(4-d)$ or smaller; γ_E is the Euler–Mascheroni constant. The ultraviolet divergence can be renormalized in the $\overline{\text{MS}}$ scheme by absorbing the pieces proportional to λ in the counterterms. In the intermediate calculations other powers in the denominator of A_f may appear. These can be related to $A_{3/2}$ and A_2 using the following recurrence relation

$$A_{f+1}(\boldsymbol{k}^2) = \frac{2(2f-d)}{f\boldsymbol{k}^2} A_f(\boldsymbol{k}^2) \,. \tag{E.5}$$

A loop integral that depends only on ΔE_{nm} appears in Secs. 9.2 and 10.1:

$$\begin{aligned} J(\Delta E_{nm})) &= \nu^{4-d} \int \frac{d^{(d-1)}q}{(2\pi)^{(d-1)}} \frac{1}{2|\boldsymbol{q}|(|\boldsymbol{q}| - \Delta E_{nm})} \\ &= \frac{\Delta E_{nm}}{8\pi^2}\left[\lambda + 2 - 2\log 2 + 2i\pi\theta\left(\Delta E_{nm}\right) - \log\left(\frac{\Delta E_n^2}{\nu^2}\right)\right]. \end{aligned} \tag{E.6}$$

In Sec. 11 loop integrals depending simultaneously on $\boldsymbol{k}^2$ and ΔE_{nm} occur. These can be reduced to the master integrals

$$B_f(\boldsymbol{k}^2, \Delta E_{nm}) = \nu^{4-d} \int_0^1 dx \int \frac{d^{(d-1)}q}{(2\pi)^{(d-1)}} \frac{1}{(\mathcal{K} - \Delta E_{nm}^2)^f} \,, \tag{E.7}$$

$$C_f(\boldsymbol{k}^2, \Delta E_{nm}) = \nu^{4-d} \int_0^1 dx \int \frac{d^{(d-1)}q}{(2\pi)^{(d-1)}} \frac{1}{\sqrt{\mathcal{K}}\,(\mathcal{K} - \Delta E_{nm}^2)^f} \,, \tag{E.8}$$

which always appear in the combination

$$K(\boldsymbol{k}^2, \Delta E_{nm}) = -\frac{1}{4\Delta E_{nm}} A_{3/2}(\boldsymbol{k}^2) + \frac{1}{2} B_2(\boldsymbol{k}^2, \Delta E_{nm})$$

$$+\frac{1}{4\Delta E_{nm}}C_1(\boldsymbol{k}^2,\,\Delta E_{nm})+\frac{\Delta E_{nm}}{2}C_2(\boldsymbol{k}^2,\,\Delta E_{nm})\,. \tag{E.9}$$

An explicit analytic result for B_2 reads

$$B_2(\boldsymbol{k}^2,\,\Delta E_{nm})=\frac{1}{8\pi|\boldsymbol{k}|}\left(\pi+2i\,\mathrm{arctanh}\,\sqrt{\frac{4\Delta E_{nm}^2}{\boldsymbol{k}^2}}\right). \tag{E.10}$$

This expression is correct in the momentum region $\boldsymbol{k}^2>4\Delta E_{nm}^2$. The analytic continuation to the region $\boldsymbol{k}^2<4\Delta E_{nm}^2$ is obtained by using the prescription $\Delta E_{nm}^2\to\Delta E_{nm}^2+i\eta$.

An analytic integration of the Feynman parameters is not possible for C_1 and C_2. Different expressions for C_1 and C_2 are possible:

$$\begin{aligned}C_1(\boldsymbol{k}^2,\,\Delta E_{nm})=\frac{1}{4\pi^2}\Bigg[&\lambda+4-\log\frac{4\Delta E_{nm}^2}{\nu^2}+i\pi\\&-\int_0^1 dx\frac{1}{\sqrt{1-x}}\sqrt{1-x\frac{4\Delta E_{nm}^2}{\boldsymbol{k}^2}}\,\mathrm{arctanh}\,\frac{1}{\sqrt{1-x\frac{4\Delta E_{nm}^2}{\boldsymbol{k}^2}}}\Bigg],\end{aligned} \tag{E.11}$$

which is valid in the momentum region $\boldsymbol{k}^2>4\Delta E_{nm}^2$ and can be analytically continued to the region $\boldsymbol{k}^2<4\Delta E_{nm}^2$ by using the prescription $\Delta E_{nm}^2\to\Delta E_{nm}^2+i\eta$. The integrand in Eq. (E.11) can be expanded for large values of $\boldsymbol{k}^2$ but not for small ones. This is because there is always a small enough value of x that makes $x/\boldsymbol{k}^2\sim 1$ for any arbitrarily small value of $\boldsymbol{k}^2$. To expand for small $\boldsymbol{k}^2$ one can use the following expression, which is valid for $\boldsymbol{k}^2<4\Delta E_{nm}^2$,

$$\begin{aligned}C_1(\boldsymbol{k}^2,\,\Delta E_{nm})=\frac{1}{4\pi^2}\Bigg[&\lambda+4-\log\left(\frac{\boldsymbol{k}^2}{\nu^2}\right)\\&-\int_0^1 dx\frac{1}{\sqrt{1-x}}\sqrt{1-x\frac{\boldsymbol{k}^2}{4\Delta E_{nm}^2}}\,\mathrm{arctanh}\,\frac{1}{\sqrt{1-x\frac{\boldsymbol{k}^2}{4\Delta E_{nm}^2}}}\Bigg].\end{aligned} \tag{E.12}$$

The last integral is

$$C_2(\boldsymbol{k}^2,\,\Delta E_{nm})=\frac{1}{8\pi^2\Delta E_{nm}^2}\int_0^1 dx\frac{x\frac{4\Delta E_{nm}^2}{\boldsymbol{k}^2}}{\sqrt{1-x}\sqrt{1-x\frac{4\Delta E_{nm}^2}{\boldsymbol{k}^2}}}\,\mathrm{arctanh}\,\frac{1}{\sqrt{1-x\frac{4\Delta E_{nm}^2}{\boldsymbol{k}^2}}}\,. \tag{E.13}$$

This expression is correct in the momentum region $\boldsymbol{k}^2>4\Delta E_{nm}^2$ and can be expanded for $\boldsymbol{k}^2\gg\Delta E_{nm}^2$. The analytic continuation to the region $\boldsymbol{k}^2<4\Delta E_{nm}^2$ is obtained by using the prescription $\Delta E_{nm}^2\to\Delta E_{nm}^2+i\eta$ and reads

$$\begin{aligned}C_2(\boldsymbol{k}^2,\,\Delta E_{nm})=-\frac{1}{8\pi^2\Delta E_{nm}^2}\Bigg[&2\\&+\int_0^1 dx\frac{x\frac{\boldsymbol{k}^2}{4\Delta E_{nm}^2}}{\sqrt{1-x}\sqrt{1-x\frac{\boldsymbol{k}^2}{4\Delta E_{nm}^2}}}\,\mathrm{arctanh}\,\frac{1}{\sqrt{1-x\frac{\boldsymbol{k}^2}{4\Delta E_{nm}^2}}}\Bigg].\end{aligned} \tag{E.14}$$

This expression can be expanded for $\boldsymbol{k}^2\ll\Delta E_{nm}^2$.

E.2 Generalized One-loop Diagram Expressions

In this appendix, we generalize the results of the one-loop contributions with electric dipole interactions to initial and final states of the hydrogen atoms with any value of the angular momentum. Nevertheless, when considering the interaction between two hydrogen atoms in an arbitrary angular momentum state, one should keep in mind that quadrupole and higher multipole moments may not vanish. These multipole couplings can give rise to tree-level interactions that can be as or more important than the one-loop van der Waals potential. For example quadrupole-quadrupole potentials, which appear when both atoms are in a state with $L \geq 2$, are parametrically larger by $\sqrt{\alpha}$ and α^2 respectively than the London and Casimir–Polder potentials.

Furthermore, we also provide the expressions for the analogous loop contributions obtained by replacing electric dipoles with magnetic dipoles. From the pNRQED Lagrangian of Eq. (4.6) we can see that the magnetic dipole operator is smaller than the electric dipole operator by a factor of order α. Since, due to parity, the two couplings on the same atom must either be both magnetic or both electric dipoles this gives two new kinds of loop contributions: one with two electric dipoles and two magnetic dipoles, and one with four magnetic dipoles. In general, all these contributions are much smaller than the ones produced with only electric dipoles.

Throughout this appendix we use the notation E, B, M to label contributions from one-loop diagrams with four electric dipoles (E), two electric dipoles and two magnetic dipoles (M), and four magnetic dipoles (B). The explicit expressions for the loop integrals $A_{3/2}$, A_2, J and K can be found in Appendix E.1. Results will be given in d space-time dimensions.

E.2.1 Short-range Regime

The one-loop matching contributions from pNRQED to the two-atom pNRQED′ potential with four electric dipole vertices given in Sec. 9.1 are independent of the initial and final states and thus valid for any angular momentum. We, now, provide the analogous contributions with four magnetic dipole vertices, and with two magnetic dipoles vertices on one atom and two electric dipole vertices on the other one. The subscripts 1 and 2 of $\boldsymbol{\mu}$ and $\boldsymbol{L}$ indicate the atom. In the first case the contributions read

$$\begin{aligned}
\widetilde{V}^{\text{1loop}}_{LO,B} &= \frac{\pi^2\alpha^2 A_{3/2}(\boldsymbol{k}^2)}{16(d-1)m_e^4}\boldsymbol{\mu}_{1\,i}\boldsymbol{\mu}_{1\,j}\boldsymbol{\mu}_{2\,k}\boldsymbol{\mu}_{2\,l} \\
&\quad\times\Big[(d-2)(\boldsymbol{k}^i\boldsymbol{k}^l\delta^{jk}+\boldsymbol{k}^j\boldsymbol{k}^k\delta^{il}-\boldsymbol{k}^i\boldsymbol{k}^k\delta^{jl}-\boldsymbol{k}^j\boldsymbol{k}^l\delta^{ik}) \\
&\quad+3\boldsymbol{k}^2\left(\delta^{il}\delta^{jk}-\delta^{ik}\delta^{jl}\right)\Big], \qquad \text{(E.15)} \\
\widetilde{V}^{\text{1loop}}_{NLO,B} &= \frac{\pi^2\alpha^2 A_2(\boldsymbol{k}^2)}{16(d-2)m_e^4}\left[\left(\boldsymbol{\mu}_{1\,i}\dot{\boldsymbol{\mu}}_{1\,j}-\dot{\boldsymbol{\mu}}_{1\,i}\boldsymbol{\mu}_{1\,j}\right)\boldsymbol{\mu}_{2\,k}\boldsymbol{\mu}_{2\,l}+\boldsymbol{\mu}_{1\,i}\boldsymbol{\mu}_{1\,j}\left(\boldsymbol{\mu}_{2\,k}\dot{\boldsymbol{\mu}}_{2\,l}-\dot{\boldsymbol{\mu}}_{2\,k}\boldsymbol{\mu}_{2\,l}\right)\right] \\
&\quad\times\left[\boldsymbol{k}^i\boldsymbol{k}^k\delta^{jl}+\boldsymbol{k}^j\boldsymbol{k}^l\delta^{ik}-\boldsymbol{k}^i\boldsymbol{k}^l\delta^{jk}-\boldsymbol{k}^j\boldsymbol{k}^k\delta^{il}+2\boldsymbol{k}^2\left(\delta^{il}\delta^{jk}-\delta^{ik}\delta^{jl}\right)\right], \qquad \text{(E.16)} \\
\widetilde{V}^{\text{1loop}}_{N^2LO,B} &= -\frac{\pi^2\alpha^2 A_{3/2}(\boldsymbol{k}^2)}{12m_e^4} \\
&\quad\times\Big\{\Big[\dot{\boldsymbol{\mu}}_{1\,i}\dot{\boldsymbol{\mu}}_{1\,j}\boldsymbol{\mu}_{2\,k}\boldsymbol{\mu}_{2\,l}+\boldsymbol{\mu}_{1\,i}\boldsymbol{\mu}_{1\,j}\dot{\boldsymbol{\mu}}_{2\,k}\dot{\boldsymbol{\mu}}_{2\,l} \\
&\quad-\frac{1}{4}\left(\boldsymbol{\mu}_{1\,i}\dot{\boldsymbol{\mu}}_{1\,j}-\dot{\boldsymbol{\mu}}_{1\,i}\boldsymbol{\mu}_{1\,j}\right)\left(\boldsymbol{\mu}_{2\,k}\dot{\boldsymbol{\mu}}_{2\,l}-\dot{\boldsymbol{\mu}}_{2\,k}\boldsymbol{\mu}_{2\,l}\right)\Big]\lambda^{ijkl}_{N^2LO,\,B}
\end{aligned}$$

$$
\left.
\begin{aligned}
&-\Big[\dot{\boldsymbol{\mu}}_{1\,i}\dot{\boldsymbol{\mu}}_{1\,j}\boldsymbol{\mu}_{2\,k}\boldsymbol{\mu}_{2\,l}+\boldsymbol{\mu}_{1\,i}\boldsymbol{\mu}_{1\,j}\dot{\boldsymbol{\mu}}_{2\,k}\dot{\boldsymbol{\mu}}_{2\,l}\\
&+\frac{1}{4}\left(\boldsymbol{\mu}_{1\,i}\dot{\boldsymbol{\mu}}_{1\,j}-\dot{\boldsymbol{\mu}}_{1\,i}\boldsymbol{\mu}_{1\,j}\right)\left(\boldsymbol{\mu}_{2\,k}\dot{\boldsymbol{\mu}}_{2\,l}-\dot{\boldsymbol{\mu}}_{2\,k}\boldsymbol{\mu}_{2\,l}\right)\Big]\lambda^{ijlk}_{N^2LO,\,B}\Big\},
\end{aligned}
\right. \tag{E.17}
$$

where $\dot{\boldsymbol{\mu}}=i\left[\boldsymbol{\mu},\hat{h}_0\right]$, and

$$
\begin{aligned}
\lambda^{ijkl}_{N^2LO,\,B} &= \Big\{(d-6)(d-4)\frac{\boldsymbol{k}^i\boldsymbol{k}^j\boldsymbol{k}^k\boldsymbol{k}^l}{\boldsymbol{k}^4}+\left(\delta^{ij}\delta^{kl}+\delta^{il}\delta^{jk}-2\delta^{ik}\delta^{jl}\right)\\
&\quad+\frac{1}{\boldsymbol{k}^2}\big[(d-4)(\boldsymbol{k}^i\boldsymbol{k}^j\delta^{kl}+\boldsymbol{k}^i\boldsymbol{k}^l\delta^{jk}+\boldsymbol{k}^k\boldsymbol{k}^l\delta^{ij}+\boldsymbol{k}^j\boldsymbol{k}^k\delta^{il})\\
&\quad+2(d-2)(\boldsymbol{k}^i\boldsymbol{k}^k\delta^{jl}+\boldsymbol{k}^j\boldsymbol{k}^l\delta^{ik})\big]\Big\}.
\end{aligned} \tag{E.18}
$$

For electric-magnetic dipole interactions the LO contribution vanishes, the following two terms read

$$
\begin{aligned}
\widetilde{V}^{1\text{loop}}_{NLO,M} &= -\frac{i\pi^2\alpha^2A_2(\boldsymbol{k}^2)}{(d-2)m_e^3}\left[\boldsymbol{L}_1^i\left(\boldsymbol{\mu}_2\times\boldsymbol{\mu}_2\right)^j+\boldsymbol{L}_2^i\left(\boldsymbol{\mu}_1\times\boldsymbol{\mu}_1\right)^j\right]\\
&\quad\times\left[(d-3)\boldsymbol{k}^i\boldsymbol{k}^j+\boldsymbol{k}^2\delta^{ij}\right],
\end{aligned} \tag{E.19}
$$

$$
\begin{aligned}
\widetilde{V}^{1\text{loop}}_{N^2LO,M} &= \frac{i2\pi^2\alpha^2A_{3/2}(\boldsymbol{k}^2)}{m_e^3\boldsymbol{k}^2}\left[\left(\boldsymbol{\mu}_1\cdot\dot{\boldsymbol{\mu}}_1+\boldsymbol{\mu}_2\cdot\dot{\boldsymbol{\mu}}_2\right)\delta^{ij}-\boldsymbol{\mu}_1^i\dot{\boldsymbol{\mu}}_1^j-\boldsymbol{\mu}_2^i\dot{\boldsymbol{\mu}}_2^j\right]\\
&\quad\times\left[(d-4)\boldsymbol{k}^i\boldsymbol{k}^j+\boldsymbol{k}^2\delta^{ij}\right].
\end{aligned} \tag{E.20}
$$

Next we provide the one-loop matching contributions from pNRQED′ to the WEFT potential of Sec. 9.2 generalized to any state of the hydrogen atoms. The first contribution corresponds to the two dipole potential exchange (diagram *(a)* of Fig. 9.4)

$$
\widetilde{W}^{(a)}_y=\sum_{m_1,m_2}{}'\,p_y(n_1,m_1)^{ij}p_y(n_2,m_2)^{kl}\lambda^{ijkl}_{(a)}\frac{A_2(\boldsymbol{k}^2)}{\Delta E_{n_1m_2}+\Delta E_{n_2m_2}},\qquad y=E,\,B\,, \tag{E.21}
$$

with

$$
\begin{aligned}
\lambda^{ijkl}_{(a)} &= \frac{1}{16d(d-2)}\Big[(d^2-4d+3)\boldsymbol{k}^i\boldsymbol{k}^j\boldsymbol{k}^k\boldsymbol{k}^l+\boldsymbol{k}^4\left(\delta^{ij}\delta^{kl}+\delta^{il}\delta^{jk}+\delta^{ik}\delta^{jl}\right)\\
&\quad+(d-1)\boldsymbol{k}^2(\boldsymbol{k}^i\boldsymbol{k}^j\delta^{kl}+\boldsymbol{k}^i\boldsymbol{k}^l\delta^{jk}+\boldsymbol{k}^k\boldsymbol{k}^l\delta^{ij}+\boldsymbol{k}^j\boldsymbol{k}^k\delta^{il})\\
&\quad-(d+1)\boldsymbol{k}^2(\boldsymbol{k}^i\boldsymbol{k}^k\delta^{jl}+\boldsymbol{k}^j\boldsymbol{k}^l\delta^{ik})\Big].
\end{aligned} \tag{E.22}
$$

The second type of diagrams corresponds to the exchange of a LO and a NLO dipole potential (diagram *(b)* of Fig. 9.4)

$$
\widetilde{W}^{(b)}_y=\sum_{m_1,m_2}{}'\,p_y(n_1,m_1)^{ij}p_y(n_2,m_2)^{kl}\lambda^{ijkl}_{(b)}\frac{A_2(\boldsymbol{k}^2)\Delta E_{n_1m_1}\Delta E_{n_2m_2}}{\Delta E_{n_1m_1}+\Delta E_{n_2m_2}},\qquad y=E,\,B\,, \tag{E.23}
$$

with

$$
\begin{aligned}
\lambda^{ijkl}_{(b)} &= \frac{1}{8(d-2)}\Big[(d-5)(d-3)\frac{\boldsymbol{k}^i\boldsymbol{k}^j\boldsymbol{k}^k\boldsymbol{k}^l}{\boldsymbol{k}^2}+(d-1)(\boldsymbol{k}^i\boldsymbol{k}^k\delta^{jl}+\boldsymbol{k}^j\boldsymbol{k}^l\delta^{ik})\\
&\quad+\boldsymbol{k}^2\left(\delta^{ij}\delta^{kl}+\delta^{il}\delta^{jk}-3\delta^{ik}\delta^{jl}\right)
\end{aligned}
$$

$$+ (d-3)(\boldsymbol{k}^i\boldsymbol{k}^j\delta^{kl} + \boldsymbol{k}^i\boldsymbol{k}^l\delta^{jk} + \boldsymbol{k}^k\boldsymbol{k}^l\delta^{ij} + \boldsymbol{k}^j\boldsymbol{k}^k\delta^{il})\Big]. \tag{E.24}$$

The velocity $\boldsymbol{v}$ (or $\dot{\boldsymbol{\mu}}$ in the magnetic case) that appears in the NLO order pNRQED' potential, involved in the calculation of diagram *(b)* of Fig. 9.4, does not appear in Eq. (E.23) for we have used $\langle n|\boldsymbol{v}|m\rangle = i\Delta E_{nm}\langle n|\boldsymbol{x}|m\rangle$ (or the equivalent for the magnetic case).

Since the LO electric-magnetic dipole potential is proportional to the energy, the corresponding two LO potential exchange diagrams give a contribution more similar to Eq. (E.23) than Eq. (E.21):

$$\begin{aligned}\widetilde{W}_M^{(a)} &= \sum_{m_1,m_1}{}' \Big[p_E(n_1,m_2)^{ij}p_B(n_2,m_2)^{kl} + p_B(n_1,m_1)^{ij}p_E(n_2,m_2)^{kl}\Big] \\ &\quad\times \left[(d-3)\boldsymbol{k}^r\boldsymbol{k}^s + \boldsymbol{k}^2\delta^{rs}\right]\epsilon^{rik}\epsilon^{sjl}\frac{A_2(\boldsymbol{k}^2)\Delta E_{n_1m_1}\Delta E_{n_2m_2}}{4(d-2)\left(\Delta E_{n_1m_1}+\Delta E_{n_2m_2}\right)}.\end{aligned} \tag{E.25}$$

The last type of diagrams are formed by a potential interaction and an ultrasoft photon (diagrams *(d)* and *(e)* of Fig. 9.4). The potential can be written as

$$\begin{aligned}\widetilde{W}_y^{(d+e)} &= -\sum_{m_1,m_2}{}' p_y(n_1,m_1)^{ij}p_y(n_2,m_2)^{kl} \\ &\quad\times\Bigg[\lambda^{ijkl}_{(d+e),\,y}\frac{\Delta E_{n_1m_1}^2 J(\Delta E_{n_1m_1}) + \Delta E_{n_2m_2}^2 J(\Delta E_{n_2m_2})}{\Delta E_{n_1m_1}+\Delta E_{n_2m_2}} \\ &\quad -\lambda^{ijlk}_{(d+e),\,y}\frac{\Delta E_{n_1m_1}^2 J(\Delta E_{n_1m_1}) - \Delta E_{n_2m_2}^2 J(\Delta E_{n_2m_2})}{\Delta E_{n_1m_1}-\Delta E_{n_2m_2}}\Bigg],\ y=E,\,B\,,\end{aligned} \tag{E.26}$$

with

$$\lambda^{ijkl}_{(d+e),\,E} = \frac{2(d-2)}{d-1}\frac{\boldsymbol{k}^j\boldsymbol{k}^l\delta^{ik}}{\boldsymbol{k}^2}\,, \tag{E.27}$$

$$\lambda^{ijkl}_{(d+e),\,B} = \frac{2(d-2)}{d-1}\frac{(\boldsymbol{k}^j\boldsymbol{k}^l - \boldsymbol{k}^2\delta^{jl})\delta^{ik}}{\boldsymbol{k}^2}\,. \tag{E.28}$$

The equivalent contribution with two electric dipoles and two magnetic dipoles vanishes.

E.2.2 Long-range Regime

The contributions to the WEFT' potential of Sec. 10.1 from the two-photon exchange diagrams in pNRQED (see Fig. 10.2) generalized to any hydrogen atom state read

$$\begin{aligned}(\widetilde{W}')^{1\text{loop}}_{LO,\,y} &= -\sum_{m_1,m_2}{}' p_y(n_1,m_1)^{ij}p_y(n_2,m_2)^{kl} \\ &\quad\times\Bigg[\frac{\sigma^{ijkl}_{LO,y}}{\Delta E_{n_1m_1}+\Delta E_{n_2m_2}}\left(\Delta E_{n_1m_1}^2 J(\Delta E_{n_1m_1}) + \Delta E_{n_2m_2}^2 J(\Delta E_{n_2m_2})\right) \\ &\quad -\frac{\sigma^{ijlk}_{LO,y}}{\Delta E_{n_1m_1}-\Delta E_{n_2m_2}}\left(\Delta E_{n_1m_1}^2 J(\Delta E_{n_1m_1}) - \Delta E_{n_2m_2}^2 J(\Delta E_{n_2m_2})\right)\Bigg],\end{aligned} \tag{E.29}$$

$$(\widetilde{W}')^{1\text{loop}}_{NLO,\,y} = -\sum_{m_1,m_2}{}' p_y(n_1,m_1)^{ij}p_y(n_2,m_2)^{kl}$$

$$\times\left[\frac{\sigma^{ijkl}_{NLO,y}}{\Delta E_{n_1m_1}+\Delta E_{n_2m_2}}\left(J(\Delta E_{n_1m_1})+J(\Delta E_{n_2m_2})\right)\right.$$
$$\left.-\frac{\sigma^{ijlk}_{NLO,y}}{\Delta E_{n_1m_1}-\Delta E_{n_2m_2}}\left(J(\Delta E_{n_1m_1})-J(\Delta E_{n_2m_2})\right)\right], \tag{E.30}$$

$$(\widetilde{W}')^{\text{1loop}}_{N^2LO,\,y}=-\sum_{m_1,m_2}{}'\,\frac{p_y(n_1,m_1)^{ij}p_y(n_2,m_2)^{kl}}{\Delta E^2_{n_1m_1}\Delta E^2_{n_2m_2}}$$
$$\times\left[\frac{\sigma^{ijkl}_{N^2LO,y}}{\Delta E_{n_1m_1}+\Delta E_{n_2m_2}}\left(\Delta E^2_{n_2m_2}J(\Delta E_{n_1m_1})+\Delta E^2_{n_1m_1}J(\Delta E_{n_2m_2})\right)\right.$$
$$\left.-\frac{\sigma^{ijlk}_{N^2LO,y}}{\Delta E_{n_1m_1}-\Delta E_{n_2m_2}}\left(\Delta E^2_{n_2m_2}J(\Delta E_{n_1m_1})-\Delta E^2_{n_1m_1}J(\Delta E_{n_2m_2})\right)\right], \tag{E.31}$$

where $y=E,\,B,\,M$. In the case of electric dipole interactions we have

$$\sigma^{ijkl}_{LO,\,E} = -\frac{1}{2(d-1)}\left[\delta^{ij}\delta^{kl}+\delta^{il}\delta^{jk}+(d^2-6d+6)\delta^{ik}\delta^{jl}\right], \tag{E.32}$$

$$\sigma^{ijkl}_{NLO,\,E} = \frac{1}{24}\left[2\left(\boldsymbol{k}^i\boldsymbol{k}^j\delta^{kl}+\boldsymbol{k}^k\boldsymbol{k}^l\delta^{ij}+\boldsymbol{k}^i\boldsymbol{k}^l\delta^{jk}+\boldsymbol{k}^j\boldsymbol{k}^k\delta^{il}\right)+4(d-4)\left(\boldsymbol{k}^i\boldsymbol{k}^k\delta^{jl}+\boldsymbol{k}^j\boldsymbol{k}^l\delta^{ik}\right)\right.$$
$$\left.+\boldsymbol{k}^2\left(\delta^{ij}\delta^{kl}+\delta^{il}\delta^{jk}+(d^2-10d+22)\delta^{ik}\delta^{jl}\right)\right], \tag{E.33}$$

$$\sigma^{ijkl}_{N^2LO,\,E} = -\frac{1}{480}\left[(d-3)\boldsymbol{k}^4\left(\delta^{ij}\delta^{kl}+\delta^{il}\delta^{jk}+(d^2-14d+46)\delta^{ik}\delta^{jl}\right)+8(d-3)\boldsymbol{k}^i\boldsymbol{k}^j\boldsymbol{k}^k\boldsymbol{k}^l\right.$$
$$+4(d-3)\boldsymbol{k}^2\left(\boldsymbol{k}^i\boldsymbol{k}^j\delta^{kl}+\boldsymbol{k}^k\boldsymbol{k}^l\delta^{ij}+\boldsymbol{k}^i\boldsymbol{k}^l\delta^{jk}+\boldsymbol{k}^j\boldsymbol{k}^k\delta^{il}\right)$$
$$\left.+6(d^2-9d+18)\boldsymbol{k}^2(\boldsymbol{k}^i\boldsymbol{k}^k\delta^{jl}+\boldsymbol{k}^j\boldsymbol{k}^l\delta^{ik}\right)\Big], \tag{E.34}$$

and, when the interaction is mediated by magnetic dipoles,

$$\sigma^{ijkl}_{LO,\,B} = -\frac{1}{2(d-1)}\left[\delta^{ij}\delta^{kl}+\delta^{il}\delta^{jk}+(d^2-2d-2)\delta^{ik}\delta^{jl}\right], \tag{E.35}$$

$$\sigma^{ijkl}_{NLO,\,B} = \sigma^{ijkl}_{NLO,\,E}\,, \tag{E.36}$$

$$\sigma^{ijkl}_{N^2LO,\,B} = \sigma^{ijkl}_{N^2LO,\,E}\,. \tag{E.37}$$

For electric dipoles interacting with magnetic dipoles the instantaneous dipole factor

$$p_M(n_1,m_1)^{ij}p_M(n_2,m_2)^{kl} \tag{E.38}$$

should be understood as

$$p_E(n_1,m_1)^{ij}p_B(n_2,m_2)^{kl}+p_B(n_1,m_1)^{ij}p_E(n_2,m_2)^{kl}, \tag{E.39}$$

and

$$\sigma^{ijkl}_{LO,\,M} = -\frac{1}{2}\left(\delta^{ij}\delta^{kl}-\delta^{il}\delta^{jk}\right), \tag{E.40}$$

$$\sigma^{ijkl}_{NLO,\,M} = \frac{d-3}{24}\epsilon^{rik}\epsilon^{sjl}\left(\boldsymbol{k}^2\delta^{rs}+2\boldsymbol{k}^r\boldsymbol{k}^s\right), \tag{E.41}$$

$$\sigma^{ijkl}_{N^2LO,\,M} = -\frac{(d-5)(d-3)\boldsymbol{k}^2}{480}\epsilon^{rik}\epsilon^{sjl}\left(\boldsymbol{k}^2\delta^{rs}+4\boldsymbol{k}^r\boldsymbol{k}^s\right). \tag{E.42}$$

The contribution to the WEFT potential from the one-loop diagram with seagull vertices in Fig. 10.3 for an arbitrary electric polarization tensor (see (8.3)) reads

$$\begin{aligned}\widetilde{W}_E^{\rm seg} = -\frac{\pi^2\alpha_{n_1}^{ij}\alpha_{n_2}^{kl}}{16(d-1)(d+1)}\Big[&2d(d-2)\boldsymbol{k}^i\boldsymbol{k}^j\boldsymbol{k}^k\boldsymbol{k}^l\\ &-(d+4)\boldsymbol{k}^2\left(\boldsymbol{k}^i\boldsymbol{k}^l\delta^{kj}+\boldsymbol{k}^j\boldsymbol{k}^k\delta^{il}+\boldsymbol{k}^i\boldsymbol{k}^k\delta^{jl}+\boldsymbol{k}^j\boldsymbol{k}^l\delta^{ik}\right)\\ &+2d\,\boldsymbol{k}^2\left(\boldsymbol{k}^i\boldsymbol{k}^j\delta^{kl}+\boldsymbol{k}^k\boldsymbol{k}^l\delta^{ij}\right)\\ &+\boldsymbol{k}^4\left(2\delta^{ij}\delta^{kl}+7(\delta^{jk}\delta^{il}+\delta^{ik}\delta^{jl})\right)\Big]\,A_{3/2}(\boldsymbol{k}^2)\,. \end{aligned} \tag{E.43}$$

Replacing the electric polarizabilities with the magnetic ones yields $\widetilde{W}_B^{\rm seg}$. For the case with electric-magnetic polarizability couplings, we obtain

$$\begin{aligned}\widetilde{W}_M^{\rm seg} = &\frac{\pi^2}{16(d-1)(d+1)}\left(\alpha_{n_1}^{ij}\beta_{n_2}^{kl}+\beta_{n_1}^{ij}\alpha_{n_2}^{kl}\right)\left(\epsilon^{rik}\epsilon^{sjl}+\epsilon^{ril}\epsilon^{sjk}\right)\\ &\times\boldsymbol{k}^2\left(\boldsymbol{k}^2\delta^{rs}+d\,\boldsymbol{k}^r\boldsymbol{k}^s\right)A_{3/2}(\boldsymbol{k}^2)\,. \end{aligned} \tag{E.44}$$

E.2.3 Intermediate-range Regime

The contribution of the one-loop pNRQED diagrams with two-photon exchanges of Fig. 11.2 to the WEFT potential for an arbitrary hydrogen atom state is

$$\begin{aligned}\widetilde{W}_y^{\rm 1loop} = &-{\sum_{m_1,m_2}}' p_y(n_1,m_1)^{ij}p_y(n_2,m_2)^{kl}\Bigg\{\\ \times\;&\left(\frac{\kappa_{y02}^{ijlk}+\kappa_{y22}^{ijlk}\Delta E_{n_1m_1}^2}{\Delta E_{n_1m_1}-\Delta E_{n_2m_2}}-\frac{\kappa_{y02}^{ijkl}+\kappa_{y22}^{ijkl}\Delta E_{n_1m_1}^2}{\Delta E_{n_1m_1}+\Delta E_{n_2m_2}}\right)J(\Delta E_{n_1m_1})\\ &-\left(\frac{\kappa_{y02}^{ijlk}+\kappa_{y22}^{ijlk}\Delta E_{n_2m_2}^2}{\Delta E_{n_1m_1}-\Delta E_{n_2m_2}}+\frac{\kappa_{y02}^{ijkl}+\kappa_{y22}^{ijkl}\Delta E_{n_2m_2}^2}{\Delta E_{n_1m_1}+\Delta E_{n_2m_2}}\right)J(\Delta E_{n_2m_2})\\ &+\left(\frac{\kappa_{y00}^{ijlk}+\kappa_{y20}^{ijlk}\Delta E_{n_1m_1}^2+\kappa_{y40}^{ijlk}\Delta E_{n_1m_1}^4}{\Delta E_{n_1m_1}-\Delta E_{n_2m_2}}-\frac{\kappa_{y00}^{ijkl}+\kappa_{y20}^{ijkl}\Delta E_{n_1m_1}^2+\kappa_{y40}^{ijkl}\Delta E_{n_1m_1}^4}{\Delta E_{n_1m_1}+\Delta E_{n_2m_2}}\right)\\ &\times K(\boldsymbol{k}^2,\,\Delta E_{n_1m_1})\\ &-\left(\frac{\kappa_{y00}^{ijlk}+\kappa_{y20}^{ijlk}\Delta E_{n_2m_2}^2+\kappa_{y40}^{ijlk}\Delta E_{n_2m_2}^4}{\Delta E_{n_1m_1}-\Delta E_{n_2m_2}}+\frac{\kappa_{y00}^{ijkl}+\kappa_{y20}^{ijkl}\Delta E_{n_2m_2}^2+\kappa_{y40}^{ijkl}\Delta E_{n_2m_2}^4}{\Delta E_{n_1m_1}+\Delta E_{n_2m_2}}\right)\\ &\times K(\boldsymbol{k}^2,\,\Delta E_{n_2m_2})\\ &-\frac{1}{4}\Bigg[\left(\kappa_{y40}^{ijkl}-\kappa_{y40}^{ijlk}\right)\left(\frac{\boldsymbol{k}^2}{4(d-1)}+\Delta E_{n_1m_1}^2+\Delta E_{n_2m_2}^2\right)\\ &-\left(\kappa_{y40}^{ijkl}+\kappa_{y40}^{ijlk}\right)\Delta E_{n_1m_1}\Delta E_{n_2m_2}\\ &+\left(\kappa_{y20}^{ijkl}-\kappa_{y20}^{ijlk}\right)\Bigg]A_{3/2}(\boldsymbol{k}^2)\Bigg\},\quad y=E,\,B,\,M\,. \end{aligned} \tag{E.45}$$

The momentum-transfer dependent coefficients read, for electric dipoles interactions

$$\kappa_{E40}^{ijkl} \;=\; \frac{1}{d(d-2)}\Bigg\{\frac{3}{\boldsymbol{k}^4}\boldsymbol{k}^i\boldsymbol{k}^j\boldsymbol{k}^k\boldsymbol{k}^l+\frac{1}{\boldsymbol{k}^2}\Big[(d-1)\left(\boldsymbol{k}^i\boldsymbol{k}^k\delta^{jl}+\boldsymbol{k}^j\boldsymbol{k}^l\delta^{ik}\right)$$

$$
\begin{aligned}
&- \quad \boldsymbol{k}^i\boldsymbol{k}^j\delta^{kl} - \boldsymbol{k}^k\boldsymbol{k}^l\delta^{ij} - \boldsymbol{k}^i\boldsymbol{k}^l\delta^{kj} - \boldsymbol{k}^j\boldsymbol{k}^k\delta^{il}\Big] \\
&+ \quad \Big[\delta^{ij}\delta^{kl} + \delta^{il}\delta^{kj} + \left(d^2 - 4d + 1\right)\delta^{ik}\delta^{jl}\Big]\Big\}, \qquad \text{(E.46)}
\end{aligned}
$$

$$
\begin{aligned}
\kappa^{ijkl}_{E20} &= \frac{1}{4d(d-2)}\Big\{\frac{2(d-3)}{\boldsymbol{k}^2}\boldsymbol{k}^i\boldsymbol{k}^j\boldsymbol{k}^k\boldsymbol{k}^l \\
&- (d-2)\left(\boldsymbol{k}^i\boldsymbol{k}^j\delta^{kl} + \boldsymbol{k}^k\boldsymbol{k}^l\delta^{ij} + \boldsymbol{k}^i\boldsymbol{k}^l\delta^{kj} + \boldsymbol{k}^j\boldsymbol{k}^k\delta^{il}\right) \\
&- (d^2 - 2d - 2)\left(\boldsymbol{k}^i\boldsymbol{k}^k\delta^{jl} + \boldsymbol{k}^j\boldsymbol{k}^l\delta^{ik}\right) \\
&- 2\boldsymbol{k}^2\Big[\delta^{ij}\delta^{kl} + \delta^{il}\delta^{kj} - (d-1)\,\delta^{ik}\delta^{jl}\Big]\Big\}, \qquad \text{(E.47)}
\end{aligned}
$$

$$
\begin{aligned}
\kappa^{ijkl}_{E00} &= \frac{1}{16d(d-2)}\Big[(d-3)(d-1)\boldsymbol{k}^i\boldsymbol{k}^j\boldsymbol{k}^k\boldsymbol{k}^l \\
&+ (d-1)\boldsymbol{k}^2\left(\boldsymbol{k}^i\boldsymbol{k}^j\delta^{kl} + \boldsymbol{k}^k\boldsymbol{k}^l\delta^{ij} + \boldsymbol{k}^i\boldsymbol{k}^l\delta^{kj} + \boldsymbol{k}^j\boldsymbol{k}^k\delta^{il}\right) \\
&- (d+1)\boldsymbol{k}^2\left(\boldsymbol{k}^i\boldsymbol{k}^k\delta^{jl} + \boldsymbol{k}^j\boldsymbol{k}^l\delta^{ik}\right) + \boldsymbol{k}^4\left(\delta^{ij}\delta^{kl} + \delta^{il}\delta^{kj} + \delta^{ik}\delta^{jl}\right)\Big], \qquad \text{(E.48)}
\end{aligned}
$$

$$
\begin{aligned}
\kappa^{ijkl}_{E22} &= \frac{1}{2d(d-2)}\Big\{\frac{3(3-d)}{\boldsymbol{k}^4}\boldsymbol{k}^i\boldsymbol{k}^j\boldsymbol{k}^k\boldsymbol{k}^l \\
&+ \frac{d-3}{\boldsymbol{k}^2}\Big[\boldsymbol{k}^i\boldsymbol{k}^j\delta^{kl} + \boldsymbol{k}^k\boldsymbol{k}^l\delta^{ij} + \boldsymbol{k}^i\boldsymbol{k}^l\delta^{kj} + \boldsymbol{k}^j\boldsymbol{k}^k\delta^{il} - (d-1)\left(\boldsymbol{k}^i\boldsymbol{k}^k\delta^{jl} + \boldsymbol{k}^j\boldsymbol{k}^l\delta^{ik}\right)\Big] \\
&+ \frac{2d-3}{d-1}\left(\delta^{ij}\delta^{kl} + \delta^{il}\delta^{kj}\right) - \frac{2d^2 - 4d + 3}{d-1}\delta^{ik}\delta^{jl}\Big\}, \qquad \text{(E.49)}
\end{aligned}
$$

$$
\begin{aligned}
\kappa^{ijkl}_{E02} &= \frac{1}{8d(d-2)}\Big[\frac{(3-d)(d-1)}{\boldsymbol{k}^2}\boldsymbol{k}^i\boldsymbol{k}^j\boldsymbol{k}^k\boldsymbol{k}^l \\
&- (d-1)\left(\boldsymbol{k}^i\boldsymbol{k}^j\delta^{kl} + \boldsymbol{k}^k\boldsymbol{k}^l\delta^{ij} + \boldsymbol{k}^i\boldsymbol{k}^l\delta^{kj} + \boldsymbol{k}^j\boldsymbol{k}^k\delta^{il}\right) \\
&+ (d+1)\left(\boldsymbol{k}^i\boldsymbol{k}^k\delta^{jl} + \boldsymbol{k}^j\boldsymbol{k}^l\delta^{ik}\right) - \boldsymbol{k}^2\left(\delta^{ij}\delta^{kl} + \delta^{il}\delta^{kj} + \delta^{ik}\delta^{jl}\right)\Big], \qquad \text{(E.50)}
\end{aligned}
$$

and for magnetic dipoles interactions

$$
\begin{aligned}
\kappa^{ijkl}_{B40} &= \kappa^{ijkl}_{E40}\,, \qquad \text{(E.51)} \\
\kappa^{ijkl}_{B20} &= \kappa^{ijkl}_{E20}\,, \qquad \text{(E.52)} \\
\kappa^{ijkl}_{B00} &= \kappa^{ijkl}_{E00}\,, \qquad \text{(E.53)} \\
\kappa^{ijkl}_{B22} &= \kappa^{ijkl}_{E22} + \frac{2(d-2)}{(d-1)}\delta^{ik}\delta^{jl}\,, \qquad \text{(E.54)} \\
\kappa^{ijkl}_{B02} &= \kappa^{ijkl}_{E02}\,. \qquad \text{(E.55)}
\end{aligned}
$$

For electric-magnetic dipole interactions the instantaneous dipole factor

$$
p_M(n_1, m_1)^{ij} p_M(n_2, m_2)^{kl} \qquad \text{(E.56)}
$$

should be understood as

$$
p_E(n_1, m_1)^{ij} p_B(n_2, m_2)^{kl} + p_B(n_1, m_1)^{ij} p_E(n_2, m_2)^{kl}, \qquad \text{(E.57)}
$$

and

$$
\kappa^{ijkl}_{M40} = \frac{\epsilon^{rik}\epsilon^{sjl}}{(d-2)\boldsymbol{k}^2}\left(-\boldsymbol{k}^r\boldsymbol{k}^s + \boldsymbol{k}^2\delta^{rs}\right), \qquad \text{(E.58)}
$$

$$\kappa_{M20}^{ijkl} = -\frac{\epsilon^{rik}\epsilon^{sjl}}{4(d-2)}\left[(d-3)\boldsymbol{k}^r\boldsymbol{k}^s + \boldsymbol{k}^2\delta^{rs}\right], \tag{E.59}$$

$$\kappa_{M00}^{ijkl} = 0\,, \tag{E.60}$$

$$\kappa_{M22}^{ijkl} = \frac{\epsilon^{rik}\epsilon^{sjl}}{2(d-2)\boldsymbol{k}^2}\left[(d-3)\boldsymbol{k}^r\boldsymbol{k}^s + \boldsymbol{k}^2\delta^{rs}\right], \tag{E.61}$$

$$\kappa_{M02}^{ijkl} = 0\,. \tag{E.62}$$

E.3 Sums over Intermediate States

In this appendix, we present some cases in which the sum over states can be explicitly performed. First, using $\mathbb{1} = \sum_m |m\rangle\langle m|$, we have

$$\sum_m \langle n|\boldsymbol{x}^i|m\rangle\langle m|\boldsymbol{x}^j|n\rangle = \langle n|\boldsymbol{x}^i\boldsymbol{x}^j|n\rangle = \langle n|(\boldsymbol{x}^i)^2|n\rangle\delta^{ij}, \tag{E.63}$$

where in the last step we have made use of the reflection symmetry $\boldsymbol{x}^i \to -\boldsymbol{x}^i$ for $i = 1, 2, 3$. Everywhere in this appendix the index i is understood as not summed.

Let $\hat{h}_0 = -\boldsymbol{\nabla}_{\boldsymbol{x}}^2/(2m_e) - \alpha/|\boldsymbol{x}|$, then it holds that

$$\begin{aligned}\sum_m \langle n|\boldsymbol{x}^i|m\rangle\Delta E_{nm}\langle m|\boldsymbol{x}^i|n\rangle &= \langle n|\boldsymbol{x}^i(E_n - \hat{h}_0)\boldsymbol{x}^i|n\rangle \\ &= \frac{1}{2}\langle n|\left[\boldsymbol{x}^i, E_n - \hat{h}_0\right]\boldsymbol{x}^i + \boldsymbol{x}^i\left[E_n - \hat{h}_0, \boldsymbol{x}^i\right]|n\rangle \\ &= \frac{i}{2m_e}\langle n|\left[\boldsymbol{x}^i, \boldsymbol{p}^i\right]|n\rangle = -\frac{1}{2m_e}\,,\end{aligned} \tag{E.64}$$

and for the case $i \neq j$

$$\begin{aligned}\sum_m \langle n|\boldsymbol{x}^i|m\rangle\Delta E_{nm}\langle m|\boldsymbol{x}^j|n\rangle &= \langle n|\boldsymbol{x}^i(E_n - \hat{h}_0)\boldsymbol{x}^j|n\rangle \\ &= \frac{1}{2}\langle n|\left[\boldsymbol{x}^i, E_n - \hat{h}_0\right]\boldsymbol{x}^j + \boldsymbol{x}^i\left[E_n - \hat{h}_0, \boldsymbol{x}^j\right]|n\rangle \\ &= \frac{i}{2m_e}\langle n|\boldsymbol{x}^i\boldsymbol{p}^j - \boldsymbol{p}^i\boldsymbol{x}^j|n\rangle = \frac{i}{2m_e}\epsilon^{ijk}\langle n|\boldsymbol{L}^k|n\rangle\,.\end{aligned} \tag{E.65}$$

Finally, when the sum over the states contains ΔE_{nm}^2, it holds that

$$\begin{aligned}\sum_m \langle n|\boldsymbol{x}^i|m\rangle\Delta E_{nm}^2\langle m|\boldsymbol{x}^j|n\rangle &= \langle n|\boldsymbol{x}^i(E_n - \hat{h}_0)^2\boldsymbol{x}^j|n\rangle \\ &= \langle n|\left[\boldsymbol{x}^i, E_n - \hat{h}_0\right]\left[E_n - \hat{h}_0, \boldsymbol{x}^j\right]|n\rangle \\ &= \frac{1}{m_e^2}\langle n|\boldsymbol{p}^i\boldsymbol{p}^j|n\rangle = \frac{1}{m_e^2}\langle n|(\boldsymbol{p}^i)^2|n\rangle\delta^{ij}.\end{aligned} \tag{E.66}$$

E.4 Fourier Transforms

To evaluate the van der Waals potentials in position space we have encountered the following Fourier transforms

$$I_{n,i_1,\ldots i_L}(\boldsymbol{R}) = \int \frac{d^3k}{(2\pi)^3}\, e^{i\boldsymbol{k}\cdot\boldsymbol{R}}\, k^n\, \hat{\boldsymbol{k}}^{i_1}\ldots\hat{\boldsymbol{k}}^{i_L}\,, \tag{E.67}$$

$$H_{n,i_1,\ldots i_L}(\boldsymbol{R}) \;=\; \int \frac{d^3k}{(2\pi)^3}\, e^{i\boldsymbol{k}\cdot\boldsymbol{R}}\, k^n\, \log k^2\, \hat{\boldsymbol{k}}^{i_1}\ldots\hat{\boldsymbol{k}}^{i_L}\,, \tag{E.68}$$

where $\hat{\boldsymbol{k}}^i = \boldsymbol{k}^i/k$, and k is the modulus of $\boldsymbol{k}$. The product of unit vectors can be decomposed into a sum of spherical harmonics with angular momentum up to the total number of unit vectors:

$$\hat{\boldsymbol{k}}^{i_1}\ldots\hat{\boldsymbol{k}}^{i_L} = \sum_{l=0}^{L}\sum_{m=-l}^{l} C^{lm}_{i_1\ldots i_L} Y_l^m(\hat{\boldsymbol{k}})\,. \tag{E.69}$$

Due to parity, $C^{lm}_{i_1\ldots i_L}$ vanishes for even (odd) values of l if the number of unit vectors is odd (even). After substituting Eq. (E.69) in Eq. (E.67) we obtain

$$I_{n,i_1,\ldots i_L}(\boldsymbol{R}) \;=\; \sum_{l=0}^{L}\sum_{m=-l}^{l} C^{lm}_{i_1\ldots i_L}\int \frac{d^3k}{(2\pi)^3}\, e^{i\boldsymbol{k}\cdot\boldsymbol{R}}\, k^n\, Y_l^m(\hat{\boldsymbol{k}})\,. \tag{E.70}$$

Using the Rayleigh expansion of the exponential, the addition theorem and orthogonality of the spherical harmonics we arrive at

$$I_{n,i_1,\ldots i_L}(\boldsymbol{R}) \;=\; \sum_{l=0}^{L}\sum_{m=-l}^{l} C^{lm}_{i_1\ldots i_L}\, Y_l^m(\hat{\boldsymbol{R}})\, I^R_{nl}\,, \tag{E.71}$$

where I^R_{nl} is defined as

$$I^R_{nl} \;=\; \frac{i^l}{2\pi^2}\int_0^\infty dk\, k^{n+2}\, j_l(Rk)\,, \tag{E.72}$$

j_l being the spherical Bessel functions and R the modulus of $\boldsymbol{R}$.

It may be convenient to rewrite (E.71) as

$$I_{n,i_1,\ldots i_L}(\boldsymbol{R}) = \sum_{l=0}^{L}(\hat{\boldsymbol{R}}^{i_1}\ldots\hat{\boldsymbol{R}}^{i_L})_l I^R_{nl}\,, \tag{E.73}$$

with

$$(\hat{\boldsymbol{R}}^{i_1}\ldots\hat{\boldsymbol{R}}^{i_L})_l = \sum_{m=-l}^{l} C^{lm}_{i_1\ldots i_L} Y_l^m(\hat{\boldsymbol{R}})\,, \tag{E.74}$$

the sum of all the terms with angular momentum l. The same procedure can be used for $H_{n,i_1,\ldots i_L}$ leading to a formula analogous to Eq. (E.73) but with I^R_{nl} replaced by

$$H^R_{nl} = \frac{i^l}{2\pi^2}\int_0^\infty dk\, k^{n+2}\, \log k^2\, j_l(Rk)\,. \tag{E.75}$$

The coefficients $C^{lm}_{i_1\ldots i_L}$ can be obtained from $\hat{\boldsymbol{R}}^{i_1}\ldots\hat{\boldsymbol{R}}^{i_L} = \sum_{l=0}^{L}\sum_{m=-l}^{l} C^{lm}_{i_1\ldots i_L} Y_l^m(\hat{\boldsymbol{R}})$ using the orthogonality relations of the spherical harmonics. Then the sum in Eq. (E.74) can be performed using the addition theorem:

$$(\hat{\boldsymbol{R}}^{i_1}\ldots\hat{\boldsymbol{R}}^{i_L})_l = (2l+1)\int \frac{d\Omega'}{4\pi}\,\hat{\boldsymbol{R}}'^{i_1}\ldots\hat{\boldsymbol{R}}'^{i_L}\, P_l(\hat{\boldsymbol{R}}'\cdot\hat{\boldsymbol{R}})\,, \tag{E.76}$$

where P_l are Legendre polynomials. Equation (E.76) can be evaluated using

$$\int \frac{d\Omega}{4\pi}\, \hat{\boldsymbol{R}}^{i_1} \dots \hat{\boldsymbol{R}}^{i_N} = \frac{\delta_{N,\,\text{even}}}{(N+1)!!} \left(\delta^{i_1 i_2} \dots \delta^{i_{N-1} i_N} + \text{permutations}\right). \tag{E.77}$$

The problem of finding the Fourier transforms of Eqs. (E.67) and (E.68) reduces then to the problem of computing the integrals I^R_{nl} and H^R_{nl} [295]. We have that

$$I^R_{nl} = i^l \frac{2^n}{\pi^{3/2} R^{n+3}} \frac{\Gamma\left(\frac{n+l+3}{2}\right)}{\Gamma\left(\frac{l-n}{2}\right)}, \qquad -(l+3) < n \text{ and } n \neq l+2s\,,\ \forall s \in \mathbb{N}\,. \tag{E.78}$$

The case $n = l$ can be obtained from the completion integral of the spherical Bessel functions

$$I^R_{ll} = i^l \frac{(2l+1)!!}{R^l} \delta^3(\boldsymbol{R})\,. \tag{E.79}$$

This expression can be generalized to cases when $n = l + 2s$, $\forall s \in \mathbb{N}$ by using the recurrence relations for the spherical Bessel functions and proceeding by induction:

$$I^R_{(l+2s)l} = i^l (-1)^s \frac{(2s)!!(2l+2s+1)!!}{R^{l+2s}} \delta^3(\boldsymbol{R})\,, \qquad \forall s \in \mathbb{N}\,. \tag{E.80}$$

The integral H^R_{nl} can be evaluated from Eq. (E.78) noticing that $\log k^2 = (k^{2\epsilon} - 1)/\epsilon$ in the limit $\epsilon \to 0$, which implies

$$H^R_{nl} = 2 \left.\frac{dI^R_{xl}}{dx}\right|_{x=n}. \tag{E.81}$$

In Table E.1 and Table E.2 we list the radial integrals of the Fourier transforms from $n = -2$ to $n = 4$ and for $l = 0$, 2, 4 for the cases without and with a $\log k^2$ respectively.

n	I_{n0}	I_{n2}	I_{n4}
-2	$1/(4\pi R)$	$-1/(8\pi R)$	$3/(32\pi R)$
-1	$1/(2\pi^2 R^2)$	$-1/(\pi^2 R^2)$	$4/(3\pi^2 R^2)$
0	$\delta^3(\boldsymbol{R})$	$-3/(4\pi R^3)$	$15/(8\pi R^3)$
1	$-1/(\pi^2 R^4)$	$-4/(\pi^2 R^4)$	$24/(\pi^2 R^4)$
2	$-6\,\delta^3(\boldsymbol{R})/R^2$	$-15\,\delta^3(\boldsymbol{R})/R^2$	$105/(4\pi R^5)$
3	$12/(\pi^2 R^6)$	$24/(\pi^2 R^6)$	$192/(\pi^2 R^6)$
4	$120\,\delta^3(\boldsymbol{R})/R^4$	$210\,\delta^3(\boldsymbol{R})/R^4$	$945\delta^3(\boldsymbol{R})/R^4$

Table E.1: Results for the radial integrals I_{nl} for n=$-2, \dots, 4$ and $l = 0$, 2, 4.

Finally, we reproduce the partial-wave decompositions (E.74) for two and four unit vectors [295]:

$$(\hat{\boldsymbol{R}}^i \hat{\boldsymbol{R}}^j)_2 = \hat{\boldsymbol{R}}^i \hat{\boldsymbol{R}}^j - \frac{1}{3}\delta^{ij}\,, \tag{E.82}$$

$$(\hat{\boldsymbol{R}}^i \hat{\boldsymbol{R}}^j)_0 = \frac{1}{3}\delta^{ij}\,, \tag{E.83}$$

$$\begin{aligned}(\hat{\boldsymbol{R}}^i \hat{\boldsymbol{R}}^j \hat{\boldsymbol{R}}^k \hat{\boldsymbol{R}}^l)_4 &= \hat{\boldsymbol{R}}^i \hat{\boldsymbol{R}}^j \hat{\boldsymbol{R}}^k \hat{\boldsymbol{R}}^l - \frac{1}{7}(\hat{\boldsymbol{R}}^i \hat{\boldsymbol{R}}^j \delta^{kl} + \text{permutations}) \\ &+ \frac{1}{35}(\delta^{ij}\delta^{kl} + \text{permutations})\,,\end{aligned} \tag{E.84}$$

$$(\hat{\boldsymbol{R}}^i \hat{\boldsymbol{R}}^j \hat{\boldsymbol{R}}^k \hat{\boldsymbol{R}}^l)_2 = \frac{1}{7}((\hat{\boldsymbol{R}}^i \hat{\boldsymbol{R}}^j)_2 \delta^{kl} + \text{permutations})\,, \tag{E.85}$$

$$(\hat{\boldsymbol{R}}^i \hat{\boldsymbol{R}}^j \hat{\boldsymbol{R}}^k \hat{\boldsymbol{R}}^l)_0 = \frac{1}{15}(\delta^{ij}\delta^{kl} + \text{permutations})\,, \tag{E.86}$$

where in the parentheses all the index permutations have to be added.

n	H_{n0}	H_{n2}	H_{n4}
-2	$-\zeta/(4\pi R)$	$(\zeta-3)/(8\pi R)$	$-(6\zeta-25)/(65\pi R)$
-1	$-\zeta/(2\pi^2R^2)$	$(\zeta-3)/(\pi^2R^2)$	$-(12\zeta-50)/(9\pi^2R^2)$
0	$-1/(2\pi R^3)$	$(3\zeta-8)/(4\pi R^3)$	$-(15\zeta-61)/(8\pi R^3)$
1	$(\zeta-3)/(\pi^2R^4)$	$(4\zeta-6)/(\pi^2R^4)$	$-(24\zeta-92)/(\pi^2R^4)$
2	$3/(\pi R^5)$	$15/(2\pi R^5)$	$-(105\zeta-352)/(4\pi R^5)$
3	$-(12\zeta-50)/(\pi^2R^6)$	$-(24\zeta-92)/(\pi^2R^6)$	$-16(12\zeta-25)/(\pi^2R^6)$
4	$-60/(\pi R^7)$	$-105/(\pi R^7)$	$-945/(2\pi R^7)$

Table E.2: Results for the radial integrals H_{nl} for n=$-2,\ldots,4$ and $l=0$, 2, 4. We have defined $\zeta=2\gamma_E+\log R^2$.

F Threshold Expansion Method of Braaten and Chen

F.1 2-body System

For simplicity, let us first consider the case in which the perturbative quarkonium is described only by the $Q\bar{Q}$ pair with the momenta p_1 and p_2. Then we can introduce Jacobi momenta for a 2-body system so that

$$p_1 = \frac{1}{2}P + \mathcal{Q}, \qquad p_2 = \frac{1}{2}P - \mathcal{Q}, \tag{F.1}$$

where $P = p_1 + p_2$ denotes the total momentum of the quarkonium, while $\mathcal{Q} = \frac{1}{2}(p_1 - p_2)$ stands for the relative momentum between the heavy quark and the heavy anti-quark.

In the laboratory frame, where the heavy quarkonium is moving (i. e. $\mathbf{p}_1 + \mathbf{p}_2 \neq 0$) we have

$$P = (\sqrt{P^2 + \mathbf{P}^2}, \mathbf{P}), \qquad \mathcal{Q} = (\sqrt{\mathcal{Q}^2 + \boldsymbol{\mathcal{Q}}^2}, \boldsymbol{\mathcal{Q}}) \tag{F.2}$$

In the rest frame of the heavy quarkonium, where $\mathbf{p}_{1,R} + \mathbf{p}_{2,R} = 0$, P_R and $\mathcal{Q}_R$ have a particularly simple form

$$\mathcal{Q}_R \equiv q = (0, \mathbf{q}), \qquad P_R = (2\sqrt{\mathbf{q}^2 + m_Q^2}, 0) \equiv (2E_q, 0), \tag{F.3}$$

with

$$\mathbf{q} \equiv \mathbf{p}_{1,R} = -\mathbf{p}_{2,R}. \tag{F.4}$$

Here $\mathbf{q}$ is indeed soft and can be used as an expansion parameter. The two frames are related by a Lorentz transformation, which means that we can express $\mathcal{Q}$ and P in terms of $\mathbf{q}$. According to [31] we have

$$\mathcal{Q}^\mu = \Lambda^\mu{}_i \mathbf{q}^i, \tag{F.5}$$

$$\Lambda^0{}_i = \frac{\mathbf{P}^i}{2E_q}, \qquad \Lambda^i{}_j = \delta^{ij} + \left(\frac{P^0}{2E_q} - 1\right)\hat{\mathbf{P}}^i\hat{\mathbf{P}}^j, \tag{F.6}$$

where

$$P^0 = \sqrt{4E_q^2 + \mathbf{P}^2}. \tag{F.7}$$

The Dirac spinors in the rest frame are given by

$$u_R(p_{1,R}) = N\begin{pmatrix} \xi \\ \frac{\mathbf{q}\cdot\boldsymbol{\sigma}}{E_q + m_Q}\xi \end{pmatrix}, \qquad v_R(p_{2,R}) = N\begin{pmatrix} \frac{-\mathbf{q}\cdot\boldsymbol{\sigma}}{E_q + m_Q}\eta \\ \eta \end{pmatrix}, \tag{F.8}$$

where N is the normalization factor. In case of relativistic normalization, it is given by $E_q + m_Q$, while in the nonrelativistic case one has $N = \frac{E_q + m_Q}{2E_q}$. When boosted to the laboratory frame they become

$$u(p_1) = \frac{1}{\sqrt{4E_q(P^0 + 2E_q)}}(2E_q + \not{P}\gamma^0)N\begin{pmatrix} \xi \\ \frac{\mathbf{q}\cdot\boldsymbol{\sigma}}{E_q + m_Q}\xi \end{pmatrix}, \tag{F.9}$$

$$v(p_2) = \frac{1}{\sqrt{4E_q(P^0 + 2E_q)}}(2E_q + \not{P}\gamma^0)N\begin{pmatrix} \frac{-\mathbf{q}\cdot\boldsymbol{\sigma}}{E_q + m_Q}\eta \\ \eta \end{pmatrix}. \tag{F.10}$$

For practical purposes, it is more convenient to work with boosted Dirac bilinears, of which we are interested only in those that transform as a vector and as an axial vector, since only they appear in the calculation of our process of interest. The two bilinears can be written as

$$\bar{u}(p_1)\gamma^\mu v(p_2) = N^2 \Lambda^\mu{}_i \left(\frac{2E_q}{E_q+m} \xi^\dagger \boldsymbol{\sigma}^i \eta - \frac{2}{(E_q+m)^2} \mathbf{q}^i \xi^\dagger \mathbf{q}\cdot\boldsymbol{\sigma}\eta \right), \tag{F.11}$$

$$\bar{u}(p_1)\gamma^\mu\gamma_5 v(p_2) = N^2 \left(\frac{m_Q}{E_q} \frac{1}{E_q+m_Q} P^\mu \xi^\dagger \eta - 2i \frac{1}{E_q+m_Q} \Lambda^\mu{}_i \xi^\dagger (\mathbf{q}\times\boldsymbol{\sigma})^i \eta \right). \tag{F.12}$$

F.2 3-body System

Let us now turn to the more relevant case of the perturbative quarkonium composed of two heavy quarks and a gluon. Here we can again introduce Jacobi momenta, this time for a 3-body system, such that

$$p_1 = \frac{1}{3}P + \mathcal{Q}_1 - \mathcal{Q}_2, \qquad p_2 = \frac{1}{3}P - \mathcal{Q}_1 - \mathcal{Q}_2, \qquad p_g = \frac{1}{3}P + 2\mathcal{Q}_2 \tag{F.13}$$

In the rest frame, where $\mathbf{p}_{1,R} + \mathbf{p}_{2,R} + \mathbf{p}_{g,R} = \mathbf{P}_R = 0$, we have

$$p_{1,R} = \frac{1}{3}P_R + q_1 - q_2, \qquad p_{2,R} = \frac{1}{3}P_R - q_1 - q_2, \qquad p_{g,R} = \frac{1}{3}P_R + 2q_2 \tag{F.14}$$

or

$$q_1 = \frac{1}{2}\left(p_{1,R} - p_{2,R}\right), \qquad q_2 = \frac{1}{6}\left(2p_{g,R} - p_{1,R} - p_{2,R}\right) \tag{F.15}$$

and in particular

$$\mathbf{p}_{1,R} = \mathbf{q}_1 - \mathbf{q}_2, \qquad \mathbf{p}_{2,R} = -\mathbf{q}_1 - \mathbf{q}_2, \qquad \mathbf{p}_{g,R} = 2\mathbf{q}_2 \tag{F.16}$$

with $\mathbf{q}_1$ and $\mathbf{q}_2$ being our soft expansion parameter. Furthermore,

$$q_1^0 = \frac{1}{2}\left(\sqrt{(\mathbf{q}_1-\mathbf{q}_2)^2+m_Q^2} - \sqrt{(\mathbf{q}_1+\mathbf{q}_2)^2+m_Q^2}\right), \tag{F.17}$$

$$q_2^0 = \frac{1}{6}\left(4|\mathbf{q}_2| - \sqrt{(\mathbf{q}_1-\mathbf{q}_2)^2+m_Q^2} - \sqrt{(\mathbf{q}_1+\mathbf{q}_2)^2+m_Q^2}\right) \tag{F.18}$$

and

$$P_R^0 = \left(2|\mathbf{q}_2| + \sqrt{(\mathbf{q}_1-\mathbf{q}_2)^2+m_Q^2} + \sqrt{(\mathbf{q}_1+\mathbf{q}_2)^2+m_Q^2}\right), \tag{F.19}$$

Since scalar products of 4-vectors are Lorentz invariant, we have

$$\mathcal{Q}_1^2 = (q_1^0)^2 - \mathbf{q}_1^2, \qquad \mathcal{Q}_1^2 = (q_2^0)^2 - \mathbf{q}_2^2, \qquad P^2 = (P_R^0)^2, \qquad P^0 = \sqrt{(P_R^0)^2 + \mathbf{P}^2}. \tag{F.20}$$

To rewrite the laboratory frame 4-momenta $\mathcal{Q}_1$ and $\mathcal{Q}_2$ in terms of the soft expansion parameters from the rest frame $\mathbf{q}_1$ and $\mathbf{q}_2$, we use that

$$\mathcal{Q}_{1/2}^\mu = \Lambda^\mu{}_\nu q_{1/2}^\nu \tag{F.21}$$

where the boost matrix now reads

$$\Lambda^0{}_0 = \sqrt{1+\frac{\mathbf{P}^2}{(P_R^0)^2}}, \qquad \Lambda^0{}_i = \Lambda^i{}_0 = \frac{\mathbf{P}^i}{P_R^0}, \qquad \Lambda^i{}_j = \delta^{ij} + \left(\sqrt{1+\frac{\mathbf{P}^2}{(P_R^0)^2}} - 1\right)\hat{\mathbf{P}}^i\hat{\mathbf{P}}^j. \tag{F.22}$$

As far as the Dirac spinors are concerned, we again begin with the rest frame, where

$$u_R(p_{1,R}) = N_1 \begin{pmatrix} \xi \\ \frac{\mathbf{p}_{1,R}\cdot\boldsymbol{\sigma}}{E_{1,R}+m_Q}\xi \end{pmatrix}, \qquad v_R(p_{2,R}) = N_2 \begin{pmatrix} \frac{\mathbf{p}_{2,R}\cdot\boldsymbol{\sigma}}{E_{2,R}+m_Q}\eta \\ \eta \end{pmatrix}, \tag{F.23}$$

with $E_{i,R} = \sqrt{\mathbf{p}_{i,R}^2 + m_Q^2}$ and $N_i = \sqrt{E_{i,R}+m_Q}$ for relativistic and $N_i = \sqrt{\frac{E_{i,R}+m_Q}{2E_{i,R}}}$ for nonrelativistic normalization respectively. The boost matrix for these spinors is given by

$$S(\Lambda) = \sqrt{\frac{P^0+P_R^0}{2P_R^0}} \begin{pmatrix} 1 & \frac{\boldsymbol{\sigma}\cdot\mathbf{P}}{(P^0+P_R^0)} \\ \frac{\boldsymbol{\sigma}\cdot\mathbf{P}}{P^0+P_R^0} & 1 \end{pmatrix}, \tag{F.24}$$

so that we arrive at

$$u(p_1) = \frac{N_1}{\sqrt{2P_R^0(P^0+P_R^0)}}(P_R^0 + \not{P}\gamma^0) \begin{pmatrix} \xi \\ \frac{\mathbf{p}_{1,R}\cdot\boldsymbol{\sigma}}{E_{1,R}+m_Q}\xi \end{pmatrix}, \tag{F.25}$$

$$v(p_2) = \frac{N_2}{\sqrt{2P_R^0(P^0+P_R^0)}}(P_R^0 + \not{P}\gamma^0) \begin{pmatrix} \frac{\mathbf{p}_{2,R}\cdot\boldsymbol{\sigma}}{E_{2,R}+m_Q}\eta \\ \eta \end{pmatrix}. \tag{F.26}$$

Again, for practical calculations it is more useful to have explicit expressions for the boosted Dirac bilinears, which read

$$\bar{u}(p_1)\gamma^\mu v(p_2) = \Lambda^\mu{}_\nu \bar{u}_R(p_{1,R})\gamma^\nu v_R(p_{2,R}), \tag{F.27}$$

$$\bar{u}(p_1)\gamma^\mu\gamma_5 v(p_2) = \Lambda^\mu{}_\nu \bar{u}_R(p_{1,R})\gamma^\nu\gamma_5 v_R(p_{2,R}), \tag{F.28}$$

where the rest frame bilinears are given by

$$\bar{u}_R(p_{1,R})\gamma^0 v_R(p_{2,R}) = N_1N_2\xi^\dagger\left(\frac{\mathbf{p}_{1,R}\cdot\boldsymbol{\sigma}}{E_{1,R}+m_Q} + \frac{\mathbf{p}_{2,R}\cdot\boldsymbol{\sigma}}{E_{2,R}+m_Q}\right)\eta, \tag{F.29}$$

$$\begin{aligned}\bar{u}_R(p_{1,R})\gamma^i v_R(p_{2,R}) = N_1N_2\xi^\dagger\Bigg(\boldsymbol{\sigma}^i + \frac{1}{E_{1,R}+m_Q}\frac{1}{E_{2,R}+m_Q}\Big(\mathbf{p}_{1,R}^i(\mathbf{p}_{2,R}\cdot\boldsymbol{\sigma}) + \mathbf{p}_{2,R}^i(\mathbf{p}_{1,R}\cdot\boldsymbol{\sigma}) \\ + (\mathbf{p}_{1,R}\cdot\mathbf{p}_{2,R})\boldsymbol{\sigma}^i - i(\mathbf{p}_{1,R}\times\mathbf{p}_{2,R})^i\Big)\Bigg)\eta,\end{aligned} \tag{F.30}$$

$$\begin{aligned}\bar{u}_R(p_{1,R})\gamma^0\gamma_5 v_R(p_{2,R}) = N_1N_2\xi^\dagger\Bigg(1 + \frac{1}{E_{1,R}+m_Q}\frac{1}{E_{2,R}+m_Q}(\mathbf{p}_{1,R}\cdot\mathbf{p}_{2,R} \\ + i\boldsymbol{\sigma}\cdot(\mathbf{p}_{1,R}\times\mathbf{p}_{2,R}))\Bigg)\eta,\end{aligned} \tag{F.31}$$

$$\bar{u}_R(p_{1,R})\gamma^0\gamma_5 v_R(p_{2,R}) = N_1N_2\xi^\dagger\left(\frac{\mathbf{p}_{1,R}^i - i(\mathbf{p}_{1,R}\times\boldsymbol{\sigma})^i}{E_{1,R}+m_Q} + \frac{\mathbf{p}_{2,R}^i + i(\mathbf{p}_{2,R}\times\boldsymbol{\sigma})^i}{E_{2,R}+m_Q}\right)\eta. \tag{F.32}$$

G Additional Short-Distance Coefficients

As was already explained in Sec. 16, not all short-distance coefficients that are obtained in the matching are relevant for our final NRQCD-factorized production cross section. As a by-product of our calculations we also determined short-distance coefficients that appear at $\mathcal{O}(v^4)$ and contribute through the dominant Fock state $|Q\bar{Q}\rangle$

$$\mathcal{A}^{J=0}_{\text{NRQCD}} + \frac{c_4^{J=0}}{m_Q^5}\langle H|\psi^\dagger\left(-\frac{i}{2}\overleftrightarrow{\mathbf{D}}\right)^4\chi|0\rangle\,, \tag{G.1}$$

$$\begin{aligned}\mathcal{A}^{J=2}_{\text{NRQCD}} &+ \frac{(c_4^{J=0})^{ij}}{m_Q^5}\langle H|\psi^\dagger\left(-\frac{i}{2}\right)^2\overleftrightarrow{\mathbf{D}}^{(i}\overleftrightarrow{\mathbf{D}}^{j)}\left(-\frac{i}{2}\overleftrightarrow{\mathbf{D}}\right)^2\chi|0\rangle \\ &+ \frac{(c_5^{J=0})^{ij}}{m_Q^4}\left(\langle H|\psi^\dagger\left(-\frac{i}{2}\right)^2\overleftrightarrow{\mathbf{D}}^{(i}\overleftrightarrow{\mathbf{D}}^{j)}\left(-\frac{i}{2}\overleftrightarrow{\mathbf{D}}\cdot\boldsymbol{\sigma}\right)\chi|0\rangle\right. \\ &\left.-\frac{2}{5}\langle H|\psi^\dagger\left(-\frac{i}{2}\right)^2\overleftrightarrow{\mathbf{D}}^{(i}\overleftrightarrow{\mathbf{D}}^{j)}\left(-\frac{i}{2}\overleftrightarrow{\mathbf{D}}\right)^2\chi|0\rangle\right).\end{aligned} \tag{G.2}$$

We provide their values in the laboratory frame

$$c_4^{J=0} = -\frac{8}{15}\bar{Q}(\boldsymbol{\ell}\cdot(\hat{\mathbf{k}}\times\boldsymbol{\varepsilon}^*)), \tag{G.3}$$

$$(c_4^{J=2})^{ij} = \frac{8}{7}\bar{Q}(\boldsymbol{\ell}\cdot(\hat{\mathbf{k}}\times\boldsymbol{\varepsilon}^*)\,\hat{\mathbf{k}}^i\hat{\mathbf{k}}^j), \tag{G.4}$$

$$\begin{aligned}(c_5^{J=2})^{ij} = \frac{1}{42}\bar{Q}\bar{r}\Big(&5\sqrt{r}(1-5\sqrt{r})(\boldsymbol{\ell}\cdot\hat{\mathbf{k}})(\hat{\mathbf{k}}^i\boldsymbol{\varepsilon}^{*j}+i\leftrightarrow j) \\ &+25r(\boldsymbol{\ell}^i\boldsymbol{\varepsilon}^{*j}+i\leftrightarrow j)-(3+17r)(\boldsymbol{\ell}\cdot\boldsymbol{\varepsilon}^*)\hat{\mathbf{k}}^i\hat{\mathbf{k}}^j\Big)\end{aligned} \tag{G.5}$$

and in the rest frame

$$c_{4,R}^{J=0} = -\frac{8}{15}\bar{Q}(\mathbf{V}\cdot(\hat{\mathbf{k}}_R\times\boldsymbol{\varepsilon}_R^*)), \tag{G.6}$$

$$(c_{4,R}^{J=2})^{ij} = \frac{8}{7}\bar{Q}(\mathbf{V}\cdot(\hat{\mathbf{k}}_R\times\boldsymbol{\varepsilon}_R^*))\hat{\mathbf{k}}_R^i\hat{\mathbf{k}}_R^j, \tag{G.7}$$

$$\begin{aligned}(c_{5,R}^{J=2})^{ij} = \frac{i}{84}\bar{Q}\Big(&50a(\mathbf{V}^i\boldsymbol{\varepsilon}_R^{*j}+i\leftrightarrow j)+5(1-8a)(\mathbf{V}\cdot\hat{\mathbf{k}}_R)(\hat{\mathbf{k}}_R^i\boldsymbol{\varepsilon}_R^{*j}+i\leftrightarrow j) \\ &-2(3+20a)(\mathbf{V}\cdot\boldsymbol{\varepsilon}_R^*)\hat{\mathbf{k}}_R^i\hat{\mathbf{k}}_R^j\Big)\end{aligned} \tag{G.8}$$

as a reference for future studies.

H Source Codes for Example Calculations using FeynCalc and FeynHelpers

H.1 Renormalization of QED at 1-loop

In[1]:=
```
$LoadAddOns = {"FeynHelpers"};
$LoadFeynArts = True;
<< FeynCalc`
$FAVerbose = 0;
```

FeynCalc 9.3.0 (development version). For help, use the documentation center, check out the wiki or write to the mailing list.

See also the supplied examples. If you use FeynCalc in your research, please cite

- V. Shtabovenko, R. Mertig and F. Orellana, Comput. Phys. Commun., 207C, 432–444, 2016, arXiv:1601.01167
- R. Mertig, M. Böhm, and A. Denner, Comput. Phys. Commun., 64, 345–359, 1991.

FeynArts 3.9 patched for use with FeynCalc, for documentation use the manual or visit www.feynarts.de.

FeynHelpers 1.0.0 loaded.

Have a look at the supplied examples. If you use FeynHelpers in your research, please cite

- V. Shtabovenko, "FeynHelpers: Connecting FeynCalc to FIRE and Package–X", TUM–EFT 75/15, arXiv:1611.06793

Furthermore, remember to cite the authors of the tools that you are calling from FeynHelpers, which are

- FIRE by A. Smirnov, if you are using the function FIREBurn.
- Package – *X* by H. Patel, if you are using the function PaXEvaluate.

In[5]:=
```
FAPatch[PatchModelsOnly -> True];
$KeepLogDivergentScalelessIntegrals = True;
```

```
Patching FeynArts models... done!
```

In[7]:=
```
params = {InsertionLevel → {Particles}, Model -> FileNameJoin[{"QED", "QED"}],
    GenericModel -> FileNameJoin[{"QED", "QED"}], ExcludeParticles → {F[2, {2 | 3}]}};
top[i_, j_] := CreateTopologies[1, i -> j,
    ExcludeTopologies -> {Tadpoles, WFCorrections, WFCorrectionCTs}];
topCT[i_, j_] := CreateCTTopologies[1, i → j,
    ExcludeTopologies -> {Tadpoles, WFCorrections, WFCorrectionCTs}];

{diagElectronSE, diagElectronSECT} =
  InsertFields[#, {F[2, {1}]} -> {F[2, {1}]}, Sequence @@ params] & /@
   {top[1, 1], topCT[1, 1]};
{diagPhotonSE, diagPhotonSECT} =
  InsertFields[#, {V[1]} -> {V[1]}, Sequence @@ params] & /@ {top[1, 1], topCT[1, 1]};
{diagVertex, diagVertexCT} =
  InsertFields[#, {F[2, {1}], V[1]} -> {F[2, {1}]}, Sequence @@ params] & /@
   {top[2, 1], topCT[2, 1]};
```

In[13]:=
```
Paint[diagElectronSE, ColumnsXRows -> {1, 1},
  SheetHeader -> None, Numbering -> None, ImageSize -> {256, 256}];
Paint[diagElectronSECT, ColumnsXRows -> {1, 1}, SheetHeader -> None,
  Numbering -> None, ImageSize -> {256, 256}];
Paint[diagPhotonSE, ColumnsXRows -> {1, 1}, SheetHeader -> None,
  Numbering -> None, ImageSize -> {256, 256}];
Paint[diagPhotonSECT, ColumnsXRows -> {1, 1}, SheetHeader -> None,
  Numbering -> None, ImageSize -> {256, 256}];
Paint[diagVertex, ColumnsXRows -> {1, 1}, SheetHeader -> None,
  Numbering -> None, ImageSize -> {256, 256}];
Paint[diagVertexCT, ColumnsXRows -> {1, 1}, SheetHeader -> None,
  Numbering -> None, ImageSize -> {256, 256}];
```

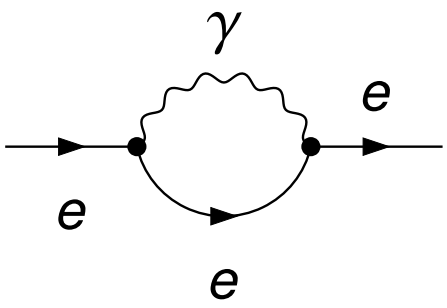

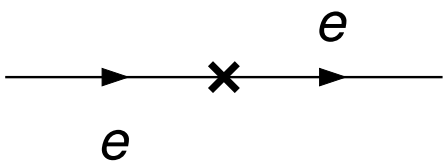

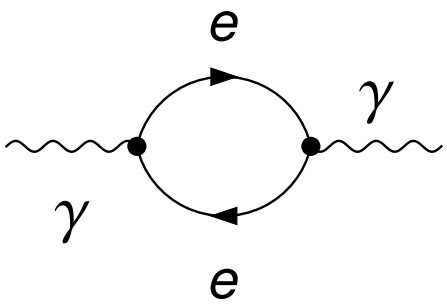
e
γ
γ
e

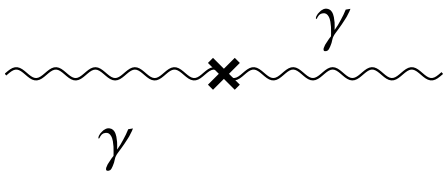
γ
γ

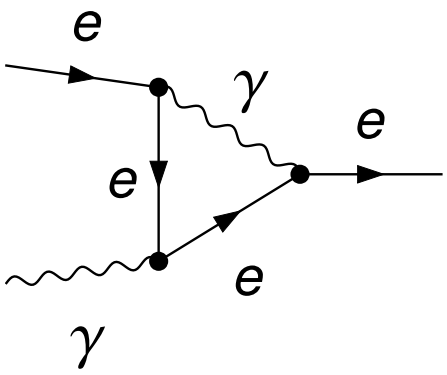
e
γ
e
e
e
γ

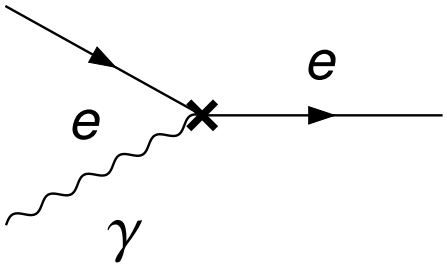

Electron self-energy

First of all we need to generate the amplitudes and convert them into FeynCalc notation. We choose l to be the loop momentum and p the external momentum.

In[19]:=
```
{ampElectronSE, ampElectronSECT} =
 Contract[FCFAConvert[CreateFeynAmp[#, Truncated -> True,
       PreFactor → 1, GaugeRules → {}], IncomingMomenta -> {p},
OutgoingMomenta -> {p}, LoopMomenta -> {l}, DropSumOver -> True,
      UndoChiralSplittings -> True, ChangeDimension -> D, List -> False, SMP -> True,
      FinalSubstitutions → {Zm → SMP["Z_m"], Zpsi → SMP["Z_psi"], SMP["e"] →
         Sqrt[4 Pi SMP["alpha_fs"]]}]] & /@ {diagElectronSE, diagElectronSECT}
```

Out[19]=
$$\left\{-\frac{4\,\pi\,\alpha\,\gamma^{\text{Lor2}}.(m_e+\gamma\cdot l).\gamma^{\text{Lor2}}}{(l^2-m_e^2).(l-p)^2}-\frac{4\,\pi\,\alpha\,(\gamma\cdot(p-l)).(m_e+\gamma\cdot l).(\gamma\cdot(l-p))}{(l^2-m_e^2).((l-p)^2)^2}+\frac{4\,\pi\,\alpha\,\xi_{V(1)}\,(\gamma\cdot(p-l)).(m_e+\gamma\cdot l).(\gamma\cdot(l-p))}{(l^2-m_e^2).((l-p)^2)^2},\right.$$
$$\left.i\,(Z_\psi-1)\,\gamma\cdot p-i\,m_e\,(Z_m\,Z_\psi-1)\right\}$$

Tensor reduction allows us to express the electron self-energy in tems of the Passarino-Veltman coefficient functions.

In[20]:=
```
ampElectronSE1 = TID[ampElectronSE, l, ToPaVe → True]
```

Out[20]=
$$\frac{1}{p^2}2\,i\,\pi^3\,\alpha\,\text{B}_0\left(p^2,\,0,\,m_e^2\right)\left(-D\left(p^2-m_e^2\right)\gamma\cdot p-2\,D\,p^2\,m_e+2\,D\,p^2\,\gamma\cdot p+m_e^2\,(-(\gamma\cdot p))+\right.$$
$$\left.2\left(p^2-m_e^2\right)\gamma\cdot p+m_e^2\,\xi_{V(1)}\,\gamma\cdot p-2\,p^2\,m_e\,\xi_{V(1)}+2\,p^2\,m_e-5\,p^2\,\gamma\cdot p+p^2\,\xi_{V(1)}\,\gamma\cdot p\right)-$$
$$\frac{2\,i\,\pi^3\,\alpha\,(1-\xi_{V(1)})\,\text{B}_0(0,\,0,\,0)\left(p^2-m_e^2\right)\gamma\cdot p}{p^2}+\frac{2\,i\,\pi^3\,\alpha\,(1-\xi_{V(1)})\left(p^2-m_e^2\right)^2\gamma\cdot p\,\text{C}_0\left(0,\,p^2,\,p^2,\,0,\,0,\,m_e^2\right)}{p^2}+$$
$$\frac{2\,i\,\pi^3\,\alpha\,(2-D)\,\gamma\cdot p\,\text{A}_0\left(m_e^2\right)}{p^2}$$

With PaxEvaluateUVIRSplit we obtain the full analytic result for the self-energy diagram

In[21]:=
```
ampElectronSE2 =
 PaXEvaluateUVIRSplit[ampElectronSE1, PaXImplicitPrefactor → 1 / (2 Pi)^D] //
   Collect2[#, DiracGamma] & // FCHideEpsilon
```

Out[21]=
$$\frac{i\,\alpha\,\Delta_{\text{UV}}\,(-m_e\,\xi_{V(1)}-3\,m_e+\xi_{V(1)}\,\gamma\cdot p)}{4\,\pi}-\frac{1}{4\,\pi\,p^4}$$
$$i\,\alpha\left(3\,p^4\,m_e\log\left(\frac{\mu^2}{m_e^2}\right)-p^4\,\xi_{V(1)}\,\gamma\cdot p\log\left(\frac{\mu^2}{m_e^2}\right)-p^2\,m_e^2\,\xi_{V(1)}\,\gamma\cdot p+m_e^4\,\xi_{V(1)}\,\gamma\cdot p\log\left(\frac{m_e^2}{m_e^2-p^2}\right)-\right.$$
$$p^4\,\xi_{V(1)}\,\gamma\cdot p\log\left(\frac{m_e^2}{m_e^2-p^2}\right)+p^4\,m_e\,\xi_{V(1)}\log\left(\frac{\mu^2}{m_e^2}\right)+2\,p^4\,m_e\,\xi_{V(1)}-p^2\,m_e^3\,\xi_{V(1)}\log\left(\frac{m_e^2}{m_e^2-p^2}\right)+$$
$$\left.p^4\,m_e\,\xi_{V(1)}\log\left(\frac{m_e^2}{m_e^2-p^2}\right)+4\,p^4\,m_e-3\,p^2\,m_e^3\log\left(\frac{m_e^2}{m_e^2-p^2}\right)+3\,p^4\,m_e\log\left(\frac{m_e^2}{m_e^2-p^2}\right)-p^4\,\xi_{V(1)}\,\gamma\cdot p\right)$$

This is the amplitude for the self-energy counter-term

In[22]:=
```
ampElectronSECT2 =
 ampElectronSECT // ReplaceAll[#, {SMP["Z_psi"] → 1 + alpha SMP["d_psi"],
        SMP["Z_m"] → 1 + alpha SMP["d_m"]}] & // Series[#, {alpha, 0, 1}] & // Normal //
  ReplaceAll[#, alpha → 1] &
```

Out[22]=
$$i\,(-\delta_\psi\,m_e-m_e\,\delta_m+\delta_\psi\,\gamma\cdot p)$$

Now we add the 1-loop SE diagram and the SE counter-term and discard all the finite pieces

In[23]:=
```
tmp[1] = SelectNotFree2[(ampElectronSECT2 + ampElectronSE2),
  {SMP["Delta_UV"], SMP["Delta_IR"], SMP["d_m"], SMP["d_psi"]}]
```

Out[23]=
$$-i\,\delta_\psi\,m_e-i\,m_e\,\delta_m+\frac{i\,\alpha\,\Delta_{\text{UV}}\,(-m_e\,\xi_{V(1)}-3\,m_e+\xi_{V(1)}\,\gamma\cdot p)}{4\,\pi}+i\,\delta_\psi\,\gamma\cdot p$$

Equating our result to zero and solving for δ_ψ and δ_m we obtain the renormalization constants in the minimal subtraction schemes.

In[24]:=
```
sol[1] = Solve[SelectNotFree2[tmp[1], DiracGamma] == 0, SMP["d_psi"]] // Flatten //
   Simplify;
sol[2] = Solve[(SelectFree2[tmp[1], DiracGamma] == 0) /. sol[1], SMP["d_m"]] //
    Flatten // Simplify;
solMS = Join[sol[1], sol[2]] /. {SMP["d_psi"] -> SMP["d_psi^MS"],
   SMP["d_m"] -> SMP["d_m^MS"], SMP["Delta_UV"] → 1 / EpsilonUV}
solMSbar = Join[sol[1], sol[2]] /. {SMP["d_psi"] -> SMP["d_psi^MSbar"],
   SMP["d_m"] -> SMP["d_m^MSbar"]}
```

Out[26]=
$$\left\{\delta_\psi^{\text{MS}}\to-\frac{\alpha\,\xi_{V(1)}}{4\,\pi\,\varepsilon_{\text{UV}}},\ \delta_m^{\text{MS}}\to-\frac{3\,\alpha}{4\,\pi\,\varepsilon_{\text{UV}}}\right\}$$

Out[27]=
$$\left\{\delta_\psi^{\overline{\text{MS}}}\to-\frac{\alpha\,\Delta_{\text{UV}}\,\xi_{V(1)}}{4\,\pi},\ \delta_m^{\overline{\text{MS}}}\to-\frac{3\,\alpha\,\Delta_{\text{UV}}}{4\,\pi}\right\}$$

For the on-shell scheme it is convenient to define the scalar product p.p as psq, since we will need to expand in this quantity

In[28]:=
```
FCClearScalarProducts[];
SPD[p, p] = psq;
```

It is also convenient to split the self-energy into a scalar (SigmaS) and a vector (SigmaV) part.

In[30]:=
```
SigmaS = Simplify[Cancel[SelectFree2[ampElectronSE1, DiracGamma] / (SMP["m_e"] I)]]
```

Out[30]=
$$-4\,\pi^3\,\alpha\,(D+\xi_{V(1)}-1)\,\mathrm{B}_0(\mathrm{psq},\,0,\,m_e^2)$$

In[31]:=
```
SigmaV =
 Simplify[Cancel[SelectNotFree2[ampElectronSE1, DiracGamma] / (FCI[GSD[p]] I)]]
```

Out[31]=
$$-\frac{1}{\mathrm{psq}}2\,\pi^3\,\alpha\left((\xi_{V(1)}-1)\,(\mathrm{psq}-m_e^2)\left((\mathrm{psq}-m_e^2)\,\mathrm{C}_0(0,\,\mathrm{psq},\,\mathrm{psq},\,0,\,0,\,m_e^2)-\mathrm{B}_0(0,\,0,\,0)\right)-\right.$$
$$\left.(D+\xi_{V(1)}-3)\,(m_e^2+\mathrm{psq})\,\mathrm{B}_0(\mathrm{psq},\,0,\,m_e^2)+(D-2)\,\mathrm{A}_0(m_e^2)\right)$$

According to the on-shell renormalization condition, the mass renormalization constant is given by the sum of SigmaS and SigmaV evaluated at p.p =0

In[32]:=
```
solOS = {SMP["d_m^OS"] -> FCHideEpsilon[
      PaXEvaluateUVIRSplit[SigmaS + SigmaV, PaXImplicitPrefactor -> 1 / (2 Pi)^D,
       PaXSeries -> {{psq, SMP["m_e"]^2, 0}}, PaXAnalytic -> True, FCVerbose -> 0]] //
   FCFactorOut[#, (-3 / (4 Pi) SMP["alpha_fs"])] &}
```

Out[32]=
$$\left\{\delta_m^{\mathrm{OS}} \to -\frac{\alpha\left(3\log\left(\frac{\mu^2}{m_e^2}\right)+3\,\Delta_{\mathrm{UV}}+4\right)}{4\,\pi}\right\}$$

For the wave-function renormalization constant we need the derivative of SigmaS+SigmaV evaluated at p.p=0

In[33]:=
```
tmp[2] =
 Simplify[(PaXEvaluateUVIRSplit[SigmaS + SigmaV, PaXImplicitPrefactor -> 1 / (2 Pi)^D,
       PaXSeries -> {{psq, SMP["m_e"]^2, 1}}, PaXAnalytic -> True, FCVerbose -> 0] -
     PaXEvaluateUVIRSplit[SigmaS + SigmaV, PaXImplicitPrefactor -> 1 / (2 Pi)^D,
       PaXSeries -> {{psq, SMP["m_e"]^2, 0}}, PaXAnalytic -> True, FCVerbose -> 0]) /
    (psq - SMP["m_e"]^2)] // FCHideEpsilon
```

Out[33]=
$$-\frac{\alpha\,\Delta_{\mathrm{IR}}\,(\xi_{V(1)}-3)}{8\,\pi\,m_e^2}-\frac{\alpha\left(-3\log\left(\frac{\mu^2}{m_e^2}\right)+\xi_{V(1)}\log\left(\frac{\mu^2}{m_e^2}\right)+2\,\xi_{V(1)}-4+3\log(4\,\pi)-3\log(\pi)-\log(64)\right)}{8\,\pi\,m_e^2}$$

as well as SigmaV at p.p=0

In[34]:=
```
tmp[3] = PaXEvaluateUVIRSplit[SigmaV, PaXImplicitPrefactor -> 1 / (2 Pi)^D,
    PaXSeries -> {{psq, SMP["m_e"]^2, 0}}, PaXAnalytic -> True] // FCHideEpsilon
```

Out[34]=
$$\frac{\alpha\,\xi_{V(1)}\left(\log\left(\frac{\mu^2}{m_e^2}\right)+2\right)}{4\,\pi}+\frac{\alpha\,\Delta_{\mathrm{UV}}\,\xi_{V(1)}}{4\,\pi}$$

Combining both pieces we can determine δ_ψ in the on-shell scheme

In[35]:=
```
{SMP["d_psi^OS"] -> Simplify[-tmp[3] - 2 SMP["m_e"]^2 tmp[2]]}
solOS = Union[Join[solOS, %]];
```

Out[35]=
$$\left\{\delta_\psi^{\text{OS}} \to -\frac{\alpha\left(3\log\left(\frac{\mu^2}{m_e^2}\right) - \Delta_{\text{IR}}\left(\xi_{V(1)} - 3\right) + \Delta_{\text{UV}}\,\xi_{V(1)} + 4\right)}{4\,\pi}\right\}$$

Photon self-energy

Again, first we obtain the amplitudes

In[37]:=
```
{ampPhotonSE, ampPhotonSECT} =
 FCTraceFactor[Contract[FCFAConvert[CreateFeynAmp[#, Truncated -> True,
       PreFactor → 1, GaugeRules → {}], IncomingMomenta -> {q},
OutgoingMomenta -> {q}, LoopMomenta -> {l}, DropSumOver -> True,
      UndoChiralSplittings -> True, ChangeDimension -> D, List -> False, SMP -> True,
      FinalSubstitutions → {ZA → SMP["Z_A"], Zpsi → SMP["Z_psi"], Zxi → SMP["Z_xi"],
        SMP["e"] → Sqrt[4 Pi SMP["alpha_fs"]]}]]] & /@ {diagPhotonSE, diagPhotonSECT}
```

Out[37]=
$$\left\{-\frac{4\,\pi\,\alpha\,\text{tr}\left((m_e - \gamma\cdot l).\gamma^{\text{Lor2}}.(m_e + \gamma\cdot(q-l)).\gamma^{\text{Lor1}}\right)}{\left(l^2 - m_e^2\right).\left((l-q)^2 - m_e^2\right)},\right.$$
$$\left. -i\,q^2\,(Z_A - 1)\,g^{\text{Lor1 Lor2}} - \frac{i\,q^{\text{Lor1}}\,q^{\text{Lor2}}\,(Z_A - Z_\xi)}{\xi_{V(1)}\,Z_\xi} + i\,(Z_A - 1)\,q^{\text{Lor1}}\,q^{\text{Lor2}}\right\}$$

then we do the tensor decomposition

In[38]:=
```
ampPhotonSE1 = TID[ampPhotonSE, l, ToPaVe → True]
```

Out[38]=
$$\frac{1}{(1-D)\,q^2} 8\,i\,\pi^3\,\alpha\,\text{B}_0\left(q^2,\,m_e^2,\,m_e^2\right)\left(-(1-D)\,q^4\,g^{\text{Lor1 Lor2}} + \right.$$
$$\left. 2\,(1-D)\,q^2\,q^{\text{Lor1}}\,q^{\text{Lor2}} + D\,q^2\,q^{\text{Lor1}}\,q^{\text{Lor2}} + 4\,q^2\,m_e^2\,g^{\text{Lor1 Lor2}} - 4\,m_e^2\,q^{\text{Lor1}}\,q^{\text{Lor2}} - q^4\,g^{\text{Lor1 Lor2}}\right) -$$
$$\frac{1}{(1-D)\,q^2} 16\,i\,\pi^3\,\alpha\,\text{A}_0\left(m_e^2\right)\left(-(1-D)\,q^2\,g^{\text{Lor1 Lor2}} - D\,q^{\text{Lor1}}\,q^{\text{Lor2}} - q^2\,g^{\text{Lor1 Lor2}} + 2\,q^{\text{Lor1}}\,q^{\text{Lor2}}\right)$$

and finally obtain the explicit results.

In[39]:=
```
ampPhotonSE2 = PaXEvaluateUVIRSplit[
    ampPhotonSE1, PaXImplicitPrefactor → 1 / (2 Pi)^D] // FCHideEpsilon
```

Out[39]=
$$\frac{1}{9\,\pi\,q^4} i\,\alpha\left(q^{\text{Lor1}}\,q^{\text{Lor2}} - q^2\,g^{\text{Lor1 Lor2}}\right)$$
$$\left(3\,q^4\log\left(\frac{\mu^2}{m_e^2}\right) + 12\,q^2\,m_e^2 + 3\,q^2\sqrt{q^2\left(q^2 - 4\,m_e^2\right)}\,\log\left(\frac{\sqrt{q^2\left(q^2 - 4\,m_e^2\right)} + 2\,m_e^2 - q^2}{2\,m_e^2}\right) + \right.$$
$$\left. 6\,m_e^2\sqrt{q^2\left(q^2 - 4\,m_e^2\right)}\,\log\left(\frac{\sqrt{q^2\left(q^2 - 4\,m_e^2\right)} + 2\,m_e^2 - q^2}{2\,m_e^2}\right) + 5\,q^4\right) + \frac{i\,\alpha\,\Delta_{\text{UV}}\left(q^{\text{Lor1}}\,q^{\text{Lor2}} - q^2\,g^{\text{Lor1 Lor2}}\right)}{3\,\pi}$$

This is the counter-term amplitude

In[40]:=
```
ampPhotonSECT2 = ampPhotonSECT // ReplaceRepeated[#, {SMP["Z_xi"] → SMP["Z_A"],
      SMP["Z_A"] → 1 + alpha SMP["d_A"]}] & // Normal // ReplaceAll[#, alpha → 1] &
```

Out[40]= $i\,\delta_A\,q^{\text{Lor1}}\,q^{\text{Lor2}} - i\,q^2\,\delta_A\,g^{\text{Lor1 Lor2}}$

Now we add the 1-loop SE diagram and the SE counter-term and discard all the finite pieces

In[41]:=
```
tmp[4] = (ampPhotonSECT2 + ampPhotonSE2) //
   SelectNotFree2[#, {SMP["Delta_UV"], SMP["d_A"]}] & // Simplify
```

Out[41]= $\frac{i\left(q^{\text{Lor1}}\,q^{\text{Lor2}} - q^2\,g^{\text{Lor1 Lor2}}\right)(3\,\pi\,\delta_A + \alpha\,\Delta_{\text{UV}})}{3\,\pi}$

Equating this to zero and solving for δ_A we obtain the wave-function renormalization constant for the photon in the minimal subtraction schemes.

In[42]:=
```
sol[3] = Solve[tmp[4] == 0, SMP["d_A"]] // Flatten;
tmp[5] = sol[3] /. {SMP["d_A"] -> SMP["d_A^MS"], SMP["Delta_UV"] → 1 / EpsilonUV}
solMS = Union[Join[solMS, tmp[5]]];
tmp[6] = sol[3] /. {SMP["d_A"] -> SMP["d_A^MSbar"]}
solMSbar = Union[Join[solMSbar, tmp[6]]];
```

Out[43]= $\left\{\delta_A^{\text{MS}} \to -\frac{\alpha}{3\,\pi\,\varepsilon_{\text{UV}}}\right\}$

Out[45]= $\left\{\delta_A^{\overline{\text{MS}}} \to -\frac{\alpha\,\Delta_{\text{UV}}}{3\,\pi}\right\}$

In[47]:=
```
SPD[q, q] = qsq;
```

Here we extract $\Pi(q^2)$

In[48]:=
```
tmp[7] = (ampPhotonSE1 // Simplify) /
   (-I FCI[qsq MTD[Lor1, Lor2] - FVD[q, Lor1] FVD[q, Lor2]])
```

Out[48]= $\frac{1}{(D-1)\,\text{qsq}}8\,\pi^3\,\alpha\left(\left((D-2)\,\text{qsq} + 4\,m_e^2\right)\text{B}_0\left(\text{qsq},\,m_e^2,\,m_e^2\right) - 2\,(D-2)\,\text{A}_0\left(m_e^2\right)\right)$

This is the derivative of $\Pi(q^2)$ evaluated at $q^2 = 0$

In[49]:=
```
tmp[8] =
 FCHideEpsilon[(PaXEvaluateUVIRSplit[qsq tmp[7], PaXImplicitPrefactor → 1 / (2 Pi)^D,
       PaXSeries → {{qsq, 0, 1}}, PaXAnalytic → True] / qsq) -
   PaXEvaluateUVIRSplit[qsq tmp3, PaXImplicitPrefactor → 1 / (2 Pi)^D,
    PaXSeries → {{qsq, 0, 0}}, PaXAnalytic → True]]
```

Out[49]= $\frac{\alpha\log\left(\frac{\mu^2}{m_e^2}\right)}{3\,\pi} + \frac{\alpha\,\Delta_{\text{UV}}}{3\,\pi}$

and from here we obtain δ_A in the on-shell scheme

In[50]:=
```
tmp[9] = {SMP["d_A^OS"] → -FCFactorOut[tmp[8], SMP["alpha_fs"] / (3 Pi)]}
solOS = Union[Join[solOS, tmp[9]]];
```

Out[50]=
$$\left\{\delta_A^{\text{OS}} \to -\frac{\alpha\left(\log\left(\frac{\mu^2}{m_e^2}\right)+\Delta_{\text{UV}}\right)}{3\,\pi}\right\}$$

Electron photon vertex

The last piece is the vertex diagram

In[52]:=
```
{ampVertex, ampVertexCT} =
 Contract[FCFAConvert[CreateFeynAmp[#, Truncated -> True, PreFactor → 1,
        GaugeRules → {}], IncomingMomenta -> {p1, k},
OutgoingMomenta -> {p2}, LoopMomenta -> {l}, DropSumOver -> True,
       UndoChiralSplittings -> True, ChangeDimension -> D, List -> False,
       SMP -> True, FinalSubstitutions → {k → p2 - p1, ZA → SMP["Z_A"],
         Zpsi → SMP["Z_psi"], Ze → SMP["Z_e"]}] & /@ {diagVertex, diagVertexCT}] //
  ReplaceAll[#, SMP["e"]^3 → 4 Pi SMP["alpha_fs"] SMP["e"]] &
```

Out[52]=
$$\left\{\frac{4\,\pi\,\alpha\,\text{e}\,\gamma^{\text{Lor3}}.(m_e+\gamma\cdot(l-\text{p1}+\text{p2})).\gamma^{\text{Lor1}}.(m_e+\gamma\cdot l).\gamma^{\text{Lor3}}}{(l^2-m_e^2).((l-\text{p1}+\text{p2})^2-m_e^2).(l-\text{p1})^2}+\right.$$
$$(4\,\pi\,\alpha\,\text{e}\,(\gamma\cdot(\text{p1}-l)).(m_e+\gamma\cdot(l-\text{p1}+\text{p2})).\gamma^{\text{Lor1}}.(m_e+\gamma\cdot l).(\gamma\cdot(l-\text{p1})))\Big/$$
$$(l^2-m_e^2).((l-\text{p1}+\text{p2})^2-m_e^2).((l-\text{p1})^2)^2-$$
$$(4\,\pi\,\alpha\,\text{e}\,\xi_{V(1)}\,(\gamma\cdot(\text{p1}-l)).(m_e+\gamma\cdot(l-\text{p1}+\text{p2})).\gamma^{\text{Lor1}}.(m_e+\gamma\cdot l).(\gamma\cdot(l-\text{p1})))\Big/$$
$$\left.(l^2-m_e^2).((l-\text{p1}+\text{p2})^2-m_e^2).((l-\text{p1})^2)^2,\ i\,\text{e}\,\gamma^{\text{Lor1}}\left(\sqrt{Z_A}\ Z_e\,Z_\psi-1\right)\right\}$$

The result of the tensor reduction is quite large, since we keep the full gauge dependence and do not specify the kinematics

In[53]:=
```
ampVertex1 = TID[ampVertex, l, ToPaVe → True, UsePaVeBasis → True]
```

Out[53]=
$$
\begin{aligned}
&-4\,i\,\pi^3\,B_0\left(p1^2-2\,(p1\cdot p2)+p2^2,\,m_e^2,\,m_e^2\right)\gamma^{Lor1}\,(-D-\xi_{V(1)}+3)\,\alpha\,e+\\
&8\,i\,(2-D)\,\pi^3\,\gamma^{Lor1}\,C_{00}\left(p1^2,\,p1^2-2\,(p1\cdot p2)+p2^2,\,p2^2,\,0,\,m_e^2,\,m_e^2\right)\alpha\,e+\\
&8\,i\,(2-D)\,\pi^3\,\gamma\cdot p1\,p1^{Lor1}\,C_{11}\left(p1^2,\,p1^2-2\,(p1\cdot p2)+p2^2,\,p2^2,\,0,\,m_e^2,\,m_e^2\right)\alpha\,e+\\
&8\,i\,(2-D)\,\pi^3\left(\gamma\cdot p2\,p1^{Lor1}+\gamma\cdot p1\,p2^{Lor1}\right)C_{12}\left(p1^2,\,p1^2-2\,(p1\cdot p2)+p2^2,\,p2^2,\,0,\,m_e^2,\,m_e^2\right)\alpha\,e+\\
&8\,i\,(2-D)\,\pi^3\,\gamma\cdot p2\,p2^{Lor1}\,C_{22}\left(p1^2,\,p1^2-2\,(p1\cdot p2)+p2^2,\,p2^2,\,0,\,m_e^2,\,m_e^2\right)\alpha\,e+\\
&4\,i\,\pi^3\,C_1\left(p1^2,\,p1^2-2\,(p1\cdot p2)+p2^2,\,p2^2,\,0,\,m_e^2,\,m_e^2\right)\alpha\,\big(-D\,(\gamma\cdot p1).\gamma^{Lor1}.(\gamma\cdot p1)+2\,(\gamma\cdot p1).\gamma^{Lor1}.(\gamma\cdot p1)-\\
&\quad 2\,(\gamma\cdot p1).\gamma^{Lor1}.(\gamma\cdot p2)-(\gamma\cdot p1).(\gamma\cdot p2).\gamma^{Lor1}-D\,(\gamma\cdot p2).\gamma^{Lor1}.(\gamma\cdot p1)+5\,(\gamma\cdot p2).\gamma^{Lor1}.(\gamma\cdot p1)+\\
&\quad (\gamma\cdot p1).(\gamma\cdot p2).\gamma^{Lor1}\,\xi_{V(1)}-(\gamma\cdot p2).\gamma^{Lor1}.(\gamma\cdot p1)\,\xi_{V(1)}+D\,\gamma^{Lor1}.(\gamma\cdot p1)\,m_e-5\,\gamma^{Lor1}.(\gamma\cdot p1)\,m_e+\\
&\quad D\,(\gamma\cdot p1).\gamma^{Lor1}\,m_e-5\,(\gamma\cdot p1).\gamma^{Lor1}\,m_e+\gamma^{Lor1}.(\gamma\cdot p1)\,\xi_{V(1)}\,m_e+(\gamma\cdot p1).\gamma^{Lor1}\,\xi_{V(1)}\,m_e+8\,p1^{Lor1}\,m_e\big)\,e-\\
&4\,i\,\pi^3\,C_2\left(p1^2,\,p1^2-2\,(p1\cdot p2)+p2^2,\,p2^2,\,0,\,m_e^2,\,m_e^2\right)\alpha\,\big(2\,(\gamma\cdot p1).\gamma^{Lor1}.(\gamma\cdot p2)+D\,(\gamma\cdot p2).\gamma^{Lor1}.(\gamma\cdot p1)-\\
&\quad 4\,(\gamma\cdot p2).\gamma^{Lor1}.(\gamma\cdot p1)+D\,(\gamma\cdot p2).\gamma^{Lor1}.(\gamma\cdot p2)-3\,(\gamma\cdot p2).\gamma^{Lor1}.(\gamma\cdot p2)+(\gamma\cdot p2).(\gamma\cdot p2).\gamma^{Lor1}+\\
&\quad (\gamma\cdot p2).\gamma^{Lor1}.(\gamma\cdot p2)\,\xi_{V(1)}-(\gamma\cdot p2).(\gamma\cdot p2).\gamma^{Lor1}\,\xi_{V(1)}-D\,\gamma^{Lor1}.(\gamma\cdot p2)\,m_e+5\,\gamma^{Lor1}.(\gamma\cdot p2)\,m_e-\\
&\quad D\,(\gamma\cdot p2).\gamma^{Lor1}\,m_e+5\,(\gamma\cdot p2).\gamma^{Lor1}\,m_e-\gamma^{Lor1}.(\gamma\cdot p2)\,\xi_{V(1)}\,m_e-(\gamma\cdot p2).\gamma^{Lor1}\,\xi_{V(1)}\,m_e-8\,p2^{Lor1}\,m_e\big)\,e-\\
&4\,i\,\pi^3\,(1-\xi_{V(1)})\,\alpha\,\big(\gamma^{Lor1}.(\gamma\cdot p1).(\gamma\cdot p1)\left(-C_0\left(0,\,p1^2,\,p1^2,\,0,\,0,\,m_e^2\right)-2\,C_1\left(0,\,p1^2,\,p1^2,\,0,\,0,\,m_e^2\right)\right)+\\
&\quad \gamma^{Lor1}.(\gamma\cdot p1)\,m_e\left(-C_0\left(0,\,p1^2,\,p1^2,\,0,\,0,\,m_e^2\right)-2\,C_1\left(0,\,p1^2,\,p1^2,\,0,\,0,\,m_e^2\right)\right)+\\
&\quad (\gamma\cdot p2).\gamma^{Lor1}.(\gamma\cdot p2)\left(-C_0\left(0,\,p2^2,\,p2^2,\,0,\,0,\,m_e^2\right)-2\,C_1\left(0,\,p2^2,\,p2^2,\,0,\,0,\,m_e^2\right)\right)-\\
&\quad \gamma^{Lor1}.(\gamma\cdot p2)\left(-C_0\left(0,\,p2^2,\,p2^2,\,0,\,0,\,m_e^2\right)-2\,C_1\left(0,\,p2^2,\,p2^2,\,0,\,0,\,m_e^2\right)\right)m_e\big)\,e+\\
&8\,i\,\pi^3\,(1-\xi_{V(1)})\,D_{00}\left(0,\,p1^2,\,p1^2-2\,(p1\cdot p2)+p2^2,\,p2^2,\,p1^2,\,p2^2,\,0,\,0,\,m_e^2,\,m_e^2\right)\alpha\\
&\quad \left(-\gamma^{Lor1}\,m_e^2-(\gamma\cdot p1).\gamma^{Lor1}\,m_e+(\gamma\cdot p2).\gamma^{Lor1}\,m_e+(\gamma\cdot p2).(\gamma\cdot p1).\gamma^{Lor1}\right)e+\\
&8\,i\,\pi^3\,(1-\xi_{V(1)})\,p1^{Lor1}\,D_{22}\left(0,\,p1^2,\,p1^2-2\,(p1\cdot p2)+p2^2,\,p2^2,\,p1^2,\,p2^2,\,0,\,0,\,m_e^2,\,m_e^2\right)\\
&\quad \alpha\left(-(\gamma\cdot p1)\,m_e^2-(\gamma\cdot p1).(\gamma\cdot p1)\,m_e+(\gamma\cdot p2).(\gamma\cdot p1)\,m_e+(\gamma\cdot p2).(\gamma\cdot p1).(\gamma\cdot p1)\right)e+\\
&8\,i\,\pi^3\,(1-\xi_{V(1)})\,p2^{Lor1}\,D_{33}\left(0,\,p1^2,\,p1^2-2\,(p1\cdot p2)+p2^2,\,p2^2,\,p1^2,\,p2^2,\,0,\,0,\,m_e^2,\,m_e^2\right)\\
&\quad \alpha\left(-(\gamma\cdot p2)\,m_e^2-(\gamma\cdot p1).(\gamma\cdot p2)\,m_e+(\gamma\cdot p2).(\gamma\cdot p2)\,m_e+(\gamma\cdot p2).(\gamma\cdot p1).(\gamma\cdot p2)\right)e+\\
&4\,i\,\pi^3\,(1-\xi_{V(1)})\,D_2\left(0,\,p1^2,\,p1^2-2\,(p1\cdot p2)+p2^2,\,p2^2,\,p1^2,\,p2^2,\,0,\,0,\,m_e^2,\,m_e^2\right)\alpha\\
&\quad \left(-\gamma^{Lor1}.(\gamma\cdot p1).(\gamma\cdot p1)\,m_e^2-(\gamma\cdot p2).\gamma^{Lor1}.(\gamma\cdot p1)\,m_e^2-\gamma^{Lor1}.(\gamma\cdot p1)\,p1^2\,m_e+\right.\\
&\quad \left.\gamma^{Lor1}.(\gamma\cdot p1)\,p2^2\,m_e+(\gamma\cdot p2).\gamma^{Lor1}.(\gamma\cdot p1)\,p1^2+\gamma^{Lor1}.(\gamma\cdot p1).(\gamma\cdot p1)\,p2^2\right)e+\\
&4\,i\,\pi^3\,(1-\xi_{V(1)})\,D_3\left(0,\,p1^2,\,p1^2-2\,(p1\cdot p2)+p2^2,\,p2^2,\,p1^2,\,p2^2,\,0,\,0,\,m_e^2,\,m_e^2\right)\alpha\\
&\quad \left(-\gamma^{Lor1}.(\gamma\cdot p1).(\gamma\cdot p2)\,m_e^2-(\gamma\cdot p2).\gamma^{Lor1}.(\gamma\cdot p2)\,m_e^2-\gamma^{Lor1}.(\gamma\cdot p2)\,p1^2\,m_e+\right.\\
&\quad \left.\gamma^{Lor1}.(\gamma\cdot p2)\,p2^2\,m_e+(\gamma\cdot p2).\gamma^{Lor1}.(\gamma\cdot p2)\,p1^2+\gamma^{Lor1}.(\gamma\cdot p1).(\gamma\cdot p2)\,p2^2\right)e-\\
&4\,i\,\pi^3\,C_0\left(p1^2,\,p2^2,\,p1^2-2\,(p1\cdot p2)+p2^2,\,m_e^2,\,0,\,m_e^2\right)\alpha\\
&\quad \left(D\,\gamma^{Lor1}\,m_e^2-3\,\gamma^{Lor1}\,m_e^2+\gamma^{Lor1}\,\xi_{V(1)}\,m_e^2-D\,\gamma^{Lor1}.(\gamma\cdot p1)\,m_e+5\,\gamma^{Lor1}.(\gamma\cdot p1)\,m_e-D\,(\gamma\cdot p2).\gamma^{Lor1}\,m_e+\right.\\
&\quad 5\,(\gamma\cdot p2).\gamma^{Lor1}\,m_e-\gamma^{Lor1}.(\gamma\cdot p1)\,\xi_{V(1)}\,m_e-(\gamma\cdot p2).\gamma^{Lor1}\,\xi_{V(1)}\,m_e-4\,p1^{Lor1}\,m_e-4\,p2^{Lor1}\,m_e+\\
&\quad \left.2\,(\gamma\cdot p1).\gamma^{Lor1}.(\gamma\cdot p2)+D\,(\gamma\cdot p2).\gamma^{Lor1}.(\gamma\cdot p1)-5\,(\gamma\cdot p2).\gamma^{Lor1}.(\gamma\cdot p1)+(\gamma\cdot p2).\gamma^{Lor1}.(\gamma\cdot p1)\,\xi_{V(1)}\right)e+\\
&8\,i\,\pi^3\,(1-\xi_{V(1)})\,D_{23}\left(0,\,p1^2,\,p1^2-2\,(p1\cdot p2)+p2^2,\,p2^2,\,p1^2,\,p2^2,\,0,\,0,\,m_e^2,\,m_e^2\right)\alpha\\
&\quad \left(-(\gamma\cdot p2)\,p1^{Lor1}\,m_e^2-\gamma\cdot p1\,p2^{Lor1}\,m_e^2-(\gamma\cdot p1).(\gamma\cdot p2)\,p1^{Lor1}\,m_e+(\gamma\cdot p2).(\gamma\cdot p2)\,p1^{Lor1}\,m_e-(\gamma\cdot p1).(\gamma\cdot p1)\right.\\
&\quad \left.p2^{Lor1}\,m_e+(\gamma\cdot p2).(\gamma\cdot p1)\,p2^{Lor1}\,m_e+(\gamma\cdot p2).(\gamma\cdot p1).(\gamma\cdot p2)\,p1^{Lor1}+(\gamma\cdot p2).(\gamma\cdot p1).(\gamma\cdot p1)\,p2^{Lor1}\right)e
\end{aligned}
$$

As we are interested in the UV piece only, there is no need to obtain the full analytic result

In[54]:=
```
tmp[10] = PaXEvaluateUV[ampVertex1, PaXImplicitPrefactor → 1 / (2 Pi)^D]
```

Out[54]=
$$\frac{i\,\alpha\,e\,\gamma^{Lor1}\,\xi_{V(1)}}{4\,\pi\,\varepsilon_{UV}}$$

This is the amplitude from the counter-term vertex

In[55]:=
```
ampVertexCT2 = Normal[Series[
    ampVertexCT /. {SMP["Z_A"] → 1 + alpha SMP["d_A"], SMP["Z_e"] → 1 + alpha SMP["d_e"],
      SMP["Z_psi"] → 1 + alpha SMP["d_psi"]}, {alpha, 0, 1}]] /. alpha → 1
```

Out[55]=
$$i\,e\,\gamma^{\text{Lor1}}\left(\frac{\delta_A}{2}+\delta_\psi+\delta_e\right)$$

Adding both amplitudes and equating them to zero gives

In[56]:=
```
tmp[11] =
  (Cancel[(tmp[10] + ampVertexCT2) / (-FCI [I SMP["e"] GAD[Lor1]])] // Simplify) == 0
```

Out[56]=
$$-\frac{2\,\pi\,\varepsilon_{\text{UV}}\,(\delta_A+2\,(\delta_\psi+\delta_e))+\alpha\,\xi_{V(1)}}{4\,\pi\,\varepsilon_{\text{UV}}}=0$$

After plugging in δ_ψ and δ_m that were determined previously, we can confirm Ward's identity which fixes the relation between
δ_A and δ_e

In[57]:=
```
Simplify[tmp[11] /. {SMP["d_psi"] -> SMP["d_psi^MS"]} /. solMS]
```

Out[57]=
$$\delta_A+2\,\delta_e=0$$

In[58]:=
```
Simplify[tmp[11] /. EpsilonUV → 1 / SMP["Delta_UV"] /.
    {SMP["d_psi"] -> SMP["d_psi^MSbar"]} /. solMSbar]
```

Out[58]=
$$\delta_A+2\,\delta_e=0$$

Finally, we want to look at the vertex in the on-shell scheme

In[59]:=
```
FCClearScalarProducts[];
SPD[p1, p1] = SMP["m_e"]^2;
SPD[p2, p2] = SMP["m_e"]^2;
```

Here we sandwich the amplitude between two spinors with 4-momenta p1 and p2.

In[62]:=
```
tmp[12] = SpinorUBarD[p2, SMP["m_e"]].ampVertex.SpinorUD[p1, SMP["m_e"]] //
    TID[#, l, UsePaVeBasis → True, ToPaVe → True] & // DiracSimplify;
```

Collecting the terms

In[63]:=
```
tmp[13] = (ExpandScalarProduct[tmp[12]] /. FCI@FVD[p1, Lor1] ->
     FCI[FVD[p1p2, Lor1] - FVD[p2, Lor1]]) // Collect2[#, LorentzIndex] &
```

Out[63]=
$$\begin{aligned}&4\,i\,\pi^3\,\alpha\,e\,(\varphi(\text{p2}, m_e)).\gamma^{\text{Lor1}}.(\varphi(\text{p1}, m_e))\\&\quad\big(D\,\text{B}_0\big(-2\,(\text{p1}\cdot\text{p2})+2\,m_e^2,\,m_e^2,\,m_e^2\big)-6\,\text{B}_0\big(-2\,(\text{p1}\cdot\text{p2})+2\,m_e^2,\,m_e^2,\,m_e^2\big)+4\,\text{B}_0\big(m_e^2,\,0,\,m_e^2\big)+\\&\qquad\xi_{V(1)}\,\text{B}_0(0,\,0,\,0)-\text{B}_0(0,\,0,\,0)+4\,(\text{p1}\cdot\text{p2})\,\text{C}_0\big(m_e^2,\,m_e^2,\,-2\,(\text{p1}\cdot\text{p2})+2\,m_e^2,\,m_e^2,\,0,\,m_e^2\big)-\\&\qquad2\,D\,\text{C}_{00}\big(m_e^2,\,2\,m_e^2-2\,(\text{p1}\cdot\text{p2}),\,m_e^2,\,0,\,m_e^2,\,m_e^2\big)+4\,\text{C}_{00}\big(m_e^2,\,2\,m_e^2-2\,(\text{p1}\cdot\text{p2}),\,m_e^2,\,0,\,m_e^2,\,m_e^2\big)\big)-\\&8\,i\,\pi^3\,\alpha\,e\,m_e\,\text{p1p2}^{\text{Lor1}}\,(\varphi(\text{p2}, m_e)).(\varphi(\text{p1}, m_e))\big(2\,\text{C}_1\big(m_e^2,\,2\,m_e^2-2\,(\text{p1}\cdot\text{p2}),\,m_e^2,\,0,\,m_e^2,\,m_e^2\big)+\\&\qquad D\,\text{C}_{11}\big(m_e^2,\,2\,m_e^2-2\,(\text{p1}\cdot\text{p2}),\,m_e^2,\,0,\,m_e^2,\,m_e^2\big)-2\,\text{C}_{11}\big(m_e^2,\,2\,m_e^2-2\,(\text{p1}\cdot\text{p2}),\,m_e^2,\,0,\,m_e^2,\,m_e^2\big)+\\&\qquad D\,\text{C}_{12}\big(m_e^2,\,2\,m_e^2-2\,(\text{p1}\cdot\text{p2}),\,m_e^2,\,0,\,m_e^2,\,m_e^2\big)-2\,\text{C}_{12}\big(m_e^2,\,2\,m_e^2-2\,(\text{p1}\cdot\text{p2}),\,m_e^2,\,0,\,m_e^2,\,m_e^2\big)\big)\end{aligned}$$

and applying Gordon decomposition we can bring the expression to the form dictated by the Lorentz covariance.

In[64]:=
```
tmp[14] = (1 / (SMP["e"] I) tmp[13] /.
    {FCI[FVD[p1p2, i_] SpinorUBarD[p2, m_].SpinorUBarD[p1, m_]] :>
      FCI[SpinorUBarD[p2, m].(2 m GAD[i] - I DiracSigma[GAD[i], GSD[p2 - p1]]).
        SpinorUD[p1, m]]}) // DotSimplify // Collect2[#, LorentzIndex] &;
```

This is $F_2(0)$

In[65]:=
```
tmp[15] = Simplify[SelectNotFree2[tmp[14], DiracSigma] /
    FCI[I / (2 SMP["m_e"]) SpinorUBarD[p2, SMP["m_e"]].
      DiracSigma[GAD[Lor1], GSD[p2 - p1]].SpinorUBarD[p1, SMP["m_e"]]]]
```

Out[65]=
$$16\,\pi^3\,\alpha\,m_e^2\,(2\,\mathrm{C}_1(m_e^2,\,2\,m_e^2-2\,(\mathrm{p1}\cdot\mathrm{p2}),\,m_e^2,\,0,\,m_e^2,\,m_e^2)+(D-2)\,(\mathrm{C}_{11}(m_e^2,\,2\,m_e^2-2\,(\mathrm{p1}\cdot\mathrm{p2}),\,m_e^2,\,0,\,m_e^2,\,m_e^2)+\mathrm{C}_{12}(m_e^2,\,2\,m_e^2-2\,(\mathrm{p1}\cdot\mathrm{p2}),\,m_e^2,\,0,\,m_e^2,\,m_e^2)))$$

its explicit value reproduces the beautiful result by Schwinger for $(g-2)/2$

In[66]:=
```
PaXEvaluateUVIRSplit[tmp[15] /. {FCI[SPD[p1, p2]] -> SMP["m_e"]^2},
 PaXImplicitPrefactor -> 1 / (2 Pi)^D]
```

Out[66]=
$$\frac{\alpha}{2\,\pi}$$

We need $F_1(0)$ to recover the on-shell renormalization condition

In[67]:=
```
tmp[16] = Cancel[DotSimplify[(tmp[14] /. p2 -> p1)] /
    FCI[SpinorUBarD[p1, SMP["m_e"]]. GAD[Lor1].SpinorUD[p1, SMP["m_e"]]]]
```

Out[67]=
$$4\,\pi^3\,\alpha\,(D\,\mathrm{B}_0(0,\,m_e^2,\,m_e^2)-6\,\mathrm{B}_0(0,\,m_e^2,\,m_e^2)+4\,\mathrm{B}_0(m_e^2,\,0,\,m_e^2)+\xi_{V(1)}\,\mathrm{B}_0(0,\,0,\,0)-\mathrm{B}_0(0,\,0,\,0)+4\,m_e^2\,\mathrm{C}_0(m_e^2,\,m_e^2,\,0,\,m_e^2,\,0,\,m_e^2)-2\,D\,\mathrm{C}_{00}(m_e^2,\,0,\,m_e^2,\,0,\,m_e^2,\,m_e^2)+4\,\mathrm{C}_{00}(m_e^2,\,0,\,m_e^2,\,0,\,m_e^2,\,m_e^2)-8\,m_e^2\,\mathrm{C}_1(m_e^2,\,0,\,m_e^2,\,0,\,m_e^2,\,m_e^2)-4\,D\,m_e^2\,\mathrm{C}_{11}(m_e^2,\,0,\,m_e^2,\,0,\,m_e^2,\,m_e^2)+8\,m_e^2\,\mathrm{C}_{11}(m_e^2,\,0,\,m_e^2,\,0,\,m_e^2,\,m_e^2)-4\,D\,m_e^2\,\mathrm{C}_{12}(m_e^2,\,0,\,m_e^2,\,0,\,m_e^2,\,m_e^2)+8\,m_e^2\,\mathrm{C}_{12}(m_e^2,\,0,\,m_e^2,\,0,\,m_e^2,\,m_e^2))$$

In[68]:=
```
tmp[17] =
 PaXEvaluateUVIRSplit[tmp[16], PaXImplicitPrefactor -> 1 / (2 Pi)^D] // FCHideEpsilon
```

Out[68]=
$$-\frac{\alpha\left(-3\log\left(\frac{\mu^2}{m_e^2}\right)-4+3\log(4\,\pi)-3\log(\pi)-\log(64)\right)}{4\,\pi}-\frac{\alpha\,\Delta_{\mathrm{IR}}\,(\xi_{V(1)}-3)}{4\,\pi}+\frac{\alpha\,\Delta_{\mathrm{UV}}\,\xi_{V(1)}}{4\,\pi}$$

Adding things up we again confirm Ward's identity, this time in the on-shell scheme

In[69]:=
```
Simplify[((tmp[17] + (ampVertexCT2 / (I SMP["e"] FCI[GAD[Lor1]])))) /.
    {SMP["d_psi"] -> SMP["d_psi^OS"]} /. solOS) == 0]
```

Out[69]=
$$\delta_A+2\,\delta_e=0$$

At the end we summarize our results

In[70]:= **solOS // TableForm**

Out[70]//TableForm=

$$\delta_A^{\text{OS}} \to -\frac{\alpha\left(\log\left(\frac{\mu^2}{m_e^2}\right)+\Delta_{\text{UV}}\right)}{3\,\pi}$$

$$\delta_m^{\text{OS}} \to -\frac{\alpha\left(3\log\left(\frac{\mu^2}{m_e^2}\right)+3\,\Delta_{\text{UV}}+4\right)}{4\,\pi}$$

$$\delta_\psi^{\text{OS}} \to -\frac{\alpha\left(3\log\left(\frac{\mu^2}{m_e^2}\right)-\Delta_{\text{IR}}\,(\xi_{V(1)}-3)+\Delta_{\text{UV}}\,\xi_{V(1)}+4\right)}{4\,\pi}$$

In[71]:= **solMS // TableForm**

Out[71]//TableForm=

$$\delta_A^{\text{MS}} \to -\frac{\alpha}{3\,\pi\,\varepsilon_{\text{UV}}}$$

$$\delta_m^{\text{MS}} \to -\frac{3\,\alpha}{4\,\pi\,\varepsilon_{\text{UV}}}$$

$$\delta_\psi^{\text{MS}} \to -\frac{\alpha\,\xi_{V(1)}}{4\,\pi\,\varepsilon_{\text{UV}}}$$

In[72]:= **solMSbar // TableForm**

Out[72]//TableForm=

$$\delta_A^{\overline{\text{MS}}} \to -\frac{\alpha\,\Delta_{\text{UV}}}{3\,\pi}$$

$$\delta_m^{\overline{\text{MS}}} \to -\frac{3\,\alpha\,\Delta_{\text{UV}}}{4\,\pi}$$

$$\delta_\psi^{\overline{\text{MS}}} \to -\frac{\alpha\,\Delta_{\text{UV}}\,\xi_{V(1)}}{4\,\pi}$$

H.2 Quark-gluon Vertex Expanded in the Relative Momentum Squared at 1-loop

```
$LoadAddOns = {"FeynHelpers"};
$LoadFeynArts = True;
<< FeynCalc`
$FAVerbose = 0;
```

FeynCalc 9.3.0 (development version). For help, use the documentation center, check out the wiki or write to the mailing list.

See also the supplied examples. If you use FeynCalc in your research, please cite

- V. Shtabovenko, R. Mertig and F. Orellana, Comput. Phys. Commun., 207C, 432–444, 2016, arXiv:1601.01167
- R. Mertig, M. Böhm, and A. Denner, Comput. Phys. Commun., 64, 345–359, 1991.

FeynArts 3.9 patched for use with FeynCalc, for documentation use the manual or visit www.feynarts.de.

FeynHelpers 1.0.0 loaded.

Have a look at the supplied examples. If you use FeynHelpers in your research, please cite

- V. Shtabovenko, "FeynHelpers: Connecting FeynCalc to FIRE and Package–X", TUM–EFT 75/15, arXiv:1611.06793

Furthermore, remember to cite the authors of the tools that you are calling from FeynHelpers, which are

- FIRE by A. Smirnov, if you are using the function FIREBurn.
- Package – *X* by H. Patel, if you are using the function PaXEvaluate.

Manohar's Results

Here we collect the results for $F_1^{(V)}$ and $F_2^{(V)}$ (abelian on-shell quark-gluon vertex) as well as $F_1^{(g)}$ and $F_2^{(g)}$ (non-abelian on-shell quark-gluon vertex)
from arXiv:hep-ph/9701294. The explicit values for these form-factors are given in Eqs. 29-30 and Eqs. 33-34 of the above-mentioned preprint.

```
F1V = ((SMP["alpha_s"] / Pi) (CF - 1 / 2 CA)
    (1 / (2 EpsilonUV) + 1 / EpsilonIR + 1 - 3 / 2 Log[m / ScaleMu] +
      q2 / m^2 (-1 / (3 EpsilonIR) - 1 / 8 + 1 / 3 Log[m / ScaleMu])))
```

$$\frac{\alpha_s\left(C_F-\frac{C_A}{2}\right)\left(\frac{1}{\varepsilon_{\text{IR}}}+\frac{\text{q2}\left(-\frac{1}{3\,\varepsilon_{\text{IR}}}+\frac{1}{3}\log\left(\frac{m}{\mu}\right)-\frac{1}{8}\right)}{m^2}-\frac{3}{2}\log\left(\frac{m}{\mu}\right)+\frac{1}{2\,\varepsilon_{\text{UV}}}+1\right)}{\pi}$$

```
F2V = (SMP["alpha_s"] / Pi) (CF - 1 / 2 CA) (1 / 2 + q2 / (12 m^2))
```

$$\frac{\left(\frac{\text{q2}}{12\,m^2}+\frac{1}{2}\right)\alpha_s\left(C_F-\frac{C_A}{2}\right)}{\pi}$$

```
F1G = (SMP["alpha_s"] / (8 Pi)) CA (2 / EpsilonUV + 4 / EpsilonIR + 4 - 6 Log[m / ScaleMu] +
      q2 / m^2 (-3 / EpsilonIR - 1 + 3 Log[m / ScaleMu]))
```

$$\frac{C_A\,\alpha_s\left(\frac{4}{\varepsilon_{\text{IR}}}+\frac{\text{q2}\left(-\frac{3}{\varepsilon_{\text{IR}}}+3\log\left(\frac{m}{\mu}\right)-1\right)}{m^2}-6\log\left(\frac{m}{\mu}\right)+\frac{2}{\varepsilon_{\text{UV}}}+4\right)}{8\,\pi}$$

```
F2G = (SMP["alpha_s"] / (8 Pi)) CA (4 / EpsilonIR + 6 - 4 Log[m / ScaleMu] +
      q2 / m^2 (4 / EpsilonIR + 1 - 4 Log[m / ScaleMu]))
```

$$\frac{C_A\,\alpha_s\left(\frac{4}{\varepsilon_{\text{IR}}}+\frac{\text{q2}\left(\frac{4}{\varepsilon_{\text{IR}}}-4\log\left(\frac{m}{\mu}\right)+1\right)}{m^2}-4\log\left(\frac{m}{\mu}\right)+6\right)}{8\,\pi}$$

Code

```
FAPatch[PatchModelsOnly -> True];
$KeepLogDivergentScalelessIntegrals = True;
```

```
Patching FeynArts models... done!
```

```
topVertex = CreateTopologies[1, 2 -> 1, ExcludeTopologies -> {WFCorrections}];
diagsVertex = InsertFields[topVertex, {F[3, {1}], V[50]} ->
        {F[3, {1}]}, InsertionLevel -> {Classes},
    Model -> FileNameJoin[{"QCDBGF", "QCDBGF"}],
    GenericModel -> FileNameJoin[{"QCDBGF", "QCDBGF"}]];
Paint[diagsVertex, ColumnsXRows -> {2, 1}, ImageSize → {512, 256},
  Numbering -> None, SheetHeader → False];
```

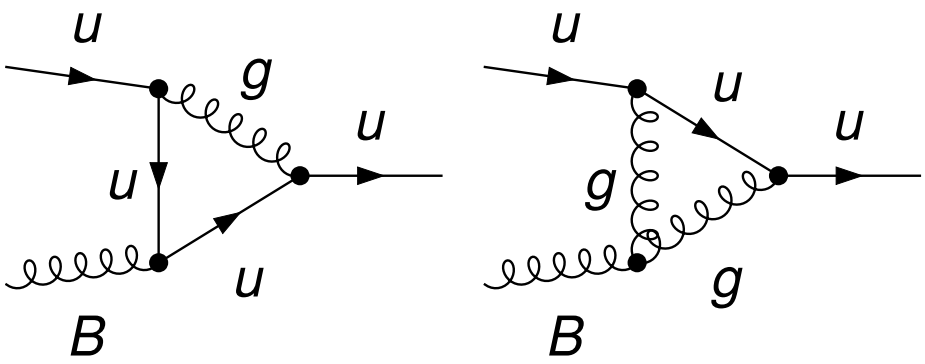

On-shell kinematics

```
FCClearScalarProducts[];
ScalarProduct[p1, p1] = m^2;
ScalarProduct[p2, p2] = m^2;
ScalarProduct[q, q] = q2;
ScalarProduct[p1, p2] = -1 / 2 FCI@ SPD[q, q] + m^2;
```

Since we are going to evaluate both diagrams one after another, it is convenient to define helper functions that will do the job.

This function obtains the amplitude for further evaluation with FeynCalc

```
ampFunc0[diag_] := FCFAConvert[
        FCPrepareFAAmp[CreateFeynAmp[diag, Truncated -> False, PreFactor → -1]],
        IncomingMomenta → {p1, q}, OutgoingMomenta → {p2},
        LoopMomenta → {l}, UndoChiralSplittings → True,
        DropSumOver → True, List → False, FinalSubstitutions →
         {SMP["m_u"] → m, q → p2 - p1, Pair[Momentum[Polarization[___], ___], ___] :> 1},
        ChangeDimension → D, SMP → True] // Contract // SUNSimplify //
    ReplaceAll[#, SUNTF[{x__}, __] :↦ SUNT[x]] & //
   SUNSimplify[#, Explicit → True] & //
  ReplaceAll[#, SMP["g_s"]^3 → 4 Pi SMP["alpha_s"] SMP["g_s"]] &
```

Tensor reduction and simplification of the Dirac algebra

```
ampFunc1[expr_] :=
  expr // TID[#, l, UsePaVeBasis → True, ToPaVe → True] & // DiracSimplify //
   Collect2[#, Spinor, Factoring → Simplify] &;
```

Gordon decomposition

```
ampFunc2[expr_] :=
  (expr /. {FCI[(FVD[p1, i_] + FVD[p2, i_]) SpinorUBarD[p2, m_].SpinorUBarD[p1, m_]] :↦
        FCI[SpinorUBarD[p2, m].(2 m GAD[i] - I DiracSigma[GAD[i], GSD[p2 - p1]]).
          SpinorUD[p1, m]]}) // DotSimplify // Collect2[#, LorentzIndex] &;
```

Expansion in q^2 up to first order

```
ampFunc3[expr_] := PaXEvaluateUVIRSplit[expr, PaXSeries → {{q2, 0, 1}},
     PaXAnalytic → True, PaXImplicitPrefactor → (2 Pi)^(-D)] //
    FCHideEpsilon // Collect2[#, LorentzIndex] &;
```

Extracts $F_1(q^2)$

```
vectorPart[expr_, fo_: 1] := ((expr // SelectFree2[#, DiracSigma] &) /
     FCI[I SMP["g_s"] SUNT[Glu2] SpinorUBarD[p2, m].GAD[Lor1].SpinorUD[p1, m]]) //
   Collect2[#, {SMP["Delta_UV"], SMP["Delta_IR"], q2},
     Factoring → FullSimplify, FCFactorOut → fo] &;
```

Extracts $F_2(q^2)$

```
scalarPart[expr_, fo_: 1] := ((expr // SelectNotFree2[#, DiracSigma] &) /
      FCI[I SMP["g_s"] SUNT[Glu2] (I / (2 m)) FCI[
         SpinorUBarD[p2, m] . DiracSigma[GAD[Lor1], GSD[p2 - p1]].SpinorUD[p1, m]]]) //
   Collect2[#, {SMP["Delta_UV"], SMP["Delta_IR"], q2},
     Factoring → FullSimplify, FCFactorOut → fo] &;
```

QCD abelian vertex

```
abelianVertex = ampFunc0[DiagramExtract[diagsVertex, 1]]
```

$$(2\,\pi\,g_s\,T^{\text{Glu2}}\,\alpha_s\,(2\,C_F - C_A)\,(\varphi(\text{p2}, m)).\gamma^{\text{Lor3}}.(\gamma\cdot(l - \text{p1} + \text{p2}) + m).\gamma^{\text{Lor1}}.(\gamma\cdot l + m).\gamma^{\text{Lor3}}.(\varphi(\text{p1}, m)))/$$
$$(l^2 - m^2).((l - \text{p1} + \text{p2})^2 - m^2).(l - \text{p1})^2$$

```
abelianVertex1 = ampFunc1[abelianVertex]
```

$$4\,i\,\pi^3\,m\,g_s\,T^{\text{Glu2}}\,\alpha_s\,(C_A - 2\,C_F)\,(\text{p1}^{\text{Lor1}} + \text{p2}^{\text{Lor1}})\,(\varphi(\text{p2}, m)).(\varphi(\text{p1}, m))$$
$$(2\,\text{C}_1(m^2, \text{q2}, m^2, 0, m^2, m^2) + (D - 2)\,(\text{C}_{11}(m^2, \text{q2}, m^2, 0, m^2, m^2) + \text{C}_{12}(m^2, \text{q2}, m^2, 0, m^2, m^2))) -$$
$$2\,i\,\pi^3\,g_s\,T^{\text{Glu2}}\,\alpha_s\,(C_A - 2\,C_F)\,((D - 6)\,\text{B}_0(\text{q2}, m^2, m^2) + 4\,\text{B}_0(m^2, 0, m^2) +$$
$$4\,m^2\,\text{C}_0(m^2, m^2, \text{q2}, m^2, 0, m^2) - 2\,\text{q2}\,\text{C}_0(m^2, m^2, \text{q2}, m^2, 0, m^2) -$$
$$2\,D\,\text{C}_{00}(m^2, \text{q2}, m^2, 0, m^2, m^2) + 4\,\text{C}_{00}(m^2, \text{q2}, m^2, 0, m^2, m^2))\,(\varphi(\text{p2}, m)).\gamma^{\text{Lor1}}.(\varphi(\text{p1}, m))$$

```
abelianVertex2 = ampFunc2[abelianVertex1];
```

```
abelianVertex3 = ampFunc3[abelianVertex2]
```

$$\frac{1}{48\,\pi\,m^3}g_s\,T^{\text{Glu2}}\,(6\,m^2 + \text{q2})\,\alpha_s\,(C_A - 2\,C_F)\,(\varphi(\text{p2}, m)).\sigma^{\text{Lor1 p2-p1}}.(\varphi(\text{p1}, m)) - \frac{1}{48\,\pi\,m^2}i\,g_s\,T^{\text{Glu2}}\,\alpha_s\,(C_A - 2\,C_F)$$
$$\left(12\,m^2\,\Delta_{\text{IR}} - 4\,\text{q2}\,\Delta_{\text{IR}} + 18\,m^2\log\left(\frac{\mu^2}{m^2}\right) - 4\,\text{q2}\log\left(\frac{\mu^2}{m^2}\right) + 6\,m^2\,\Delta_{\text{UV}} + 24\,m^2 - 18\,m^2\log(4\,\pi) + 18\,m^2\log(\pi) +\right.$$
$$\left.m^2\log(68\,719\,476\,736) - 3\,\text{q2} + 4\,\text{q2}\log(4\,\pi) - 4\,\text{q2}\log(\pi) - \text{q2}\log(256)\right)(\varphi(\text{p2}, m)).\gamma^{\text{Lor1}}.(\varphi(\text{p1}, m))$$

This is $F_1^{(V)}$

```
vectorPart[abelianVertex3, SMP["alpha_s"] (CF - CA / 2) 1 / Pi]
```

$$\frac{1}{\pi}\alpha_s\left(C_F - \frac{C_A}{2}\right)\left(\frac{\Delta_{\text{IR}}}{2} - \frac{\text{q2}\,\Delta_{\text{IR}}}{6\,m^2} + \frac{3}{4}\log\left(\frac{\mu^2}{m^2}\right) - \frac{\text{q2}\left(4\log\left(\frac{\mu^2}{m^2}\right) + 3\right)}{24\,m^2} + \frac{\Delta_{\text{UV}}}{4} + 1\right)$$

and this is $F_2^{(V)}$

```
scalarPart[abelianVertex3, SMP["alpha_s"] (CF - CA / 2) 1 / Pi]
```

$$\frac{\left(\frac{\text{q2}}{12\,m^2} + \frac{1}{2}\right)\alpha_s\left(C_F - \frac{C_A}{2}\right)}{\pi}$$

Comparing our result to the literature

```
Simplify[(PowerExpand[FCShowEpsilon[vectorPart[abelianVertex3]] /.
      {ScaleMu^2 → ScaleMu^2 E^EulerGamma / (4 Pi), 1 / EpsilonIR → 2 / EpsilonIR,
       1 / EpsilonUV → 2 / EpsilonUV}]) - F1V, Assumptions → {ScaleMu > 0, m > 0}]
```

0

```
Simplify[(PowerExpand[FCShowEpsilon[scalarPart[abelianVertex3]] /.
      {ScaleMu^2 → ScaleMu^2 E^EulerGamma / (4 Pi), 1 / EpsilonIR → 2 / EpsilonIR,
       1 / EpsilonUV → 2 / EpsilonUV}]) - F2V, Assumptions → {ScaleMu > 0, m > 0}]
```

0

QCD non-abelian vertex

```
nonAbelianVertex = ampFunc0[DiagramExtract[diagsVertex, 2]];
```

```
nonAbelianVertex1 = ampFunc1[nonAbelianVertex];
```

```
nonAbelianVertex2 = ampFunc2[nonAbelianVertex1];
```

```
nonAbelianVertex3 = ampFunc3[nonAbelianVertex2];
```

This is $F_1^{(g)}$

```
vectorPart[nonAbelianVertex3, SMP["alpha_s"] CA / (8 Pi)]
```

$$\frac{1}{8\pi} C_A \alpha_s \left(2\,\Delta_{\text{IR}} - \frac{3\,\text{q2}\,\Delta_{\text{IR}}}{2\,m^2} + 3\log\left(\frac{\mu^2}{m^2}\right) - \frac{\text{q2}\left(3\log\left(\frac{\mu^2}{m^2}\right)+2\right)}{2\,m^2} + \Delta_{\text{UV}} + 4\right)$$

and this is $F_2^{(g)}$

```
scalarPart[nonAbelianVertex3, SMP["alpha_s"] CA / (8 Pi)]
```

$$\frac{1}{8\pi} C_A \alpha_s \left(2\,\Delta_{\text{IR}} + \frac{2\,\text{q2}\,\Delta_{\text{IR}}}{m^2} + 2\left(\log\left(\frac{\mu^2}{m^2}\right)+3\right) + \frac{\text{q2}\left(2\log\left(\frac{\mu^2}{m^2}\right)+1\right)}{m^2}\right)$$

Comparing our result to the literature

```
Simplify[(PowerExpand[FCShowEpsilon[vectorPart[nonAbelianVertex3]] /.
      {ScaleMu^2 → ScaleMu^2 E^EulerGamma / (4 Pi), 1 / EpsilonIR → 2 / EpsilonIR,
       1 / EpsilonUV → 2 / EpsilonUV}]) - F1G, Assumptions → {ScaleMu > 0, m > 0}]
```

0

```
Simplify[(PowerExpand[FCShowEpsilon[scalarPart[nonAbelianVertex3]] /.
      {ScaleMu^2 → ScaleMu^2 E^EulerGamma / (4 Pi), 1 / EpsilonIR → 2 / EpsilonIR,
       1 / EpsilonUV → 2 / EpsilonUV}]) - F2G, Assumptions → {ScaleMu > 0, m > 0}]
```

```
0
```

H.3 Higgs Decay to Two Gluons

In[1]:=
```
$LoadAddOns = {"FeynHelpers"};
$LoadFeynArts = True;
<< FeynCalc`
$FAVerbose = 0;
```

FeynCalc 9.3.0 (development version). For help, use the documentation center, check out the wiki or write to the mailing list.

See also the supplied examples. If you use FeynCalc in your research, please cite

- V. Shtabovenko, R. Mertig and F. Orellana, Comput. Phys. Commun., 207C, 432–444, 2016, arXiv:1601.01167
- R. Mertig, M. Böhm, and A. Denner, Comput. Phys. Commun., 64, 345–359, 1991.

FeynArts 3.9 patched for use with FeynCalc, for documentation use the manual or visit www.feynarts.de.

FeynHelpers 1.0.0 loaded.

Have a look at the supplied examples. If you use FeynHelpers in your research, please cite

- V. Shtabovenko, "FeynHelpers: Connecting FeynCalc to FIRE and Package–X", TUM–EFT 75/15, arXiv:1611.06793

Furthermore, remember to cite the authors of the tools that you are calling from FeynHelpers, which are

- FIRE by A. Smirnov, if you are using the function FIREBurn.
- Package – *X* by H. Patel, if you are using the function PaXEvaluate.

In[5]:=
```
diagsHiggsToGG = InsertFields[CreateTopologies[1, 1 -> 2], {S[1]} -> {V[5], V[5]},
   InsertionLevel -> {Particles}, Model -> "SMQCD"];
```

In[6]:=
```
Paint[DiagramExtract[diagsHiggsToGG, {3, 6}], ColumnsXRows -> {2, 1},
  Numbering -> None, SheetHeader -> None, ImageSize -> {512, 256}];
```

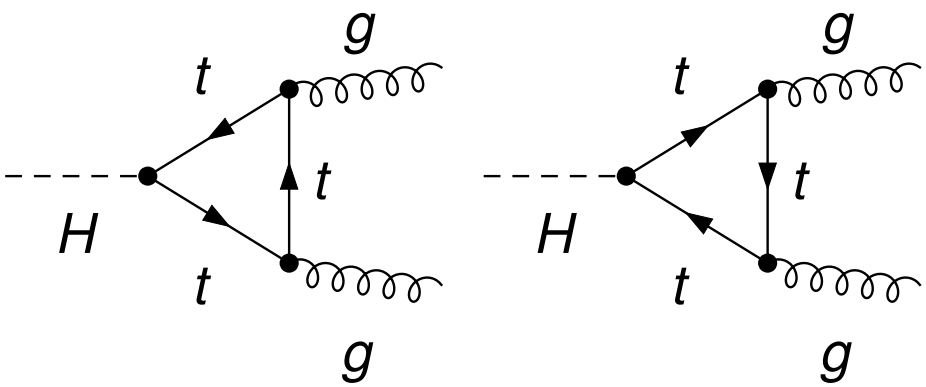

The initial and final state particles are put on-shell.

In[7]:=
```
FCClearScalarProducts[];
ScalarProduct[k1, k1] = 0;
ScalarProduct[k2, k2] = 0;
ScalarProduct[pH, pH] = SMP["m_H"]^2;
ScalarProduct[k1, k2] = (SMP["m_H"]^2) / 2;
```

This is the sum of both amplitudes

In[12]:=
```
ampHiggsToTwoGluons =
 FCFAConvert[CreateFeynAmp[DiagramExtract[diagsHiggsToGG, {3, 6}],
       PreFactor -> -1], IncomingMomenta -> {pH}, OutgoingMomenta -> {k1, k2},
      LoopMomenta -> {q}, List -> False, TransversePolarizationVectors -> {k1, k2},
ChangeDimension -> D, DropSumOver -> True,
      SMP -> True, UndoChiralSplittings -> True] //
     Contract // FCTraceFactor // SUNSimplify
```

Out[12]=
$$\left(\mathrm{e}\, g_s^2\, m_t\, \delta^{\mathrm{Glu2\,Glu3}}\, \mathrm{tr}\left((m_t-\gamma\cdot(\mathrm{k1}+\mathrm{k2}-q)).(\gamma\cdot\varepsilon^*(\mathrm{k2})).(m_t-\gamma\cdot(\mathrm{k1}-q)).(\gamma\cdot\varepsilon^*(\mathrm{k1})).(m_t+\gamma\cdot q)\right)\right)/$$
$$\left(2\, m_W\, (\sin(\theta_W))\, (q^2-m_t^2).((q-\mathrm{k1})^2-m_t^2).((-\mathrm{k1}-\mathrm{k2}+q)^2-m_t^2)\right)$$

Tensor reduction is straight-forward, after which we end up with coefficient functions

In[13]:=
```
ampHiggsToTwoGluons2 =
 TID[ampHiggsToTwoGluons, q, ToPaVe → True] // Collect2[#, B0, C0] &
```

Out[13]=
$$-\Big(\big(2\, i\, \pi^2\, (D-4)\, \mathrm{e}\, g_s^2\, m_t^2\, \delta^{\mathrm{Glu2\,Glu3}}\, \mathrm{B}_0\left(m_H^2,\, m_t^2,\, m_t^2\right)\left(m_H^2\left(\varepsilon^*(\mathrm{k1})\cdot\varepsilon^*(\mathrm{k2})\right)-2\left(\mathrm{k1}\cdot\varepsilon^*(\mathrm{k2})\right)\left(\mathrm{k2}\cdot\varepsilon^*(\mathrm{k1})\right)\right)\big)/$$
$$\left((D-2)\, m_H^2\, m_W\, (\sin(\theta_W))\right)\Big) - \frac{1}{(D-2)\, m_H^2\, m_W\, (\sin(\theta_W))} i\, \pi^2\, \mathrm{e}\, g_s^2\, m_t^2\, \delta^{\mathrm{Glu2\,Glu3}}$$
$$\left(D\, m_H^2-2\, m_H^2-8\, m_t^2\right)\mathrm{C}_0\left(0,\, 0,\, m_H^2,\, m_t^2,\, m_t^2,\, m_t^2\right)\left(m_H^2\left(\varepsilon^*(\mathrm{k1})\cdot\varepsilon^*(\mathrm{k2})\right)-2\left(\mathrm{k1}\cdot\varepsilon^*(\mathrm{k2})\right)\left(\mathrm{k2}\cdot\varepsilon^*(\mathrm{k1})\right)\right)$$

The coefficient functions are evaluated with Package-X

In[14]:=
```
ampHiggsToTwoGluons3 =
 PaXEvaluate[ampHiggsToTwoGluons2, PaXImplicitPrefactor → 1 / (2 Pi)^D] //
  Simplify
```

Out[14]=
$$\frac{1}{32\,\pi^2\, m_H^4\, m_W\, (\sin(\theta_W))}$$
$$i\, \mathrm{e}\, g_s^2\, m_t^2\, \delta^{\mathrm{Glu2\,Glu3}}\left(m_H^2\left(\log^2\left(\frac{\sqrt{m_H^4-4\, m_H^2\, m_t^2}-m_H^2+2\, m_t^2}{2\, m_t^2}\right)-4\right)-4\, m_t^2\log^2\left(\frac{\sqrt{m_H^4-4\, m_H^2\, m_t^2}-m_H^2+2\, m_t^2}{2\, m_t^2}\right)\right)$$
$$\left(2\left(\mathrm{k1}\cdot\varepsilon^*(\mathrm{k2})\right)\left(\mathrm{k2}\cdot\varepsilon^*(\mathrm{k1})\right)-m_H^2\left(\varepsilon^*(\mathrm{k1})\cdot\varepsilon^*(\mathrm{k2})\right)\right)$$

As the result is finite, it is safe to switch from D to 4 dimensions.

In[15]:=
```
ampHiggsToTwoGluons4 = ChangeDimension[ampHiggsToTwoGluons3, 4];
```

We square the amplitude and sum over the polarizations of the gluons

In[16]:=
```
ampSq = ampHiggsToTwoGluons4 ComplexConjugate[ampHiggsToTwoGluons4] //
      DoPolarizationSums[#, k1, k2] & // DoPolarizationSums[#, k2, k1] & // Simplify //
SUNSimplify[#, SUNNToCACF -> False] &
```

Out[16]=
$$\frac{e^2 \left(N^2-1\right) g_s^4 m_t^4 \left(m_H^2 \left(\log^2\left(\frac{\sqrt{m_H^4-4 m_H^2 m_t^2}-m_H^2+2 m_t^2}{2 m_t^2}\right)-4\right)-4 m_t^2 \log^2\left(\frac{\sqrt{m_H^4-4 m_H^2 m_t^2}-m_H^2+2 m_t^2}{2 m_t^2}\right)\right)^2}{512 \pi^4 m_H^4 m_W^2 (\sin(\theta_W))^2}$$

Multiplying the result by the phase space factor we obtain the total decay rate

In[17]:=
```
$Assumptions = {SMP["m_H"] > 0, SMP["m_t"] > 0};
decayRateTotal = (1 / 2 * 1 / (16 Pi SMP["m_H"])) * (ampSq /. SUNN → 3)) //
ReplaceAll[#, {SMP["e"]^2 -> 4 Pi SMP["alpha_fs"],
      SMP["g_s"]^4 -> 16 Pi^2 SMP["alpha_s"]^2}] & //
  Simplify
```

Out[18]=
$$\frac{\alpha m_t^4 \alpha_s^2 \left(m_H^2 \left(\log^2\left(\frac{m_H \sqrt{m_H^2-4 m_t^2}-m_H^2+2 m_t^2}{2 m_t^2}\right)-4\right)-4 m_t^2 \log^2\left(\frac{m_H \sqrt{m_H^2-4 m_t^2}-m_H^2+2 m_t^2}{2 m_t^2}\right)\right)^2}{32 \pi^2 m_H^5 m_W^2 (\sin(\theta_W))^2}$$

For convenience, we can eliminate the fine-structure constant and sine of the Weinberg angle in favor of Fermi's constant

In[19]:=
```
decayRateTotal2 =
 Simplify[decayRateTotal /. { SMP["m_t"] → SMP["m_H"] / (2 Sqrt[τ]), SMP["alpha_fs"] →
      Sqrt[2] / Pi SMP["m_W"]^2 SMP["sin_W"]^2 SMP["G_F"]}]
```

Out[19]=
$$\frac{G_F m_H^3 \alpha_s^2 \left((\tau-1) \log^2\left(2\left(\sqrt{\frac{\tau-1}{\tau}}-1\right)\tau+1\right)-4\tau\right)^2}{256\sqrt{2}\,\pi^3 \tau^4}$$

To compare to the literature (arXiv:hep-ph/9504378) we extract the function $A^2(\tau)$

In[20]:=
```
aSq = decayRateTotal2 /
   (SMP["alpha_s"]^2 SMP["G_F"] SMP["m_H"]^3 / (36 Sqrt[2] Pi^3) 9 / 16)
```

Out[20]=
$$\frac{\left((\tau-1) \log^2\left(2\left(\sqrt{\frac{\tau-1}{\tau}}-1\right)\tau+1\right)-4\tau\right)^2}{4\tau^4}$$

The plots show that our results coincide with those of Spira et al.

In[21]:=
```
aSqLit[x_] := Piecewise[{{(2 (x + (x - 1) ArcSin[Sqrt[x]]^2) / x^2)^2, 0 < x ≤ 1},
    {(2 (x + (x - 1) (-1 / 4 (Log[(1 + Sqrt[1 - 1 / x]) / (1 - Sqrt[1 - 1 / x])] - I Pi)^2)) / x^2)^2,
     x > 1}}]
```

In[22]:=
```
aSqLitBT = (2 (τ + (τ - 1) ArcSin[Sqrt[τ]]^2) / τ^2)^2;
aSqLitAT =
  (2 (τ + (τ - 1) (-1/4 (Log[(1 + Sqrt[1 - 1/τ]) / (1 - Sqrt[1 - 1/τ])] - I Pi)^2)) / τ^2)^2;
```

In[24]:=
```
plot1 = Plot[{Re[aSq], Re[aSqLit[τ]]},
  {τ, 0, 2}, PlotStyle → {{Dashed, Red}, {DotDashed, Blue}},
  PlotLegends → {Re[A_FeynCalc^2], Re[A_Literature^2]}, AxesLabel → {τ, Re[A^2]}]
plot2 = Plot[{Im[aSq], Im[aSqLit[τ]]}, {τ, 0, 2},
  PlotStyle → {{Dashed, Cyan}, {DotDashed, Black}},
  PlotLegends → {Im[A_FeynCalc^2], Im[A_Literature^2]}, AxesLabel → {τ, Im[A^2]}]
```

Out[24]=

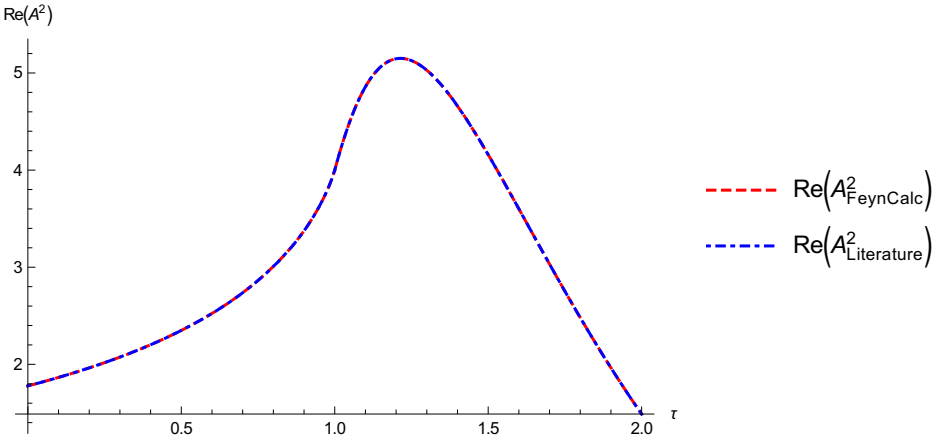

Out[25]=

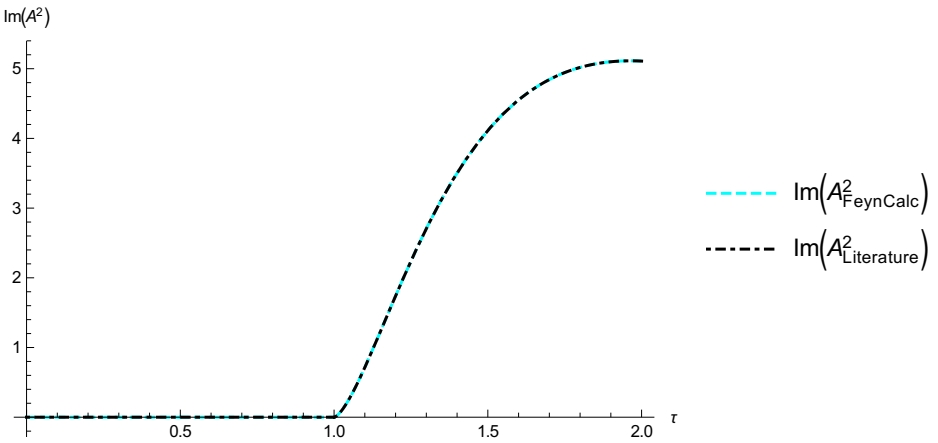

H.4 2-loop Self-energies in Massless QED

In[1]:=
```
$LoadAddOns = {"FeynHelpers"};
$LoadFeynArts = True;
<< FeynCalc`
$FAVerbose = 0;
```

FeynCalc 9.3.0 (development version). For help, use the documentation center, check out the wiki or write to the mailing list.

See also the supplied examples. If you use FeynCalc in your research, please cite

- V. Shtabovenko, R. Mertig and F. Orellana, Comput. Phys. Commun., 207C, 432–444, 2016, arXiv:1601.01167
- R. Mertig, M. Böhm, and A. Denner, Comput. Phys. Commun., 64, 345–359, 1991.

FeynArts 3.9 patched for use with FeynCalc, for documentation use the manual or visit www.feynarts.de.

FeynHelpers 1.0.0 loaded.

Have a look at the supplied examples. If you use FeynHelpers in your research, please cite

- V. Shtabovenko, "FeynHelpers: Connecting FeynCalc to FIRE and Package–X", TUM–EFT 75/15, arXiv:1611.06793

Furthermore, remember to cite the authors of the tools that you are calling from FeynHelpers, which are

- FIRE by A. Smirnov, if you are using the function FIREBurn.
- Package – *X* by H. Patel, if you are using the function PaXEvaluate.

Vacuum polarization in massless QED at 2-loops

In[5]:=
```
topsPol = CreateTopologies[2, 1 -> 1, ExcludeTopologies -> {Tadpoles}];
diagsVacuumPol =
  InsertFields[topsPol, {V[1]} -> {V[1]}, InsertionLevel -> {Particles},
   ExcludeParticles → {V[2 | 3], S[_], U[_], F[1 | 3 | 4]}];
Paint[DiagramExtract[diagsVacuumPol, {1, 4, 7}], ColumnsXRows → {2, 1},
  SheetHeader -> False,  Numbering -> None, ImageSize -> {512, 256}];
```

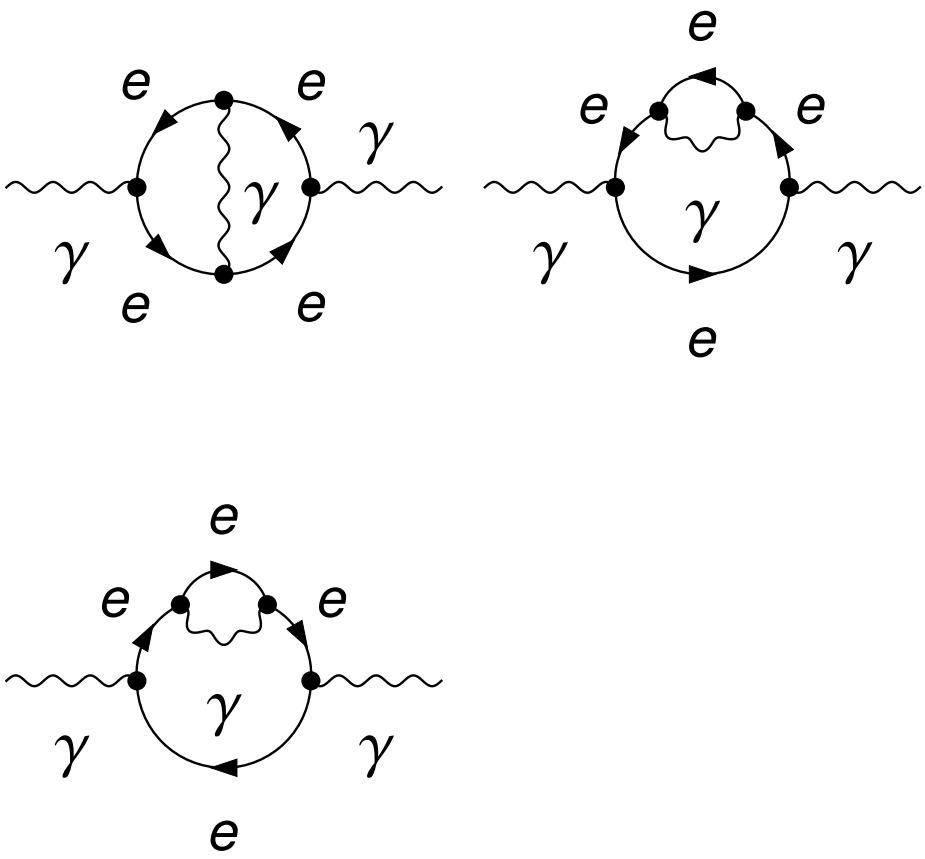

First of all we need to generate the amplitudes and convert them into FeynCalc notation. We choose l1 and l2 to be the loop momenta and p the external momentum

In[8]:=
```
ampsVacuumPol =
 FCFAConvert[CreateFeynAmp[DiagramExtract[diagsVacuumPol, {1, 4, 7}],
       Truncated -> True, PreFactor -> -1, GaugeRules → {}],
  IncomingMomenta -> {p}, OutgoingMomenta -> {p}, LoopMomenta -> {l1, l2},
      DropSumOver → True, ChangeDimension -> D, UndoChiralSplittings -> True,
      List → False, SMP → True, LorentzIndexNames → {μ, ν}] //
    ReplaceAll[#, SMP["m_e"] → 0] & // Contract // FCTraceFactor
```

Out[8]=
$$-\Big(i\, e^4\, \xi_A\, \mathrm{tr}\big((\gamma\cdot(l2-p)).\gamma^\nu.(\gamma\cdot l2).(\gamma\cdot(l1+l2)).(\gamma\cdot l1).\gamma^\mu.(\gamma\cdot(-l1-p)).(\gamma\cdot(-l1-l2))\big)\Big)\Big/ \\ l1^2.l2^2.\big((l1+l2)^2\big)^2.(l2-p)^2.(l1+p)^2 + \\ \Big(2\,i\, e^4\, \xi_A\, \mathrm{tr}\big((\gamma\cdot(l1-p)).\gamma^\nu.(\gamma\cdot l1).\gamma^\mu.(\gamma\cdot(l1-p)).(\gamma\cdot(l1-l2-p)).(\gamma\cdot l2).(\gamma\cdot(-l1+l2+p))\big)\Big)\Big/ \\ l1^2.l2^2.\big((l1-p)^2\big)^2.\big((-l1+l2+p)^2\big)^2 + \\ \Big(i\, e^4\, \mathrm{tr}\big((\gamma\cdot(l2-p)).\gamma^\nu.(\gamma\cdot l2).\gamma^{\mathrm{Lor4}}.(\gamma\cdot l1).\gamma^\mu.(\gamma\cdot(-l1-p)).\gamma^{\mathrm{Lor4}}\big)\Big)\Big/ l1^2.l2^2.(l1+l2)^2.(l2-p)^2.(l1+p)^2 - \\ \Big(2\,i\, e^4\, \mathrm{tr}\big((\gamma\cdot(l1-p)).\gamma^\nu.(\gamma\cdot l1).\gamma^\mu.(\gamma\cdot(l1-p)).\gamma^{\mathrm{Lor4}}.(\gamma\cdot l2).\gamma^{\mathrm{Lor4}}\big)\Big)\Big/ l1^2.l2^2.\big((l1-p)^2\big)^2.(-l1+l2+p)^2 + \\ \Big(i\, e^4\, \mathrm{tr}\big((\gamma\cdot(l2-p)).\gamma^\nu.(\gamma\cdot l2).(\gamma\cdot(l1+l2)).(\gamma\cdot l1).\gamma^\mu.(\gamma\cdot(-l1-p)).(\gamma\cdot(-l1-l2))\big)\Big)\Big/ \\ l1^2.l2^2.\big((l1+l2)^2\big)^2.(l2-p)^2.(l1+p)^2 - \\ \Big(2\,i\, e^4\, \mathrm{tr}\big((\gamma\cdot(l1-p)).\gamma^\nu.(\gamma\cdot l1).\gamma^\mu.(\gamma\cdot(l1-p)).(\gamma\cdot(l1-l2-p)).(\gamma\cdot l2).(\gamma\cdot(-l1+l2+p))\big)\Big)\Big/ \\ l1^2.l2^2.\big((l1-p)^2\big)^2.\big((-l1+l2+p)^2\big)^2$$

Calculation of the Dirac trace and tensor reduction

In[9]:=
```
AbsoluteTiming[ampsVacuumPol1 =
    (ampsVacuumPol /. DiracTrace → Tr) // FCMultiLoopTID[#, {l1, l2}] &] // First
```

Out[9]= 22.6071

Simplification of the loop integrals using shifts in the loop momenta

In[10]:=
```
ampsVacuumPol2 = ampsVacuumPol1 // FDS[#, l1, l2] &;
```

IBP-Reduction using FIRE

In[11]:=
```
ampsVacuumPol3 = FIREBurn[ampsVacuumPol2, {l1, l2}, {p}] // FDS[#, l1, l2] &
```

```
FIREBurn: Processing integral 1 of 13; IBP-reduction done, timing: 2.121
FIREBurn: Processing integral 2 of 13; IBP-reduction done, timing: 1.403
FIREBurn: Processing integral 3 of 13; IBP-reduction done, timing: 1.804
FIREBurn: Processing integral 4 of 13; IBP-reduction done, timing: 1.542
FIREBurn: Processing integral 5 of 13; IBP-reduction done, timing: 1.505
FIREBurn: Processing integral 6 of 13; IBP-reduction done, timing: 2.516
FIREBurn: Processing integral 7 of 13; IBP-reduction done, timing: 1.625
FIREBurn: Processing integral 8 of 13; IBP-reduction done, timing: 1.613
FIREBurn: Processing integral 9 of 13; IBP-reduction done, timing: 1.641
FIREBurn: Processing integral 10 of 13; IBP-reduction done, timing: 1.430
FIREBurn: Processing integral 11 of 13; IBP-reduction done, timing: 1.639
FIREBurn: Processing integral 12 of 13; IBP-reduction done, timing: 1.630
FIREBurn: Processing integral 13 of 13; IBP-reduction done, timing: 1.584
```

Out[11]=
$$-\Big(2\,i\,e^4\,\big(21\,D^4\,p^2\,\xi_A\,g^{\mu\nu}-228\,D^3\,p^2\,\xi_A\,g^{\mu\nu}+879\,D^2\,p^2\,\xi_A\,g^{\mu\nu}-1392\,D\,p^2\,\xi_A\,g^{\mu\nu}+720\,p^2\,\xi_A\,g^{\mu\nu}-15\,D^4\,p^2\,g^{\mu\nu}-14\,D^4\,p^\mu\,p^\nu+134\,D^3\,p^2\,g^{\mu\nu}+182\,D^3\,p^\mu\,p^\nu-431\,D^2\,p^2\,g^{\mu\nu}-784\,D^2\,p^\mu\,p^\nu+568\,D\,p^2\,g^{\mu\nu}+1336\,D\,p^\mu\,p^\nu-208\,p^2\,g^{\mu\nu}-768\,p^\mu\,p^\nu\big)\Big)\Big/\big(3\,(D-4)^2\,(D-1)\,p^2\,l1^2.(l1-l2)^2.(l2-p)^2\big)+\Big(2\,i\,e^4\,\big(21\,D^4\,p^2\,\xi_A\,g^{\mu\nu}-228\,D^3\,p^2\,\xi_A\,g^{\mu\nu}+879\,D^2\,p^2\,\xi_A\,g^{\mu\nu}-1392\,D\,p^2\,\xi_A\,g^{\mu\nu}+720\,p^2\,\xi_A\,g^{\mu\nu}-3\,D^4\,p^2\,g^{\mu\nu}-26\,D^4\,p^\mu\,p^\nu+26\,D^3\,p^2\,g^{\mu\nu}+290\,D^3\,p^\mu\,p^\nu-23\,D^2\,p^2\,g^{\mu\nu}-1192\,D^2\,p^\mu\,p^\nu-200\,D\,p^2\,g^{\mu\nu}+2104\,D\,p^\mu\,p^\nu+368\,p^2\,g^{\mu\nu}-1344\,p^\mu\,p^\nu\big)\Big)\Big/\big(3\,(D-4)^2\,(D-1)\,p^2\,l1^2.(l1-l2)^2.(l2-p)^2\big)+\frac{2\,i\,(D-2)\,\big(D^2-7\,D+16\big)\,e^4\,\big(p^\mu\,p^\nu-p^2\,g^{\mu\nu}\big)}{(D-4)\,(D-1)\,l1^2.l2^2.(l1-p)^2.(l2-p)^2}$$

Nicer form. Notice that the gauge dependence dropped out in the final result, as it should.

In[12]:=
```
ampsVacuumPol4 =
 ampsVacuumPol3 // Collect2[#, {FeynAmpDenominator}, Factoring → Factor2] &
```

Out[12]=
$$\frac{8\,i\,(2-D)\,(3-D)\,\big(D^2-4\,D+8\big)\,e^4\,\big(p^\mu\,p^\nu-p^2\,g^{\mu\nu}\big)}{(1-D)\,(4-D)^2\,p^2\,l1^2.(l1-l2)^2.(l2-p)^2}-\frac{2\,i\,(2-D)\,\big(D^2-7\,D+16\big)\,e^4\,\big(p^\mu\,p^\nu-p^2\,g^{\mu\nu}\big)}{(1-D)\,(4-D)\,l1^2.l2^2.(l1-p)^2.(l2-p)^2}$$

This is $\Pi_2(p^2)$ up to the $\frac{1}{(2\pi)^{2D}}$ prefactor

In[13]:=
```
resVacuumPol =
 Cancel[ampsVacuumPol4 / (-I FCI[(FVD[p, μ] FVD[p, ν] - SPD[p, p] MTD[μ, ν])])] //
  FullSimplify
```

Out[13]=
$$\frac{2\,(D-2)\,e^4\left(\frac{4\,(D-3)\,((D-4)\,D+8)}{l1^2.(l1-l2)^2.(l2-p)^2}-\frac{(D-4)\,((D-7)\,D+16)\,p^2}{l1^2.l2^2.(l1-p)^2.(l2-p)^2}\right)}{(D-4)^2\,(D-1)\,p^2}$$

Check with Eq. 5.18 from Grozin's Lectures on QED and QCD (hep-ph/0508242)

In[14]:=
```
resGrozinVacuumPol = FCI[SMP["e"]^4 2 (D - 2) / ((D - 1) (D - 4))
      (-(D^2 - 7 D + 16) FAD[l1, l2, l1 - p, l2 - p] + 4 (D - 3) (D^2 - 4 D + 8) / (D - 4)
        (1 / SPD[p, p]) FAD[l1, l1 - l2, l2 - p])] // Cancel // FullSimplify
```

Out[14]=
$$\frac{2\,(D-2)\,e^4\left(\frac{4\,(D-3)\,((D-4)\,D+8)}{l1^2.(l1-l2)^2.(l2-p)^2}-\frac{(D-4)\,((D-7)\,D+16)\,p^2}{l1^2.l2^2.(l1-p)^2.(l2-p)^2}\right)}{(D-4)^2\,(D-1)\,p^2}$$

In[15]:=
```
Simplify[resVacuumPol - resGrozinVacuumPol]
```

Out[15]= 0

Electron self-energy in massless QED at 2-loops

In[16]:=
```
topsSE = CreateTopologies[2, 1 -> 1, ExcludeTopologies -> {Tadpoles}];
diagsSE =
  InsertFields[topsSE, {F[2, {1}]} -> {F[2, {1}]}, InsertionLevel -> {Particles},
   ExcludeParticles → {V[2 | 3], S[_], U[_], F[1 | 3 | 4]}];
Paint[DiagramExtract[diagsSE, {1, 2, 5}], ColumnsXRows → {2, 1},
  SheetHeader -> False,  Numbering -> None, ImageSize -> {512, 256}];
```

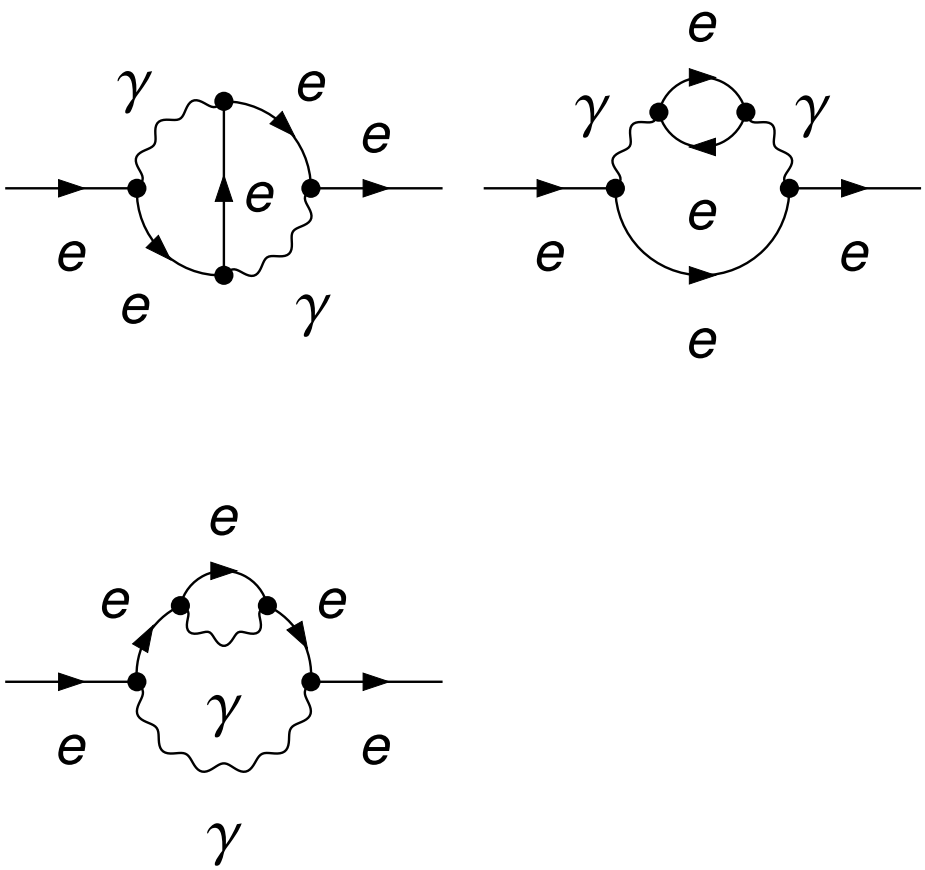

First of all we need to generate the amplitudes and convert them into FeynCalc notation. We choose l1 and l2 to be the loop momenta and p the external momentum

In[19]:=
```
ampsSE =
  FCFAConvert[CreateFeynAmp[DiagramExtract[diagsSE, {1, 2, 5}], Truncated -> True,
      PreFactor -> -1, GaugeRules → {}],
IncomingMomenta -> {p}, OutgoingMomenta -> {p}, LoopMomenta -> {l1, l2},
    DropSumOver → True, ChangeDimension -> D, UndoChiralSplittings -> True,
    List → False, SMP → True, LorentzIndexNames → {μ}] //
   ReplaceAll[#, SMP["m_e"] → 0] & // Contract // FCTraceFactor;
```

Calculation of the Dirac trace, tensor reduction and simplification of the Dirac algebra

In[20]:=
```
AbsoluteTiming[ampsSE1 = (ampsSE /. DiracTrace → Tr) //
    FCMultiLoopTID[#, {l1, l2}] & // DiracSimplify] // First
```

Out[20]= 48.1153

Simplification of the loop integrals using shifts in the loop momenta

In[21]:=
```
ampsSE2 = ampsSE1 // FDS[#, l1, l2] &;
```

IBP-Reduction using FIRE

In[22]:=
```
ampsSE3 = FIREBurn[ampsSE2, {l1, l2}, {p}] // FDS[#, l1, l2] &
```

```
FIREBurn: Processing integral 1 of 27; IBP-reduction done, timing: 1.751
FIREBurn: Processing integral 2 of 27; IBP-reduction done, timing: 1.708
FIREBurn: Processing integral 3 of 27; IBP-reduction done, timing: 3.060
FIREBurn: Processing integral 4 of 27; IBP-reduction done, timing: 1.725
FIREBurn: Processing integral 5 of 27; IBP-reduction done, timing: 1.478
FIREBurn: Processing integral 6 of 27; IBP-reduction done, timing: 1.522
FIREBurn: Processing integral 7 of 27; IBP-reduction done, timing: 1.714
FIREBurn: Processing integral 8 of 27; IBP-reduction done, timing: 1.611
FIREBurn: Processing integral 9 of 27; IBP-reduction done, timing: 1.733
FIREBurn: Processing integral 10 of 27; IBP-reduction done, timing: 1.605
FIREBurn: Processing integral 11 of 27; IBP-reduction done, timing: 1.446
FIREBurn: Processing integral 12 of 27; IBP-reduction done, timing: 1.545
FIREBurn: Processing integral 13 of 27; IBP-reduction done, timing: 1.567
FIREBurn: Processing integral 14 of 27; IBP-reduction done, timing: 1.655
FIREBurn: Processing integral 15 of 27; IBP-reduction done, timing: 1.627
FIREBurn: Processing integral 16 of 27; IBP-reduction done, timing: 1.606
FIREBurn: Processing integral 17 of 27; IBP-reduction done, timing: 1.761
FIREBurn: Processing integral 18 of 27; IBP-reduction done, timing: 1.629
FIREBurn: Processing integral 19 of 27; IBP-reduction done, timing: 1.725
FIREBurn: Processing integral 20 of 27; IBP-reduction done, timing: 1.700
FIREBurn: Processing integral 21 of 27; IBP-reduction done, timing: 1.756
FIREBurn: Processing integral 22 of 27; IBP-reduction done, timing: 2.155
FIREBurn: Processing integral 23 of 27; IBP-reduction done, timing: 1.935
FIREBurn: Processing integral 24 of 27; IBP-reduction done, timing: 2.270
FIREBurn: Processing integral 25 of 27; IBP-reduction done, timing: 1.562
FIREBurn: Processing integral 26 of 27; IBP-reduction done, timing: 1.744
FIREBurn: Processing integral 27 of 27; IBP-reduction done, timing: 1.692
```

Out[22]=
$$-\Big(i\, e^4 \left(4 D^3 \xi_A^2 + D^3 \xi_A - 28 D^2 \xi_A^2 - 13 D^2 \xi_A + 64 D \xi_A^2 + 46 D \xi_A - 48 \xi_A^2 - 48 \xi_A - 2 D^3 + 15 D^2 - 62 D + 96\right) \gamma\cdot p\Big)\Big/ \left(2 (D-4)\, p^2\, l1^2.(l1-l2)^2.(l2-p)^2\right) +$$
$$\Big(i\, e^4 \left(D^4 \xi_A^2 + D^4 \xi_A - 11 D^3 \xi_A^2 - 19 D^3 \xi_A + 36 D^2 \xi_A^2 + 124 D^2 \xi_A - 36 D \xi_A^2 - 324 D \xi_A + 288 \xi_A - D^4 + 16 D^3 - 128 D^2 + 496 D - 656\right) \gamma\cdot p\Big)\Big/ \left(2 (D-6)(D-4)\, p^2\, l1^2.(l1-l2)^2.(l2-p)^2\right) + \frac{i (D-2)\, e^4 \left(D \xi_A^2 - 2 \xi_A^2 + D - 6\right) \gamma\cdot p}{4\, l1^2.l2^2.(l1-p)^2.(l2-p)^2}$$

Nicer form

In[23]:=
```
ampsSE4 = ampsSE3 // Collect2[#, {FeynAmpDenominator}, Factoring → FullSimplify] &
```

Out[23]=
$$\frac{i (D-2)\, e^4 \left((D-2) \xi_A^2 + D - 6\right) \gamma\cdot p}{4\, l1^2.l2^2.(l1-p)^2.(l2-p)^2} -$$
$$\Big(i (D-2)\, e^4 \left((D-6)(D-3)(3D-8) \xi_A^2 - D\left((D-9) D + 6\right) - 40\right) \gamma\cdot p\Big)\Big/\left(2 (D-6)(D-4)\, p^2\, l1^2.(l1-l2)^2.(l2-p)^2\right)$$

This is $\Sigma_{2\,V}(p^2)$ up to the $\frac{1}{(2\pi)^{2D}}$prefactor

In[24]:=
```
resSE = Cancel[ampsSE4 / (-I FCI[(GSD[p])])] // FullSimplify
```

Out[24]=
$$\Bigg((D-2)\, e^4 \Bigg(\left(2\left((D-6)(D-3)(3D-8) \xi_A^2 - D\left((D-9) D + 6\right) - 40\right)\right)\Big/ l1^2.(l1-l2)^2.(l2-p)^2 - \frac{(D-6)(D-4)\, p^2 \left((D-2) \xi_A^2 + D - 6\right)}{l1^2.l2^2.(l1-p)^2.(l2-p)^2}\Bigg)\Bigg)\Big/\left(4 (D-6)(D-4)\, p^2\right)$$

Check with Eq. 5.51 from Grozin's Lectures on QED and QCD (hep-ph/0508242)

In[25]:=
```
resGrozinSE =
 FCI[SMP["e"]^4 (D - 2) ( 2 (D - 2) / (D - 6) (1 / SPD[p, p]) FAD[l1, l1 - l2, l2 - p] -
       1 / 4 ((D - 2) (GaugeXi[A])^2 + D - 6) FAD[l1, l2, l1 - p, l2 - p]
       + (1 / 2) (D - 3) / (D - 4) ((3 D - 8) (GaugeXi[A])^2 - D - 4) (1 / SPD[p, p])
        FAD[l1, l1 - l2, l2 - p])] // Cancel // FullSimplify
```

Out[25]=
$$-\left(\left((D-2)\,\mathrm{e}^4\left(\frac{(D-6)\,(D-4)\,p^2\left((D-2)\,\xi_A^2+D-6\right)}{\mathrm{l1}^2.\mathrm{l2}^2.(\mathrm{l1}-p)^2.(\mathrm{l2}-p)^2}+\left(2\left(-(D-6)\,(D-3)\,(3\,D-8)\,\xi_A^2+D\left((D-9)\,D+6\right)+40\right)\right)\Big/\right.\right.\right.$$
$$\left.\left.\left.\mathrm{l1}^2.(\mathrm{l1}-\mathrm{l2})^2.(\mathrm{l2}-p)^2\right)\right)\Big/\left(4\,(D-6)\,(D-4)\,p^2\right)\right)$$

In[26]:=
```
Simplify[resSE - resGrozinSE]
```

Out[26]= 0

I Source Codes for Example Calculations using FeynCalc and FeynOnium

I.1 Exclusive Electromagnetic Decay $J/\psi \to 3\gamma$ at $\mathcal{O}(\alpha_s^0 v^0)$

Tree-level matching between QCD and NRQCD for QQbar -> 3 gamma

Load FeynCalc, FeynArts and FeynOnium

In[1]:=
```
$LoadAddOns = {"FeynOnium"};
$LoadFeynArts = True;
<< FeynCalc`
$FAVerbose = 0;
```

FeynCalc 9.3.0 (development version). For help, use the documentation center, check out the wiki or write to the mailing list.

See also the supplied examples. If you use FeynCalc in your research, please cite

- V. Shtabovenko, R. Mertig and F. Orellana, Comput. Phys. Commun., 207C, 432–444, 2016, arXiv:1601.01167
- R. Mertig, M. Böhm, and A. Denner, Comput. Phys. Commun., 64, 345–359, 1991.

FeynArts 3.9 patched for use with FeynCalc, for documentation use the manual or visit www.feynarts.de.

FeynOnium 0.5.0 loaded.

Have a look at the supplied examples. If you use FeynOnium in your research, please cite

- N. Brambilla, V. Shtabovenko and A.Vairo, TUM–EFT 92/17, in preparation

Generate Feynman diagrams

In[5]:=
```
diags=InsertFields[CreateTopologies[0,2->3],{F[3,{2}],
-F[3,{2}]}->{V[1],V[1],V[1]},InsertionLevel->{Classes},Model->"SMQCD"];
Paint[diags,ColumnsXRows->{3,2},Numbering->None,
SheetHeader->False,ImageSize->{512,256}];
```

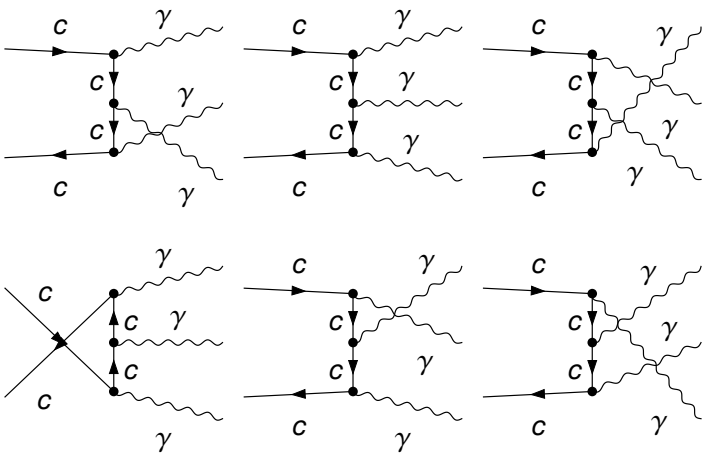

In[7]:=
```
ampsRaw=((3/2)^3 SMP["e_Q"]^3*FCFAConvert[CreateFeynAmp[diags,
Truncated->False,PreFactor->-1],IncomingMomenta->{p1,p2},
OutgoingMomenta->{k1,k2,k3},UndoChiralSplittings->True,List->False,
TransversePolarizationVectors->{k1,k2,k3},ChangeDimension->4,
List->True,SMP->True,DropSumOver->True,
FinalSubstitutions->{SMP["m_c"]->SMP["m_Q"],SUNFDelta[__]:>1}])//Contract
```

Out[7]=
$$\frac{27}{8} e_Q^3 \Big(\Big(8 i e^3 \Big(\varphi\big(-\overline{\text{p2}}, m_Q\big)\Big).(\overline{\gamma}\cdot\overline{\varepsilon^*}(\text{k1})).\Big(\overline{\gamma}\cdot\Big(\overline{\text{k1}}-\overline{\text{p2}}\Big)+m_Q\Big).(\overline{\gamma}\cdot\overline{\varepsilon^*}(\text{k2})).\Big(\overline{\gamma}\cdot\Big(\overline{\text{k1}}+\overline{\text{k2}}-\overline{\text{p2}}\Big)+m_Q\Big).(\overline{\gamma}\cdot\overline{\varepsilon^*}(\text{k3})).\Big(\varphi\big(\overline{\text{p1}}, m_Q\big)\Big)\Big)\Big/\big(27\,((\text{p2}-\text{k1})^2-m_Q^2)\,((-\text{k1}-\text{k2}+\text{p2})^2-m_Q^2)\big) + \Big(8 i e^3 \Big(\varphi\big(-\overline{\text{p2}}, m_Q\big)\Big).(\overline{\gamma}\cdot\overline{\varepsilon^*}(\text{k2})).\Big(\overline{\gamma}\cdot\Big(\overline{\text{k2}}-\overline{\text{p2}}\Big)+m_Q\Big).(\overline{\gamma}\cdot\overline{\varepsilon^*}(\text{k1})).\Big(\overline{\gamma}\cdot\Big(\overline{\text{k1}}+\overline{\text{k2}}-\overline{\text{p2}}\Big)+m_Q\Big).(\overline{\gamma}\cdot\overline{\varepsilon^*}(\text{k3})).\Big(\varphi\big(\overline{\text{p1}}, m_Q\big)\Big)\Big)\Big/\big(27\,((\text{p2}-\text{k2})^2-m_Q^2)\,((-\text{k1}-\text{k2}+\text{p2})^2-m_Q^2)\big) + \Big(8 i e^3 \Big(\varphi\big(-\overline{\text{p2}}, m_Q\big)\Big).(\overline{\gamma}\cdot\overline{\varepsilon^*}(\text{k1})).\Big(\overline{\gamma}\cdot\Big(\overline{\text{k1}}-\overline{\text{p2}}\Big)+m_Q\Big).(\overline{\gamma}\cdot\overline{\varepsilon^*}(\text{k3})).\Big(\overline{\gamma}\cdot\Big(\overline{\text{k1}}+\overline{\text{k3}}-\overline{\text{p2}}\Big)+m_Q\Big).(\overline{\gamma}\cdot\overline{\varepsilon^*}(\text{k2})).\Big(\varphi\big(\overline{\text{p1}}, m_Q\big)\Big)\Big)\Big/\big(27\,((\text{p2}-\text{k1})^2-m_Q^2)\,((-\text{k1}-\text{k3}+\text{p2})^2-m_Q^2)\big) + \Big(8 i e^3 \Big(\varphi\big(-\overline{\text{p2}}, m_Q\big)\Big).(\overline{\gamma}\cdot\overline{\varepsilon^*}(\text{k3})).\Big(\overline{\gamma}\cdot\Big(\overline{\text{k3}}-\overline{\text{p2}}\Big)+m_Q\Big).(\overline{\gamma}\cdot\overline{\varepsilon^*}(\text{k1})).\Big(\overline{\gamma}\cdot\Big(\overline{\text{k1}}+\overline{\text{k3}}-\overline{\text{p2}}\Big)+m_Q\Big).(\overline{\gamma}\cdot\overline{\varepsilon^*}(\text{k2})).\Big(\varphi\big(\overline{\text{p1}}, m_Q\big)\Big)\Big)\Big/\big(27\,((\text{p2}-\text{k3})^2-m_Q^2)\,((-\text{k1}-\text{k3}+\text{p2})^2-m_Q^2)\big) + \Big(8 i e^3 \Big(\varphi\big(-\overline{\text{p2}}, m_Q\big)\Big).(\overline{\gamma}\cdot\overline{\varepsilon^*}(\text{k2})).\Big(\overline{\gamma}\cdot\Big(\overline{\text{k2}}-\overline{\text{p2}}\Big)+m_Q\Big).(\overline{\gamma}\cdot\overline{\varepsilon^*}(\text{k3})).\Big(\overline{\gamma}\cdot\Big(\overline{\text{k2}}+\overline{\text{k3}}-\overline{\text{p2}}\Big)+m_Q\Big).(\overline{\gamma}\cdot\overline{\varepsilon^*}(\text{k1})).\Big(\varphi\big(\overline{\text{p1}}, m_Q\big)\Big)\Big)\Big/\big(27\,((\text{p2}-\text{k2})^2-m_Q^2)\,((-\text{k2}-\text{k3}+\text{p2})^2-m_Q^2)\big) + \Big(8 i e^3 \Big(\varphi\big(-\overline{\text{p2}}, m_Q\big)\Big).(\overline{\gamma}\cdot\overline{\varepsilon^*}(\text{k3})).\Big(\overline{\gamma}\cdot\Big(\overline{\text{k3}}-\overline{\text{p2}}\Big)+m_Q\Big).(\overline{\gamma}\cdot\overline{\varepsilon^*}(\text{k2})).\Big(\overline{\gamma}\cdot\Big(\overline{\text{k2}}+\overline{\text{k3}}-\overline{\text{p2}}\Big)+m_Q\Big).(\overline{\gamma}\cdot\overline{\varepsilon^*}(\text{k1})).\Big(\varphi\big(\overline{\text{p1}}, m_Q\big)\Big)\Big)\Big/\big(27\,((\text{p2}-\text{k3})^2-m_Q^2)\,((-\text{k2}-\text{k3}+\text{p2})^2-m_Q^2)\big)\Big)$$

Eliminate k3 using momentum conservation

In[8]:=
```
amps=(MomentumExpand[ampsRaw]/.Momentum[k3]->Momentum[p1+p2-k1-k2])//
MomentumExpand
```

Out[8]=
$$\frac{27}{8} e_Q^3 \Big(\Big(8 i e^3 \Big(\varphi\big(-\overline{\text{p2}}, m_Q\big)\Big).(\overline{\gamma}\cdot\overline{\varepsilon^*}(\text{k3})).\Big(-\Big(\overline{\gamma}\cdot\overline{\text{k1}}\Big)-\overline{\gamma}\cdot\overline{\text{k2}}+\overline{\gamma}\cdot\overline{\text{p1}}+m_Q\Big).(\overline{\gamma}\cdot\overline{\varepsilon^*}(\text{k2})).\Big(-\Big(\overline{\gamma}\cdot\overline{\text{k1}}\Big)+\overline{\gamma}\cdot\overline{\text{p1}}+m_Q\Big).(\overline{\gamma}\cdot\overline{\varepsilon^*}(\text{k1})).\Big(\varphi\big(\overline{\text{p1}}, m_Q\big)\Big)\Big)\Big/\big(27\,((\text{k1}-\text{p1})^2-m_Q^2)\,((\text{k1}+\text{k2}-\text{p1})^2-m_Q^2)\big) + \Big(8 i e^3 \Big(\varphi\big(-\overline{\text{p2}}, m_Q\big)\Big).(\overline{\gamma}\cdot\overline{\varepsilon^*}(\text{k3})).\Big(-\Big(\overline{\gamma}\cdot\overline{\text{k1}}\Big)-\overline{\gamma}\cdot\overline{\text{k2}}+\overline{\gamma}\cdot\overline{\text{p1}}+m_Q\Big).(\overline{\gamma}\cdot\overline{\varepsilon^*}(\text{k1})).\Big(-\Big(\overline{\gamma}\cdot\overline{\text{k2}}\Big)+\overline{\gamma}\cdot\overline{\text{p1}}+m_Q\Big).(\overline{\gamma}\cdot\overline{\varepsilon^*}(\text{k2})).\Big(\varphi\big(\overline{\text{p1}}, m_Q\big)\Big)\Big)\Big/\big(27\,((\text{k2}-\text{p1})^2-m_Q^2)\,((\text{k1}+\text{k2}-\text{p1})^2-m_Q^2)\big) + \Big(8 i e^3 \Big(\varphi\big(-\overline{\text{p2}}, m_Q\big)\Big).(\overline{\gamma}\cdot\overline{\varepsilon^*}(\text{k1})).\Big(\overline{\gamma}\cdot\overline{\text{k1}}-\overline{\gamma}\cdot\overline{\text{p2}}+m_Q\Big).(\overline{\gamma}\cdot\overline{\varepsilon^*}(\text{k3})).\Big(-\Big(\overline{\gamma}\cdot\overline{\text{k2}}\Big)+\overline{\gamma}\cdot\overline{\text{p1}}+m_Q\Big).(\overline{\gamma}\cdot\overline{\varepsilon^*}(\text{k2})).\Big(\varphi\big(\overline{\text{p1}}, m_Q\big)\Big)\Big)\Big/\big(27\,((\text{p2}-\text{k1})^2-m_Q^2)\,((\text{k2}-\text{p1})^2-m_Q^2)\big) + \Big(8 i e^3 \Big(\varphi\big(-\overline{\text{p2}}, m_Q\big)\Big).(\overline{\gamma}\cdot\overline{\varepsilon^*}(\text{k2})).\Big(\overline{\gamma}\cdot\overline{\text{k2}}-\overline{\gamma}\cdot\overline{\text{p2}}+m_Q\Big).(\overline{\gamma}\cdot\overline{\varepsilon^*}(\text{k3})).\Big(-\Big(\overline{\gamma}\cdot\overline{\text{k1}}\Big)+\overline{\gamma}\cdot\overline{\text{p1}}+m_Q\Big).(\overline{\gamma}\cdot\overline{\varepsilon^*}(\text{k1})).\Big(\varphi\big(\overline{\text{p1}}, m_Q\big)\Big)\Big)\Big/\big(27\,((\text{k1}-\text{p1})^2-m_Q^2)\,((\text{p2}-\text{k2})^2-m_Q^2)\big) + \Big(8 i e^3 \Big(\varphi\big(-\overline{\text{p2}}, m_Q\big)\Big).(\overline{\gamma}\cdot\overline{\varepsilon^*}(\text{k1})).\Big(\overline{\gamma}\cdot\overline{\text{k1}}-\overline{\gamma}\cdot\overline{\text{p2}}+m_Q\Big).(\overline{\gamma}\cdot\overline{\varepsilon^*}(\text{k2})).\Big(\overline{\gamma}\cdot\overline{\text{k1}}+\overline{\gamma}\cdot\overline{\text{k2}}-\overline{\gamma}\cdot\overline{\text{p2}}+m_Q\Big).(\overline{\gamma}\cdot\overline{\varepsilon^*}(\text{k3})).\Big(\varphi\big(\overline{\text{p1}}, m_Q\big)\Big)\Big)\Big/\big(27\,((\text{p2}-\text{k1})^2-m_Q^2)\,((-\text{k1}-\text{k2}+\text{p2})^2-m_Q^2)\big) + \Big(8 i e^3 \Big(\varphi\big(-\overline{\text{p2}}, m_Q\big)\Big).(\overline{\gamma}\cdot\overline{\varepsilon^*}(\text{k2})).\Big(\overline{\gamma}\cdot\overline{\text{k2}}-\overline{\gamma}\cdot\overline{\text{p2}}+m_Q\Big).(\overline{\gamma}\cdot\overline{\varepsilon^*}(\text{k1})).\Big(\overline{\gamma}\cdot\overline{\text{k1}}+\overline{\gamma}\cdot\overline{\text{k2}}-\overline{\gamma}\cdot\overline{\text{p2}}+m_Q\Big).(\overline{\gamma}\cdot\overline{\varepsilon^*}(\text{k3})).\Big(\varphi\big(\overline{\text{p1}}, m_Q\big)\Big)\Big)\Big/\big(27\,((\text{p2}-\text{k2})^2-m_Q^2)\,((-\text{k1}-\text{k2}+\text{p2})^2-m_Q^2)\big)\Big)$$

On-shell kinematics

In[9]:=
```
QMass=SMP["m_Q"];
QCharge=SMP["e_Q"];
```

In[11]:=
```
FCClearScalarProducts[];
SP[k1, k1] = 0;
SP[k2, k2] = 0;
SP[k3, k3] = 0;
SP[p1, p1] = QMass^2;
SP[p2, p2] = QMass^2;
```

In[17]:=
```
TemporalMomentum[Polarization[k1|k2|k3,___]]=0;
TC[q]=0;
TC[p1]=Eq;
TC[p2]=Eq;
TC[k1]=k1abs;
TC[k2]=k2abs;
TC[k3]=k3abs;
TC[aux]=1;
CSP[k1hat,Polarization[k1,-I]]=0;
CSP[k2hat,Polarization[k2,-I]]=0;
CSP[k3hat,Polarization[k3,-I]]=0;
CSP[k1hat,k1hat]=1;
CSP[k2hat,k2hat]=1;
CSP[k3hat,k3hat]=1;
CSP[k1hat,k2hat]=1/(k1abs k2abs) (2 Eq^2-2  Eq (k1abs+k2abs)+ k1abs*k2abs);
CartesianMomentum[k1]:=k1abs CartesianMomentum[k1hat];
CartesianMomentum[k2]:=k2abs CartesianMomentum[k2hat];
CartesianMomentum[k3]:=k3abs CartesianMomentum[k3hat];
CartesianMomentum[p1]:=qabs CartesianMomentum[qhat];
CartesianMomentum[p2]:=-qabs CartesianMomentum[qhat];
CartesianMomentum[q]:=qabs CartesianMomentum[qhat];
CartesianMomentum[aux]=0;

Eq=Series[Sqrt[qabs^2+QMass^2],{qabs,0,0}]//Normal//PowerExpand;
k1abs=Eq x1;
k2abs=Eq x2;
```

Calculation of the total decay rate in QCD

Simplify the Dirac algebra, rewrite Dirac chains in terms of Pauli chains and decompose all 4 - vectors into temporal components and 3 - vectors

In[42]:=
```
amps2=amps//DiracSimplify//
FMSpinorChainExplicit2[#,FMSpinorNormalization->"nonrelativistic"]&//
Contract//PropagatorDenominatorExplicit//LorentzToCartesian;
```

Expand in qabs up to 0th order

In[43]:=
```
amps3=amps2//EpsEvaluate//ExpandScalarProduct//DotSimplify//
Series[#,{qabs,0,0}]&//Normal;
```

Extract the spin triplet contribution

In[44]:=
```
ampST=Collect2[SelectNotFree2[amps3,PauliSigma],
PauliSigma,Polarization,FCFactorOut->QCharge^3]//
ReplaceAll[#,{PauliEta[-I].PauliSigma[x_].PauliXi[I]:>
CartesianPair[CartesianMomentum[ST],x],
PauliXi[-I].PauliSigma[x_].PauliEta[I]:>
CartesianPair[CartesianMomentum[STcc],x]}]&;
```

Compute amplitude squared

In[45]:=
```
ampSTSquared1=(ComplexConjugate[ampST/.ST->STcc] ampST);
```

Sum over polarizations of the photons

In[46]:=
```
ampSTSquared2=ampSTSquared1//DoPolarizationSums[#,k1,aux]&//
DoPolarizationSums[#,k2,aux]&//
DoPolarizationSums[#,k3,aux]&//LorentzToCartesian//Collect2[#,{ST,STcc}]&;
```

Eliminate k3hat

In[47]:=
```
ampSTSquared3=ampSTSquared2//
Uncontract[#,k3hat,CartesianPair->All]&//
ReplaceRepeated[#,{CartesianMomentum[k3hat]:>
-k1abs/k3abs CartesianMomentum[k1hat]-
k2abs/k3abs CartesianMomentum[k2hat],k3abs->2Eq-k1abs-k2abs}]&//
ExpandScalarProduct//Contract//Collect2[#,k1hat,k2hat]&
```

Out[47]=
$$-\frac{4\,e^6\,e_Q^6\,(x1+x2-1)^2\left(\overline{\mathbf{k1hat}}\cdot\overline{\mathbf{STcc}}\right)\left(\overline{\mathbf{k2hat}}\cdot\overline{\mathbf{ST}}\right)}{x1\,x2\,m_Q^4\,(x1+x2-2)^2}-\frac{4\,e^6\,e_Q^6\,(x1+x2-1)^2\left(\overline{\mathbf{k1hat}}\cdot\overline{\mathbf{ST}}\right)\left(\overline{\mathbf{k2hat}}\cdot\overline{\mathbf{STcc}}\right)}{x1\,x2\,m_Q^4\,(x1+x2-2)^2}-$$
$$\left(4\,e^6\,e_Q^6\left(2\,x1^2+2\,x1\,x2-4\,x1+x2^2-2\,x2+2\right)\left(\overline{\mathbf{k1hat}}\cdot\overline{\mathbf{ST}}\right)\left(\overline{\mathbf{k1hat}}\cdot\overline{\mathbf{STcc}}\right)\right)\Big/\left(x2^2\,m_Q^4\,(x1+x2-2)^2\right)-$$
$$\left(4\,e^6\,e_Q^6\left(x1^2+2\,x1\,x2-2\,x1+2\,x2^2-4\,x2+2\right)\left(\overline{\mathbf{k2hat}}\cdot\overline{\mathbf{ST}}\right)\left(\overline{\mathbf{k2hat}}\cdot\overline{\mathbf{STcc}}\right)\right)\Big/\left(x1^2\,m_Q^4\,(x1+x2-2)^2\right)+$$
$$\Big(8\,e^6\,e_Q^6\left(x1^4+2\,x1^3\,x2-4\,x1^3+3\,x1^2\,x2^2-9\,x1^2\,x2+7\,x1^2+2\,x1\,x2^3-9\,x1\,x2^2+$$
$$13\,x1\,x2-6\,x1+x2^4-4\,x2^3+7\,x2^2-6\,x2+2\right)\left(\overline{\mathbf{ST}}\cdot\overline{\mathbf{STcc}}\right)\Big)\Big/\left(x1^2\,x2^2\,m_Q^4\,(x1+x2-2)^2\right)$$

Average over k1hat and k2hat (corresponds to the angular integration)

In[48]:=
```
ampSTSquared4=FMCartesianTensorDecomposition[ampSTSquared3,
{k1hat,k2hat},0]//Simplify
```

Out[48]=
$$\Big(16\,e^6\,e_Q^6\left(x1^4+2\,x1^3\,(x2-2)+x1^2\left(3\,x2^2-9\,x2+7\right)+x1\left(2\,x2^3-9\,x2^2+13\,x2-6\right)+(x2-1)^2\left(x2^2-2\,x2+2\right)\right)$$
$$\left(\overline{\mathbf{ST}}\cdot\overline{\mathbf{STcc}}\right)\Big)\Big/\left(3\,x1^2\,x2^2\,m_Q^4\,(x1+x2-2)^2\right)$$

Obtain the total decay rate

In[49]:=
```
QCDDecayRate=ReplaceRepeated[QMass^2/(192 Pi^3) ampSTSquared4,{SMP["e"]->
2 Sqrt[Pi SMP["alpha_fs"]]},
(x1^4+2 x1^3 (-2+x2)+(-1+x2)^2 (2-2 x2+x2^2)+x1^2 (7-9 x2+3 x2^2)+
x1 (-6+13 x2-9 x2^2+2 x2^3))/(x1^2 x2^2 (-2+x1+x2)^2)->1/2(Pi^2-9)}]
```

Out[49]=
$$\frac{8\left(\pi^2-9\right)\alpha^3\, e_Q^6\left(\overline{\mathbf{ST}}\cdot\overline{\mathbf{STcc}}\right)}{9\, m_Q^2}$$

FYI: This is how the integral over x1 and x2 is calculated

In[50]:=
```
(*tmp=Integrate[(x1^4+2 x1^3 (-2+x2)+(-1+x2)^2 (2-2 x2+x2^2)+x1^2 (7-
9 x2+3 x2^2)+x1 (-6+13 x2-9 x2^2+2 x2^3))/(x1^2 x2^2 (-2+x1+x2)^2),
{x2,1-x1,1}]
Integrate[Normal[tmp],{x1,0,1}]*)
```

Matching between QCD and NRQCD

The total decay rate in NRQCD at leading order in velocity is simply

In[51]:=
```
NRQCDDecayRate= 2ImFem3S1/QMass^2FCI[ CSP[ST,STcc]]
```

Out[51]=
$$\frac{2\,\mathrm{ImFem3S1}\left(\overline{\mathbf{ST}}\cdot\overline{\mathbf{STcc}}\right)}{m_Q^2}$$

Equating the two decay rates we can read off the value of the matching coefficient

In[52]:=
```
matchingCoeff[ImFem3S1]=Solve[QCDDecayRate==NRQCDDecayRate,{ImFem3S1}]//
Flatten
```

Out[52]=
$$\left\{\mathrm{ImFem3S1}\to\frac{4}{9}\left(\pi^2-9\right)\alpha^3\, e_Q^6\right\}$$

So that our final NRQCD factorized decay rate is given by

In[53]:=
```
NRQCDDecayRateFinal=NRQCDDecayRate/.matchingCoeff[ImFem3S1]
```

Out[53]=
$$\frac{8\left(\pi^2-9\right)\alpha^3\, e_Q^6\left(\overline{\mathbf{ST}}\cdot\overline{\mathbf{STcc}}\right)}{9\, m_Q^2}$$

Check with the literature

In[54]:=
```
resLit=(8 (-9+π^2) CSP[ST,STcc] SMP["alpha_fs"]^3 SMP["e_Q"]^6)/
(9 SMP["m_Q"]^2);
Print["Check with Eq.1 in arXiv:1210.6337: ",
            If[FCI[resLit]-NRQCDDecayRateFinal===0,
            "CORRECT.", "!!! WRONG !!!"]];
```

Check with Eq.1 in arXiv:1210.6337: CORRECT.

I.2 Exclusive Electromagnetic Decays $\eta_c \to 2\gamma$ and $\chi_{cJ} \to 2\gamma$ at $\mathcal{O}(\alpha_s^0 v^4)$

Tree-level matching between QCD and NRQCD for QQbar -> 2 gamma

Load FeynCalc, FeynArts and FeynOnium

In[1]:=
```
$LoadAddOns={"FeynOnium"};
$LoadFeynArts = True;
<<FeynCalc`
$FAVerbose=0;
```

FeynCalc 9.3.0 (development version). For help, use the documentation center, check out the wiki or write to the mailing list.

See also the supplied examples. If you use FeynCalc in your research, please cite

- V. Shtabovenko, R. Mertig and F. Orellana, Comput. Phys. Commun., 207C, 432–444, 2016, arXiv:1601.01167
- R. Mertig, M. Böhm, and A. Denner, Comput. Phys. Commun., 64, 345–359, 1991.

FeynArts 3.9 patched for use with FeynCalc, for documentation use the manual or visit www.feynarts.de.

FeynOnium 0.5.0 loaded.

Have a look at the supplied examples. If you use FeynOnium in your research, please cite

- N. Brambilla, V. Shtabovenko and A.Vairo, TUM–EFT 92/17, in preparation

Generate Feynman diagrams

In[5]:=
```
diags=InsertFields[CreateTopologies[0,2->2],{F[3,{2,col1}],
    -F[3,{2,col2}]}->{V[1],V[1]},InsertionLevel->{Classes}];
Paint[diags,ColumnsXRows->{2,1},Numbering->None,SheetHeader->False,
ImageSize->{512,256}];
```

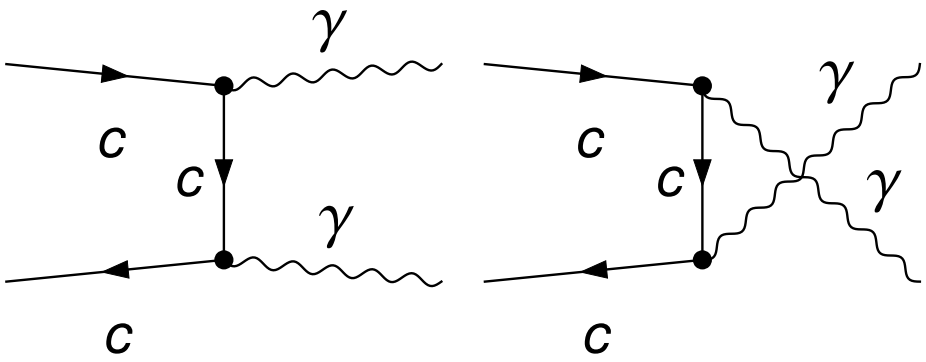

In[7]:=
```
amps=((3/2)^2SMP["e_Q"]^2*FCFAConvert[CreateFeynAmp[diags,Truncated->False,
PreFactor->-1],IncomingMomenta->{p1,p2},OutgoingMomenta->{k1,k2},
UndoChiralSplittings->True,List->False,
TransversePolarizationVectors->{k1,k2},
ChangeDimension->4,List->True,SMP->True,
FinalSubstitutions->{SMP["m_c"]->SMP["m_Q"],
SUNFDelta[__]:>1}])//Contract
```

Out[7]=
$$\frac{9}{4} e_Q^2 \left(\left(4\, i\, e^2 \left(\varphi\left(-\overline{p2}, m_Q\right)\right).\left(\overline{\gamma}\cdot\overline{\varepsilon^*}(k1)\right).\left(\overline{\gamma}\cdot\left(\overline{k1}-\overline{p2}\right)+m_Q\right).\left(\overline{\gamma}\cdot\overline{\varepsilon^*}(k2)\right).\left(\varphi\left(\overline{p1}, m_Q\right)\right)\right)\Big/\left(9\left((p2-k1)^2-m_Q^2\right)\right)+\left(4\, i\, e^2 \left(\varphi\left(-\overline{p2}, m_Q\right)\right).\left(\overline{\gamma}\cdot\overline{\varepsilon^*}(k2)\right).\left(\overline{\gamma}\cdot\left(\overline{k2}-\overline{p2}\right)+m_Q\right).\left(\overline{\gamma}\cdot\overline{\varepsilon^*}(k1)\right).\left(\varphi\left(\overline{p1}, m_Q\right)\right)\right)\Big/\left(9\left((p2-k2)^2-m_Q^2\right)\right)\right)$$

On-shell kinematics

In[8]:=
```
QMass=SMP["m_Q"];
QCharge=SMP["e_Q"];
```

In[10]:=
```
FCClearScalarProducts[];
SP[k1, k1] = 0;
SP[k2, k2] = 0;
SP[p1, p1] = QMass^2;
SP[p2, p2] = QMass^2;
```

In[15]:=
```
TemporalMomentum[Polarization[k1|k2,___]]=0;
TC[q]=0;
TC[p1]=Eq;
TC[p2]=Eq;
TC[k1]=kabs;
TC[k2]=kabs;
CSP[khat,Polarization[k1,-I,Transversality->True]]=0;
CSP[khat,Polarization[k2,-I,Transversality->True]]=0;
CSP[khat,khat]=1;
CSP[qhat,qhat]=1;
CSP[qhatp,qhatp]=1;
CartesianMomentum[k1]:=kabs CartesianMomentum[khat];
CartesianMomentum[k2]:=-kabs CartesianMomentum[khat];
CartesianMomentum[p1]:=qabs CartesianMomentum[qhat];
CartesianMomentum[p2]:=-qabs CartesianMomentum[qhat];
CartesianMomentum[q]:=qabs CartesianMomentum[qhat];
CartesianMomentum[qp]:=qabs CartesianMomentum[qhatp];
CartesianMomentum[aux]=0;
Eq=Series[Sqrt[qabs^2+QMass^2],{qabs,0,4}]//Normal//PowerExpand;
kabs=Eq;
```

Evaluation of the QCD amplitude, nonrelativistic normalization

Simplify the Dirac algebra, rewrite Dirac chains in terms of Pauli chains and decompose all 4 - vectors into temporal components and 3-vectors

In[35]:=
```
AbsoluteTiming[amps2=amps//DiracSimplify//FMSpinorChainExplicit2[#,
    FMSpinorNormalization->"nonrelativistic"]&//Contract//
    PropagatorDenominatorExplicit//LorentzToCartesian;]//First
```

Out[35]= 0.802219

Expand in qabs up to 4th order

In[36]:=
```
AbsoluteTiming[amps3=amps2//EpsEvaluate//ExpandScalarProduct//
    DotSimplify//Series[#,{qabs,0,4}]&//Normal;]//First
```

Out[36]= 0.085773

Prepare the amplitude for angular projections

In[37]:=
```
AbsoluteTiming[amps4=amps3//ReplaceAll[#,
PauliEta[-I].PauliSigma[x_].PauliXi[I]:>
    CartesianPair[CartesianMomentum[ST],x]]&//Collect2[#,
    {ST,PauliXi,PauliEta,qhat}]&;]//First
```

Out[37]= 0.017054

Project out J=0,1,2 contributions

In[38]:=
```
ampQCDJ0=FMCartesianTensorDecomposition[amps4,{qhat,ST},0]//
Collect2[#,qhat,ST,qabs]&;
ampQCDJ1=FMCartesianTensorDecomposition[amps4,{qhat,ST},1]//
Collect2[#,qhat,ST,qabs]&;
ampQCDJ2tmp=FMCartesianTensorDecomposition[amps4,{qhat,ST},2]//
Collect2[#,qhat,ST,qabs]&;
```

As expected, there is no J = 1 contribution

In[41]:=
```
ampQCDJ1===0
```

Out[41]= True

The J = 2 contribution can be further simplified using Schouten identity in 3 dimensions

In[42]:=
```
ampQCDJ2=FixedPoint[FMCartesianSchoutenBruteForce[#,{khat,khat,
qhat,qhat,Polarization[k1,-I,Transversality->True],
Polarization[k2,-I,Transversality->True]},FCVerbose->-1]&,ampQCDJ2tmp];
```

Final QCD amplitudes for matching

In[43]:=
```
ampQCDJ0
ampQCDJ1
ampQCDJ2
```

Out[43]=
$$-\frac{e^2\, e_Q^2\, \eta^\dagger.\xi\, \bar{\epsilon}^{\overline{\text{khat}}\,\bar{\varepsilon}^*(k1)\,\bar{\varepsilon}^*(k2)}}{m_Q} - \frac{8\, e^2\, \text{qabs}^4\, e_Q^2\, \eta^\dagger.\xi\, \bar{\epsilon}^{\overline{\text{khat}}\,\bar{\varepsilon}^*(k1)\,\bar{\varepsilon}^*(k2)}}{15\, m_Q^5} + \frac{2\, e^2\, \text{qabs}^2\, e_Q^2\, \eta^\dagger.\xi\, \bar{\epsilon}^{\overline{\text{khat}}\,\bar{\varepsilon}^*(k1)\,\bar{\varepsilon}^*(k2)}}{3\, m_Q^3} +$$
$$\frac{7\, i\, e^2\, \text{qabs}^3\, e_Q^2 \left(\overline{\mathbf{qhat}}\cdot\overline{\mathbf{ST}}\right)\left(\bar{\varepsilon}^*(k1)\cdot\bar{\varepsilon}^*(k2)\right)}{6\, m_Q^4} - \frac{i\, e^2\, \text{qabs}\, e_Q^2 \left(\overline{\mathbf{qhat}}\cdot\overline{\mathbf{ST}}\right)\left(\bar{\varepsilon}^*(k1)\cdot\bar{\varepsilon}^*(k2)\right)}{m_Q^2}$$

Out[44]=
$$0$$

Out[45]=
$$\frac{8\, e^2\, \text{qabs}^4\, e_Q^2\, \eta^\dagger.\xi\, (\overline{\mathbf{khat}}\cdot\overline{\mathbf{qhat}})^2\, \bar{\epsilon}^{\overline{\text{khat}}\,\bar{\varepsilon}^*(k1)\,\bar{\varepsilon}^*(k2)}}{7\, m_Q^5} - \frac{1}{42\, m_Q^4}$$
$$17\, i\, e^2\, \text{qabs}^3\, e_Q^2 \left(\overline{\mathbf{qhat}}\cdot\overline{\mathbf{ST}}\right)\left(\bar{\varepsilon}^*(k1)\cdot\bar{\varepsilon}^*(k2)\right)(\overline{\mathbf{khat}}\cdot\overline{\mathbf{qhat}})^2 - \frac{e^2\, \text{qabs}^2\, e_Q^2\, \eta^\dagger.\xi\, (\overline{\mathbf{khat}}\cdot\overline{\mathbf{qhat}})^2\, \bar{\epsilon}^{\overline{\text{khat}}\,\bar{\varepsilon}^*(k1)\,\bar{\varepsilon}^*(k2)}}{m_Q^3} -$$
$$\frac{8\, e^2\, \text{qabs}^4\, e_Q^2\, \eta^\dagger.\xi\, \bar{\epsilon}^{\overline{\text{khat}}\,\bar{\varepsilon}^*(k1)\,\bar{\varepsilon}^*(k2)}}{21\, m_Q^5} + \frac{16\, i\, e^2\, \text{qabs}^3\, e_Q^2 \left(\overline{\mathbf{khat}}\cdot\overline{\mathbf{qhat}}\right)\left(\overline{\mathbf{khat}}\cdot\overline{\mathbf{ST}}\right)\left(\bar{\varepsilon}^*(k1)\cdot\bar{\varepsilon}^*(k2)\right)}{21\, m_Q^4} +$$
$$\frac{e^2\, \text{qabs}^2\, e_Q^2\, \eta^\dagger.\xi\, \bar{\epsilon}^{\overline{\text{khat}}\,\bar{\varepsilon}^*(k1)\,\bar{\varepsilon}^*(k2)}}{3\, m_Q^3} - \frac{i\, e^2\, \text{qabs}\, e_Q^2 \left(\overline{\mathbf{khat}}\cdot\overline{\mathbf{qhat}}\right)\left(\overline{\mathbf{khat}}\cdot\overline{\mathbf{ST}}\right)\left(\bar{\varepsilon}^*(k1)\cdot\bar{\varepsilon}^*(k2)\right)}{m_Q^2} +$$
$$\frac{25\, i\, e^2\, \text{qabs}^3\, e_Q^2 \left(\overline{\mathbf{qhat}}\cdot\overline{\mathbf{ST}}\right)\left(\overline{\mathbf{qhat}}\cdot\bar{\varepsilon}^*(k1)\right)\left(\overline{\mathbf{qhat}}\cdot\bar{\varepsilon}^*(k2)\right)}{21\, m_Q^4} +$$
$$\frac{16\, i\, e^2\, \text{qabs}^3\, e_Q^2 \left(\overline{\mathbf{ST}}\cdot\bar{\varepsilon}^*(k1)\right)\left(\overline{\mathbf{qhat}}\cdot\bar{\varepsilon}^*(k2)\right)}{21\, m_Q^4} + \frac{16\, i\, e^2\, \text{qabs}^3\, e_Q^2 \left(\overline{\mathbf{qhat}}\cdot\bar{\varepsilon}^*(k1)\right)\left(\overline{\mathbf{ST}}\cdot\bar{\varepsilon}^*(k2)\right)}{21\, m_Q^4} -$$
$$\frac{43\, i\, e^2\, \text{qabs}^3\, e_Q^2 \left(\overline{\mathbf{qhat}}\cdot\overline{\mathbf{ST}}\right)\left(\bar{\varepsilon}^*(k1)\cdot\bar{\varepsilon}^*(k2)\right)}{42\, m_Q^4} - \frac{i\, e^2\, \text{qabs}\, e_Q^2 \left(\overline{\mathbf{ST}}\cdot\bar{\varepsilon}^*(k1)\right)\left(\overline{\mathbf{qhat}}\cdot\bar{\varepsilon}^*(k2)\right)}{m_Q^2} -$$
$$\frac{i\, e^2\, \text{qabs}\, e_Q^2 \left(\overline{\mathbf{qhat}}\cdot\bar{\varepsilon}^*(k1)\right)\left(\overline{\mathbf{ST}}\cdot\bar{\varepsilon}^*(k2)\right)}{m_Q^2} + \frac{i\, e^2\, \text{qabs}\, e_Q^2 \left(\overline{\mathbf{qhat}}\cdot\overline{\mathbf{ST}}\right)\left(\bar{\varepsilon}^*(k1)\cdot\bar{\varepsilon}^*(k2)\right)}{m_Q^2}$$

Evaluation of the NRQCD amplitude, nonrelativistic normalization

Tell FeynCalc that the J=2 short distance coefficients should be treated as tensors.This is important to make Uncontract work with these objects.

In[46]:=
```
DataType[c1J2,FCTensor]=True;
DataType[c2J2,FCTensor]=True;
DataType[c3J2,FCTensor]=True;
DataType[c4J2,FCTensor]=True;
DataType[c5J2,FCTensor]=True;
```

Convenient shortcuts for entering parts of the J=2 NRQCD amplitude

In[51]:=
```
symmTraceless1[i_,j_]:=FCI[CV[q,i]CV[ST,j]/2+CV[q,j]CV[ST,i]/2-
1/3 KD[i,j]CSP[q,ST]];
symmTraceless2[i_,j_]:=FCI[CV[q,i]CV[q,j]-1/3 KD[i,j]CSP[q,q]];
```

Final NRQCD amplitudes for matching

In[53]:=
```
ampNRQCDJ0=((c0J0/QMass) PauliEta[-I].PauliXi[I]+
(c1J0/QMass^2)CSP[q,ST]+
(c2J0/QMass^3)CSP[q,q]PauliEta[-I].PauliXi[I]+
(c3J0/QMass^4)CSP[q,ST]CSP[q,q]+
(c4J0/QMass^5)CSP[q,q]^2 PauliEta[-I].PauliXi[I])//FCI;
```

In[54]:=
```
ampNRQCDJ2=((1/QMass^2)c1J2[CartesianIndex[i],CartesianIndex[j]]*
symmTraceless1[i,j]+
(1/QMass^3)c2J2[CartesianIndex[i],CartesianIndex[j]]symmTraceless2[i,j]*
PauliEta[-I].PauliXi[I]+
(1/QMass^4)c3J2[CartesianIndex[i],CartesianIndex[j]]symmTraceless1[i,j]*
CSP[q,q]+
(1/QMass^5)c4J2[CartesianIndex[i],CartesianIndex[j]]symmTraceless2[i,j]*
CSP[q,q]PauliEta[-I].PauliXi[I]+
(1/QMass^4)c5J2[CartesianIndex[i],CartesianIndex[j]](symmTraceless2[i,j]*
CSP[q,ST]-
2/5 symmTraceless1[i,j]CSP[q,q]))//Contract;
```

Matching QCD to NRQCD

J=0

The determination of the scalar short distance coefficients is easy

In[55]:=
```
tmp=(Coefficient[ampQCDJ0,qabs,0]==Coefficient[ampNRQCDJ0,qabs,0])
sdCoeff[c0J0]=Solve[tmp,c0J0]//Flatten
```

Out[55]=
$$-\frac{e^2\, e_Q^2\, \eta^\dagger.\xi\, \overline{\text{khat}\cdot\vec{\epsilon}^*}(\text{k1})\,\vec{\epsilon}^*(\text{k2})}{m_Q} = \frac{\text{c0J0}\,\eta^\dagger.\xi}{m_Q}$$

Out[56]=
$$\left\{\text{c0J0} \to e^2\, e_Q^2 \left(-\overline{\text{khat}\cdot\vec{\epsilon}^*}(\text{k1})\,\vec{\epsilon}^*(\text{k2})\right)\right\}$$

In[57]:=
```
tmp=(Coefficient[ampQCDJ0,qabs,1]==Coefficient[ampNRQCDJ0,qabs,1])
sdCoeff[c1J0]=Solve[tmp,c1J0]//Flatten
```

Out[57]=
$$-\frac{i\, e^2\, e_Q^2 \left(\overline{\text{qhat}\cdot\text{ST}}\right)\left(\vec{\epsilon}^*(\text{k1})\cdot\vec{\epsilon}^*(\text{k2})\right)}{m_Q^2} = \frac{\text{c1J0}\left(\overline{\text{qhat}\cdot\text{ST}}\right)}{m_Q^2}$$

Out[58]=
$$\left\{\text{c1J0} \to -i\, e^2\, e_Q^2 \left(\vec{\epsilon}^*(\text{k1})\cdot\vec{\epsilon}^*(\text{k2})\right)\right\}$$

In[59]:=
```
tmp=(Coefficient[ampQCDJ0,qabs,2]==Coefficient[ampNRQCDJ0,qabs,2])
sdCoeff[c2J0]=Solve[tmp,c2J0]//Flatten
```

Out[59]= $\frac{2\,e^2\,e_Q^2\,\eta^\dagger.\xi\,\overline{\epsilon^{\overline{khat}\,\vec{\varepsilon}^*(k1)\,\vec{\varepsilon}^*(k2)}}}{3\,m_Q^3} = \frac{c2J0\,\eta^\dagger.\xi}{m_Q^3}$

Out[60]= $\left\{c2J0 \to \frac{2}{3}\,e^2\,e_Q^2\,\overline{\epsilon^{\overline{khat}\,\vec{\varepsilon}^*(k1)\,\vec{\varepsilon}^*(k2)}}\right\}$

In[61]:=
```
tmp=(Coefficient[ampQCDJ0,qabs,3]==Coefficient[ampNRQCDJ0,qabs,3])
sdCoeff[c3J0]=Solve[tmp,c3J0]//Flatten
```

Out[61]= $\frac{7\,i\,e^2\,e_Q^2\left(\overline{\mathbf{qhat}}\cdot\overline{\mathbf{ST}}\right)\left(\vec{\boldsymbol{\varepsilon}}^*(k1)\cdot\vec{\boldsymbol{\varepsilon}}^*(k2)\right)}{6\,m_Q^4} = \frac{c3J0\left(\overline{\mathbf{qhat}}\cdot\overline{\mathbf{ST}}\right)}{m_Q^4}$

Out[62]= $\left\{c3J0 \to \frac{7}{6}\,i\,e^2\,e_Q^2\left(\vec{\boldsymbol{\varepsilon}}^*(k1)\cdot\vec{\boldsymbol{\varepsilon}}^*(k2)\right)\right\}$

In[63]:=
```
tmp=(Coefficient[ampQCDJ0,qabs,4]==Coefficient[ampNRQCDJ0,qabs,4])
sdCoeff[c4J0]=Solve[tmp,c4J0]//Flatten
```

Out[63]= $-\frac{8\,e^2\,e_Q^2\,\eta^\dagger.\xi\,\overline{\epsilon^{\overline{khat}\,\vec{\varepsilon}^*(k1)\,\vec{\varepsilon}^*(k2)}}}{15\,m_Q^5} = \frac{c4J0\,\eta^\dagger.\xi}{m_Q^5}$

Out[64]= $\left\{c4J0 \to -\frac{8}{15}\,e^2\,e_Q^2\,\overline{\epsilon^{\overline{khat}\,\vec{\varepsilon}^*(k1)\,\vec{\varepsilon}^*(k2)}}\right\}$

J=2

The determination of the tensor short distance coefficients is cumbersome to automatize.

Usually, it is easier to look at the equality A_QCD = A_NRQCD at the given order in qabs and guess the correct short distance coefficient.

In[65]:=
```
sdCoeff[c1J2]={c1J2[CartesianIndex[i_],CartesianIndex[j_]]->
FCI[- I(CV[Polarization[k2,-I,Transversality->True],j]*
CV[Polarization[k1,-I,Transversality->True],i]+CV[Polarization[k2,-I,
Transversality->True],i] CV[Polarization[k1,-I,Transversality->True],j]+
CV[khat,i] CSP[Polarization[k2,-I,Transversality->True],
    Polarization[k1,-I,Transversality->True]] CV[khat,j])*
    SMP["e"]^2 QCharge^2]}
```

Out[65]= $\left\{c1J2(\mathbf{i\_},\,\mathbf{j\_}) \to -i\,e^2\,e_Q^2\left(\vec{\boldsymbol{\varepsilon}}^{*\,i}(k2)\,\vec{\boldsymbol{\varepsilon}}^{*\,j}(k1) + \vec{\boldsymbol{\varepsilon}}^{*\,i}(k1)\,\vec{\boldsymbol{\varepsilon}}^{*\,j}(k2) + \overline{\mathbf{khat}}^{\,i}\,\overline{\mathbf{khat}}^{\,j}\left(\vec{\boldsymbol{\varepsilon}}^*(k1)\cdot\vec{\boldsymbol{\varepsilon}}^*(k2)\right)\right)\right\}$

In[66]:=
```
sdCoeff[c2J2]={c2J2[CartesianIndex[i_],CartesianIndex[j_]]->
-CV[khat,i] CV[khat,j] SMP["e"]^2 QCharge^2 CLC[][khat,
Polarization[k1,-I,Transversality->True],Polarization[k2,-I,
Transversality->True]]}
```

Out[66]= $\left\{c2J2(\mathbf{i\_},\,\mathbf{j\_}) \to e^2\,e_Q^2\left(-\overline{\mathbf{khat}}^{\,i}\right)\overline{\mathbf{khat}}^{\,j}\,\overline{\epsilon^{\overline{khat}\,\vec{\varepsilon}^*(k1)\,\vec{\varepsilon}^*(k2)}}\right\}$

In[67]:=
```
sdCoeff[c3J2]={c3J2[CartesianIndex[i_],CartesianIndex[j_]]->
1/5 I (3 CSP[Polarization[k1,-I,Transversality->True],
Polarization[k2,-I,Transversality->True]] CV[khat,i] CV[khat,j]+
5 CV[Polarization[k1,-I,Transversality->True],j] *
CV[Polarization[k2,-I,Transversality->True],i]+
5 CV[Polarization[k1,-I,Transversality->True],i] CV[Polarization[k2,-I,
    Transversality->True],j]) SMP["e"]^2 QCharge^2}
```

Out[67]=
$$\left\{\text{c3J2}(\text{i\_},\ \text{j\_}) \to \frac{1}{5} i\, e^2\, e_Q^2 \left(5\, \vec{\varepsilon}^{*i}(\text{k2})\, \vec{\varepsilon}^{*j}(\text{k1}) + 5\, \vec{\varepsilon}^{*i}(\text{k1})\, \vec{\varepsilon}^{*j}(\text{k2}) + 3\, \overline{\text{khat}^i}\, \overline{\text{khat}^j}\, \left(\vec{\varepsilon}^{*}(\text{k1}) \cdot \vec{\varepsilon}^{*}(\text{k2})\right)\right)\right\}$$

In[68]:=
```
sdCoeff[c4J2]={c4J2[CartesianIndex[i_],CartesianIndex[j_]]->
FCI[8/7 CV[khat,i] CV[khat,j] SMP["e"]^2 QCharge^2 *
CLC[][khat,Polarization[k1,-I,Transversality->True],
Polarization[k2,-I,Transversality->True]]]}
```

Out[68]=
$$\left\{\text{c4J2}(\text{i\_},\ \text{j\_}) \to \frac{8}{7} e^2\, e_Q^2\, \overline{\text{khat}^i}\, \overline{\text{khat}^j}\, \overline{\epsilon^{\overline{\text{khat}}\,\vec{\varepsilon}}(\text{k1})\, \vec{\varepsilon}^{*}(\text{k2})}\right\}$$

In[69]:=
```
sdCoeff[c5J2]={c5J2[CartesianIndex[i_],CartesianIndex[j_]]->
    FCI[1/42 I (-17 CSP[Polarization[k1,-I,Transversality->True],
Polarization[k2,-I,Transversality->True]] CV[khat,i] CV[khat,j]+
25 CV[Polarization[k1,-I,Transversality->True],j] CV[Polarization[k2,-I,
Transversality->True],i]+25 CV[Polarization[k1,-I,
Transversality->True],i] CV[Polarization[k2,-I,
    Transversality->True],j]) SMP["e"]^2 QCharge^2]};
```

Consistency check for the short distance coefficients

Let us check that our short distance coefficients are correct, i.e. that we have A_QCD - A_NRQCD = 0 order by order in qabs

In[70]:=
```
AmpQCDMinusAmpNRQCDJ0=Simplify[(ampNRQCDJ0/.sdCoeff[c0J0]/.sdCoeff[c1J0]
/.sdCoeff[c2J0]/.sdCoeff[c3J0]/.sdCoeff[c4J0])-ampQCDJ0]
```

Out[70]= 0

In[71]:=
```
AmpQCDMinusAmpNRQCDJ2=Simplify[Contract[Uncontract[ampNRQCDJ2,All]/.
sdCoeff[c1J2]/.sdCoeff[c2J2]/.sdCoeff[c3J2]/.sdCoeff[c4J2]/.
sdCoeff[c5J2]]-ampQCDJ2]
```

Out[71]= 0

List of the obtained short-distance coefficients

In[72]:=
```
sdCoeff[c0J0]
sdCoeff[c1J0]
sdCoeff[c2J0]
sdCoeff[c3J0]
sdCoeff[c4J0]
```

Out[72]= $\left\{\text{c0J0} \to \text{e}^2\, e_Q^2 \left(-\overline{\epsilon}^{\overline{\text{khat}}\,\overline{\boldsymbol{\varepsilon}}^*(\text{k1})\,\overline{\boldsymbol{\varepsilon}}^*(\text{k2})}\right)\right\}$

Out[73]= $\left\{\text{c1J0} \to -i\,\text{e}^2\, e_Q^2 \left(\overline{\boldsymbol{\varepsilon}}^*(\text{k1}) \cdot \overline{\boldsymbol{\varepsilon}}^*(\text{k2})\right)\right\}$

Out[74]= $\left\{\text{c2J0} \to \frac{2}{3}\,\text{e}^2\, e_Q^2\, \overline{\epsilon}^{\overline{\text{khat}}\,\overline{\boldsymbol{\varepsilon}}^*(\text{k1})\,\overline{\boldsymbol{\varepsilon}}^*(\text{k2})}\right\}$

Out[75]= $\left\{\text{c3J0} \to \frac{7}{6}\,i\,\text{e}^2\, e_Q^2 \left(\overline{\boldsymbol{\varepsilon}}^*(\text{k1}) \cdot \overline{\boldsymbol{\varepsilon}}^*(\text{k2})\right)\right\}$

Out[76]= $\left\{\text{c4J0} \to -\frac{8}{15}\,\text{e}^2\, e_Q^2\, \overline{\epsilon}^{\overline{\text{khat}}\,\overline{\boldsymbol{\varepsilon}}^*(\text{k1})\,\overline{\boldsymbol{\varepsilon}}^*(\text{k2})}\right\}$

In[77]:=
```
sdCoeff[c1J2]
sdCoeff[c2J2]
sdCoeff[c3J2]
sdCoeff[c4J2]
sdCoeff[c5J2]
```

Out[77]= $\left\{\text{c1J2}(\mathbf{i\_},\ \mathbf{j\_}) \to -i\,\text{e}^2\, e_Q^2 \left(\overline{\boldsymbol{\varepsilon}}^{*\,i}(\text{k2})\,\overline{\boldsymbol{\varepsilon}}^{*\,j}(\text{k1}) + \overline{\boldsymbol{\varepsilon}}^{*\,i}(\text{k1})\,\overline{\boldsymbol{\varepsilon}}^{*\,j}(\text{k2}) + \overline{\mathbf{khat}}^{\,i}\,\overline{\mathbf{khat}}^{\,j} \left(\overline{\boldsymbol{\varepsilon}}^*(\text{k1}) \cdot \overline{\boldsymbol{\varepsilon}}^*(\text{k2})\right)\right)\right\}$

Out[78]= $\left\{\text{c2J2}(\mathbf{i\_},\ \mathbf{j\_}) \to \text{e}^2\, e_Q^2 \left(-\overline{\mathbf{khat}}^{\,i}\right) \overline{\mathbf{khat}}^{\,j}\, \overline{\epsilon}^{\overline{\text{khat}}\,\overline{\boldsymbol{\varepsilon}}^*(\text{k1})\,\overline{\boldsymbol{\varepsilon}}^*(\text{k2})}\right\}$

Out[79]= $\left\{\text{c3J2}(\mathbf{i\_},\ \mathbf{j\_}) \to \frac{1}{5}\,i\,\text{e}^2\, e_Q^2 \left(5\,\overline{\boldsymbol{\varepsilon}}^{*\,i}(\text{k2})\,\overline{\boldsymbol{\varepsilon}}^{*\,j}(\text{k1}) + 5\,\overline{\boldsymbol{\varepsilon}}^{*\,i}(\text{k1})\,\overline{\boldsymbol{\varepsilon}}^{*\,j}(\text{k2}) + 3\,\overline{\mathbf{khat}}^{\,i}\,\overline{\mathbf{khat}}^{\,j} \left(\overline{\boldsymbol{\varepsilon}}^*(\text{k1}) \cdot \overline{\boldsymbol{\varepsilon}}^*(\text{k2})\right)\right)\right\}$

Out[80]= $\left\{\text{c4J2}(\mathbf{i\_},\ \mathbf{j\_}) \to \frac{8}{7}\,\text{e}^2\, e_Q^2\, \overline{\mathbf{khat}}^{\,i}\,\overline{\mathbf{khat}}^{\,j}\, \overline{\epsilon}^{\overline{\text{khat}}\,\overline{\boldsymbol{\varepsilon}}^*(\text{k1})\,\overline{\boldsymbol{\varepsilon}}^*(\text{k2})}\right\}$

Out[81]= $\left\{\text{c5J2}(\mathbf{i\_},\ \mathbf{j\_}) \to \frac{1}{42}\,i\,\text{e}^2\, e_Q^2 \left(25\,\overline{\boldsymbol{\varepsilon}}^{*\,i}(\text{k2})\,\overline{\boldsymbol{\varepsilon}}^{*\,j}(\text{k1}) + 25\,\overline{\boldsymbol{\varepsilon}}^{*\,i}(\text{k1})\,\overline{\boldsymbol{\varepsilon}}^{*\,j}(\text{k2}) - 17\,\overline{\mathbf{khat}}^{\,i}\,\overline{\mathbf{khat}}^{\,j} \left(\overline{\boldsymbol{\varepsilon}}^*(\text{k1}) \cdot \overline{\boldsymbol{\varepsilon}}^*(\text{k2})\right)\right)\right\}$

Final matching coefficients

(*Decay rates according to Eqs. 2.39-2.42 from arXiv:hep-ph/0604190, omitting matrix elements that contain chromoelectric or chromomagnetic fields*)

In[82]:=
```
decayRateEtaC= 2im[{"f_em","1S0"}]/QMass^2 PauliEta[-I].PauliXi[I] *
PauliXi[-I].PauliEta[I]+
2im[{"g_em","1S0"}]/QMass^2 qabs^2 PauliEta[-I].PauliXi[I] *
PauliXi[-I].PauliEta[I]+
2im[{"h'_em","1S0"}]/QMass^4 qabs^4 PauliEta[-I].PauliXi[I] *
PauliXi[-I].PauliEta[I]+
2im[{"h''_em","1S0"}]/QMass^4 qabs^4 PauliEta[-I].PauliXi[I] *
PauliXi[-I].PauliEta[I];
```

In[83]:=
```
decayRateChiC0= (2im[{"f_em","3P0"}]/QMass^4 qabs^2 CSP[qhat,ST]*
CSP[qhatp,STcc]/3+2im[{"g_em","3P0"}]/QMass^6 qabs^4 CSP[qhat,ST]*
CSP[qhatp,STcc]/3)//FCI;
```

In[84]:=
```
decayRateChiC2= (2im[{"f_em","3P2"}]/QMass^4 symmTraceless1[i,j]*
(symmTraceless1[i,j]/.{qhat->qhatp,ST->STcc}) +
2im[{"g_em","3P2"}]/QMass^6 qabs^2 symmTraceless1[i,j]*
(symmTraceless1[i,j]/.{qhat->qhatp,ST->STcc}))//Contract;
```

These LDMEs do not appear in the decay formulas for eta_c or chi_c, but the corresponding contributions do appear on the QCD side of the matching, since they are allowed by symmetries. Therefore, when matching QCD and NRQCD amplitudes/decay rates to each other, we must also include these LDMEs

In[85]:=
```
extraLDMEs=(2im[{"g_em","3P2,3F2"}]/QMass^6 *
Contract[(1/2symmTraceless2[i,j]CSP[q,ST]-
1/5 symmTraceless1[i,j]CSP[q,q])(symmTraceless1[i,j]/.
{qhat->qhatp,ST->STcc})+
((1/2symmTraceless2[i,j]CSP[qp,ST]- 1/5 symmTraceless1[i,j]CSP[q,q])/.
{qhat->qhatp,ST->STcc})(symmTraceless1[i,j]))]+
2im[{"h_em","1D2"}]/QMass^6 Contract[symmTraceless2[i,j]*
(symmTraceless2[i,j]/.{qhat->qhatp,ST->STcc})];
```

In[86]:=
```
repRuleJ0=Join[sdCoeff[c0J0],sdCoeff[c1J0],sdCoeff[c2J0],sdCoeff[c3J0],
sdCoeff[c4J0]];
repRuleJ0cc=ComplexConjugate[repRuleJ0];
repRuleJ2=Join[sdCoeff[c1J2],sdCoeff[c2J2],sdCoeff[c3J2],sdCoeff[c4J2],
sdCoeff[c5J2]];
repRuleJ2cc=(rd[#[[1]],ComplexConjugate[#[[2]]]]&/@repRuleJ2)/.
rd->Rule;
```

In[90]:=
```
decayRateNRQCDJ0pert=Series[ampNRQCDJ0 ComplexConjugate[ampNRQCDJ0//.
{qhat->qhatp,ST->STcc}/.{h:c0J0|c1J0|c2J0|c3J0|c4J0:>Conjugate[h]}],
{qabs,0,4}]//Normal;
decayRateNRQCDJ2pert=(Series[ampNRQCDJ2 ComplexConjugate[ampNRQCDJ2//.
{qhat->qhatp,ST->STcc}/.
{(h:c1J2|c2J2|c3J2|c4J2|c5J2)[x__]:>h["cc",x]},{qabs,0,4}]//Normal//
Uncontract[#,All]&)//FMCartesianTensorDecomposition[#,
{qhat,qhatp,ST,STcc},0]&//Uncontract[#,All]&;
```

In[92]:=
```
getMatchingCoeffJ0[n_]:=(1/(16Pi))(Coefficient[decayRateNRQCDJ0pert,qabs,n]/.
{Conjugate[x_]:>(x/.ComplexConjugate[repRuleJ0])}/.repRuleJ0/.
{SMP["e"]->2Sqrt[Pi SMP["alpha_fs"]]})//DoPolarizationSums[#,k1,aux]&//
DoPolarizationSums[#,k2,aux]&//LorentzToCartesian//Simplify
```

In[93]:=
```
getMatchingCoeffJ2[n_]:=(1/(16Pi))(Coefficient[decayRateNRQCDJ2pert,qabs,n]/.
{(h:c1J2|c2J2|c3J2|c4J2|c5J2)["cc",x__]:>(h[x]/.repRuleJ2cc)}/.repRuleJ2/.
{SMP["e"]->2Sqrt[Pi SMP["alpha_fs"]]})//DoPolarizationSums[#,k1,aux]&//
DoPolarizationSums[#,k2,aux]&//LorentzToCartesian//Simplify
```

This precisely reproduces Eqs. 3.4-3.12 from arXiv:hep-ph/0604190

In[94]:=
```
Solve[SelectFree2[getMatchingCoeffJ0[0],ST]==
    Coefficient[decayRateEtaC,qabs,0],{im[{"f_em","1S0"}]}]
Solve[SelectFree2[getMatchingCoeffJ0[2],ST]==
    Coefficient[decayRateEtaC,qabs,2],{im[{"g_em","1S0"}]}]
Solve[SelectNotFree2[getMatchingCoeffJ0[2],ST]==
    Coefficient[decayRateChiC0,qabs,2],{im[{"f_em","3P0"}]}]
Solve[SelectNotFree2[getMatchingCoeffJ2[2],ST]==
    (Coefficient[decayRateChiC2,qabs,2]),{im[{"f_em","3P2"}]}]
Solve[SelectFree2[getMatchingCoeffJ2[4],ST]==
    Coefficient[SelectFree[extraLDMEs,ST],qabs,4],{im[{"h_em","1D2"}]}]
Solve[SelectFree2[getMatchingCoeffJ0[4],ST]==
    Coefficient[decayRateEtaC,qabs,4],{im[{"h'_em","1S0"}]}]
Solve[SelectNotFree2[getMatchingCoeffJ0[4],ST]==
    Coefficient[decayRateChiC0,qabs,4],{im[{"g_em","3P0"}]}]
Solve[SelectNotFree2[getMatchingCoeffJ2[4],ST]==
    ((Coefficient[decayRateChiC2+SelectNotFree2[extraLDMEs,ST],qabs,4])/.
        {im[{"g_em","3P2,3F2"}]->-20/21 SMP["alpha_fs"]^2 SMP["e_Q"]^4 Pi
})),{im[{"g_em","3P2"}]}]
```

Out[94]= $\{\{\text{im}(\{\text{f\_em, 1S0}\}) \to \pi \alpha^2 e_Q^4\}\}$

Out[95]= $\left\{\left\{\text{im}(\{\text{g\_em, 1S0}\}) \to -\frac{4 \pi \alpha^2 e_Q^4}{3 m_Q^2}\right\}\right\}$

Out[96]= $\{\{\text{im}(\{\text{f\_em, 3P0}\}) \to 3 \pi \alpha^2 e_Q^4\}\}$

Out[97]= $\left\{\left\{\text{im}(\{\text{f\_em, 3P2}\}) \to \frac{4}{5} \pi \alpha^2 e_Q^4\right\}\right\}$

Out[98]= $\left\{\left\{\text{im}(\{\text{h\_em, 1D2}\}) \to \frac{2}{15} \pi \alpha^2 e_Q^4 \eta^\dagger.\xi \xi^\dagger.\eta\right\}\right\}$

Out[99]= $\left\{\left\{\text{im}(\{\text{h'\_em, 1S0}\}) \to \frac{68 \pi \alpha^2 e_Q^4 - 45 m_Q^2 \text{im}(\{\text{h''\_em, 1S0}\})}{45 m_Q^2}\right\}\right\}$

Out[100]= $\{\{\text{im}(\{\text{g\_em, 3P0}\}) \to -7 \pi \alpha^2 e_Q^4\}\}$

Out[101]= $\left\{\left\{\text{im}(\{\text{g\_em, 3P2}\}) \to -\frac{8}{5} \pi \alpha^2 e_Q^4\right\}\right\}$

Check with the the known results

In[102]:=
```
Print["Check with the known results: ",
      If[{AmpQCDMinusAmpNRQCDJ0,AmpQCDMinusAmpNRQCDJ2}=={0,0},
      "CORRECT.", "!!! WRONG !!!"]];
```

Check with the known results: CORRECT.

I.3 Matching Coefficients of the Dimension six 4-fermion Operators in NRQCD (Unequal Mass Case)

One-loop matching between QCD and NRQCD for QQbar' -> QQbar'

Load FeynCalc, FeynArts and FeynHelpers and FeynOnium

In[1]:=
```
$LoadAddOns={"FeynHelpers","FeynOnium"};
$LoadFeynArts = True;
<<FeynCalc`
$FAVerbose=0;
```

FeynCalc 9.3.0 (development version). For help, use the documentation center, check out the wiki or write to the mailing list.

See also the supplied examples. If you use FeynCalc in your research, please cite

- V. Shtabovenko, R. Mertig and F. Orellana, Comput. Phys. Commun., 207C, 432–444, 2016, arXiv:1601.01167
- R. Mertig, M. Böhm, and A. Denner, Comput. Phys. Commun., 64, 345–359, 1991.

FeynArts 3.9 patched for use with FeynCalc, for documentation use the manual or visit www.feynarts.de.

FeynHelpers 1.0.0 loaded.

Have a look at the supplied examples. If you use FeynHelpers in your research, please cite

- V. Shtabovenko, "FeynHelpers: Connecting FeynCalc to FIRE and Package–X", TUM–EFT 75/15, arXiv:1611.06793

Furthermore, remember to cite the authors of the tools that you are calling from FeynHelpers, which are

- FIRE by A. Smirnov, if you are using the function FIREBurn.
- Package – *X* by H. Patel, if you are using the function PaXEvaluate.

FeynOnium 0.5.0 loaded.

Have a look at the supplied examples. If you use FeynOnium in your research, please cite

- N. Brambilla, V. Shtabovenko and A.Vairo, TUM–EFT 92/17, in preparation

Generate Feynman diagrams

In[5]:=
```
diags = InsertFields[CreateTopologies[1, 2 -> 2,BoxesOnly],
{F[3, {1,Col1}],-F[3, {2,Col2}]} -> {F[3, {1,Col3}],
-F[3, {2,Col4}]}, InsertionLevel -> {Classes}, Model -> "SMQCD",
ExcludeParticles -> {S[_], V[1|2|3|4]}];
Paint[diags, ColumnsXRows -> {2, 1}, Numbering -> None,
SheetHeader->None,ImageSize->{512,256}];
```

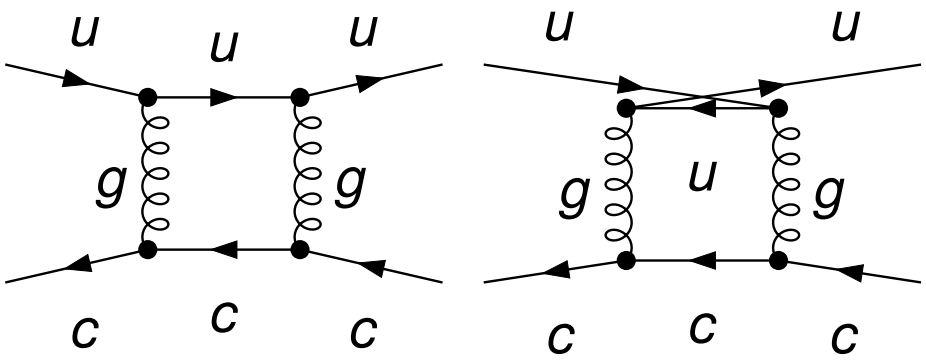

In[7]:=
```
amp=FCFAConvert[CreateFeynAmp[diags,PreFactor->-1],
IncomingMomenta->{p1,p2},OutgoingMomenta->{p3,p4},
LoopMomenta->{l},DropSumOver->True,ChangeDimension->D,
UndoChiralSplittings->True,List->False,SMP->True,
FinalSubstitutions->{SMP["m_u"]->m1,SMP["m_c"]->m2}]//Contract
```

Out[7]=
$$-\Big(\big(g_s^4\ T^{\text{Glu5}}_{\text{Col5 Col1}}\ T^{\text{Glu6}}_{\text{Col2 Col6}}\ T^{\text{Glu6}}_{\text{Col3 Col5}}\ T^{\text{Glu5}}_{\text{Col6 Col4}}\ (\varphi(\text{p3},\text{m1})).\gamma^{\text{Lor4}}.(\gamma\cdot l+\text{m1}).\gamma^{\text{Lor1}}.(\varphi(\text{p1},\text{m1}))\\ (\varphi(-\text{p2},\text{m2})).\gamma^{\text{Lor4}}.(\gamma\cdot(-l-\text{p2}+\text{p3})+\text{m2}).\gamma^{\text{Lor1}}.(\varphi(-\text{p4},\text{m2}))\big)\Big/\\ \big(l^2-\text{m1}^2\big).(l-\text{p3})^2.\big((l+\text{p2}-\text{p3})^2-\text{m2}^2\big).(l+\text{p2}-\text{p3}-\text{p4})^2\big)-\\ \Big(\big(g_s^4\ T^{\text{Glu5}}_{\text{Col5 Col1}}\ T^{\text{Glu5}}_{\text{Col2 Col6}}\ T^{\text{Glu6}}_{\text{Col3 Col5}}\ T^{\text{Glu6}}_{\text{Col6 Col4}}\ (\varphi(-\text{p2},\text{m2})).\gamma^{\text{Lor1}}.(\gamma\cdot(-l-\text{p2})+\text{m2}).\gamma^{\text{Lor3}}.(\varphi(-\text{p4},\text{m2}))\\ (\varphi(\text{p3},\text{m1})).\gamma^{\text{Lor3}}.(\gamma\cdot(-l-\text{p2}+\text{p3}+\text{p4})+\text{m1}).\gamma^{\text{Lor1}}.(\varphi(\text{p1},\text{m1}))\big)\Big/\\ l^2.\big((l+\text{p2})^2-\text{m2}^2\big).(l+\text{p2}-\text{p4})^2.\big((l+\text{p2}-\text{p3}-\text{p4})^2-\text{m1}^2\big)$$

In[8]:=
```
ruleColor={SUNTF[{SUNIndex[a_],SUNIndex[b_]},
i1_SUNFIndex,i2_SUNFIndex] SUNTF[{SUNIndex[a_],SUNIndex[b_]},
i3_SUNFIndex,i4_SUNFIndex]:>
CF hold[(CA/2-CF)]SUNFDelta[i1,i2]SUNFDelta[i3,i4]-
2hold[(CA/2-CF)] SUNTF[{SUNIndex[a]},i1,i2]SUNTF[{SUNIndex[a]},i3,i4],

SUNTF[{SUNIndex[a_],SUNIndex[b_]},
i1_SUNFIndex,i2_SUNFIndex] SUNTF[{SUNIndex[b_],SUNIndex[a_]},
i3_SUNFIndex,i4_SUNFIndex]:>
CF hold[(CA/2-CF)]SUNFDelta[i1,i2]SUNFDelta[i3,i4]+
(CF-hold[(CA/2-CF)]) SUNTF[{SUNIndex[a]},i1,i2]SUNTF[{SUNIndex[a]},i3,i4]};
```

On-shell kinematics

In[9]:=
```
FCClearScalarProducts[];
SPD[p1,p1]=m1^2;
SPD[p2,p2]=m2^2;
SPD[p3,p3]=m1^2;
SPD[p4,p4]=m2^2;
SPD[p1,p2]=m1 m2;
SPD[p3,p4]=m1 m2;
SPD[p1,p3]=m1^2;
SPD[p2,p4]=m2^2;
SPD[p1,p4]=m1 m2;
SPD[p2,p3]=m1 m2;
```

In[20]:=
```
TC[p1]= m1;
TC[p2]= m2;
TC[p3]= m1;
TC[p4]= m2;
CartesianMomentum[p1,D-1]=0;
CartesianMomentum[p2,D-1]=0;
CartesianMomentum[p3,D-1]=0;
CartesianMomentum[p4,D-1]=0;
CartesianMomentum[p1]=0;
CartesianMomentum[p2]=0;
CartesianMomentum[p3]=0;
CartesianMomentum[p4]=0;
```

Calculation of the box amplitudes in QCD

Tensor reduction of the 1-loop integrals and simplification of the Dirac algebra

In[32]:=
```
AbsoluteTiming[amp1=TID[amp,l,UsePaVeBasis->True,ToPaVe->True,
Isolate->False]//DiracSimplify//DiracSimplify;]//First
```

Out[32]= 9.04557

Using "naive" scheme for Pauli matrices in D-1 dimensions, i.e. the anticommutator relation is applied with a D-1 dimensional epsilon tensor

In[33]:=
```
FCSetPauliSigmaScheme["Naive"];
```

Nonrelativistic expansion of spinor chains

In[34]:=
```
AbsoluteTiming[amp2=amp1//Collect2[#,DiracSpinor]&//
FMSpinorChainExplicit2[#,FMSpinorNormalization->"nonrelativistic"]&//
    ReplaceAll[#,{PauliEta[-I].PauliSigma[x_,D-1].PauliEta[I]:>
    CartesianPair[CartesianMomentum[ST1,D-1],x],
    PauliXi[-I].PauliSigma[x_,D-1].PauliXi[I]:>
    CartesianPair[CartesianMomentum[ST2,D-1],x]}]&//Contract//
    Collect2[#,{ST1,ST2}]&;]//First
```

Out[34]= 3.26004

Evaluation of the Passarino-Veltman functions

In[35]:=
```
AbsoluteTiming[amp3=amp2//Collect2[#,{PaVe,D0}]&//
ReplaceAll[#,(x:_PaVe|_D0):>PaXEvaluateUVIRSplit[x,
PaXAnalytic->True,PaXImplicitPrefactor->1/(2Pi)^D]]&//
FCHideEpsilon;]//First
```

Out[35]= 3.65069

This simulates the prescription of arXiv:hep-ph/9802365, i.e. eps^ijk eps^ijk' = (D-2) d^kk'

In[36]:=
```
amp4=(amp3/.{FCI[CSPD[ST1,ST2]]->FCI[CSPD[ST1,ST2]]/(D-3)});
```

Expanding around eps=0 for D=4-2eps

In[37]:=
```
AbsoluteTiming[amp5=Series[amp4//FCReplaceD[#,D->4-2EpsilonIR]&//
DotSimplify//FCShowEpsilon,{EpsilonIR,0,0}]//Normal//
FCHideEpsilon;]//First
```

Out[37]= 1.67247

Pick up the finite part and separate color singlet and color octet contributions from each other

In[38]:=
```
{finitePart,divergentPart}=FCSplit[amp5,{SMP["Delta_IR"]}];
AbsoluteTiming[finitePartEval=(finitePart/.D->4)//SUNSimplify//
Expand2[#,SUNTF]&//ReplaceAll[#,ruleColor]&;]//First
```

Out[39]= 4.96062

Final splitting into spin singlet, spin triplet, color singlet and color octet pieces

In[40]:=
```
{spinSingletFin,spinTripletFin}=FCSplit[finitePartEval,{ST1,ST2}];
{spinSingletColorSingletFin,spinSingletColorOctetFin}=
FullSimplify/@(FCSplit[spinSingletFin,{SUNTF}]);
{spinTripletColorSingletFin,spinTripletColorOctetFin}=
FullSimplify/@(FCSplit[spinTripletFin,{SUNTF}]);
```

Final matching coefficients

In[43]:=
```
getMatchingCoeff[ex_,ru_]:=
(m1 m2 I ex//PowerExpand//Simplify//ReplaceAll[#,ru]&//
ReplaceAll[#,{SMP["g_s"]^4->16Pi^2 SMP["alpha_s"]^2,
FCI[CSP[ST1,ST2]]:>1,DOT[x_,y_]:>1,
SUNFDelta[__]:>1,SUNTF[__]:>1}]&//Simplify)/.hold->Identity
```

In[44]:=
```
matchingCoeff["d_ss"]=getMatchingCoeff[spinSingletColorSingletFin,
{Log[m1]->1/2Log[(m1/ScaleMu)^2]+
Log[ScaleMu],Log[m2]->1/2Log[(m2/ScaleMu)^2]+Log[ScaleMu]}]
```

Out[44]=
$$-\left(\left(C_F\,\alpha_s^2\left(\frac{C_A}{2}-C_F\right)\left(3\,\text{m1}^2\log\left(\frac{\text{m2}^2}{\mu^2}\right)-3\,\text{m2}^2\log\left(\frac{\text{m1}^2}{\mu^2}\right)+\text{m1}^2-\text{m2}^2\right)\right)\Big/(3\,(\text{m1}-\text{m2})\,(\text{m1}+\text{m2}))\right)$$

In[45]:=
```
matchingCoeff["d_sv"]=getMatchingCoeff[spinTripletColorSingletFin,
{Log[m1]->1/2Log[(m1/m2)^2]+Log[m2]}]
```

Out[45]=
$$\frac{\text{m1}\,\text{m2}\,C_F\,\alpha_s^2\left(\frac{C_A}{2}-C_F\right)\log\left(\frac{\text{m1}^2}{\text{m2}^2}\right)}{\text{m1}^2-\text{m2}^2}$$

In[46]:=
```
matchingCoeff["d_vs"]=getMatchingCoeff[spinSingletColorOctetFin,
{Log[m1]->1/2Log[(m1/ScaleMu)^2]+Log[ScaleMu],
Log[m2]->1/2Log[(m2/ScaleMu)^2]+Log[ScaleMu]}]//Collect2[#,CA,CF]&
```

Out[46]=
$$\left(C_A\,\alpha_s^2\left(3\,\text{m1}^4\log\left(\frac{\text{m2}^2}{\mu^2}\right)+10\,\text{m1}^4+9\,\text{m1}^3\,\text{m2}\log\left(\frac{\text{m2}^2}{\mu^2}\right)+3\,\text{m1}^3\,\text{m2}-3\,\text{m2}^4\log\left(\frac{\text{m1}^2}{\mu^2}\right)-\right.\right.$$
$$\left.\left.9\,\text{m1}\,\text{m2}^3\log\left(\frac{\text{m1}^2}{\mu^2}\right)-3\,\text{m1}\,\text{m2}^3-10\,\text{m2}^4\right)\right)\Big/(12\,\text{m1}\,\text{m2}\,(\text{m1}-\text{m2})\,(\text{m1}+\text{m2}))-$$
$$\left(2\,C_F\,\alpha_s^2\left(3\,\text{m1}^2\log\left(\frac{\text{m2}^2}{\mu^2}\right)-3\,\text{m2}^2\log\left(\frac{\text{m1}^2}{\mu^2}\right)+\text{m1}^2-\text{m2}^2\right)\right)\Big/(3\,(\text{m1}-\text{m2})\,(\text{m1}+\text{m2}))$$

In[47]:=
```
matchingCoeff["d_vv"]=getMatchingCoeff[spinTripletColorOctetFin,
{Log[m1]->1/2Log[(m1/ScaleMu)^2]+
Log[ScaleMu],Log[m2]->1/2Log[(m2/ScaleMu)^2]+Log[ScaleMu]}]//
Collect2[#,CA,CF]&
```

Out[47]=
$$\frac{1}{4\,(\text{m1}-\text{m2})\,(\text{m1}+\text{m2})}$$
$$C_A\,\alpha_s^2\left(\text{m1}^2\log\left(\frac{\text{m2}^2}{\mu^2}\right)-\text{m2}^2\log\left(\frac{\text{m1}^2}{\mu^2}\right)-3\,\text{m1}\,\text{m2}\log\left(\frac{\text{m1}^2}{\mu^2}\right)+3\,\text{m1}^2+3\,\text{m1}\,\text{m2}\log\left(\frac{\text{m2}^2}{\mu^2}\right)-3\,\text{m2}^2\right)+$$
$$\frac{2\,\text{m1}\,\text{m2}\,C_F\,\alpha_s^2\left(\log\left(\frac{\text{m1}^2}{\mu^2}\right)-\log\left(\frac{\text{m2}^2}{\mu^2}\right)\right)}{(\text{m1}-\text{m2})\,(\text{m1}+\text{m2})}$$

Check with the literature

Compare our results to arXiv:hep-ph/9802365, Eq. 3.1 - 3.4

In[48]:=
```
matchingCoeffPinedaSoto["d_ss"]=- CF(CA/2-CF) SMP["alpha_s"]^2/
(m1^2-m2^2)(m1^2(Log[m2^2/ScaleMu^2]+1/3)-m2^2(Log[m1^2/ScaleMu^2]+1/3));
matchingCoeffPinedaSoto["d_sv"]= CF(CA/2-CF) SMP["alpha_s"]^2/
(m1^2-m2^2)m1 m2 Log[m1^2/m2^2];
matchingCoeffPinedaSoto["d_vs"]= -2CF SMP["alpha_s"]^2/
(m1^2-m2^2)(m1^2(Log[m2^2/ScaleMu^2]+1/3)-m2^2(Log[m1^2/ScaleMu^2]+
1/3))+CA SMP["alpha_s"]^2/(4(m1^2-m2^2))(
3(m1^2(Log[m2^2/ScaleMu^2]+1/3)-m2^2(Log[m1^2/ScaleMu^2]+1/3))
+1/(m1 m2) (m1^4(Log[m2^2/ScaleMu^2]+10/3)-m2^4(Log[m1^2/ScaleMu^2]+10/3)));
matchingCoeffPinedaSoto["d_vv"]= 2CF SMP["alpha_s"]^2/
(m1^2-m2^2) m1 m2 Log[m1^2/m2^2]+CA SMP["alpha_s"]^2/
(4(m1^2-m2^2))((m1^2(Log[m2^2/ScaleMu^2]+3)-
m2^2(Log[m1^2/ScaleMu^2]+3))-3 m1 m2 Log[m1^2/m2^2]);
```

In[52]:=
```
resLit=(8 (-9+π^2) CSP[ST,STcc] SMP["alpha_fs"]^3 SMP["e_Q"]^6)/
(9 SMP["m_Q"]^2);
Print["Check with Eq. 3.1-3.4 in arXiv:hep-ph/9802365: ",
            If[Simplify[PowerExpand[{matchingCoeff["d_ss"]-
            matchingCoeffPinedaSoto["d_ss"],
matchingCoeff["d_sv"]-matchingCoeffPinedaSoto["d_sv"],
matchingCoeff["d_vs"]-matchingCoeffPinedaSoto["d_vs"],
matchingCoeff["d_vv"]-matchingCoeffPinedaSoto["d_vv"]}]]==={0,0,0,0},
"CORRECT.", "!!! WRONG !!!"]];
```

Check with Eq. 3.1–3.4 in arXiv:hep–ph/9802365: CORRECT.

Acknowledgments

First of all, I would like to thank God for giving me strength and endurance to finish this thesis.

My sincere gratitude goes to my supervisors Nora Brambilla and Antonio Vairo for guiding me through my PhD and helping me to stay focused on the research but also to learn many new methods and techniques by going to conferences and schools. Without their support I would not have become the scientist I am today. They always made me feel like being part of the T30f family.

I would also like to thank my collaborators Michael Benzke, Jaume Tarrús Castellà, Rolf Mertig, Frederik Orellana, Yu Jia and Wen Chen for our productive work together. I'm particularly indebted to Yu Jia and York Schroeder for providing recommendation letters during my searches for a postdoc position.

My time at the TUM would not have been so enjoyable without my colleagues Michael Benzke, Matthias Berwein, Simone Biondini, Jaume Tarrús Castellà, Miguel Escobedo, Sungmin Hwang, Kie Sang Jeong, Javad Komijani, Wai Kin Lai, Hector Martinez, Thomas Rosenhammer, Jorge Segovia, Sebastian Steinbeißer and Johannes Weber. I will never forget all the moments that we spent together inside and outside of the Physics Department. I'm also very grateful to our secretaries Susanne Tillich, Laura Darabas and Karin Ramm, who always kindly navigated me through the paperwork jungle and helped organizing various events.

Finally, I would like to thank my family for being with me in all these years of university studies. I love you very much.

List of Figures

Bibliography

[1] S. Weinberg, Phenomenological Lagrangians, Physica, **A96**, 327–340, (1979).

[2] K. Wilson, Confinement of quarks, Phys. Rev. D, **10**, 2445–2459, (1974).

[3] N. Brambilla, A. Pineda, J. Soto, and A. Vairo, Effective field theories for heavy quarkonium, Rev. Mod. Phys., **77**, 1423, (2005), arXiv:hep-ph/0410047.

[4] N. Brambilla et al., Heavy Quarkonium Physics, CERN Yellow Report, **CERN-2005-005**, 487p., (2005), arXiv:hep-ph/0412158.

[5] W. Caswell and G. Lepage, Effective lagrangians for bound state problems in QED, QCD, and other field theories, Phys. Lett. B, **167**, 437–442, (1986).

[6] A. Pineda and J. Soto, The Lamb Shift in Dimensional Regularization, Phys. Lett. B, **420**, 391–396, (1998), arXiv:hep-ph/9711292.

[7] G. T. Bodwin, E. Braaten, and G. P. Lepage, Rigorous QCD Analysis of Inclusive Annihilation and Production of Heavy Quarkonium, Phys. Rev. D, **51**, 1125–1171, (1995), arXiv:hep-ph/9407339.

[8] A. Pineda and J. Soto, Effective Field Theory for Ultrasoft Momenta in NRQCD and NRQED, Nucl.Phys.Proc.Suppl., **64**, 428–432, (1998), arXiv:hep-ph/9707481.

[9] N. Brambilla, A. Pineda, J. Soto, and A. Vairo, Potential NRQCD: an effective theory for heavy quarkonium, Nucl. Phys. B, **566**, 275, (2000), arXiv:hep-ph/9907240.

[10] W. Heisenberg, A quantum-theoretical reinterpretation of kinematic and mechanical relations, Z. Phys., **33**, 879–893, (1925).

[11] F. London, Zur Theorie und Systematik der Molekularkräfte, Z. Phys., **63**, 245–279, (1930).

[12] H. B. G. Casimir and D. Polder, The Influence of Retardation on the London-van der Waals Forces, Phys. Rev., **73**, 360–372, (1948).

[13] V. A. Parsegian, (2005), Van der Waals Forces: A Handbook for Biologists, Chemists, Engineers, and Physicists, (Cambridge University Press).

[14] H. Fujii and D. Kharzeev, Long-Range Forces of QCD, Phys. Rev. D, **60**, 114039, (1999), arXiv:hep-ph/9903495.

[15] N. Brambilla, G. Krein, J. Tarrús Castellà, and A. Vairo, Long-range properties of $1S$ bottomonium states, Phys. Rev., **D93**, 054002, (2016), arXiv:1510.05895.

[16] N. Brambilla et al., QCD and Strongly Coupled Gauge Theories: Challenges and Perspectives, Eur. Phys. J., **C74**, 2981, (2014), arXiv:1404.3723.

[17] J. J. Aubert et al., Experimental Observation of a Heavy Particle J, Phys. Rev. Lett., **33**, 1404–1406, (1974).

[18] J. E. Augustin et al., Discovery of a Narrow Resonance in e^+e^- - Annihilation, Phys. Rev. Lett., **33**, 1406–1408, (1974).

[19] T. Appelquist and H. D. Politzer, Orthocharmonium and e+ e- Annihilation, Phys. Rev. Lett., **34**, 43, (1975).

[20] R. Mertig, M. Böhm, and A. Denner, Feyn Calc - Computer-algebraic calculation of Feynman amplitudes, Comput. Phys. Commun., **64**, 345–359, (1991).

[21] V. Shtabovenko, R. Mertig, and F. Orellana, New Developments in FeynCalc 9.0, Comput. Phys. Commun., **207**, 432–444, (2016), arXiv:1601.01167.

[22] F. Feng and R. Mertig, FormLink/FeynCalcFormLink : Embedding FORM in Mathematica and FeynCalc, arXiv:1212.3522.

[23] A. V. Smirnov and V. A. Smirnov, FIRE4, LiteRed and accompanying tools to solve integration by parts relations, Comput. Phys. Commun., **184**, 2820–2827, (2013), arXiv:1302.5885.

[24] A. V. Smirnov, FIRE5: a C++ implementation of Feynman Integral REduction, Comput. Phys. Commun., **189**, 182–191, (2015), arXiv:1408.2372.

[25] J.-X. Wang, Progress in FDC project, Nucl. Instrum. Meth. A, **534**, 241–245, (2004), arXiv:hep-ph/0407058.

[26] J. P. Ma and Q. Wang, Corrections For Two Photon Decays of χ_{c0} and χ_{c2} and Color Octet Contributions, Phys. Lett. B, **537**, 233–240, (2002), arXiv:hep-ph/0203082.

[27] N. Brambilla, E. Mereghetti, and A. Vairo, Electromagnetic quarkonium decays at order v^7, JHEP, **0608**, 039, (2006), arXiv:hep-ph/0604190.

[28] Y.-J. Li, G.-Z. Xu, K.-Y. Liu, and Y.-J. Zhang, Relativistic Correction to J/psi and Upsilon Pair Production, JHEP, **07**, 051, (2013), arXiv:1303.1383.

[29] K.-T. Chao, Z.-G. He, D. Li, and C. Meng, Search for $C = +$ charmonium states in $e^+e^- \to \gamma + X$ at BEPCII/BESIII, arXiv:1310.8597.

[30] G.-Z. Xu, Y.-J. Li, K.-Y. Liu, and Y.-J. Zhang, $\alpha_s v^2$ corrections to η_c and χ_{cJ} production recoiled with a photon at e^+e^- colliders, JHEP, **1410**, 71, (2014), arXiv:1407.3783.

[31] E. Braaten and Y.-Q. Chen, Helicity Decomposition for Inclusive J/ψ Production, Phys. Rev. D, **54**, 3216–3227, (1996), arXiv:hep-ph/9604237.

[32] G. T. Bodwin, F. Petriello, S. Stoynev, and M. Velasco, Higgs boson decays to quarkonia and the Hccbar coupling, Phys. Rev. D, **88,**, 053003, (2013), arXiv:1306.5770.

[33] G. T. Bodwin, H. S. Chung, J.-H. Ee, J. Lee, and F. Petriello, Relativistic corrections to Higgs boson decays to quarkonia, Phys. Rev. D, **90,**, 113010, (2014), arXiv:1407.6695.

[34] M. Gell-Mann, Quarks, Acta Phys. Austriaca Suppl., **9**, 733–761, (1972).

[35] H. Fritzsch and M. Gell-Mann, Current algebra: Quarks and what else?, eConf, **C720906V2**, 135–165, (1972), arXiv:hep-ph/0208010.

[36] H. Fritzsch, M. Gell-Mann, and H. Leutwyler, Advantages of the Color Octet Gluon Picture, Phys. Lett., **B47**, 365–368, (1973).

[37] C.-N. Yang and R. L. Mills, Conservation of Isotopic Spin and Isotopic Gauge Invariance, Phys. Rev., **96**, 191–195, (1954).

[38] H. D. Politzer, Reliable Perturbative Results for Strong Interactions?, Phys. Rev. Lett., **30**, 1346–1349, (1973).

[39] D. J. Gross and F. Wilczek, Ultraviolet Behavior of Nonabelian Gauge Theories, Phys. Rev. Lett., **30**, 1343–1346, (1973).

[40] C. Patrignani et al., Review of Particle Physics, Chin. Phys., **C40**, 100001, (2016).

[41] A. Bazavov et al., Determination of α_s from the QCD static energy, Phys. Rev., **D86**, 114031, (2012), arXiv:1205.6155.

[42] A. Bazavov et al., Determination of α_s from the QCD static energy: An update, Phys. Rev., **D90**, 074038, (2014), arXiv:1407.8437.

[43] F. J. Dyson, The S matrix in quantum electrodynamics, Phys. Rev., **75**, 1736–1755, (1949).

[44] J. S. Schwinger, On the Green's functions of quantized fields. 2., Proc. Nat. Acad. Sci., **37**, 455–459, (1951).

[45] J. S. Schwinger, On the Green's functions of quantized fields. 1., Proc. Nat. Acad. Sci., **37**, 452–455, (1951).

[46] J. C. Collins, D. E. Soper, and G. Sterman, Factorization of Hard Processes in QCD, Adv.Ser.Direct.High Energy Phys., **5:1-91**, (1988), arXiv:hep-ph/0409313.

[47] N. Brambilla et al., Heavy quarkonium: progress, puzzles, and opportunities, Eur.Phys.J.C, **71:1534,2011**, (2010), arXiv:1010.5827.

[48] R. Aaij et al., Observation of $J/\psi p$ Resonances Consistent with Pentaquark States in $\Lambda_b^0 \to J/\psi K^- p$ Decays, Phys. Rev. Lett., **115**, 072001, (2015), arXiv:1507.03414.

[49] E. Braaten, How the $Z_c(3900)$ Reveals the Spectra of Quarkonium Hybrid and Tetraquark Mesons, Phys. Rev. Lett., **111**, 162003, (2013), arXiv:1305.6905.

[50] E. Braaten and M. Kusunoki, Exclusive production of the X(3872) in B meson decay, Phys. Rev., **D71**, 074005, (2005), arXiv:hep-ph/0412268.

[51] M. Berwein, N. Brambilla, J. Tarrús Castellà, and A. Vairo, Quarkonium Hybrids with Nonrelativistic Effective Field Theories, Phys. Rev., **D92**, 114019, (2015), arXiv:1510.04299.

[52] J. M. Pendlebury et al., Revised experimental upper limit on the electric dipole moment of the neutron, Phys. Rev., **D92**, 092003, (2015), arXiv:1509.04411.

[53] R. D. Peccei and H. R. Quinn, CP Conservation in the Presence of Instantons, Phys. Rev. Lett., **38**, 1440–1443, (1977).

[54] R. D. Peccei and H. R. Quinn, Constraints Imposed by CP Conservation in the Presence of Instantons, Phys. Rev., **D16**, 1791–1797, (1977).

[55] F. Englert and R. Brout, Broken Symmetry and the Mass of Gauge Vector Mesons, Phys. Rev. Lett., **13**, 321–323, (1964).

[56] P. W. Higgs, Broken Symmetries and the Masses of Gauge Bosons, Phys. Rev. Lett., **13**, 508–509, (1964).

[57] P. W. Higgs, Broken symmetries, massless particles and gauge fields, Phys. Lett., **12**, 132–133, (1964).

[58] G. S. Guralnik, C. R. Hagen, and T. W. B. Kibble, Global Conservation Laws and Massless Particles, Phys. Rev. Lett., **13**, 585–587, (1964).

[59] K. Abe et al., Search for proton decay via $p \to \nu K^+$ using 260 kiloton-year data of Super-Kamiokande, Phys. Rev., **D90**, 072005, (2014), arXiv:1408.1195.

[60] S. Aoki et al., Review of lattice results concerning low-energy particle physics, Eur. Phys. J., **C74**, 2890, (2014), arXiv:1310.8555.

[61] S. L. Adler, Axial vector vertex in spinor electrodynamics, Phys. Rev., **177**, 2426–2438, (1969).

[62] J. S. Bell and R. Jackiw, A PCAC puzzle: pi0 –> gamma gamma in the sigma model, Nuovo Cim., **A60**, 47–61, (1969).

[63] W. Heisenberg, On the structure of atomic nuclei, Z. Phys., **77**, 1–11, (1932).

[64] W. Heisenberg and W. Pauli, On Quantum Field Theory. (In German), Z. Phys., **56**, 1–61, (1929).

[65] W. Heisenberg and W. Pauli, On Quantum Field Theory. 2. (In German), Z. Phys., **59**, 168–190, (1930).

[66] M. Gell-Mann and F. Low, Bound states in quantum field theory, Phys. Rev., **84**, 350–354, (1951).

[67] M. E. Peskin and D. V. Schroeder, (1995), An Introduction to quantum field theory.

[68] F. J. Dyson, The Radiation theories of Tomonaga, Schwinger, and Feynman, Phys. Rev., **75**, 486–502, (1949).

[69] G. C. Wick, The Evaluation of the Collision Matrix, Phys. Rev., **80**, 268–272, (1950), [,592(1950)].

[70] H. Lehmann, K. Symanzik, and W. Zimmermann, On the formulation of quantized field theories, Nuovo Cim., **1**, 205–225, (1955).

[71] R. P. Feynman, Space-time approach to nonrelativistic quantum mechanics, Rev. Mod. Phys., **20**, 367–387, (1948).

[72] K. Bleuler, A New method of treatment of the longitudinal and scalar photons, Helv. Phys. Acta, **23**, 567–586, (1950).

[73] S. N. Gupta, Theory of longitudinal photons in quantum electrodynamics, Proc. Phys. Soc., **A63**, 681–691, (1950).

[74] L. D. Faddeev and V. N. Popov, Feynman Diagrams for the Yang-Mills Field, Phys. Lett., **25B**, 29–30, (1967).

[75] C. Becchi, A. Rouet, and R. Stora, Renormalization of the Abelian Higgs-Kibble Model, Commun. Math. Phys., **42**, 127–162, (1975).

[76] C. Becchi, A. Rouet, and R. Stora, Renormalization of Gauge Theories, Annals Phys., **98**, 287–321, (1976).

[77] I. V. Tyutin, Gauge Invariance in Field Theory and Statistical Physics in Operator Formalism, arXiv:0812.0580.

[78] N. D. Christensen and C. Duhr, FeynRules - Feynman rules made easy, Comput. Phys. Commun., **180**, 1614–1641, (2008), arXiv:0806.4194.

[79] G. 't Hooft and M. Veltman, Regularization and renormalization of gauge fields, Nucl. Phys. B, **44**, 189–213, (1972).

[80] P. Breitenlohner and D. Maison, Dimensional renormalization and the action principle, Communications in Mathematical Physics, **52**, 11–38, (1977).

[81] A. Pineda, Review of Heavy Quarkonium at weak coupling, Prog. Part. Nucl. Phys., **67**, 735–785, (2012), arXiv:1111.0165.

[82] F. Schwabl, (1990), Quantum mechanics.

[83] A. Pich, Effective field theory: Course, arXiv:hep-ph/9806303.

[84] S. Weinberg, Effective Field Theory, Past and Future, PoS, **CD09**, 001, (2009), arXiv:0908.1964.

[85] A. J. Buras, Weak Hamiltonian, CP violation and rare decays, arXiv:hep-ph/9806471.

[86] J. F. Donoghue, Leading quantum correction to the Newtonian potential, Phys. Rev. Lett., **72**, 2996–2999, (1994), arXiv:gr-qc/9310024.

[87] J. F. Donoghue, General relativity as an effective field theory: The leading quantum corrections, Phys. Rev., **D50**, 3874–3888, (1994), arXiv:gr-qc/9405057.

[88] N. Brambilla, D. Gromes, and A. Vairo, Poincare' invariance constraints on NRQCD and potential NRQCD, Phys. Lett. B, **576:314-327,2003**, (2003), arXiv:hep-ph/0306107.

[89] M. Beneke and V. A. Smirnov, Asymptotic expansion of Feynman integrals near threshold, Nucl. Phys. B, **522**, 321–344, (1998), arXiv:hep-ph/9711391.

[90] B. Jantzen, Foundation and generalization of the expansion by regions, JHEP, **12**, 076, (2011), arXiv:1111.2589.

[91] A. Manohar, The HQET/NRQCD Lagrangian to order α/m^3, Phys. Rev. D, **56**, 230–237, (1997), arXiv:hep-ph/9701294.

[92] W. Heisenberg and H. Euler, Consequences of Dirac's theory of positrons, Z. Phys., **98**, 714–732, (1936), arXiv:physics/0605038.

[93] A. G. Grozin, Introduction to effective field theories. 1. Heisenberg-Euler effective theory, decoupling of heavy flavours, arXiv:0908.4392.

[94] A. Denner, Techniques for the calculation of electroweak radiative corrections at the one-loop level and results for W-physics at LEP200, Fortschr.Phys., **41:307-420,1993**, (2007), arXiv:0709.1075.

[95] N. Brambilla and A. Vairo, Quark confinement and the hadron spectrum, arXiv:hep-ph/9904330.

[96] J. Gasser and H. Leutwyler, Chiral Perturbation Theory to One Loop, Annals Phys., **158**, 142, (1984).

[97] J. Gasser and H. Leutwyler, Chiral Perturbation Theory: Expansions in the Mass of the Strange Quark, Nucl. Phys., **B250**, 465–516, (1985).

[98] N. Isgur and M. B. Wise, Weak Decays of Heavy Mesons in the Static Quark Approximation, Phys. Lett., **B232**, 113–117, (1989).

[99] N. Isgur and M. B. Wise, WEAK TRANSITION FORM-FACTORS BETWEEN HEAVY MESONS, Phys. Lett., **B237**, 527–530, (1990).

[100] E. Eichten and B. R. Hill, STATIC EFFECTIVE FIELD THEORY: 1/m CORRECTIONS, Phys. Lett., **B243**, 427–431, (1990).

[101] H. Georgi, An Effective Field Theory for Heavy Quarks at Low-energies, Phys. Lett., **B240**, 447–450, (1990).

[102] B. Grinstein, The Static Quark Effective Theory, Nucl. Phys., **B339**, 253–268, (1990).

[103] C. W. Bauer, S. Fleming, and M. E. Luke, Summing Sudakov logarithms in B —> X(s gamma) in effective field theory, Phys. Rev., **D63**, 014006, (2000), arXiv:hep-ph/0005275.

[104] C. W. Bauer, S. Fleming, D. Pirjol, and I. W. Stewart, An Effective field theory for collinear and soft gluons: Heavy to light decays, Phys. Rev., **D63**, 114020, (2001), arXiv:hep-ph/0011336.

[105] C. W. Bauer and I. W. Stewart, Invariant operators in collinear effective theory, Phys. Lett., **B516**, 134–142, (2001), arXiv:hep-ph/0107001.

[106] C. W. Bauer, D. Pirjol, and I. W. Stewart, Soft collinear factorization in effective field theory, Phys. Rev., **D65**, 054022, (2002), arXiv:hep-ph/0109045.

[107] C. W. Bauer, S. Fleming, D. Pirjol, I. Z. Rothstein, and I. W. Stewart, Hard scattering factorization from effective field theory, Phys. Rev., **D66**, 014017, (2002), arXiv:hep-ph/0202088.

[108] M. Beneke, A. P. Chapovsky, M. Diehl, and T. Feldmann, Soft-collinear effective theory and heavy-to-light currents beyond leading power, Nucl. Phys. B, **643**, 431–476, (2002), arXiv:hep-ph/0206152.

[109] N. Brambilla, J. Ghiglieri, A. Vairo, and P. Petreczky, Static quark-antiquark pairs at finite temperature, Phys. Rev., **D78**, 014017, (2008), arXiv:0804.0993.

[110] M. B. Wise, Chiral perturbation theory for hadrons containing a heavy quark, Phys. Rev., **D45**, R2188, (1992).

[111] G. Burdman and J. F. Donoghue, Union of chiral and heavy quark symmetries, Phys. Lett., **B280**, 287–291, (1992).

[112] T.-M. Yan et al., Heavy quark symmetry and chiral dynamics, Phys. Rev., **D46**, 1148–1164, (1992), [Erratum: Phys. Rev.D55,5851(1997)].

[113] S. Fleming and T. Mehen, Hadronic Decays of the X(3872) to chi(cJ) in Effective Field Theory, Phys. Rev., **D78**, 094019, (2008), arXiv:0807.2674.

[114] B. Povh, K. Rith, C. Scholz, and F. Zersche, (1995), Particles and nuclei: An Introduction to the physical concepts.

[115] G. T. Bodwin, H. S. Chung, D. Kang, J. Lee, and C. Yu, Improved determination of color-singlet nonrelativistic QCD matrix elements for S-wave charmonium, Phys. Rev., **D77**, 094017, (2008), arXiv:0710.0994.

[116] R. Barbieri, M. Caffo, R. Gatto, and E. Remiddi, Strong QCD Corrections to p Wave Quarkonium Decays, Phys. Lett., **B95**, 93–95, (1980).

[117] A. Gunawardana and G. Paz, On HQET and NRQCD Operators of Dimension 8 and Above, (2017), arXiv:1702.08904.

[118] N. Brambilla, E. Mereghetti, and A. Vairo, Hadronic quarkonium decays at order v^7, Phys. Rev. D, **79:074002,2009;**, Erratum–ibid.D83:079904,2011, (2008), arXiv:0810.2259.

[119] A. Pineda and J. Soto, Matching at one loop for the four-quark operators in NRQCD, Phys. Rev. D, **58**, 114011, (1998), arXiv:hep-ph/9802365.

[120] S. Fleming, I. Z. Rothstein, and A. K. Leibovich, Power counting and effective field theory for charmonium, Phys. Rev., **D64**, 036002, (2001), arXiv:hep-ph/0012062.

[121] M. B. Einhorn and S. D. Ellis, Hadronic Production of the New Resonances: Probing Gluon Distributions, Phys. Rev., **D12**, 2007, (1975).

[122] S. D. Ellis, M. B. Einhorn, and C. Quigg, Comment on Hadronic Production of Psions, Phys. Rev. Lett., **36**, 1263, (1976).

[123] C. E. Carlson and R. Suaya, Hadronic Production of psi/J Mesons, Phys. Rev., **D14**, 3115, (1976).

[124] P. Cho and A. K. Leibovich, Color-octet quarkonia production II, Phys.Rev. D, **53**, 6203–6217, (1996), arXiv:hep-ph/9511315.

[125] N. Brambilla, D. Eiras, A. Pineda, J. Soto, and A. Vairo, Inclusive Decays of Heavy Quarkonium to Light Particles, Phys. Rev. D, **67**, 034018, (2003), arXiv:hep-ph/0208019.

[126] G. T. Bodwin, J. Lee, and R. Vogt, Inclusive heavy quarkonium production in hadronic collisions, arXiv:hep-ph/0305034.

[127] J. M. Campbell, F. Maltoni, and F. Tramontano, QCD corrections to J/psi and Upsilon production at hadron colliders, Phys. Rev. Lett., **98**, 252002, (2007), arXiv:hep-ph/0703113.

[128] P. Artoisenet, J. M. Campbell, J. P. Lansberg, F. Maltoni, and F. Tramontano, Υ Production at Fermilab Tevatron and LHC Energies, Phys. Rev. Lett., **101**, 152001, (2008), arXiv:0806.3282.

[129] Z.-B. Kang, J.-W. Qiu, and G. Sterman, Heavy quarkonium production and polarization, Phys. Rev. Lett., **108**, 102002, (2012), arXiv:1109.1520.

[130] Z.-B. Kang, Y.-Q. Ma, J.-W. Qiu, and G. Sterman, Heavy Quarkonium Production at Collider Energies: Factorization and Evolution, Phys. Rev., **D90**, 034006, (2014), arXiv:1401.0923.

[131] S. Fleming, A. K. Leibovich, T. Mehen, and I. Z. Rothstein, The Systematics of Quarkonium Production at the LHC and Double Parton Fragmentation, Phys. Rev., **D86**, 094012, (2012), arXiv:1207.2578.

[132] S. Fleming, A. K. Leibovich, T. Mehen, and I. Z. Rothstein, Anomalous dimensions of the double parton fragmentation functions, Phys. Rev., **D87**, 074022, (2013), arXiv:1301.3822.

[133] G. T. Bodwin, X. Garcia i Tormo, and J. Lee, Factorization theorems for exclusive heavy-quarkonium production, Phys. Rev. Lett., **101**, 102002, (2008), arXiv:0805.3876.

[134] G. T. Bodwin, X. Garcia i Tormo, and J. Lee, Factorization in exclusive quarkonium production, Phys. Rev., **D81**, 114014, (2010), arXiv:1003.0061.

[135] G. T. Bodwin, X. Garcia i Tormo, and J. Lee, Closing a Loophole in Factorization Proofs, AIP Conf. Proc., **1343**, 317–319, (2011), arXiv:1011.5899.

[136] G. C. Nayak, J.-W. Qiu, and G. Sterman, Fragmentation, NRQCD and NNLO Factorization Analysis in Heavy Quarkonium Production, Phys. Rev. D, **72**, 114012, (2005), arXiv:hep-ph/0509021.

[137] G. C. Nayak, J.-W. Qiu, and G. F. Sterman, NRQCD Factorization and Velocity-dependence of NNLO Poles in Heavy Quarkonium Production, Phys. Rev., **D74**, 074007, (2006), arXiv:hep-ph/0608066.

[138] M. Butenschoen and B. A. Kniehl, World data of J/psi production consolidate NRQCD factorization at NLO, Phys. Rev., **D84**, 051501, (2011), arXiv:1105.0820.

[139] H. Bethe and E. Salpeter, A Relativistic Equation for Bound-State Problems, Phys. Rev., **84**, 1232–1242, (1951).

[140] T. Kinoshita and M. Nio, Radiative corrections to the muonium hyperfine structure. 1. The alpha**2 (Z-alpha) correction, Phys. Rev., **D53**, 4909–4929, (1996), arXiv:hep-ph/9512327.

[141] P. Labelle, S. M. Zebarjad, and C. P. Burgess, NRQED and next-to-leading hyperfine splitting in positronium, Phys. Rev., **D56**, 8053–8061, (1997), arXiv:hep-ph/9706449.

[142] A. H. Hoang, P. Labelle, and S. M. Zebarjad, The Single photon annihilation contributions to the positronium hyperfine splitting to order m(e) alpha**6, Phys. Rev. Lett., **79**, 3387–3390, (1997), arXiv:hep-ph/9707337.

[143] R. J. Hill, New value of m(muon) / m(e) from muonium hyperfine splitting, Phys. Rev. Lett., **86**, 3280–3283, (2001), arXiv:hep-ph/0010130.

[144] R. J. Hill and G. P. Lepage, Order (alpha**2 Gamma) binding effects in orthopositronium decay, Phys. Rev., **D62**, 111301, (2000), arXiv:hep-ph/0003277.

[145] R. J. Hill, G. Lee, G. Paz, and M. P. Solon, NRQED Lagrangian at order $1/M^4$, Phys. Rev., **D87**, 053017, (2013), arXiv:1212.4508.

[146] R. Harlander, T. Seidensticker, and M. Steinhauser, Complete corrections of Order alpha alpha-s to the decay of the Z boson into bottom quarks, Phys. Lett., **B426**, 125–132, (1998), arXiv:hep-ph/9712228.

[147] T. Seidensticker, Automatic application of successive asymptotic expansions of Feynman diagrams, arXiv:hep-ph/9905298.

[148] T. Hahn, Generating Feynman Diagrams and Amplitudes with FeynArts 3, Comput. Phys. Commun., **140**, 418–431, (2001), arXiv:hep-ph/0012260.

[149] P. Nogueira, Automatic Feynman graph generation, J. Comput. Phys., **105**, 279–289, (1993).

[150] M. Jamin and M. E. Lautenbacher, TRACER version 1.1, Comput. Phys. Commun., **74**, 265–288, (1993).

[151] M. Sjödahl, ColorMath - A package for color summed calculations in SU(Nc), Eur. Phys. J., **C73**, 2310, (2013), arXiv:1211.2099.

[152] T. Hahn and M. Perez-Victoria, Automatized One-Loop Calculations in 4 and D dimensions, Comput. Phys. Commun., **118**, 153–165, (1999), arXiv:hep-ph/9807565.

[153] G. Cullen et al., GoSam-2.0: a tool for automated one-loop calculations within the Standard Model and beyond, Eur. Phys. J. C, **74**, 8, 3001, (2014), arXiv:1404.7096.

[154] G. Belanger et al., GRACE at ONE-LOOP: Automatic calculation of 1-loop diagrams in the electroweak theory with gauge parameter independence checks, Phys. Rept., **430**, 117–209, (2006), arXiv:hep-ph/0308080.

[155] H. H. Patel, Package-X: A Mathematica package for the analytic calculation of one-loop integrals, Comput. Phys. Commun., **197**, 276–290, (2015), arXiv:1503.01469.

[156] M. Wiebusch, HEPMath: A Mathematica Package for Semi-Automatic Computations in High Energy Physics, Comput. Phys. Commun., **195**, 172–190, (2014), arXiv:1412.6102.

[157] J. A. M. Vermaseren, New features of FORM, arXiv:math-ph/0010025.

[158] E. R. Caianiello and S. Fubini, On the algorithm of Dirac spurs, Nuovo Cim, **9**, 1218–1226, (1952).

[159] J. S. R. Chisholm, Calculation of S-matrix elements, (Cambridge Univ Press), Vol. 48 02.

[160] J. S. R. Chisholm, Relativistic scalar products of γ matrices, Il Nuovo Cimento (1955-1965), **30**, 426, (1963).

[161] J. Chisholm, Generalisation of the Kahane algorithm for scalar products of λ-matrices, Comput. Phys. Commun., **4**, 205–207, (1972).

[162] M. Veltman, Gammatrica, Nucl. Phys. B, **319**, 253–270, (1989).

[163] J. C. Collins, (1986), Renormalization, Cambridge Monographs on Mathematical Physics, (Cambridge University Press, Cambridge), Vol. 26.

[164] F. Jegerlehner, Facts of life with gamma(5), Eur.Phys.J.C, **18:673-679,2001**, (2001), arXiv:hep-th/0005255.

[165] P. A. Baikov and V. A. Ilyin, Status of gamma(5) in dimensional regularization, Theor. Math. Phys., **88**, 789–809, (1991), [Teor. Mat. Fiz.88,163(1991)].

[166] J. G. Korner, D. Kreimer, and K. Schilcher, A Practicable gamma(5) scheme in dimensional regularization, Z. Phys., **C54**, 503–512, (1992).

[167] T. L. Trueman, Spurious anomalies in dimensional renormalization, Z. Phys., **C69**, 525–536, (1996), arXiv:hep-ph/9504315.

[168] S. Weinzierl, Equivariant dimensional regularization, arXiv:hep-ph/9903380.

[169] T. H. West, FeynmanParameter and trace - programs for expressing Feynman amplitudes as integrals over Feynman parameters, Comput. Phys. Commun., **77**, 286–298, (1993).

[170] P. Cvitanović, Group theory for Feynman diagrams in non-Abelian gauge theories, Phys. Rev. D, **14**, 1536–1553, (1976).

[171] K. Chetyrkin and F. Tkachov, Integration by parts: The algorithm to calculate β-functions in 4 loops, Nucl. Phys. B, **192**, 159–204, (1981).

[172] J. H. Kuhn, J. Kaplan, and E. G. O. Safiani, Electromagnetic Annihilation of e+ e- Into Quarkonium States with Even Charge Conjugation, Nucl. Phys., **B157**, 125–144, (1979).

[173] B. Guberina, J. H. Kuhn, R. D. Peccei, and R. Ruckl, Rare Decays of the Z0, Nucl. Phys., **B174**, 317–334, (1980).

[174] G. T. Bodwin and A. Petrelli, Order-v^4 corrections to S-wave quarkonium decay, Phys. Rev. D, **66**, 094011, (2002), arXiv:1301.1079, [Erratum: Phys. Rev.D87,no.3,039902(2013)].

[175] M. Butenschoen, Photoproduction of the J/psi meson at HERA at next-to-leading order within the framework of nonrelativistic QCD, Ph.D. thesis, (Hamburg U.), (2009).

[176] F. Feng, $Apart: A Generalized Mathematica Apart Function, Comput. Phys. Commun., **183**, 2158–2164, (2012), arXiv:1204.2314.

[177] K. G. Chetyrkin, A. L. Kataev, and F. V. Tkachov, New approach to evaluation of multiloop Feynman integrals: The Gegenbauer polynomial x-space technique, Nuclear Physics B, **174**, 345–377, (1980).

[178] E. Braaten and Y.-Q. Chen, Dimensional regularization in quarkonium calculations, Phys. Rev., **D55**, 2693–2707, (1997), arXiv:hep-ph/9610401.

[179] G. Feinberg and J. Sucher, General Theory of the van der Waals Interaction: A Model-Independent Approach, Phys. Rev. A, **2**, 2395–2415, (1970).

[180] G. Feinberg, The dispersion theory of dispersion forces, Physics Reports, **180**, 83–157, (1989).

[181] G. Bhanot and M. E. Peskin, Short-distance analysis for heavy-quark systems, Nucl. Phys. B, **156**, 391–416, (1979).

[182] S. J. Brodsky, I. A. Schmidt, and G. F. de Teramond, NUCLEAR BOUND QUARKONIUM, Phys. Rev. Lett., **64**, 1011, (1990).

[183] M. Luke, A. V. Manohar, and M. J. Savage, A QCD Calculation of the Interaction of Quarkonium with Nuclei, Phys. Lett. B, **288**, 355–359, (1992), arXiv:hep-ph/9204219.

[184] S. J. Brodsky and G. A. Miller, Is J/psi-Nucleon Scattering Dominated by the Gluonic van der Waals Interaction?, Phys. Lett. B, **412**, 125–130, (1997), arXiv:hep-ph/9707382.

[185] S. R. Beane et al., Quarkonium-Nucleus Bound States from Lattice QCD, Phys. Rev., **D91**, 114503, (2015), arXiv:1410.7069.

[186] M. B. Voloshin, Charmonium, Prog. Part. Nucl. Phys., **61**, 455–511, (2008), arXiv:0711.4556.

[187] I. A. Perevalova, M. V. Polyakov, and P. Schweitzer, On LHCb pentaquarks as a baryon-ψ(2S) bound state: prediction of isospin-$\frac{3}{2}$ pentaquarks with hidden charm, Phys. Rev., **D94**, 054024, (2016), arXiv:1607.07008.

[188] S. Elhatisari, S. König, D. Lee, and H. W. Hammer, Causality, universality, and effective field theory for van der Waals interactions, Phys. Rev., **A87**, 052705, (2013), arXiv:1303.5261.

[189] L. H. Ford, M. P. Hertzberg, and J. Karouby, Quantum Gravitational Force Between Polarizable Objects, Phys. Rev. Lett., **116**, 151301, (2016), arXiv:1512.07632.

[190] B. R. Holstein, Long Range Electromagnetic Effects involving Neutral Systems and Effective Field Theory, Phys. Rev. D, **78**, 013001, (2008), arXiv:0802.2266.

[191] J. Sucher, Casimir and beyond: Long-range forces between neutral and charged particles, Comments Mod. Phys., **D1**, 227–242, (2000).

[192] A. Vairo, pNRQCD: Review of selected results, arXiv:hep-ph/0010191.

[193] G. Maroulis, (2006), Atoms, Molecules and Clusters in Electric Fields: Theoretical Approaches to the calculation of electric polarizability, (World Scientific), Vol. 1.

[194] B. R. Holstein, D. Drechsel, B. Pasquini, and M. Vanderhaeghen, Higher order polarizabilities of the proton, Phys. Rev., **C61**, 034316, (2000), arXiv:hep-ph/9910427.

[195] D. B. Kaplan, Five lectures on effective field theory, arXiv:nucl-th/0510023.

[196] H. W. Griesshammer, Nucleon polarisabilities from Compton scattering off the one- and few-nucleon system, Prog. Part. Nucl. Phys., **55**, 215–227, (2005), arXiv:nucl-th/0411080.

[197] M. O'Carroll and J. Sucher, Exact Computation of the van der Waals Constant for Two Hydrogen Atoms, Phys. Rev. Lett., **21**, 1143–1146, (1968).

[198] J. O. Hirschfelder and W. J. Meath, (2007), The Nature of Intermolecular Forces, (John Wiley & Sons, Inc.), pp. 3–106.

[199] G. Feinberg, J. Sucher, and C. K. Au, The Dispersion Theory of Dispersion Forces, Phys. Rept., **180**, 83, (1989).

[200] N. Brambilla, G. Krein, J. Tarrus Castella, and A. Vairo, TUM-EFT-69-15, (in preparation).

[201] Y. Bai, S. Lu, and J. Osborne, Beauty-full Tetraquarks, arXiv:1612.00012.

[202] M. Giordano and E. Meggiolaro, Remarks on the static dipole-dipole potential at large distances, Phys. Rev., **D92**, 096007, (2015), arXiv:1507.07215.

[203] H. S. Chung, J. Lee, and C. Yu, Exclusive heavy quarkonium + gamma production from e+ e- annihilation into a virtual photon, Phys. Rev. D, **78**, 074022, (2008), arXiv:0808.1625.

[204] W.-L. Sang and Y.-Q. Chen, Higher Order Corrections to the Cross Section of e+e- to Quarkonium plus gamma, Phys. Rev. D, **81**, 034028, (2010), arXiv:0910.4071.

[205] D. Li, Z.-G. He, and K.-T. Chao, Search for $C = +$ charmonium and bottomonium states in $e^+e^- \to \gamma + X$ at B factories, Phys. Rev. D, **80**, 114014, (2009), arXiv:0910.4155.

[206] B.-Q. Li and K.-T. Chao, Higher Charmonia and X,Y,Z states with Screened Potential, Phys.Rev.D, **79**, 094004, (2009), arXiv:0903.5506.

[207] R. Molina and E. Oset, The Y(3940), Z(3930) and the X(4160) as dynamically generated resonances from the vector-vector interaction, Phys. Rev. D, **80**, 114013, (2009), arXiv:0907.3043.

[208] B.-Q. Li, C. Meng, and K.-T. Chao, Search for $\chi_{c_J}(2P)$ from Higher Charmonim E1 Transitions and X,Y,Z States, arXiv:1201.4155.

[209] F.-K. Guo and U.-G. Meißner, Where is the $\chi_{c0}(2P)$?, Phys. Rev. D, **86**, 091501, (2012), arXiv:1208.1134.

[210] S. L. Olsen, Is the $X(3915)$ the $\chi_{c0}(2P)$?, Phys. Rev. D, **91**, 057501, (2014), arXiv:1410.6534.

[211] BESIII Collaboration, Observation of $e^+e^- \to \gamma X(3872)$ at BESIII, Phys. Rev. Lett., **112**, 092001, (2013), arXiv:1310.4101.

[212] G. T. Bodwin, J. Lee, and E. Braaten, Exclusive double charmonium production from e^+e^- annihilation into two virtual photons, Phys. Rev., **D67**, 054023, (2003), arXiv:hep-ph/0212352, [Erratum: Phys. Rev.D72,099904(2005)].

[213] E. Braaten and Y.-Q. Chen, Renormalons in Electromagnetic Annihilation Decays of Quarkonium, Phys. Rev. D, **57**, 4236–4253, (1998), arXiv:hep-ph/9710357.

[214] I. Maksymyk, Comment concerning relativistic corrections in NRQCD, arXiv:hep-ph/9710291.

[215] E. Braaten and J. Lee, Exclusive double charmonium production from e+ e- annihilation into a virtual photon, Phys. Rev., **D67**, 054007, (2003), arXiv:hep-ph/0211085, [Erratum: Phys. Rev.D72,099901(2005)].

[216] E. Braaten, S. Fleming, and T. C. Yuan, Production of Heavy Quarkonium in High-Energy Colliders, Annual Review of Nuclear and Particle Science, **46**, 197–235, (1996).

[217] D. A. Bolotin and S. V. Poslavsky, Introduction to Redberry: a computer algebra system designed for tensor manipulation, arXiv:1302.1219.

[218] M. Gremm and A. Kapustin, Annihilation of S-wave quarkonia and the measurement of $alpha_s$, Phys. Lett. B, **407**, 323–330, (1997), arXiv:hep-ph/9701353.

[219] W. L. Sang, Quarkonium annihilation into photons, talk given at the 9th International Workshop on Heavy Quarkonium in Beijing, (2013).

[220] Y.-J. Li, G.-Z. Xu, K.-Y. Liu, and Y.-J. Zhang, Search for $C = +$ charmonium and XYZ states in $e^+e^- \to \gamma + H$ at BESIII, JHEP, **01**, 022, (2014), arXiv:1310.0374.

[221] E. Eichten and C. Quigg, Quarkonium wave functions at the origin, Phys. Rev. D, **52**, 1726–1728, (1995).

[222] W.-L. Sang, F. Feng, and Y.-Q. Chen, Relativistic corrections to Y exclusive decay into double $S-$wave charmonia, (year?), arXiv:1502.01499v2.

[223] M. Ablikim et al., Two-photon widths of the $\chi_{c0,2}$ states and helicity analysis for $\chi_{c2} \to \gamma\gamma$, Phys. Rev., **D85**, 112008, (2012), arXiv:1205.4284.

[224] R. Barbieri, R. Gatto, and R. Kogerler, Calculation of the Annihilation Rate of P Wave Quark - anti-Quark Bound States, Phys. Lett., **60B**, 183–188, (1976).

[225] K. G. Chetyrkin, J. H. Kuhn, and M. Steinhauser, RunDec: A Mathematica package for running and decoupling of the strong coupling and quark masses, Comput. Phys. Commun., **133**, 43–65, (2000), arXiv:hep-ph/0004189.

[226] B. Schmidt and M. Steinhauser, CRunDec: a C++ package for running and decoupling of the strong coupling and quark masses, Comput. Phys. Commun., **183**, 1845–1848, (2012), arXiv:1201.6149.

[227] A. Denner, J. Küblbeck, R. Mertig, and M. Böhm, Electroweak radiative corrections to $e^+e^- \to HZ$, Z. Phys. C, **56**, 261–272, (1992).

[228] W. Beenakker, A. Denner, S. Dittmaier, R. Mertig, and T. Sack, High-energy approximation for on-shell W-pair production, Nucl. Phys. B, **410**, 245–279, (1993).

[229] W. Beenakker et al., Electroweak one-loop contributions to top pair production in hadron colliders, Nucl. Phys. B, **411**, 343–380, (1994).

[230] W. Beenakker, A. Denner, S. Dittmaier, and R. Mertig, On-shell W-pair production in the TeV range, Phys. Lett. B, **317**, 622–630, (1993).

[231] R. Mertig and W. L. van Neerven, The calculation of the two-loop spin splitting functions $P_{ij}^{(1)}(x)$, Z. Phys. C, **70**, 637–653, (1996), arXiv:hep-ph/9506451.

[232] R. Mertig and R. Scharf, TARCER - A Mathematica program for the reduction of two-loop propagator integrals, Comput. Phys. Commun., **111**, 265–273, (1998), arXiv:hep-ph/9801383.

[233] O. V. Tarasov, Connection between Feynman integrals having different values of the space-time dimension, Phys. Rev. D, **54**, 6479–6490, (1996), arXiv:hep-th/9606018.

[234] O. V. Tarasov, Generalized Recurrence Relations for Two-loop Propagator Integrals with Arbitrary Masses, Nucl. Phys. B, **502**, 455–482, (1997), arXiv:hep-ph/9703319.

[235] M. Buechler, G. Colangelo, J. Kambor, and F. Orellana, Dispersion relations and soft pion theorems for $K \to \pi\pi$, Phys. Lett. B, **521**, 22–28, (2001), arXiv:hep-ph/0102287.

[236] M. Tentyukov and J. Fleischer, A Feynman Diagram Analyser DIANA, Comput. Phys. Commun., **132**, 124–141, (2000), arXiv:hep-ph/9904258.

[237] G. Passarino and M. Veltman, One Loop Corrections for e^+e^- Annihilation Into $\mu^+\mu^-$ in the Weinberg Model, Nucl. Phys., **B160**, 151, (1979).

[238] A. Buckley et al., LHAPDF6: parton density access in the LHC precision era, Eur. Phys. J. C, **75**, (2015).

[239] P. Cho and A. Leibovich, Color-octet quarkonia production, Phys. Rev. D, **53**, 150–162, (1996), arXiv:hep-ph/9505329.

[240] Y.-J. Zhang and K.-T. Chao, Double charm production $e^+e^- \to J/\psi + c\bar{c}$ at B factories with next-to-leading order QCD corrections, Phys. Rev. Lett., **98**, 092003, (2007), arXiv:hep-ph/0611086.

[241] A. Petrelli, M. Cacciari, M. Greco, F. Maltoni, and M. L. Mangano, NLO Production and Decay of Quarkonium, Nucl. Phys. B, **514**, 245–309, (1998), arXiv:hep-ph/9707223.

[242] Y. Jia, X.-T. Yang, W.-L. Sang, and J. Xu, $\mathcal{O}\left(\alpha_s v^2\right)$ correction to pseudoscalar quarkonium decay to two photons, J. High Energ. Phys., **2011**, (2011), arXiv:arXiv:1104.1418.

[243] C. O. Dib, R. Rosenfeld, and A. Zerwekh, Double Higgs Production and Quadratic Divergence Cancellation in Little Higgs Models with T Parity, JHEP, **0605**, 074, (2006), arXiv:hep-ph/0509179.

[244] D. Buttazzo et al., Investigating the near-criticality of the Higgs boson, J. High Energ. Phys., **2013**, (2013), arXiv:arXiv:1307.3536.

[245] D. de Florian and J. Mazzitelli, Higgs Boson Pair Production at Next-to-Next-to-Leading Order in QCD, Phys. Rev. Lett., **111**, 201801, (2013), arXiv:1309.6594.

[246] B. Xiao, Y.-K. Wang, Z.-Q. Zhou, and S. hua Zhu, Edge Charge Asymmetry in Top Pair Production at the LHC, Phys. Rev. D, **83**, 057503, (2011), arXiv:1101.2507.

[247] M. Fael, L. Mercolli, and M. Passera, Radiative μ and τ leptonic decays at NLO, JHEP, **1507**, 153, (2015), arXiv:1506.03416.

[248] L. S. Geng, J. M. Camalich, L. Alvarez-Ruso, and M. J. V. Vacas, Nucleon-to-Delta axial transition form factors in relativistic baryon chiral perturbation theory, Phys. Rev. D, **78**, 014011, (2008), arXiv:0801.4495.

[249] D. R. Phillips, M. R. Schindler, and R. P. Springer, An effective-field-theory analysis of low-energy parity-violation in nucleon-nucleon scattering, Nucl. Phys. A, **822**, 1–19, (2009), arXiv:0812.2073.

[250] J. Kopp, V. Niro, T. Schwetz, and J. Zupan, DAMA/LIBRA data and leptonically interacting dark matter, Phys. Rev. D, **80**, (2009), arXiv:arXiv:0907.3159.

[251] J. M. Cline, A. R. Frey, and F. Chen, Metastable dark matter mechanisms for INTEGRAL 511 keV γ rays and DAMA/CoGeNT events, Phys. Rev. D, **83**, 083511, (2010), arXiv:1008.1784.

[252] S. Bray, J. S. Lee, and A. Pilaftsis, Heavy Majorana Neutrino Production at e-gamma Colliders, Phys. Lett. B, **628**, 250–261, (2005), arXiv:hep-ph/0508077.

[253] R. Laha, B. Dasgupta, and J. F. Beacom, Constraints on New Neutrino Interactions via Light Abelian Vector Bosons, Phys. Rev. D, **89,**, 093025, (2013), arXiv:1304.3460.

[254] B. Dasgupta and J. Kopp, A ménage à trois of eV-scale sterile neutrinos, cosmology, and structure formation, Phys. Rev. Lett., **112,**, 031803, (2013), arXiv:1310.6337.

[255] S. Foffa and R. Sturani, Dynamics of the gravitational two-body problem at fourth post-Newtonian order and at quadratic order in the Newton constant, Phys. Rev. D, **87**, (2013), arXiv:1206.7087.

[256] J. R. Gaunt and M. Stahlhofen, The Fully-Differential Quark Beam Function at NNLO, JHEP, **1412**, 146, (2014), arXiv:1409.8281.

[257] F. Feng, Y. Jia, and W.-L. Sang, Can Nonrelativistic QCD Explain the $\gamma\gamma^* \to \eta_c$ Transition Form Factor Data?, Phys. Rev. Lett., **115**, 222001, (2015), arXiv:1505.02665.

[258] A. V. Smirnov, FIESTA 3: cluster-parallelizable multiloop numerical calculations in physical regions, Comput. Phys. Commun., **185**, 2090–2100, (2013), arXiv:1312.3186.

[259] S. Borowka, J. Carter, and G. Heinrich, Numerical evaluation of multi-loop integrals for arbitrary kinematics with SecDec 2.0, Comput. Phys. Commun., **184**, 396–408, (2012), arXiv:1204.4152.

[260] R. N. Lee, Presenting LiteRed: a tool for the Loop InTEgrals REDuction, arXiv:1212.2685.

[261] C. Studerus, Reduze - Feynman Integral Reduction in C++, Comput. Phys. Commun., **181**, 1293–1300, (2009), arXiv:0912.2546.

[262] C. Anastasiou and A. Lazopoulos, Automatic Integral Reduction for Higher Order Perturbative Calculations, JHEP, **0407**, 046, (2004), arXiv:hep-ph/0404258.

[263] F. Feng, Automated One-loop Computation in Quarkonium Process within NRQCD Framework, J. Phys. Conf. Ser., **523**, 012041, (2014), arXiv:1307.5587.

[264] M. R. Fiorentin, FaRe: a Mathematica package for tensor reduction of Feynman integrals, Int. J. Mod. Phys., **C27**, 1650027, (2015), arXiv:1507.03527.

[265] J. Küblbeck, M. Böhm, and A. Denner, Feyn arts — computer-algebraic generation of Feynman graphs and amplitudes, Comput. Phys. Commun., **60**, 165–180, (1990).

[266] G. Ossola, C. G. Papadopoulos, and R. Pittau, Reducing full one-loop amplitudes to scalar integrals at the integrand level, Nucl. Phys. B, **763**, 147–169, (2007), arXiv:hep-ph/0609007.

[267] G. van Oldenborgh, FF - a package to evaluate one-loop Feynman diagrams, Comput. Phys. Commun., **66**, 1–15, (1991).

[268] S. Carrazza, R. K. Ellis, and G. Zanderighi, QCDLoop: a comprehensive framework for one-loop scalar integrals, Comput. Phys. Commun., **209**, 134–143, (2016), arXiv:1605.03181.

[269] A. van Hameren, OneLOop: for the evaluation of one-loop scalar functions, Comput. Phys. Commun., **182**, 2427–2438, (2011), arXiv:1007.4716.

[270] G. Cullen et al., Golem95C: A library for one-loop integrals with complex masses, Comput. Phys. Commun., **182**, 2276–2284, (2011), arXiv:1101.5595.

[271] J. Fleischer and T. Riemann, A complete algebraic reduction of one-loop tensor Feynman integrals, Phys. Rev. D, **83**, 073004, (2011), arXiv:1009.4436.

[272] A. Denner, S. Dittmaier, and L. Hofer, Collier: a fortran-based Complex One-Loop LIbrary in Extended Regularizations, Comput. Phys. Commun., **212**, 220–238, (2017), arXiv:1604.06792.

[273] A. Denner and S. Dittmaier, Reduction schemes for one-loop tensor integrals, Nucl. Phys. B, **734**, 62–115, (2006), arXiv:hep-ph/0509141.

[274] R. K. Ellis and G. Zanderighi, Scalar one-loop integrals for QCD, JHEP, **0802**, 002, (2008), arXiv:0712.1851.

[275] P. W. Angel, Y. Cai, N. L. Rodd, M. A. Schmidt, and R. R. Volkas, Testable two-loop radiative neutrino mass model based on an $LLQd^cQd^c$ effective operator, JHEP, **10**, 118, (2013), arXiv:1308.0463.

[276] A. Ilakovac and L. Popov, LOOL: Mathematica package for evaluating leading order one loop functions, arXiv:1407.2727.

[277] S. Laporta, High-precision calculation of multi-loop Feynman integrals by difference equations, Int. J. Mod. Phys. A, **15**, 5087–5159, (2000), arXiv:hep-ph/0102033.

[278] P. A. Baikov, Explicit solutions of the 3–loop vacuum integral recurrence relations, Phys. Lett. B, **385**, 404–410, (1996), arXiv:hep-ph/9603267.

[279] A. V. Smirnov and V. A. Smirnov, S-bases as a tool to solve reduction problems for Feynman integrals, Nucl. Phys. Proc. Suppl., **160**, 80–84, (2006), arXiv:hep-ph/0606247.

[280] F. Feng, APart 2: A generalized Mathematica Apart function, Comput. Phys. Commun., **198**, 260–261, (2016).

[281] M. Bohm, A. Denner, and H. Joos, Gauge theories of the strong and electroweak interaction, Stuttgart, Germany: Teubner, 784 p, (2001).

[282] J. Schwinger, On Quantum-Electrodynamics and the Magnetic Moment of the Electron, Phys. Rev., **73**, 416–417, (1948).

[283] C. Degrande, Automatic evaluation of UV and R2 terms for beyond the Standard Model Lagrangians: a proof-of-principle, Comput. Phys. Commun., **197**, 239–262, (2015), arXiv:1406.3030.

[284] D. J. Broadhurst, N. Gray, and K. Schilcher, Gauge-invariant on-shellZ 2 in QED, QCD and the effective field theory of a static quark, Zeitschrift für Physik C Particles and Fields, **52**, 111–122, (1991).

[285] L. Abbott, The background field method beyond one loop, Nucl. Phys. B, **185**, 189–203, (1981).

[286] L. Abbott, Introduction to the Background Field Method, Acta Phys. Polon., **B13**, 33, (1982).

[287] M. Spira, A. Djouadi, D. Graudenz, and P. M. Zerwas, Higgs boson production at the LHC, Nucl. Phys. B, **453**, 17–82, (1995), arXiv:hep-ph/9504378.

[288] A. Grozin, Lectures on QED and QCD, arXiv:hep-ph/0508242.

[289] A. Ore and J. L. Powell, Three photon annihilation of an electron - positron pair, Phys. Rev., **75**, 1696–1699, (1949).

[290] F. Feng, Y. Jia, and W.-L. Sang, Reconciling the nonrelativistic QCD prediction and the $J/\psi \to 3\gamma$ data, Phys. Rev., **D87**, 051501, (2013), arXiv:1210.6337.

[291] G. S. Adkins, Analytic evaluation of the amplitudes for orthopositronium decay to three photons to one-loop order, Phys.Rev.Lett., **76:4903-4906,1996**, (Phys.Rev.Lett.76:4903-4906,1996), arXiv:hep-ph/0506213.

[292] A. K. Cyrol, M. Mitter, and N. Strodthoff, FormTracer - A Mathematica Tracing Package Using FORM, (2016), arXiv:1610.09331.

[293] L. L. Foldy and S. A. Wouthuysen, On the Dirac theory of spin 1/2 particle and its nonrelativistic limit, Phys. Rev., **78**, 29–36, (1950).

[294] S. Tani, Connection between Particle Models and Field Theories, I The Case Spin 1/2, Progress of Theoretical Physics, **6**, 267–285, (1951).

[295] G. S. Adkins, Three-dimensional Fourier transforms, integrals of spherical Bessel functions, and novel delta function identities, arXiv:1302.1830.